The Cretaceous-Paleogene transition and Chicxulub impact ejecta in the northwestern Gulf of Mexico: Paleoenvironments, sequence stratigraphic setting and target lithologies

Zur Erlangung des akademischen Grades eines

Doktors der Naturwissenschaften

an der Fakultät für Bauingenieur-, Geo- und Umweltwissenschaften

der

Universität Karlsruhe

genehmigte

DISSERTATION

von

Peter Schulte

aus St. Ingbert (Saarland)

Karlsruhe 2003

Peter Schulte
Geologisches Institut
Universität (TH) Karlsruhe
Postfach 6980
D-76128 Karlsruhe, Germany
Tel.: +49-721-6082943
Fax. +49-721-6082138
Email 1: peter.schulte@bio-geo.uni-karlsruhe.de
Email 2: email@peterschulte.de

Abstract

The Cretaceous-Paleogene (K-P) transition is characterized by a period of mass extinctions, the Chicxulub impact event, sea-level changes, and considerable climate changes (e.g., cooling). The Gulf of Mexico region is a key area for addressing these issues, specifically because of the proximity to the large Chicxulub impact structure in southern Mexico, and because of its shallow shelf areas throughout the Maastrichtian to Danian period. This study presents the results of a multidisciplinary investigation of Chicxulub impact ejecta and marine sediments from the K-P transition in the western Gulf of Mexico. Sedimentological, mineralogical, and geochemical aspects of K-P sections and cores from northeastern Mexico, Texas, and Alabama have been by studied with focus on Chicxulub ejecta, long- or short-term facies change, and sequence stratigraphic setting.

The Chicxulub ejecta (or impact spherule) deposits from northeastern Mexico and Texas revealed an unexpected complex and localized ejecta composition. Fe-Mg-rich chlorite- as well as Si-Al-K-rich glass-spherules are the predominant silicic ejecta components in northeastern Mexico, whereas in Texas, spherules of Mg-rich smectite compositions were encountered. Spherules contain Fe-Ti-K-rich schlieren, Fe-Mg-rich globules, and rare μm-sized metallic and sulfidic Ni-Co-(Ir-?) rich inclusions. This composition provides evidence for a distinct range of target rocks of mafic to intermediate composition, presumably situated in the northwestern sector of the Chicxulub impact structure, in addition to the possibility of contamination by meteoritic material. The absence of spinels and the ubiquitous presence of hematite and goethite points to high oxygen fugacity during the impact process. Besides these silicic phases, the most prominent ejecta component is carbonate. Carbonate is found in ejecta deposits as unshocked clasts, accretionary lapilli-like grains, melt globules (often with quenching textures), and as microspar, suggesting that this area received ejecta mainly from shallow, carbonate-rich lithologies at the impact site on the Yucatán carbonate platform.

Albeit the ejecta spherules are mostly altered to clay minerals and iron oxides, the microfacies and internal textures of the ejecta particles show a variety of distinct features, including welding and fusing of components and evidence for liquid immiscibility between silicic-silicic and carbonate-silicic melts. No evidence for binary mixing of ejecta phases was found. Therefore, it is assumed that ejecta in northeastern Mexico derived from less energetic parts of the ejecta curtain. The welding features of ejecta particles suggest an initial ground surge-like ejecta-dispersion mode.

The specific morphological features and the compositional range of Chicxulub ejecta, as well as the results of petrological and rock magnetic characteristics reveal similarities to Chicxulub ejecta from K-P sections in the Gulf of Mexico area, the Caribbean, the Atlantic, the Pacific, and Northern America (Western Interior). In addition, Mg-rich smectite, K-feldspar, and iron oxide-rich microspherules are characteristic for the K-P boundary clay layer in sections from the Atlantic and Tethyan realm, suggestive of a relationship between the Chicxulub impact event and the basal K-P boundary clay layer.

The Chicxulub ejecta deposits are commonly associated with an event deposit that shows a complex succession of deposition from high-energetic (channelized) debris flows or turbidity currents derived from multiple source areas, followed by a period of decreasing current energy and intermittent periods of reworking. The uppermost parts of these deposits are often bioturbated, pointing to longer periods of deposition, as also sustained by the complex internal subdivision of the K-P event deposits.

In northeastern Mexico, Chicxulub ejecta is also locally embedded within latest Maastrichtian marls, though common soft-sediment deformation opposes a clear age assignation of these deposits. However, individual spherule layers in the slumped and in the channelized spherule deposits are of similar petrological, mineralogical, and geochemical composition with no size-sorting and

abrasion of ejecta, hence pointing to an origin from a single impact event (Chicxulub) and provid-
ing no evidence for extended periods between reworking of individual spherule layers.

In the Brazos core from Texas, a m-thick shale interval, almost devoid of micro- and macro-
fossils and therefore of unclear stratigraphic age, is sandwiched between Chicxulub impact ejecta
and the first appearance of Paleocene microfossils, indicating a period (of enhanced reworking?)
between these two events. However, no mm-thick ferruginous layer with Ni-rich spinels, smectite
spherules, and shocked quartz that defines the K-P boundary in the Global Stratotype Section and
Point (GSSP) at El Kef, Tunisia, and elsewhere has been observed in any of the sections and cores
studied. Therefore, an unequivocal positioning of the K-P boundary is difficult for the northwestern
Gulf of Mexico region.

The long-term record of clay mineral species during the K-P transition of northeastern Mexico,
Texas, and Alabama shows remarkably localized compositional patterns, indicating local sedi-
ment influx from topographically, petrologically, and probably climatically distinct source regions.
Chlorite-illite-dominated clay assemblages in northwestern Mexico indicate mafic source rocks,
predominance of physical weathering, and cooler climates, probably associated with the uplift of
the Sierra Madre Oriental, whereas a smectite-dominated clay assemblage in Texas indicates semi-
arid-humid climates. In central Alabama, a distinct trend from tropically humid and warm climates
to more seasonal and drier climate that already started in the late Maastrichtian was inferred from
a prominent change of a kaolinite- to a smectite-dominated clay mineral assemblage. Hence, no
unique climate conditions and distinct climate trends can be inferred for the northwestern Gulf of
Mexico area from the data provided by this study.

The sequence stratigraphic setting of the Maastrichtian to Danian strata in northeastern Mexico,
Texas, and Alabama is also quite complex. The deep-water marls in northeastern Mexico were not
amenable to a clear sequence stratigraphic subdivision, though the similar mineralogical (and geo-
chemical) composition of the Maastrichtian to Danian marls provided no evidence for a distinct ma-
jor facies change during this interval. In Texas, no facies change was observed for the (highstand)
shale interval that includes the event bed, though a gradual sea-level lowering took place upon the
appearance of the earliest Paleocene microfossils. A sequence boundary is present in the earliest
Danian and overlain by transgressive systems tract. In central Alabama, a pronounced sea-level
shallowing was recognized during a highstand systems tract in the late Maastrichtian, topped by a
sequence boundary and subsequent (strongly) rising sea level throughout the latest Maastrichtian
and the early Danian. Rapid and intense water-depth fluctuations are inferred from middle Danian
carbonate-rich strata concomitant to a change from a mixed siliciclastic-carbonate depositional
system to a more stable carbonate platform in central Alabama during this period. In summary, no
universal pattern of facies and related sea-level changes was obtained from the northwestern Gulf
of Mexico area, and particularly, no evidence for adverse an- or dysoxic sedimentary conditions
were observed for the Maastrichtian to Danian interval governed by this study.

Kurzfassung

Der Übergang von der Kreide zum Paläozän ist charakterisiert durch ein außergewöhnliches Massensterben, den Chicxulub Impakt, signifikante Meeresspiegel-Veränderungen, und beträchtliche Klimaveränderungen (u.a. Abkühlung). Aufgrund seiner Nähe zur Chicxulub Impakt Struktur und durch seine ausgedehnten Schelfgebiete die während des Maastricht und des Dan existierten ist der Golf von Mexiko ist eine entscheidende Region für das Studium dieser Ereignisse und Umweltveränderungen. Diese Doktorarbeit zeigt die Resultate einer multidisziplinären Untersuchung von Sedimenten und Chicxulub Ejekta Material aus dem Kreide-Paläozän (K-P)-Übergang im nordwestlichen Golf von Mexiko. Im Zuge dieser Arbeit wurden die Sedimentologie, Mineralogie und Geochemie von Profilen und Bohrkernen aus Nordost-Mexiko, Texas und Alabama untersucht. Die Schwerpunkte der Untersuchungen lagen bei der Charakterisierung der Chicxulub-Ejekta-Lagen, der kurz- und langzeitlichen Faziesveränderungen und der sequenzstratigraphischen Interpretation dieser Profile.

Die gut erhaltenen Impakt-Ejekta-Lagen (so genannte „Spherule- oder Mikrotektit-Lagen") aus Nordost-Mexiko und Texas zeigen eine unerwartet komplexe, lokal unterschiedliche mineralogische und geochemische Zusammensetzung. Fe-Mg-reiche chloritische Mikrotektite sowie Si-Al-K-reiche Glas-Mikrotektite sind die vorherrschenden silikatischen Ejekta-Komponenten in Nordost-Mexiko, während in Texas in erster Linie Mg-reiche smektitische Mikrotektite gefunden wurden, aber auch chloritische Ejektapartikel vorhanden sind. Spherules beinhalten Fe-, Ti-, K-reiche Schlieren, Fe-Mg-reich Globules, und μm-große metallische und sulfidische Ni-, Co- (Ir-?) reiche Einschlüsse. Diese Ejekta-Zusammensetzung deutet auf eine Abstammung von Gesteinen mit mafischen bis intermediären petrologischen Charakter aus dem nordwestlichen Bereich der Chicxulub-Impakt-Struktur hin, zudem besteht die Möglichkeit der Kontamination mit meteoritischem Material. Das Fehlen von Spinellen und das häufige Auftreten von Hämatit und Goethit weist auf hohe Sauerstoff-Fugazitäten während des Impakt-Prozesses hin.

Alle Chicxulub Ejekta-Lagen zeigen einen außerordentlich hohen Anteil an Karbonat. Das Karbonat liegt als ungeschockte und geschockte (aufgeschmolzene) Klasten (oftmals mit kristallinen Abschreckungstexturen), als akkretionäre Lapilli und als mikritischer Sparit vor. Diese Zusammensetzung des Karbonates und seine Häufigkeit lassen darauf schließen, dass in Nordost-Mexiko und Texas vorwiegend Ejekta aus flachen karbonatreichen stratigraphischen Horizonten der Chicxulub-Impakt-Struktur auf der Yucatán-Karbonatplattform in Südmexiko abgelagert wurden.

Obwohl die Mikrotektite zumeist zu Tonmineralen und Eisenoxiden alteriert sind, zeigen die Ejektalagen und ihre Komponenten eine charakteristische Mikrofazies und interne Strukturen, die vor allem Sintertexturen zwischen Ejektapartikeln und Unmischbarkeitstexturen zwischen karbonatischen und silikatischen Ejektaphasen umfassen. Hinweise für eine binäre Mischung dieser silikatischen und karbonatischen Phasen, wie sie z.B. für die Spherules in Beloc, Haiti, charakteristisch sind, wurden nicht gefunden. Dies legt den Schluss nahe, dass in Nordost-Mexiko vor allem Ejekta aus niedrigenergetischen Bereichen der Impakt-generierten Glutwolke abgelagert wurde.

Die speziellen morphologischen Eigenschaften der Spherules im nordwestlichen Golf von Mexiko sind kongruent zu Mikrotektiten und mikrokristallinen Ejektapartikeln aus Profilen des Kreide-Paläozän-Übergangs im Golf von Mexiko, der Karibik, dem Atlantik, dem Pazifik, und Nordamerika. Zudem sind Mg-reiche Smektitspherules ebenso wie K-reiche und eisenoxidreiche Mikrospherules charakteristisch für die basale Tonschicht an der Kreide-Paläozän-Grenze in der Tethys. Dies deutet auf eine kausale Beziehung zwischen dem Chicxulub Impakt Ereignis und der basalen Impakt-Lage der Kreide-Paläozän Grenztons hin.

Die Spherules in Nordost Mexiko, Texas und Alabama sind assoziiert mit einer Eventablagerungs-Sequenz, die eine komplexe Ablagerungsabfolge von hochenergetischen Massenströmen („debris-flows") mit jeweils verschiedenen Liefergebieten darstellt. Diese Abfolge wird überlagert

von Ablagerungen mit abnehmender Strömungsenergie. Die obersten Lagen dieser Ablagerungen sind häufig bioturbiert, was zusammen mit ihrem komplexen internen Aufbau auf längere und intermittierende Aufarbeitungsperioden hinweist. Chicxulub-Ejekta wurde in Nordost-Mexiko aber auch lokal eingeschaltet in Mergel des späten Maastrichts gefunden, obwohl sedimentäre Deformationsstrukturen („Slumps") und Rutschungen hier keine eindeutige (bio-) stratigraphische Einstufung erlauben. Allerdings sind die verschiedenen Ejektalagen in Nordost-Mexiko unter sedimentologischen, mineralogischen und geochemischen Gesichtspunkten sehr ähnlich was auf sehr kurze Zeiträume zwischen Ablagerung und Aufarbeitung schließen lässt. Im Kreide-Paläozän-Übergang des Bohrkerns aus Brazos, Texas, sind die Chicxulub Ejekta-Ablagerungen von etwa 1.6 m mächtigen, karbonat- und fossilarmen Schiefertonen unklarer stratigraphischer Zuordnung überlagert, auf die karbonatreiche Schiefertone mit den ersten Mikrofossilien des Paläozäns folgen.

Eine mm-dicke eisenreiche Tonlage mit smektitischen Spherules und Ni-reichen Spinellen (und geschockten Mineralen), die die K-P Grenze im K-P Typusprofil von El Kef in Tunesien (und vielen anderen K-P Profilen weltweit) darstellt, wurde in keinem der untersuchten Profile und Bohrkerne gefunden. Dies erschwert eine eindeutige Positionierung der K-P Grenze im untersuchten nordwestlichen Teil des Golfes von Mexiko.

Die Tonmineralfazies vom späten Maastricht zum Dan zeigt in den untersuchten Profilen und Bohrkernen aus Nordost-Mexiko, Texas und Alabama eine sehr komplexe und lokal verschiedene Zusammensetzung mit Einflüssen von topographisch, petrologisch und vermutlich auch klimatisch unterschiedlichen Regionen. Für den unmittelbaren K-P Übergang wurden für diese Gebiete keine einheitlichen klimatischen Trends aus den vorherrschenden Tonmineralspezies festgestellt. Nur in dem Bohrkern aus Zentral-Alabama zeigt sich anhand des Wechsels von einer Kaolinit- zu einer Smektit-dominierten Tonmineralfazies ein genereller Trend von humid-feuchten Klimabedingungen während des Maastrichts zu saisonalen und trockeneren Klimaten während des Dans.

Die sequenzstratigraphische Untersuchung der Profile und Bohrkerne ergab für den unmittelbaren K-P-Übergang in Texas und Alabama ein stark lokalisiertes Schema der Meeresspiegelveränderungen, während die Tiefwasser-Mergel in Nordost-Mexiko keine sequenzstratigraphische Analyse zuließen. Hinweise auf ausgedehnte an- oder dys-oxische sedimentäre Bedingungen wurden nicht gefunden. In Texas zeigt die Sedimentologie der Tonsteine aus dem späten Maastricht keine spezifischen proximal-distalen Trends an, und sie wurden deshalb als „highstand systems tract" mit stabilem Meeresspiegelniveau interpretiert. Eine Sequenzgrenze wurde anhand verschiedener Proxies in den Sedimenten des frühesten Dans gefunden, die von transgressiven Einheiten überlagert wird. In Zentral-Alabama deuten die Sedimente des späten Maastrichts auf einen ausgeprägten Meeresspiegel-Tiefstand hin, gefolgt von einer Sequenzgrenze und transgressivem Meeresspiegelverhalten über die K-P Grenze hinweg bis in das früheste Dan hinein. Während des mittleren Dans treten dann in Alabama starke Meeresspiegelveränderungen zugleich mit einem Wechsel von einem siliziklastisch- zu einem karbonat-dominierten Ablagerungsraum auf, etwa 1-2 Mio. Jahre nach der K-P Grenze.

Acknowledgements

Preface

This thesis consists of a series of chapters on the themes of Chicxulub impact ejecta and environmental changes (sea-level fluctuations, climate change) in northeastern Mexico, Texas, and Alabama during a 2 Ma interval enclosing the Cretaceous-Paleogene (K-P) boundary at 65 Ma. Each chapter has its own introduction, methodology, discussion, conclusions, and references and therefore may be printed as an independent part of this thesis.

Chapter 1 introduces the major events during the Cretaceous-Paleogene transition and outlines the aims of this thesis. It also introduces the temporal framework used in this study, the lithologic expression of the K-P boundary, and the global distribution pattern of Chicxulub impact ejecta.

Chapter 2 consists of a multidisciplinary investigation of Chicxulub ejecta deposits and the K-P transition in northeastern Mexico. Excerpts of this study, with focus on the La Sierrita area in northeastern Mexico, were co-authored with W. Stinnesbeck, D. Stüben, U. Kramar, Z. Berner, G. Keller, and T. Adatte, and were published in the International Journal of Earth Sciences (2003), 92(1): 114-142.

Chapter 3 is a multidisciplinary investigation of two cores across the K-P transition in Brazos, Texas, a region where so far little evidence on nature and composition of Chicxulub ejecta exists.

Chapter 4 provides a sequence stratigraphic study and describes climatic changes through an extended interval from the late Maastrichtian to the late Danian of the Antioch Church core from central Alabama.

Chapter 5 presents the general conclusions and synthesis of the results of Chapter 2 to 4.

This thesis was accomplished following the recommendations of the commission on "*Selbstkontrolle in der Wissenschaft*: *Vorschläge zur Sicherung guter wissenschaftlicher Praxis*", published by the German Science Foundation (DFG) in January 1998. Geological mapping, as well as sampling and description of outcrops and cores were done by the author. The Antioch Church core is stored at the Geological Department of Princeton University, Princeton, USA, and the Brazos cores are stored at the Geological Department of the Washington University, Bellingham, USA

The author prepared all samples for mineralogical and geochemical analysis and evaluated the X-ray diffractograms. All samples, thin-sections, photographs, and analytical data are stored at the Geological Institute of the University Karlsruhe, and at the institution where they have been produced. Planktic foraminifera biostratigraphy for outcrops in La Sierrita, northeastern Mexico, was made by Gerta Keller, Princeton University, USA. Robert Speijer from the University of Bremen provided the planktic foraminifera biostratigraphy and benthic foraminifera fauna analysis for the Brazos cores. Hartmut Mai from the University of Bremen conducted the calcareous nannoplankton stratigraphy for the two Brazos cores and the Antioch Church core. Thierry Adatte made the XRD measurements at the University of Neuchâtel, Switzerland. Doris Stüben and Utz Kramar provided the major- and trace-element analysis, as well as stable isotope data, which were performed at the Institute for Mineralogy und Geochemistry at the University of Karlsruhe. Analyses with the electron microprobe were conducted under supervision by Volker Zibat at the Laboratory for Electron Microscopy, University of Karlsruhe. Rock magnetic data was accomplished at the Institute for Paleontology und Mineralogy, University Heidelberg, supervised by Agnes Kontny.

Table of Contents

1. Introduction to the Cretaceous-Paleogene transition

1.1 The Maastrichtian-Danian world and the Chicxulub impact

The late Maastrichtian to early Danian period (about 68-64 Ma) corresponds to an array of prominent environmental and faunal changes in Earth history including the onset of a global cooling interval, major sea-level changes, flood basalt volcanism, the Chicxulub impact event, and, quite outstanding, a period of global mass extinctions (Ryder et al., 1996; MacLeod et al., 1997; Barrera and Johnson, 1999; Courtillot, 2002; Koeberl and MacLeod, 2002). These severe extinctions affected reptiles (e.g., dinosaurs), marine invertebrates (e.g., ammonites), and marine planktonic fauna (e.g., foraminifera), and led not only to a diversity reduction in excess of 65 % (Sepkoski, 1996; Hallam, 1998), but are also associated with a significant drop in biogenic productivity (e.g., Zachos et al., 1989; Kaiho et al., 1999). However, the exact timing and pattern of these extinctions remain largely unknown (Hallam, 1998; MacLeod, 1998; Kiessling and Claeys, 2001), and most faunal groups flourished well up to the Cretaceous-Paleogene (K-P)

boundary (e.g., Gartner, 1996; Pospichal, 1996; Arenillas et al., 2000; Steuber et al., 2002), whereas some faunal groups, locally may show a pre-K-P boundary decline in species abundance (e.g., planktic foraminifera, Keller et al., 1993a; Abramovich et al., 1998). In addition, the recovery and repopulation pattern following the biotic crisis are still discussed (e.g., Hart, 1996; D'Hondt et al., 1998; Harries, 1999; Beerling et al., 2001; Stilwell, 2003).

Many studies invoked the impact of a large meteorite at the K-P boundary as the causative event for the mass extinctions at the K-P boundary (impact-extinction hypothesis, Alvarez et al., 1980), and suggested that they have been triggered by the "Chicxulub impact" that generated a 180-300 km-in diameter impact structure at the Yucatán peninsula in southern Mexico (Fig. 1.1, Hildebrand et al., 1991; Sharpton et al., 1992; 1993). Specifically, the massive release of the climatically sensitive gases CO_2 and SO_2 by this impact into the 3 km-thick carbonate- and evaporite-bearing Yucatán platform, as well as the ejection of water and dust in the atmosphere, are generally postulated to have caused a brief inter-
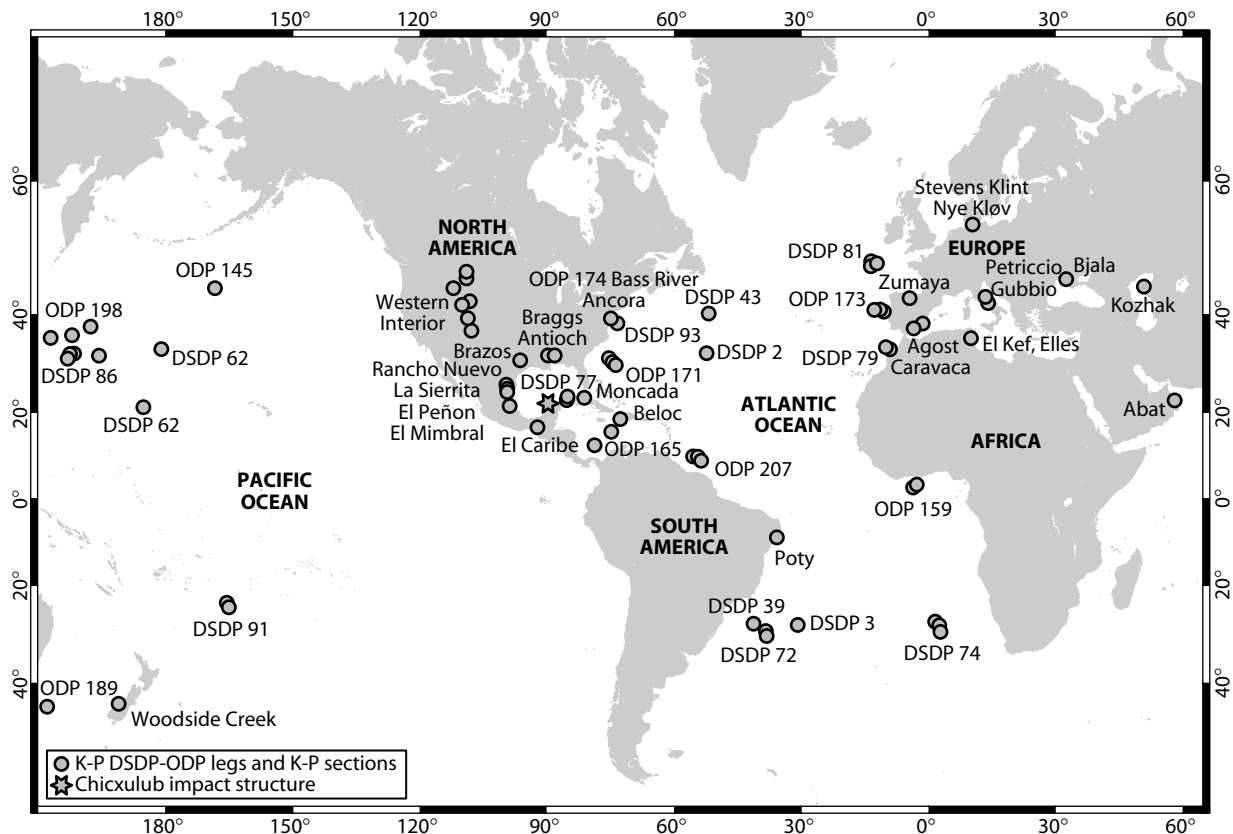
Figure 1.1 Overview on sections and DSDP/ODP Legs and terrestrial outcrops that include Maastrichtian and Danian strata and the K-P boundary interval. Most of these sites yield also evidence for Chicxulub impact ejecta. For details and references see text and Tables 2.1 and 3.5, as well as Fig. 1.3.

val of cooling and darkness ("impact winter", e.g., Toon et al., 1997; Pierazzo et al., 1998; Gupta et al., 2001; Luder et al., 2003).

The impact-induced immediate cooling of the average global surface temperature is estimated between 12-19 °C during the month or years following the impact, and possibly related to the sunlight shading of dust and sulfuric acid aerosols in the atmosphere (calculations from Pierazzo et al., 1998; Gupta et al., 2001). Although the complex palynoflora within the ejecta fallout layer in North America, as well as the thickness (about 3-30 mm) of the global Chicxulub ejecta fallout layer (e.g., Sweet et al., 1999; Sweet, 2001; Pope, 2002), counters scenarios of complete darkness and freezing, a brief interval (some decades) of cooling was inferred from characteristic changes of microfossil, pollen and spore assemblages at the K-P boundary (e.g., Brinkhuis et al., 1998; Sweet, 2001; Vajda et al., 2001; Galeotti and Coccioni, 2002). This impact-related cooling was probably accompanied by a short period of acid rain from the atmospheric washout of sulfur oxides, as shown by numerical modeling or from observations of bleached paleosols at the K-P boundary in North America (e.g., Sigurdsson et al., 1992; D'Hondt et al., 1994; Pollastro and Bohor, 1993; Retallack, 1996), albeit acid rain might have become local buffered by the calcium dispersed by the impact (Maruoka and Koeberl, 2003).

The immediate post-K-P interval of drastic environmental changes was probably superseded by a prolonged greenhouse-warming event resulting from the impact-related high CO_2 concentrations in the atmosphere (Pierazzo et al., 1998). According to Lomax et al. (2001), this elevated CO_2 concentrations may have also mediated the post-impact recovery of ecosystems by stimulating photosynthetic productivity. However, studies by Galbrun et al. (1997) and D'Hondt et al. (1998) suggested that productivity was depressed for at least up to 3 Ma (!) following the K-P impact event. Such a long recovery time seems to be astonishing in view of the month-year interval of cooling and sunlight-blocking in the aftermath of the K-P impact event (e.g., Lomax et al., 2001; Pierazzo and Hahmann, 2002). Particularly, since these studies suggest that the climate change associated with the impact was probably of short duration, followed by a complete recovery of the climate to pre-impact conditions within less than 10-100 years.

Consequently, it becomes evident that estimations of the environmental consequences of large impact events are currently in flux and require further verification and evaluation via the sedimentological and fossil record. Model calculation studies generally include distinct error ranges, resulting from (i) the input data (quantity of anhydrite at Yucatán?), (ii) the physical conditions during the impact (amount of calcium vaporization?), and (iii) the numerical modeling of related climate effects (e.g., Pierazzo and Hahmann, 2002; Luder et al., 2003). However, a comparison of the K-P impact scenario, for instance, to the last Pleistocene intervals of glaciations, which also led to sudden (within <50 years) changes in mean regional annual temperatures of about 5 °C (tropics) to 10-15 °C (high latitudes) for several thousands of years (e.g., Shackleton and Kennett, 1975), shows that each glacial stage is obviously not related to a major extinction event and followed by quite rapidly local faunal recovery (e.g., Cronin, 1999). Therefore, the K-P mass extinctions must also be regarded within the specific climatic and oceanographic context during the late Maastrichtian to Danian period.

Recently, a number of studies started addressing the complex temporal relationships and possible feedback effects between the environmental consequences of the K-P impact and other, more long-term environmental changes and events during the late Maastrichtian to early Danian period (e.g., Li and Keller, 1998; Dessert et al., 2001; Wilf et al., 2003). These studies emphasized the presence of prominent climate and sea-level trends, specifically for the Campanian-Maastrichtian period. During this period, the late Cretaceous 'hot greenhouse' (average global temperature of about +2 to +5 °C compared to the present) was superseded by 'cool greenhouse' conditions (5-6 °C temperature lowering) that lasted into the early Paleocene (e.g., Li and Keller, 1998; Barrera and Johnson, 1999).

Some 0.5 Ma before the K-P boundary, however, this cool greenhouse condition was punctuated by a brief warming interval lasting for some 300-400 ka. This "late Maastrichtian warming event" has probably raised mean annual temperatures by about 3-4 °C. It apparently coincided with the major eruptive phase of a large flood basalt-province (Deccan Traps) in India, suggesting a genetic link by the release of CO_2 and SO_2 during Deccan Trap volcanism. However, the Deccan Traps are estimated to have induced global warming of at most 1 °C during an interval of about 1 Ma across the K-P boundary, which makes a direct relationship less obvious (Wignall, 2001; Courtillot and Renne, 2003).

Several sequence stratigraphic studies and paleo-bathymetric studies have inferred a major sea-level lowstand (about 50 to 80 m) during the latest Maastrichtian (65.5-65.2 Ma), which could have additionally stressed parts of the marine fauna by reducing the ratio of shallow to deep marine continental-shelf environments (e.g., Donovan et al., 1988; Keller and Stinnesbeck, 1996; Pardo et al., 1996; Li et al., 2000; Smith et al., 2001; Alegret et al., 2003), though the relationship of a global warming interval to a concurrent rapid global sea-level lowering is not clear yet. In addition, the K-P boundary clay is commonly associated with a maximum flooding event (e.g., Adatte et al., 2002) or transgressive sea-level behavior (Olsson et al., 2002), which could have led to the expansion of the oxygen minimum zone across large shelf areas and hence, may have further promoted environmental stress in shelfal sedimentary environments (Hallam and Wignall, 1999).

This brief excursion into the Maastrichtian to Danian period demonstrates not only the complexity and still inadequate understanding of mutually interrelated processes (e.g., effects of a large meteorite impact, sea level fluctuations, and climate change), which probably require a more 'holistic' approach. This excursion also stresses that despite 20 years of K-P boundary research, we are still far from knowing even the principal mechanisms of the K-P mass extinctions (e.g., Hallam, 1998; Courtillot, 2002). Therefore, scenario-independent systematic studies of this interval are required, incorporating multiple data sets, to provide insights in biotic and environmental changes, as well as specifically for the disastrous Chicxulub impact event that presumably terminated the Cretaceous period. The northern and northwestern Gulf of Mexico is a key region for studying many issues of the K-P transition (e.g., ejecta deposits, sea-level and climate change), because of the proximity to the Chicxulub structure and the excellent exposure of K-P sections along the Gulf of Mexico coastal plain, though there are few multidisciplinary studies on these issues (as envisioned in this thesis), except for the Beloc K-P section in Haiti (Stüben et al., 2002b).

1.2 Aims of this thesis

The main objectives of this thesis focus on the Maastrichtian to Danian transition in the northwestern part of the Gulf of Mexico, a region close to the Chicxulub impact site, and specifically evaluate the following points by an integrated multidisciplinary approach:

(1) The petrology and mineralogy of Chicxulub ejecta to provide details on the involved target lithologies and the amounts of carbonate ejected during the impact (Chapter 2 and 3).

(2) The sedimentology and microfacies characteristics of Chicxulub ejecta to constrain the impact melting, ejection, and dispersal process (Chapter 2 and 3).

(3) The stratigraphical and compositional aspects of Chicxulub ejecta in comparison with other ejecta deposits at, or close to the K-P boundary on a regional to global scale to reveal ejecta distribution patterns (Chapter 2 and 3).

(4) The facies development and sequence stratigraphic setting of the late Maastrichtian to Danian sediments (including the ejecta layers) to constrain characteristics of the depositional environment, timing and magnitude of lithofacies shifts, and possible sea-level fluctuations (Chapter 3 and 4).

(5) The climate development in this area inferred from clay mineral assemblages and stable isotope ratios (Chapter 3 and 4).

The temporal framework used in this thesis, and the defining characteristics of the Cretaceous-Paleogene boundary, including the lithological expression of the K-P transition in different settings worldwide, are documented in the following section. This section also includes details on the composition and distribution pattern of ejecta from the Chicxulub impact event, though a detailed discussion of the Chicxulub impact structure is beyond the scope of this thesis introduction; for details on this topic, the reader is referred to instructive summaries provided in Hildebrand et al. (1998), Morgan et al. (1997; 2002), and Sharpton et al. (1996).

1.3 Chrono- and lithostratigraphy of the K-P transition

1.3.1 Late Maastrichtian to Danian biostratigraphic framework

A tight chronostratigraphic framework, which is based on a combination of magnetochronology and biostratigraphy, has been established for the K-P transition by several previous studies (Fig 1.2). This combination allows the determination of the absolute duration of biozones relative to magnetochrons with a resolution that is generally better than 50-100 ka and therefore even below the error range

usually given for radiometric dating (Aubry, 1995). However, some limitations may occur, particularly for the time-slice governed by this study, as outlined in the following:

(1) Hiatuses frequently affect K-P boundary sections, hence, the completeness of biozones is difficult to assess (e.g., MacLeod and Keller, 1991; Keller et al., 1993b). Moreover, the severe faunal changes across the K-P boundary include the problematic of large-scale reworking of Cretaceous taxa during the early Paleocene, particularly for the μm-sized calcareous nannofossils (see Gartner, 1996; Pospichal, 1996).

(2) First and last occurrence of index taxa may be diachronous in different sections, as inferred from their position relative to magnetochron, or relative to other taxa. The calibration of biozones to magnetochrons that is necessary to estimate the absolute duration of the biozones is accomplished only for few K-P sections (see discussion in Berggren et al., 1995; Pardo et al., 1996) and even lacking for the El Kef section, Tunisia, which is the Global Stratotype Section and Point (GSSP) for the Cretaceous-Tertiary boundary (see below and Cowie et al., 1989; Odin, 1992).

(3) The index taxa for biozones may be restricted to a certain latitude or water depth (ecological exclusion, e.g., Pardo et al., 1999; Smith et al., 2001). Therefore, their absence may not always be an indication that sediments of the age of the related biozone are indeed missing.

(4) The uncertainty in determining the actual timing of the demise or appearance of individual taxa is pointed out by the "Signor-Lipps effect" (Signor and Lipps, 1982). This effect is a particular problem for species that are rare in the assemblage and therefore may not be detected in the small samples that are used in faunal studies; hence, last and first appearances may underestimate the truth extinction and origination datum (Gradstein and Agterberg, 1998). Similarly, reworking and bioturbation can extend the last appearance of species.

1.3.2 Definition of the K-P boundary position

According to Cowie (1989 p. 82), the International Commission on Stratigraphy has made the decision for "…the base of the boundary clay at El Kef, Tunisia, to be the Global Stratotype Section and Point (GSSP) for the Cretaceous-Tertiary boundary." This section includes a prominent and abrupt lithological break from limestones to a 0.5 m-thick interval of almost carbonate-free mudstones ("K P boundary

clay", see Fig. 1.3 and Keller et al., 1995; Remane et al., 1999). The base of this mudstone interval ("a 2-mm-thick red layer") contains anomalously high iridium values, Ni-Cr-rich spinels, goethite and hematite spherules, and is strongly enriched in smectite (e.g., Lindinger, 1988; Robin and Rocchia, 1998; Rocchia and Robin, 1998; Ortega-Huertas et al., 1998). In addition, the K-P boundary clay layer is marked by nano-sized iron and iron-titanium particles and a distinct anomaly of the magnetic susceptibility, resulting from globally distributed iron-rich fallout and the presence of magnetite spherules (see Fig. 1.3 and Worm and Banerjee, 1987; Griscom et al., 1999; 2003; Wdowiak et al., 2001; Verma et al., 2002). Also, the carbonate content drops sharply to almost zero at the base of the boundary clay layer and the carbon isotopes show a prominent negative excursion (see Fig. 1.3 and Lindinger, 1988; Zachos et al., 1989; Hollander et al., 1993).

The specific constituents and characteristics of the K-P boundary clay outlined above are related to (i) the globally distributed fallout from the K-P impact event (presumably the Chicxulub impact), (ii) a sharp drop in plankton productivity, and (iii) to the mass extinction of tropical planktic foraminifera and many calcareous nannoplankton species (e.g., Lindinger, 1988; Zachos et al., 1989; Hollander et al., 1993; D'Hondt et al., 1998; Kaiho et al., 1999; Stüben et al., 2002a).

The unique and joint occurrence of these mineralogical and geochemical characteristics in a mm-thick clay layer, including the presence of a strong iridium anomaly, Ni-Cr-rich spinels, shocked quartz, microspherules, δ^{13}C shift, Fe-rich nanophases, and/or faunal changes virtually assures an almost isochronous formation of the K-P boundary layer. However, not all known K-P sections bear a complete record of these characteristic markers, and K-P sections, for instance in the Gulf of Mexico, may not show a distinct 'mm-thick boundary clay' but reveal the dispersion of the 'classical' boundary markers over an interval of several meters in thickness. Therefore, correlation and unequivocal positioning of the K-P boundary in these sections is difficult, and in absence of a mm-thick boundary clay it is more appropriate to consider this interval as 'K-P transition' or 'K-P contact' (see Fig. 1.3 and discussion in Odin, 1992; Remane et al., 1996).

1.3.3 Characteristics of the K-P boundary

A synoptic view of the lithological expression of the K-P transition in marine sections and cores from

Figure 1.2 content:

Magneto-stratigraphy Cande & Kent (1992, 1995)	Planktic foraminifera Berggren et al. (1995) Bralower et al. (1995)	Planktic foraminifera Keller (1993), Keller et al. (1995) Pardo et al. (1996)	Calcareous nannoplankton Perch-Nielsen (1985) Berggren et al. (1995)
Danian — C27R	P1c	P1d — _Morozovella trinidadensis_	NP4 — _Ellipsolithus macellus_
C28N (62.5, 63.0)		P1c(2)	
	Globanomalina compressa / _Praemurica inconstans_ (FA)	? — _Morozovella inconstans_	NP3
C28R (63.5)	P1b	P1c(1)	_Chiasmolithus danicus_
C29N (64.0, 64.5)		? — _Subbotina varianta_	
	Subbotina triloculinoides (FA)	P1b	NP2 — _Cruciplacolithus tenuis_
	P1a	P1a(2) — _P. eugubina/P. longiapertura_; _Subbotina pseudobulloides_	NP1
C29R (65.0)	Pα — _Parvularugoglobigerina eugubina_	P1a(1) — _P. eugubina/P. longiapertura_	_Markalius astroporus_; _Biantholithus sparsus_; faunal change; _Micula_ spp.
	P0* — _Abathomphalus mayaroensis_ Extinction of all tropical species	P0 — _Plummerita hantkeninoides_	
	A. mayaroensis	CF1 — _Plummerita reicheli_	CC26b — _Micula prinsii_
Maastrichtian — C30N (65.5)		CF2 — _Gansserina gansseri_	CC26 — _Nephrolithus frequens_
		CF3	CC25 — _Micula murus_

Legend:
⊥ First appearance
⊤ Last appearance
* P0 = _Guembelitria cretacea_ acme

Figure 1.2 Chronostratigraphic framework of the K-P transition adopted for this study, including the geomagnetic polarity timescale by Cande and Kent (1992, 1995), the planktic foraminifera and calcareous nannofossils zonation, as well as datum events of zonal marker species by Keller (1993), Keller et al. (1995), Bralower et al. (1995), and Berggren et al. (1995). Additional details of the immediate K-P interval can be found in Gartner (1996), Pospichal (1996), Gardin and Monechi (1998), and Keller et al. (2002c).

different ocean basins and from terrestrial settings in North America and New Zealand reveals that the characteristics of the K-P boundary depend mainly on the distance to the Chicxulub crater (compare Fig. 1.1 and 1.3) (see Montanari and Koeberl, 2000; Kring and Durda, 2002; Croskell et al., 2002; Koeberl and Martínez-Ruiz, 2003). The deposition of the material ballistically ejected from the crater resulted in a distinct layer, or a series of deposits, that separate Cretaceous from Paleocene sediments (Fig. 1.3).

The distinctive dispersed ejecta was mostly derived from (i) the laterally expanding turbulent front of the melted target rocks ("ejecta curtain") and (ii) the vertically expanding hot "vapor plume" of vaporized meteorite and target material; this bimodal ejecta dispersion process led to the regional and global ejecta distribution, respectively (Pollastro and Bohor, 1993; Alvarez et al., 1995; Bohor and Glass,

1995; Pierazzo and Melosh, 1999). Therefore, at localities proximal to the Chicxulub crater greater contributions existed to the ejecta from Chicxulub target rocks (melted and unmelted rocks; "spherules"), whereas distal sites received a relatively higher contribution of molten target rocks (microspherules and microkrystites) and extraterrestrial material (iridium anomaly, spinels). This particular 'ejecta distribution pattern' is reflected in the lithology, mineralogy, and geochemistry of the K-P boundary in the regions outlined in the following.

Gulf of Mexico and Caribbean

In the regions close to the Chicxulub crater, i.e., in the Gulf of Mexico and the Caribbean, the lithological expression of the K-P transition is highly variable and usually by far more complex than in the Tunisian K-P stratotype and point section El Kef outlined above. At these sites the ejecta can be divided in (i)

a thick blanket and carbonate megabreccias extending radially some 500-800 km around the Chicxulub structure on the Yucatan peninsula (ii) an area occurring around the Gulf of Mexico and the Caribbean characterized by m-thick ejecta deposits, locally followed by siliciclastic units. At these localities, K-P boundary ejecta deposits comprise material of variable composition, ranging from pure carbonate to silicate melt and mixtures of these two end-members commonly altered to clay minerals.

In the Guatemala K-P sections (e.g., El Caribe) the ejecta layer is composed of glass spherules altered to well-crystallized Mg-rich smectite and overlies Maastrichtian limestones and dolomites and underlies Paleocene marls (e.g., Stinnesbeck et al., 1997; Debrabant et al., 1999). In the Belize K-P sites (Albion Island), an altered smectite-rich spheroid- and diamictite-bed overlies dolomitized limestones of late Cretaceous (Maastrichtian?) age (e.g., Pope et al., 1999; Fouke et al., 2002).

Multiple smectite- and carbonate-rich spherule deposits are present at Beloc, Haiti (e.g., Maurrasse and Sen, 1991; Izett, 1991; Koeberl and Sigurdsson, 1992; Lyons and Officer, 1992; Stüben et al., 2002b). The spherule deposits are found about 0.5 m below the first occurrence of the Danian *P. eugubina* (Zone P1a) and immediate above latest Maastrichtian marls (Biozone CF1, Stinnesbeck et al., 1999; Keller et al., 2001), This indicates that at Haiti, these spherules have been reworked, probably by turbidites, whereas other sections indicate subsequent slumping, faulting, and thrusting of ejecta (Keller et al., 2001). In two cores of the Caribbean ODP Leg 165, Site 1001, one graded smectite- and carbonate-rich spherule deposit overlies late Maastrichtian sediments and underlies earliest Paleocene sediments (Biozone P1a, Sigurdsson et al., 1997).

The northeastern Mexican K-P sections, spanning more than 300 km, include an up to 1 m thick carbonaceous chlorite- and chlorite-smectite-rich spherule deposit at the base of a channelized "siliciclastic deposit" (Stinnesbeck et al., 1993; 1996; Smit et al., 1992; 1996). A series of subdued iridium-anomalies starts in the top of the "siliciclastic deposit" and extends into the overlying Paleocene marls (Smit et al., 1996). This 'siliciclastic deposit' has been interpreted as a short-term Chicxulub impact-triggered megatsunami or gravity flow deposit immediately at the K-P boundary (e.g., Smit et al., 1992; 1996; Smit, 1999; Bohor, 1996; Alegret et al., 2001; Arz et al., 2001). Alternatively, it has been interpreted as long-term sea-level lowstand deposit and deposition

occurred sometime during the last 100-200 ka of the Maastrichtian, placing the Chicxulub impact several hundred thousand years before the K-P boundary (e.g., Stinnesbeck et al., 1993; 1996; Keller et al., 1997; Ekdale and Stinnesbeck, 1998).

Recent findings of multiple lens-like spherule deposits locally embedded within latest Maastrichtian hemipelagic marls in some northeastern Mexican K-P sections, however, may suggest that the Chicxulub impact occurred during the latest Maastrichtian biozone CF1 (Stinnesbeck et al., 2001; Keller et al., 2002b). On the other hand, these multiple spherule deposits are commonly associated with soft-sediment deformation and faulting (Soria et al., 2001; Schulte et al., 2003), and therefore the suggestion of an additional late-Maastrichtian impact is not universally accepted (but see discussion in Keller et al., 2002a; Soria et al., 2002).

North America (Western Interior)

In the Western Interior of North America, sections encompassing the K-P boundary comprise a cm-thick dual layer sequence in a terrestrial backwater swamp setting: A lower (kaolinitic) spherule-rich clay layer with rare shocked minerals directly underlies a laminated (smectitic) clay layer rich in shocked minerals, iridium, siderophile elements, and Ni-rich spinels (e.g., Izett, 1990; Sharpton et al., 1990; Schmitz, 1992; Bohor and Glass, 1995; Ortega-Huertas et al., 2002). This layer also marks the onset of a strong negative δ^{13}C shift (Arens and Jahren, 2000; 2002; Beerling et al., 2001).

Certain ejecta components are restricted to one layer or the other within both layers, some components, however, are common to both layers but in different amounts. Consequently, partitioning of components allows distinction in the mode of ejection, dispersion, and deposition of each layer and suggests one causative event (Pollastro and Bohor, 1993) instead of two temporally disparate impact events (Fastovsky and McSweeney, 1987). According to Pollastro and Bohor (1993), the lower spherule-rich layer represented the initial Chicxulub melt-ejecta, followed by more-long-term fallout from stratospherically and globally dispersed ejecta reflected in the iridium-rich upper layer (Pollastro and Bohor, 1993; Alvarez et al., 1995; Bohor and Glass, 1995; Croskell and Collins, 2002). Palynological studies by Lerbekmo (1999) and Sweet and Bramann (2001) have shown that these two layers are separated by a "micro-diastem" of days-month in duration, which
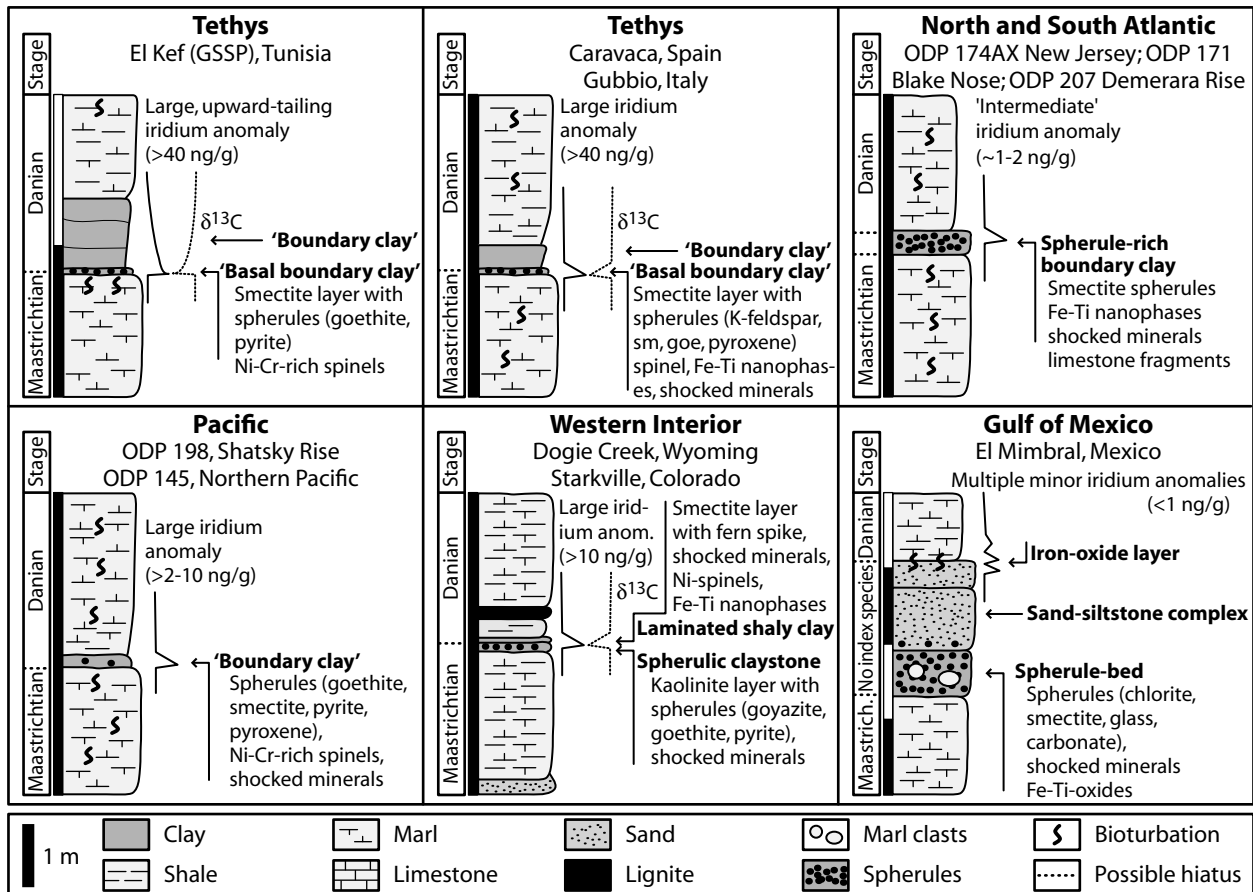
Figure 1.3 Generalized summary of the lithology of the K-P transition and the immediate K-P boundary from different ocean basin and terrestrial settings, including the mineralogical and geochemical markers found at, or close to the K-P boundary. Note the absence of a distinct K-P boundary clay in the Gulf of Mexico and dispersion of the 'classical' boundary markers over an interval of several meters in thickness. The iridium-anomaly and the negative $\delta^{13}C$ excursion are drawn schematically. Details on the (bio-) stratigraphic setting and references are given in the text.

agrees with the ejecta-dispersal model outlined by Pollastro and Bohor (1993).

U-Pb dating of single shocked zircons from the K-P boundary clay in the Western Interior and from the Haitian spherule deposits at Beloc, as well as from the suevite from within the Chicxulub impact structure, revealed similar source ages, suggesting that these zircons derived from a common basement that contains lithologies with two distinct ages of about 418±6 Ma and 540±10 Ma (see Table 2.6 and Krogh et al., 1993a; 1993b; Kamo and Krogh, 1995).

In addition, the grain-size distribution of shocked quartz in the North American K-P sections shows a grain-size decrease towards south, and on the Pacific Ocean towards east, pointing to an origin by an impact event in the Caribbean as well (see Appendix 1.1 and Bohor and Izett, 1986; Kring, 1995; Kring and Durda, 2002; Kyte et al., 1996; Croskell et al., 2002). Combined, these data suggest a relationship between the Chicxulub impact event and the iridium-rich K-P boundary clay layer in the Western Interior. Notably,

the K-P boundary ejecta distribution predicted the size and location of the Chicxulub crater even before this crater structure was actually located in southern Mexico (e.g., Bohor and Izett, 1986; Hildebrand and Stansberg, 1992).

Atlantic Ocean

In the northwestern Atlantic, a 1 to 20 cm thick clayey spherule-rich layer with shocked quartz, carbonate clasts overlain by a limonitic calcareous layer that includes an Ir anomaly is "sandwiched" between late Maastrichtian sediments below and early Danian sediments above. At the New Jersey coastal plane, western Atlantic (ODP Leg 174AX), a thin smectite-rich spherule layer interpreted as an original in-situ ejecta fallout deposit from the Chicxulub impact separates early Danian (Biozone P0 or P1a) from late Maastrichtian sediments (Olsson et al., 1997; 2002). Three cores from the Blake Nose Plateau, western Atlantic (ODP Leg 171B) include reworked Chicxulub ejecta (smectite spherules) that overlies disturbed latest Maastrichtian sediments

(Biozone CC26b) and underlies sediments of early Danian age (Biozone P1a, see Fig. 3.5 and Norris et al., 1999; 2000; Klaus et al., 2000; MacLeod and Huber, 2001; Martínez-Ruiz et al., 2001a; 2001b; Self-Trail, 2001).

The ODP Leg 207 drilled at the Demerara Rise off Suriname, South America, resulted in the recovery of six copies of extended and undisturbed K-P sequences from three deep-water sites (Site 1258-1260, Erbacher et al., 2003). Each of these intervals contains a 1-2 cm-thick graded smectite-spherule ejecta bed, presumably resulting from fallout of the Chicxulub impact event. The graded spherule layers overlie latest Maastrichtian chalks (Biozone CC26b and CF1) and underlie sediments of earliest Danian age (Biozone P0 and P1a).

Tethyan realm

In the Tethyan K-P sections in Spain (Caravaca), Italy (e.g., Gubbio), and Denmark (e.g., Stevens Klint), as well as in the GSSP El Kef stratotype in Tunisia, a 1-50 cm thick K-P boundary clay with a basal mm-thick impact-fallout layer separates latest Maastrichtian (Biozone CF1) and early Danian sediments (Biozone P0 or P1a, see Fig. 1.3 and Montanari, 1991; Keller et al., 1995; Martínez-Ruiz et al., 1997; Kaiho et al., 1999; Ortega-Huertas et al., 2002). The basal thin "fallout" layer includes a strong iridium anomaly, shocked minerals, K-feldspar spherules, glass fragments, and often contains evidence of a brief period of dysoxic or anoxic conditions, including framboidal pyrite and high TOC contents (e.g., Martínez-Ruiz et al., 1999; Tribovillard et al., 2000; Frei and Frei, 2002).

Pacific Ocean

In the Pacific K-P sections recently drilled by the ODP Leg 198 (Bralower et al., 2002a; 2002b), the lithologic sequence in the K-P boundary interval is similar to previous K-P sections from several Pacific DSDP and ODP Legs, though with better biostratigraphic resolution (see Fig. 1.3 and summary in Kyte et al., 1996; Kyte and Vakulenko, 2001). The K-P boundary succession in the ODP Leg 198 includes latest Maastrichtian (Biozone CC26b), white to pale orange, slightly indurated, nannofossil ooze overlain by a 10-cm thick layer of basal Paleocene (Biozone P0-P1a) grayish orange foraminiferal ooze. This layer grade into 20-cm thick white foraminiferal nannofossil chalks, then into grayish orange nannofossil ooze. The boundary between the late Maastrichtian and the lowermost Paleocene is bioturbated and contains brown to amber Chicxulub ejecta spherules up to 100-150 μm in diameter (Bralower et al., 2002a; 2002b).

The mm-thick K-P boundary clay layer in terrestrial and near-shore marine K-P sections in New Zealand (e.g., in Woodside Creek) includes abundant goethite spherules, shocked quartz, and an iridium anomaly (Brooks et al., 1985; Schmitz, 1988). These K-P sections also show the instant, extensive destruction of land plants immediately followed by a fern spike, which both are similar to the floral succession observed in the Northern American K-P sections (Vajda et al., 2001).

1.4 References

Abramovich S, Almogi-Labin A, Benjamini C (1998) Decline of the Maastrichtian pelagic ecosystem based on planktic foraminiferal assemblage changes: Implications for the terminal Cretaceous faunal crisis. *Geology* **26**(1): 63-66.

Adatte T, Keller G, Stinnesbeck W (2002) Late Cretaceous to early Paleocene climate and sea-level fluctuations: The Tunisian record. *Palaeogeogr Palaeoclimatol Palaeoecol* **178**(3-4): 165-196.

Alegret L, Molina E, Thomas E (2001) Benthic foraminifera at the Cretaceous-Tertiary boundary around the Gulf of Mexico. *Geology* **29**(10): 891-894.

Alegret L, Molina E, Thomas E (2003) Benthic foraminiferal turnover across the Cretaceous/Paleogene boundary at Agost (southeastern Spain): Paleoenvironmental inferences. *Mar Micropaleontol* **48**(3-4): 251-279.

Alvarez LW, Alvarez W, Asaro F, Michel HV (1980) Extraterrestrial cause for the Cretaceous-Tertiary extinction. *Science* **208**: 1095-1108.

Alvarez W, Claeys P, Kieffer SW (1995) Emplacement of Cretaceous-Tertiary boundary shocked quartz from Chicxulub crater. *Science* **269**: 930-935.

Alvarez W, Smit J, Lowrie W, Asaro F, Margolis SV, Claeys P, Kastner M, Hildebrand AR (1992) Proximal impact deposits at the Cretaceous-Tertiary boundary in the Gulf of Mexico: A restudy of DSDP Leg 77, Sites 536 and 540. *Geology* **20**(8): 697-700.

Arenillas I, Arz JA, Molina E, Dupuis C (2000) An independent test of planktic foraminiferal turnover across the Cretaceous/Paleogene (K/P) boundary at El Kef, Tunisia: Catastrophic mass extinction and possible survivorship. *Micropaleontology* **46**(1): 31-49.

Arens NC, Jahren AH (2000) Carbon isotope excursion in atmospheric CO_2 at the Cretaceous-Tertiary boundary: Evidence from terrestrial sediments. *Palaios* **15**(4): 314-322.

Arens NC, Jahren AH (2002) Chemostratigraphic correlation of four fossil-bearing sections in southwest North Dakota. In: Hartman JH, Johnson KR, Nichols DJ (eds) The Hell Creek Formation and the Cretaceous-Tertiary boundary in the northern Great Plains – An integrated continental record of the end of the Cretaceous. *Geol Soc Am Spec Pap* **361**: 75-93.

Arz JA, Arenillas I, Soria AR, Alegret L, Grajales-Nishimura JM, Liesa CL, Melendez A, Molina E, Rosales MC (2001) Micropaleontology and sedimentology across the Cretaceous/Tertiary boundary at La Ceiba (Mexico): Impact-generated sediment gravity flows. *Jour South Am Earth Sci* **14**(5): 505-519.

Aubry M-P (1995) From chronology to stratigraphy: Interpreting the lower and middle Eocene stratigraphic record in the Atlantic Ocean. In: Berggren WA, Kent DV, Aubry M-P et al. (eds) Geochronology, time scales, and global stratigraphic correlation. *Soc Econ Paleont Miner Spec Pub* **54**: 213-274.

Barrera E, Johnson CC (eds) (1999) Evolution of the Cretaceous ocean-climate system. *Geol Soc Am Spec Pap* **332**: 1-445.

Beerling DJ, Lomax BH, Upchurch GRJ, Nichols DJ, Pillmore CL, Handley LL, Scrimgeour CM (2001) Evidence for the recovery of terrestrial ecosystems ahead of marine primary production following a biotic crisis at the Cretaceous-Tertiary boundary. *Jour Geol Soc Lond* **158**(5): 737-740.

Berggren WA, Kent DV, Swisher CC, Aubry M-P (1995) A revised Cenozoic geochronology and chronostratigraphy. In: Berggren WA, Kent DV, Aubry M-P et al. (eds) Geochronology, time scales, and global stratigraphic correlation. *Soc Econ Paleont Miner Spec Pub* **54**: 129-212.

Bohor BF (1996) A sediment gravity flow hypothesis for siliciclastic units at the K/T boundary, northeastern Mexico. In: Ryder G, Fastovsky D, Gartner S (eds) The Cretaceous-Tertiary boundary event and other catastrophes in Earth history. *Geol Soc Am Spec Pap* **307**: 183-195.

Bohor BF, Glass BP (1995) Origin and diagenesis of K/T impact spherules – From Haiti to Wyoming and beyond. *Meteoritics* **30**: 182-198.

Bohor BR, Izett GA (1986) Worldwide size distribution of shocked quartz at the K/T boundary: Evidence for a North American impact site (abstract). *Lun Planet Sci* **17**: 68-69.

Bostwick JA, Kyte FT (1996) The size and abundance of shocked quartz in Cretaceous-Tertiary boundary sediments from the Pacific basin. In: Ryder G, Fastovsky D, Gartner S (eds) The Cretaceous-Tertiary boundary event and other catastrophes in Earth history. *Geol Soc Am Spec Pap* **307**: 403-415.

Bralower TJ, Premoli Silva I, Malone MJ (2002a) Shipboard Scientific Party: Leg 198 summary. Proceedings of the Ocean Drilling Program. *Initial Results* **198**: 1-148.

Bralower TJ, Leckie RM, Sliter WV, Thierstein HR (1995) An integrated Cretaceous microfossil biostratigraphy. In: Berggren WA, Kent DV, Aubry M-P et al. (eds) Geochronology, time scales and global stratigraphic correlation. *Soc Econ Paleont Miner Spec Pub* **54**: 65-79.

Bralower TJ, Premoli-Silva I, Malone MJ, Scientific Participants of ODP Leg 198 (2002b) New evidence for abrupt climate change in the Cretaceous and Paleogene: An Ocean Drilling Program expedition to Shatsky Rise, northwest Pacific. *GSA Today* **12**(4): 4-10.

Brinkhuis H, Bujak JP, Smit J, Versteegh GJM, Visscher H (1998) Dinoflagellate-based sea surface temperature reconstructions across the Cretaceous-Tertiary boundary. *Palaeogeogr Palaeoclimatol Palaeoecol* **141**(1-2): 67-83.

Brooks RR, Hoek PL, Reeves RD, Wallace RC, Johnston JH, Ryan DE, Holzbecher J, Collen JD (1985) Weathered spheroids in a Cretaceous/Tertiary boundary shale at Woodside Creek, New Zealand. *Geology* **13**(10): 738-740.

Cande SC, Kent DV (1992) A new geomagnetic polarity time scale for the Late Cretaceous and Cenozoic. *Jour Geophys Res* **97**(10): 13,917-13,951.

Cande SC, Kent DV (1995) Revised calibration of the geomagnetic polarity timescale for the Late Cretaceous and Cenozoic. *Jour Geophys Res* **100**(4): 6093-6095.

Courtillot V (2002) Evolutionary catastrophes: The science of mass extinction. Cambridge University Press, Cambridge: 1-173.

Courtillot V, Renne P (2003) On the age of flood basalt events. *CRAS II* **335**(1): 113-140.

Cowie JW, Zieger W, Remane J (1989) Stratigraphic Commission accelerates progress, 1984-1989. *Episodes* **12**(2): 79-83.

Cronin TM (1999) Principles of paleoclimatology. *Perspectives in paleobiology and Earth history*. Columbia University Press, New York: 1-560.

Croskell MS, Collins GS (2002) Formation of the double K/T boundary layer in North America (abstract). *Lun Planet Sci* **33**: #1103 (CD-ROM).

Croskell MS, Warner M, Morgan J (2002) Annealing of shocked quartz during atmospheric re-entry. *Geophy Res Lett* **29**(20): 1-4.

D'Hondt S, Donaghay P, Luttenberg D, Lindinger M (1998) Organic carbon fluxes and ecological recovery from the Cretaceous-Tertiary mass extinction. *Science* **282**: 276-278.

D'Hondt S, Pilson MEQ, Sigurdsson H, Hanson AKJ, Carey S (1994) Surface water acidification and extinction at the K/T boundary. *Geology* **22**(11): 983-986.

Debrabant P, Fourcade E, Chamley H, Rocchia R, Robin E, Bellier J-P, Gardin S, Thiébault F (1999) Les argiles de la transition Crétacé-Tertiaire au Guatemala, témoins d'un impact d'asteroide. *Bull Soc Géol Fr* **170**(5): 643-660.

Dessert C, Dupré B, François LM, Schott J, Gaillardet J, Chakrapani G, Bajpai S (2001) Erosion of Deccan Traps determined by river geochemistry: Impact on the global climate and the 87Sr/86Sr ratio of seawater. *Earth Planet Sci Lett* **188**(3-4): 459-474.

Doehne E, Margolis SV (1990) Trace-element geochemistry and mineralogy of the Cretaceous/Tertiary boundary: Identification of extraterrestrial components. In: Sharpton VL, Ward PD (eds) Global catastrophes in Earth history: An interdisciplinary conference on impacts, volcanism, and mass mortality. *Geol Soc Am Spec Pap* **247**: 367-382.

Donovan AD, Baum GR, Blechschmidt GL, Loutit TS, Pflum CE, Vail PR (1988) Sequence stratigraphic setting of the Cretaceous-Tertiary boundary in central Alabama. In: Wilgus CK, Hastings BS, Kendall CG et al. (eds) Sea-level changes: An integrated approach. *Soc Econ Paleont Miner Spec Pub* **42**: 299-307.

Ekdale AA, Stinnesbeck W (1998) Trace fossils in Cretaceous-Tertiary (KT) boundary beds in Northeastern Mexico: Implications for sedimentation during the KT boundary event. *Palaios* **13**(1): 1-23.

Erbacher J, Mosher DC, Malone MJ, Berti D et al. (2003) Shipboard Scientific Party: Leg 207 Preliminary report. Proceedings of the Ocean Drilling Program. *Initial Results* **207**: 1-63.

Fastovsky DE, McSweeney K (1987) Paleosols spanning the Cretaceous-Paleogene transition, eastern Montana and western North Dakota. *Geol Soc Am Bull* **99**(1): 66-77.

Fouke BW, Zerkle AL, Alvarez W, Pope KO, Ocampo AC, Wachtman RJ, Grajales-Nishimura JM, Claeys P, Fischer AG (2002) Cathodoluminescence, petrography and isotope geochemistry of KT impact ejecta deposited 360 km from the Chicxulub crater, at Albion Island, Belize. *Sedimentology* **49**(1): 117-138.

Frei R, Frei KM (2002) A multi-isotopic and trace element investigation of the Cretaceous-Tertiary boundary layer at Stevns Klint, Denmark – Inferences for the origin and nature of siderophile and lithophile element geochemical anomalies. *Earth Planet Sci Lett* **203**(2): 691-708.

Galbrun B, Louvel V, Cottilon P, Leckie M et al. (1997) Signature sédimentaire d'événements globaux post-mésozoiques en mer des Caraïbes: Résultats préliminaires de la campagne ODP 165. *CRAS II* **325**(7): 505-510.

Galeotti S, Coccioni R (2002) Changes in coiling direction of *Cibicidoides pseudoacutus* (Nakkady) across the Cretaceous/Tertiary boundary of Tunisia: Palaeoecological

and biostratigraphic implications. *Palaeogeogr Palaeoclimatol Palaeoecol* **178**(3-4): 197-210.

Gardin S, Monechi S (1998) Paleoecological change in middle to low latitude calcareous nannoplankton at the Cretaceous/ Tertiary boundary. *Bull Soc Géol Fr* **169**(5): 709-723.

Gartner S (1996) Calcareous nannofossils at the Cretaceous-Tertiary boundary. In: MacLeod N, Keller G (eds) Cretaceous-Tertiary boundary mass extinction: Biotic and environmental changes. Norton Press, New York: 27-48.

Gradstein FM, Agterberg FP (1998) Uncertainty in stratigraphic correlation. In: Gradstein FM, Sandvik KO, Milton NJ (eds) Sequence stratigraphy – Concepts and applications. *Norwegian Petroleum Society (NPF) Special Publication* **8**. Elsevier, Amsterdam: 9-30.

Griscom Dl, Beltrán-López V, Merzbacher CI, Bolden E (1999) Electron spin resonance of 65-million-year-old glasses and rocks from the Cretaceous/Tertiary boundary. *Jour Non-Crystal Solids* **253**(1-3): 1-22.

Griscom Dl, Beltrán-López V, Pope KO, Ocampo AC (2003) New geochemical insights from electron-spin-resonance studies of Mn^{2+} and SO_3^- in calcites: Quantitative analyses of Chicxulub crater ejecta from Belize and southern Mexico with comparison to limestones from distal Cretaceous-Tertiary boundary sites. In: Koeberl C, Martínez-Ruiz F (eds) Impact markers in the stratigraphic record. *Impact studies.* Springer, Heidelberg: 229-270.

Gupta SC, Ahrens TJ, Yang W (2001) Shock-induced vaporization of anhydrite and global cooling from the K/T impact. *Earth Planet Sci Lett* **188**(3-4): 399-412.

Hallam A (1998) Mass extinctions in Phanerozoic time. In: Grady MM, Hutchison R, McCall GJH et al. (eds) Meteorites: Flux with time and impact effects. *Geol Soc Lond Spec Pub* **140**: 259-274.

Hallam A, Wignall PB (1999) Mass extinctions and sea-level changes. *Earth-Sci Rev* **48**(3-4): 217-250.

Harries PJ (1999) Repopulations from Cretaceous mass extinctions: Environmental and/or evolutionary controls? In: Barrera E, Johnson CC (eds) Evolution of the Cretaceous ocean-climate system. *Geol Soc Am Spec Pap* **332**: 345-364.

Hart MB (ed) (1996) Biotic recovery from mass extinction events. *Geol Soc Lond Spec Pap* **102**: 1-392.

Hildebrand AR, Stansberg JA (1992) K/T boundary ejecta distribution predicts size and location of the Chicxulub crater (abstract). *Lun Planet Sci* **23**: 537-538.

Hildebrand AR, Penfield GT, Kring DA, Pilkington M, Camargo AZ, Jacobsen SB, Boynton WV (1991) Chicxulub Crater: A possible Cretaceous/Tertiary boundary impact crater on the Yucatán peninsula, Mexico. *Geology* **19**(9): 867-871.

Hildebrand AR, Pilkington M, Ortiz-Aleman C, Chavez RE, Urrutia-Fucugauchi J, Connors M, Graniel-Castro E, Camara-Zi A, Halpenny J, Niehaus D (1998) Mapping Chicxulub crater structure with overlapping gravity and seismic reflection data. In: Grady MM, Hutchison R, McCall GJH et al. (eds) Meteorites: Flux with time and impact effects. *Geol Soc Lond Spec Pub* **140**: 155-176.

Hollander DJ, McKenzie JA, Hsü KJ (1993) Carbon isotope evidence for unusual plankton blooms and fluctuations of surface water CO_2 in "Strangelove Ocean" after terminal Cretaceous event. *Palaeogeogr Palaeoclimatol Palaeoecol* **104**(1-4): 229-237.

Izett GA (1990) The Cretaceous/Tertiary boundary interval, Ration basin, Colorado and New Mexico, and its content of shock-metamorphosed minerals: Evidence relevant to the K/T boundary impact-extinction event. *Geol Soc Am Spec Pap* **249**: 1-100.

Izett GA (1991) Tektites in Cretaceous-Tertiary boundary rocks on Haiti and their bearing on the Alvarez impact extinction hypothesis. *Jour Geophys Res* **96**(E4): 20879-20905.

Kaiho K, Kajiwara Y, Tazaki K, Ueshima M, Takeda N, Kawahata H, Arinobu T, Ishiwatari R, Hirai A, Lamolda MA (1999) Oceanic primary productivity and dissolved oxygen levels at the Cretaceous-Tertiary boundary: Their decrease, subsequent warming, and recovery. *Paleoceanography* **14**(4): 511-524.

Kamo SL, Krogh TE (1995) Chicxulub Crater source for shocked zircon crystals from the Cretaceous-Tertiary boundary layer, Saskatchewan: Evidence from new U-Pb data. *Geology* **23**(3): 281-284.

Keller G (1993) The Cretaceous-Tertiary boundary transition in the Antarctic Ocean and its global implications. *Mar Micropaleontol* **21**(1-2): 1-45.

Keller G, Stinnesbeck W (1996) Sea-level changes, clastic deposits, and megatsunamis across the Cretaceous-Tertiary boundary. In: MacLeod N, Keller G (eds) Cretaceous-Tertiary boundary mass extinction: Biotic and environmental changes. Norton Press, New York: 415-450.

Keller G, Li L, MacLeod N (1995) The Cretaceous/Tertiary boundary stratotype section at El Kef, Tunisia: How catastrophic was the mass extinction? *Palaeogeogr Palaeoclimatol Palaeoecol* **119**(3-4): 221-254.

Keller G, Stinnesbeck W, Adatte T (2002a) Comment: "Slumping and a sandbar deposit at the Cretaceous-Tertiary boundary in the El Tecolote section (northeastern Mexico): An impact-induced sediment gravity flow". *Geology* **30**(4): 382-383.

Keller G, Barrera E, Schmitz B, Mattson E (1993a) Gradual mass extinction, species survivorship, and long-term environmental changes across the Cretaceous-Tertiary boundary in high latitudes. *Geol Soc Am Bull* **105**(8): 979-997.

Keller G, MacLeod N, Lyons JB, Officer CB (1993b) Is there evidence for Cretaceous-Tertiary boundary-age deep-water deposits in the Caribbean and Gulf of Mexico? *Geology* **21**(9): 776-780.

Keller G, López-Oliva J-G, Stinnesbeck W, Adatte T (1997) Age, stratigraphy and deposition of near-K/T siliciclastic deposits in Mexico: Relation to bolide impact? *Geol Soc Am Bull* **109**(6): 410-428.

Keller G, Adatte T, Stinnesbeck W, Stüben D, Berner Z (2001) Age, chemo- and biostratigraphy of Haiti spherule-rich deposits: A multievent K-T scenario. *Can Jour Earth Sci* **38**(2): 197-227.

Keller G, Adatte T, Stinnesbeck W, Affolter M, Schilli L, López-Oliva J-G (2002b) Multiple spherule layers in the late Maastrichtian of northeastern Mexico. In: Koeberl C, MacLeod KG (eds) Catastrophic events and mass extinctions: Impacts and beyond. *Geol Soc Am Spec Pap* **356**: 145-162.

Keller G, Adatte T, Stinnesbeck W, Luciani V, Karoui-Yaakoub N, Zaghbib-Turki D (2002c) Paleoecology of the Cretaceous/Tertiary mass extinction in planktonic foraminifera. *Palaeogeogr Palaeoclimatol Palaeoecol* **178**(3-4): 257-297.

Kiessling W, Claeys P (2001) A geographic database approach to the KT boundary. In: Buffetaut E, Koeberl C (eds) Geological and biological effects of impact events. *Impact Studies.* Springer, Heidelberg: 83-140.

Klaus A, Norris RD, Kroon D, Smit J (2000) Impact-induced mass wasting at the K-T boundary: Blake Nose, western North Atlantic. *Geology* **28**(4): 319-322.

Koeberl C, Sigurdsson H (1992) Geochemistry of impact glasses from the K/T boundary in Haiti: Relation to smectites and a new type of glass. *Geochim Cosmochim Acta* **56**: 2113-2129.

Koeberl C, MacLeod KG (eds) (2002) Catastrophic events and mass extinctions: Impacts and beyond. *Geol Soc Am Spec Pap* **356**: 1-746.

Koeberl C, Martínez-Ruiz FC (eds) (2003) Impact markers in the stratigraphic record. *Impact Studies.* Springer, Heidelberg: 1-347.

Kring DA (1995) The dimensions of the Chicxulub impact crater and impact melt sheet. *Jour Geophys Res* **100**(E8): 16,979-16,986.

Kring DA, Durda DD (2002) Trajectories and distribution of material ejected from the Chicxulub impact crater: Implications for postimpact wildfires. *Jour Geophys Res* **107**(E8): 1-22.

Kring DA, Hildebrand AR, Boynton WV (1994) Provenance of mineral phases in the Cretaceous-Tertiary boundary sediments exposed on the southern peninsula of Haiti. *Earth Planet Sci Lett* **128**(3-4): 629-641.

Krogh TE, Kamo SL, Bohor BF (1993a) Fingerprinting the K/T impact site and determining the time of impact by U-Pb dating of single shocked zircons from distal ejecta. *Earth Planet Sci Lett* **119**(3): 425-429.

Krogh TE, Kamo SL, Sharpton VL, Marin LE, Hildebrand AR (1993b) U-Pb ages of single shocked zircons linking distal K/T ejecta to the Chicxulub crater. *Nature* **366**: 731-734.

Kyte FT, Vakulenko M (2001) KT boundary impact debris from DSDP Site 577 (abstract). Meteoritical Society, 64th Annual Meeting: #5423 (CD-ROM).

Kyte FT, Bostwick JA, Zhou L (1996) The Cretaceous-Tertiary boundary on the Pacific plate: Composition and distribution of impact debris. In: Ryder G, Fastovsky D, Gartner S (eds) The Cretaceous-Tertiary boundary event and other catastrophes in Earth history. *Geol Soc Am Spec Pap* **307**: 389-401.

Lerbekmo JF, Sweet AR, Davidson RA (1999) Geochemistry of the Cretaceous-Tertiary (K-T) boundary interval: South-central Saskatchewan and Montana. *Can Jour Earth Sci* **36**(5): 717-724.

Li L, Keller G (1998) Abrupt deep-sea warming at the end of the Cretaceous. *Geology* **26**(11): 995-998.

Li L, Keller G, Adatte T, Stinnesbeck W (2000) Late Cretaceous sea level changes in Tunisia: A multi-disciplinary approach. *Jour Geol Soc Lond* **157**: 447-458.

Lindinger M (1988) The Cretaceous/Tertiary boundaries of El Kef and Caravaca: Sedimentological, geochemical, and clay mineralogical aspects. *PhD Thesis*, ETH Zürich: 1-253.

Lomax BH, Beerling DJ, Upchurch G, Otto-Bliesner B (2001) Rapid (10-yr) recovery of terrestrial productivity in a simulation study of the terminal Cretaceous impact event. *Earth Planet Sci Lett* **192**(2): 137-144.

Luder T, Benz W, Stocker TF (2003) A model for long-term climatic effects of impacts. *Jour Geophys Res* **108**(E7): 5074.

Lyons JB, Officer CB (1992) Mineralogy and petrology of the Haiti Cretaceous/Tertiary section. *Earth Planet Sci Lett* **109**(1): 205-224.

MacLeod KG (1998) Impacts and marine invertebrate extinctions. In: Grady MM, Hutchison R, McCall GJH et al. (eds) Meteorites: Flux with time and impact effects. *Geol Soc Lond Spec Pub* **140**: 217-246.

MacLeod KG, Huber BT (2001) The Maastrichtian record at Blake Nose (western North Atlantic) and implications for global palaeoceanographic and biotic changes. In: Kroon D, Norris RD, Klaus A (eds) Western North Atlantic Paleogene and Cretaceous paleoceanography. *Geol Soc Lond Spec Pub* **183**: 111-130.

MacLeod N, Keller G (1991) How complete are Cretaceous/Tertiary boundary sections? A chronostratigraphic estimate based on graphic correlation. *Geol Soc Am Bull* **103**(11): 1439-1457.

MacLeod N, Rawson PF, Forey PL, Banner FT et al. (1997) The Cretaceous-Tertiary biotic transition. *Jour Geol Soc Lond* **154**(2): 265-292.

Martínez-Ruiz F, Ortega-Huertas M, Palomo-Delgado I (1999) Positive Eu anomaly development during diagenesis of the K/T boundary ejecta layer in the Agost section (SE Spain): Implications for trace-element remobilization. *Terra Nova* **11**(6): 290-296.

Martínez-Ruiz F, Ortega-Huertas M, Palomo-Delgado I, Acquafredda P (1997) Quench textures in altered spherules from the Cretaceous-Tertiary boundary layer at Agost and Caravaca, SE Spain. *Sediment Geol* **113**(1-2): 137-147.

Martínez-Ruiz F, Ortega-Huertas M, Palomo-Delgado I, Smit J (2001a) K-T boundary spherules from Blake Nose (ODP Leg 171B) as a record of the Chicxulub ejecta deposits. In: Kroon D, Norris RD, Klaus A (eds) Western North Atlantic Paleogene and Cretaceous paleoceanography. *Geol Soc Lond Spec Pub* **183**: 149-161.

Martínez-Ruiz F, Ortega-Huertas M, Kroon D, Smit J, Palomo-Delgado I, Rocchia R (2001b) Geochemistry of the Cretaceous-Tertiary boundary at Blake Nose (ODP Leg 171B). In: Kroon D, Norris RD, Klaus A (eds) Western North Atlantic Paleogene and Cretaceous paleoceanography. *Geol Soc Lond Spec Pub* **183**: 131-148.

Maruoka T, Koeberl C (2003) Acid-neutralizing scenario after the Cretaceous-Tertiary impact event. *Geology* **31**(6): 489–492.

Maurrasse FJ, Sen G (1991) Impacts, tsunamis, and the Haitian Cretaceous-Tertiary boundary layer. *Science* **252**: 1690-1693.

Montanari A (1991) Authigenesis of impact spheroids in the K/T boundary clay from Italy: New constraints for high-resolution stratigraphy of terminal Cretaceous events. *Jour Sediment Petrol* **61**(3): 315-339.

Montanari A, Koeberl C (2000) Impact stratigraphy. *Lecture notes in Earth sciences* **93**. Springer, Heidelberg: 1-364.

Morgan J, Warner M, Grieve RAF (2002) Geophysical constraints on the size and structure of the Chicxulub impact crater. In: Koeberl C, MacLeod KG (eds) Catastrophic events and mass extinctions: Impacts and beyond. *Geol Soc Am Spec Pap* **356**: 39-46.

Morgan JV, Warner MR, Brittan J, Buffler RT et al. (1997) Size and morphology of the Chicxulub impact crater. *Nature* **390**: 472-476.

Norris RD, Huber BT, Self-Trail BT (1999) Synchroneity of the K-T oceanic mass extinction and meteorite impact: Blake Nose, western North Atlantic. *Geology* **27**(5): 419-422.

Norris RD, Firth J, Blusztain JL, Ravizza G (2000) Mass failure of the North Atlantic margin triggered by the Cretaceous-Paleogene bolide impact. *Geology* **28**(12): 1119-1122.

Odin GS (1992) New stratotypes for the Paleogene, the Cretaceous/Paleogene, Eocene/Oligocene and Paleogene/Neogene boundaries. *Neues Jahrb Geol Paläontol Abh* **186**(1-2): 7-20.

Olsson RK, Miller KG, Browning JV, Habib D, Sugarmann PJ (1997) Ejecta layer at the Cretaceous-Tertiary boundary, Bass River, New Jersey (Ocean Drilling Program Leg 174AX). *Geology* **25**(8): 759-762.

Olsson RK, Miller KG, Browning JV, Wright JD, Cramer BS (2002) Sequence stratigraphy and sea-level changes across the Cretaceous-Tertiary boundary on the New Jersey passive margin. In: Koeberl C, MacLeod KG (eds) Catastrophic events and mass extinctions: Impacts and beyond. *Geol Soc Am Spec Pap* **356**: 97-108.

Ortega-Huertas M, Palomo-Delgado I, Martínez-Ruiz F, Gonzalez I (1998) Geological factors controlling clay mineral patterns across the Cretaceous-Tertiary boundary in Mediterranean and Atlantic sections. *Clay Miner* **33**(3): 483-500.

Ortega-Huertas M, Martínez-Ruiz F, Palomo-Delgado I, Chamley H (2002) Review of the mineralogy of the Cretaceous-Tertiary boundary clay: Evidence supporting a major extraterrestrial catastrophic event. *Clay Miner* **37**(3): 395-411.

Pardo A, Ortiz N, Keller G (1996) Latest Maastrichtian and Cretaceous-Tertiary foraminiferal turnover and environmental changes at Agost, Spain. In: MacLeod N, Keller G (eds) Cretaceous-Tertiary boundary mass extinction: Biotic and environmental changes. Norton Press, New York: 139-171.

Pardo A, Adatte T, Keller G, Oberhänsli H (1999) Palaeoenvironmental changes across the Cretaceous-Tertiary boundary at Koshak, Kazakhstan, based on planktic foraminifera and clay mineralogy. *Palaeogeogr Palaeoclimatol Palaeoecol* **154**(3-4): 247-273.

Pierazzo E, Melosh HJ (1999) Hydrocode modeling of Chicxulub as an oblique impact event. *Earth Planet Sci Lett* **165**(2): 163-176.

Pierazzo E, Hahmann AN (2002) Chicxulub and climate: Investigating the climate sensitivity to stratospheric injections of impact-generated S-bearing gases (abstract). *Lun Planet Sci* **33**: #1269 (CD-ROM).

Pierazzo E, Kring DA, Melosh HJ (1998) Hydrocode simulations of the Chicxulub impact event and the production of climatically active gases. *Jour Geophys Res* **103**(E12): 28607-28625.

Pollastro RM, Bohor BF (1993) Origin and clay-mineral genesis of the Cretaceous/Tertiary boundary unit, Western Interior of North America. *Clays Clay Miner* **41**(1): 7-25.

Pope KO (2002) Impact dust not the cause of the Cretaceous-Tertiary mass extinction. *Geology* **30**(2): 99-102.

Pope KO, Ocampo AC, Fischer AG, Alvarez W, Fouke BW, Webster CL, Vega FJ, Smit J, Fritsche AE, Claeys P (1999) Chicxulub impact ejecta from Albion Island, Belize. *Earth Planet Sci Lett* **170**(4): 351-364.

Pospichal JJ (1996) Calcareous nannoplankton mass extinction at the Cretaceous/Tertiary boundary: An update. In: Ryder G, Fastovsky D, Gartner S (eds) The Cretaceous-Tertiary boundary event and other catastrophes in Earth history. *Geol Soc Am Spec Pap* **307**: 335-360.

Remane J, Keller G, Hardenbol J, Ben Haj Ali M (1999) Report on the international workshop on Cretaceous-Paleogene transitions. *Episodes* **22**(1): 47–48.

Remane J, Bassett MG, Cowie JW, Gohrbandt KH, Lane HR, Michelsen O, Naiwen W (1996) Revised guidelines for the establishment of global chronostratigraphic standards by the International Commission on Stratigraphy (ICS). *Episodes* **19**(3): 77-81.

Retallack GJ (1996) Acid trauma at the Cretaceous-Tertiary boundary in eastern Montana. *GSA Today* **6**(5): 1-7.

Robin E, Rocchia R (1998) Ni-rich spinel at the Cretaceous-Tertiary boundary of El Kef, Tunisia. *Bull Soc Géol Fr* **169**(3): 365-372.

Rocchia R, Robin E (1998) L'iridium à la limite Crétacé-Tertiaire du site d'El Kef, Tunisie. *Bull Soc Géol Fr* **169**(4): 515-526.

Ryder G, Fastovsky D, Gartner S (eds) (1996) The Cretaceous-Tertiary event and other catastrophes in Earth history. *Geol Soc Am Spec Pap* **307**: 1-556.

Schmitz B (1988) Origin of microlayering in worldwide distributed Ir-rich marine Cretaceous/Tertiary boundary clays. *Geology* **16**(12): 1068-1072.

Schmitz B (1992) Chalcophile elements and Ir in continental Cretaceous-Tertiary boundary clays from the Western Interior of the USA. *Geochim Cosmochim Acta* **56**: 1695-1703.

Schulte P, Stinnesbeck W, Stüben D, Kramar U, Berner Z, Keller G, Adatte T (2003) Fe-rich and K-rich mafic spherules from slumped and channelized Chicxulub ejecta deposits at the northern La Sierrita area, NE Mexico. *Int Jour Earth Sci* **92**(1): 114-142.

Self-Trail JM (2001) Biostratigraphic subdivision and correlation of upper Maastrichtian sediments from the Atlantic Coastal Plain and Blake Nose, western Atlantic. In: Kroon D, Norris RD, Klaus A (eds) Western North Atlantic Paleogene and Cretaceous paleoceanography. *Geol Soc Lond Spec Pub* **183**: 93-110.

Sepkoski JJ (1996) Patterns of Phanerozoic extinction: A perspective from global data bases. In: Walliser OH (ed) Global events and event stratigraphy in the Phanerozoic. Springer, Heidelberg: 35-51.

Shackleton NJ, Kennett JP (1975) Paleotemperature history of the Cenozoic and the initiation of Antarctic glaciation; oxygen and carbon isotope analyses in DSDP Sites 277, 279, and 281. Deep Sea Drilling Project. *Initial Results* **29**: 743-755.

Sharpton VL, Schuraytz BC, Burke K, Murali AV, Ryder G (1990) Detritus in K/T boundary clays of western North America: Evidence against a single oceanic impact. In: Sharpton VL, Ward PD (eds) Global catastrophes in Earth history: An interdisciplinary conference on impacts, volcanism, and mass mortality. *Geol Soc Am Spec Pap* **247**: 349-357.

Sharpton VL, Dalrymple GB, Marín LE, Ryder G, Schuraytz BC, Urrutia-Fucugauchi J (1992) New links between the Chicxulub impact structure and the Cretaceous/Tertiary boundary. *Nature* **359**: 819-821.

Sharpton VL, Marín LE, Carney JL, Lee S, Ryder G, Schuraytz BC, Ikora P, Spudis PD (1996) A model of the Chicxulub impact basin based on evaluation of geophysical data, well-logs, and drill core samples. In: Ryder G, Fastovsky D, Gartner S (eds) The Cretaceous-Tertiary boundary event and other catastrophes in Earth history. *Geol Soc Am Spec Pap* **307**: 55-74.

Sharpton VL, Burke K, Camargo-Zanoguera A, Hall SA, Lee S, Marín LE, Suárez-Reynoso G, Quezada-Muñeton JM, Spudis PD, Urrutia-Fucugauchi J (1993) Chicxulub multiring impact basin: Size and other characteristics derived from gravity analysis. *Science* **261**: 1564-1567.

Signor PW, Lipps JH (1982) Sampling bias, gradual extinction patterns and catastrophes in the fossil record. In: Silver LT, Schultz PH (eds) Geological implications of impacts of large asteroids and comets on the Earth. *Geol Soc Am Spec Pap* **190**: 291-296.

Sigurdsson H, D'Hondt S, Carey S (1992) The impact of the Cretaceous/Tertiary bolide on evaporite terrane and generation of major sulfuric acid aerosol. *Earth Planet Sci Lett* **109**(3/4): 543-559.

Sigurdsson H, Leckie RM, Acton GD (1997) Shipboard Scientific Party: Caribbean volcanism, Cretaceous/Tertiary impact, and ocean climate history: Synthesis of Leg 165. Proceedings of the Ocean Drilling Program. *Initial Reports*: 377-400.

Smit J (1999) The global stratigraphy of the Cretaceous-Tertiary boundary impact ejecta. *Ann Rev Earth Planet Sci* **27**: 75-113.

Smit J, Alvarez W, Montanari A, Claeys P, Grajales-Nishimura JM (1996) Coarse-grained, clastic sandstone complex at the K/T boundary around the Gulf of Mexico: Deposition by tsunami waves induced by the Chicxulub impact? In: Ryder G, Fastovsky D, Gartner S (eds) The Cretaceous-Tertiary boundary event and other catastrophes in Earth history. *Geol Soc Am Spec Pap* **307**: 151-182.

Smit J, Montanari A, Swinburn NHM, Alvarez W, Hildebrand AR, Margolis SV, Claeys P, Lowrie W, Asaro F (1992) Tektite-bearing, deep-water clastic unit at the Cretaceous-Tertiary boundary in northeastern Mexico. *Geology* **20**(1): 99-103.

Smith AB, Gale AS, Monks NEA (2001) Sea-level change and rock-record bias in the Cretaceous: A problem for extinction and biodiversity studies. *Paleobiology* **27**(2): 241-253.

Soria AR, Liesa CL, Mata MP, Arz JA, Alegret L, Arenillas I, Meléndez A (2001) Slumping and a sandbar deposit at the Cretaceous-Tertiary boundary in the El Tecolote section (northeastern Mexico): An impact-induced sediment gravity flow. *Geology* **29**(3): 231-234.

Soria AR, Liesa CL, Mata MP, Arz JA, Alegret L, Arenillas I, Meléndez A (2002) Reply: "Slumping and a sandbar deposit at the Cretaceous-Tertiary boundary in the El Tecolote section (northeastern Mexico): An impact-induced sediment gravity flow". *Geology* **30**(4): 382-383.

Steuber T, Mitchell SF, Buhl D, Gunter G, Kasper HU (2002) Catastrophic extinction of Caribbean rudist bivalves at the Cretaceous-Tertiary boundary. *Geology* **30**(11): 999-1002.

Stilwell JD (2003) Patterns of biodiversity and faunal rebound following the K-T boundary extinction event in Austral Palaeocene molluscan faunas. *Palaeogeogr Palaeoclimatol Palaeoecol* **195**(3-4): 319-356.

Stinnesbeck W, Keller G, Adatte T, López-Oliva J-G, MacLeod N (1996) Cretaceous-Tertiary boundary clastic deposits in NE Mexico: Bolide impact or sea-level lowstand? In: MacLeod N, Keller G (eds) The Cretaceous-Tertiary boundary mass extinction: Biotic and environmental events. Norton Press, New York: 471-517.

Stinnesbeck W, Keller G, de la Cruz J, de Léon C, MacLeod N, Whittacker JE (1997) The Cretaceous-Tertiary boundary in Guatemala-Limestone breccia deposits from the South Peten Basin. *Int Jour Earth Sci* **86**(4): 686-709.

Stinnesbeck W, Keller G, Adatte T, Stüben D, Kramar U, Berner Z, Desremeaux C, Molière E (1999) Beloc, Haiti, revisited: Multiple events across the K/T boundary in the Caribbean. *Terra Nova* **11**(5): 303-310.

Stinnesbeck W, Barbarin JM, Keller G, López-Oliva J-G, Pivnik DA, Lyons JB, Officer CB, Adatte T, Graup G, Rocchia R, Robin E (1993) Deposition of channel deposits near the Cretaceous-Tertiary boundary in northeastern Mexico: Catastrophic or "normal" sedimentary deposits? *Geology* **21**(7): 797-800.

Stinnesbeck W, Schulte P, Lindenmaier F, Adatte T et al. (2001) Late Maastrichtian age of spherule deposits in northeastern Mexico: Implication for Chicxulub scenario. *Can Jour Earth Sci* **38**(2): 229-238.

Stüben D, Kramar U, Berner Z, Stinnesbeck W, Keller G, Adatte T (2002a) Trace elements, stable isotopes, and clay mineralogy of the Elles II K/T boundary section in Tunisia: Indications for sea level fluctuations and primary productivity. *Palaeogeogr Palaeoclimatol Palaeoecol* **178**(3-4): 321-345.

Stüben D, Kramar U, Berner Z, Eckhardt J-D, Stinnesbeck W, Keller G, Adatte T, Heide K (2002b) Two PGE anomalies above the Cretaceous/Tertiary boundary at Beloc/Haiti: Geochemical context and consequences for the impact scenario. In: Koeberl C, MacLeod KG (eds) Catastrophic events and mass extinctions: Impacts and beyond. *Geol Soc Am Spec Pap* **356**: 163-188.

Sweet AR (2001) Plants, a yardstick for measuring the environmental consequences of the Cretaceous/Tertiary boundary event. *Geosci Can* **28**(3): 127-138.

Sweet AR, Braman DR, Lerbekmo JF (1999) Sequential palynological changes across the composite Cretaceous-Tertiary (K-T) boundary claystone and contiguous strata, western Canada and Montana, USA. *Can Jour Earth Sci* **36**(5): 743-768.

Tada R, Nakano Y, Iturralde-Vinent MA, Yamamoto S et al. (2002) Complex tsunami waves suggested by the Cretaceous-Tertiary boundary deposit at the Moncada section, western Cuba. In: Koeberl C, MacLeod KG (eds) Catastrophic events and mass extinctions: Impacts and beyond. *Geol Soc Am Spec Pap* **356**: 109-124.

Toon OB, Zahnle K, Morrison D, Turco RP, Covey C (1997) Environmental perturbations caused by the impacts of asteroids and comets. *Rev Geophys* **35**(1): 41-78.

Tribovillard N, Dupuis C, Robin E (2000) Sedimentological and diagenetical conditions of the impact level of the Cretaceous/Tertiary boundary in Tunisia: No anoxia required. *Bull Soc Géol Fr* **171**(6): 629-636.

Vajda V, Raine JI, Hollis CJ (2001) Indication of global deforestation at the Cretaceous-Tertiary boundary by New Zealand fern spike. *Science* **294**: 1700-1702.

Verma HC, Upadhyay C, Tripathi A, Tripathi RP, Bhandari N (2002) Thermal decomposition pattern and particle size estimation of iron minerals associated with the Cretaceous-Tertiary boundary at Gubbio. *Meteor Planet Sci* **37**(7): 901-909.

Wdowiak TJ, Armendarez LP, Agresti DG, Wade ML, Wdowiak YS, Claeys P, Izett GA (2001) Presence of an iron-rich nanophase material in the upper layer of the Cretaceous-Tertiary boundary clay. *Meteor Planet Sci* **36**(1): 123-133.

Wignall PB (2001) Large igneous provinces and mass extinctions. *Earth-Sci Rev* **53**(1-2): 1-33.

Wilf P, Johnson KR, Huber BT (2003) Correlated terrestrial and marine evidence for global climate changes before mass extinction at the Cretaceous-Paleogene boundary. *Proc Natl Acad Sci* **100**(2): 599-604.

Worm HU, Banerjee SK (1987) Rock magnetic signature of the Cretaceous-Tertiary boundary. *Geophy Res Lett* **14**(11): 1083-1086.

Zachos JC, Arthur MA, Dean WE (1989) Geochemical evidence for suppression of pelagic marine productivity at the Cretaceous/Tertiary boundary. *Nature* **337**: 61-64.

2. The Cretaceous-Paleogene transition and Chicxulub impact ejecta in northeastern Mexico: Target lithologies, impact processes and depositional scenario

2.1 Introduction

Spherules are a salient component of many localities that include the Cretaceous-Paleogene (K-P) boundary (e.g., Ryder et al., 1996; Smit, 1999; Montanari and Koeberl, 2000; Claeys et al., 2002). These spherules are interpreted to be of impact ejecta origin and are generally ascribed to the Chicxulub impact on the Yucatán peninsula, Mexico (e.g., Izett, 1991; Smit et al., 1992b; Bohor and Glass, 1995; Martínez-Ruiz et al., 1997; Claeys et al., 2002). In this context, ejecta formations, such as spherule deposits, and their spatial distribution, composition, and degree of shock metamorphism are instrumental in determining pre-impact target lithology, extent of excavation, trajectory of the projectile, and P/T conditions during the impact (e.g., Melosh, 1989; Engelhardt et al., 1997; Pierazzo and Melosh, 1999; Kettrup et al.,

2000; Montanari and Koeberl, 2000). This information is crucial for estimating the amount of water, carbonate, sulfate, and dust released by the impact that is required for modeling the resulting environmental and climatic effects of this event (Covey et al., 1994; Ivanov et al., 1996; Pope et al., 1997; Toon et al., 1997; Pierazzo et al., 1998; Gupta et al., 2001; Luder et al., 2003).

Accurate knowledge of these perturbations is important for evaluating the significance of the Chicxulub impact event compared to other 'events' (e.g., Deccan Trap volcanism) that took place during the K-P transition, and presumably contributed to the biological crisis at the end of the Cretaceous period (MacLeod et al., 1997; Toon et al., 1997; Barrera and Savin, 1999; Hallam and Wignall, 1999; Wignall, 2001; Kiessling and Claeys, 2001; Courtillot, 2002). In addition, impactoclastic layers may
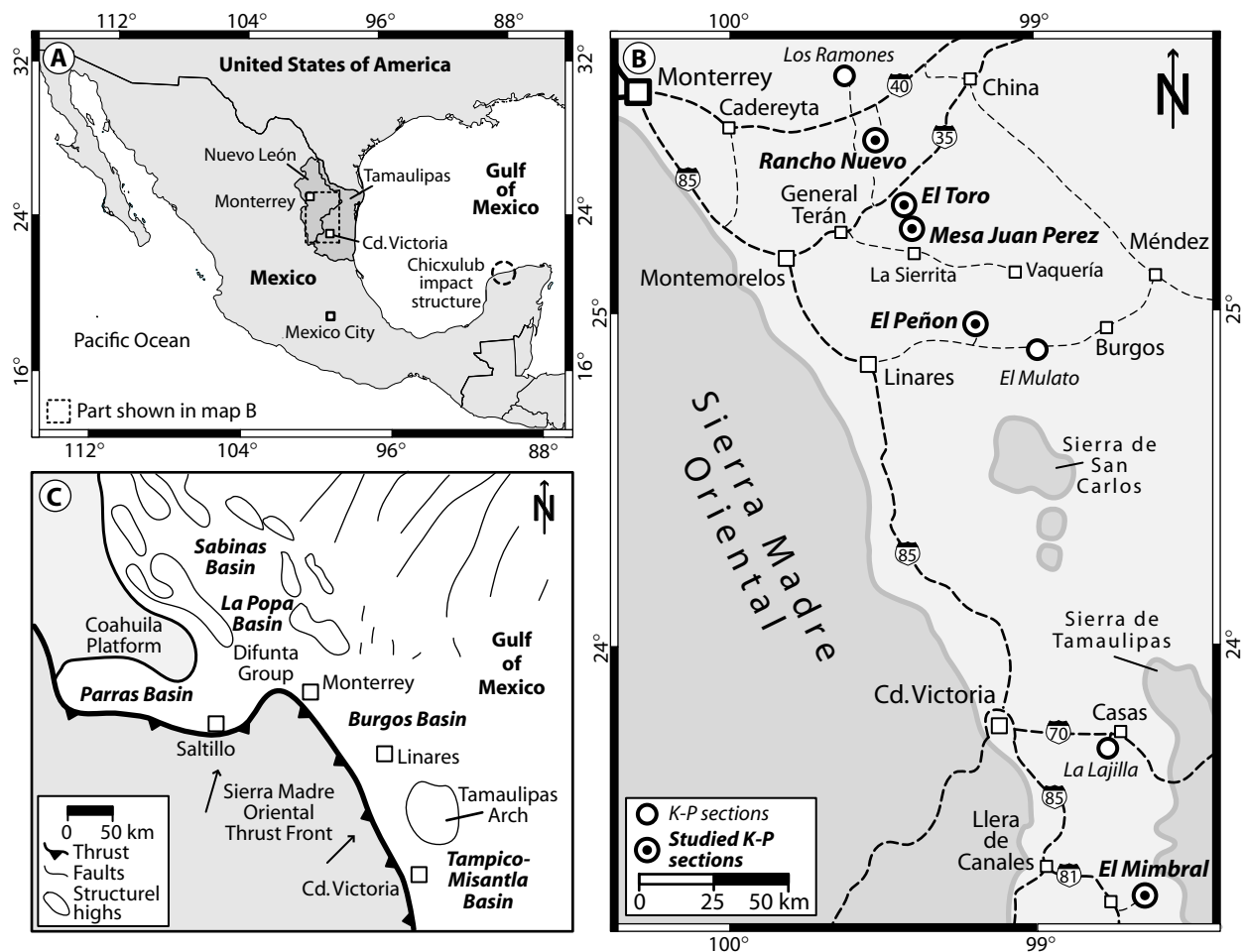
Figure 2.1 Map of Mexico (**A**) and northeastern Mexico (**B**) showing the locations of the K-P sections referred to in this study. Details of the Mesa Juan Perez and El Peñon area are provided in Fig. 2.2. (**C**) Paleogeographic overview of northeastern Mexico with main structural elements. Modified after Echanove (1986), Perez Cruz (1992), and Goldhammer and Johnson (2001).

document the mechanism of ejecta dispersion and deposition, as well as later reworking (e.g., McHugh et al., 1998; Tsikalas et al., 1998; Smit, 1999; Ormö and Lindström, 2000; Sturkell et al., 2000).

2.1.1 Characteristics of Chicxulub impact ejecta

Two major types of ejecta spherules are generally present in K-P boundary sites: (i) "microtektite"-like mm-cm sized vesiculated glassy or clayey spherules, suggestive of silicic and carbonaceous progenitor phases, and (ii) ~0.1 mm-sized microcrystalline spherules ("microkrystites") of pyroxene, K-feldspar, or iron-oxide crystals that all are alteration products of unknown (mafic?) precursor lithologies, albeit Ni-rich and Cr-rich inclusions may indicate contamination by meteoritic material (Table 2.1 and Montanari, 1991; Smit et al., 1992a; Bohor and Glass, 1995; Martínez-Ruiz et al., 1997). In addition, microtektite spherules and microkrystites may be embedded in a ferruginous and iridium-enriched clayey phase that also bears abundant shocked minerals. The wide compositional range, mode of occurrence, and relative quantity of these ejecta phases in K-P sites reflect not only different formation processes, but also point to a geologically complex target area at the Chicxulub structure.

Smit et al. (1992a) and Pollastro and Bohor (1993) proposed that microtektite spherules formed exclusively from molten target rocks and were dispersed ballistically by the impact ejecta-curtain in regions 'close' to the impact (e.g., Montanari and Koeberl, 2000). In contrast, microkrystites may have formed by condensation from the vaporized target-rock and meteoritic materials in the expanding vapour plume cloud ("fireball", Pollastro and Bohor, 1993); their elevation well above the atmospheric heights presumably led to their almost global distribution concomitant to the iridium-rich dust (e.g., Alvarez et al., 1995; Croskell et al., 2002; Kring and Durda, 2002).

The composition of glass and smectite spherules suggests that they derived from silicate rocks of upper crustal, gneiss-granite-like composition with admixture of variable amounts of a calcium- and sulfur-rich endmember (e.g., Izett, 1991; Koeberl and Sigurdsson, 1992; Bohor and Glass, 1995; Stüben et al., 2002). This composition is congruent to the known basement and carbonaceous (limestone, anhydrite) sedimentary cover of the Yucatán peninsula (e.g., Schuraytz et al., 1994), as further shown by isotope and geochemical studies on ejecta and isotopes (e.g., Blum et al., 1993). However, studies of

Sm-Nd isotopes by Kettrup et al. (2000) and Kettrup and Deutsch (2003) suggested the admixture of a distinct mafic precursor phase to account for the observed mixing trend that is not solely explained by the granite-gneiss basement. Additional findings of amphibolite clasts in suevite drilled at the Chicxulub structure further corroborated these results (Kring and Boynton, 1992; Kettrup, 2002). These mafic lithologies may also be the parental phase to the K-feldspar and pyroxene microkrystites found at several K-P sites, though the formation conditions of these microkrystites are still unknown (Table 2.1 and Kettrup and Deutsch, 2003).

Recent studies of the Yaxcopoil drillcore from the Chicxulub impact structure confirmed not only the presence of mafic lithologies (e.g., Kring et al., 2003), but also revealed the pervasive alkali metasomatism and potassic alteration of the suevite, for which the precursor phases that provided the large amounts of potassium, are not clear yet (Hecht et al., 2003). Consequently, a significant contribution may have existed to the ejecta from mafic lithologies in the subsurface of the Chicxulub structure, besides the contribution from silicic and carbonaceous target rocks, though such mafic lithologies have, so far, rarely been reported from the Yucatán peninsula (e.g., from PEMEX drillcores, Ward et al., 1995).

In this general context, the findings of mafic phases in proximal Chicxulub ejecta deposits at La Sierrita and La Lajilla in northeastern Mexico by Kontny et al. (2002), Schulte et al. (2002; 2003), and Kettrup et al. (2003) are quite stimulating. Previous investigations of the K-P sections in northeastern Mexico have primarily aimed on the particular siliciclastic depositional sequence associated with the ejecta deposits in this area, which is considered either as impact-generated tsunamite (e.g., Smit et al., 1992b; 1996; Smit, 1999; Bohor, 1996; Alegret et al., 2001; Arz et al., 2001) or as sea-level lowstand deposit (e.g., Stinnesbeck et al., 1993; 1996; Keller et al., 1997; Ekdale and Stinnesbeck, 1998), instead of focusing on the mineralogical and geochemical properties of the ejecta components. However, ejecta deposits from the La Sierrita outcrops in northeastern Mexico show an extraordinary iron-rich, as well as K-rich mafic composition with pristinely preserved microfacies characteristics and abundance of carbonate (Schulte et al., 2002; 2003). Moreover, besides the common presence of a spherule layer at the base of the 'siliciclastic K-P deposit' in the La Sierrita area, spherule deposits are locally embedded within hemipelagic marls of latest Maastrichtian age

Table 2.1 Published occurrences and compositional characteristics of microtektites (spherules) and microkrystites from Chicxulub ejecta deposits and the basal K-P boundary clay in K-P sections.

Location	Type and mineralogy of spherules	Grain-size in mm (max)	References
Gulf of Mexico			
Rancho Nuevo, La Sierrita, El Peñon, El Mimbral; NE Mexico	Chlorite, K-feldspar, carbonate, glass (andesitic), pyroxene, chlorite-smectite, Si-Al-K-rich glass, illite, smectite,	0.5-2 (~16)	Smit et al. (1992a); Premo et al. (1995); Adatte et al. (1996); Bell and Sharpton (1996); this study
Brazos River; Texas	Smectite, chlorite, carbonate	0.25-1 (~2)	Smit et al. (1996); Yancey (1996); Chapter 3
Moscow Landing, Shell Creek; Alabama	Smectite, chlorite, carbonate	0.5-2 (3)	Pitakpaivan (1994); Smit et al. (1996); Chapter 4
DSDP Leg 77 Site 536-540	Glass (andesitic), smectite, K-feldspar		Alvarez et al. (1992)
Moncada; Cuba	Chlorite, smectite, goethite, carbonate, pyroxene	~1 mm	Tada et al. (2002; 2003)
Caribbean Sea			
Beloc; Haiti	Glass (andesitic), smectite, carbonate, chlorite, palagonite	0.5-2 (8)	Izett (1991); Koeberl and Sigurdsson (1992); Bohor and Glass (1995); Stüben et al. (2002a)
ODP Leg 165 Site 999, 1001	Smectite, carbonate	1.5 (~8)	Sigurdsson et al. (1997)
Albion Island; Belize	Smectite, carbonate, palagonite	3 (~10)	Pope et al. (1999)
North America			
Hell Creek, Dogie Creek, Sussex, Lance Creek, Teapot Dome, Raton Basin; Montana, Wyoming, Colorado	Kaolinite, smectite, goyazite, goethite	0.5-1 (~1)	Bohor et al. (1987); Bohor and Glass (1995); Izett (1990); Schmitz (1992); Pollastro and Bohor (1993); Sweet et al. (1999, 2001)
Atlantic Ocean			
ODP Leg 174AX Bass River Site	"Clay", carbonate	0.2-1 (~1.1)	Olsson et al. (1997; 2002)
DSPD Leg 43 Site 386, 390	Smectite, chlorite, carbonate. glauconite	0.5-1 (~1.5)	Klaver et al. (1987); Bohor and Betterton (1989); Norris et al. (2000)
ODP Leg 171 Site 1049-1053	Smectite, carbonate	1-2 (~3)	Norris et al. (1999); Martínez-Ruiz et al. (2001a, b; 2002)
ODP Leg 207 Site 1258-1260	Smectite, carbonate	0.2-0.5 (~1)	Erbacher et al. (2003)
Zumaya; Spain	Smectite, goethite, magnetite, pyroxene, K-feldspar	~ 0.2-0.4	Doehne and Margolis (1990); Smit et al. (1992a)
DSDP Leg 73 Site 524	Goethite, magnetite	~ 0.2	Hsü (1984); Cisowski (1990)
Tethyan realm			
Stevns Klint, Nye Kløv; Denmark	Pyrite, goethite, Fe-Ni-spherules (magnetite), Fe(0), glass (andesitic)	~ 0.1-0.3	Schmitz et al. (1988); Graup et al. (1992); Morden (1993); Bauluz et al. (2000)
Agost, Caravaca; Spain	Smectite, goethite, pyrite, K-feldspar	~ 0.05-0.2	Varenkamp and Thomas (1982); DePaolo et al. (1983); Lindinger (1988); Martínez-Ruiz et al. (1997)
Bottachione, Furlo, Gubbio, Petriccio, Pontedazzo; Italy	Smectite, glauconite, goethite, K-feldspar	~ 0.2-0.5	Varenkamp and Thomas (1982); Smit and Kyte (1984); Worm and Banerjee (1987); Montanari (1991); Montanari and Koeberl (2000)
El Kef, Elles; Tunisia	Glauconite, goethite, K-feldspar	~ 0.3-0.5	Smit (1982); Lindinger (1988)
Abat, Buraymi; Oman		~ 0.5-0.1	Le Callonnec et al. (1998); MacDonald et al. (2002); Ellwood et al. (2003)
Pacific Ocean			
DSDP Leg 89 Site 585-586; Leg 91 Site 595-596; ODP Leg 145 Site 886; Leg 198 Site 1209-1212	"Clay", ca-rich pyroxene, K-feldspar, magnetite, goethite	0.1-0.15 (1.5)	Ingram (1995); Kyte et al. (1996); Kyte and Vakulenko (2001); Bralower et al. (2002a, b)
DSDP Leg 62 Site 465; Leg 96 Site 577	Smectite, clinopyroxene, K-feldspar	~ 0.1	Varenkamp and Thomas (1982); Smit et al. (1992a); Kyte et al. (1996); Kyte and Vakulenko (2001)
Woodside Creek; New Zealand	Goethite, hematite	~ 0.3	Brooks et al. (1985); Vajda et al. (2001)

and show soft-sedimentary deformation structures (Soria et al., 2001; Stinnesbeck et al., 2001; Schulte et al., 2003).

These preliminary findings raised several questions, regarding not only possibly constraints on the depositional nature of these ejecta deposits and the temporal placement of the Chicxulub impact relative to the K-P boundary (Soria et al., 2001; Stinnesbeck et al., 2001), but also whether these mafic phases are present in other localities in northeastern Mexico as well, and why they have so far only rarely been encountered in other well-known proximal K-P sites with spherule deposits. This information is critical for determining the stratigraphic location and the amount of such mafic phases in the Yucatán basement. A closer study of the K-P outcrops in northeastern Mexico may provide also further insights into the depositional mode of the ejecta.

In this study the results of a multidisciplinary investigation in four outcrop areas in northeastern Mexico (Rancho Nuevo, La Sierrita, El Peñon, El Mimbral) are reported that (i) documents the spatial and stratigraphic distribution of the various spherule deposits and the K-P sand-siltstone complex to distinguish between the sedimentary processes that originated these deposits, (ii) examines their sedimentological and petrological characteristics to obtain further details on the ejecta dispersion and deposition mode, (iii) analyzes their mineralogical and geochemical composition to evaluate the origin of the spherules, and (iv) investigates the rock magnetic properties to reveal inferences on physical processes and target rocks.

2.1.2 Locations and geological setting

Localities: The Mexican K-P boundary outcrop areas are situated in the Gulf coastal plain of northeastern Mexico in the State of Nuevo León and Tamaulipas (Fig. 2.1A). For this study, the K-P outcrop areas at La Sierrita and El Peñon, as well as the outcrops Rancho Nuevo and El Mimbral, were geologically mapped and sampled (Fig. 2.2). The Rancho Nuevo outcrop can be reached via highway 40, from which a small paved road turns southward about three kilometers to the east following the large crossing at Los Ramones. The Rancho Nuevo outcrop (latitude 25°29'25''N; longitude 99°33'57''W) is found at the northern riverbank of the Rio San Juan, several hundred meters upstream from the ford southwest of the hamlet Rancho Nuevo.

The La Sierrita outcrop area is found adjacent to the small hamlet of La Sierrita near the road that connects General Terán and Vaquerías (Fig. 2.1A, B). They are exposed along the flanks of a series of low-lying hills to the south and the north of the Mesa Juan Perez (25°13'45''N; 99°31'05''W). The El Peñon outcrop area (25°58'05''N; 99°12'50''W) is located close to the unpaved road from Linares to the hamlet of Burgos (Fig. 2.1C). The outcrops are located about 2 km northwest of the Porvenir Lake at a series of low-lying hills west of the main road close to the Rancho El Peñon. The El Mimbral outcrop (23°13'10''N; 98°40'05''W) is found about 10 km to the southeast of Llera de Canales on the southwestern bank of the El Mimbral Creek and can be reached via an unpaved road that branch of from the Mexican Highway 81 to the east at the radio antenna.

Geological setting: Northeastern Mexico with the states of Nuevo León and Tamaulipas consists principally of two geologic departments (Weidie and Murray, 1967; Morán-Zenteno, 1994; Goldhammer and Johnson, 2001): The Gulf of Mexico coastal plain to the east, where the studied sections are situated, and the Sierra Madre Oriental to the west (Fig. 2.1C). This area has been the site of interaction of the North American Cordilleran fold and thrust belt of western America with the passive margin of the Gulf of Mexico (Ross and Scotese, 1988; Marton and Buffler, 1999). The compressional deformation by the Laramide orogeny that resulted in the generation of large thrust sheets and the uplift of the Sierra Madre Oriental started in the late Cretaceous, but main phases of deformation occurred in the middle Paleogene.

The Sierra Madre Oriental consists of folded late Jurassic to late Cretaceous carbonates, evaporites, and terrigeneous sediments. A series of through-like foreland basins was formed along the NNE-SSW trending Sierra Madre Oriental because of the rapid uplift of the Sierra Madre Oriental and the large-scale overthrusting from the southwest: The Sabinas, La Popa, and Parras basins in the northern part, the Burgos basin in the northeast, including the outcrop areas at Rancho Nuevo, La Sierrita, and El Peñon, and the Tampico-Misantla basin in the southeast with the El Mimbral outcrop (Weidie et al., 1972; Bitter, 1993; Perez Cruz, 1993). Today, these basins constitute the Gulf coastal plain and are characterized by km-thick sedimentary infill by Jurassic to Cretaceous carbonates, deep-water marls, shales, and Paleocene shallow-water or terrestrial sediments.

During the late Cretaceous to early Paleogene period, the Sabinas, La Popa, and Parras foreland basins were filled with coarse-grained sediments from the west, including volcaniclastics and shallow marine and deltaic terrigeneous siliciclastic of the Difunta Group (Weidie et al., 1972; Bitter, 1993). In contrast, fine-grained deep-water shales and marls of the Campanian-Maastrichtian Méndez and Danian Velasco Formation characterize the Burgos and Tampico-Misantla foreland basins. The maximum thickness (~1.6 km) of the Méndez Formation is present in the northern part of the Burgos basin, close to the Coahuila platform. A gradual decrease is observed from west to east and from north to south (e.g., Muir, 1936; Perez Cruz, 1993). Perez Cruz (1993) has shown that rapid thickness reduction of the Méndez Formation to the south in the area of the Sierra San Carlos indicates the existence of a shallower threshold ("Tamaulipas arch"), separating the Burgos and the Tampico-Misantla basin.

Thickness, marly-shaley nature, and deep-water environment of the Méndez Formation imply an increase in siliciclastic influx from the west, and eastward dipping of both basins during Campanian-Maastrichtian time (Perez Cruz, 1993). These characteristics suggest a synorogenic origin for the Méndez deposits associated with the foredeep of the Sierra Madre Oriental fold and thrust belt. The Danian Velasco Formation was deposited in shallow to deep marine environments and is dominated by slope-fan system tracts. These successions documents the eastward propagation of the coastline from the area west of Monterrey during the Late Cretaceous up to the present position resulting from the progressive fill by terrigeneous input and the rapid propagation (and uplift) of the Sierra Madre Oriental (diachronous from South to North, Echanove, 1986; Perez Cruz, 1993; Goldhammer and Johnson, 2001).

K-P transition: The following generalized lithology of the K-P succession in northeastern Mexico resulted from the detailed studies outlined below (see also Stinnesbeck et al., 1996; Schulte et al., 2003). The K-P transition in this area is characterized by the intermittent presence of a channelized or sheet-like spherule and sand-siltstone deposit, which overlies uniform Maastrichtian Méndez marls (named 'K-P sand-siltstone complex' in this paper). The channel levee complex in these channelized deposits is often dislocated relative to the central part of the channel ("thalweg"), with a vertical offset of several meters. Individual parts of the central channel may be displaced vertically against each other by up to 20 meters. Locally, slumped, 'brecciated', or lens-like spherule deposits are interbedded in the Méndez marls associated with the sand-siltstone deposit (as outlined below).

The K-P sand-siltstone deposit is characterized by three distinct units: (i) a cm-m thick basal spherule deposit (unit 1), partly with intercalated thin layers of quartzose to calcareous, or foraminiferal sandstone, (ii) the overlying unit 2 is 0.2-10 m thick structureless-massive or slightly laminated sandstone consisting of quartz, carbonate clasts, feldspar, and occasional foraminifera tests, which contains large marl clasts, plant debris, and rare spherules at the base, and (iii) the topmost unit 3 presents 0.1-1.5 m thick alternating silt-sandstones with similar composition as unit 2, but with abundant benthic and planktic foraminifera. Its top is orange-stained, rippled, and bioturbated by *Chondrites*, *Planolites*, and *Ophiomorpha*.

In most sections, there is an erosional surface atop of the sand-siltstone deposit, with no sediments preserved above, and only in few sections marls of the Paleocene Velasco Formation disconformably overlie unit 3, though no distinct ferruginous K-P boundary clay has been observed. Locally, the very base of the Velasco shale is made of a 2-10 cm thick orange-stained and indurated limestone devoid of microfossils, in addition, elevated PGE concentrations are present in this layer (0.3-0.9 ng/g Iridium), as well as in the topmost part of unit 3 (0.3-0.4 ng/g Iridium, cf. Smit et al., 1996; Lindenmaier et al., 1999). Besides the locations investigated for this study, comparable K-P sequences, though with variable thickness, petrological composition, and amount of bioturbation have been reported from some other K-P outcrop areas in northeastern Mexico, including Los Ramones, Loma Cerca, El Mulato, and La Lajilla (see Fig. 2.1 and Smit et al., 1992b; 1996; Stinnesbeck et al., 1993; 1996; Keller et al., 1994; 1997; Soria et al., 2001).

2.2 Analytical techniques

The following analytical techniques were used to characterize the sediments of the K-P transition in northeastern Mexico; for the geochemical and mineralogical analyses, samples were dried, crushed, and finely ground in an agate mill.

Biostratigraphy: Samples were prepared for planktic foraminiferal biostratigraphic analysis by using two size fractions (38-63 μm and >63 μm) after methods given by Pardo et al. (1996). Planktic

foraminifera from the La Sierrita area were analyzed by Gerta Keller, Princeton University.

Nonclay and clay mineralogy was analyzed by X-ray diffractometry (XRD) at the Geological In-

stitute of the University of Neuchâtel, Switzerland, with a SCINTAG XRD 2000 diffractometer and Cu-kα-radiation. Diffractograms were evaluated with the MacDIFF software (freeware by R. Petschick,
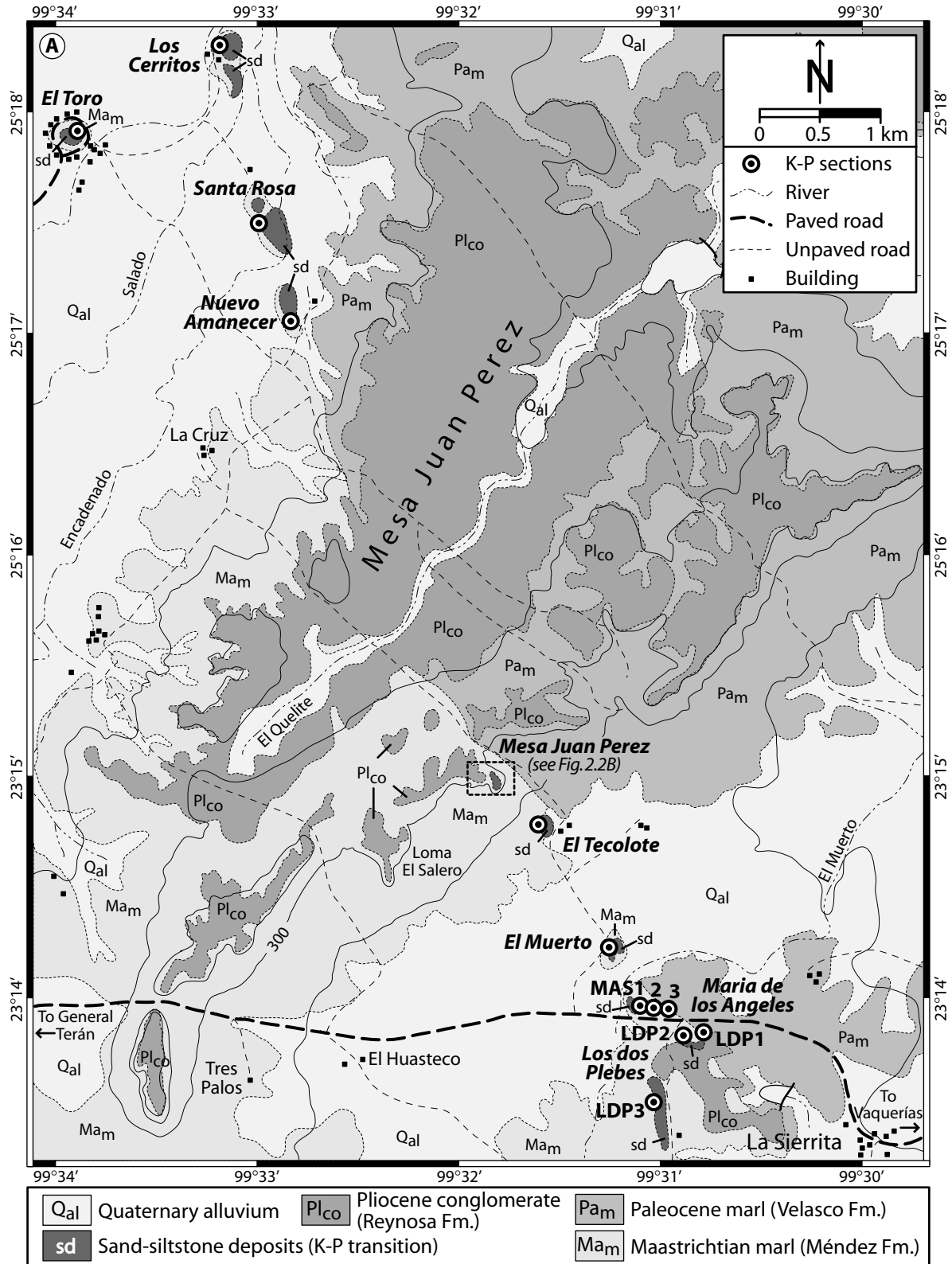
Figure 2.2A Geological map of the La Sierrita areawith locatiopns of K-P sections. It reveals the channel-like lateral persistence of the NNW/SSE-trending sand-siltstone complex, with exception of the El Toro section that is found about 0.5 km to the West of the main channel axis. General dip of the units is towards NEE (about 5-10°).

University of Frankfurt, details in Petschick et al., 1996) and methods outlined in Appendix 3.1. In order to ease comparison with non-weighted datasets, the raw-data, including peak position, height, and area, is given in the Appendix 2.1.

Major elements were determined by wavelength-dispersive X-ray fluorescence spectrometry (WDS) at the Institute for Mineralogy and Geochemistry, University of Karlsruhe, with a SRS 303 AS XRF. For these analyses, fused glass discs were prepared from a mixture of 1 g ignited powder of each sample and 4 g of SPECTROMELT. Major elements were evaluated by a fundamental parameter calibration procedure.

Trace elements (Cr, Ni, Cu, Zn, As, Rb, Sr, Y, Zr, Ba, La, Ce, and Pb) were analyzed from bulk powder samples (5 g) by energy-dispersive X-ray fluorescence spectrometry (EDS) with a SPECTRACE 5000 X-ray analyzer at the Institute for Mineralogy and Geochemistry, University of Karlsruhe. Trace elements were determined using a Compton and intensity matrix correction procedure. Detailed analytical procedures, detection limits, and standards used were compiled by Kramar (1997).

Electron microprobe: Wavelength-dispersive (WDS) and energy-dispersive (EDS) electron microprobe analyses, as well as back-scattered electron (BSE) images were performed with a CAMECA SX50 microprobe on polished, carbon-coated thin

sections at the Laboratory for Electron Microscopy, University of Karlsruhe. Detailed sample preparation techniques and analytical methods are summarized in Reed (1996). The SX50 microprobe is equipped with four crystal spectrometers, an EDS system and an electron backscatter detector. Quantitative (WDS) microprobe analyses were carried out using the crystals TAP (Si, Al), PET (Ti, Ca, K, P), RAP (Mg, Na) and LiF (Fe, Mn). All quantitative major element analyses were calibrated with the following standards: Fe: Fe_2O_3; Si: Wollastonite; Mg: MgO; K: Orthoclase; Ca, Al: Anorthite; Ti: $MnTiO_3$; Na: Albite; Ni: NiO. Accelerating voltage was set to 15-20 kV with a primary beam of 15 nA and counting times of 20-40 seconds were used per element. Detection limits are in the range between 0.5 and 1 wt‰. Oxide percentages were calculated using the ZAF correction program and natural silicate and oxide standards.

Cathodoluminiscence: Polished thin sections were examined on a CITL CCL 8200mk3 cold cathodoluminoscope in the Geological Institute at the University of Heidelberg, which operates at a vacuum voltage of 20 kV and with a beam current of 380 μA. The resulting cathode luminescence was documented with a LEICA camera on regular 100 ASA KODAK slide film.

Volume magnetic susceptibilities (κ) from various ejecta deposits and enclosing sedimentary rocks
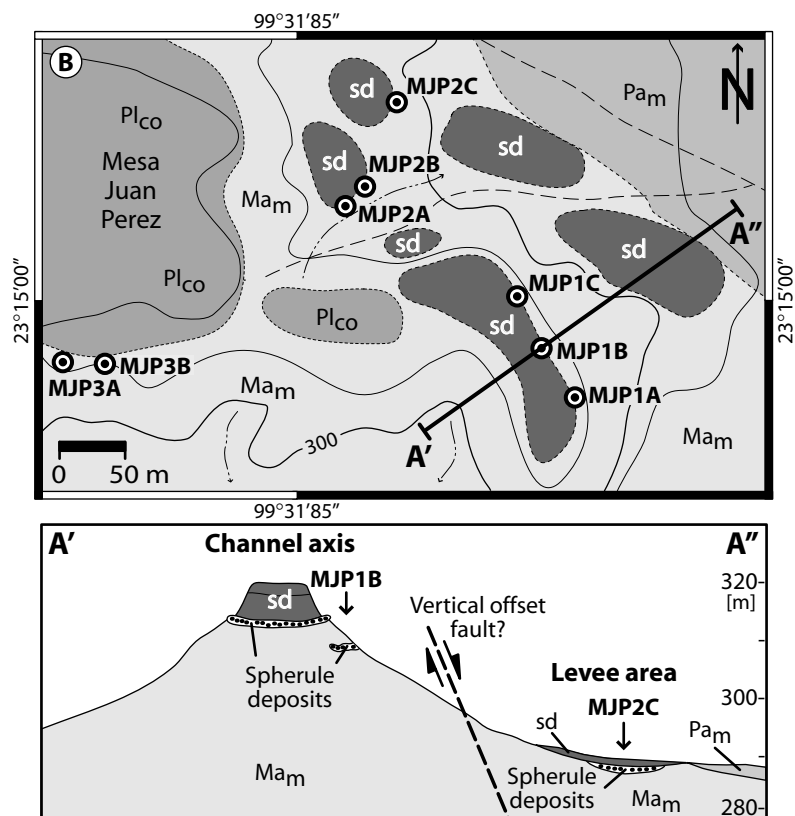
Figure 2.2B Close-up of the Mesa Juan Perez area (upper illustration) and the crosscut (A'-A'' below), revealing the spatial and stratigraphic relationships of spherule- and sand-siltstone deposits. Note lateral discontinuity of spherule deposits within Méndez marls and vertical offset of spherule-sandstone deposits by postsedimentary faulting. A legend is provided in Fig. 2A.
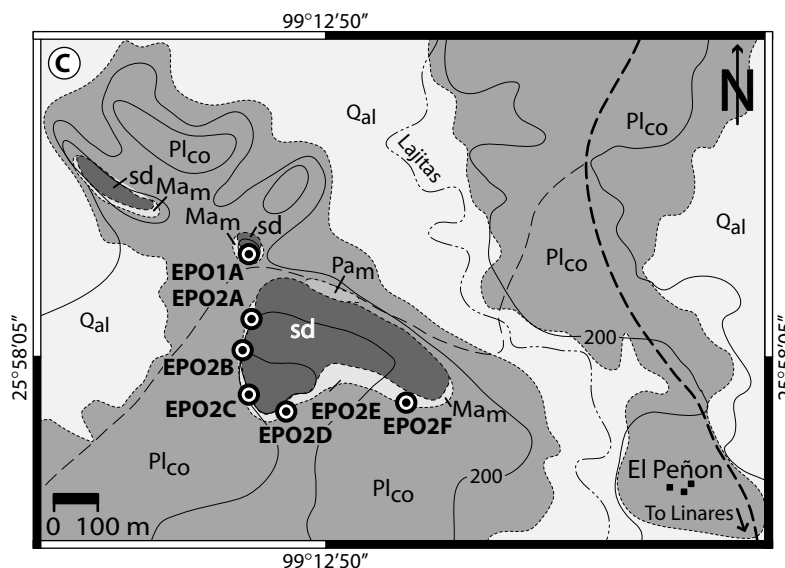
Figure 2.2C Geological map of the El Peñon area with locatiopns of K-P sections. General dip of the units is towards NEE (about 5-10°). A legend is provided in Fig. 2A.

(marls, sandstones) were determined in low fields (300 A/m, 1200 Hz) with a Kappabridge KLY-3 (AGICO). About 3-4 aliquots with 7 g bulk powder of every sample were measured.

Temperature dependent susceptibility (κ-T curve) was measured over the temperature range of –192 to 700 °C in an argon atmosphere (110 ml/min) to avoid oxidation during heating using the KLY-2 Kappabridge (AGICO), fitted with the CS-2/CS-L furnace apparatus (Hrouda, 1994). The sensitivity of this Kappabridge is given with 4×10^{-8} (in SI units) using a standard pickup unit for 10 cm^3 nominal volume (KLY-2.1). During the cooling run from –192 to 0 °C, and the subsequent heating/cooling cycles from room temperature to 700 °C (heating rate 10 °/min) temperatures and susceptibilities were recorded. The raw data were corrected for the empty furnaces and normalized to the susceptibility magnitude at zero °C (low-temperature) and room temperature (high-temperature).

Remanent magnetization measurements were made with a JR5A spinner magnetometer (AGICO). The vectorial composition and stability have been analyzed by detailed stepwise alternating field (AF) demagnetization at room temperature and by isothermal remanent magnetization (IRM). Ten steps (2.5, 5, 7.5, 10, 25, 50, 75, 100 mT) until peak fields of 160 mT were used for alternating-filed demagnetization. The acquisition of isothermal remanent magnetization was performed in fields up to 1000 mT.

2.3 Results

2.3.1 Stratigraphy and lithology

The lithological and sedimentological characteristics of the four outcrop areas investigated for this study are provided in the following section. Additional comprehensive outlines of the geology at the specific localities, are given in Bohor (1996), Keller et al. (1994; 1997; 2002), Smit et al. (1992b; 1996), Soria et al. (2001), and Stinnesbeck et al. (1993; 1996; 2001).

Rancho Nuevo

The Rancho Nuevo (RNO) outcrop (locality in Fig. 2.1) exposes about 20 m of Méndez marls. Two 'U'-shaped channelized spherule-sandstone depos-

Figure 2.3 (page 23) Photos of sections in northeastern Mexico; hammer as scale (30 cm). (**A**) Rancho Nuevo outcrop with the massive sandstones of unit 2 and 3. Note the weathered (white) spherule-rich deposit (SRD) at the base of the sandstone. (**B**) Deeply incised sand-siltstone deposit at Rancho Nuevo. The boundary of the channelized sandstone is marked by arrows. (**C**) Flow and dewatering structures marked by arrows at the base of the sand-siltstone deposit at Rancho Nuevo. Flow direction of 'escaping' water is from the base to the top. (**D**) Strongly inclined indurated calcareous spherule-rich layer (unit 1) at the base of the sand-siltstone deposit in the Mesa Juan Perez 1A section. Spherule-layer is under- and overlain by 20-40 cm thick marl-spherule breccia. (**E**) El Peñon outcrop 2A. The top of hammer marks position of the sandy limestone layer (SLL), and its black handle marks the upper part pf the greenish spherule bed (unit 1). (**F**) Spherule deposit (unit 1) in El Mimbral at meter-mark 6 Note through-like wavy upper surface of the Méndez marls and presence of thin bentonite layer (BL) below the laminated spherule bed. (**G**) 'Tepee-like' structures (arrow) of the sandy limestone layer ("SLL") at El Mimbral (meter mark 48). (**H**) Graded and laminated spherule deposit at El Mimbral. Note coarse, cm-sized ejecta clasts at the base grading into finer sand-sized ejecta.
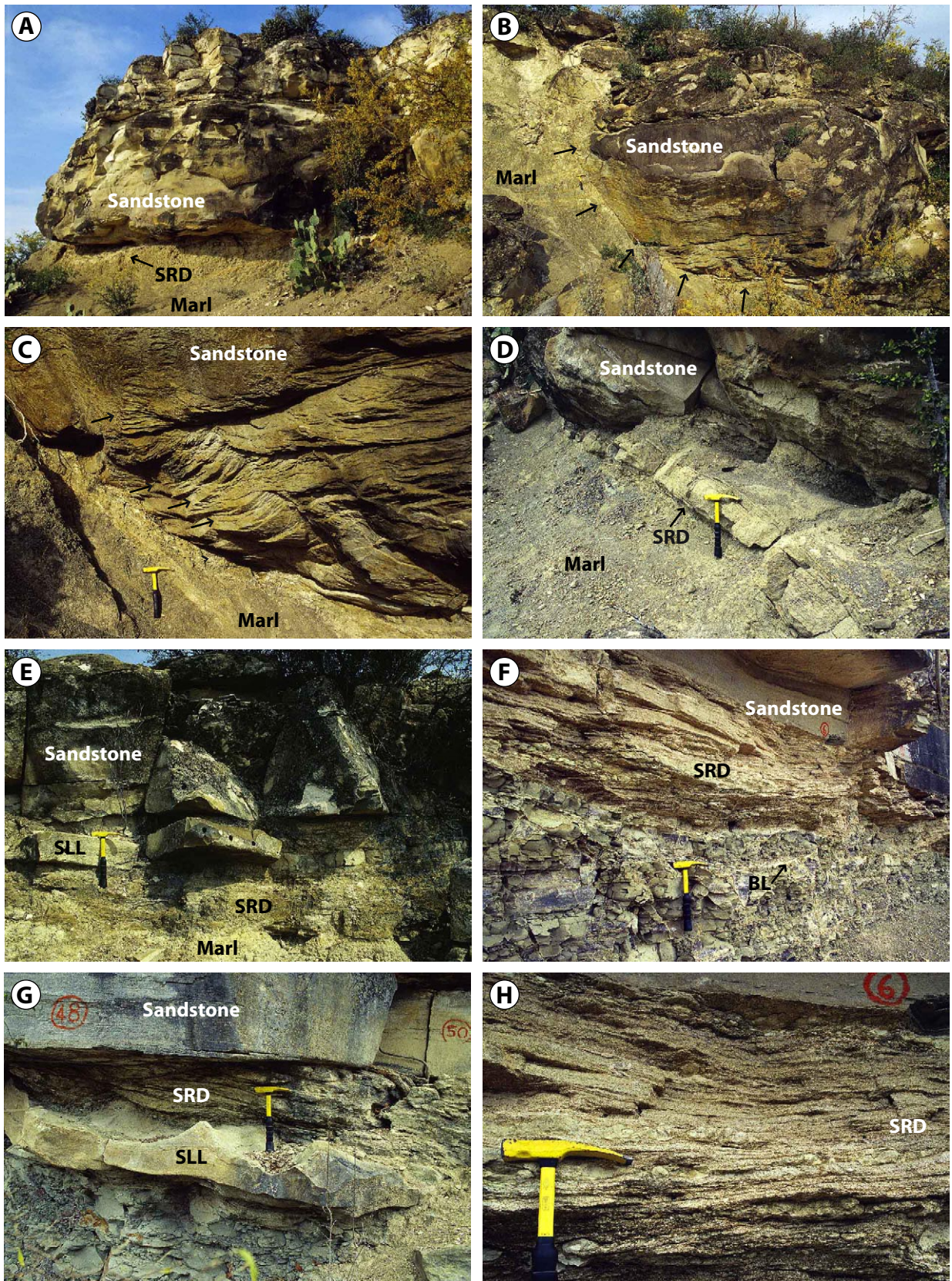
Figure 2.3 (caption on page 22).

its are deeply incised into these marls, each about 50-80 m in horizontal, and about 3-8 m in vertical extent (Figs. 2.3A-C, 2.6). The direction of the channel axis is about 320° and the channels have a strike/dip of about 60°/10° to 80°/15°. Both channels expose an analogous succession of strata that are exemplary depicted in Fig. 2.6; the measured section corresponds to the central part of the eastern, lower-lying channel.

The base of the channel fills is characterized by the intermittent presence of a 5-25 cm thick marly coarse-grained spherule deposit (unit 1). Unit 1 often includes large Méndez marl clasts and is locally disturbed by diapir-like protrusions of Méndez marls. No spherule deposits have been found within Méndez marls on the exposed slope. The spherule deposit is disconformably overlain by the up to 6 m thick massive to laminated fine-grained sandstone of unit 2. The sandstone shows prominent dewatering structures at its edges, and distinct flute casts indicate a current direction from NW or NNW. Unit 2 has quartz, limestone clasts, feldspar, and occasional foraminifera. The topmost part of unit 2 is rippled and may be assigned to unit 3. However, the top of the sand-siltstone complex is an erosive surface, without overlying sediments.

La Sierrita area

The **Mesa Juan Perez sections** (MJP) **1A-C** and **2A**, **B** are located along the eastern flank of a prominent southward protrusion of the Mesa Juan Perez, 300 m northwest of the Rancho El Tecolote (Fig. 2.2B). The Mesa Juan Perez section 1A comprises a 30 cm thick lens-like and marl clast-rich spherule deposit, embedded in Méndez marls, about three meters below the sand-siltstone complex (Figs. 2.3D, 2.7A). The contact to the under- and overlying Méndez marls is gradational, and the lens-like spherule deposit is traceable over one meter laterally. In contrast, the spherule deposit at the base of the sand-siltstone complex can be traced about ten meters laterally and has a 20-30 cm thick indurated spherule layer that shows boudinage, and pinches out to the north-

west. It is under- and overlain by 20-40 cm of marl-spherule mixtures with many flattened marl clasts (Figs. 2.4A, 2.7A). This 'marl clast-spherule breccia' has sharp contacts to the indurated spherule horizon and the overlying sandstone of unit 2, as well as a gradational contact to the underlying Méndez marls.

The Mesa Juan Perez section 1B and 1C each contain a single, well-indurated 20-30 cm thick, lens-like spherule deposit that is traceable over several meters (Fig. 2.7A). Up to 2-3 m of Méndez marls, separate this spherule deposits from the spherule layer at the base of the sand-siltstone complex (unit 1). The lower, discontinuous spherule deposit is contorted, without marl clasts, has sharp upper and lower contacts to the Méndez marls, and constitutes an overturned fold in the Mesa Juan Perez 1C section. This fold is inclined to the W, with the direction of the fold axis at 140-160°. Their core contains spherules and large rounded marl clasts. The upper (unit 1) spherule layer is 20-30 cm thick, weathered with a friable matrix and contains a cm-thick sandy limestone. The lower contact with the Méndez marls is gradational, and the upper contact with the overlying sandstone (unit 2) is sharp.

The **Mesa Juan Perez sections 2A** and **2B** contain scattered, 10-40 cm thick, breccia-like marly spherule deposits, rich in rounded to angular marl clasts interbedded within Méndez marls (Fig. 2.4G, H) and one 20 cm thick, quartz-rich, and weathered spherule deposit at the base of the sand-siltstone complex (unit 1) (Fig. 2.7A). The former have usually gradational transitions with the Méndez marls, whereas the latter has a sharp contact to the overlying sandstone (unit 2). These scattered 'sedimentary breccias' extend over 2-8 m vertically. Thickness and sedimentological features of the sand-siltstone units 2 and 3 are variable with respect to the relative position in the channel system; details are depicted in Fig. 2.7A.

The **Mesa Juan Perez sections 3A** and **3B** are located on a ridge-like southward projection of the Mesa Juan Perez, about 200 m from the main out-

Figure 2.4 (page 25) Photos of sections in northeastern Mexico; hammer as scale (30 cm). (**A**) Close-up from unit 1 at the Mesa Juan Perez 1A section in Fig. 2.3D showing alternating layers of weathered marl and spherule layers under- and overlying the indurated calcareous spherule layer. (**B**) Close-up of the laminated spherule layers at El Mimbral in Fig. 2.3.H showing alternating white layers of carbonaceous and green spherule-rich ejecta. (**C**) Spherule layer embedded within slope-debris at the El Peñon section 2D. (**D**) 'Breccia-like' Méndez marl with intermixed spherule deposits in the Mesa Juan Perez 3B section. (**E**) Recumbent folded spherule deposit with large marl clasts in the core of the fold in the Mesa Juan Perez 3A section. The axis of the slump fold has a northeastern trend and the fold is open towards southeast. (**F**) Indurated carbonaceous core of the fold depicted in (E), illustrating the armored marl clasts and the marl-clast-spherule breccia. (**G**) and (**H**) Squeezing and mixing of spherule deposits with Méndez marl at the Mesa Juan Perez 2A section, interpreted as slump-slide or liquefaction structures.
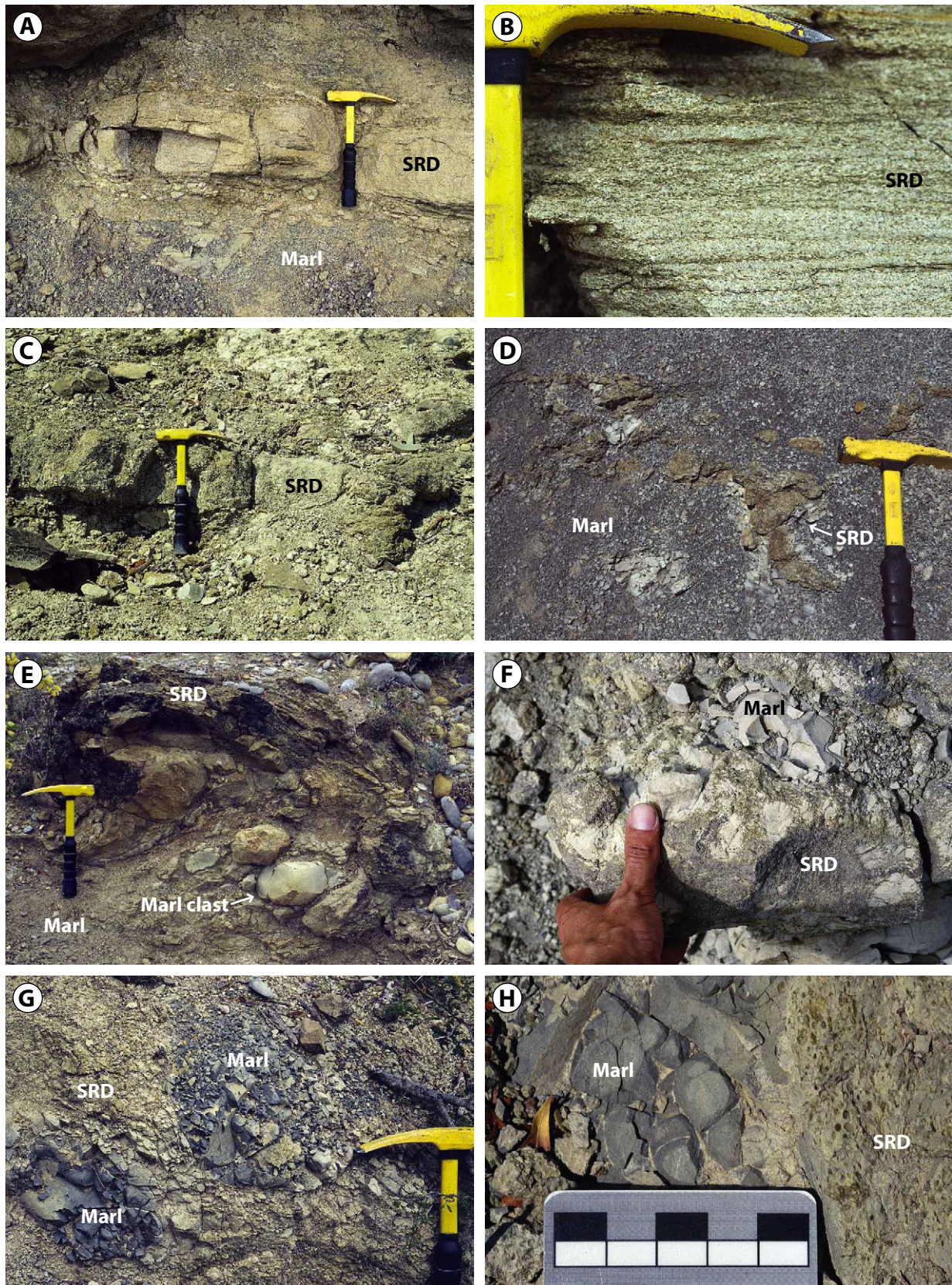
Figure 2.4 (caption on page 24).

Sandstone	Foraminifera-sandstone	Siltstone	Limestone	Conglomerate
Spherules	Marl	Shale-Claystone	Marl clasts	Plant remains
Lamination	Ripples	Grading	Bioturbation	Tractability of units

MF = Microfacies-type of spherule deposit   **U** = Unit of siliciclastic deposit   **SLL** = Sandy limestone layer
CF1 = *P. hantkeninoides* Zone   **CF2** = *P. palpebra* Zone   **P1a** = *P. eugubina* Zone

Figure 2.5 Explanation for lithologic symbols and abbreviations used in the stratigraphic columns.

crop axis (Fig. 2.2A, B). A 20-30 cm thick spherule deposit is present in the Mesa Juan Perez section 3A in a prominent 60 cm thick fold within the Méndez marl (Figs. 2.4E-F, 2.7A). The fold is inclined to the SSE and the fold axis has a direction of about 80-90°. The core of the fold contains large rounded marl clasts, in part armored with spherules, and an indurated calcareous spherule layer with sharp upper and lower contacts. This spherule layer is exposed laterally over about 10 m. Isolated spherule-rich lenses are present in the marls below the fold. From this fold and along the steep slope, the spherule layers

grade laterally in irregular spherule-rich domains floating in a reconstituted marl matrix. These spherule-marl breccias can be traced towards the east up to the Mesa Juan Perez 3B section, where they are patchily distributed along the slope over 4-8 m in vertical and 10 m in horizontal direction (Fig. 2.4D). Conglomerates of the Paleocene Reynosa Formation disconformably overlie the Méndez marls in both sections (Figs. 2.2, 2.4E, 2.7A).

The **Maria de los Angeles section** (MAS) **1** is located on the southeastern flank of the hill, 400 m southeast of the Rancho El Tecolote (Fig. 2.2A). An
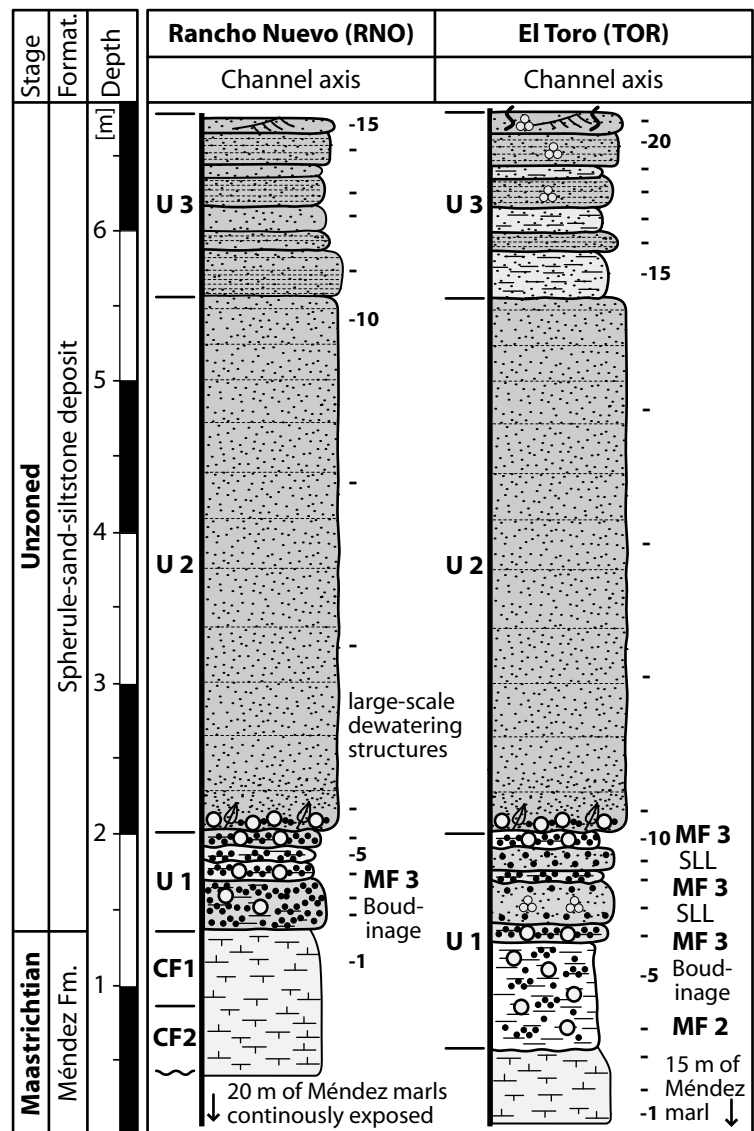
Figure 2.6 Lithology and stratigraphy of the Rancho Nuevo and El Toro section. Biostratigraphic assignation for the Rancho Nuevo section is from López-Oliva and Keller (1996) and Keller et al. (1997). A key to the lithologic symbols is provided in Fig. 2.5.

indurated, 20-30 cm-thick folded spherule deposit is present at the slope, extending about 2 m laterally (Fig. 2.7B). Three meters of Méndez marls separates this spherule layer from the spherule layer at the base of the sand-siltstone complex (unit 1). The lower spherule deposit is devoid of marl clasts, has sharp upper and lower contacts to the Méndez marls, and constitutes an overturned fold inclined to SSE, with the direction of the fold-axis about 70-90°. The core of the fold contains spherules and rounded marl clasts that are armored by spherules. The unit 1-spherule layer is 20-30 cm thick and indurated or, locally, weathered. The lower contact with the Méndez marls is gradational, whereas the upper contact with the overlying sandstone (unit 2) is sharp. The lithology of the spherule deposits and the sandstone units of the Maria de los Angeles 2 and 3 section is shown in Fig. 2.7B.

At the **El Toro**, **Los Cerritos**, **Santa Rosa**, **Nuevo Amanacer**, **El Tecolote**, **El Muerto**, and **Los dos Plebes** (LDP) outcrops (see Fig. 2.2A), a spherule layer (unit 1) is present at the base of a 1 to 8 m-thick sand-siltstone deposit (El Toro and Los dos Plebes are exemplarily shown in Figs. 2.6, 2.7B). Unit 1 varies in thickness, composition, and degree of weathering. It is between 20-60 cm thick and has alternating friable to indurated layers rich in either spherules, fragments, carbonate clasts, and sand, or spherule-marl mixtures, besides the presence of large round or flattened marl clasts (>25 cm in diameter). These marl clasts locally accumulate as 'marl clast breccias'. Occasionally, sandy limestone layers ("SLL" of Stinnesbeck et al., 1993) are interbedded. The indurated spherule- and sand-layers are structureless or slightly laminated, and not bioturbated. They often show boudinage and are tilted in an upward direction. The transition to the underlying Méndez marl is gradational in most sections, whereas, locally, the base of unit 1 is a sharp, scoured surface atop of the Méndez marls. The upper contact with the overlying sandstone (unit 2 or 3) is abrupt and at the base of this sandstone, horizons of interbedded spherules, plant fragments, and large marl clasts occur, aside from flute casts that show a current from the northwest during deposition. This current direction is confirmed by the common presence of NW-SE trending gutter casts.

The thickness and lithology of the units 2 and 3 in these sections are highly variable and depend primarily on the position of the outcrop relative to the channel axis. Unit 2 is generally massive quartz-feldspar-carbonate-rich sandstone with lamination in its upper part, whereas unit 3 consists of alternating layers of sand-siltstone with either lamination or current ripples, as well as bioturbation in its upper part. These sand-siltstone layers are rich in quartz and carbonate clasts, albeit often the topmost part is foraminifera sandstone, made of abundant tests of planktic and (rare) benthic foraminifera.

El Peñon area

The El Peñon section (EPO) 1A is located about hundred meters in front of the main El Peñon outcrop area, at the top of a small hill some ten meters to the north of the dirt road (Fig. 2.2C). The slope of this hill consists of about 8-10 m of debris-covered Méndez marls. At its topmost part, a 10-60 cm thick spherule deposit, partly covered by, or admixed with, Méndez marls, is intermittently exposed in the southeastern sector (Fig. 2.8). This spherule deposit is overlain by weathered, 2-3 m thick massive to laminated sand-siltstones (unit 2). The strike and dip of this sandstone complex are in the range between 0°/10° and 15°/25°.

The main outcrop (El Peñon section 2A) is found at the abandoned quarry (Fig. 2.2C) and has a ~7 m thick clastic deposit that constitutes the top of the low-lying hill (Fig. 2.3E). It dips about 5-10° to the northeast and shows a strike of 10-20°. The spherule layer (unit 1) at the main outcrop area is 10-60 cm thick and overlies about 1 m of Méndez marls with an undulatory surface to the underlying Méndez marls, and small-scale soft-sediment deformation features (Fig. 2.8). A white, friable cm-thick chalky layer marks the contact between the marls and the spherule deposit surface. Within the slightly graded, but otherwise massive spherule deposit, a prominent 10-20 cm thick sandy limestone layer (SLL) is intermittently present showing boudinage and "tepee-like" structures. This sandy limestone has quartz, limestone clasts, feldspar, and occasional spherules. The SLL eventually disappears about 25 m to the West from the main outcrop (El Peñon 2B).

The spherule deposit is disconformably overlain by the massive, fine-grained sandstone of unit 2, which includes large marl clasts (>10 cm in diameter) and spherules at their base, as well as flutecasts that indicate a current direction from the northwest. The sandstone has quartz, limestone clasts, and feldspar; occasionally plant remains are present in the basal part. Some 0.5 to 1.5 cm thick J-shaped and spherule-filled burrows are present at the base of unit 2 (see Ekdale and Stinnesbeck, 1998), though no evidence for widespread colonization of the unit 2-sands is

present. Unit 2 is conformably overlain by the alternating laminated sand-siltstones of unit 3. The topmost part of unit 3 shows ripples and is bioturbated by multiple horizons of *Thalassinoides*, *Planolites*, *Chondrites*, and rare *Zoophycos*. The rippled and bioturbated beds of unit 3 in the northern part of the outcrop, close to the dirt road, are disconformably overlain by the marls-shales of the Velasco Formation; though no distinct 'red boundary clay' has been observed (Fig. 2.2C).

The gently inclined, and debris covered slopes in the western part of the El Peñon 2 outcrop area consisted of weathered Méndez marls intermixed with occasional sandstone clasts and spherule deposits. The sand-siltstone complex is here found about 6-10 m above the dirt path, suggesting the presence of syn- or postsedimentary faults at the transition of the channel axis to the channel margin-levee complex.

Along the slope, about 10-20 cm thick, lens-like spherule deposits are irregularly exposed for a few centimeters to several meters. They show structures indicative of soft-sediment deformation (contortion and folding). These lens-like spherule deposits are hardly traceable for more than a few meters, and it is difficult to judge weather they are actual in place or not; in addition, strike-dip measurement on these irregular lenses showed widely varying directions, not consistent with the directions found for the sand-siltstone deposit. Several short sections have been documented, though (see Figs. 2.2C, 2.8): (i) section El Peñon 2C with a folded, highly weathered spherule deposit, (ii) El Peñon 2D, which included one 10-20 cm indurated spherule deposit (Fig. 2.4C), (iii) El Peñon 2E with two indurated spherule deposits that are intermittently found on the debris-covered slope, with both layers separated by about 1.5 m, and (iv) El Peñon 2F which includes an indurated spherule deposit at the base of a 30 cm thick, horizontally lying laminated sandstone, though it is difficult to judge if both are indeed in place. The sand-siltstone complex is consistently exposed about three to four meters above these spherule-bearing sections. However, debris and shrubs extensively cover the sand-siltstones. Particularly, the basal part of the sand-siltstones is not exposed, including the unit 1 spherule deposit and the transition to the Méndez marls below. Therefore, the relationship with the lower-lying spherule and the general stratal architecture of these, apparently not allochthonous, spherule deposits are not comprehensible (Fig. 2.8).

El Mimbral

The El Mimbral (ELM) outcrop extends for about 200 m along the stream bank and is marked with red meter marks that ease orientation (see Stinnesbeck et al., 1993, Fig. 1). It exposes a steep slope having 5-10 meters of dark grey and uniform Méndez marls with occasional cm-thick light grey bentonite layers (Fig. 2.3F). The marls have a strike and dip between 260°/5° and 280°/10°. They are disconformably overlain by the spherule deposits of unit 1 that constitute three, broadly incised channel-like structures with pinch and swell structures; each channel is about 15-20 m wide and about 10-100 cm thick. The thickness of the spherule deposits roughly equals the depth of scouring; in addition, the channel-like structures may be accentuated by loading. The uppermost meter of the Méndez marls is locally affected by soft-sediment deformation and thrusting, leading to oversteepened and overturned channel margins, for instance at meter mark 38, where the spherule deposit is deformed to an overturned slump fold, vergent to northeast that includes large Méndez marl clasts in its core. Adjacent to this slump fold, a 4 m wide diapir-like protrusion of the Méndez marls has been observed. To account for the differences in lithology of each part of the outcrop, two sections were documented and sampled: One section at meter mark 26 in the central part of the eastern, higher channel (El Mimbral 1) and another at meter mark 44, in the central part of the western, lower channel (El Mimbral 2); their lithology is depicted in Fig. 2.9.

The spherule deposit is general of massive appearance, but occasionally shows normal grading with extraordinary coarse spherules at the base (meter mark 44), and contains many, generally deformed, large marl clasts. A slight low-angle or horizontal lamination with lighter calcite-rich layers and darker spherule-rich layers is developed in the upper part of unit 1 (Figs. 2.3H, 2.4B). Within the spherule deposit, a 10-20 cm thick sandy limestone layer (SLL) is intermittently intercalated, showing charac-

---

Figure 2.7A (page 29) Lithology and stratigraphy of sections with spherule deposits in the La Sierrita area: Mesa Juan Perez. A key to the lithologic symbols is provided in Fig. 2.5. Sections studied for biostratigraphy (by Gerta Keller, Princeton), are marked with an asterisk. Note the lithologic variability and lateral discontinuity of spherule deposits embedded in marls of the late Maastrichtian. The large J-shaped burrow in the MJP1B section is interpreted as an escape-burrow (Bromley, 1996).

Figure 2.7A (caption on page 28).
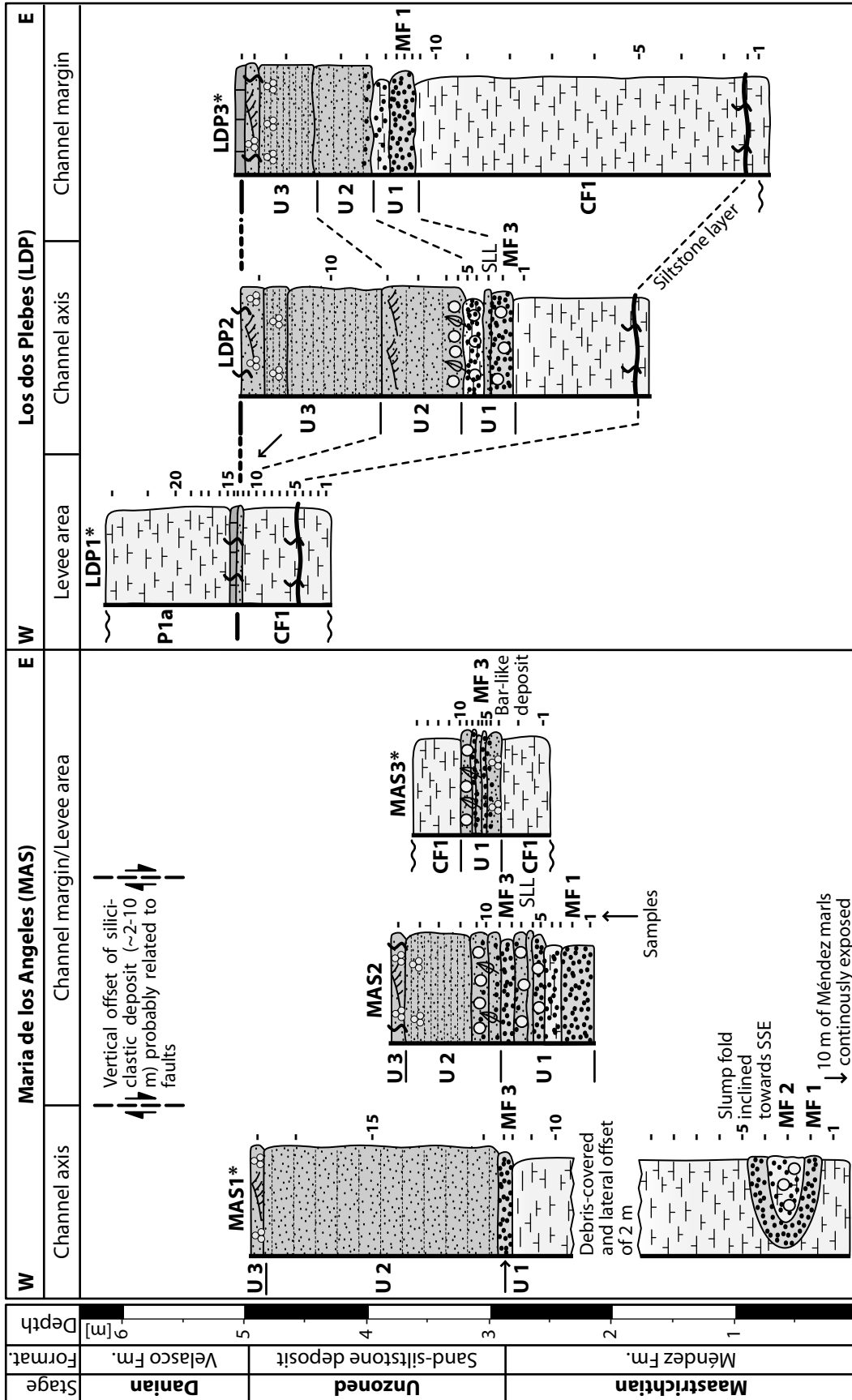
Figure 2.7B Lithology and stratigraphy of sections with spherule deposits in the La Sierrita area: Maria de los Angeles and Los dos Plebes. A key to the lithologic symbols is provided in Fig. 2.5. Sections studied for biostratigraphy (by Gerta Keller, Princeton) are marked with an asterisk. Note the lithologic variability and lateral discontinuity of spherule deposits embedded in marls of the late Maastrichtian.
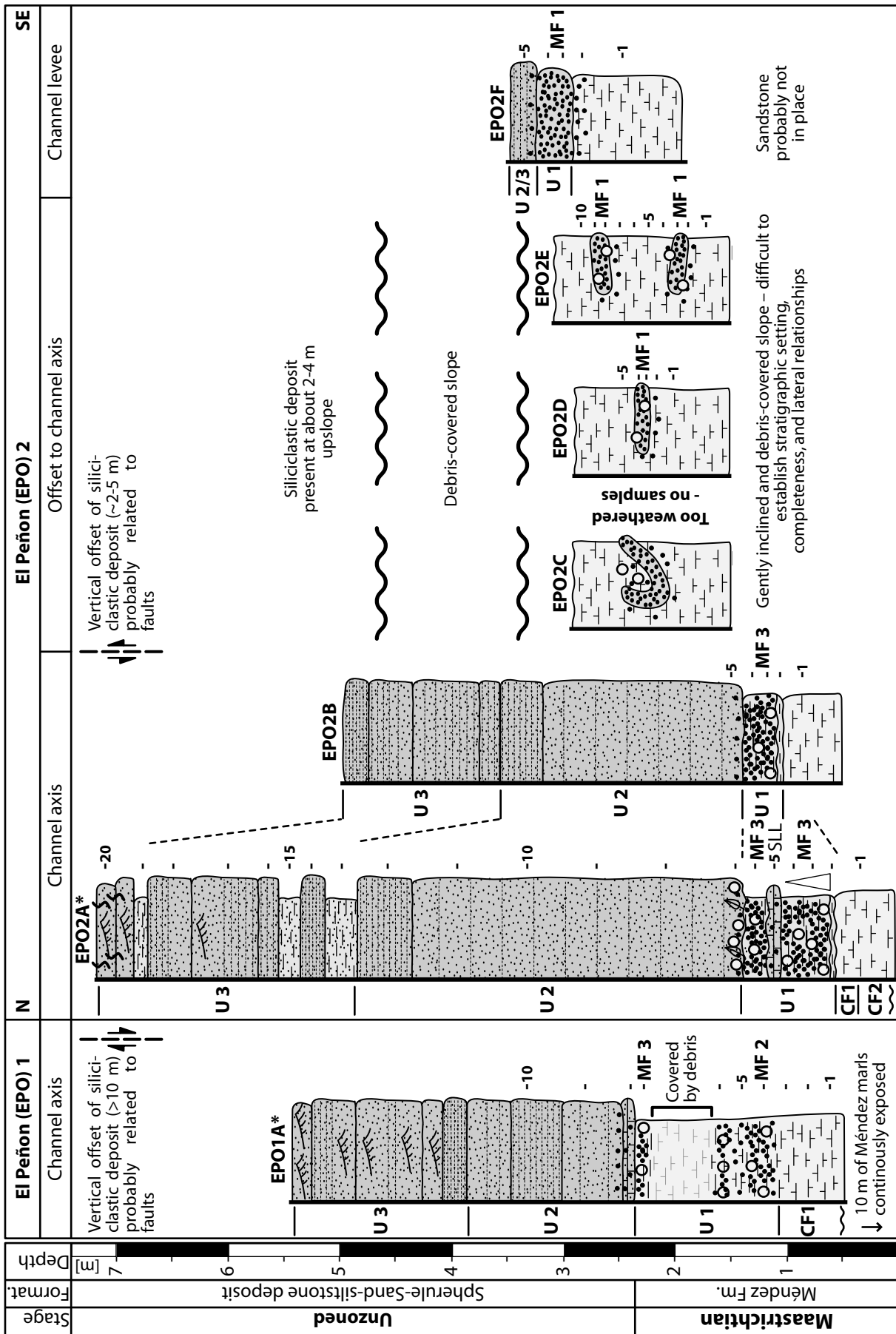
Figure 2.8 Lithology and stratigraphy of sections with spherule deposits in the El Peñon area. A key to the lithologic symbols is provided in Fig. 2.5. Biostratigraphic assignation of sections marked with an asterisk is from López-Oliva and Keller (1996) and Keller et al. (1997).
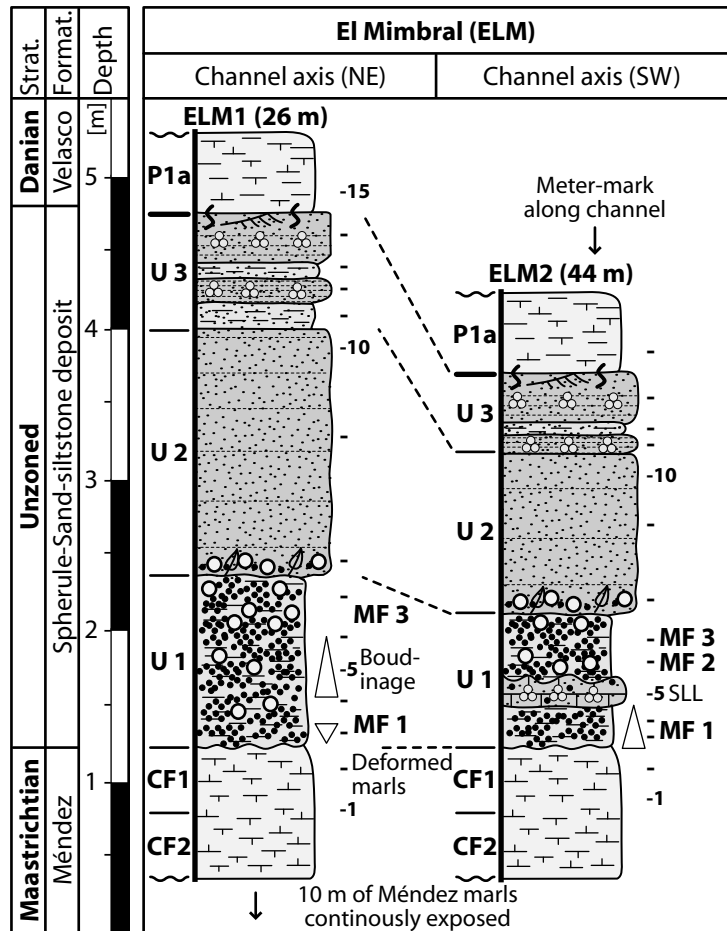
Figure 2.9 Lithology and stratigraphy of the El Mimbral sections with spherule deposits. A key to the lithologic symbols is provided in Fig. 2.5. Biostratigraphic assignation is from Keller et al. (1994; 1997) and López-Oliva and Keller (1996).

teristic boundinage structures and a 'tepee-like' upper surface (Fig. 2.3G). The "SLL" is foraminiferal packstone with rare terrigeneous detritus.

The basal unit 1 is disconformably overlain by the well indurated, massive and, in its upper part, laminated fine-grained sandstone of unit 2. Unit 2 is made of quartz, carbonate, and minor feldspar. In some laminae, foraminifers dominate the sand-fraction; other laminae are rich in quartz and feldspar. Minor amounts of biotite crystals and charcoal fragments occur as well. Unit 2 has an erosional base that cuts into the spherule deposits, and locally, even into the underlying Méndez marls. However, in contrast to the channel-like geometry of the spherule deposit, unit 2 has a more sheet-like character, since

it spans almost along the whole outcrop area with a thickness between 1-2 m. It finally pinches out at meter mark 60. Its base is decorated with groove casts, flute casts, abundant large pieces of plant debris, and spherules, and it includes round marl clasts of 5-40 cm in diameter. Remarkably, lamination and deformation within this unit are convoluted around upward protrusions of the underlying unit 1. The sand-silt-shale layers of unit 3 conformably overlie unit 2 across most of the outcrop area. Unit 3 has sand- to silt-sized quartz, carbonate, and feldspar. In some laminae, foraminifers dominate the sand-fraction. Unit 3 is made of horizontally laminated basal sandstone and a thinning and fining-upward sequence of multiple sand-silt layers with current

Figure 2.10 (page 33) Thin section microphotographs of spherule deposits in northeastern Mexico (plane polarized light). (**A**) "Grainstone"-like microfacies-type 1 from La Sierrita with spherules, (ejecta-) fragments, and carbonate clasts within microspar. The matrix-supported texture suggests that some carbonate had to be part of the original deposit. Note the random orientation of grains and presence of ejecta-fragments with characteristic internal flow-patterns (Sample MJP1B-3). (**B**) "Dense" variety of microfacies-type 1 with less spherules than in (A), but with more (ejecta-) fragments and enclosed limestone and accretionary lapilli grains. Note the particular "cauliflower"-shaped blocky calcite around fragments (MAS1-2). (**C**) Microfacies-type 3 with spherules, fragments, carbonate, clasts, and minor terrigeneous debris (e.g., quartz, feldspar), revealing bimodal grain-size distribution and slight preferred dimensional orientation of grains. Note presence of delicate-shaped spherules and fragments (MJP1A-14). (**D**) Microfacies-type 1 from El Mimbral with abundant spherules, limestone clasts, and blocky carbonate. Note translucent ribbon-like ejecta-fragments enclosing spherules, the near absence of terrigenous detritus, and the presence of composite spherules with Si-Al-K-rich glassy cores and outer dark chlorite shell (ELM1-5).
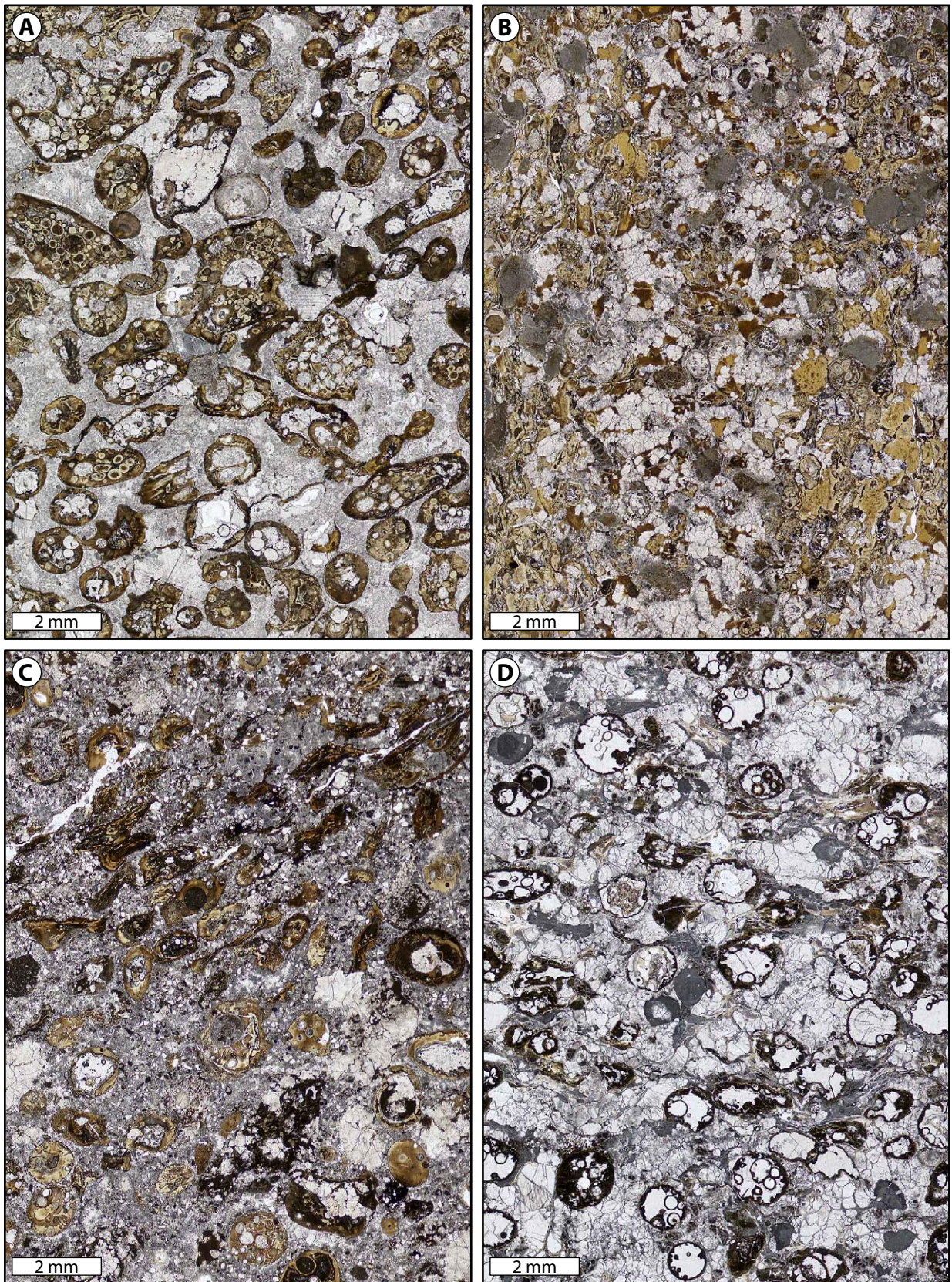
Figure 2.10 (caption on page 32).

ripples in its upper part. The uppermost 5-10 cm of unit 3 are bioturbated by *Thalassinoides*, *Planolites*, and *Chondrites* burrows and red-stained by iron oxides. The Paleocene marls of the Velasco Formation overlie the rippled beds.

2.3.2 Biostratigraphy and paleowater depth

Late Maastrichtian Méndez marl: Biostratigraphic analysis of the topmost 1-5 m of the Méndez marls in several sections of the La Sierrita area (marked with an asterisk in Fig. 2.7) revealed the sporadic presence of *Plummerita hantkeninoides* (Zone CF1). According to Pardo et al. (1996) and the magnetostratigraphic calibration by Cande and Kent (1995), this indicates deposition of these Méndez marls during the last 200-300 ka of the Maastrichtian.

For the sections at Rancho Nuevo, El Peñon, and El Mimbral, no biostratigraphic analysis was conducted for this study, since these outcrops are well-dated by biostratigraphic studies, including planktic foraminifera (Keller et al., 1994; 1997; Longoria and Gamper, 1995; López-Oliva and Keller, 1996; Soria et al., 2001) and calcareous nannofossils (Pospichal, 1996); the biozonation of these sections is shown in the Figs. 2.6, 2.8, and 2.9. These studies suggested that the 10-40 cm thick marls of the Méndez formation below the sand-siltstone deposit at Rancho Nuevo, El Peñon, and El Mimbral are of latest Maastrichtian age and commonly belong to the planktic foraminifera *P. hantkeninoides* Zone CF1. The presence of the calcareous nannofossil *Micula murus* (Zone CC26) and the occasional presence of *Micula prinsii* (Zone CC26b) in the uppermost meters of the Méndez marls corroborated this age assignation (Pospichal, 1996). However, the first appearance of the index marker for the latest Maastrichtian (*P. hantkeninoides*) below the sand-siltstone deposit is highly variable and is observed intermittently within 0.2 to 11 m below the base of the spherule-sand-siltstone deposit, suggesting the presence of a variable hiatus and/or local variations in the sedimentation rate. In addition, lateral movements of marls because of loading with the thick sand-siltstone deposit, as well as erosion at the channel base may have influenced the thickness distribution of the late Maastrichtian biozones (Soria et al., 2001; Schulte et al., 2003).

K-P boundary: There is a considerable agreement about the late Cretaceous age of the Méndez Formation and the early Paleocene age of the Velasco Formation. However, the stratigraphic age of the interbedded sand-siltstone deposits, and particularly, the placement of the K-P boundary, is controversial: Some authors placed the K-P boundary at the base of the sand-siltstone complex, arguing that this position coincides with the first occurrence of ejecta and the last occurrence of an indigenous Cretaceous fauna (e.g., Pospichal, 1996; Smit et al., 1996; Soria et al., 2001; Alegret et al., 2002). Conversely, other studies have placed the K-P boundary atop of the sand-siltstone sequence, coincident with the first appearance of Paleocene microfossils (e.g., López-Oliva, 1996; Keller et al., 1997; Stinnesbeck et al., 1996; 2001). However, (i) no distinctive ferruginous and mm-thick K-P boundary clay with characteristics comparable to the Global K-P Stratotype Section and Point at El Kef, Tunisia (e.g., peak iridium values, presence of spherules, Ni-rich spinels) has been described from any outcrop in northeastern Mexico (this study and Smit et al., 1996; Stinnesbeck et al., 1996; Keller et al., 1997; Lindenmaier et al., 1999), (ii) shocked quartz and spherules are confined to the basal part of the sand-siltstone deposit (Smit et al., 1992b; Keller et al., 2002), and (iii) multiple peak iridium values occur across an interval of about 50 cm, beginning within unit 3 of the sand-siltstone deposit (Smit et al., 1996; Keller et al., 1997; Lindenmaier et al., 1999). Since this study is designated to the sedimentology and petrography of the sand-siltstone complex, and specifically to the ejecta deposits, no distinct stratigraphic age was assigned to the sand-siltstone deposit ('unzoned').

Figure 2.11 (page 35) Thin section microphotographs of spherule deposits in northeastern Mexico (plane polarized light). (**A**) and (**B**) "Microbreccia-like texture of ejecta beds in the La Sierrita area with distinct, large cauliflower-shaped calcite crystals enclosing ejecta fragments to the left and the accretionary lapilli to the right in (A). Note texture with welded and amalgamated spherules and fragments, as well as enclosed fossil debris in (B) (both samples MAS1-2). (**C**) Detail of the spherule deposit at El Mimbral (ELM1-5) showing composite spherules enclosed by glassy, ribbon-like fragments. Note "cauliflower"-like texture of carbonate within the fragment in the middle part of the image. (**D**) Spherules with thick carbonate overgrowth and internal opaque phases (MAS2-2). (**E**) Ribbon-like chlorite ejecta fragment from La Sierrita (MAS1-2) that encloses benthic foraminifera. (**F**) A ribbon-like Si-Al-K-rich glass fragments from El Mimbral (ELM1-5), with opaque internal schlieren encloses cauliflower-shaped carbonate particles. (**G**) Two attached spherules with related internal deformation of vesicles and schlieren. Vesicles are filled by calcite, clay minerals, or silicic phases (tridymite?). (**H**) Typical fluidal texture within a chlorite spherule from La Sierrita (MJP1C-2).
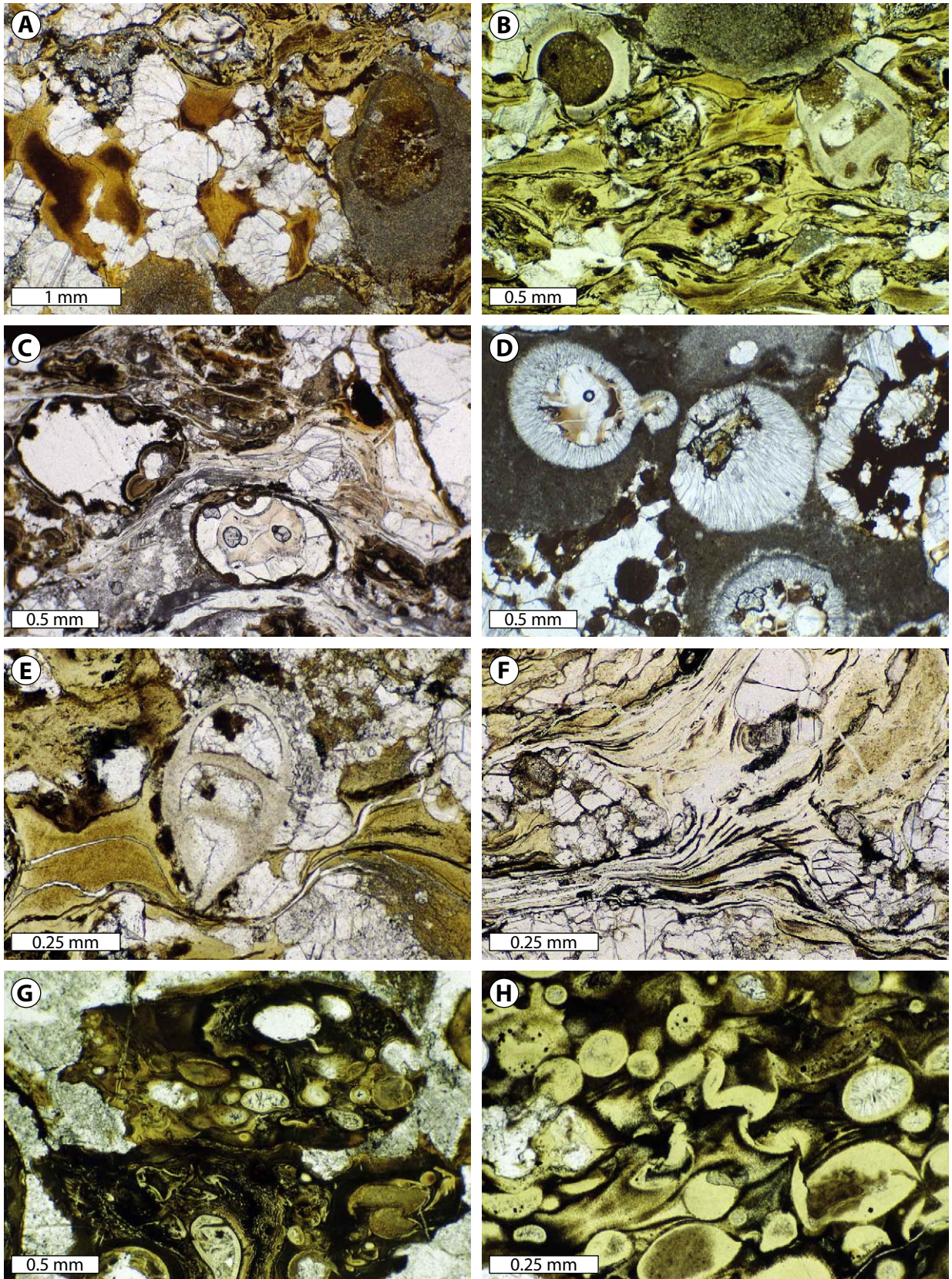
Figure 2.11 (caption on page 34).

Table 2.2 Modal compositions of spherule deposits from the Rancho Nuevo, La Sierrita, El Peñon, and El Mimbral area in northeastern Mexico as determined by analysis of petrographic thin-sections (see text). Data is given as vol%. Note the large variability of composition, but the similarity in ranges of all three microfacies-types observed. Asterisk indicates that large marl clasts (1-25 cm) are present.

	Microfacies-type	Spherules	Fragments	Carbonate clasts	Detritus (Qtz/Fdsp)	Marl clasts	Mean Ø of spherules	Max Ø of spherules
		vol%	vol%	vol%	vol%	vol%	mm	mm
Rancho Nuevo	MF 3	5-20	30-60	10-20	5-20	rare	~0.8 mm	5
La Sierrita	MF 1	15-40	30-70	15-30	<5	rare-common	~0.8 mm	8
	MF 2	20-40	25-35	10-20	<5	frequent*	~1 mm	8
	MF 3	5-20	30-60	15-30	5-20	rare*	~0.8 mm	8
El Peñon	MF 1	15-30	10-20	30-60	<5	rare-common	~0.6 mm	15
	MF 3	5-20	15-20	30-60	5-10	rare*	~0.9 mm	14
El Mimbral	MF 1	15-40	20-30	10-30	<5	rare-common	~0.8 mm	16
	MF 2	10-30	10-15	10-30	<5	frequent*	~0.6 mm	10
	MF 3	5-20	20-30	10-30	5-10	rare*	~0.7 mm	9

Danian Velasco marl: Sediments of Paleocene age, and hence of the Velasco formation, have been encountered only at La Sierrita, El Peñon, and at El Mimbral. López-Oliva and Keller (1996), Keller et al. (1994; 1997), and Pospichal (1996) have assigned an earliest Danian age (planktonic foraminifera Biozone P0 and/or P1a *Parvularugoglobigerina eugubina*, calcareous nannofossil Biozone NP1 *Neobiscutum parvulum*) to these marls. The abrupt onset of several Danian species immediate above the sand-siltstone deposits in these outcrops suggests a hiatus and/or condensed sedimentation (e.g., Keller et al., 1997).

Bathymetry: Paleowater depth studies by Alegret and Thomas (2001), Alegret et al. (2001), Soria et al. (2001), and Keller et al. (2002) on benthic foraminifera suggests that sediment deposition occurred in middle and lower bathyal environments at a water depth of about 500-1000 m, with slight shallower (upper bathyal) conditions in the northernmost sections (e.g., Rancho Nuevo). In contrast, mixed neritic-bathyal faunas were present in the clastic unit indicating redeposition from shallower settings into deeper parts of the Burgos basin.

2.3.3 Microfacies analysis

The ejecta deposits in NE Mexico can be subdivided into three different microfacies types based on thin section and BSE image analysis (Fig. 2.10). Their characteristics are briefly summarized below, though gradual transitions between these microfacies exist locally. Characteristic microfacies features (e.g., abundances and sizes of components) unique to each outcrop area are also tabulated in Table 2.2.

Microfacies-type 1 has a dense, chaotic, grain-supported texture, resembling a sedimentary polymict microbreccia, though sometimes constituents are loosely 'floating' in grey microspar with a distinct matrix-supported texture (Fig. 2.10A, B, C). Constituents include all types of ejecta particles (spherules, fragments, carbonate clasts, accretionary lapilli), as well as marl clasts, and occasional benthic foraminifera. Microfacies-type 1 is generally devoid of terrigeneous detritus. In this microfacies, many spherules and fragments appear welded together and large clusters are present with concave-convex contacts and concomitant deformation of internal structures. In addition, spherules and fragments, as well as marl clasts appear to have been reshaped

Figure 2.12 (page 37) Thin section microphotographs of spherule deposits in northeastern Mexico (plane-polarized light). (**A**) Spherule from El Mimbral (sample ELM1-3) showing distinct, garland-shaped opaque lamellae. These lamellae are made of tiny (sub-μm-sized), microcrystalline Fe-Ti oxides and rutile. Note the spherule-inward increase in grain-size of the crystallites. (**B**) Si-Al-K-rich glass spherule from La Sierrita (SRS-1). Note the cavity that is filled with feathery pyroxene whiskers. (**C**) Altered K-feldspar crystals within a spherule from La Sierrita. Note lath-shaped K-feldspar crystallites with slanted end-phases indicating rapid quenching from a (mafic) melt phase (MJP3A-4). (**D**) Euhedral branched skeletal microliths within a spherule, presumably quenched olivine, or pyroxene (LDP3-14). (**E**) Two spherules from El Peñon: The right part shows a glass-spherule with an enclosed droplet of chlorite composition. This spherule has a thick rim of microcrystalline carbonate ("feathery calcite"). To the left a part of a large carbonate globule with enclosed translucent glass shards is shown (EPO2A-4). (**F**) Spherule-fragment rimmed by radially-orientated, bent and needle-like calcite crystals ("feathery calcite", crossed nicols; MAS2-2). (**G**) and (**H**) Lithoclasts from La Sierrita with concentric internal structure interpreted as accretionary lapilli-like ejecta (MJP1A-14, MAS2-2).
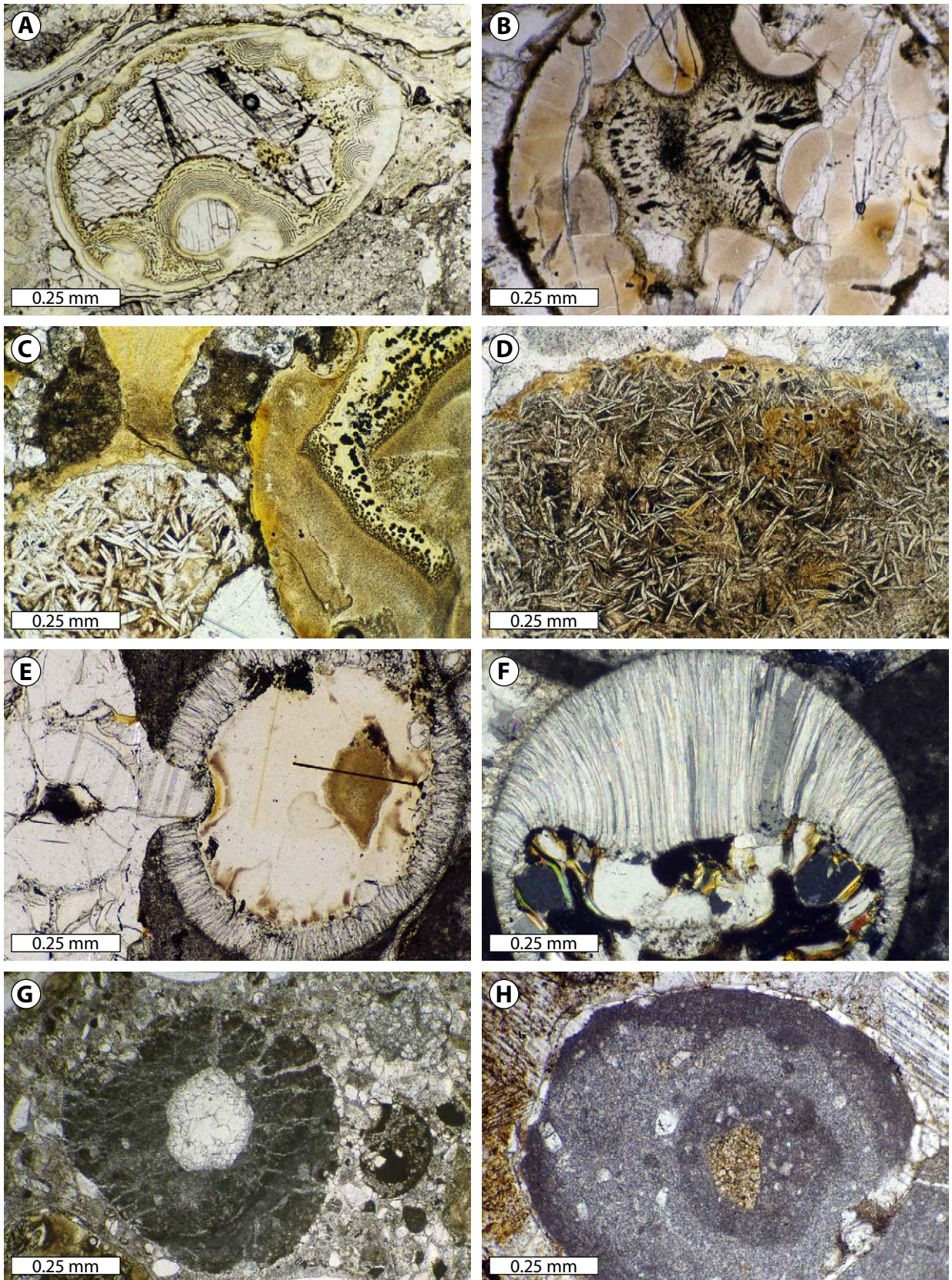
Figure 2.12 (caption on page 36).

plastically along their contacts and, most eminently, large cm-sized filaments envelop other constituents, giving an 'amalgamated' appearance to this microfacies. Locally, microfacies-type 1 shows a distinct spherule-enrichment (up to 70 vol%), resulting in the relative depletion of fragments and carbonate clasts. In this microfacies, planktic and benthic foraminifera are rare and mainly comprise miliolids and rotaliids; the genera *Anomalina*, *Cibicidoides*, *Lenticulina*, *Neoflabellina*, *Tritaxia*, and *Palmula* have been identified (R. Speijer, written communication 2000).

Microfacies-type 2 is distinguished from type 1 by its micritic (marly) matrix and a mud-supported texture, revealing a variable mixture with Méndez marls. In contrast to microfacies 1, welding and amalgamation of constituents are rarely observed. The main constituents of microfacies 2 and their relative abundances are similar to microfacies-type 1 (Table 2.2). Terrestrial detritus is present only in the fine fraction (<63 μm) of the marl matrix. In this microfacies-type, mainly late Cretaceous planktic foraminifera are present, whereas benthic foraminifera are rare and no identifiable individuals have been detected.

Microfacies-type 3 shows a grain- to matrix-supported texture with microspar (Fig. 2.10C). Spherule deposits of this microfacies-type have spherules, fragments, carbonate clasts, and accretionary lapilli, besides a variable, amount of detritus (5-25 %) such as quartz and feldspar (Table 2.2). Rounded marl clasts are present as minor components. Analogous to microfacies-type 2, welding and amalgamation of constituents are rarely present. Planktic or benthic foraminifera are rare in this microfacies, and no identifiable genera have been detected.

The classification of the ejecta deposits in the individual outcrops into the microfacies-types 1-3 is provided in Figs. 2.6 to 2.9: At Rancho Nuevo, spherule deposits show no welding features and are generally diluted by marl or detritus. At the Mesa Juan Perez area, all types of spherule deposits are present, though the occurrence of microfacies-type 1 is not restricted to spherule deposits embedded in Méndez marls, but has been also observed at the base of the sand-siltstone deposits (unit 1) at the Mesa Juan Perez 2C and Los dos Plebes 3 outcrops. An analogous situation occurs in the El Peñon outcrops, though microfacies type 1 is restricted to the spherule deposits within Méndez marls. Unit 1 at the base of the siliciclastic deposit in the El Mimbral section shows an excellently preserved microfacies-type 1,

which are very similar to the ejecta deposits at La Sierrita and comprise large ribbon-like fragments that envelop other ejecta components (Fig. 2.10D).

2.3.4 Petrographic analysis

Based on microscope examination of petrographic thin-sections and backscattered electron (BSE) images, the main components of the studied spherule deposits in northeastern Mexico are ejecta spherules and fragments (as defined below), particles with concentric accretionary features (lapilli), as well as carbonate clasts and globules (Table 2.2, Figs. 2.10-12, 2.16). In addition, intrabasinal marl clasts, benthic and planktic foraminifera, opaque phases, and extrabasinal siliciclastic detritus, such as quartz and feldspar, are present.

Spherules and fragments: The morphologies and surface features of spherules and fragments are highly variable in all ejecta deposits and many features are gradational, making a rigorous classification difficult (Fig. 2.10A). Therefore, they may be considered as endmembers of 'morphological mixing lines' between 'spherules', which are generally round, elongate or teardrop- to dumbbell-shaped and 'fragments', which are irregularly shaped, in blocky, or ribbon-like forms. Occasionally, spherules and fragments are broken with fractures that cut through internal structures and cavities. The relative amount of spherules to fragments varies between 1:1 and 3:1 and these particles are generally between sub-millimeters to about one centimeter, and at maximum two centimeters in size.

The eject particles generally are made of one or more distinct compositional phases (see Figs. 2.10-12, 16), including (i) a phase with intense green, brown-orange colors with high birefringence under crossed nicols, corresponding to chlorite, or other clay minerals (palagonite?) (Fig. 2.10A), (ii) an opaque phase, which corresponds to diverse iron-oxides (hematite, goethite, palagonite) (Fig. 2.11D), (iii) a translucent glass phase, which remains black under crossed nicols (Fig. 2.11C), and (iv) a carbonate phase that may also fill cavities and forms thick rims having outward-radiating fine crystals and suggest rapid quenching (Fig. 2.10A, D). The amount of these individual phases in each ejecta particle is highly variable, and they may consist, for instance entirely of chlorite or carbonate, conversely, all the phases (i-iv) are present in one particle (Fig. 2.16C, F, G). These compositional phases may be arranged in different modes: (a) 'Foam- or pumice-like' with stretched-out and attenuated films between carbon-

ate-silicic or silicic-silicic phases (Fig. 2.16D), (b) circular or brain-like structures with alternating carbonate-silicic phases (Fig. 2.16F), (c) distinct patterns of carbonate veins (Fig. 2.16B), and (d) thin coatings of silicic phases on carbonate globules (Fig. 2.16F). The broken and irregular outlines of some silicic cores inside individual ejecta clasts suggest that cooling of these phases was finished before they were enveloped by further compositional phases (Fig. 2.16G).

Additional internal structures in ejecta particles include schlieren with a distinct flow-pattern (Figs. 2.11H, 2.16A), vesicles, cracks, light-colored globular structures of round, elongate, or twisted shape (Fig. 2.11H), and irregular to rounded inclusions of dark micrite. Some ejecta particles are even 'hollow' and may be partly filled with 'aggregates' of secondary clay minerals. Vesicles reach up to 75 % of the spherule volume and have smooth internal surfaces, exhibiting peeled 'onion-ring-like' opaque coatings that have tiny hematite or rutile crystals. They are filled with calcite, micrite, and zeolites. Most calcite infillings are coarse sparite, and no concentrically zoned drusy mosaic-like spar or geopetal

Table 2.3 X-ray diffraction analysis of nonclay minerals from bulk (powder) samples and summarized clay mineralogy from the glycolated <2 μm fraction of spherule deposits in the La Sierrita, El Peñon, and El Mimbral area (raw data for the clay mineral analysis in Appendix 2.1). Results are arranged according to their microfacies-types and localities. Abbreviations: S, smectite; Ch, chlorite; I, illite; K, kaolinite; I-S, illite-smectite; Ch-S, chlorite-smectite mixed layers. Abbreviations for the section names are given in the text.

Sample	MF	Quartz	K-Feldspar	Plagioclase	Calcite	Clay mineral assemblage	Ch (002/001)	I (001)/ Ch (001)	I (002/001)
		counts/second					peak intensity ratio		
MJP1C-2	MF 1	162	10	10	5830	Ch, I	1.57	0.07	0.16
MJP1C-3	MF 1	285	17	31	2571	Ch, Ch-S, I, I-S	2.00	0.21	0.18
MJP1C-4	MF 1	13	<5	11	4195	Ch, I	2.57	0.03	0.24
MJP3A-4	MF 1	21	10	10	5852	Ch, I-S	1.07	0.01	0.27
MJP3A-5	MF 1	59	<5	<5	2587	Ch, I-S	1.62	0.04	0.16
MJP3A-6	MF 1	118	<5	<5	6844	Ch, I-S	1.70	0.04	0.09
MJP3A-8	MF 1	63	<5	12	6245	Ch, I	2.13	0.06	0.16
MJP1B-3	MF 1	96	12	34	7695	Ch, I, I-S	1.62	0.19	0.13
MAS1-2	MF 1	61	11	18	8677	Ch, I	3.80	0.03	0.31
MAS2-2	MF 1	80	10	10	6487	Ch, I, I-S	1.71	0.60	0.08
LPD3-14	MF 1	152	10	10	5046	Ch, I	1.90	0.21	0.10
MJP2B-8	MF 2	649	33	128	1404	Ch, I, I-S, C-S	1.81	0.23	0.22
MJP2B-10	MF 2	869	32	148	4592	Ch, I, I-S, C-S	0.96	0.61	0.36
MJP2B-12	MF 2	965	45	221	1937	Ch, I, I-S, C-S	2.05	0.42	0.60
MJP2B-23	MF 3	815	45	309	617	I, S, I-S, C-S	–	–	0.29
MAS1-14	MF 3	463	10	277	5420	Ch, I, S	1.46	0.13	0.16
LPD2-2	MF 3	515	12	21	4328	I, Ch	3.83	4.22	0.75
SRS-1	MF 3	151	11	110	4533	I, Ch, S	2.61	1.67	0.18
SRS-2	MF 3	527	31	43	5871	Ch, I	1.70	0.10	0.17
MJP1A-14	MF 3	231	28	147	2148	Ch, I	2.63	0.07	0.48
MJP1A-15	MF 3	225	20	85	4339	Ch, I	2.80	0.11	0.19
EPO2D-3	MF 1	41	12	19	2949	I, Ch	0.42	2.52	0.37
EPO2E-2	MF 1	39	<5	<5	18876	S, Ch-S, I, I-S	0.50	1.29	0.65
EPO2E-8	MF 1	31	<5	<5	5924	S, I, Ch, Ch-S, I-S	0.63	1.04	0.23
EPO2F-3	MF 1	102	<5	<5	5940	Ch, Ch-S, I, I-S, S	0.30	0.95	0.26
EPO2A-3	MF 3	510	17	85	2913	S, Ch, Ch-S, I, I-S	0.16	0.72	0.19
EPO2A-4	MF 3	665	<5	231	4744	Ch, Ch-S, S, I, I-S	0.17	0.42	0.36
EPO2A-6	MF 3	539	<5	212	10418	Ch, Ch-S, S, I, I-S	0.07	0.91	0.35
EPO2B-3	MF 3	388	125	70	3470	Ch, I, Ch-S, I-S	0.29	0.09	0.42
EPO2A-2	Lime	110	<5	<5	4209	S, Ch-S, I-S	–	–	–
ELM1-3	MF 1	237	10	148	3917	Ch, Ch-S, I-S	0.78	0.53	0.23
ELM1-5	MF 1	305	18	113	3766	Ch, Ch-S, I-S	0.65	0.74	0.41
ELM2-3	MF 1	330	12	128	3045	Ch, Ch-S, I-S	1.14	0.32	0.40
ELM2-4	MF 1	37	<5	18	6875	Ch, I-S	0.63	0.07	0.35
ELM2-6	MF 2	125	<5	380	3320	Ch, I, I-S	0.66	0.21	0.98
ELM1-7	MF 3	426	10	252	3917	Ch, Ch-S, I, I-S	0.48	0.13	0.56
Marl	(n=19)	2775	38	215	2240	I, Ch, I-S, C-S, (S)	0.86	2.35	0.31
	stdv	912	12	45	419		0.33	1.21	0.07

calcite mineralization was observed. Larger vesicles are embedded with smaller ones, resembling 'composite' spherules. The ejecta particles are generally devoid of microliths, though small twinned crystals with swallowtails and a typical criss-crossing texture, dark, hairlike whiskers, or thin skeletal and branching crystals occur. In addition, garland-like arranged opaque micro-crystallites are present in ejecta particles, which show an inward-directed increase of the crystallite-size (Figs. 2.12A, 2.24).

Accretionary lapilli: The concentric lapilli clasts are similar to lapilli from volcanic pyroclastic and have rounded shapes, as well as deformed irregular outlines with grain sized from 0.5 to >2 mm (Fig. 2.12G, H). Some lapilli grains are broken. The lapilli grains are made of fine-grained particles and show a pronounced concentric structure with several continuous layers. Subsequent layers may show slight variations in grain size and color and document multiple episodes of accretion. Some lapilli grains have distinct cores of either irregular limestone fragments, or calcite aggregates, or even spherule fragments.

The spherule deposit from the Rancho Nuevo section comprises altered and variable mm-sized glassy and clayey (chlorite) spherules, as well as an abundance of mm-sized carbonate fragments and globules. The spherule deposits from the Mesa Juan Perez area have mainly mm-sized green-brown ejecta clayey spherules and fragments (chlorite) with only sporadic occurrences of glass (see also Schulte et al., 2003). In addition, abundant mm-sized carbonate fragments and globules, as well as accretionary lapilli are present. The spherule deposits from the El Peñon area are generally characterized by mm- to cm-sized ejecta particles of variable composition including glassy, clayey (chlorite), carbonaceous, or opaque spherules and fragments. The spherule deposit from the El Mimbral section has glassy and clayey (chlorite) spherules and large ribbon-like fragments, as well as plentiful carbonate clasts, accretionary lapilli, and tiny marl clasts.

2.3.5 Bulk rock mineralogy

The bulk rock analysis of the spherule deposits by X-ray diffractometry revealed a relatively homogenous composition. At all localities, the dominate mineralogic phase is calcite, added by minor, or even trace amounts of quartz, plagioclase, and K-feldspar (Table 2.3). In addition, trace amounts of gypsum, ankerite, hematite, goethite, and dolomite are present. The microfacies-types can be well distinguished in all localities, with the microfacies-types 1 and 3 revealing strong similarities and only minor detrital influx, whereas the Méndez marl admixed in microfacies-type 2 is reflected by increased quartz and feldspar and less abundant calcite.

The analysis of oriented and glycolated samples of the <2 μm fraction by X-ray diffractometry shows a distinct local variability in the clay mineral assemblage of the spherule deposits: The spherule-deposits in the La Sierrita area are characterized by well-defined peaks of chlorite and low amounts of illite and diverse mixed-layers, whereas the samples from El Peñon and El Mimbral show an abundance of highly variable chlorite-smectite and illite-smectite mixed-layers besides discrete smectite, chlorite and illite (see also Appendix 2.1). The ubiquitous presence of mixed-layer clay minerals and the different morphotypes of chlorite in the spherule deposits and in the Méndez marls with a very different Ch(001/002) peak intensity ratio, as specified below, suggests that these samples are not amenable to an accurate semiquantitative estimation of clay mineral abundances (see discussion in Moore and Reynolds, 1997). Consequently, no percent abundances of individual clay minerals are given. Instead, only the dominant clay mineral species are estimated based on the relative peak intensities and the general clay mineral assemblage is determined. The clay mineral data for the spherule deposits and the Méndez marls are summarized below and outlined for individual samples in Table 2.3.

The **spherule deposits** from the **La Sierrita** area show a chlorite dominated clay mineral assemblage with low illite (I001/Ch001 intensity ratio of 0.18) and illite-smectite content, as well as low amounts of chlorite-smectite mixed-layers (Table 2.3). The chlorite-smectite has high chlorite content, generally exceeding 80-90 %, as estimated according to the method provided by Moore and Reynolds (1997). Compositional differences in the clay mineralogy between the various sample localities (and microfacies-types) exist primarily in the addition of significant illite, probably because of dilution by Méndez marls in the microfacies-type 2. Only one sample from the La Sierrita area furnished meaningful amounts of smectite (SRS-1).

The **spherule deposits** from the **El Peñon** area show a smectite and illite-smectite dominated clay mineral assemblage with additional chlorite and chlorite-smectite (smectite ~10-25 %). No pronounced difference in clay mineral composition has been recognized between the sample locations.
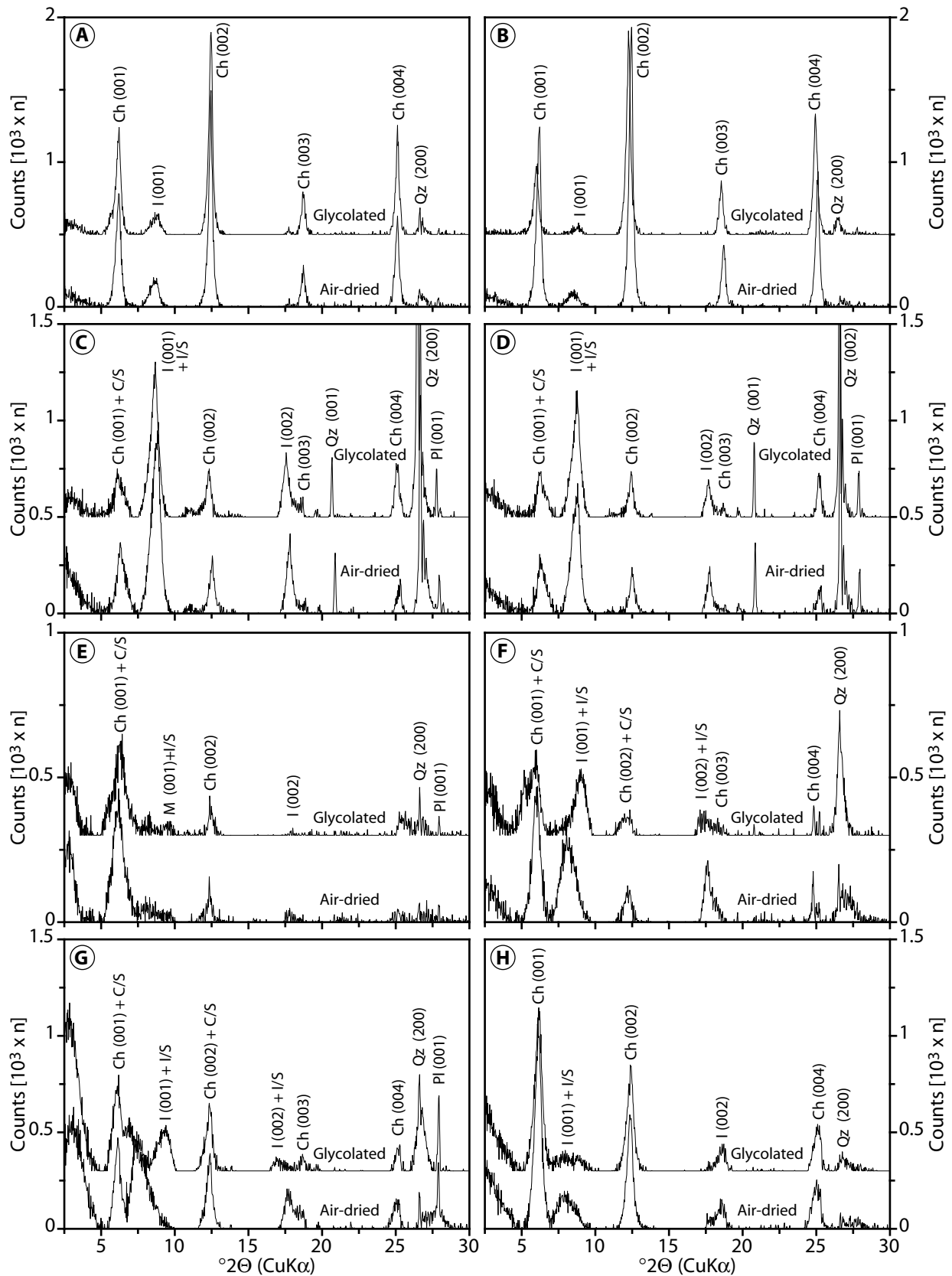
Figure 2.13 Representative X-ray diffractograms of the <2 μm fraction from air-dried and glycolated specimens of ejecta deposits, Méndez marl (50 cm below K-P), and Velasco marl (50 cm above K-P) in northeastern Mexico. Abbreviations: S, smectite; Ch, chlorite; I, illite; I-S, illite-smectite mixed layers; Ch-S, chlorite-smectite mixed layers; Q, quartz; Pl, Plagioclase. (**A**) Mesa Juan Perez: Microfacies-type 1 (Sample MJP1C-3); (**B**) Mesa Juan Perez: Microfacies-type 3 (MJP1A-14); (**C**) Méndez marl (LDP1-8), (**D**) Velasco marl (LDP1-18); (**E**) Microfacies-type 3: El Peñon (EPO2A-3); (**F**) Microfacies-type 1: El Peñon (EPO2F-3); (**G**) Microfacies-type 3: El Mimbral (ELM2-7); (**H**) Microfacies-type 1: El Mimbral (ELM5-2).

The **spherule deposit** from **El Mimbral** shows a chlorite and illite-smectite dominated clay mineral assemblage with additional chlorite-vermiculite mixed layers (?), occasionally in considerable amounts, and minor chlorite-smectite (chlorite ~80-90 %). The strong variations in the illite-smectite 001/002 and 002/003 peak positions suggests strong variations of the illite-smectite composition, with up to 40 % smectite in some samples, though, the broad range of peaks in the 16-17.7 °2Θ area, makes it difficult to give a well-constrained estimation of the smectite-content.

The **Méndez marls** are characterized by an illite and illite-smectite dominated clay mineral assemblage with high amounts of chlorite and chlorite-smectite (I001/Ch001 intensity ratio of 2.35±1.2). The clay mineralogy of the Méndez marls across the K-P boundary in the Los dos Plebes 1 section shows little variation (see also Table 2.3 and Appendix 2.1), though a smectite-rich thin, siltstone layer is intercalated in the late Maastrichtian part (see Fig. 2.7B), suggesting minor volcanic influx. These results are in keeping with major- and trace element studies of this section by Lindenmaier (1999), who found, besides the intercalation of the siltstone layer limestone-layer, no particular trends in the geochemical composition across the K-P boundary, except for the upper part of Biozone P1a, where increased terrigeneous detritus content suggested enhanced weathering and/or proximity to the coastline. The moderate burial depth (<1 km) did not lead to large scale clay mineral transformations (see discussion and Keller et al., 1997). Therefore, the illite- and chlorite-dominated clay mineral facies of the Méndez and basal Danian Velasco marls may have originated from areas with rocks of predominant mafic character, associated with dominance of physical over chemical weathering (e.g., Chamley, 1989; 1997; Müller et al., 2001). The provenance of these clay mineral species may be found in the approaching Sierra Madre Oriental to the West, with a pronounced phase of uplift during the K-P transition (e.g., Echanove, 1986; Goldhammer and Johnson, 2001).

Origin of chlorite and illite

The incorporation of details on the specific mineralogical properties of the predominant clay minerals (chlorite and illite) allows constraining possible origins of these clay mineral species.

The **chlorite** found in the spherule deposits of the La Sierrita area shows well-defined peaks with a crystallinity index (FWHM, full width at half maximum peak height above background, Kübler, 1987; Moore and Reynolds, 1997) of about 0.36±0.05 °2Θ, implying a high degree of 'crystallinity'. This may suggesting that a large part of this chlorite formed as an authigenic phase from the alteration of glassy ejecta material of mafic composition, instead of derivation from detrital input, as also revealed by EMP analysis (see Fig. 2.13, Arkai and Sadek Ghabrial, 1997; Shata and Hesse, 1998).

In contrast, the chlorites in the Méndez marls of this area show a distinctly lower crystallinity (FWHM 0.56±0.9 °2Θ), indicating a certain degree of disorder typical for detrital chlorite (see Fig. 2.13). However, chlorites in the Méndez marls have also a different mineralogical structure, as shown by their different chlorite (002/001) peak intensity ratio of 0.85±0.3 compared to the chlorites in the spherule deposits, which have a chlorite (002/001) peak intensity ratio of 2.1±0.8. Therefore, a direct comparison of crystallinity indexes is difficult and regarded as tentative. However, the chlorite (002/001) peak intensity ratios suggest that the chlorites in the Méndez marls have low contents of Fe in the silicate and hydroxide sheets, whereas the chlorites in the spherule deposits have high Fe contents in the silicate and hydroxide sheets (Moore and Reynolds, 1997). The chlorites in the spherule deposit from the El Peñon and El Mimbral area show a wide range of crystallinity index values (FWHM ~0.4 to 0.8 °2Θ), suggesting variable degrees of admixture by Méndez marls or the presence of different chlorite morphotypes, though the few samples analyzed and the common presence of smectite and illite interlayers, do not allow further specification.

The 'octahedral character' of the **illites** was determined by using the illite (002/001) peak intensity ratio. It shows an average value of 0.25±0.17 for the illite of the spherule deposits and an average value of 0.3±01 for the Méndez marls (Table 2.3). These results indicate an intermediate di- and trioctahedral composition of the illites, since values <0.15 correspond to 'biotitic' illites and values >0.4 correspond to Al-rich ('muscovitic') illites (Bengtsson and Stevens, 1998). Spherule deposits at El Peñon and El Mimbral show a wider range of illite (002/001) peak intensity ratios from about 0.3 to 0.8, indicating the dominance of dioctahedral illite over trioctahedral illite.

2.3.6 Bulk rock geochemistry

The results from major and trace element composition from bulk-rock wavelength-dispersive (WDS)

Locality + Lithology (samples)	Si/Al [mol/mol] 0 2 5	Ti/Al [mol/mol] 0.01 0.03 0.04	Fe/Al [mol/mol] 0 0.5 1	Mg/Al [mol/mol] 0 0.4 0.8	K/Al [mol/mol] 0 0.1 0.3	Sr/Ca [mmol/mol] 0.6 1.2 1.8	Zr/Ti [mmol/mol] 10 30 50

RN: Marl(24), MF 3(5)

La Sierrita: MF 1(12), MF 2(8), MF 3(10), Sand(4)

El Peñon: MF 1(4), MF 3(4), Sand(2)

El Mimbral: MF 1(4), MF 2(1), MF 3(1), Sand(2)

Scale: 0 2 5 | 0.01 0.03 0.04 | 0 0.5 1 | 0 0.4 0.8 | 0 0.1 0.3 | 0.6 1.2 1.8 | 10 30 50
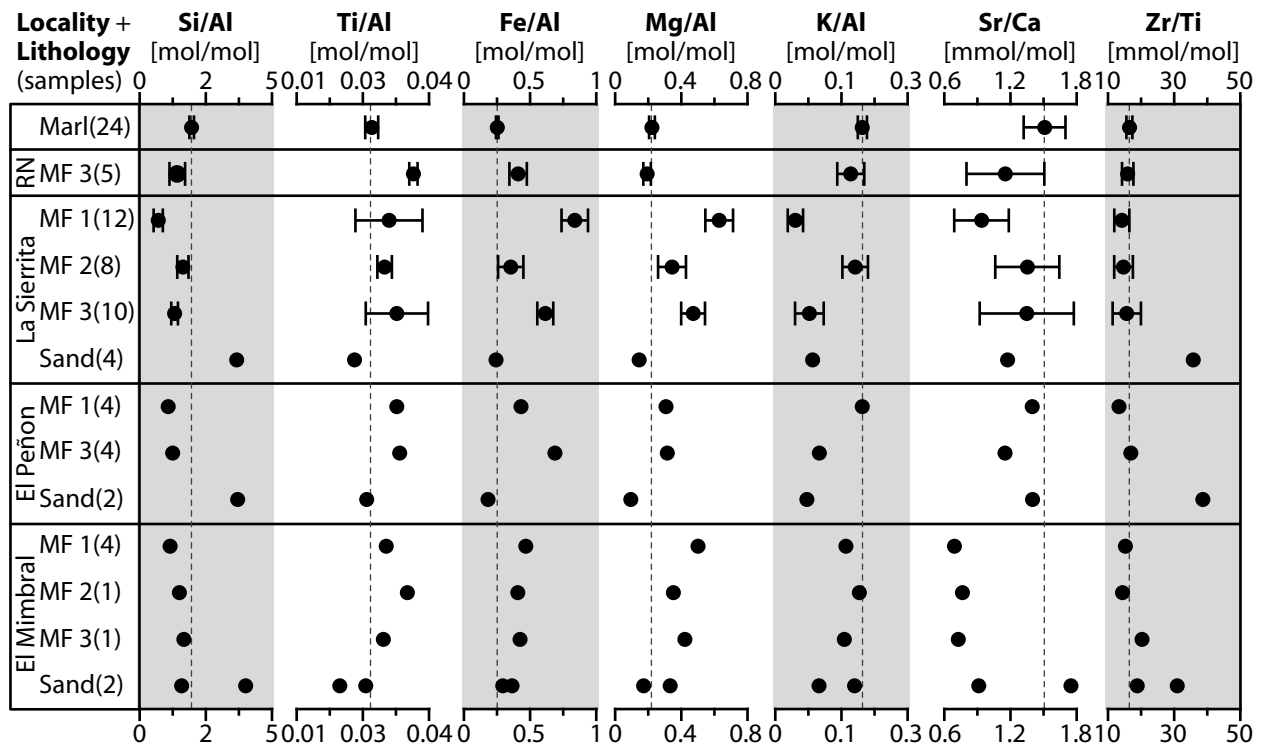
Figure 2.14 Synoptic view of selected major and trace element contents derived from wavelength-dispersive X-ray fluorescence spectrometry (WDS) and energy-dispersive X-ray fluorescence spectrometry (EDS) from spherule deposits in northeastern Mexico. The major element abundances have been normalized to Al (values in Appendix 2.2), and are arranged according to their microfacies type. In addition, the Sr/Ca and Zr/Ti ratio is shown. Data for the Méndez marl (average of 24 analysis), the sandy limestone layer ('SLL'), and the basal sandstones of unit 2 ('Sand') have been included. All values shown are mean values, except for the single analysis of the "SLL" and unit 1. For lithologic units with five and more analyses, the standard deviation is depicted as error bars.

and energy dispersive (EDS) analyses of ejecta deposits in northeastern Mexico have been arranged according to locality and microfacies-type, and selected element ratios (Si, Ti, Fe, Mg, and K versus Al, Sr/Ca, Zr/Ti) are synoptically depicted in Fig. 2.14; original results are included in Appendix 2.2.

The ejecta deposits from each locality show a variable major-element composition with SiO_2 contents of 4-48 wt% and CaO contents of 25-45 wt%, besides Fe_2O_3 and Al_2O_3 with about 5-15 wt% each, and minor MgO (~2-7 wt%). K_2O and Na_2O range between 0.1 and 3 wt%, whereas TiO_2, MnO, and P_2O_5 are generally below 1 wt%. The trace elements show uniform values only for the Cu contents (20-30 ppm), the Y contents (4-26 ppm), and the La contents (3-26 ppm), with As and Pb generally below 10 ppm, except for the Rancho Nuevo samples, which show higher values. In contrast, most other trace element concentrations show considerable scattering: The Rb contents (4-90 ppm), Zn contents (30-100 ppm), the Sr contents (240-800 ppm), the Ce contents (3-55 ppm), and specifically the Ba contents (100-7000 ppm). The results for the elements Cr and Ni measured by EDS, are below or near the detection limit (Cr, Ni: 50 ppm), and are therefore not listed in Appendix 2.2.

Samples from sand-siltstone deposit and the Méndez marls have been included in the analyses to constrain the effects of mixing with ejecta phases. The sand-siltstone deposit and the "SLL" show a wide compositional range, with SiO_2 contents of 20-50 wt% and CaO contents of 20-38 wt%, aside from Al_2O_3 with about 5-8 wt%, and minor Fe_2O_3 (~1-3 wt%). According to data from this study and data from Lindenmaier (1999), the Méndez marls show a more limited compositional range with SiO_2 ~40-44 wt%, Al_2O_3 ~10-12 wt%, CaO ~18 wt%, and Fe_2O_3 ~4 wt%, all other elements are below 1 wt%.

The composition of the samples from Rancho Nuevo mirrors the intense mixing with Méndez marl and silicic detritus (Fig. 2.14 and Appendix 2.2). Samples from the microfacies-types 1 and 3 from the La Sierrita area are very similar in their major and trace element composition (though with elevated SiO_2 contents in microfacies-type 3 by silicic detritus). The geochemical composition of microfacies-type 2 spherule deposits – with higher SiO_2, K_2O, and Na_2O, and lower CaO, Fe_2O_3, and MgO contents – reflects the admixture of Méndez marls.
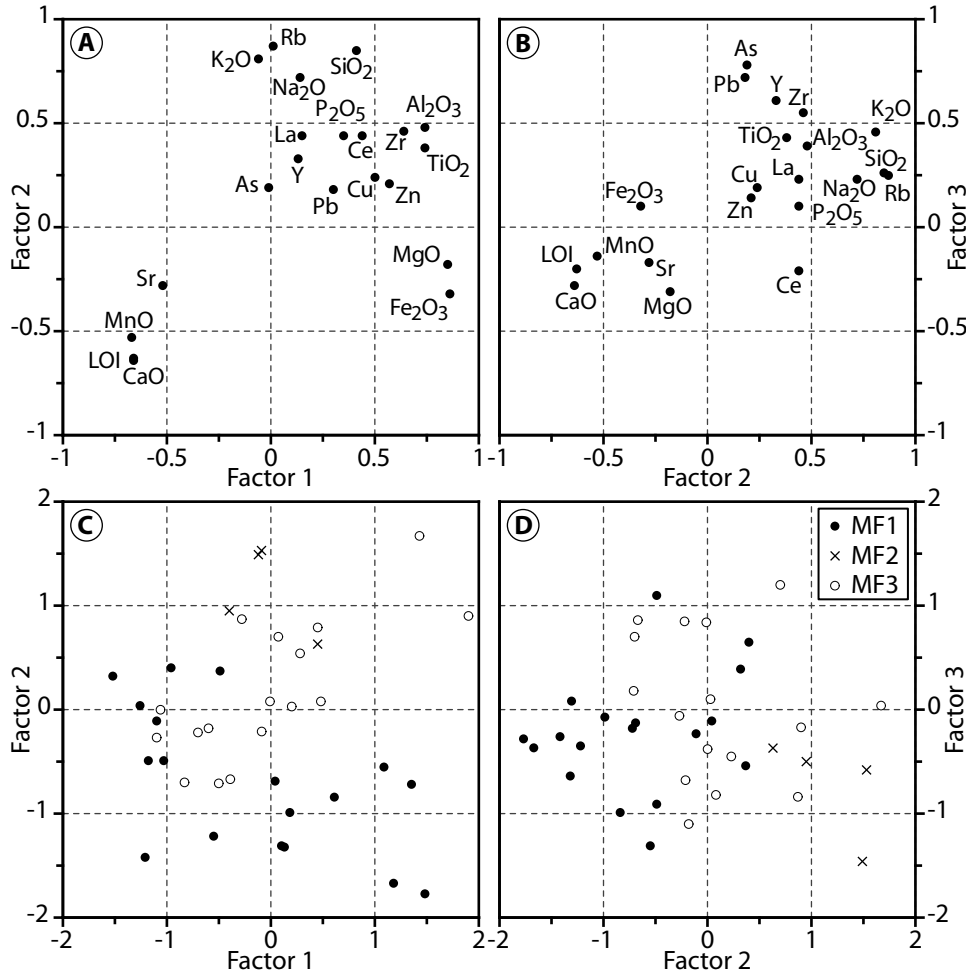
Figure 2.15 Plots of the three factors extracted by principal component analysis from Spearman rank correlation matrix of bulk samples from spherule deposits in northeastern Mexico (**A**) and (**B**) crossplot of factor loadings for individual elements, (**C**) and (**D**) crossplot of factor values for the samples arranged according to their microfacies-type (see text and Appendix 2.3 and 2.4 with numeric results).

Samples from microfacies-type 2 show also higher Rb contents, slightly elevated Zr contents, and more limited range of Ba concentrations. A clear distinction between the microfacies-types of the spherule deposits from the El Peñon and El Mimbral sections are difficult to make based solely on the bulk geochemical phases. Particularly, samples from the El Peñon area show a very narrow compositional range, hardly reflecting influx from Méndez marl or silicic

detritus. This similarity exists also in terms of trace element compositions.

Factor analysis

The set of geochemical phases was investigated by factor analysis to give a qualitative discrimination between the various ejecta phases in the spherule deposits. Specifically, this statistic approach may be useful to establish the differences between the

---

Figure 2.16 (page 45) BSE images of spherule deposits from northeastern Mexico. Abbreviations: Fe-, K-, Ti-rich schlieren, S; calcite, Cz; chlorite, Ch; calcite globules, Cz-g; Fe-Mg-rich globules, Fe-g. (**A**) Chlorite-spherule from La Sierrita with internal Ti- and K-rich schlieren and collapsed cavities (vesicles?). (**B**) Si-Al-K-rich glass spherule from El Peñon with rim of radially arranged calcite and irregular, internal calcite veins. (**C**) Si-Al-K-rich glass-carbonate spherule from El Peñon with two rounded inclusions of chlorite (bright areas) and characteristic "marble-like" texture of the carbonate and the curved menisci that delimit the glass-carbonate boundary. (**D**) Irregular "foamy" chlorite-carbonate spherule from El Peñon with complex intermingled carbonate and silicic phases. (**E**) Large ribbon-like Si-Al-K-rich glass fragments from El Mimbral. This glass fragment encloses carbonate globules and limestone fragments. (**F**) Spherule from El Mimbral with typical "tektite-in-tektite" pattern consisting of three different phases: Si-Al-K-rich glass in the center with abundant garland-shaped cracks. This glass is surrounded by blocky calcite, which in turn is enclosed by a chlorite phase. (**G**) Spherule from El Mimbral, similar to (F), illustrating the contrasting compositional phases and the occurrence of bright, Ti-rich phases that concentrically line the outer rim of the spherule. (**H**) Ti-rich (rutile) and Ni-S-rich inclusions in a spherules from El Mimbral.
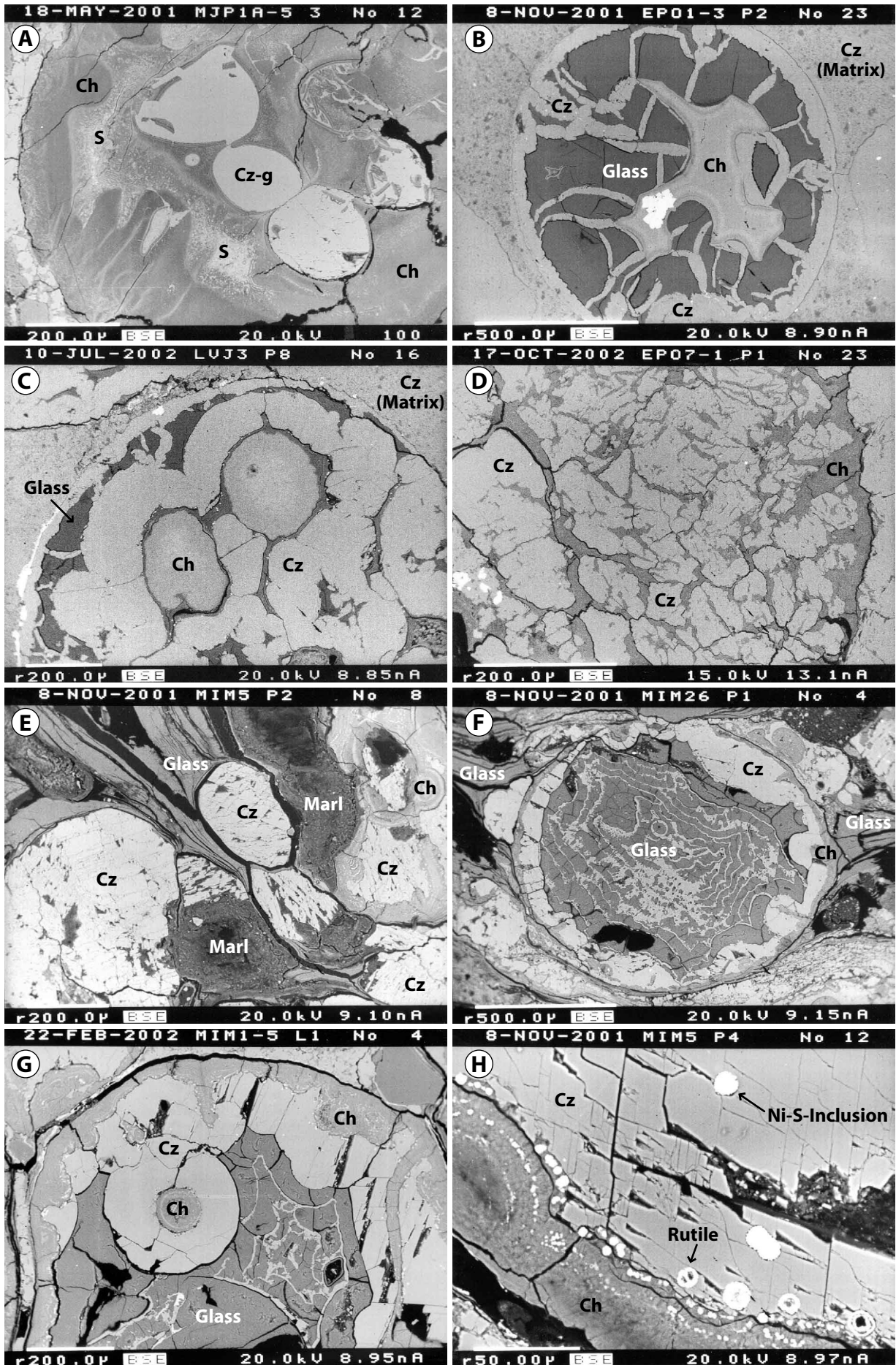
Figure 2.16 (caption on page 44).

various microfacies on a more objective base and to point out constrains on the ejecta target rocks and on the influx of reworking process. Therefore, factors were extracted for the spherule deposits, as well as independently for the Méndez marls. Since the matrix data are unlikely to be distributed normally, the parameter-free Spearman rank correlation was used instead of the Pearson correlation matrix. The resulting factor loadings for the major and trace elements are illustrated in Fig. 2.15 and shown in Appendix 2.3; the corresponding individual factor values for each sample are shown in Appendix 2.4.

Spherule deposits: Factor 1 accounts for 27 % relative variance and shows high positive loadings for TiO_2, Al_2O_3, Fe_2O_3, MgO, and to a lesser degree for SiO_2, Cu, Zn, Zr, K_2O, Zn, and Rb, whereas high negative loadings are present for MnO, CaO, LOI, and Sr. This pattern of element distribution reflect elements typically bound in minerals of terrigenous origin, here mainly derived from rocks of mafic composition, as well as elements associated with a carbonate component. Sr shows a high communality with the elements of the carbonate fraction, pointing to its almost exclusive association with this fraction. Factor 2 explains 26 % of the relative variance with high factor loading for SiO_2, Na_2O, K_2O, Rb, and again, negative factor loadings are present for MnO, CaO, LOI, and Sr. This pattern of element distribution again reflects elements typically bound in

minerals of terrigenous origin, but instead suggests felsic precursor rocks, and the additional existence of a carbonate component. Factor 3 accounts only for 14 % of the relative variance and shows high positive loadings for As, Y, Zr, and Pb, though this result must be taken with caution, since As and Pb are commonly very close to their detection limits.

Méndez marls: The factor analysis for the Méndez marls shows a different picture compared to the spherule deposits: Factor 1 is also associated with high factor loadings for Al_2O_3, Fe_2O_3, MgO, and Zr, similarly to Factor 1 derived for the spherule deposits, but shows high factor loadings for K_2O and Rb as well. Factor 2 shows high factor loadings almost exclusively for SiO_2 and Na_2O, and is clearly distinct from the high silicate Factor 2 of the spherule deposits. Factor 3 is associated exclusively with P_2O_5 and Y.

The tabulation of individual factor values, arranged according to the microfacies-types of the samples, is depicted in Appendix 2.4. Highest values for Factor 1 are almost equally assigned to samples from microfacies 1 as well as microfacies-type 3 from the outcrops at the La Sierrita area and Rancho Nuevo. Neutral or intermediate values for Factor 1 come from samples mostly assigned to microfacies-type 2 and the lowest, negative values for Factor 1 are again derived from microfacies-types 1 and 3, though here, assigned to the El Peñon and
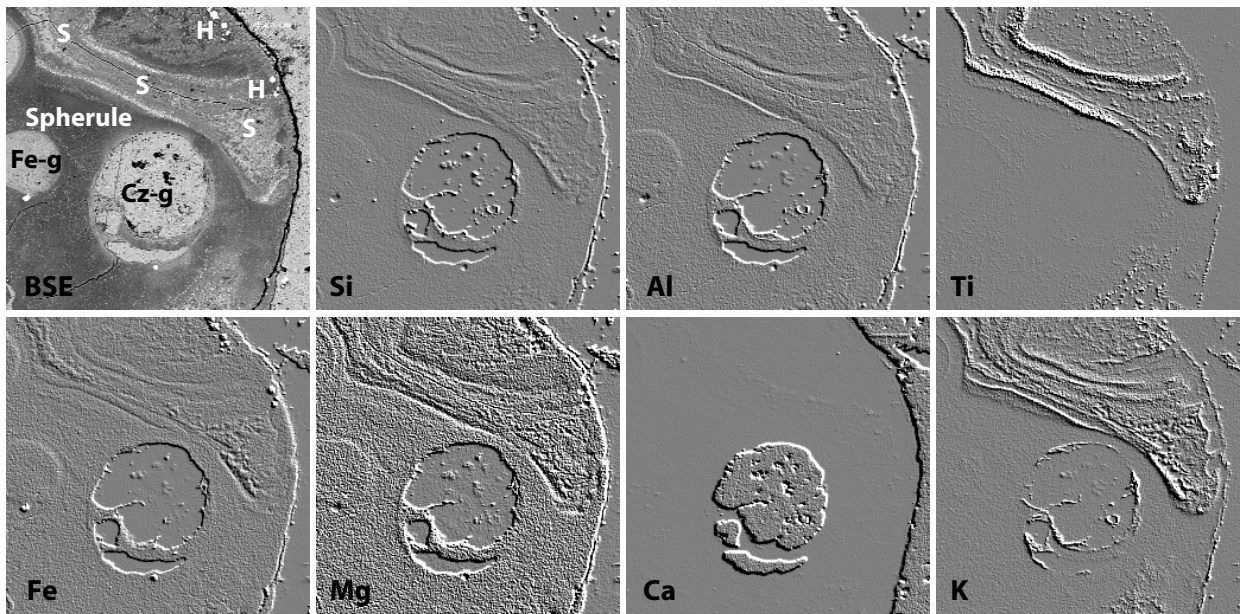
Figure 2.17 BSE image and artificially illuminated qualitative element-distribution maps of a spherule from the Mesa Juan Perez section 1B (sample 3). Length of each field is 0.5 mm. High relief indicates high concentrations (illumination from the upper right). These maps show the Fe-, Al-, and Mg-rich spherule composition with K-, Ti-rich schlieren (S) and calcite globules/vesicles? (Cz-g). In addition, small globules enriched in Fe and Mg (Fe-g) are present and crystals of hematite (H) line the spherule-rim.
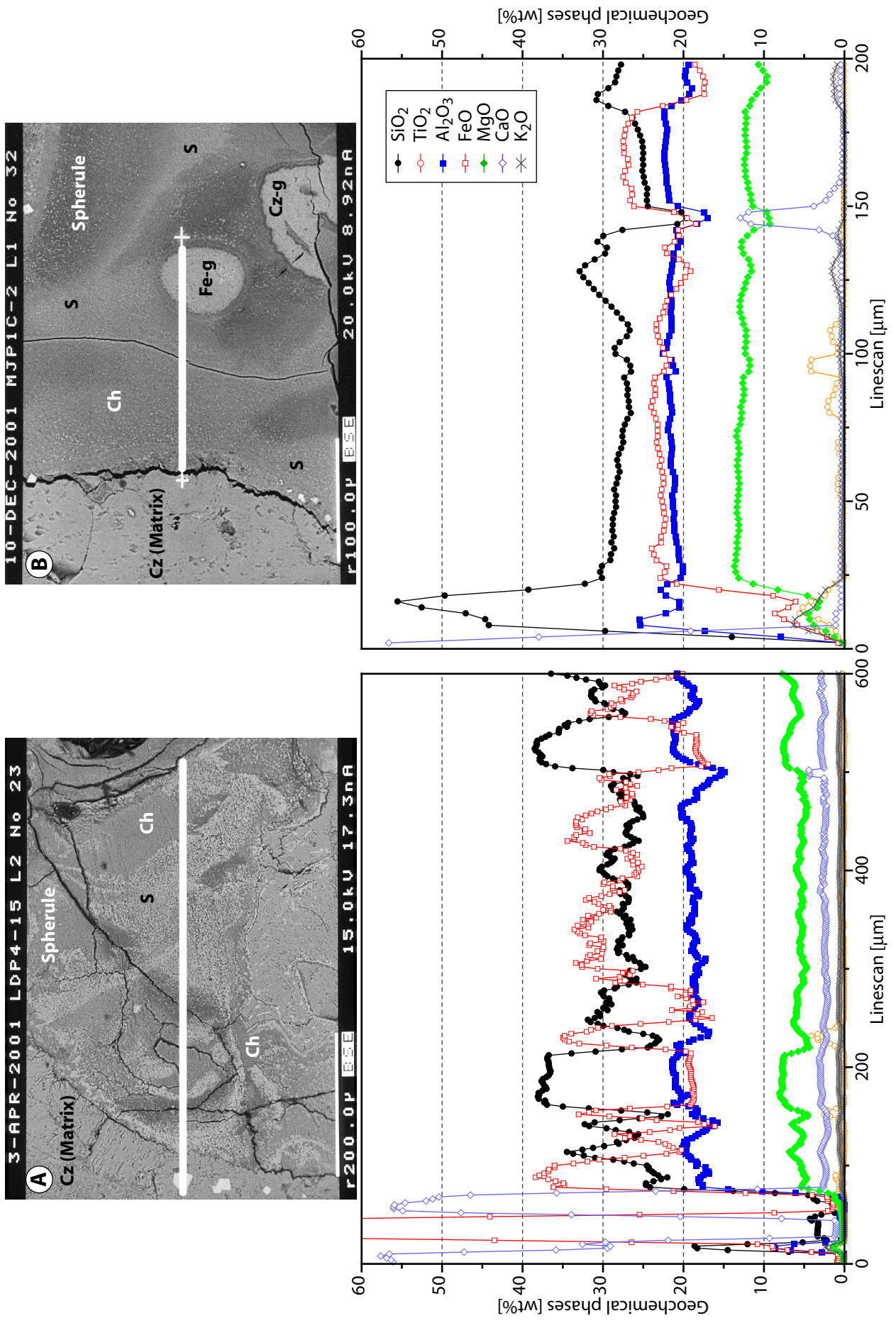
Figure 2.18 Backscattered electron images and representative quantitative electron microprobe linescans of ejecta spherules from spherule deposits in La Sierrita. (**A**) Los dos Plebes, (**B**) Mesa Juan Perez. Abbreviations in Fig. 2.16.
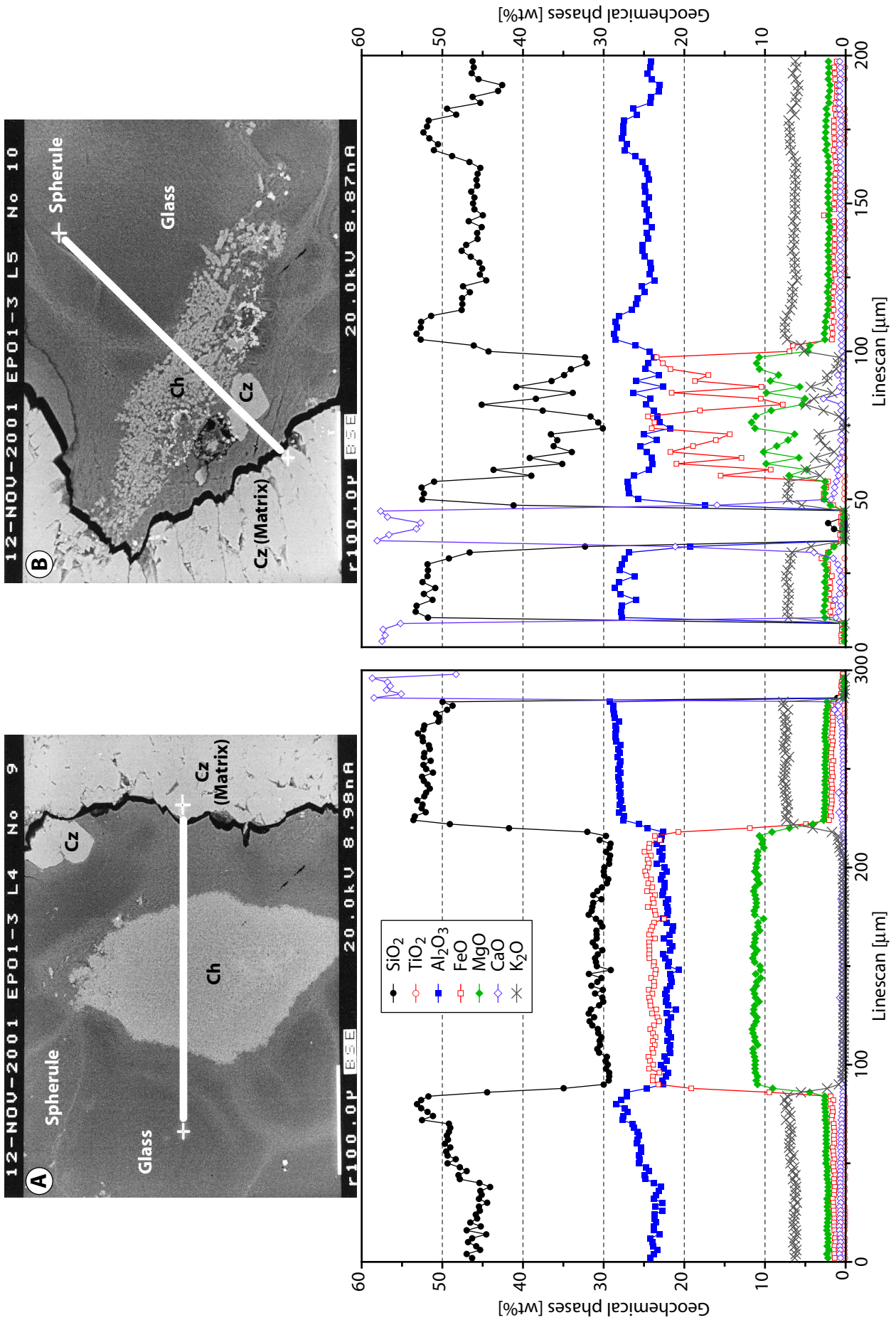
Figure 2.19 Backscattered electron images images and representative quantitative electron microprobe linescans of ejecta spherules from spherule deposits at El Peñon. Abbreviations are provided in Fig. 2.16.
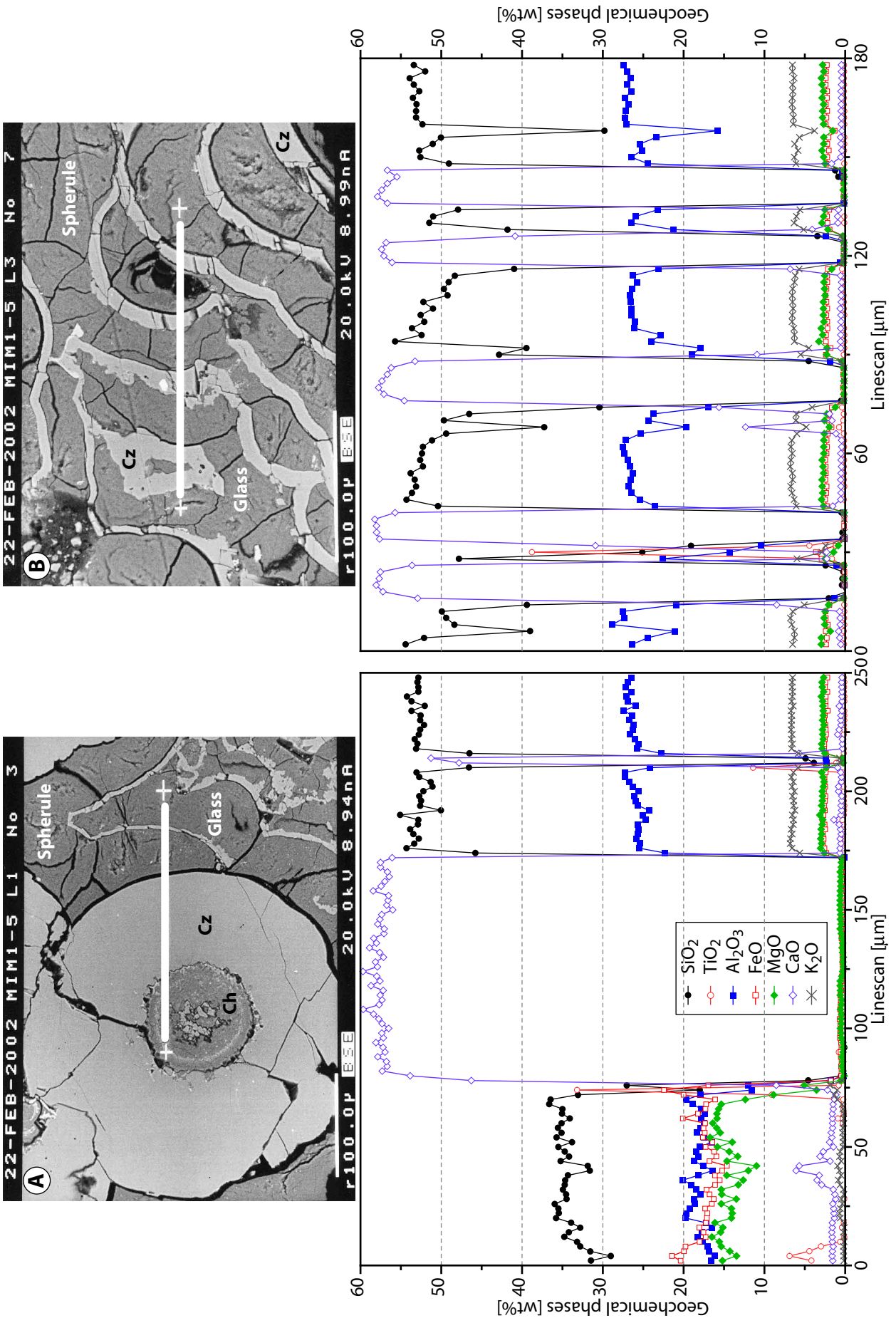
Figure 2.20 Backscattered electron images images and representative quantitative electron microprobe linescans of ejecta spherules from spherule deposits at El Mimbral. Abbreviations are provided in Fig. 2.16.
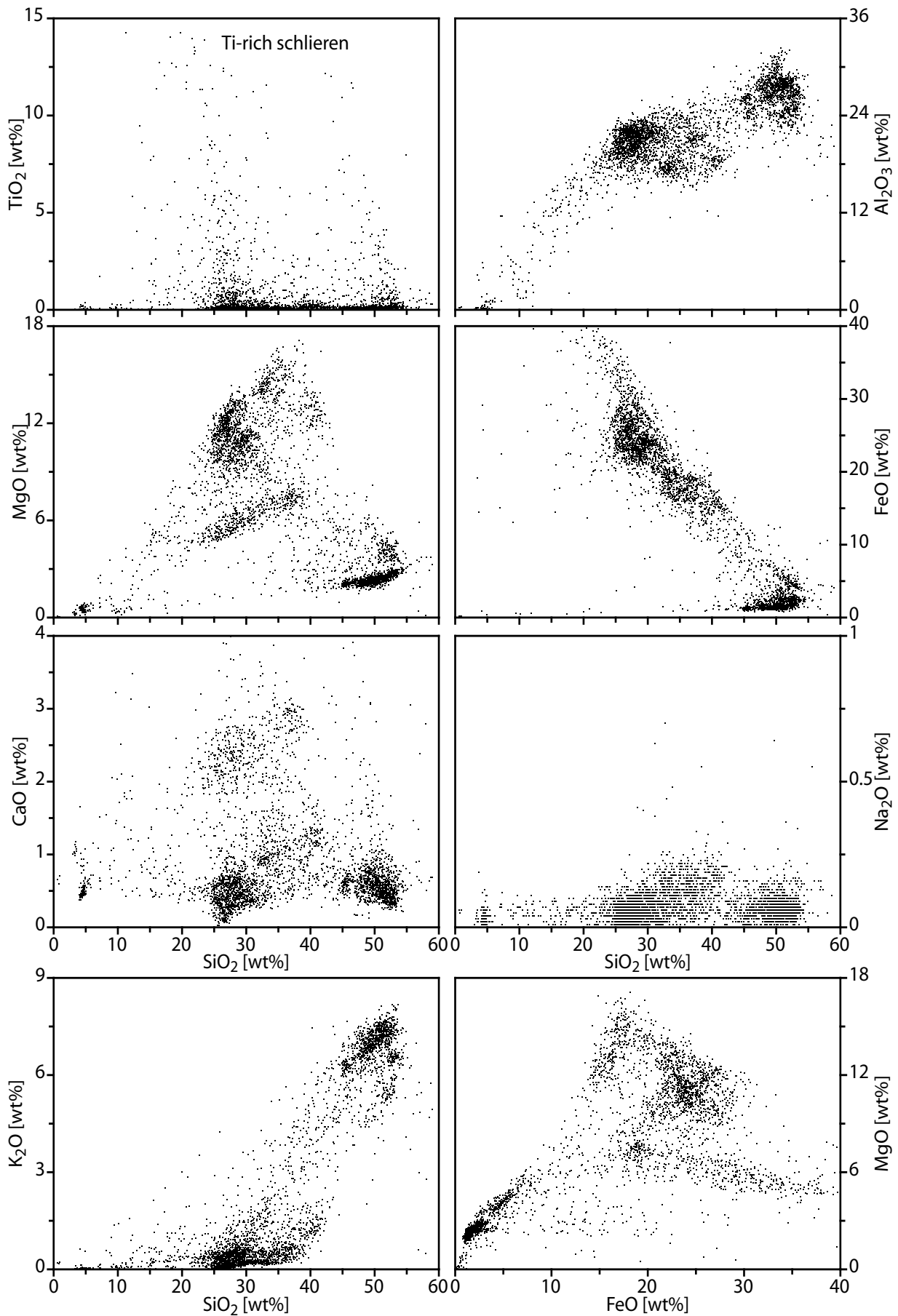
Figure 2.21 Oxide-correlation diagrams ("*Harker* diagrams") of spherules and fragments from La Sierrita, El Peñon, and El Mimbral with the results from individual microprobe analyses (n = 3500, totals >80 wt%). Note the wide range in element concentrations, though with several distinct compositional batches. Summaries of these microprobe analyses are provided in Table 2.4 and Appendix 2.5.

El Mimbral samples. This distribution of the factor values supports the results from petrological and microfacies analysis that, on the one hand no particular grain-sorting effects are apparent between spherule deposits in the various stratigraphic settings. However, this distribution suggests that Fe-Mg-rich chlorite spherules are predominant at the two northernmost localities, Rancho Nuevo and La Sierrita, whereas Si-Al-K-rich glass spherules are prevailing over chlorite spherule compositions at El Peñon and El Mimbral. The highest values for Factor 2 are almost exclusively derived from microfacies-type 2 samples from the Mesa Juan Perez area, as well as from Rancho Nuevo, whereas the lowest, negative values are found for the microfacies-type 1 deposits at the Mesa Juan Perez area. Therefore, the admixture of Méndez marl, which is lowest in microfacies-type 1 deposits, slightly elevated in the microfacies-type 3, and particularly high in the microfacies-type 2 spherule deposits, probably explains Factor 2.

2.3.7 Electron microprobe analysis

Petrographic thin-sections of the spherule deposits were first examined by electron microprobe (EMP) via backscattered electron (BSE) images and energy-dispersive spectrometry (EDS) to get an overview on the compositional variability and to determine representative ejecta particles suitably for quantitative analysis. In a second step, some 15-20 individual points were analyzed by wavelength-dispersive spectrometry (WDS) for each melt phase on selected

ejecta particles to assure good average values and to get a measure for the compositional variability in a thin section. In a third step, linescans of ejecta particles were made to assess possible zonation or inhomogenities. These linescans usually have a point-to-point distance of two μm and include 50 to 400 points each. The BSE images, element mappings, and results of the quantitative EMP analysis are shown in Figs. 2.17 to 2.21. A summary of the quantitative analytical data is provided in Table 2.4 and Appendix 2.5; Table 2.4 also includes a comparison with compositions of target rocks and suevite from the Chicxulub structure. BSE images and major element compositions of six representative linescans are shown in Figs 2.18 to 2.20. Based on methods outlined in Newman (1987), the stoichiometric conversions of oxide-weight percentage into molar abundances of cations were performed for representative points of characteristic geochemical composition (Table 2.5).

Silicic ejecta phases

The silicic phases within ejecta particles are compositionally very heterogeneous and show a wide range for the average SiO_2 (10-60 wt%), MgO (1-18 wt%), Fe_2O_3 (1-45 wt%), and K_2O (0.1-9 wt%) contents. However, the distribution of oxide abundances depicted in the *Harker* diagrams in Fig. 2.21 allows the recognition of three compositionally distinct silicic ejecta phases outlined in the following section:

Table 2.4 Summary of major element data from the electron microprobe analyses. The compositional data has been grouped into three compositionally distinct batches based on the relative oxide abundances plotted in Fig. 2.21. Distinct outliers within each group are noted in brackets. All Fe is noted as FeO. For comparison, major element data from the Chicxulub melt and target lithologies provided by Kettrup et al. (2000) and Kettrup and Deutsch (2003) were added. Data for the Si-Ca-rich glass from El Mimbral (marked by an asterisk) is from Smit et al. (1992b).

	SiO_2	TiO_2	Al_2O_3	FeO	MgO	CaO	Na_2O	K_2O	Totals
	wt%	wt%	wt%	wt%	wt%	wt%	wt%	wt%	wt%
NE Mexico (this study)									
(1) Chlorite	24-32	0.1-0.5 (4)	18-24	22-30 (35)	8-14 (18)	<1	<0.1	0.1-1	84-90
(2) Chlorite-Smectite	32-42	0.1-0.5 (2)	16-22	15-24	10-15 (7)	1-4	0.1-0.3	0.2-1.2	86-88
(3) Si-Al-K-rich glass	42-54	0.1-0.5 (2)	25-32	1-6 (10)	2-5	<1	<0.1	6-8 (5)	88-96
(4) Si-Ca-rich glass*	52-66	0.1-0.8	12-18	4-12	1-9	1-23	0.1-4	0.5-3	98-99
Chicxulub impact lithologies									
C-1 impact breccia	61.1	0.8	15.9	5.5	2.9	7.2	4.7	1.8	100
Y-6 impact breccia	34.4	0.4	9.6	3	5.5	41.4	2	0.6	100
Y-6 impact melt	51.2	0.8	12.4	6.3	6.7	18.3	3.3	0.8	100
Y-6 impact melt (*)	65.3	0.3	14.5	4.1	2.6	8.4	3.3	1.4	100
Chicxulub basement									
Y-6 gneiss	68.4	<0.1	20.1	0.2	0.1	1.6	7.8	2	100
Y-6 gneiss	84.3	<0.1	8.9	<0.1	<0.1	0.1	2.2	4.5	100
Y-6 gneiss	67.9	0.2	16.7	3.9	1.7	0.9	7.1	1.6	100
Y-6 amphibolite	52.2	2.2	14.9	14.5	7.9	3.1	3.3	1.9	100
Y-6 granite	81.9	0.2	8.5	4.1	0.1	1.3	2.3	1.6	100

Table 2.5 Mineralogical formulae calculated stoichiometrically from representative electron microprobe analyses of ejecta particles of spherule deposits in NE Mexico. The analysis (1) to (5) correspond to di,trioctahedral chlorites on basis of $O_{10}(OH)_8$, the analysis (6) to 11) corresponds to trioctahedral chlorites on basis of $O_{10}(OH)_8$, whereas analysis (12) to (14) are similar to muscovite-phengite micas on basis of $O_{10}(OH)_2$. Abbreviations: Tetra, tetrahedral; Octa, octahedral; Inter, interlayered; abbreviations for the section names are given in the text. Total iron is given as FeO.

Locality	MIM	MJP	MIM	MIM	MJP	EPO	MJP	MJP	MIM	EPO	MJP	MJP	EPO	MIM
Number	(1)	(2)	(3)	(4)	(5)	(6)	(7)	(8)	(9)	(10)	(11)	(12)	(13)	(14)
Element	wt%	wt%	wt%	wt%	wt%	wt%	wt%	wt%	wt%	wt%	wt%	wt%	wt%	wt%
SiO_2	43.03	38.94	39.52	36.62	32.53	30.8	25.16	28.36	26.55	24.99	25.35	50.79	53.02	53.34
TiO_2	0.13	0.05	1.03	0.23	0.07	0.09	0.21	0.05	0.01	0.03	0.03	0.31	0.58	0.34
Al_2O_3	20.1	21.35	18.15	18.86	21.39	22.62	18.90	21.60	22.42	20.03	22.32	30.37	23.21	25.45
FeO	13.8	18.85	17.83	17.22	25.04	24.62	37.76	26.74	25.4	32.29	27.62	1.34	4.12	2.75
MgO	11.71	7.79	13.88	15.34	6.43	11.4	5.34	12.97	12.99	10.07	12.51	2.06	4.22	2.92
CaO	1.05	2.99	1.26	1.5	2.86	0.37	2.15	0.29	0.2	0.54	0.14	0.63	0.35	0.53
Na_2O	0.19	0.14	0.11	0.08	0.15	0.13	0.05	0.06	0.04	0.03	0.04	0.13	0.11	0.06
K_2O	1.9	0.76	0.91	0.37	0.53	0.22	0.31	0.16	0.07	0.12	0.03	7.37	8.14	6.81
Total	92.03	90.86	92.83	90.34	89.00	90.29	89.90	90.24	87.75	88.19	88.05	93.02	93.83	92.21
numbers of cations per half structural unit cell														
Si	3.92	3.74	3.69	3.52	3.35	3.08	2.82	2.90	2.78	2.74	2.69	3.32	3.50	3.52
Al(IV)	0.08	0.26	0.31	0.48	0.65	0.92	1.18	1.10	1.22	1.26	1.31	0.68	0.50	0.48
∑ (Tetra)	4	4	4	4	4	4	4	4	4	4	4	4	4	4
Al(VI)	2.08	2.16	1.68	1.66	1.95	1.75	1.31	1.50	1.55	1.32	1.47	1.66	1.30	1.51
Fe	1.05	1.52	1.39	1.39	2.16	2.06	3.53	2.28	2.23	2.96	2.45	0.07	0.23	0.15
Mg	1.59	1.12	1.93	2.20	0.99	1.70	0.89	1.97	2.03	1.64	1.98	0.20	0.42	0.29
Ti	0.02	0.01	0.14	0.03	0.01	0.01	0.04	0.01	0.01	0.01	0.01	0.03	0.06	0.03
∑ (Octa)	4.74	4.80	5.15	5.28	5.11	5.53	5.77	5.76	5.82	5.93	5.91	1.96	2.00	1.98
Ca	0.05	0.15	0.06	0.08	0.16	0.02	0.13	0.02	0.01	0.03	0.01	0.02	0.01	0.02
Na	0.02	0.01	0.01	0.01	0.01	0.01	0.01	0.01	0.01	0.01	0.01	0.01	0.01	0.01
K	0.19	0.08	0.09	0.04	0.06	0.02	0.04	0.02	0.01	0.01	0.01	0.52	0.58	0.48
∑ (Inter)	0.25	0.25	0.16	0.12	0.23	0.06	0.17	0.04	0.03	0.06	0.03	0.55	0.59	0.51
Fe/(Fe+Mg)	0.40	0.58	0.42	0.39	0.69	0.55	0.80	0.54	0.52	0.64	0.55	0.27	0.35	0.35

(1) Chlorite ejecta spherules and fragments have FeO contents of 24-32 wt%, Al_2O_3 contents of 18-24 wt%, MgO contents of 8-14 wt%, and about 24-32 wt% SiO_2. The alkali content is generally low and well below 1 wt%, albeit some ejecta clasts may have a CaO enrichment of up to 4 wt%, which is paired with a significant lower MgO contents (~5-7 wt%). Table 2.5 shows that the stoichiometric formulas derived from the oxide-weight percentage and normalized to $O_{10}(OH)_8$ yield reasonable cation sums identifying this phase as chlorite, suggesting that the mineral analyzes are principally affirmative. The characteristic cations for the octahedral sheets between 5.6 and 5.9 are comparable to trioctahedral chlorite (Newman and Brown, 1987). The predominance of Fe in the octahedral sheet (e.g., #7 in Table 2.5) suggests that these chlorites belong to the chamosite group (Newman and Brown, 1987; Bailey, 1988). Ejecta particles consisting of this compositional phase have been found in all K-P spherule deposits investigated for this study, although this compositional phase is by far most predominant at the La Sierrita

area, whereas it is significantly less abundant at El Peñon and El Mimbral.

(2) Chlorite-smectite and chlorite-illite ejecta spherules and fragments have FeO contents of 16-24 wt%, Al_2O_3 contents of 16-22 wt%, MgO contents of 8-15 wt%, and about 32-42 wt% SiO_2. This compositional phase has low amounts of CaO and alkalis (~1-4 wt% each). Normalization to $O_{10}(OH)_8$ revealed cation sums indicative of a chlorite mineralogy (Newman and Brown, 1987; Bailey, 1988). However, in contrast to the trioctahedral chlorites shown above, their number of octahedral cations per formula unit is significantly lower and between 4.7 and 5.1 (#1-#5 in Table 2.5), corresponding to di,trioctahedral chlorites (Newman and Brown, 1987). The variable dominance of either Fe (e.g., #1 in Table 2.5) or Mg (e.g., #3) in the octahedral layer suggests a chamosite- or chlorite-like composition, albeit (i) the high silica content (Si 3.3-3.9 per formula unit), (ii) the Al^{VI} content (1.6-2.1) much larger than the Al^{IV} (0.1-0.6) content, and (iii) low octahedral occupation, suggest that some illite or smectite interlayers are present (Shau et al., 1991). These illite or smec-

tite interlayers may also account for the presence of Ca, Na, and K in the interlayers; alternatively, these cations may be regarded as impurities (Newman and Brown, 1987). Ejecta particles having this compositional phase are present in all spherule deposits from the four K-P localities investigated for this study, though they are most abundant at the El Mimbral ejecta bed.

(3) Si-Al-K-rich glassy spherules and fragments have high contents of SiO_2 of about 42-55 wt%, Al_2O_3 contents of 25-32 wt%, and 6-8 wt% K_2O, with low FeO and MgO contents (<2-5 wt% each). A more narrow range of the compositional variability than the Fe-Mg-rich chlorite phase outlined above characterizes this phase. Remarkably, the stoichiometric formulas obtained from the oxide-weight percentage yield reasonable cation sums pointing to a mica-like (muscovite, phengite) mineralogy (analysis #12-14 in Table 2.5 and Newman and Brown, 1987), though only the most hydrous Si-Al-K-rich ejecta phases (<90 wt% total) show petrographic characteristics (by the thin-section analysis) that are indicative of mica (bright interference colors etc.). Ejecta particles consisting of

this compositional phase have been found in all spherule deposits though they are most abundant in the ejecta deposits from the El Peñon and El Mimbral sections, and rarely present at Rancho Nuevo or La Sierrita.

Aside from the silicic phases presented above, several studies have reported rare glassy spherules of andesitic composition with considerable Ca enrichment from the El Mimbral outcrop (Smit et al., 1992b; Stinnesbeck et al., 1993; Premo et al., 1995; Bell and Sharpton, 1996). This analysis extends the compositional range of the ejecta particles outlined above even into the range of felsic rocks, well comparable to ejecta particles from Beloc, Haiti (Izett, 1991; Koeberl and Sigurdsson, 1992; Stüben et al., 2002). However, such glasses have not been encountered during this study, likely resulting from the exclusive usage of thin-sections in contrast to the washing and dissolution techniques employed by these authors.

Total oxides values: The oxide totals for the altered glasses/ejecta particles are relatively low and show a bimodal distribution, with 85-90 wt% for the chlorite phase, which is a typical total value for
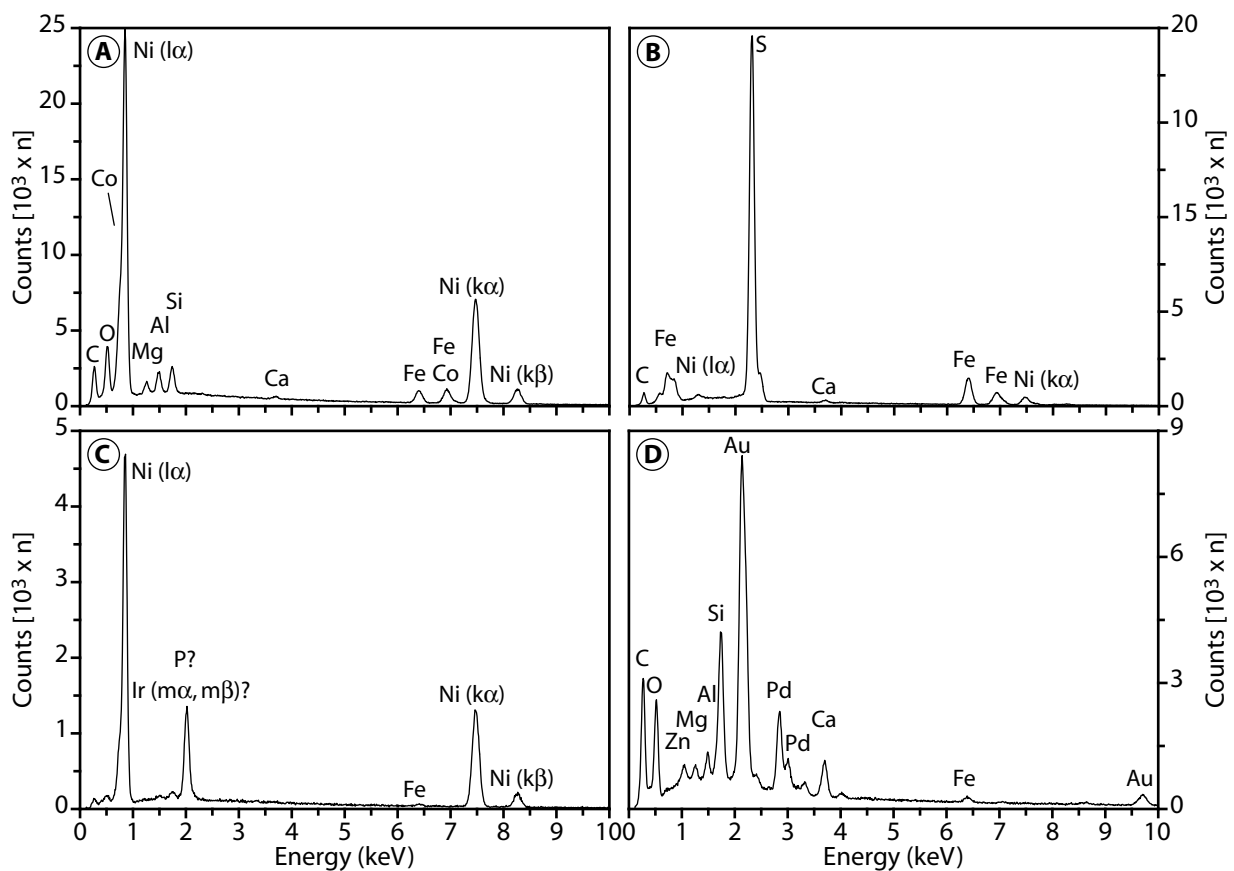
Figure 2.22 Energy-dispersive X-ray fluorescence (EDS) spectra of 'metallic' and 'sulfidic' Ni-, Co-rich inclusions in spherules and carbonates from La Sierrita and El Mimbral (with 15 keV acceleration voltage). (**A**) Sample MAS2-2; (**B**) MAS1-3; (**C**) MIM1-5; (**D**) MIM1-5. The weak Mg-, Al-, Si-, and Fe-peaks in (A, D) and Ca peaks in (B) derived from the enclosing spherule and carbonate, respectively.

such clay minerals (Newman and Brown, 1987), and 90-96 wt% for the Si-Al-K-rich glass. These values are relatively low when compared to common glass analysis of tektites (Heider et al., 1993; Koeberl, 1994), implying copious amounts of volatile phases and strong hydration. In addition, submicroscopic porosity may be substantial, because some spots revealed oxide totals less than 80 wt%, and natural glasses with such low totals are rare (Bouska, 1993). However, individual microprobe analyses totaling <80 wt% have been rejected from further consideration.

Compositional domains in ejecta particles: In support of the petrographic results, the electron microprobe analysis show that individual ejecta particles may consist exclusively of one of the compositional phases outlined above (homogeneous particles), though, often, there are multiple different compositional phases within one ejecta particle ('tektite in tektite' configuration). However, the electron microprobe investigation by linescans showed that individual melt phases in one ejecta particle are mostly well confined and phase-changes occur in a few μm instead of with broad, gradational transitions (see Figs. 2.18-20). Instead, these two endmembers generally occur as distinct irregular inclusions, globules, or schlieren in the respective host phase, providing no support for two- or three-component mixing.

Besides these 'principal' mineralogical and geochemical phases in spherules and fragments, several textural domains in the ejecta particles show a markedly different composition: (i) schlieren that are enriched either in FeO, TiO_2 or K_2O (Fig. 2.16A), (ii) globules (sometimes distorted) that are slightly enriched in FeO and MgO, and depleted in SiO_2 (Fig. 2.11H), (iii) hexagonal and octahedral hematite, rutile, and Ti-Fe oxides, about 10-20 μm in diameter (Fig. 2.24) that are slightly enriched in SiO_2 (5-10 wt%) and in NiO (~0.4 wt%); Ti-Fe oxides may show a dendritic or skeletal appearance, or present garland-shaped lamellae with crystal sizes of the oxides growing towards the interior of grains (see section on rock magnetic properties and Fig. 2.10), and (iv) rare μm-sized globular or irregular inclu-

sions of either Fe-Ni-Co-rich metallic or Ni-rich sulfide composition (Figs. 2.16, 2.24). The EDX spectra of some Ni-rich inclusions showed a strong peak at about 2.0 keV (Fig. 2.22C), which may represent the α-line of phosphorus (at 2.012 keV), or the double mα-, mβ-line of iridium (1.98 and 2.054 keV). However, by EDX analysis no further specification of these inclusions was possible.

Carbonaceous ejecta phases

The ejecta deposits contain abundant carbonate as irregular clasts, as globules, as overgrowths, and as inclusions in individual ejecta particles. Linescans showed that the carbonate overgrowths and inclusion phase are often characterized by a distinct Fe- and Mg-enrichment, which averages about 0.6 to 1 wt% for the Fe_2O_3 contents and about 0.2 to 0.6 wt% for the MgO contents (see Appendix 2.5). The Fe-Mg enrichment may vary along a linescan, and usually become close to zero at the outermost rim. Notably, this Fe-Mg enrichment is not interrelated with the geochemical composition of the adjacent or even enclosing silicic phase(s). The analysis of the MnO contents of the carbonate revealed amounts between 0.1 and 0.2 wt% (not shown) that may occasionally reach up to 0.4 wt% MnO. The distinct Si-enrichment up to a few wt% that is occasionally present (see Figs. 2.18-20), is not considered as evidence for a true mixture of carbonate with silicate melt phases and may be an artifact of porosity.

Accretionary lapilli

The electron microprobe analysis showed very low totals for the accretionary 'lapilli-like' grains, comparable to calcite (~50-60 wt%), with high porosity, and some silica- and aluminum-enriched areas (SiO_2 contents about 20-40 wt%, Al_2O_3 about 10-20 wt%). However, these low totals do not allow further constraining the mineralogy of these phases by means of EMP analysis.

2.3.8 Cathodoluminiscence analysis

Cathodoluminiscence petrography is a basic tool for characterizing the origin of carbonates and their

---

Figure 2.23 (page 55) Representative paired plane light (left) and cathodoluminiscence (right) photomicrographs of spherule deposits. (**A**, **B**) and (**C**, **D**) Radially arranged blocky calcite crystals with typical "cauliflower-texture" enclosing ejecta fragments (sample MJP3A-6). The blocky calcite shows typical dark red (to brown) luminescence colors, which is in contrast to the bright yellow luminescence of the matrix. The dull luminescence may be related to "luminescence-quenching" due to the high amount of Fe and Mg (0.5 to 1 wt%) in the calcite. Note that the carbonate inside the carbonate spherule to the upper right in (A) shows bright yellow luminescence colors. (**E**, **F**) Two carbonate-silicate spherules with dark red luminescence (EPO2A-3). Note the worm-like appearance of the carbonate in the left spherule and the complex carbonate veins in the right spherule. (**G**, **H**) Part of a carbonate-silicate spherule (EPO2A-3). This spherule shows a prominent radially arranged calcite overgrowth ('feathery calcite').
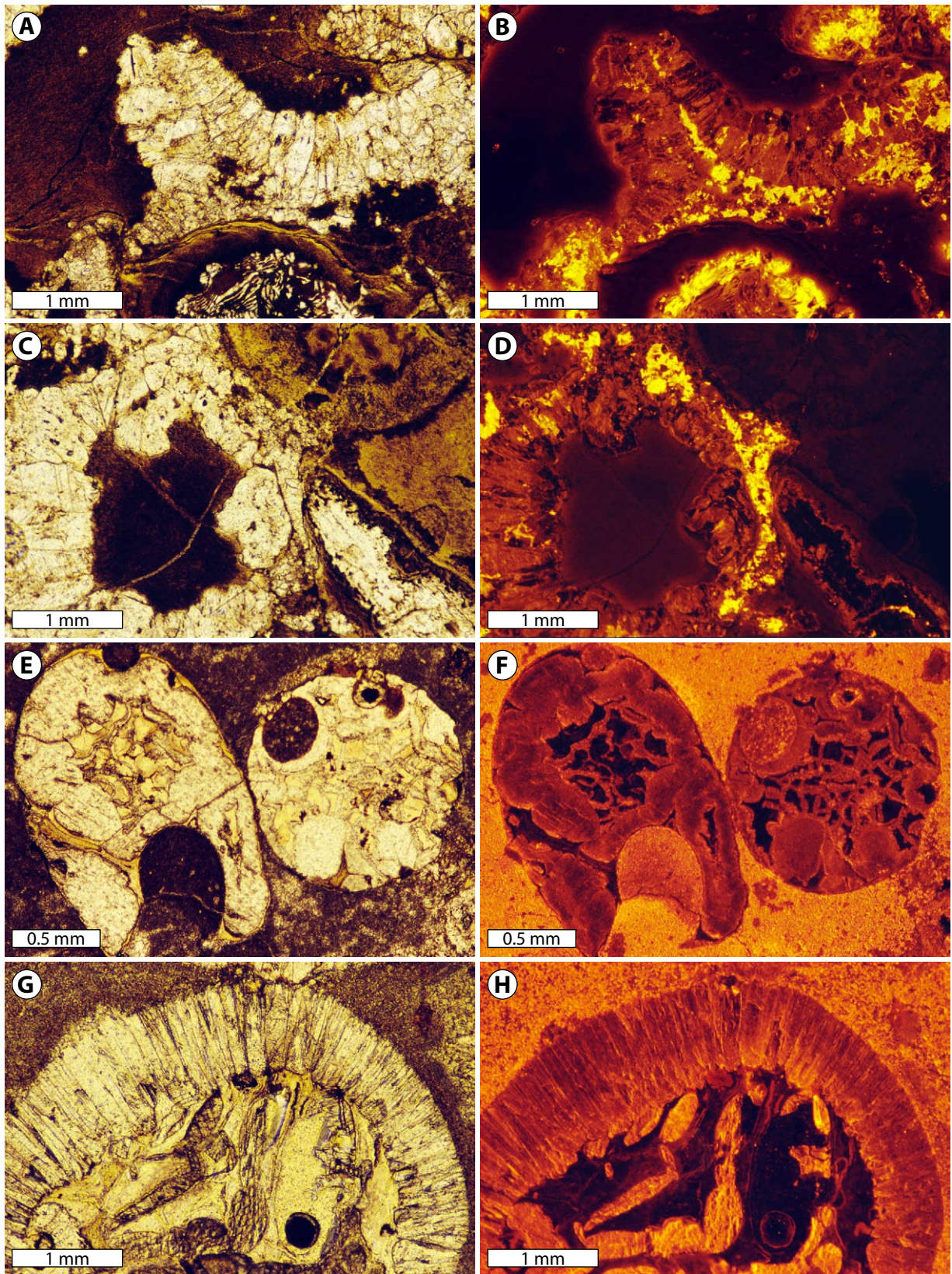
Figure 2.23 (caption on page 54).

diagenetic history, specifically when complemented by electron microprobe analysis (e.g., Machel, 2000). With this technique, distinct zones of similar carbonate composition (in terms of major- and trace-element abundances) can be mapped easily using their individual color, extending the resolution of the electron microprobe.

Cathodoluminiscence (CL) is produced by the counterbalance between activator- and quencher-ions, as well as by defects in the lattice structure (Pagel et al., 2000). According to Amieux (1982), Mn^{2+} is the primary activator-ion and even very low concentrations in the range of 10-100 ppm causes bright yellow to red emission-colors; chemical pure carbonate should yield a blue CL-color caused by the defects in the lattice structure. The most common quencher ions are Fe^{2+} and Ni^{2+}. Complete quenching of CL by >1.5 wt% Fe^{2+} results in absence of luminescence, whereas lower Fe^{2+} concentrations will induce a dull brown luminescence. However, Fe and Mn tend to occur together in carbonate minerals, therefore, mutual degrees of activation and quenching is expected to occur. In carbonates with <1 wt% Fe, the Mn/Fe relation is the determining factor in CL intensity and the presence of appropriate amounts of both, Fe and Mn, will lead to a brown CL color, as shown by Fairchild (1983). The substitution of Mg^{2+} for Mn^{2+} produces more reddish CL colors (Amieux, 1982), and generally, Mg-poor calcites have a yellow CL resulting from the dominant Mn luminescence, whereas Mg-rich calcites have an orange to red CL color.

The focus of this study was on the carbonate clasts and globules in the ejecta deposits with textures indicative of quenching from a melt, which, according to the microprobe analysis, show a distinct iron- and magnesium-enrichment of up to 1 wt%. As outlined above, such amounts of Fe and Mg, in concert with the manganese content (between 0.1 to 0.4 wt%), should result either in the total quenching of luminescence, or in a dull-brown luminescence. However, is conceivable that the probably defect-rich lattice structure of these quenched carbonate

crystals (from high cooling rates) induce a bright luminescence, since defects in the crystal-structure are activators of luminescence.

The results of the CL investigation show that the quenched carbonate clast and globules, as well as the carbonate in ejecta particles, have a very low dark ('brick') red to dull-brown luminescence or show even total absence of luminescence (Fig. 2.23). Therefore, the CL-quenching effects resulting from the Fe-and Mg-enrichment appear to take priority over the CL induced by lattice-defects. Moreover, the brick red or dull brown luminescence color of the radially arranged carbonate crystals stands out clearly against the yellow to orange colored luminescence of the microspar and marly matrix to the spherules; no concentric zoning has been observed that could give proof of multiple stages of diagenetic precipitation of carbonate. In addition, non-quenched carbonate clasts, as well as vesicle infillings by calcite, commonly show orange or yellow luminescence, and occasionally bluish shining radially arranged crystals, probably zeolites, have been observed in vesicles in spherules. However, no evidence for the presence of organic material, which commonly shows intensive blue fluorescence, has been observed. The survey of more than twenty thin sections from spherule deposits in Rancho Nuevo, La Sierrita, El Peñon, and El Mimbral, shows that this luminescence behavior appears to be a characteristic feature of the carbonate clasts and the quenched calcite in all outcrops studied, independent of the microfacies-type of the ejecta deposit.

2.3.9 Magnetic mineralogy

The optical microscopy allows the detection and the evaluation of opaque phases, which are generally related to paramagnetic, antiferromagnetic, and ferrimagnetic phases, for instance chlorite, hematite, or magnetite (e.g., Haggerty, 1991). Further constraints on these opaque phases can be made by BSE imaging and sustaining EMP analysis, which are powerful tools to monitor their mineralogy and geochemistry since these phases generally have high

Figure 2.24 (page 57) BSE-images showing magnetic mineral phases and Fe-Ti oxide textures from spherule deposits in northeastern Mexico. Abbreviations: Fe-Ti-K-rich schlieren, S; calcite, Cz; chlorite, Ch; calcite globules, Cz-g; Fe and Mg-rich globules, Fe-g. (**A**) and (**B**) 5-15 μm-sized hematite crystals in ejecta particles (A in chlorite; B in calcite). Some crystals have a zoned composition with a distinct Si (5-10 wt%) and Ni (~0.4 wt%) enrichment in the core. (**C**), (**D**), and (**E**) Ti- and Fe-rich lamellae in a chlorite spherules with rhythmic garland-shaped textures. Crystal sizes of Ti-Fe-oxides, as well as the Ti content, increases towards the carbonaceous interior of the ejecta particles with rutile as an end member; brightest points have the highest Ti-contents. (**F**) Skeletal growth of Ti-Fe oxides (up to 50 μm in size) within a chlorite spherule, resembling a spinifex texture (cf. Kontny et al., 2003). Note the lath- and hourglass-shaped and cruciform Ti-Fe oxides with slanted end-phases. (**G**) Carbonate globule with Fe-oxides (goethite and hematite). (**H**) Carbonate spherule with radially arranged intergrown calcite crystals (bright phases) and Fe-Ti-oxides (dark).
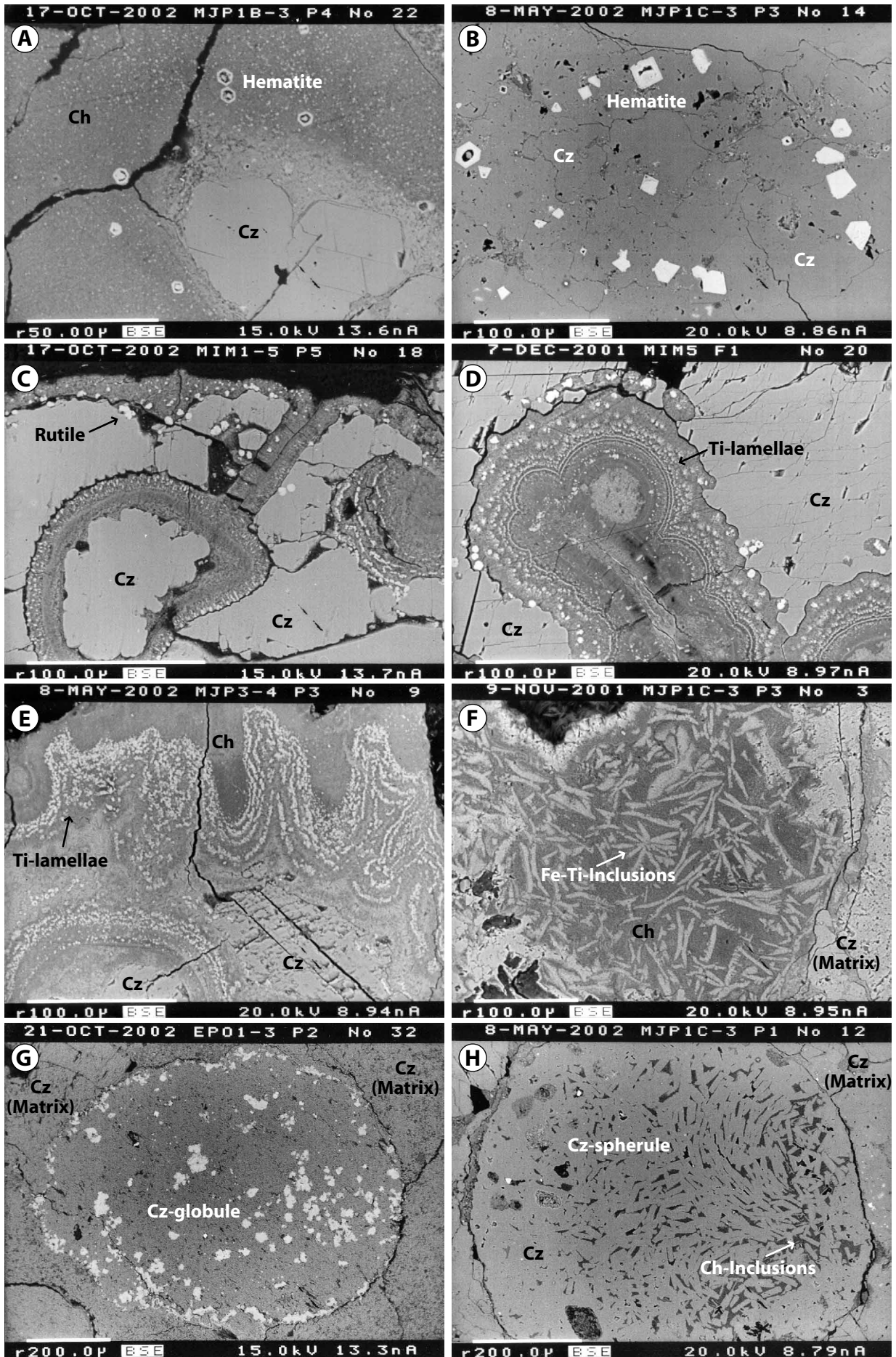
Figure 2.24 (caption on page 56).

Z elements (e.g., Fe, Ti, Ni) that provide good optical contrast to the enclosing host phase, which generally has low *Z* elements (e.g., Si, Ca).

The optical microscopy, the BSE images, and the EMP analysis of spherule deposits from northeastern Mexico show that opaque phases in Fe- and Mg-rich chlorite spherules and fragments are goethite, hematite, rutile, and Ti-Fe oxides (Fig. 2.24). Opaque phases occur as tiny μm-sized grains that constitute either single, isolated crystals, occasionally with dendritic or skeletal shape, or they are arranged as garland-shaped lamellae (Fig. 2.24A-F). Goethite may also occur as agglomerated rounded masses, preferentially inside cavities. These opaque phases are even present in the carbonate phase in spherules, as well as in carbonate globules (Fig. 2.24G-H). In contrast, in the sparitic or micritic matrix to the ejecta particles, opaque phases are significantly less abundant.

The cubic and hexagonal goethite crystals are about 5 to 20 μm in size and frequently show a zonar composition with elevated SiO_2 (4-8 wt%) and NiO (up to 0.4 wt%) concentrations in the cores of crystals (Fig. 2.24A, B). The goethite and hematite may have formed either authigenically or as replacement product of cubic minerals, such as magnetite or pyrite, during diagenesis, which both would explain their rather unusual cubic- and hexagonal-formed grains. The precursor minerals to the goethite and hematite, including magnetite or pyrite, may then have formed primary from melt or during subsequent diagenesis.

The prominent garland-shaped Ti- and Fe-rich lamellae in the chlorite spherules and fragments often have a distinct 'onion-ring-like' appearance with multiple stacked rings (Fig.2.24C-E). The grain sizes of the opaque minerals in these lamellae range from below the resolution of the EMP with crystal size growing towards the interior of grains up to 5-10 μm. These inclusions become essentially pure rutile (TiO_2) at the edge of the carbonate interior of the spherule. This characteristic pattern of grain-inward directed concomitant increasing crystal sizes, and Ti contents may indicate progressive 'expelling' of incompatible elements (e.g., Ti) from the melt during rapid cooling, or it may be related to diagenetic processes. However, the presence of these lamellae in tiny broken spherule fragments that are 'swim-
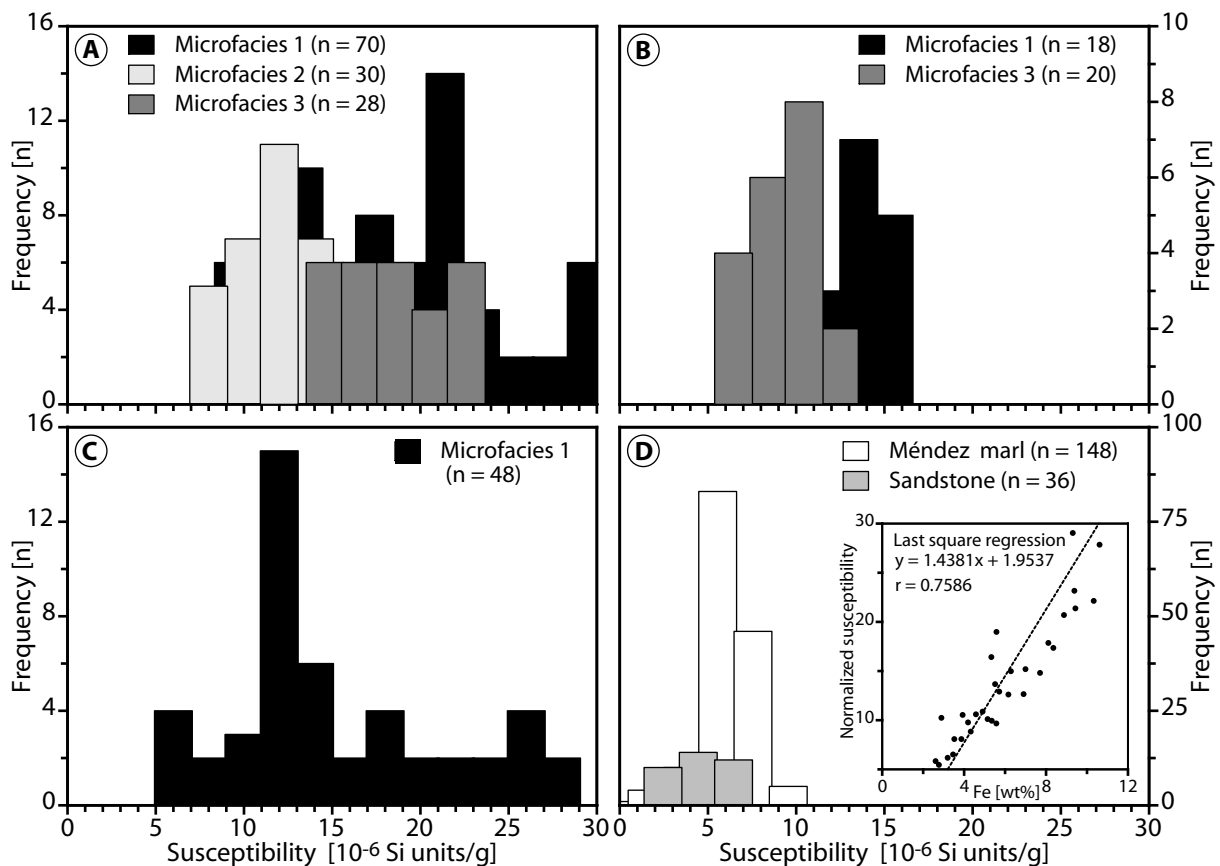
Figure 2.25 Frequency distribution of volume magnetic susceptibility for spherule deposits according to their microfacies and outcrop localities: (**A**) La Sierrita area, (**B**) El Peñon area, and (**C**) El Mimbral, compared to (**D**) the enclosing marls and sandstones. The inset in (**D**) shows a scatterplot with the bulk Fe_2O_3 content (from WDS analysis) drawn against the magnetic susceptibility, illustrating the high correlation between both.

ming' in the carbonate blebs inside spherules, rather suggests a primary origin and consequently suggest prolonged cooling inside the grain, probably related to the enlarged thermal diffusivity of the carbonate melt when compared to the siliceous melt (Treiman, 1989), as outlined in the petrology section.

Quite outstanding petrological textures of the iron-rich chlorite spherules are 10-40 μm-sized cruciform, lath-shaped, and dendritic-skeletal crystals of Ti-Fe oxides (Fig. 2.24F). Their crystal shape and arrangement are similar to 'spinifex textures' in the rims of oceanic pillow basalts and, by analogy, suggests rapid quenching from a melt (Bryan, 1972).

2.3.10 Volume susceptibility

The volume magnetic susceptibility of a rock reflects the contents of dia- (e.g., calcite), para- (e.g., chlorite), and ferromagnetic (e.g., magnetite) phases per volume unit (Dunlop and Özdemir, 1997; Butler, 1998). Diamagnetic minerals have low negative susceptibilities (below about -10^{-6} SI) and paramagnetic minerals have low- to intermediate susceptibilities (10^{-6}-10^{-3} SI), whereas ferromagnetic minerals show very high susceptibilities $>10^{-3}$ SI (Hunt et al., 1995; Dunlop and Özdemir, 1997). Therefore, the volume

magnetic susceptibility is a very sensitive tool to detect even low amounts of ferromagnetic phases.

The ejecta deposits from northeastern Mexico show uniform paramagnetic values of the volume magnetic susceptibility (Fig. 2.25). Samples from the La Sierrita area show paramagnetic magnetic susceptibility values that range between 6 and 30 x 10^{-6} SI/g and that correlate well with the bulk Fe-content (correlation coefficient r ~0.76; inset in Fig. 2.25D). The microfacies-type 1 ejecta deposits cover the broadest range from about 8 to 30 x 10^{-6} SI/g, whereas the microfacies-type 2 show the lowest values and a limited range (7 to 14 x 10^{-6} SI/g). The microfacies-type 3 shows similar high MS values as the microfacies-type 1, but a more limited range (14 to 24 x 10^{-6} SI/g). The samples from the El Peñon sections (microfacies-type 1 and 3) show a smaller range from 6 to 16 x 10^{-6} SI/g, whereas the samples from the El Mimbral locality (microfacies-type 1-3) have a very broad range with susceptibilities from 5 to 28 x 10^{-6} SI/g.

The Méndez marls and the sand-siltstones display distinctly lower volume magnetic susceptibility values compared to the ejecta deposits, that cover a more limited range from about zero to 10 x 10^{-6} SI/g.
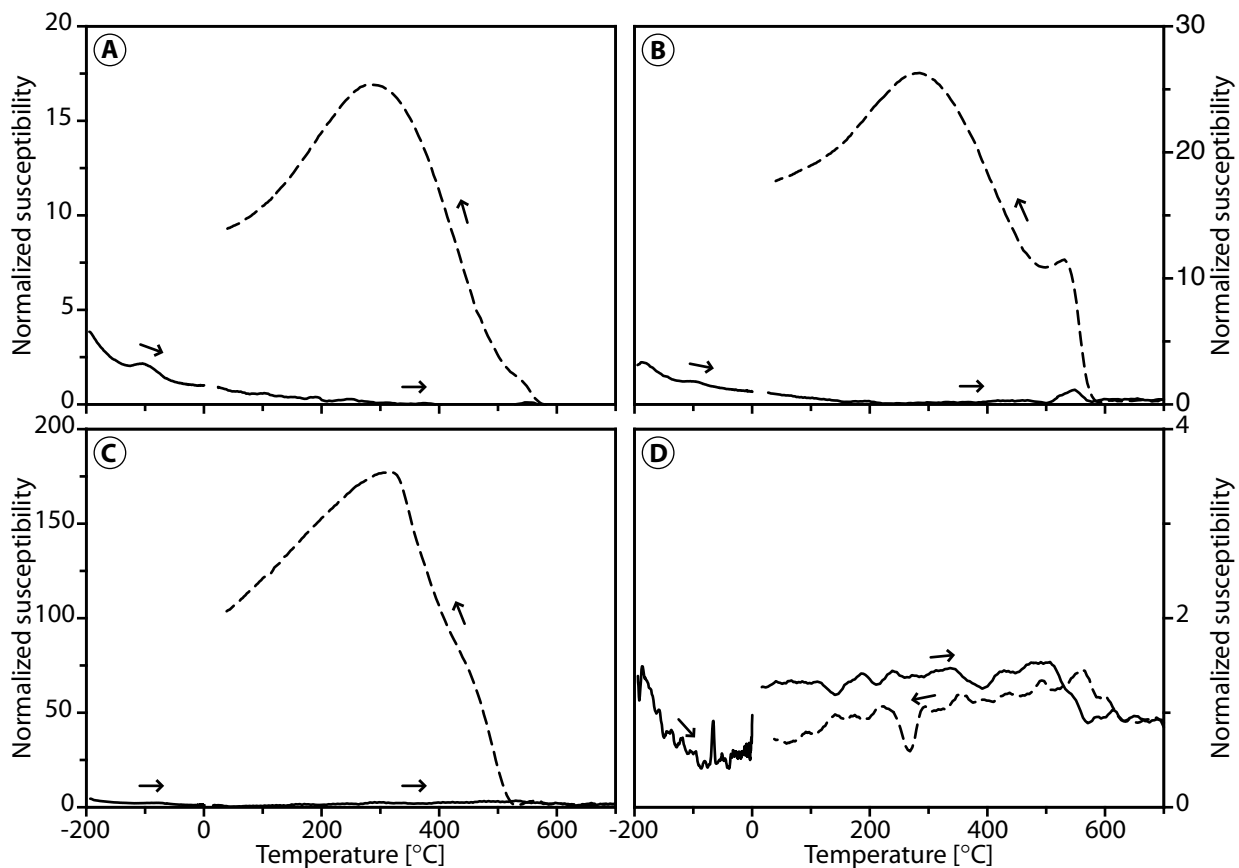
Figure 2.26 Typical curves showing the temperature-dependence of MS and Curie temperatures of the studied spherule deposits in northeastern Mexico. (**A**) Microfacies-type 1 (Sample MJP1B-3); (**B**) microfacies-type 1 (LDP3-14); (**C**) microfacies-type 3 (MJP1A-14); (**D**) sandstone (MJP1B-1).

Remarkably, the range of the magnetic susceptibility values is closely related to the respective microfacies-type, with a distinctive wider range for the microfacies-type 1. Microfacies-type 1 is considered as 'almost' pristine ejecta fallout, with little reworking and dilution. The higher magnetic susceptibility values for these deposits in the La Sierrita and El Mimbral area confirm this petrographic assignation. The similar range of the slight sandy microfacies-type 3 spherule deposits sustains the low degree of reworking and dilution that has been revealed from petrological, mineralogical, and geochemical methods. In contrast, the significant lower magnetic susceptibility values of the marly microfacies-type 2 reflect progressive admixture of Méndez marls during soft-sediment mass-movements and reworking.

2.3.11 Temperature-dependence of susceptibility

The temperature-dependent susceptibility allows identification of the different magnetic phases (minerals) by monitoring their characteristic phase transitions and the related temperatures (e.g., Curie or Néel temperature Dunlop and Özdemir, 1997; Butler, 1998).

The κ-T curves in Fig. 2.26 show that the samples from spherule deposits in northeastern Mexico behave in very similar ways: The temperature-dependent magnetic susceptibility from –192 to 700 °C shows low values and an exponential decrease, indicating mainly a paramagnetic behavior. However, a small peak is superimposed at –80 °C on the paramagnetic curve either suggesting a Curie or Néel temperature or reflecting grain-size effects of a not yet identified ferromagnetic phase (Dunlop and Özdemir, 1997). The heating and cooling runs are irreversible and the heating leg of several samples shows

a small peak at 560-580 °C that may be diagnostic for the presence of fine-grained (single domain) magnetite. The heating is associated with a pronounced color change from the grey-brown sample to a brick red color. Considerable amounts of weight were lost during the heating process (as shown by the large zero drift), presumably by water released from hydrated minerals. The cooling leg displays two Curie temperatures at 570 and 480 °C, indicating transformation during heating of paramagnetic iron-bearing minerals into magnetite or magnetite-near phases. Resulting from the inert argon atmosphere, a reduction of Fe^{3+}-bearing phases into magnetite is assumed to cause this irreversibility. However, no characteristic Curie temperature related either to goethite or to hematite has been detected; this absence could be linked to the observed impurities (Si, Al, Ni) or non-stoichiometry.

2.3.12 Remanent magnetization

The isothermal remanent magnetization (IRM) acquisition and alternating field (AF) demagnetization are methods employed for inferring magnetic domain behavior, for instance to characterize magnetically "soft" (e.g., magnetite) and "hard" (e.g., goethite) phases (e.g., Lowrie, 1990; Dunlop and Özdemir, 1997; Butler, 1998).

Four samples of spherule deposits from La Sierrita, El Peñon, and El Mimbral were prepared to use in IRM and AF experiments by coring cylinders with a diameter of 2.5 cm and length of 2 cm from well-indurated specimens. The measurements show that the intensity of the natural remanent magnetization (NRM) of these samples is very small and shows maximum values of about 0.3-0.7 mA/m (Fig. 2.27). In fields below 10 mT, the alternating field-demag-
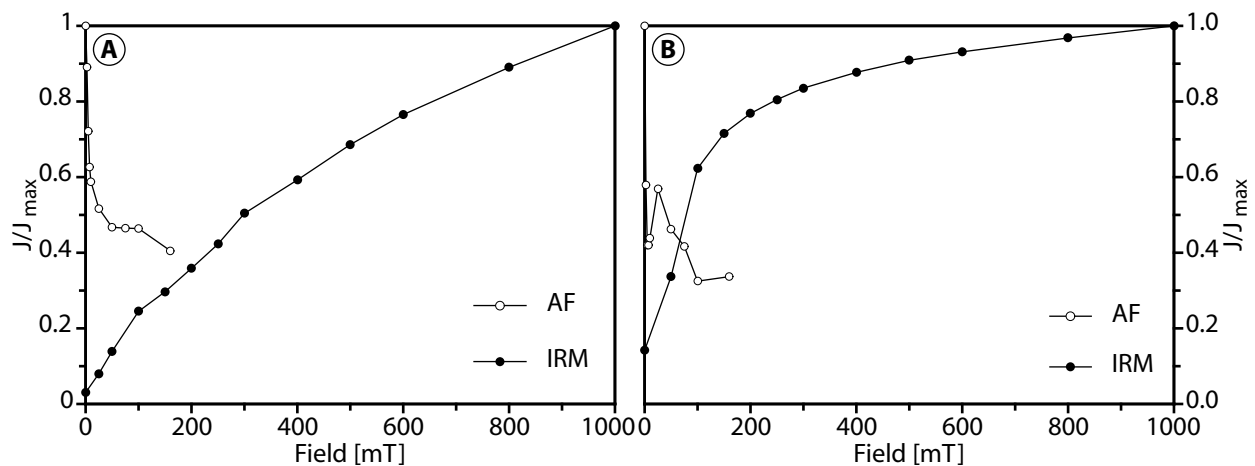
Figure 2.27 Alternating field demagnetization and isothermal remanent magnetization in peak fields up to 160 mT of natural remanent magnetization for typical ejecta samples from the La Sierrita area comprising (**A**) microfacies-type 1 (Sample MJP3A-1), and (**B**) microfacies-type 3 (MJP1A-5).

netization of NRM shows an initial rapid decrease of about 50 % of the original intensity, whereas in fields of 160 mT no further demagnetization occurs. The induced remanent magnetization (IRM) acquisition curves show that some studied samples are nearly saturated in fields of 1000 mT while others are not. Furthermore, the IRM data confirm the dominant presence of high coercive minerals, for instance hematite and goethite (Dunlop and Özdemir, 1997).

2.4 Interpretation and discussion 1: Target lithologies and impact processes

Spherule deposits from K-P outcrops in northeastern Mexico are texturally and compositionally complex and exhibit various petrologic features and geochemical ranges that allow the evaluation of their origin and comparison with spherule deposits in other K-P boundary localities.

2.4.1 Origin of spherule deposits

The characteristic morphological features of spherules, including their fluidal-shaped form and internal textures, such as vesicles and schlieren are indicative of an origin as molten droplets from highly fluid melt with subsequent exsolution of a gas phase because of pressure release and cooling (Shelley, 1993; Engelhardt et al., 1995). The abundance of spherical particles suggests surface tension control on their shape, implying low viscosity, probably at temperatures well above the solidus (Freundt and Schmincke, 1998). The same applies to the angular fragments with similar flow-textures, though their irregular shapes and less abundant vesicles point to a different thermal history and indicate either fragmentation in a ductile-rigid state by turbulence in the air, or by thermal stress owed to quenching with water (Glass et al., 1997). Pyroclasts of comparable size and shape have been described for impact ejecta (Stähle, 1972; Graup, 1981; Glass, 1990; Izett, 1991; Engelhardt et al., 1995; Dressler and Reimold, 2001), and for specific volcanic processes (Cas and Wright, 1987; Fisher and Schmincke, 1984; Robin et al., 1996). However, a volcanic origin seems unlikely because of the following observations:

(1) The coarse grain size of the spherule deposits in northeastern Mexico would require a nearby vent (Fisher and Schmincke, 1984) and to date no volcanic source is known close to these outcrops (e.g., Perez Cruz, 1993).

(2) The multiple compositional phases (Fe-Mg-rich and Si-Al-K-rich phases, carbonate, lithic inclu-

sions) that are present even in single spherules indicate the simultaneous ejection of several batches of compositionally distinct melt and sediment into the air, which is incompatible with known volcanogenic sources that also generally have a more narrow compositional range (e.g., Fisher and Schmincke, 1984). In addition, these distinct compositions are unlike differentiation and fractionation trends commonly observed in sub-volcanic, magmatic systems (Kring and Boynton, 1992).

(3) Further evidence sustaining an impact origin of the spherule deposits is concluded from the presence of shocked quartz in the spherule beds of El Mimbral and Loma Cerca, in the southern La Sierrita area (Smit et al., 1992b; Keller et al., 2002 p. 148), and from trace element studies in K-P sections from spherule deposits at northeastern Mexico by the working group of Doris Stüben, IMG Karlsruhe (written communication, 2003). Their plot of first-row transition element (V, Cr, Ni) versus immobile element (Zr, Ti, Al) concentrations in the discrimination diagram of Andreozzi et al. (1997) showed that all samples from spherule deposits are in the field for terrigeneous sediments, providing no evidence for a volcaniclastic component. A similar conclusion was drawn by this group for spherule deposits at Beloc, Haiti (Stüben et al., 2002).

Consequently, an impact-origin appears to be the most reasonable explanation and is consistent with the interpretation of morphologically similar K-P boundary spherules that have been attributed to the Chicxulub impact on the Yucatán peninsula (Table 2.1 with references).

2.4.2 Implications from petrological characteristics

The salient petrological features of the ejecta particles (e.g., schlieren, tektite in tektite structures, liquid immiscibility textures, accretionary clasts) and the microfacies characteristics of the spherule beds (welding textures) provide not only further compelling evidence for an impact-origin of the spherule deposits but also provides constrains to the physical conditions during, and immediately following, the impact process.

Schlieren, microliths, and opaque inclusions in ejecta particles

The **Fe-Ti-K-rich schlieren**, as well as marl-carbonate-inclusions, and the general absence of microliths in ejecta particles may document the rapid and

violent mixing of melt from different origins, contamination with (unmolten) lithic clasts, and rapid quenching (Stähle, 1972; Engelhardt et al., 1995; See et al., 1998). Such fast melting and cooling prevents the melt from homogenization and crystal growth (Glass, 1990; Izett, 1991). These features are characteristic of impact glasses (e.g., Stähle, 1972; Glass, 1990; Engelhardt et al., 1995; See et al., 1998; Dressler and Reimold, 2001) and are rarely observed in volcanogenic pyroclasts (Fisher and Schmincke, 1984; Cas and Wright, 1987). Schlieren are also a prominent feature of spherules from the K-P transition in Beloc, Haiti, though these schlieren are distinct by their Ca- and S-enrichment (e.g., Izett, 1991; Bohor and Glass, 1995; Stüben et al., 2002).

The **microliths** in ejecta particles are interpreted as devitrification products that developed during somewhat slower cooling (Shelley, 1993). This occurs during quenching in response to high degrees of undercooling and supersaturation, and low nucleation densities (Donaldson, 1976). Albeit these microliths are now pseudomorphically replaced by calcite or chlorite, their characteristic shapes may constrain their initial mineralogy. It is distinguished between (i) thin skeletal and branching crystals that are analogous to pyroxene and olivine textures observed in quenched mafic melt by laboratory experiments as well as in impact glasses of mafic composition (Donaldson, 1976; Jones et al., 2000; Hörz and See, 2000), (ii) characteristic crisscross patterns with twinned individuals, similar to quenched K-feldspar (Lofgren, 1974; Shelley, 1993), and (iii) dark radial hairlike crystals, analogous to pyroxene-whiskers observed in impact glass from the Ries impact structure (Stähle, 1972; Engelhardt et al., 1995). Such microliths have rarely been observed in spherules from the K-P transition in other localities (e.g., Izett, 1991; Bohor and Glass, 1995), but are characteristic features of microkrystites from the K-P boundary clay layer (e.g., Montanari, 1991; Smit et al., 1992a; Smit, 1999; Martínez-Ruiz et al., 1997), as well as from late Eocene microtektites (e.g., Glass and Koeberl, 1999).

The **Fe-Mg-rich globules** in the chlorite ejecta particles may be interpreted as exsolution or segregation of distinct phases in the melt, according to similar observations in igneous rocks (e.g., Philpotts, 1990) and impact-generated glasses (Delano and Hanson, 1996). The elongated and twisted forms of the globules argue against an exclusive diagenetic origin. Such immiscible melt globules may have been stretched by flow movements of the melt and

suggest that quenching preceded completion of the mixing process (Delano and Hanson, 1996). They are unique to spherules from northeastern Mexico and have not been found in other K-P localities to date.

The **hematite** and **goethite crystals** formed either primary from melt or as replacement product of cubic minerals such as magnetite or pyrite during diagenesis (Philpotts, 1990), as outlined in the rock magnetic section.

The μm-sized **metallic** or **sulfidic Ni-Co-rich inclusions** may indicate contamination from meteoritic material as refractory grains or condensed droplets since these elements are commonly concentrated in extraterrestrial matter (see Grieve et al., 1980; Schmidt et al., 1997; Koeberl, 1998; Hart et al., 2002). An analogous explanation may apply to the μm-sized P(?)- or Ir(?)-Ni-rich grains found in the El Mimbral spherule bed. They may either be indicative of the phosphide minerals schreibersite $(Fe,Ni)_3P$, barringerite $(Fe,Ni)_2P$, or rhabdite $(Fe,Ni)P$ (e.g., Japel et al., 2002). Alternatively, they may be interpreted as Ni-Ir rich inclusions, resulting from contamination by extraterrestrial material (e.g., Hart et al., 2002). A contribution from extraterrestrial material could also account for the rather unusual Ni-enrichment in hematite crystals. Ni-rich iron oxides have also been reported by Soria et al. (2001) for spherules from northeastern Mexico and are common in from microkrystites from the K-P boundary clay (e.g., Doehne and Margolis, 1990; Montanari, 1991; Martínez-Ruiz et al., 1997; Bauluz et al., 2000; Claeys et al., 2002). In summary, the presence of several types of Ni-Co-and possibly Ir-rich metallic and sulfidic inclusions strongly suggest a distinct contamination by meteoritic material.

Liquid immiscibility in ejecta particles

The ejecta particles are principally made of carbonate and compositionally distinct silicate phases, which all show a range of particular petrological features including alternating layers of contrasting composition ('tektite in tektite' configuration) or radially oriented needle-like calcite crystals. These unique features may be attributed to diagenetic processes such as incipient to pervasive stages of particle alteration (Bohor and Glass, 1995; Morris et al., 1998) or inorganic carbonate precipitation (e.g., Tucker and Wright, 1992). However, several observations are difficult to reconcile with an exclusive diagenetic origin of these petrological features: (i) irregular and broken silica particles with abrasion

textures in the cores of spherules which are mutually enclosed by layers of carbonate and silicate phases, (ii) the elongated and twisted forms of the Fe-Mg-globules in spherules suggest a liquid precursor state, and (iii) knife-sharp transitions between compositionally distinct silicic phases. In addition, the carbonate phase reveals further characteristic textures: (a) individual calcite globules are confined to the spherule deposits and show no traces of later infilling by diagenesis ('marble-like' carbonate texture), (b) the 'emulsion-like' textures of carbonate intermingling with silicate, (c) the coalesced calcite globules in spherules and ejecta-fragments, and (d) the curved concave-convex menisci with sharp boundaries between spherules, fragments, and carbonate overgrowths or inclusions. These textures are interrupted along fractures of broken spherules, fragments, and carbonates, and therefore appear to predate diagenesis.

According to petrologic and experimental data provided by Graup (1999), Jones et al. (2000), and Osinski et al. (2001), these microtextures are indicative of liquid immiscibility with different silicate melts and large parts of the calcite initially being in a liquid state. Hence, the presence of multiple geochemical phases in single ejecta particles provides evidence for the coexistence of compositionally different melts and melt in variable cooling stages up to cooled silicic fragments that were subsequently surrounded by carbonate melt and finally by silicic melt again. The carbonate overgrowths on spherules and fragments with radially aligned elongate, needle-like calcite crystals ('feathery calcite') are in keeping with this interpretation as they may attest to rapid cooling from a carbonate melt (Graup, 1999). Ejecta particles with analogous textures are present in suevite from the Ries impact structure, Germany (Graup, 1999), the Haughton impact structure, Canada (Martinez et al., 1994; Graup, 1999; Osinski and Spray, 2001), and the Chicxulub impact structure (Jones et al., 2000), whereas evidence for a volcanic origin is generally restricted to carbonatites and alkali-basaltic volcanism (e.g., Philpotts, 1990; Graup, 1999).

Reasonable explanations for the ubiquitous presence of immiscibility features observed in the spherule deposits at northeastern Mexico derive from the physical properties of the compositionally melt phases. For polymerized silicic melts, the physical properties depend on the amounts of polymer modifiers (e.g., Mg) versus polymer formers (e.g., Si), which results in specific liquidus temperatures,

for instance ~750 °C for a granitic and ~1100 °C for a basaltic melt at atmospheric pressure, as well as in a lower viscosity for basaltic melts (e.g., Philpotts, 1990; Heide et al., 2001; Osinski and Spray, 2001). In contrast, carbonate melts are unpolymerized ionic liquids and do not associate with the silicate anions in the melt, resulting in the effect known as "carbonate-silicic liquid immiscibility" (Graup, 1999). The liquidus temperature of carbonate melts is about 500-600 °C, which is several hundred degrees lower than for silicate melts, as outlined above (e.g., Philpotts, 1990; Osinski and Spray, 2001). Therefore, carbonate melts may be slightly longer in a liquid state, whereas the silicic melt fraction has already quenched to glasses or is in a more viscous state (Barker, 1989). This behavior may explain the thick carbonate overgrowths on spherules and fragments, indicating that the carbonaceous matrix was a hot liquid, whereas the silicate melt was at least partly solid.

This 'delayed' cooling of the carbonate phase may be enhanced by the low thermal diffusivity of carbonate melt which is more than a magnitude smaller than for basaltic melt, so that carbonatite melts will cool distinctly more slowly than siliceous melts (Dawson et al., 1990). Moreover, the viscosity of carbonate melts is extremely low (10^{-2} poise) and comparable to the viscosity of water (Treiman, 1989), resulting in an enormous wetting power with the potential to infiltrate thin cracks or porous media. These physical properties may explain the complex carbonate veins observed in the spherules (Graup, 1999; Osinski and Spray, 2001). The repeatedly surrounding by hot molten carbonaceous ejecta melts may have induced thermal stress inside the 'cool' host grains, leading to their partial melting and disruption and the subsequent intrusion of carbonate into the cracks. Hence, the particular multiple coated ejecta particles ('tektite in tektite' textures) record the time-temperature path from ejection of the melt until cooling at the water surface, well comparable to "coated gneiss" bombs observed at the Popigai impact structure (Masaitis and Deutsch, 1999; Kettrup et al., 2003). Such impact glass shells may have originated when the ejected spherules and fragments passed through different parts of the turbulent vapour cloud above the growing crater, and their trajectory passed the ejecta curtain or the expanding fireball (Kerschhofer et al., 2000).

In conclusion, these observations provide unequivocal evidence not only for the silicic glasses, but also for large parts of the calcite as initially being

in a liquid state. The coexistence of compositionally distinct silicic and carbonaceous melt phases, however, suggests that in this part of the ejecta curtain (or fireball), the thermal energy, turbulences, and pressure may have been already low enough to allow their coexistence without the necessity to produce homogenized melts. In other words, the expansion or cooling of the ejecta curtain was already in an advanced stage that precluded intense mixture and melt homogenization. It is remarkable that, with exception of marl and carbonate clasts, no lithic clasts with lower degrees of shock state (i.e., basement clasts or diaplectic glasses) have been observed in the spherule deposits, therefore, the spherule deposits appear to be comprised entirely of former liquid-state glasses and hence are indicative of "shock state IV," comprising shock pressures of 60-80 Gpa and postshock temperatures of 1300-3000 °C (Stöffler, 1971; Engelhardt et al., 1997; French, 1998).

Accretionary lapilli-like ejecta

Accretionary lapilli has been observed in deposits of active and ancient explosive volcanoes throughout the world, and it is especially common in phreato-magmatic tephra deposits forming in laterally-expanding turbulent wet ash clouds (cf. Schumacher and Schmincke, 1995 and references therein). Two possible modes of lapilli origination have been distinguished by Schumacher and Schminke (1991; 1995): (i) in co-ignimbrite ashfall from the eruptive ash cloud and (ii) in pyroclastic flows and surges. In addition, lapilli may be associated with the direct explosive "blast surge" and may form during lateral spreading of the surge (see Schumacher and Schmincke, 1995; Glicken, 1996). Accretionary lapilli has also been reported from impact ejecta deposits of the Ries impact structure, Germany (Graup, 1981), the Alamo impact structure, Texas (Warme et al., 2002), and the Chicxulub impact structure from the Gulf of Mexico area (Chapter 3 and Pope et al., 1999; Salge et al., 2000; Yancey, 2002).

The genesis of accretionary lapilli is probably analogous for volcanic- and impact-generated lapilli, and therefore related to cooling and condensation of moisture in the ash cloud or ejecta curtain, which leads to the rapid agglutinization of ash forming cores of accretionary lapilli (Graup, 1981; Schumacher and Schmincke, 1991; Gilbert and Lane, 1994; Schumacher and Schmincke, 1995; Warme et al., 2002). During the later fall or movement through the ash cloud or ejecta curtain, ash adhering to the outer surface of the lapillus builds up an outer shell. Aside

from moisture and van-der-Waals forces, electrostatic forces may be also responsible for this process, leading to an outward growth of these particles (e.g., Schumacher and Schmincke, 1995). Multiple accretionary layers in lapilli particles may be produced by passage through several successive envelopes of the cloud or ejecta curtain probably associated with turbulent currents.

For the Chicxulub impact structure, the marine conditions at the target area on the water-saturated Yucatán carbonate platform therefore may have favored the generation of accretionary lapilli by providing large amounts of water in the ejecta curtain or ejecta ash cloud. During crater-outward movement of the ejecta curtain atop of the sea surface, water may have become incorporated by vaporization, analogous to the expansion of volcanic pyroclastic flows in marine settings (e.g., Cas and Wright, 1991; Allen and Cas, 2001). Considering the impact-generated accretionary lapilli found in northeastern Mexico and in Texas (Yancey, 2002 and Chapter 3), an origin by direct fallout from the impact cloud appears to be unlikely because of the large distance of these locations to the impact crater rather points to ballistic transport. Therefore, an origin associated with the expanding ejecta curtain or its collapse seems to be conceivable and is in keeping with petrological data from the basal units of the Chicxulub suevite (Stöffler et al., 2003) and welding of ejecta particles in northeastern Mexico, as outlined below.

Welding and amalgamation of ejecta particles

Welding and amalgamation of ejecta particles as well as the enveloping of carbonate clasts, marl, and benthic foraminifera, could have resulted from compaction by sediment overload (Tucker and Wright, 1992; Collinson, 1994; Bohor, 1996). Most of these particles, however, show a random grain orientation. Particularly, the fragile accretionary lapilli show no signs of flattening, nor are the long axes of the flattened vesicles or internal structures aligned parallel to the bedding plane. Combined with the three-dimensional mesh-like fabric, the pore space, and the good preservation of components, this suggests that these structures originated in a ductile state before cooling (Cas and Wright, 1991; Kokelaar and Busby, 1992; Freundt and Schmincke, 1998). Further evidence for a primary origin of these particular welding-features comes from the observation that they are essentially restricted to the microfacies-type 1-ejecta deposits and have not been observed in the microfacies-type 3 deposits, though both ejecta
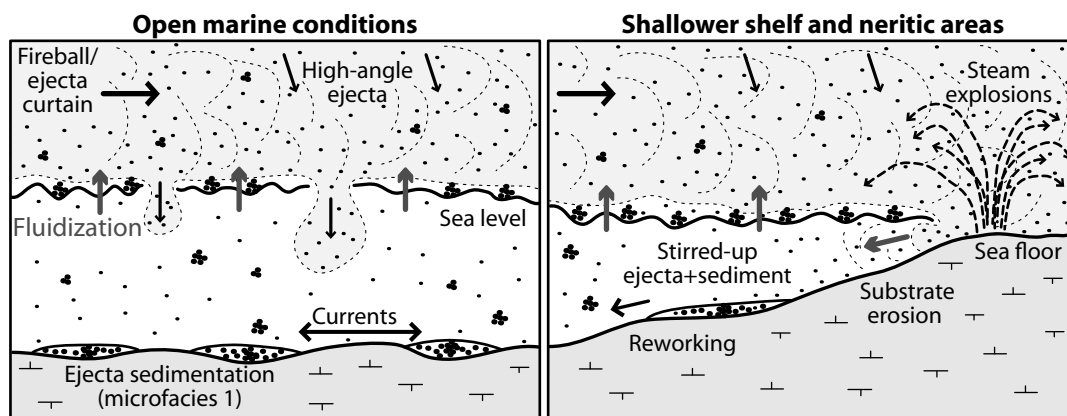
Figure 2.28 Conceptual sketch based on the hypothesis that the ejecta curtain of the Chicxulub impact behaves similar to a pyroclastic flow. It demonstrates the initial ejecta-dispersion by the vapor-rich ejecta curtain, gliding over the sea and entering shallower marine settings, causing large steam explosions; modified after Cas and Wright (1991) and Freundt and Schminke (1998). Legend provided in Fig. 2.5.

deposits underwent the same post-depositional history and burial depth. Such a selective occurrence is not compatible with an exclusively diagenetic origin of these features by sediment overload. In addition, transport and emplacement as hot ejecta on the sea floor at high temperatures is unlikely, because of the paleowater depth of 300-1000 m (Alegret et al., 2001; Soria et al., 2001) and the small thickness of the deposits (e.g., Cas and Wright, 1991).

Consequently, another mechanism is required to account for these features. Following the interpretation of volcanic ignimbrite deposits by Freundt and Schminke (1998), the amalgamated, and welded ejecta particles may have formed by accretion and mingling of compositionally distinct ejected melts at a range of temperatures during transport in the expanding ejecta curtain. A possible scenario for ejecta dispersion is shown in Fig. 2.28 and based on observations from volcanic pyroclastics. Welded ejecta particles imply a hot transport system in which the particles possibly remained in a liquid or viscous state for a considerable time. The hot liquid ejecta droplets completely coalesced to form dense, smooth rims, whereas cooler, more viscous ejecta particles variably and mutually welded-amalgamated with, or enveloped other particles. The significance of composite and sintered particles is that they document the viscous coalescence of liquid droplets during high temperature transport. The high temperatures during ejection and initial transport in impact events correspond to low melt viscosities, facilitating particle coalescence and hence, thorough welding of particles (e.g., French, 1998). The turbulent conditions in the ejecta curtain or plume (fireball), however, are opposed to this inclination of particle behavior, since it leads to particle disruption

and abrasion during collisions. Therefore, the ejecta cloud must be significantly diluted before considerable agglomeration of particles can happen.

2.4.3 Alteration of silicic ejecta phases

To reconstruct parental phases to the ejecta found in northeastern Mexico, and to constrain possible target lithologies, it is important to evaluate diagenetic effects as well as to discriminate original and secondary signatures before conducting a comparative analysis to ejecta material from other localities and melt rocks of the Chicxulub impact structure.

The results from the mineralogical and geochemical analysis of spherules and fragments from northeastern Mexico suggest that they originally quenched from impact melts of variable, though predominantly mafic to intermediate felsic composition. The ubiquitous presence of secondary phases (e.g., chlorite, chlorite-smectite, Fe-oxides and -hydroxides) and the low oxide totals of the Si-Al-K-rich glass suggest the pervasive submarine alteration of the former glass phase (see Fisher and Schmincke, 1984; Berger et al., 1994; Mørk et al., 2001; Utzmann et al., 2002). By that, the chlorite may either have formed by direct replacement of the glass phase or of secondary phases such as Fe-Mg-rich smectite or palagonite that replaced the glass during early diagenesis (e.g., Fisher and Schmincke, 1984; Daux et al., 1994; Utzmann et al., 2002), whereas the Si-Al-K-rich glass may show a more pristine composition. However, the following observations suggest that the influx of diagenesis did not alter the general compositional trends of the ejecta particles fundamentally, hence, they may indeed represent multiple ejecta phases of originally different composition that is

now reflected in the Fe-Mg-rich chlorite and Si-Al-K-rich glassy ejecta phases:

(1) A progenitor of mafic composition is in line with the relict crystals in spherules and fragments, interpreted to be pseudomorphs of rapidly cooled pyroxene, feldspar, and olivine crystals (cf. Lofgren, 1974; Carstens, 1975; Donaldson, 1976).

(2) Elements such as Ti, Al, and Fe are relatively insoluble in natural waters of almost neutral pH, and their amounts are therefore assumed to remain largely unchanged during rock alteration, though some solution and precipitation may occur as documented by their entrapment in secondary phases (e.g., Crovisier et al., 1987; Daux et al., 1994; Stroncik and Schmincke, 2002; Utzmann et al., 2002).

(3) The excellent preservation of ejecta components with delicate microstructures, including geochemically distinct internal domains (schlieren, globules), argues against a destructive diagenetic overprint that obliterated any primary geochemical signals (e.g., Mørk et al., 2001). Particularly, the 'microtektite in microtektite' configuration, with sharply contrasting compositional phases found 'side by side' in single ejecta particles attests to a genuine feature of these compositional differences.

(4) No hydrothermal influx was recognized, nor has been reported from elsewhere in the Méndez Formation that could explain the chloritization of spherules and fragments (Perez Cruz, 1993) and, according to Keller et al. (1997 p. 419), the 500 to 1000 m of sediments which are assumed to have overlain the clastic K-P sequence in this region are "…insufficient to cause significant transformation of clay minerals (e.g., from smectite to illite-smectite mixed layers and to illite)." This interpretation is inline with the results of Hower et al. (1976) who suggested that a significant clay mineral transformation in buried sediments from the Gulf of Mexico usually occurs at a burial depth in excess of 3 km. The preservation of thin smectitic bentonite layers intercalated within the mineralogically quite distinct (illite-chlorite) Méndez marls further corroborates this assignation (see also Adatte et al., 1996).

Therefore, it is concluded that alteration processes alone do not explain the observed compositional trends and hence, an important contribution existed to the impact melt from mainly target rocks of mafic to intermediate composition, though a contribution from felsic target lithologies may also be present, as shown by the glasses of andesitic composition found at the El Mimbral locality (Smit et al., 1992b;

Stinnesbeck et al., 1993; Premo et al., 1995). Details of the alteration processes, however, are inadequately understood, including the question whether these alterations, for instance the transformation of glass to chlorite, occurred during post-depositional burial diagenesis or whether these processes possibly are related to the hydrolysis and oxidation upon contact of the presumably hot ejecta particles with the sea surface following the cratering event. The good preservation of petrological features of the eject components may be explained by their rapid embedding via slumping within the clay-rich Méndez marls, or rapid covering by the sandstones of unit 2 and 3.

2.4.4 Constraints on Chicxulub target rocks

As shown in the previous section, the major element composition of the ejecta particles in northeastern Mexico (see Table 2.4, Fig. 2.21) suggests a suite of mafic to intermediate progenitor rocks, as also revealed by the altered K-feldspar and pyroxene microliths. Although the majority of (granitic-gneiss) basement clasts and the andesitic composition of the Chicxulub suevite found in numerous drillcores from the Yucatán peninsula both imply a predominance of intermediate to felsic rocks in the subsurface of the Chicxulub structure, mafic lithologies are also known from the southeastern part of the Gulf of Mexico (e.g., DSDP Leg 77, Schlager et al., 1984) and the Yucatan peninsula (Bateson and Hall, 1977; Rebolledo-Vieyra et al., 2000) and have been related to extension during the late Cretaceous in the attenuated ('transitional') continental crust of the Yucatán peninsula and the southernmost Gulf of Mexico area. For instance, at DSDP Hole 538 several hundred kilometers to the north of the Yucatán peninsula, post-tectonic diabase dikes intruded an association of variably mylonitic felsic gneisses and interlayered amphibolites (Dallmeyer, 1984). Mafic dikes have also been found in the (granitic) Maya Mountain in Belize (Bateson and Hall, 1977). The northern extension of these granite plutons is assumed to constitute a large part of the Chicxulub basement (Banks, 1975; López-Ramos, 1975; Steiner and Walker, 1996; Rebolledo-Vieyra et al., 2000). These granites possibly formed during period of crustal extension during the Silurian.

In addition, mafic lithologies are present in the Chicxulub suevite and impact breccia: Kring and Boynton (1992) observed diabase, pyroxenite, and amphibolite fragments (see also Kring et al., 2003) and Kettrup and Deutsch (2003) found an amphibo-

lite clast in the Yucatán 6 well from the center of the Chicxulub structure (Y6 amphibolite in Table 2.4). Remarkably, Deutsch and Kettrup (2003) have shown a close similarity between this 'Y6 amphibolite' and chlorite spherules from northeastern Mexico (La Lajilla) in terms of trace element compositions (Rb, Sr, Sm, Nd) and isotope ratios ($^{87}Sr/^{86}Sr$, $^{143}Nd/^{144}Nd$). However, the range of element abundances and diverse element ratios (Si/Al, Fe/Mg) found in the Fe-Mg-rich chlorite spherules from northeastern Mexico does not allow clear correlation to amphibolite rocks (see Table 2.4). Besides diagenetic effects (though probably minor as outlined above), this inconsistency may also derive from the complex mixing and fractionation processes within the impact melt as observed at various impact structures (Attrep et al., 1991; Mittlefehldt et al., 1992; Hörz et al., 1998; Koeberl, 1998; See et al., 1999; Dressler and Reimold, 2001). According to these authors, such mixing and fractionation processes may lead to melt compositions that are not correlated directly to specific target rock melts. The presence of Fe-Ti-K-rich schlieren in spherules and fragments with individual element-enrichments up to 25 wt% may document such processes. Alternatively, additional mafic precursor phases are present inside the impact structure and have so far not been observed in the Chicxulub drillcores.

The precursor phase to the Si-Al-K-rich glass is more difficult to constrain, since there are few types of rocks with similarly low Si:Al ratios and hence, are undersaturated with respect to SiO_2. Therefore, either melt-fractionation processes during the impact have to be considered (see above) and/or K-feldspar- to mica-rich rock types (e.g., schists) that provided high amount of potassium and aluminum to the melt. However, such rock types have only rarely been reported from the Yucatán peninsula and from the Chicxulub impact breccia (see Table 2.4), albeit a pervasive potassium metasomatism has been reported from the Chicxulub suevite (e.g., Hecht et al., 2003), for which the lithologies that released this large amount of potassium are not clear yet.

On the other hand, K-feldspar-rich 'biotite leucogranite' has been found in a suite of granitic rocks in the Maya Mountains from central Belize (Steiner and Walker, 1996). A contribution of similar leucogranitic rock-types of Silurian age from the subsurface of Yucatán to the Chicxulub ejecta seems possible, particularly since Lopez-Ramos (1975) reported a Silurian age (Rb-Sr age of about 410 Ma) for the basement (schists) found in the Yucatán No. 1 well drilled in the central Yucatán peninsula. These crustal ages are in line with:

(1) U-Pb dating of shocked zircons from the K-P boundary clay in the Western Interior and from the Haitian spherule deposits at Beloc, as well as from the suevite from inside the Chicxulub impact structure, which revealed source ages of about 418±6 Ma (e.g., Krogh et al., 1993a; 1993b; Kamo and Krogh, 1995),

(2) the 418±4 U-Pb ages derived from (unshocked) zircons of granites in the Maya Mountains, Belize, as reported by Steiner and Walker (1996).

A compilation of all Chicxulub-related U-Pb ages, and further conclusions on possible source rocks by trace elements and isotope rations can also be found in Table 2.6 and in Kettrup and Deutsch (2003).

The high amount of allochthonous carbonate (40-70 wt%) in bulk rock ejecta samples that occurs as (i) microcrystalline sparite, (ii) as distinct melt phase (e.g., globules with 'feathery calcite' or

Table 2.6 Compilation of resetting and formation ages from the Chicxulub impact site, various K-P boundaries, and rocks eqivalent to the potential basement of the Yucatán target region (e.g., Maya Mountains, Belize).

Locality	Material	Impact age (Ma)	Basement age (Ma)	Method	References
(a) Chicxulub crater impactites, (b) K-P spherule deposit Beloc, Haiti, (c) laminated K-P boundary clay in Colorado	Shocked zircons	57 ± 4	545 ± 5; 418 ± 6	U-Pb	Krogh et al. (1993a, b)
Laminated K-P boundary-clay in Colorado	Shocked zircons	66 ± 3; 65.2 ± 9.2	550 ± 10; 571 ± 6	U-Pb	Krogh et al. (1993a); Premo and Izett (1993)
Laminated K-P boundary clay in Saskatchewan	Shocked zircons	59 ± 10	548 ± 8	U-Pb	Kamo and Krogh (1995)
Yucatán No. 1 corehole (rhyolite porphyries)	Zircons		410	Rb-Sr	López-Ramos (1975)
Silurian plutons, Maja Mountains	Zircons		418 ± 4; 404 ± 3; 420	U-Pb	Steiner and Walker (1996)
Paleozoic granite	Zircons		595 ± 69; 680 ± 69	U-Pb	Lopez et al. (2001)

in spherules), and (iii) as limestone clasts, points to a carbonate-rich target, supports an impact on a carbonate platform, and therefore strengthens the correlation between the spherule deposits in northeastern Mexico and the Chicxulub impact structure with its thick sequence of Cretaceous carbonates (López-Ramos, 1975; Ward et al., 1995; Smit et al., 1996; Jones et al., 2000). These high amounts of carbonate imply not only that the dispersion of carbonate by the Chicxulub impact event was substantial in this area, as unshocked clasts and as melt, but also emphasize that northeastern Mexico received ejecta mainly from the sedimentary cover of the Yucatán peninsula, and hence, from shallower target areas. However, evidence for a significant contribution by 'sulfur-rich' lithologies (anhydrite or gypsum) was not found, though this may also be a diagenetic effect related to the preferential dissolution of such sediments (Tucker and Wright, 1992).

The origin of the microcrystalline carbonate in the spherule deposits (microspar in the matrix-supported microfacies-type 1) is not clear, and it may have originated from dust dispersed by the impact event, and/or as secondary products derived from the recombination of CO_2 and solid oxides (CaO), as suggested by Deutsch et al. (1998). An exclusive diagenetic origin seems unlikely because of the matrix-supported texture of these spherule deposits (cf. Fig. 2.10).

2.4.5 Chicxulub ejecta and the K-P boundary

The petrological and mineralogical characteristics of northeastern Mexican ejecta spherules and fragments generally show a resemblance to the microtektites (spherules) and microkrystites that are found in K-P spherule deposits 'proximal' to the Chicxulub structure in the Gulf of Mexico region, the Caribbean, the Western Interior, the Atlantic, and the Pacific (see Table 2.1 and Izett, 1990; 1991; Bohor and Glass, 1995; Ingram, 1995; Kyte et al., 1996; Smit et al., 1996; Martínez-Ruiz et al., 2002; Stüben et al., 2002). Specifically, this similarity exists in analogous unique morphological details of the ejecta particles, including the presence of mm-sized, smooth, hollow and composite spherules.

Spherules from northeastern Mexico and microspherules and microkrystites from the K-P boundary clay layer in the Tethyan realm, 'distal' to the Chicxulub impact site, have also several compositional aspects in common, as both include potassium-rich phases, iron oxides, fibroradial pyroxene, K-feldspar crystals, Mg-rich smectite, and chlorite, and often

have Ni- or Ni-Cr-rich inclusions (see Table 2.1 and Smit and Klaver, 1981; Schmitz, 1988; Izett, 1990; Montanari, 1991; Schmitz, 1992; Bohor and Glass, 1995; Martínez-Ruiz et al., 1997; Ortega-Huertas et al., 1998; 2002; Bauluz et al., 2000; Wdowiak et al., 2001).

Although this morphological and compositional similarities suggest a relationship between the Chicxulub impact and the impact fallout at the global K-P boundary, the link of these ejecta phases to possible origination modes, for instance, condensation from the vapor plume and contamination by projectile matter, has yet to be established (see Smit et al., 1992a; Evans et al., 1994; Barnouin-Jha et al., 1999a; 1999b; Griscom et al., 2003). However, the complex mineralogical and geochemical composition of the microtektites and microkrystites found in the Chicxulub ejecta in the Gulf of Mexico and the K-P boundary clay layer is unique and different to the known ejecta compositions found in strewnfields from other craters. For instance, the microtektites and clinopyroxene spherules linked to the Chesapeake Bay and Popigai impact structures have a distinctly more narrow compositional range (e.g., Glass and Koeberl, 1999; Kettrup et al., 2003). A very narrow compositional range was also observed for the distal ejecta of the Ries impact crater, Germany (Buchner et al., 2003).

2.4.6 Implications from rock magnetic properties

The elevated magnetic susceptibility of the Chicxulub ejecta deposits compared to the enclosing lithologies in northeastern Mexico is apparently caused by the occurrence of Fe-rich chlorite spherules and ejecta-fragments from the Chicxulub impact on the Yucatán peninsula, southern Mexico. The susceptibility is, in good approximation, proportional to the iron content, and since the bulk of the iron is found in the chlorite spherules (25-35 wt% iron), the susceptibility is directly proportional to the abundance of these spherules, suggesting a close relationship between the petrographic characteristics and the magnetic properties.

The carriers of the paramagnetic behavior may be found in the chlorite groundmass of the spherules, with chlorites having susceptibility between 20 to 130 x 10^{-6} SI/g (Borradaile et al., 1987; Borradaile and Werner, 1994). In addition, opaque inclusions in ejecta spherule and fragments, including Ti-Fe oxides and, more important, Fe-oxides (goethite, hematite) may have further enhanced the paramagnetic

signal. In combination, these paramagnetic phases lead to the observed susceptibility values of about 15 to 30 x 10^{-6} SI/g for the spherule deposits. Evidence for ferrimagnetic phases other than goethite and hematite, however, is rare and restricted to small peaks in the κ-T-curves at 560 to 580 °C, which are possibly linked to a subordinate and fine-grained magnetite phase (Morden, 1993).

Goethite and hematite in the ejecta particles formed either primary from melt or as replacement product of cubic minerals such as magnetite or pyrite during diagenesis. In any case, the occurrence of goethite and hematite, as well as their possible precursor phase magnetite points to highly oxidizing conditions during or after ejecta formation. Such conditions may have prevented the origination of stronger ferromagnetic phases (magnetite) or destroyed them. If goethite and hematite replaced pyrite, locally reducing conditions may have occurred.

Compared to the Chicxulub ejecta deposits in Beloc (Haiti) that have an iron content below 4 wt% (bulk rock, Stüben et al., 2002), and for which susceptibility measurements have shown very low paramagnetic values (Senftle et al., 1993; Thorpe et al., 1994), the data from northeastern Mexico reflect the different composition of the ejecta phases (mafic vs. andesitic origin), and hence the input of ferruginous and potential magnetic phases in these regions. In addition, the contrasting susceptibility values of the spherule deposits of these areas suggest a different ejecta dispersal mechanism: for the Haitian glasses, the formation of oxides was suppressed during homogenization and rapid quenching (see also Werner and Borradaile, 1998), whereas the ubiquitous presence of iron and the probably prolonged cooling history of ejecta from northeastern Mexico allowed the formation of Fe- and Fe-Ti oxides, contributing to the higher paramagnetic susceptibilities. The characteristic Ca-rich schlieren in the Si-rich Chicxulub ejecta glasses from Beloc, Haiti, sustain this interpretation and indicate incipient homogenization of the carbonate and silicic melt. In contrast, the ejecta phases in northeastern Mexico show 'liquid immiscibility' that suggest less intense mixture and probably lower energy during formation and dispersion. Moreover, the inferred base-surge like transportation mechanism for the northeastern Mexican spherule deposits may have further delayed cooling, in contrast to the ballistic emplacement via upper atmospheric levels for the Haitian spherule deposits.

The mm-thick basal part of the K-P boundary clay in more distal settings to the Chicxulub impact structure are generally characterized by a strong anomaly of the magnetic susceptibility which is associated with peak iridium values, high amounts of siderophile elements, Fe-rich and Fe-Ti-rich nanophases, as well as microkrystites containing magnetite and Ni-rich spinels in a goethite-hematite host phase (e.g., Worm and Banerjee, 1987; Morden, 1993; Griscom et al., 1999; Wdowiak et al., 2001; Bralower et al., 2002a). The magnetic susceptibility of the basal layer of the boundary clay is approximately proportional to the contents of the magnetic microkrystites. However, microkrystites do not entirely account for the boundary layers' magnetic properties and magnetically 'hard' phases (goethite-hematite) in the groundmass possibly increase their coercivity (Worm and Banerjee, 1987). Therefore, the microkrystites have been interpreted to form in low oxygen fugacity, probably in the ejecta plume rising well above the atmosphere, whereas the goethite-hematite mineralogy of the fine-grained matrix of the boundary clay layer is characteristic of an oxidizing environment (Wdowiak et al., 2001; Bhandari et al., 2002; Verma et al., 2002).

The low bulk rock susceptibility and scarcity of ferrimagnetic phases (e.g., magnetite) in the spherule deposits of northeastern Mexico suggest that quenching and strongly oxidizing conditions during the impact event may have prevented the formation of these magnetic phases or destroyed them. This hypothesis agrees with the inferred base-surge ejecta-distribution mode in these proximal settings, which presumably correspond to a highly oxidizing environment. However, diagenetic effects may have further enhanced the oxidization of ferrimagnetic phases.

2.5 Interpretation and discussion 2: Depositional processes

The sedimentological study of selected outcrops presented here is intended to supply the sedimentological framework for the ejecta deposits in northeastern Mexico. In addition to previous sedimentological studies by Bohor (1996), Smit et al. (1992b; 1996) and Stinnesbeck et al. (1993; 1996), petrological, microfacies, and geochemical data were incorporated to constrain reworking of the ejecta masses and to develop a depositional scenario for the Chicxulub ejecta and sand-siltstone deposits.

2.5.1 Sedimentology of ejecta and the K-P sand-siltstone deposits

A detailed "bed-to-bed" analysis as recommended by Shanmugam (2002) was conducted to reveal the depositional mode of the spherule deposits and the sand-siltstone complex.

Spherule deposits embedded in Méndez marl

The coarse-grained spherule deposits in Méndez marls are about 10-40 cm thick, and commonly have a massive appearance without grading or current-induced sedimentary structures. In some outcrops, however, faint lamination, which has alternating layers rich in carbonate and spherules, is visible and occasionally, rounded marl clasts are present. All types of these spherule deposits have in common that no bioturbation has been observed. These features suggest that the massive beds may represent an original ejecta fallout deposit from combined air-water settling (e.g., Bitschene and Schmincke, 1991; Nakayama and Yoshikawa, 1997), whereas laminated spherule deposits may have been reworked by debris flows (e.g., Shanmugam, 1996). The absence of bioturbation and hardgrounds in the spherule deposits points to rapid coverage by marls.

The petrological characteristics of the microfacies-type 1 spherule deposits corroborate this interpretation: The type-1 microfacies shows loosely packed welded or clustered components exhibiting random grain orientation, poor sorting, and absence of grading, suggesting an origin as rapidly settled fallout-ejecta (Cas and Wright, 1987; Bitschene and Schmincke, 1991; d'Atri et al., 1999). In addition, mineralogical and geochemical analyses show that the amount of admixed Méndez marl in these spherule deposits is negligible, sustaining a predominant 'fallout'-character. The presence of lateral flow indicators such as alignment of platy fragments in the laminated beds suggests localized reworking by currents. However, (i) the absence of particle rounding, (ii) the microbreccia-like texture of these ejecta deposits, including partly welded, highly fragile vesicular and schlieren-like ejecta particles, and (iii) the presence of accretionary lapilli, all emphasize that transport by mass flows was restricted and localized, countering long-term transport on the sea floor (Bitschene and Schmincke, 1991; d'Atri et al., 1999). Particularly, since the accretionary 'lapilli' clasts are prone to reworking (e.g., Fisher and Schmincke, 1984; Cas and Wright, 1987). This interpretation is also consistent with the occurrence of this microfacies in the interchannel area (as primary fallout),

and in the channel margin to levee area, where mass-flows or currents may have redistributed them locally.

After their initial deposition, spherule deposits embedded in Méndez marls in the La Sierrita and El Peñon area have been modified by further mass-movements because they constitute isolated and lenticular units of either: (i) contorted and recumbent folded layers with curvilinear fold hinges that bear characteristic outsized marl clasts in their cores, or (ii) disaggregated (breccia-like) spherule deposits of chaotic appearance. According to the criteria provided by Martinson (1994), Mulder and Cochonat (1996), and Hampton et al. (1997), these sedimentary features are indicative of downslope sediment movements associated with soft-sediment deformation (see also Soria et al., 2001; 2002). The contorted and recumbent folded deposits are interpreted as coherent to semi-coherent slump structures (Corbett, 1973; Elliot and Williams, 1988; Martinsen, 1994). The characteristic outsized marl clasts in their cores may have been derived from up-slope directed parts of the slump sheet and point to the presence of erosive high-energy currents, presumably associated with the slumping of these beds. This indicates that, in these localities, spherule deposits were not entirely buried by sediments before slumping took place and therefore slumping likely affected superficial spherule deposits ("open-cast slumps", Corbett, 1973). The 'breccia-like' appearance of spherule deposits may indicate local acceleration of slumps down-slope into a sedimentary mass flow-slide in which internal cohesion is lost (Corbett, 1973; Elliot and Williams, 1988; Guiraud and Plaziat, 1993; Martinsen, 1994). Also, they may be interpreted as the result of liquefaction of marls and spherule layers (Decker, 1990; Nichols, 1995). These processes are schematically depicted in Fig. 2.28.

Unit 1 of the K-P sand-siltstone complex

In contrast to the intermittent occurrence of spherule deposits embedded within Méndez marls, the unit 1 spherule deposits are consistently present at the base of the sand-siltstone deposit (see also Lindenmaier, 1999; Schulte, 1999; Affolter, 2000; Ifrim, 2000; Schilli, 2000). The thickness of this unit 1 spherule deposit is about 10-20 cm at Rancho Nuevo, 10-40 cm in the La Sierrita area, 20-80 cm in the El Peñon area, and reaches a maximum thickness of about 1 m (!) at El Mimbral, indicating a distinct increase in thickness towards the south. Remarkably, this range in thickness does not only exceed

the thickness for the spherule deposits embedded in Méndez marls as outlined above, but also shows a reciprocal behavior to the thickness of the sand-siltstone complex, which becomes progressively thinner towards the south.

The spherule deposits at the base of the sand-siltstone complex have very similar sedimentary characteristics when compared to the spherule deposits embedded within Méndez marl, including a massive appearance with faint lamination, alternating layers rich in spherules and carbonate, as well as the absence of bioturbation. This similarity also exists in the local presence of marl clasts and marl clast-spherule deposit breccia. In addition, syn- or postdepositional soft sediment deformation, probably induced by loading with the sand-siltstone units is ubiquitous in this layer, since, for instance at El Mimbral, an overturned slump fold is present in unit 1, whereas in other outcrops at La Sierrita unit 1 is squeezed and shows boudinage (Knaust, 2002; Strachan, 2002). Therefore, the depositional processes recorded in unit 1 appear to be similar to the processes involved in deposition of spherules embedded in Méndez marls (e.g., Shanmugam, 1996). These processes may therefore have included fall-out sedimentation, locally followed by multiple phases of channelized debris flows (e.g., Martinsen, 1994; Johansson and Stow, 1995; Mulder and Cochonat, 1996; Stow et al., 1996; Stow and Mayall, 2000).

The preservation of fragile marl and ejecta clasts is explained by laminar flow, albeit over short transportation distances (Shanmugam, 1996). However, unit 1 is distinguished by locally inverse or normal graded intervals (e.g., El Mimbral) and by the sandy limestone layer ("SLL"). In addition, marl-spherule intervals are occasionally embedded in the channel axis area. The local spherule-marl clast breccias and outsized marl clasts point to deposition by erosive high-velocity currents and may have been generated by the undercutting and collapse of channel margins, causing intra-extrachannel slumping and sliding (Shanmugam et al., 1994; Johansson and Stow, 1995; Mulder and Cochonat, 1996; Stow and Mayall, 2000; Stow and Johansson, 2000). A schematic model for the generation of these channels is depicted in Fig. 2.29.

The microfacies-characteristics of this spherule deposit reflect the sedimentary processes outlined above: (i) the presence of texturally and compositionally immature 'microbreccia-like' spherule deposits (comprising microfacies-type 1) with welded constituents and fragile, flaser-like ejecta particles at the base of the sand-siltstone complex at El Mimbral, and at the channel-margin area in the La Sierrita area suggests fallout possibly followed by only short transportation on the sea-floor without admixture of terrigeneous detritus. (ii) The variable, though minor contents in terrigenous detritus as well as the absence of welding features in the unit 1 spherule deposits in the channel axis area point to fallout deposition followed by reworking and transport in debris flows (e.g., Bitschene and Schmincke, 1991; Stix, 1991; d'Atri et al., 1999).

The detritus content and the embedded sandstone-layers both suggest local influx from nearshore or more proximal shelf areas. However, the complete lack of significant abrasion, sorting, and the preservation of delicate ejecta components imply a short transport that is difficult to reconcile with the more long-term transport of the siliciclastic detritus that presumably derived from proximal shelf or coastal areas. A possible explanation could be that strong basin-ward directed submarine currents carried sand in turbulent suspension or within debris flows from distal nearshore or shallow shelf areas and incorporated surficial non-consolidated ejecta deposits from proximal areas along their pathway. The incorporation of surficial ejecta deposits is also indicated by the similar mineralogical and geochemical composition of the microfacies-type 1 and 3 spherule deposits, arguing against intense mixing with Méndez marls before deposition (Fisher and Schmincke, 1984; Cas and Wright, 1987; Johansson and Stow, 1995; d'Atri et al., 1999).

The interpretation outlined above is consistent with the occurrence of these deposits at the base of the sand-siltstone complex in the channel axis area. Additional constraints on the reworking of unit 1 spherule deposits versus the spherule deposits embedded within Mendez marls may be derived from the 'adoption' and application of criteria originally developed to distinguish resedimented volcaniclastic layers from their primary counterparts (e.g., Clayton et al., 1996; Nakayama and Yoshikawa, 1997; d'Atri et al., 1999; Schneider et al., 2001):

(1) Reworking is only for a selected subset of the originally deposited components possible. Spherule deposits embedded in Méndez marl or unit 1 spherule deposits show no major compositionally bias: both types of deposits contain an equally diverse ejecta assemblage, including spherules, fragments, carbonate clasts, accretionary lapilli, ribbon-like ejecta clasts, welded and amalgamated ejecta particles.

(2) Reworking should cause relative abundance changes of the components, biased towards break-resistant forms, they should not reflect the proportions present in the original sediments from which they were derived. However, the unit 1 spherule deposit has relative abundances of ejecta components in the same range as the spherule deposits within Méndez marls.

(3) Reworking should cause the severe abrasion and sorting of components, though no particular abrasion features have been observed in any of the spherule deposits in question, even delicate shapes and forms are present, including ribbon-like cm-sized fragments, welded constituents, and accretionary lapilli.

(4) Reworking should be clearly reflected in the grain-size distribution of the components because of winnowing and sorting effects by currents. No difference in the grain-size distribution has been observed between spherule deposits embedded in Méndez marl or at the base of the sand-siltstone complex.

(5) Reworking should cause important changes in the whole rock mineralogical and geochemical composition resulting from mixing with background sediments during the periods of normal hemipelagic sedimentation (dilution effect). Significant dilution by Méndez marls has been observed only for spherule-marl breccias (microfacies-type 2 deposits), whereas spherule deposits embedded in Méndez marl and at the base of the sand-siltstone complex are very similar in bulk rock mineralogy and geochemistry. The factor analysis of the various spherule deposits also showed analogous amounts of the geochemical phases.

(6) The thickness of reworked ejecta deposits would be expected to be largest for the original deposit and increasingly reduced for reworked deposits. However, the thickness of the unit 1 spherule deposits in the northeastern Mexican outcrops is almost equivalent (20-60 cm), or even larger (1 m), than the thickness of the spherule deposits embedded within Méndez marls (about 20-40 cm).

Consequently, the strong similarity of spherule deposits embedded within Méndez marl and unit 1 in terms of composition and petrology, in concert with the absence of clear sedimentary features commonly related to the reworking and resedimentation over extended periods, suggests contemporaneous or quasi-contemporaneous formation of both types of deposits. Therefore, sedimentary mass movements, soft-sediment deformation, and syn- or postdepo-

sitional faulting may explain the apparent stratigraphic offset between these types of deposits, in keeping with the sedimentological results. However, other authors (e.g., Stinnesbeck et al., 2001; Keller et al., 2002) have concluded otherwise and based on their stratigraphic data from the Loma Cerca section, which is located 10 km to the south of La Sierrita, these authors suggested that distinct periods of 270 ka, 215 ka and 50 ka separated the three lens-like and folded (Affolter, 2000; Schilli, 2000) spherule deposits in this outcrop from the early Paleocene strata atop of the sand-siltstone deposit. Hence, further critical evaluation by sedimentological and biostratigraphic data is needed to resolve this divergent views, though the sedimentological data presented by this study clearly points to only minor intervals of time that separate these deposits since no argument was found from the earlier established criteria (points 1-6 above) for extended intervals between reworking and resedimentation.

Sandy limestone layer (SLL) in unit 1

The intercalation of the structureless 10-20 cm thick carbonaceous and foraminiferal sands of the sandy limestone layer ('SLL') in the spherule deposits of unit 1 show a sudden change in provenance of the sediments. The massive appearance of this layer, combined with the general absence of clear sedimentary structures points to a debris flow origin and rapid deposition (e.g., Shanmugam, 2002). Rapid deposition and subsequent burial are also shown by the absence of burrowed hardgrounds atop of the "SLL" and by the particular 'tepee-structures' at its upper surface: These "tepee-structures" typically indicate vertical sediment movement related to immediate loading by the sands-siltstone deposit in an unconsolidated state (Pettijohn et al., 1987; Nichols, 1995; Knaust, 2002; Strachan, 2002). Compositionally, the carbonaceous sands in the "SLL" layer of the northern outcrops and the foraminiferal sands in the "SLL" of the El Mimbral outcrop suggest an abrupt switch between proximal (landward) and to open-marine sedimentary sources during deposition of unit 1. However, the different composition of this layer in widely separated outcrop areas argues against a common source. The fauna in the foraminiferal sands of El Mimbral, with predominance of planktic forms and only rare benthic foraminifera may be derived via winnowing of surficial sedimentary layers from adjacent shelf areas.

Unit 2 of the K-P sand-siltstone complex

The 0.2 to 8 m (!) thick massive fine-grained sandstone of unit 2 shows a slight grading, resulting from intercalated spherules and variably sized marl clasts, partly armored with spherules, at the base; however, the grain size of the sand does not change upsection. Grove and flute casts at the base of this sandstone show generally a current direction from the north or northwest. At the El Mimbral outcrop, large (>15 cm long!) plant fragments have been observed outcrop and suggest close proximity to the shoreline, whereas only tiny plant fragments are present at the other outcrops in northeastern Mexico. The middle to upper part of this unit is laminated, with alternating layers of coarser and finer grains, and has occasionally current ripples. These characteristics are consistent with an interpretation as (laminar) debris flow deposit with traction deposition by bottom currents in the upper part during waning flow energy. Sandy debris flows represent a continuous spectrum of processes between cohesive and cohesionless gravity flows (see review in Shanmugam, 1996, 2002). In some outcrops, however, the basal marl clast-rich parts of this unit have a distinct chaotic debris flow character that may be linked to channel-wall slumping or collapse. In several outcrops, but particularly at Rancho Nuevo, water escape structures have been found that are attributed to rapid sedimentation associated with enhanced pore-pressures (see Fig. 9 in Stow and Johansson, 2000).

Bioturbation of unit 2 has only been observed in the El Peñon outcrop, as shown by Ekdale and Stinnesbeck (1998), where a few J-shaped burrows are present in the lower part, and in the Mesa Juan Perez 1A outcrop, where one large J-shaped burrow has been observed (Schulte, 1999). Ekdale and Stinnesbeck (1998 p. 585) suggested that "…the burrows were emplaced during, not following, the sedimentation of unit 2." In addition, they mentioned that the burrows "…could have been excavated very quickly." This implies that living endobenthic individuals may have been introduced with the sediment and started to escape (so-called "doomed pioneers") once the sediment came to a rest, as suggested by Föllmi and Grimm (1990) and Frey and Goldring (1992). Grimm and Föllmi (1994) concluded that such "…allochthonous tracemakers are likely a geologically-common phenomenon." However, no bioturbation was observed in the up to 10 m thick, massive sands of unit 2 at Rancho Nuevo, at the La Sierrita area (see also Lindenmaier, 1999; Schulte, 1999; Affolter, 2000; Schilli, 2000), at the El Mu-lato area (see also Ifrim, 2000), and at El Mimbral (see also Smit et al., 1992a; Stinnesbeck et al., 1993). This suggests that the entrainment of tracemakers is rather a rare phenomenon in the northeastern Mexican area and provides no substantiation for long intervals of colonialization. Therefore, brief changes in the hydrodynamic regime and local entrainment of tracemakers are likely to account for the faint and very restricted bioturbation of this unit. This interpretation is in line with Frey and Goldring (1992 p. 329), who pointed out that "…colonialization of new or defaunated substrates is indicated not by sporadic occurrences of individual traces, but rather by broadly distributed diagnostic patterns of burrowing activity."

Unit 3 of the K-P sand-siltstone complex

The sand-siltstone beds of unit 3 range in thickness from cm to meter scale, but resulting from erosion, the very top of this unit is rarely exposed. The alternating layers of contrasting grain-size (silt-sand) in combination with diverse sedimentary structures comprising intervals with lamination, which are alternating layers rich in coarse foraminifera and finer quartz-rich layers, contorted laminae, and various kinds of, partly mud-draped, current ripples suggest tractional deposition by currents of variable strength and sediment load (e.g., Shanmugam, 1996; 2002). Therefore, the transition from unit 2 to unit 3 may reflect a change from an upper flow regime (lamination) to a lower flow regime (current ripples). However, albeit grain-sizes in unit 3 are more variable than in unit 2, no distinct upward grading is present in unit 3. Even the topmost rippled and indurated layer is rich in planktic foraminifera and, therefore, is generally coarser than the underlying units.

The sheet-like, thin layers of the rippled unit 3 sandstones are often found in areas next to the main channel axis and are therefore interpreted as channel levee deposits associated with sediment-overspill (Clark and Pickering, 1996a). However, the strong vertical displacement (>10-20 m) suggests syn- or postdepositional faulting. Bioturbation is ubiquitous in unit 3 and has been recognized in most northeastern Mexican K-P outcrops (Ekdale and Stinnesbeck, 1998). Tracemakers are diverse and comprise *Thalassinoides*, *Chondrites*, and *Zoophycos*. Sometimes, multiple levels of bioturbation ("tiering") have been found in the uppermost centimeters of unit 3, for instance at El Peñon, and suggest prolonged periods of colonialization during a low hydrodynamic regime associated with slow accretion or brief still-

stands in sedimentation (Bromley, 1996; Ekdale and Stinnesbeck, 1998). At El Mimbral, the upper 10 cm of unit 3 also include the onset of a series of peak iridium values (Smit et al., 1996; Keller et al., 1997). An analogous set of observations, including the start of elevated iridium anomalies and multiple bioturbated levels, has been made for the uppermost part of the spherule-rich event deposit at Brazos, Texas (Chapter 3 and Rocchia et al., 1996; Yancey, 1996; Heymann et al., 1998).

2.5.2 Soft-sediment deformation and faulting of the K-P succession

Considering the small scale of the soft-sediment mass movements in the La Sierrita and El Peñon area, the lens-like and irregular shapes of spherule deposits within Méndez marls and their limited lateral correlation between outcrops some 10 m apart indicate local phenomena, instead of truly sheet-like (Corbett, 1973). The vertical extension of intermittent breccia-like spherule deposits in the Mesa Juan Perez sections suggests that soft sediment deformation and mass movements may have affected the upper 4-8 m of the Méndez marls in the La Sierrita area (see Fig. 2.4), whereas for the El Peñon outcrops, an estimate is difficult because of the

coverage by debris. However, these characteristics combined with the relative 'integrity' of deformed spherule layers, advocate for a minor transportation distance (tens to hundreds of meters?) of slumps or slides (Maltman, 1994a; Martinsen, 1994), though, the limited outcrop scale, the vertical offset between outcrops, and the absence of distinct glide planes in the almost structureless Méndez marls do not allow further evaluation of size and extension of the slump or slide masses.

The cause of these sedimentary mass movements is difficult to establish, though such rapidly deposited, and coarse-grained deposits are particularly prone to soft-sediment disturbances (e.g., Collinson, 1994), and the paleobathymetric outer shelf to bathyal setting of the northeastern Mexican K-P sections (Alegret et al., 2001; Soria et al., 2001; Keller et al., 2002) presumably promoted these processes (e.g., Shanmugam et al., 1994; Hampton et al., 1997). In the Maria de los Angeles 1 and the Mesa Juan Perez 3A sections the slump fold axis parallels the assumed direction of the paleoslope (inclined towards SSE, Perez Cruz, 1993; Keller et al., 1994; Bohor, 1996) and the inferred current direction of the sandstones, pointing to gravity- or current-driven processes. Considering the suggested outer shelf to
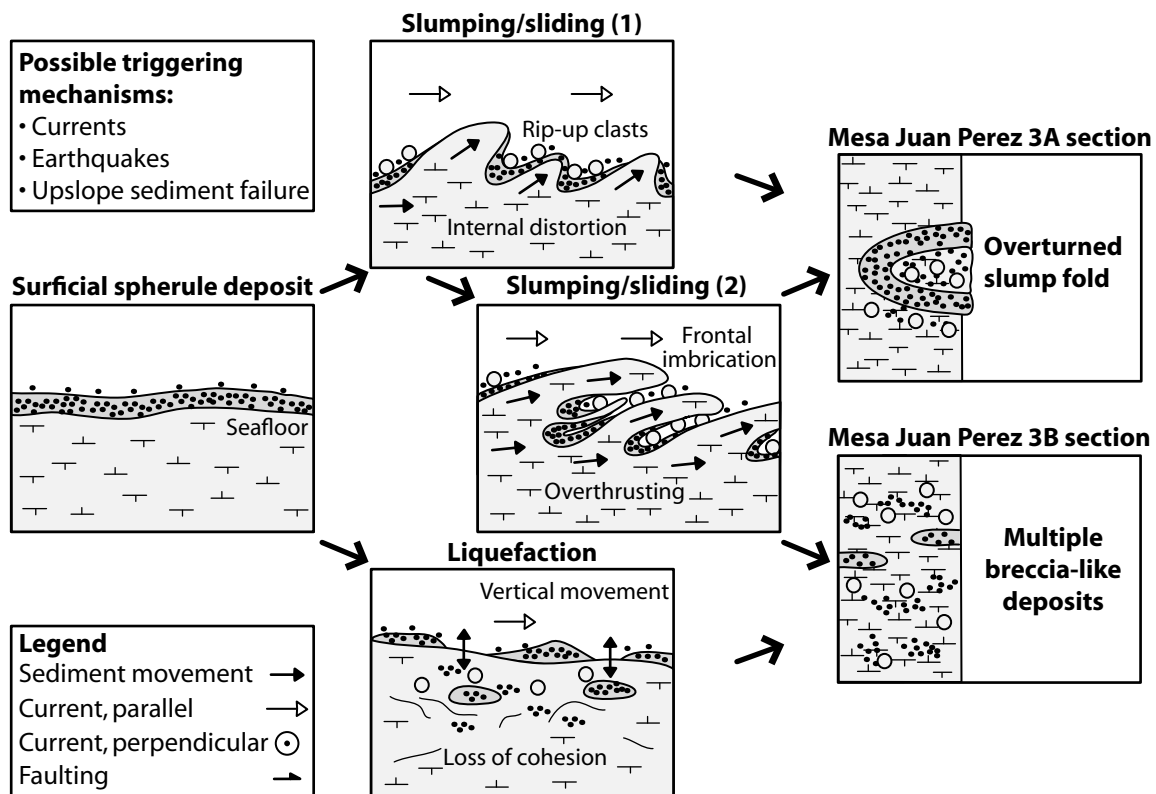
Figure 2.29 Schematic model demonstrating the supposed generation and related sedimentological features of soft-sediment deformation features at the La Sierrita and El Peñon area; modified after Corbett (1973) and Maltman (1994a). Legend to the lithologic symbols provided in Fig. 2.5.

bathyal setting of these deposits, well below storm wave-base, seismic shaking, strong bottom currents, or upslope sediment failure could have been plausible trigger mechanisms (e.g., Morton, 1993; Maltman, 1994b; Stow et al., 1996; Hampton et al., 1997). However, it appears unlikely that these triggering mechanisms were directly associated with the ejecta-generation by the Chicxulub impact, because they affected 'thick' ejecta deposits with ejecta that has already traveled several hundred meters through the water column.

The tilting, boudinage, and lateral movement of unit 1-spherule deposits in the Mesa Juan Perez section, may have been induced by loading with the up to 10 m (!) thick sand-siltstone complex. Such loading may have also induced local relief adjacent to the channel, resulting in destabilization of channel margin-levee areas associated with later, secondary mass movements and faulting as observed at the Maria de los Angles 1C section, where the slump fold axis parallels the channel axis of the sand-siltstone complex. Such secondary mass movements may provide an explanation for the apparent vertical dislocation between parts of the sand-siltstone deposit against each other by up to 10 m, in the La Sierrita, and the El Peñon area, where preferentially the channel margin-levee area was moved down relative to the channel axis (e.g., in the sections with multiple spherule deposits). The considerable postdepositional vertical displacement of the sand-siltstone complex that may exceed 50 m (!), is specifically shown in Fig. 2 of Keller et al. (2002) and further corroborates this assignation. In addition, differential compaction (marl vs. sand-siltstone) may have caused or enhanced this vertical offset (Johansson et al., 1998).

2.5.3 Facies association and architectural style of the K-P succession

The stratigraphic framework of the ejecta deposits and the K-P sand-siltstone complex in northeastern Mexico suggests upper slope to upper bathyal settings (Alegret and Thomas, 2001; Alegret et al., 2001; Keller et al., 2002) and therefore, probably encounters strong variations in the gradient. Slope settings may have steep gradients, whereas in the upper bathyal, gradients become lower and reach a basin-plain setting (e.g., Mutti and Normark, 1987). This setting is consistent with the observation that the 10 to 30 m of Méndez marls and Danian Velasco marls, which bracket the sand-siltstones in the K-P outcrops, are quiet uniform and have a low sandstone-to-marl ratio. The suite of depositional facies

observed in the studied interval, including channelized silty-sandy debris flow strata, slumps, slides and other structures indicative of sediment instability (e.g., faulting) are also agreeing with the various genetic facies associations characteristic of slope and upper bathyal settings (e.g., Reading and Richards, 1994; Galloway, 1998; Richards et al., 1998; Ricketts and Evenchick, 1999).

The strata architecture of the K-P sand-siltstone beds shows a high variability, albeit a distinct change in the channel geometry has been observed: deeply incised, narrow U-shaped channels, comprising unit 1, 2 and 3, are present at some of the northern outcrops (Rancho Nuevo, La Sierrita), with a sheet-like character of unit 3, whereas in the southern outcrops (El Peñon, El Mimbral, and El Mulato, Smit et al., 1992b; 1996; Ifrim, 2000), the incised channels apparently have a shallow incision depth and the sand-siltstone deposit (especially unit 3) has a sheet-like character (except for unit 1). Following the channel classification of Clark and Pickering (1996b), the sand-siltstone deposits in the northern part area are therefore considered as simple, isolated, and confined channels with low sinuosity, while the sand-siltstone deposits in the southern and western part are interpreted as isolated lobes. The exact length-wide ratio and connectivity of these channels are, however, difficult to assess, though from geological mapping of the La Sierrita area, one channel of about 0.5 km width could be traced along 20 km in length, giving a moderate length-wide ratio of about 40 : 1 (see also Schulte, 1999; Affolter, 2000; Schilli, 2000).

A systematic decrease in thickness of the sand-siltstone complex from the northern to the southern K-P outcrops in northeastern Mexico has been observed. The variable thickness of the sand-siltstone complex at the northern sections (Rancho Nuevo to El Peñon) in combination with the greatly decreased thickness at the southern sections (e.g., El Mimbral) suggests a multitude of separate channels (see also Smit et al., 1996; Stinnesbeck et al., 1996). The vertical displacement and tilting affected individual channel segments, parallel channel branches, and channel thalweg versus levee deposits. Such processes are typical for channels, especially at slope settings (Clark and Pickering, 1996a). However, as outlined below, all K-P sand-siltstone deposits lack characteristics common in multiple stacked, mature channelized sandstones that aggregated during long periods of time including (i) marl intercalations, reflecting abandonment of the channel, (ii) sideward

movement of the channel axis, (ii) absence of distinct hardgrounds in the sand-siltstone deposit, and (iv) multiple stacked sets of graded units with basal conglomeratic parts (Clark and Pickering, 1996a; 1996b; Stow and Johansson, 2000; Stow and Mayall, 2000). These characteristics stress the specific 'event character' of these deposits and argue against long-term built-up of a channel system, s for instance observed in the Mississippi slope systems of the Gulf of Mexico (see Clark and Pickering, 1996a). The switch in the architectural style of the channel geometry from the northern to the southern K-P outcrops may be associated with either local conditions (e.g., relief, gradient) or with differences in current speed and sediment supply.

The different petrological composition of individual sandstone units (calcareous arenites vs. foraminiferal sands) in each locality suggests that the sandstones were deposited from several point sources along the shelf (-edge?), instead of from a unique source in the northwest (e.g., the Difunta Group, Fig. 2.1C). In addition, the petrological composition (rare volcanic fragments/clast, abundant foraminifera) of the sandstones is distinguished from the volcanic-rock fragment-dominated sediment petrography of the Difunta sandstones (McBride et al., 1975).

Deposition of the K-P sand-siltstone complex

The amalgamated beds of units 1 to 3 represent multiple depositional events by debris flows and traction deposition from bottom currents, providing no support for an interpretation as turbidite flow or parts of a turbidite flow, as concluded by Bohor (1996). Many observed sedimentary features are incompat-

ible with settling from turbulent suspension (no size grading, intercalated layers of spherules and marl clasts, alternating sand-silt layers in unit 3). These sedimentary features also counter an origin by tsunami-like impact-megawaves, as proposed by Smit et al. (1996), since no evidence for deposition from waves has been found; evidence for alternating current directions is restricted to few outcrops and few layers (see also Schulte, 1999; Affolter, 2000; Ifrim, 2000). In addition, the paleowater depth, which is estimated between 300-500 m, or even deeper (Alegret and Thomas, 2001; Alegret et al., 2001), opposes a wave-related depositional mechanism.

The absence of thoroughly bioturbated intercalated layers or hardgrounds in the massive sands of unit 2, does not attest to long-term breaks in sedimentation, but instead point to a geologically 'brief' interval for deposition (see also Ekdale and Stinnesbeck, 1998). In contrast, the bioturbated topmost layer(s) of unit 3 may have been repeatedly reworked and bioturbated at some locations, suggesting a prolonged period of (local) current activity and resedimentation. Accurate time estimates, however, are difficult to constrain, but, by analogy to bioturbated turbidite currents and tempestite deposits (e.g., Einsele, 1998), a rather brief interval is tentatively concluded, not exceeding more than a few years-decades; an estimation that is well within the (lower) range given by Ekdale and Stinnesbeck (1998) for this period. Consequently, the time between the diverse depositional events represented by the three sand-siltstone units was probably quite short, maybe several days-weeks, with an extended period for the uppermost part of unit 3.
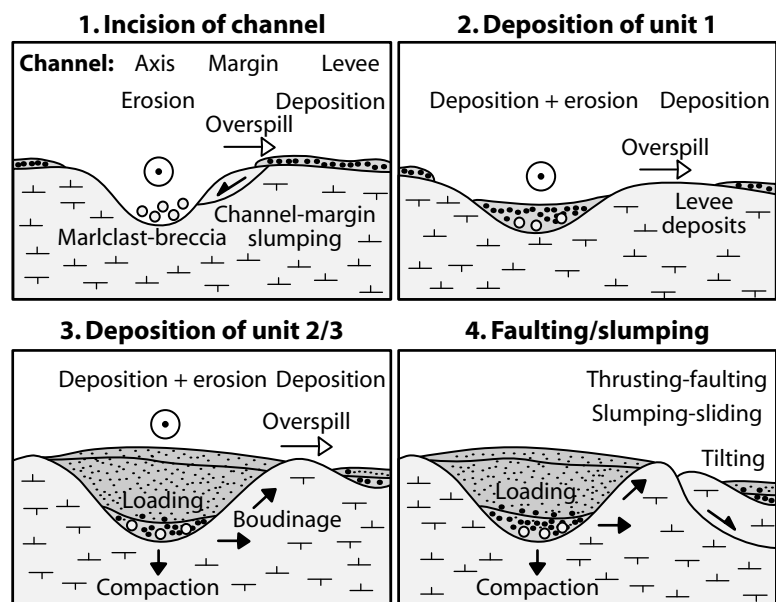
Figure 2.30 Schematic model demonstrating the supposed generation and related sedimentological features of channelized deposits in northeastern Mexico, modified after Clark and Pickering (1996a). Legend in Fig. 2.5 and 2.28.

The sand-siltstone units are always found atop of the spherule deposit, hence, a direct relationship to the initial disturbances of the Chicxulub impact, probably earthquakes or tsunamis, appears to be unlikely (see also Stinnesbeck and Keller, 1996). However, the ultimate cause of this multiple gravity flows is not amenable to the geological and sedimentological analysis. Activation of such submarine landslides could have resulted from storm activity, sediment instability (resulting from earthquakes and/or ejecta deposition), lowered sea level (see also Stinnesbeck and Keller, 1996), a series of upslope or shelf retrogressive failures, accelerated creep, and other processes (e.g., Nilsen, 2000). However, without preservation of the more proximal parts of this system, it is clearly difficult to be certain of the triggering mechanism(s).

2.6 Scenario for ejecta dispersal and emplacement

From the observations outline in the first part of the discussion, one possible scenario for ejecta dispersion by the Chicxulub impact event combined with amalgamation and welding of components incorporates the generation of a hot, fluidized and outward radiating curtain of molten ejecta, entrained clasts, vapor, and admixed seawater by the impact (Alvarez et al., 1995). This 'ejecta curtain' may behave analogous to a volcanic-generated pyroclastic flow and may be transported over long distances on top of the sea surface as depicted in Fig. 2.28 (e.g., Cas and Wright, 1991; Ormö and Lindström, 2000).

A hot, very turbulent "nuée ardente"-like transportation mechanism has been interpreted to have emplaced the basal units of the Chicxulub suevite (Stöffler et al., 2003) and the lateral outward extending ground surge could account for the wide distribution of such coarse ejecta more than five crater radii from the Yucatán peninsula (Cas and Wright, 1991; Ormö and Lindström, 2000; Sturkell et al., 2000). In addition, this mechanism provides favorable conditions for the formation of accretionary lapilli as outlined above. Finally, steam-explosions during the entry of the ground surge in shallow-water areas, as observed for pyroclastic flows (e.g., Freundt and Schmincke, 1998), could account for the incorporation of marl and benthic foraminifera by erosion of the Mexican shelf and mixing with the hot ejecta since some of the benthic foraminifera observed in this microfacies-type include *Anomalina*, *Cibicidoides*, *Lenticulina*, *Neoflabellina*, *Tritaxia*, and

Palmula, which are not characteristic carbonate-platform occupants (Murray, 1991). Analogous to observations from other marine impact structures, subsequent resurge currents presumably contributed to the re-distribution of settling ejecta towards offshore areas (McHugh et al., 1998; Ormö and Lindström, 2000; Dalwigk and Ormö, 2001; Poag, 2002).

A succession of multiple interacting depositional and reworking events that followed the ejecta generation/dispersion by the Chicxulub impact event can be constructed from the sedimentological and petrological data. This succession of depositional events is summarized in the following steps, though their relative timing is difficult to constrain, and during steps 1 to 4, repetitive shelf destabilization, current-scour, and instant loading may have induced concurrent or subsequent down-slope as well as intra- and extrachannel sedimentary mass movements (see Fig. 2.29 and 2.30).

Step 1: Origination and blanket-like distribution of spherules, fragments, and carbonate clasts by the Chicxulub impact on the Yucatán peninsula occurred by the mechanisms outlined above (e.g., fluidization; see Fig. 2.28). Subsequent settling of ejecta through the water column took place, probably locally accompanied by enhanced currents, resulting in delayed ejecta deposition on the sea floor and in local reworking. Fallout deposits without reworking are found only in sectors less affected by currents.

Step 2: The ejecta (unit 1) was consecutively reworked and redeposited by channelized sedimentary gravity flows, with stepwise (increasing) incorporation of extrabasinal detritus from more proximal shoreface areas and alternating provenance areas (foraminiferal sands vs. calcareous arenites).

Step 3: The siliciclastic units 2 and 3 were deposited by a series of successive debris flows. Unit 2 was deposited in a more restricted thalweg facies. In contrast, unit 3 was deposited in the immediate channel area and in attached/detached overspill deposits (off-channel facies; see Fig. 2.29), and covered adjacent fallout-ejecta deposits.

Step 4: Loading of sediments by the thick units of the sand-siltstone sequence and ejecta masses induced (local) shelf destabilization and may have induced simultaneous or following intra- and extrachannel as well as down-slope sedimentary mass movements (see Figs. 2.29 and 2.30).

2.7 Conclusions

On the basis of the multidisciplinary evaluation of the Chicxulub ejecta and the K-P transition in northeastern Mexico conclusions concerning the following issues are presented:

Origin of spherules

(1) Spherule deposits consist of mm-cm sized spherical to drop-shaped vesiculated spherules, angular to ribbon-like fragments, and abundant carbonate. Morphological and petrological features (e.g., shapes, schlieren) of these particles, and the presence of carbonate with microtextures indicative of quenching and/or liquid immiscibility, as well as the close proximity of northeastern Mexico to the Yucatán peninsula, suggest that the spherule deposits originated as ejecta from the Chicxulub impact event.

(2) Differences in ejecta composition exist between locations to the north (La Sierrita, El Peñon), which show a chlorite-dominated mineralogy, and the southernmost outcrop at El Mimbral, where Si-K-rich glasses are the main ejecta phases. These trends have been confirmed by bulk rock analysis of main elements and by principal component analysis; they are also reflected in the clay mineral composition of these deposits. These compositional trends may suggest highly localized patterns of melt dispersion from specific sectors in the target area.

Chicxulub target lithologies

(1) Albeit possible ejecta fractionation or mixing processes and alteration make a clear evaluation difficult, the particular composition of the ejecta phases suggests that they originated from mafic lithologies, aside from a contribution from intermediate-felsic rocks, and the possibility of meteoritic contamination. Hence, the target rocks in the northwestern sector of the Chicxulub impact structure may show a considerable compositional range from rocks with mafic character to rocks of andesitic composition, though the exact assignation of the ejecta phases in northeastern Mexico to distinct target lithologies (amphibolites?) known from the Chicxulub impact breccia and suevite has yet to be established. Specifically, the composition of the Si-Al-K-rich glasses is difficult to bring into account with possible target lithologies since they show a low Si:Al ratio of about 1.5 and high amounts of potassium (6-9 wt%), suggesting a mica-rich precursor phase.

(2) The high amount of CaO (25-35 wt %) in the spherule deposits in northeastern Mexico, as revealed by petrological and major element analysis, suggests that this area may have received ejecta mainly from shallow carbonaceous lithologies stratigraphic units of the Yucatán peninsula. Carbonaceous ejecta phases were dispersed as unshocked clasts and as highly shocked melt. The microspar in the spherule deposits, and their matrix-supported texture suggests that microcrystalline carbonate and spherules were ejected and deposited simultaneously. Evidence for a significant contribution by anhydrite or gypsum was not found.

Regional-global correlation of Chicxulub ejecta

(1) Spherules correspond morphologically to glass-smectite spherules found in the K-P transition of the Gulf of Mexico, Northern America (Western Interior), the western Atlantic, and the eastern Pacific. In the northeastern Mexican outcrops, however, ejecta spherules and fragments are distinct by their Fe-Mg-rich chlorite composition and the presence of Si-Al-K-rich glass. They also contain Fe-Ti-K-rich schlieren, Fe-Mg-rich globules, and rare μm-sized metallic and sulfidic Ni-Co-rich inclusions. Welded and amalgamated ejecta constituents, as well as enveloping of marl and benthic foraminifera by spherules, suggest an initial (ground surge-like) dispersion of the ejecta.

(2) Ejecta spherules and fragments have also several compositional aspects in common with microkrystites found in the basal layer of the globally occurring K-P boundary clay, suggesting a close relationship between the Chicxulub impact event and the impact fallout at the global K-P boundary. These aspects include the presence of potassium-enriched phases, altered K-feldspar and pyroxene crystallites with fibroradial texture, and an abundance of fine-grained iron-titanium oxides and iron oxides.

Implications from rock magnetic properties

(1) The spherule deposits comprise elevated magnetic susceptibility compared to the enclosing lithologies. This elevated susceptibility is caused by the occurrence of Fe-rich chlorite-spherules from the Chicxulub impact event.

(2) The ubiquitous occurrence of goethite and hematite in the spherule deposits points to highly oxidizing conditions during or after ejecta formation, in keeping with the inferred ground surge-like ejecta dispersion mode. Such oxidizing conditions may have prevented the extensive origination of

stronger ferromagnetic phases (magnetite) or destroyed them. Therefore, goethite and hematite in the ejecta particles formed either primary from melt or as replacement product of cubic minerals such as magnetite or pyrite during diagenesis. Remanence measurements indicate the presence of only goethite or hematite as high coercitive phases at room temperature. Evidence for ferrimagnetic phases other than goethite and hematite, is rare and restricted to small peaks in the κ-T-curves at 560-580 °C, possibly indicating the presence of a subordinate fine-grained magnetite phase.

(3) The small grain-sizes of inclusions and dendritic-skeletal crystals of Ti-Fe oxides ('spinifex texture') are indicative of rapid quenching from a melt. This fine-grained Fe-Ti-phase, also found in the global K-P boundary clay, may explain the small peak at –80 °C in the low-temperature susceptibility behavior that is characteristic for the ejecta deposits.

Deposition of the K-P succession

(1) In two K-P outcrop areas in northeastern Mexico (La Sierrita and El Peñon), spherule deposits are locally embedded in late Maastrichtian marls, constitute air-water fallout deposits with little reworking, and have been affected by remolding and reworking resulting from slumps-slides, liquefaction, and debris flows after original deposition.

(2) The laterally more widespread channelized spherule deposit at the base of the K-P sand-siltstone complex is interpreted as the result of multiple confined debris flows, in part with incorporation of terrigeneous influx from proximal shelf areas.

(3) Petrological, mineralogical, and geochemical criteria suggest that ejecta components from the various spherule deposits are similar, with multiple deposits produced by minor remolding and resedimentation, though size sorting and abrasion of ejecta has not been observed. The sedimentological, petrological, and mineralogical data as well as the statistical evaluation provided no support for long intervals between deposition of individual slumped and channelized spherule deposits, therefore suggesting nearly contemporaneous formation.

(4) The main part of the channelized sand-siltstone sequence, including the basal ejecta layer, has been deposited by a series of debris flows under variable, though high current energies; a distinctly lowered current energy was noticed for the uppermost part. Compositional differences (sandy and calcareous sandstone vs. foraminiferal sandstone) between individual depositional units suggest alternating influx from multiple provenance areas (line-sources) to the sand-siltstone sequence. Bioturbation of the uppermost layers suggests longer, intermittent periods of deposition for this unit.

(5) Postdepositional displacement (faulting) with offsets >10 m transected not only individual channel axis (thalweg) segments against each other, but also the channel levee complex relative to the main channel axis and possibly promoted the generation of multiple lens-like spherule deposits embedded in Méndez marl adjacent to the channel.

2.8 References

Adatte T, Stinnesbeck W, Keller G (1996) Lithostratigraphic and mineralogic correlations of near K/T boundary clastic sediments in NE Mexico: Implications for origin and nature of deposition. In: Ryder G, Fastovsky D, Gartner S (eds) The Cretaceous-Tertiary boundary event and other catastrophes in Earth history. *Geol Soc Am Spec Pap* **307**: 211-226.

Affolter M (2000) Etude des depots clastiques de la limite Cretace-Tertiare dans la region de la Sierrita, Nuevo Leon, Mexique. *Unpublished Master Thesis*, Université de Neuchâtel: 1-133.

Alegret L, Thomas E (2001) Upper Cretaceous and lower Paleogene benthic foraminifera from northeastern Mexico. *Micropaleontology* **47**(4): 269-316.

Alegret L, Molina E, Thomas E (2001) Benthic foraminifera at the Cretaceous-Tertiary boundary around the Gulf of Mexico. *Geology* **29**(10): 891-894.

Alegret L, Arenillas I, Arz JA, Liesa C, Mélendez A, Molina E, Soria AR, Thomas E (2002) The Cretaceous/Tertiary boundary: Sedimentology and micropaleontology at the El Mulato section, NE Mexico. *Terra Nova* **14**(5): 330-336.

Allen SR, Cas RAF (2001) Transport of pyroclastic flows across the sea during the explosive, rhyolitic eruption of the Kos Plateau, Tuff, Greece. *Bull Volcanol* **62**(6-7): 441-456.

Alvarez W, Claeys P, Kieffer SW (1995) Emplacement of Cretaceous-Tertiary boundary shocked quartz from Chicxulub crater. *Science* **269**: 930-935.

Alvarez W, Smit J, Lowrie W, Asaro F, Margolis SV, Claeys P, Kastner M, Hildebrand AR (1992) Proximal impact deposits at the Cretaceous-Tertiary boundary in the Gulf of Mexico: A restudy of DSDP Leg 77, Sites 536 and 540. *Geology* **20**(8): 697-700.

Amieux P (1982) La cathodoluminescence: Methode d'etude sedimentologiques des carbonates. *Bulletin des Centres de Recherches Exploration-Production Elf-Aquitaine* **6**(2): 437-483.

Andreozzi M, Dinelli E, Tateo F (1997) Geochemical and mineralogical criteria for the identification of ash layers in the stratigraphic framework of a foredeep: The Early Miocene Mt. Cervarola Sandstones, northern Italy. *Chem Geol* **137**(1-2): 23-39.

Arkai P, Sadek Ghabrial D (1997) Chlorite crystallinity as an indicator of metamorphic grade of low-temperature meta-igneous rocks: A case study from the Bukk Mountains, Northeast Hungary. *Clay Miner* **32**(2): 205-222.

Arz JA, Arenillas I, Soria AR, Alegret L, Grajales-Nishimura JM, Liesa CL, Melendez A, Molina E, Rosales MC (2001) Micropaleontology and sedimentology across the Cretaceous/Tertiary boundary at La Ceiba (Mexico): Impact-

generated sediment gravity flows. *Jour South Am Earth Sci* **14**(5): 505-519.

Attrep M, Orth CJ, Quintana LR, Shoemaker CS, Shoemeker EM, Taylor SR (1991) Chemical fractionation of siderophile elements in impactites from Australian meteorite craters (abstract). *Lun Planet Sci* **22**: 39-40.

Bailey SW (1988) Chlorites: Structures and crystal chemistry. In: Bailey SW (ed) Hydrous phyllosilicates (exclusive of micas). *Reviews in Mineralogy* **19**. Mineralogical Society of America: 347-403.

Banks PO (1975) Basement rocks bordering the Gulf of Mexico and the Caribbean. In: Nairn AEM, Stehli FG (eds) Ocean basins and margins: The Gulf of Mexico and the Caribbean **3**. Plenum Press, New York: 181-196.

Barker DS (1989) Field relations of carbonatites. In: Bell K (ed) Carbonatites: Genesis and evolution. Unwin Hyman, London: 38-69.

Barnouin-Jha OS, Schultz PH, Lever JH (1999a) Investigating the interactions between an atmosphere and an ejecta curtain: 2, Numerical experiments. *Jour Geophys Res* **104**(E11): 27,117-27,132.

Barnouin-Jha OS, Schultz PH, Lever JH (1999b) Investigating the interactions between an atmosphere and an ejecta curtain: 1, Wind tunnel tests. *Jour Geophys Res* **104**(E11): 27,105-27,116.

Barrera E, Savin SM (1999) Evolution of late Campanian-Maastrichtian marine climates and oceans. In: Barrera E, Johnson CC (eds) Evolution of the Cretaceous ocean-climate system. *Geol Soc Am Spec Pap* **332**: 245-282.

Bateson JH, Hall IHS (1977) The geology of the Maya Mountains, Belize. *Overseas Memoir* **3**. Institute of Geological Sciences, London: 1-43.

Bauluz B, Peacor DR, Elliott WC (2000) Coexisting altered glass and Fe/Ni oxides at the Cretaceous/Tertiary boundary, Stevns Klint (Denmark): Direct evidence of meteorite impact. *Earth Planet Sci Lett* **182**: 127-136.

Bell MS, Sharpton VL (1996) Small scale heterogeneities in K-T boundary tektites from Mimbral (abstract). *Lun Planet Sci* **27**: 91-92.

Bengtsson H, Stevens RL (1998) Source and grain-size influences upon the clay mineral distribution in the Skagerrak and northern Kattegat. *Clay Miner* **33**(1): 3-13.

Berger G, Claparols C, Guy C, Daux V (1994) Dissolution rate of a basalt glass in silica-rich solutions: Implications for long-term alteration. *Geochim Cosmochim Acta* **58**(22): 4875-4886.

Bhandari N, Verma HC, Upadhyay C, Tripathi A, Tripathi RP (2002) Global occurrence of magnetic and superparamagnetic iron phases in Cretaceous-Tertiary boundary clays. In: Koeberl C, MacLeod KG (eds) Catastrophic events and mass extinctions: Impacts and beyond. *Geol Soc Am Spec Pap* **356**: 201-212.

Bitschene PR, Schmincke H-U (1991) Fallout tephra layers: Composition and significance. In: Heling D, Rothe P, Förstner U et al. (eds) Sediments and environmental geochemistry. Springer, Heidelberg: 48-82.

Bitter MR (1993) Sedimentation and provenance of Chicontepec sandstones with implications for uplift of the Sierra Madre Oriental and Teziutlán massif, east-central Mexico. Society of Economic Paleontologists and Mineralogists Foundation, Gulf Coast Section, 3th Annual Research Conference Proceedings: 155-172.

Blum JD, Chamberlain CP, Hingston MP, Koeberl C, Marín LE, Schuraytz BC, Sharpton VL (1993) Isotopic comparison of K/T boundary impact glasses with melt rock from the Chicxulub and Manson impact structures. *Nature* **364**: 325-327.

Bohor BF (1996) A sediment gravity flow hypothesis for siliciclastic units at the K/T boundary, northeastern Mexico. In:

Ryder G, Fastovsky D, Gartner S (eds) The Cretaceous-Tertiary boundary event and other catastrophes in Earth history. *Geol Soc Am Spec Pap* **307**: 183-195.

Bohor BF, Betterton WJ (1989) Glauconite spherules and shocked quartz at the K-T boundary in DSDP Site 603 B (abstract). *Lun Planet Sci* **20**: 92-93.

Bohor BF, Glass BP (1995) Origin and diagenesis of K/T impact spherules – From Haiti to Wyoming and beyond. *Meteoritics* **30**: 182-198.

Bohor BF, Triplehorn DM, Nichols DJ, Millard HTJ (1987) Dinosaurs, spherules, and the "magic" layer: A new K-T boundary clay site in Wyoming. *Geology* **15**(10): 896-899.

Borradaile GJ, Werner T (1994) Magnetic anisotropy of some phyllosilicates. *Tectonophysics* **235**(3): 223-248.

Borradaile GJ, Keeler W, Alford C, Sarvas P (1987) Anisotropy of magnetic susceptibility of some metamorphic minerals. *Phys Earth Planet Inter* **48**(1-2): 161-166.

Bouska V (ed) (1993) Natural glasses. *Ellis Holdswood Series.* Academia, Praha: 1-354.

Bralower TJ, Premoli Silva I, Malone MJ (2002a) Shipboard Scientific Party: Leg 198 summary. Proceedings of the Ocean Drilling Program. *Initial Results* **198**: 1-148.

Bralower TJ, Premoli-Silva I, Malone MJ, Scientific Participants of ODP Leg 198 (2002b) New evidence for abrupt climate change in the Cretaceous and Paleogene: An Ocean Drilling Program expedition to Shatsky Rise, northwest Pacific. *GSA Today* **12**(4): 4-10.

Bromley RG (1996) Trace fossils: Biology, taphonomy and applications. Chapman & Hall, London: 1-361.

Brooks RR, Hoek PL, Reeves RD, Wallace RC, Johnston JH, Ryan DE, Holzbecher J, Collen JD (1985) Weathered spheroids in a Cretaceous/Tertiary boundary shale at Woodside Creek, New Zealand. *Geology* **13**(10): 738-740.

Bryan WB (1972) Morphology of quench crystals in submarine basalts. *Jour Geophys Res* **77**(29): 5812-5819.

Buchner E, Seyfried H, Bogaard Pvd (2003) ^{40}Ar/^{39}Ar laser probe age determination confirms the Ries impact crater as the source of glass particles in Graupensand sediments (Grimmelfingen Formation, North Alpine Foreland Basin). *Int Jour Earth Sci* **92**(1): 1-6.

Butler RF (1998) Paleomagnetism: Magnetic domains to geologic terranes (electronic edition). Department of Geosciences, Tucson, Arizona: 1-238.

Cande SC, Kent DV (1995) Revised calibration of the geomagnetic polarity timescale for the Late Cretaceous and Cenozoic. *Jour Geophys Res* **100**(4): 6093-6095.

Carstens H (1975) Thermal history of impact melt rocks in the Fennoscandian Shield. *Contrib Mineral Petrol* **50**(2): 145-155.

Cas RAF, Wright JV (1987) Volcanic successions, modern and ancient: A geological approach to processes, products and successions. Allen & Unwin, London: 1-528.

Cas RAF, Wright JV (1991) Subaqueous pyroclastic flows and ignimbrites: An assessment. *Bull Volcanol* **53**(3): 357-380.

Chamley H (1989) Clay sedimentology. Springer, Heidelberg: 1-623.

Chamley H (1997) Clay mineral sedimentation in the ocean. In: Paquet H, Clauer N (eds) Soils and sediments. Springer, Heidelberg: 269-302.

Cisowski SM (1990) The significance of magnetic spheroids and magnesioferrite occurring in K/T boundary sediments. In: Sharpton VL, Ward PD (eds) Global catastrophes in Earth history: An interdisciplinary conference on impacts, volcanism, and mass mortality. *Geol Soc Am Spec Pap* **247**: 359-365.

Claeys P, Kiessling W, Alvarez W (2002) Distribution of Chicxulub ejecta at the Cretaceous-Tertiary boundary. In: Koeberl C, MacLeod KG (eds) Catastrophic events and mass

extinctions: Impacts and beyond. *Geol Soc Am Spec Pap* **356**: 55-68.

Clark JD, Pickering KT (1996a) Submarine channels: Processes and architecture. Vallis Press, London: 1-229.

Clark JD, Pickering KT (1996b) Architectural elements and growth patterns of submarine channels: Application to hydrocarbon exploration. *Am Ass Petrol Geol Bull* **80**(2): 194-221.

Clayton T, Francis JE, Hiller SJ, Hodson F, Saunders RA, Stone J (1996) The implications of the reworking on the mineralogy and chemistry of lower Carboniferous K-bentonites. *Clay Miner* **31**(3): 377-390.

Collinson JD (1994) Sedimentary deformation structures. In: Maltman AJ (ed) The geological deformation of sediments. Chapman & Hall, London: 95-125.

Corbett KD (1973) Open-cast slump sheets and their relationship to sandstone beds in an upper Cambrian flysch sequence, Tasmania. *Jour Sediment Petrol* **43**(1): 147-159.

Courtillot V (2002) Evolutionary catastrophes: The science of mass extinction. Cambridge University Press, Cambridge: 1-173.

Covey C, Thompson SL, Weissman PR, MacCracken MC (1994) Global climatic effects of atmospheric dust from an asteroid or comet impact on Earth. *Glob Planet Change* **9**: 263-273.

Croskell MS, Warner M, Morgan J (2002) Annealing of shocked quartz during atmospheric re-entry. *Geophy Res Lett* **29**(20): 1-4.

Crovisier JL, Honnorez J, Eberhart JP (1987) Dissolution of basaltic glass in seawater: Mechanism and rate. *Geochim Cosmochim Acta* **51**(11): 2977-2990.

d'Atri A, Dela Pierre F, Lanza R, Ruffini R (1999) Distinguishing primary and resedimented vitric volcaniclastic layers in the Burdigalian carbonate shelf deposits in Monferrato (NW Italy). *Sediment Geol* **129**(1-2): 143-163.

Dallmeyer RD (1984) 40Ar/39Ar ages from a pre-Mesozoic crystalline basement penetrated at Holes 537 and 538a of the Deep Sea Drilling Project Leg 77, southeastern Gulf of Mexico: Tectonic implications. Deep Sea Drilling Program. *Initial Reports* **77**: 497-504.

Dalwigk Iv, Ormö J (2001) Formation of resurge gullies at impacts at sea: The Lockne crater, Sweden. *Meteor Planet Sci* **36**(3): 359-369.

Daux V, Crovisier JL, Hemond C, Petit JC (1994) Geochemical evolution of basaltic rocks subjected to weathering: Fate of the major elements, rare earth elements, and thorium. *Geochim Cosmochim Acta* **58**(22): 4941-4954.

Dawson JB, Pinkerton H, Norton GE, Pyle DM (1990) Physical properties of alkali carbonatite lavas: Data from the 1988 eruption of Oldoinyo Lengai, Tanzania. *Geology* **18**(2): 260-263.

Decker PL (1990) Style and mechanics of liquefaction-related deformation; lower Absaroka Volcanic Supergroup (Eocene), Wyoming. *Geol Soc Am Spec Pap* **240**: 71.

Delano JW, Hanson B (1996) Liquid immiscibility: Cause of compositional heterogeneity in tektites (abstract). *Lun Planet Sci* **27**: 305-306.

DePaolo DJ, Kyte FT, Marshall BD, O'Neil JR, Smit J (1983) Rb-Sr, Sm-Nd, K-Ca, O, and H isotopic study of Cretaceous-Tertiary boundary sediments, Caravaca, Spain: Evidence for an oceanic impact site. *Earth Planet Sci Lett* **64**(3): 356-373.

Deutsch A, Schärer U, Agrinier P (1998) Evidence for back-reacted carbonates in distant of the Chicxulub impact event? An experimental approach (abstract). *Lun Planet Sci* **29**: #1363 (CD-ROM).

Doehne E, Margolis SV (1990) Trace-element geochemistry and mineralogy of the Cretaceous/Tertiary boundary: Identification of extraterrestrial components. In: Sharpton VL,

Ward PD (eds) Global catastrophes in Earth history: An interdisciplinary conference on impacts, volcanism, and mass mortality. *Geol Soc Am Spec Pap* **247**: 367-382.

Donaldson CH (1976) An experimental investigation of olivine morphology. *Contrib Mineral Petrol* **57**(2): 187-213.

Dressler BO, Reimold WU (2001) Terrestrial impact melt rocks and glasses. *Earth-Sci Rev* **56**(1-4): 205-284.

Dunlop DJ, Özdemir Ö (1997) Rock magnetism: Fundamentals and frontiers. Cambridge University Press, Cambridge: 1-573.

Echanove OE (1986) Geología petrolera de la Cuenca de Burgos (Parte 1): Considerations geólogico-petroleras. *Asociatión Mexicana de Geólogos Petroleros Bolletin* **38**: 1-39.

Einsele G (1998) Event stratigraphy: Recognition and interpretation of sedimentary event horizons. In: Doyle P, Bennet M (eds) Unlocking the stratigraphical record: Advances in modern stratigraphy. John Wiley & Sons, New York: 145-194.

Ekdale AA, Stinnesbeck W (1998) Trace fossils in Cretaceous-Tertiary (KT) boundary beds in Northeastern Mexico: Implications for sedimentation during the KT boundary event. *Palaios* **13**(1): 1-23.

Elliot CG, Williams PE (1988) Sediment slump structures: A review of diagnostic criteria and application to an example from Newfoundland. *Jour Struct Geol* **10**(2): 171-182.

Ellwood BB, MacDonald WD, Wheeler CW, Benoist SL (2003) The K-T boundary in Oman: Identified using magnetic susceptibility field measurements with geochemical confirmation. *Earth Planet Sci Lett* **206**(3-4): 529-540.

Engelhardt Wv, Arndt J, Fecker B, Pankau HG (1995) Suevite breccia from the Ries crater, Germany: Origin, cooling history and devitrification of impact glasses. *Meteoritics* **30**: 279-293.

Engelhardt Wv, Arndt J, Fecker B, Pankau HG (1997) Suevite breccia from the Ries impact crater, Germany: Petrography, chemistry and shock metamorphism of crystalline rock clasts. *Meteor Planet Sci* **32**(5): 545-554.

Erbacher J, Mosher DC, Malone MJ, Berti D et al. (2003) Shipboard Scientific Party: Leg 207 Preliminary report. Proceedings of the Ocean Drilling Program. *Initial Results* **207**: 1-63.

Evans NJ, Shahinpoor M, Ahrens TJ (1994) Hypervelocity impact: Ejecta velocity, angle, and composition. In: Dressler BO, Grieve RAF, Sharpton VL (eds) Large meteorite impacts and planetary evolution. *Geol Soc Am Spec Pap* **293**: 93-101.

Fairchild IJ (1983) Chemical controls of cathodoluminescence of natural dolomites and calcites: New data and review. *Sedimentology* **30**(4): 579-583.

Fisher RV, Schmincke H-U (1984) Pyroclastic rocks. Springer, Heidelberg: 1-472.

Föllmi KB, Grimm KA (1990) Doomed pioneers: Gravity-flow deposition and bioturbation in oxygen-deficient environments. *Geology* **18**(11): 1069-1072.

French BM (1998) Traces of catastrophe: A handbook of shock-metamorphic effects in terrestrial meteorite impact structures. *LPI Contribution* **954**. Lunar and Planetary Institute, Houston, Texas: 1-130.

Freundt A, Schmincke H-U (1998) Emplacement of ash layers related to high-grade ignimbrite P1 in the sea around Gran Canaria. Proceedings of the Ocean Drilling Program. *Scientific Results* **157**: 201-218.

Frey RW, Goldring R (1992) Marine event beds and recolonization surfaces as revealed by trace fossil analysis. *Geol Mag* **129**(3): 325-335.

Galloway WE (1998) Siliciclastic slope and base-of-slope depositional systems: Component facies, stratigraphic architecture, and classification. *Am Ass Petrol Geol Bull* **82**(4): 569-595.

Gilbert JS, Lane SJ (1994) The origin of accretionary lapilli. *Bull Volcanol* **56**(5): 398-411.

Glass BP (1990) Tektites and microtektites: Key facts and inferences. *Tectonophysics* **171**: 393-404.

Glass BP, Koeberl C (1999) Ocean Drilling Project Hole 689B spherules and upper Eocene microtektite and clinopyroxene-bearing spherule strewn fields. *Meteor Planet Sci* **34**(2): 197-208.

Glass BP, Muenow DW, Bohor BF, Meeker GP (1997) Fragmentation and hydration of tektites and microtektites. *Meteor Planet Sci* **32**(3): 333-341.

Glicken (1996) Rockslide-debris avalanche of May 18, 1980, Mount St. Helens volcano, Washington. *Open-File Report 96-677*. US Geological Survey, Reston, Virginia: 1-98.

Goldhammer RK, Johnson CA (2001) Middle Jurassic - Upper Cretaceous paleogeographic evolution and sequence-stratigraphic framework of the northwestern Gulf of Mexico rim. In: Bartolini C, Buffler RT, Cantú-Chapa A (eds) The western Gulf of Mexico basin: Tectonics, sedimentary basins and petroleum systems. *Am Ass Petrol Geolog Spec Mem* **75**: 45-82.

Graup G (1981) Terrestrial chondrules, glass spheres and accretionary lapilli from the suevite, Ries Crater, Germany. *Earth Planet Sci Lett* **55**: 407-418.

Graup G (1999) Carbonate-silicate liquid immiscibility upon impact melting: Ries Crater, Germany. *Meteor Planet Sci* **34**(3): 425-438.

Graup G, Palme H, Spettel B (1992) Trace element stratification in the Stevns Klint Cretaceous/Tertiary boundary layers (abstract). *Lun Planet Sci* **23**: 445-446.

Grieve RAF, Palme H, Plant AG (1980) Siderophile-rich particles in the melt rocks at the East Clearwater Impact structure, Quebec: Their characteristics and relationship to the impacting body. *Contrib Mineral Petrol* **75**(2): 187-198.

Grimm KA, Föllmi KB (1994) Doomed pioneers: Allochthonous crustacean tracemarkers in anaerobic basinal strata, Oligo-Miocene San Gregorio Formation, Baja California Sur, Mexico. *Palaios* **9**: 313-334.

Griscom Dl, Beltrán-López V, Merzbacher CI, Bolden E (1999) Electron spin resonance of 65-million-year-old glasses and rocks from the Cretaceous/Tertiary boundary. *Jour Non-Crystal Solids* **253**(1-3): 1-22.

Griscom Dl, Beltrán-López V, Pope KO, Ocampo AC (2003) New geochemical insights from electron-spin-resonance studies of Mn^{2+} and SO_3^- in calcites: Quantitative analyses of Chicxulub crater ejecta from Belize and southern Mexico with comparison to limestones from distal Cretaceous-Tertiary boundary sites. In: Koeberl C, Martínez-Ruiz F (eds) Impact markers in the stratigraphic record. *Impact studies*. Springer, Heidelberg: 229-270.

Guiraud M, Plaziat J-C (1993) Seismites in the fluviatile Bima sandstones: Identification of paleoseisms and discussion of their magnitudes in a Cretaceous synsedimentary strike-slip basin (Upper Benue, Nigeria). *Tectonophysics* **225**: 493-522.

Gupta SC, Ahrens TJ, Yang W (2001) Shock-induced vaporization of anhydrite and global cooling from the K/T impact. *Earth Planet Sci Lett* **188**(3-4): 399-412.

Haggerty SE (1991) Oxide textures: A mini-atlas. In: Lindsley DH (ed) Oxide Minerals: Petrologic and magnetic significance. *Reviews in Mineralogy* **25**. Mineralogical Society of America: 129-219.

Hallam A, Wignall PB (1999) Mass extinctions and sea-level changes. *Earth-Sci Rev* **48**(3-4): 217-250.

Hampton MA, Lee HJ, Locat J (1997) Submarine landslides. *Rev Geophys* **34**(1): 33-59.

Hart RJ, Cloete M, McDonald I, Carlson RW, Andreoli MAG (2002) Siderophile-rich inclusions from the Morokweng impact melt sheet, South Africa: Possible fragments of a chondritic meteorite. *Earth Planet Sci Lett* **198**(1-2): 49-62.

Hecht L, Schmitt RT, Wittmann A (2003) Hydrothermal alteration of the impactites at the ICDP drill site Yax-1 (Chicxulub Crater) (abstract). *Lun Planet Sci* **34**: #1583 (CD-ROM).

Heide K, Heide G, Kloess G (2001) Glass chemistry of tektites. *Planet Space Sci* **49**(8): 839-844.

Heider F, Koerner U, Bitschene PR (1993) Volcanic ash particles as carriers of remanent magnetization in deep-sea sediments from the Kerguelen Plateau. *Earth Planet Sci Lett* **118**(1-4): 121-134.

Heymann D, Yancey TE, Wolbach WS, Thiemens MH, Johnson EA, Roach D, Moecker S (1998) Geochemical markers of the Cretaceous-Tertiary boundary event at Brazos River, Texas, USA. *Geochim Cosmochim Acta* **62**(1): 173-181.

Hörz F, See TH (2000) Quenched olivines and pyroxenes in impact melts from Meteor Crater, AZ (abstract). *Lun Planet Sci* **31**: #1737 (CD-ROM).

Hörz F, See TH, Yang V, Mittlefehldt DW (1998) Major element composition of ballistically dispersed melt particles from Meteor Crater, AZ (abstract). *Lun Planet Sci* **29**: #1777 (CD-ROM).

Hower JC, Eslinger E, Hower ME, Perry EA (1976) Mechanism of burial metamorphism of argillaceous sediment: 1. Mineralogical and chemical evidence. *Geol Soc Am Bull* **87**(5): 725-737.

Hrouda F (1994) A technique for the measurement of thermal changes of MS of weakly magnetic rocks by the CS-2 apparatus and KLY-2 kappabridge. *Geophys Jour Int* **118**: 604-612.

Hsü KJ (1984) A scenario for the terminal Cretaceous event. Deep Sea Drilling Project. *Initial Reports* **73**: 755-763.

Hunt CP, Moskowitz BM, Banerjee SK (1995) Magnetic properties of rocks and minerals. In: Ahrens TJ (ed) A handbook of physical constants: Rock physics and phase relations. *AGU Reference Shelf* **3**. American Geophysical Union, San Francisco, California: 189-204.

Ifrim C (2000) Geologische, sedimentologische und geochemische Untersuchungen zum Kreide-Tertiär Übergang zwischen El Porvenir, Nuevo León, und El Mulato, Tamaulipas. *Unpublished Master Thesis*, Universität Karlsruhe: 1-137.

Ingram BL (1995) Ichthyolith strontium isotopic stratigraphy of deep-sea clays: Sites 885 and 886 (North Pacific transect). Proceedings of the Ocean Drilling Program. *Scientific Results* **145**: 399-412.

Ivanov BA, Badukov DD, Yakovlev OI, Gerasimov MV, Dikov YP, Pope KO, Ocampo AC (1996) Degassing of sedimentary rocks due to the Chicxulub impact: Hydrocode and physical simulations. In: Ryder G, Fastovsky D, Gartner S (eds) The Cretaceous-Tertiary boundary event and other catastrophes in Earth history. *Geol Soc Am Spec Pap* **307**: 125-139.

Izett GA (1990) The Cretaceous/Tertiary boundary interval, Ration basin, Colorado and New Mexico, and its content of shock-metamorphosed minerals: Evidence relevant to the K/T boundary impact-extinction event. *Geol Soc Am Spec Pap* **249**: 1-100.

Izett GA (1991) Tektites in Cretaceous-Tertiary boundary rocks on Haiti and their bearing on the Alvarez impact extinction hypothesis. *Jour Geophys Res* **96**(E4): 20879-20905.

Japel S, Prewitt C, Boctor N, Veblen D (2002) Iron-nickel phosphides at high pressures and temperatures (abstract). *EOS Trans AGU* **83**(47)(Fall Meeting Supplement): Abstract #MR61A-1025.

Johansson M, Stow DAV (1995) A classification scheme for shale clasts in deep water sandstones. In: Hartley AJ, Prosser DJ (eds) Characterization of deep marine clastic systems. *Geol Soc Lond Spec Pub* **94**: 221-241.

Johansson M, Braakenburg NE, Stow DAV, Faugeres J-C (1998) Deep-water massive sands: facies, processes and channel geometry in the Numidian Flysch, Sicily. *Sediment Geol* **115**(1-4): 233-265.

Jones AP, Claeys P, Heuschkel S (2000) Impact melting of carbonates from the Chicxulub impact crater. In: Gilmour I, Koeberl C (eds) Impacts and the Early Earth. *Lecture Notes in Earth Sciences* **91**. Springer, Heidelberg: 343-361.

Kamo SL, Krogh TE (1995) Chicxulub Crater source for shocked zircon crystals from the Cretaceous-Tertiary boundary layer, Saskatchewan: Evidence from new U-Pb data. *Geology* **23**(3): 281-284.

Keller G, Stinnesbeck W, López-Oliva J-G (1994) Age, deposition and biotic effects of the Cretaceous/Tertiary boundary event at Mimbral, NE Mexico. *Palaios* **9**: 144-157.

Keller G, López-Oliva J-G, Stinnesbeck W, Adatte T (1997) Age, stratigraphy and deposition of near-K/T siliciclastic deposits in Mexico: Relation to bolide impact? *Geol Soc Am Bull* **109**(6): 410-428.

Keller G, Adatte T, Stinnesbeck W, Affolter M, Schilli L, López-Oliva J-G (2002) Multiple spherule layers in the late Maastrichtian of northeastern Mexico. In: Koeberl C, MacLeod KG (eds) Catastrophic events and mass extinctions: Impacts and beyond. *Geol Soc Am Spec Pap* **356**: 145-162.

Kerschhofer L, Kettrup B, Deutsch A, Masaitis V (2000) Al-rich orthopyroxenes in impact melt coatings of gneiss bombs from Popigai, Russia (abstract). *Lun Planet Sci* **31**: #1360 (CD-ROM).

Kettrup B (2002) Impact lithologies and target rocks of the impact craters Popigai, Russia, and Chicxulub, Mexico: Geochemical investigations. *PhD Thesis*, Westfälische Wilhelms Universität Münster: 1-88.

Kettrup B, Deutsch A (2003) Geochemical variability of the Yucatán basement: Constraints from crystalline clasts in Chicxulub impactites. *Meteor Planet Sci*: (in press).

Kettrup B, Deutsch A, Masaitis VL (2003) Homogeneous impact melts produced by a heterogeneous target? Sr-Nd isotopic evidence from the Popigai crater, Russia. *Geochim Cosmochim Acta* **67**(4): 733-750.

Kettrup B, Deutsch A, Ostermann M, Agrinier P (2000) Chicxulub impactites: Geochemical clues to the precursor rocks. *Meteor Planet Sci* **35**(6): 1229-1238.

Kiessling W, Claeys P (2001) A geographic database approach to the KT boundary. In: Buffetaut E, Koeberl C (eds) Geological and biological effects of impact events. *Impact Studies.* Springer, Heidelberg: 83-140.

Klaver GT, Van Kempen TMG, Bianchi FR (1987) Green spherules as indicators of the Cretaceous/Tertiary boundary in Deep Sea Drilling Project Hole 603B. Deep Sea Drilling Project. *Initial Reports* **93**: 1039-1047.

Knaust D (2002) Pinch-and-swell structures at the Middle/Upper Muschelkalk boundary (Triassic): Evidence of earthquake effects (seismites) in the Germanic Basin. *Int Jour Earth Sci* **91**(2): 291-303.

Koeberl C (1994) Tektite origin by hypervelocity asteroidal or cometary impact: Target rocks, source craters, and mechanisms. In: Dressler BO, Grieve RAF, Sharpton VL (eds) Large meteorite impacts and planetary evolution. *Geol Soc Am Spec Pap* **293**: 133-151.

Koeberl C (1998) Identification of meteoritic components in impacites. In: Grady MM, Hutchison R, McCall GJH et al. (eds) Meteorites: Flux with time and impact effects. *Geol Soc Lond Spec Pub* **140**: 133-153.

Koeberl C, Sigurdsson H (1992) Geochemistry of impact glasses from the K/T boundary in Haiti: Relation to smectites and a new type of glass. *Geochim Cosmochim Acta* **56**: 2113-2129.

Kokelaar P, Busby C (1992) Subaqueous explosive eruption and welding of pyroclastic deposits. *Science* **257**: 196-200.

Kontny A, Schulte P, Stinnesbeck W (2002) Rock magnetic properties of iron-rich Chicxulub impact ejecta from La Sierrita, northeastern Mexico. *EOS Trans AGU* **83(47)** (Fall Meeting Supplement): Abstract #OS22C-0294.

Kontny A, Vahle C, de Wall H (2003) Characteristic magnetic behavior of subaerial and submarine lava units from the Hawaiian Scientific Drilling Project (HSDP-2). *Geochem Geophys Geosyst* **4**(2): 1-31.

Kramar U (1997) Advances in energy-dispersive X-ray fluorescence. *Jour Geochem Exploit* **58**: 73-80.

Kring DA, Boynton WV (1992) Petrogenesis of an augite-bearing melt rock in the Chicxulub structure and its relationship to K/T impact spherules in Haiti. *Nature* **358**: 141-143.

Kring DA, Durda DD (2002) Trajectories and distribution of material ejected from the Chicxulub impact crater: Implications for postimpact wildfires. *Jour Geophys Res* **107**(E8): 1-22.

Kring DA, Hörz F, Zürcher L (2003) Initial assessment of the excavation and deposition of impact lithologies exposed by the Chicxulub Scientific Drilling Project, Yaxcopoil, Mexico (abstract). *Lun Planet Sci* **34**: #1641 (CD-ROM).

Krogh TE, Kamo SL, Bohor BF (1993a) Fingerprinting the K/T impact site and determining the time of impact by U-Pb dating of single shocked zircons from distal ejecta. *Earth Planet Sci Lett* **119**(3): 425-429.

Krogh TE, Kamo SL, Sharpton VL, Marin LE, Hildebrand AR (1993b) U-Pb ages of single shocked zircons linking distal K/T ejecta to the Chicxulub crater. *Nature* **366**: 731-734.

Kübler B (1987) Cristallinité de l'illite, méthodes normalisées de préparations, méthodes normalisées de mesures. **Série ADX**. Cahiers de l'Institute Géologique de Neuchâtel, Suisse: 1-13.

Kyte FT, Vakulenko M (2001) KT boundary impact debris from DSDP Site 577 (abstract). Meteoritical Society, 64th Annual Meeting: #5423 (CD-ROM).

Kyte FT, Bostwick JA, Zhou L (1996) The Cretaceous-Tertiary boundary on the Pacific plate: Composition and distribution of impact debris. In: Ryder G, Fastovsky D, Gartner S (eds) The Cretaceous-Tertiary boundary event and other catastrophes in Earth history. *Geol Soc Am Spec Pap* **307**: 389-401.

Le Callonnec L, Renard M, Rocchia R, Bourdillon C, Galbrun B, Razin P, Roger J (1998) Approche géochimique (isotopes du carbone et iridium) de la limite Crétacé/Paléocène dans les montagnes d'Oman: Un événement "catastrophique" au sein d'une succession d'événements geologiques au cours du Maastrichtien et du Danien. *Bull Soc Géol Fr* **169**(4): 503-514.

Lindenmaier F (1999) Geologie und Geochemie an der Kreide/Tertiär-Grenze im Nordosten von Mexico. *Unpublished Master Thesis*, Universität Karlsruhe: 1-90.

Lindenmaier F, Stüben D, Kramar U, Stinnesbeck W, Keller G, López-Oliva J-G (1999) Chemostratigraphy of the K/T-boundary at La Sierrita and La Lajilla, NE Mexico (abstract). Annual Meeting. *Abstracts with Programs* **31**. Geol Soc Am: 123.

Lindinger M (1988) The Cretaceous/Tertiary boundaries of El Kef and Caravaca: Sedimentological, geochemical, and clay mineralogical aspects. *PhD Thesis*, ETH Zürich: 1-253.

Lofgren G (1974) An experimental study of plagioclase crystal morphology: Isothermal crystallization. *Am Jour Sci* **274**(3): 243 -273.

Longoria JF, Gamper MA (1995) Plankton foraminiferal faunas across the Cretaceous-Tertiary succession of Mexico: Implications for the Cretaceous-Tertiary boundary problem. *Geology* **23**(4): 329-332.

Lopez R, Cameron KL, Jones NW (2001) Evidence for Paleoproterozoic, Grenvillian, and Pan-African age Gond-

wanan crust beneath northeastern Mexico. *Precamb Res* **107**(3-4): 195-214.

López-Oliva J-G (1996) Stratigraphy of the Cretaceous/ Tertiary (K/T) boundary transition in northeastern and east-central Mexico. *PhD Thesis*, Princeton University: 1-246.

López-Oliva J-G, Keller G (1996) Age and stratigraphy of near-K/T boundary clastic deposits in northeastern Mexico. In: Ryder G, Fastovsky D, Gartner S (eds) The Cretaceous-Tertiary boundary event and other catastrophes in Earth history. *Geol Soc Am Spec Pap* **307**: 227-242.

López-Ramos E (1975) Geological summary of the Yucatán Peninsula. In: Nairn AEM, Stehli FG (eds) Ocean basins and margins: The Gulf of Mexico and the Caribbean **3**. Plenum Press, New York: 257-282.

Lowrie W (1990) Identification of ferromagnetic minerals in a rock by coercivity and unblocking temperature properties. *Geophy Res Lett* **17**(2): 159-162.

Luder T, Benz W, Stocker TF (2003) A model for long-term climatic effects of impacts. *Jour Geophys Res* **108**(E7): 5074.

MacDonald WD, Ellwood BB, Wheeler CW, Benoist SL (2002) Magnetic susceptibility variations across the Cretaceous-Tertiary boundary in Oman (abstract). American Geophysical Union, Spring Meeting: #GP32C-03.

Machel HG (2000) Application of cathodoluminescence to carbonate diagenesis. In: Pagel M, Barbin V, Blanc P et al. (eds) Cathodoluminescence in geosciences. Springer, Heidelberg: 271-301.

MacLeod N, Rawson PF, Forey PL, Banner FT et al. (1997) The Cretaceous-Tertiary biotic transition. *Jour Geol Soc Lond* **154**(2): 265-292.

Maltman AJ (1994a) Deformation structures preserved in rocks. In: Maltman AJ (ed) The geological deformation of sediments. Chapman & Hall, London: 261-303.

Maltman AJ (ed) (1994b) The geological deformation of sediments. Chapman & Hall, London: 1-362.

Martinez I, Agrinier P, Schärer U, Javoy M (1994) A SEM-ATEM and stable isotope study of carbonates from the Haughton impact crater, Canada. *Earth Planet Sci Lett* **121**: 559-574.

Martínez-Ruiz F, Ortega-Huertas M, Palomo-Delgado I, Acquafredda P (1997) Quench textures in altered spherules from the Cretaceous-Tertiary boundary layer at Agost and Caravaca, SE Spain. *Sediment Geol* **113**(1-2): 137-147.

Martínez-Ruiz F, Ortega-Huertas M, Palomo-Delgado I, Smit J (2001a) K-T boundary spherules from Blake Nose (ODP Leg 171B) as a record of the Chicxulub ejecta deposits. In: Kroon D, Norris RD, Klaus A (eds) Western North Atlantic Paleogene and Cretaceous paleoceanography. *Geol Soc Lond Spec Pub* **183**: 149-161.

Martínez-Ruiz F, Ortega-Huertas M, Palomo-Delgado I, Smit J (2002) Cretaceous-Tertiary boundary at Blake Nose (Ocean drilling Program Leg 171B): A record of the Chicxulub impact ejecta. In: Koeberl C, MacLeod KG (eds) Catastrophic events and mass extinctions: Impacts and beyond. *Geol Soc Am Spec Pap* **356**: 189-200.

Martínez-Ruiz F, Ortega-Huertas M, Kroon D, Smit J, Palomo-Delgado I, Rocchia R (2001b) Geochemistry of the Cretaceous-Tertiary boundary at Blake Nose (ODP Leg 171B). In: Kroon D, Norris RD, Klaus A (eds) Western North Atlantic Paleogene and Cretaceous paleoceanography. *Geol Soc Lond Spec Pub* **183**: 131-148.

Martinsen OJ (1994) Mass movements. In: Maltman AJ (ed) The geological deformation of sediments. Chapman & Hall, London: 127-165.

Marton GL, Buffler RT (1999) Jurassic-early Cretaceous tectono-paleogeographic evolution of the southeastern Gulf of Mexico basin. In: Mann P (ed) Caribbean Basins. *Sedimentary basins of the World* **4**. Elsevier, Amsterdam: 63-91.

Masaitis VL, Deutsch A (1999) Popigai: Gneiss bombs coated with impact melt – heating in the fireball? (abstract). *Lun Planet Sci* **30**: #1237 (CD-ROM).

McBride EF, Weidie AE, Wolleben JA (1975) Deltaic and associated deposits of Difunta Group (Late Cretaceous to Paleocene), Parras and La Popa Basins, northeastern Mexico. In: Broussard ML (ed) Deltas, models for exploration. Geological Society, Houston, Texas: 485-522.

McHugh CMG, Snyder SW, Miller KG (1998) Upper Eocene ejecta of the New Jersey continental margin reveal dynamics of Chesapeake Bay impact. *Earth Planet Sci Lett* **160**(3-4): 353-367.

Melosh HJ (1989) Impact cratering. Oxford University Press, New York: 1-245.

Mittlefehldt DW, See TH, Hörz F (1992) Dissemination and fractionation of projectile materials in the impact melts from the Wabar Crater, Saudi Arabia. *Meteoritics* **27**: 361-370.

Montanari A (1991) Authigenesis of impact spheroids in the K/T boundary clay from Italy: New constraints for high-resolution stratigraphy of terminal Cretaceous events. *Jour Sediment Petrol* **61**(3): 315-339.

Montanari A, Koeberl C (2000) Impact stratigraphy. *Lecture notes in Earth sciences* **93**. Springer, Heidelberg: 1-364.

Moore DM, Reynolds RC (1997) X-ray diffraction and the identification and analysis of clay minerals. Oxford University Press, Oxford: 1-378.

Morán-Zenteno DJ (1994) Geology of the Mexican Republic. *Am Ass Petrol Geol Stud Geol* **39**, Tulsa, Oklahoma: 1-150.

Morden SJ (1993) Magnetic analysis of K/T boundary layer clay from Stevns Klint, Denmark. *Meteoritics* **28**(4): 595-599.

Mørk MBE, Leith DA, Fanavoll S (2001) Origin of carbonate-cemented beds on the Naglfar Dome, Vøring Basin, Norwegian Sea. *Mar Petrol Geol* **18**(2): 223-234.

Morris RV, Golden DC, Allen CC, Ming DW, Mertzman SA, Thompson DR (1998) Major element fractionation during hydrolytic and sulfuric weathering on Mauna Kea volcano: Implications for weathering on Mars (abstract). *Lun Planet Sci* **29**: #1953 (CD-ROM).

Morton RA (1993) Attributes and origins of ancient submarine slides and filled embayments: Examples from the Gulf Coast Basin. *Am Ass Petrol Geol Bull* **77**(6): 1064-1081.

Muir JM (1936) Geology of the Tampico region, Mexico. Am Ass Petrol Geol, Tulsa, Oklahoma: 1-280.

Mulder T, Cochonat P (1996) Classification of offshore mass movements. *Jour Sediment Res* **66**(1): 43-57.

Müller J, Oberhänsli H, Melles M, Schwab M, Rachold V, Hubberten H-W (2001) Late Pliocene sedimentation in Lake Baikal: Implications for climatic and tectonic change in SE Siberia. *Palaeogeogr Palaeoclimatol Palaeoecol* **174**(4): 305-326.

Murray JW (1991) Ecology and palaeoecology of benthic foraminifera. Longman Scientific, London: 1-397.

Mutti E, Normark WR (1987) Comparing examples of modern and ancient turbidite systems: Problems and concepts. In: Legett JR, Zuffa GG (eds) Marine clastic sedimentology: Concepts and case studies. Graham & Trotman, London: 1-37.

Nakayama K, Yoshikawa S (1997) Depositional processes of primary to reworked volcaniclastics on an alluvial plain: An example from the lower Pliocene Ohta tephra bed of the Tokai Group, central Japan. *Sediment Geol* **107**(3-4): 211-229.

Newman ACD, Brown G (1987) The chemical constitution of clays. In: Newman ACD (ed) Chemistry of clays and cay minerals. *Mineralogical Society Monograph* **6**. Longman Scientific, London: 1-128.

Nichols RJ (1995) The liquification and remobilization of sandy sediments. In: Hartley AJ, Prosser DJ (eds) Character-

ization of deep marine clastic systems. *Geol Soc Lond Spec Pub* **94**: 63-76.

Nilsen TH (2000) The Hilt Bed, an Upper Cretaceous compound basin–plain seismoturbidite in the Hornbrook Forearc Basin of southern Oregon and northern California, USA. *Sediment Geol* **135**: 51-63.

Norris RD, Huber BT, Self-Trail BT (1999) Synchroneity of the K-T oceanic mass extinction and meteorite impact: Blake Nose, western North Atlantic. *Geology* **27**(5): 419-422.

Norris RD, Firth J, Blusztain JL, Ravizza G (2000) Mass failure of the North Atlantic margin triggered by the Cretaceous-Paleogene bolide impact. *Geology* **28**(12): 1119-1122.

Olsson RK, Miller KG, Browning JV, Habib D, Sugarmann PJ (1997) Ejecta layer at the Cretaceous-Tertiary boundary, Bass River, New Jersey (Ocean Drilling Program Leg 174AX). *Geology* **25**(8): 759-762.

Olsson RK, Miller KG, Browning JV, Wright JD, Cramer BS (2002) Sequence stratigraphy and sea-level changes across the Cretaceous-Tertiary boundary on the New Jersey passive margin. In: Koeberl C, MacLeod KG (eds) Catastrophic events and mass extinctions: Impacts and beyond. *Geol Soc Am Spec Pap* **356**: 97-108.

Ormö J, Lindström M (2000) When a cosmic impact strikes the sea bed. *Geol Mag* **137**(1): 67-80.

Ortega-Huertas M, Palomo-Delgado I, Martínez-Ruiz F, Gonzalez I (1998) Geological factors controlling clay mineral patterns across the Cretaceous-Tertiary boundary in Mediterranean and Atlantic sections. *Clay Miner* **33**(3): 483-500.

Ortega-Huertas M, Martínez-Ruiz F, Palomo-Delgado I, Chamley H (2002) Review of the mineralogy of the Cretaceous-Tertiary boundary clay: Evidence supporting a major extraterrestrial catastrophic event. *Clay Miner* **37**(3): 395-411.

Osinski GR, Spray JG (2001) Impact-generated carbonate melts: Evidence from the Haughton structure, Canada. *Earth Planet Sci Lett* **194**(1-2): 17-29.

Pagel M, Barbin V, Blanc P, Ohnenstetter D (2000) Cathodoluminescence in geosciences: An introduction. In: Pagel M, Barbin V, Blanc P et al. (eds) Cathodoluminescence in geosciences. Springer, Heidelberg: 1-21.

Pardo A, Ortiz N, Keller G (1996) Latest Maastrichtian and Cretaceous-Tertiary foraminiferal turnover and environmental changes at Agost, Spain. In: MacLeod N, Keller G (eds) Cretaceous-Tertiary boundary mass extinction: Biotic and environmental changes. Norton Press, New York: 139-171.

Perez Cruz GA (1993) Geologic evolution of the Burgos basin, Northeastern Mexico. *PhD Thesis*, Rice University: 1-155.

Petschick R, Kuhn G, Gingele F (1996) Clay mineral distribution in surface sediments of the South Atlantic: Sources, transport, and relation to oceanography. *Mar Geol* **130**(3): 203-229.

Pettijohn FJ, Potter PE, Siever R (1987) Sand and sandstone. Springer, Heidelberg: 1-552.

Philpotts AR (1990) Principles of igneous and metamorphic rocks. Prentice Hall, New Jersey: 1-498.

Pierazzo E, Melosh HJ (1999) Hydrocode modeling of Chicxulub as an oblique impact event. *Earth Planet Sci Lett* **165**(2): 163-176.

Pierazzo E, Kring DA, Melosh HJ (1998) Hydrocode simulations of the Chicxulub impact event and the production of climatically active gases. *Jour Geophys Res* **103**(E12): 28607-28625.

Pitakpaivan K, Byerly GR, Hazel JE (1994) Pseudomorphs of impact spherules from a Cretaceous-Tertiary boundary section at Shell Creek, Alabama. *Earth Planet Sci Lett* **124**(1): 49-56.

Poag CW (2002) Synimpact-postimpact transition inside Chesapeake Bay crater. *Geology* **30**(11): 995-998.

Pollastro RM, Bohor BF (1993) Origin and clay-mineral genesis of the Cretaceous/Tertiary boundary unit, Western Interior of North America. *Clays Clay Miner* **41**(1): 7-25.

Pope KO, Baines KH, Ocampo AC, Ivanov BA (1997) Energy, volatile production, and climate effects of the Chicxulub Cretaceous/Tertiary impact. *Jour Geophys Res* **E102**(9): 21645-21664.

Pope KO, Ocampo AC, Fischer AG, Alvarez W, Fouke BW, Webster CL, Vega FJ, Smit J, Fritsche AE, Claeys P (1999) Chicxulub impact ejecta from Albion Island, Belize. *Earth Planet Sci Lett* **170**(4): 351-364.

Pospichal JJ (1996) Calcareous nannofossils and clastic sediments at the K/T boundary, northeastern Mexico. *Geology* **24**(3): 255-258.

Premo WR, Izett GA (1993) U-Pb provenance ages of shocked zircons from the K-T boundary, Raton basin, Colorado (abstract). *Lun Planet Sci* **24**: 1171-1172.

Premo WR, Izett GA, Meeker GP (1995) Major-element and isotopic compositions of relic tektites and glass-like shards from the K/T boundary spherule bed at El Mimbral, Mexico (abstract). *Lun Planet Sci* **26**: 1139-1140.

Reading HG, Richards M (1994) Turbidite systems in deepwater basin margins classified by grain size and feeder system. *Am Ass Petrol Geol Bull* **78**(5): 792-822.

Rebolledo-Vieyra M, Vera-Sánchez P, Urrutia-Fucugauchi J, Marin LE (2000) Physical characteristics of deposition of impact breccias Pan-African basement affinities of Chicxulub crater (abstract). Catastrophic events and mass extinctions: Impacts and beyond. *LPI Contribution* **1053**. Lunar and Planetary Institute, Houston, Texas: 180-181.

Reed SJB (1996) Electron microprobe analysis and scanning electron microscopy in geology. Cambridge University Press, Cambridge: 1-199.

Richards M, Bowman M, Reading HG (1998) Submarine-fan systems i: Characterization and stratigraphic prediction. *Mar Petrol Geol* **15**(7): 689-717.

Ricketts BD, Evenchick CA (1999) Shelfbreak gullies, products of sea-level lowstand and sediment failure: Examples from Bowser Basin, northern British Columbia. *Jour Sediment Res* **69**(6): 1232-1240.

Robin E, Swinburn NHM, Froget L, Rocchia R, Gayraud J (1996) Characteristics and origin of the glass spherules from the Paleocene flood basalt province of western Greenland. *Geochim Cosmochim Acta* **60**(5): 815-830.

Rocchia R, Robin E, Froget L, Gayraud J (1996) Stratigraphic distribution of extraterrestrial markers at the Cretaceous-Tertiary boundary in the Gulf of Mexico area: Implications for the temporal complexity of the event. In: Ryder G, Fastovsky D, Gartner S (eds) The Cretaceous-Tertiary boundary event and other catastrophes in Earth history. *Geol Soc Am Spec Pap* **307**: 279-286.

Ross MI, Scotese CR (1988) A hierarchical tectonic model of the Gulf of Mexico and the Caribbean region. *Tectonophysics* **155**: 139-168.

Ryder G, Fastovsky D, Gartner S (eds) (1996) The Cretaceous-Tertiary event and other catastrophes in Earth history. *Geol Soc Am Spec Pap* **307**: 1-556.

Salge T, Tagle R, Claeys P (2000) Accretionary lapilli from the K-T boundary site of Guayal, Mexico: Preliminary insights of expansion plume formation (abstract). Meteoritical Society, 63th Annual Meeting: #5124 (CD-ROM).

Schilli L (2000) Etude de la limite K-T dans la region de la Sierrita, Nuevo Leon, Mexique. *Unpublished Master Thesis*, Université de Neuchâtel: 1-138.

Schlager W, Buffler RT, Angstadt D, Phair R (1984) Geologic history of the southeastern Gulf of Mexico. Deep Sea Drilling Project. *Initial Reports* **77**: 715-738.

Schmidt G, Palme H, Kratz KL (1997) Highly siderophile elements (Re, Os, Ir, Ru, Rh, Pd, Au) in impact melts from

three European impact craters (Saaksjarvi, Mien, and Dellen): Clues to the nature of the impacting bodies. *Geochim Cosmochim Acta* **61**(14): 2977-2987.

Schmitz B (1988) Origin of microlayering in worldwide distributed Ir-rich marine Cretaceous/Tertiary boundary clays. *Geology* **16**(12): 1068-1072.

Schmitz B (1992) Chalcophile elements and Ir in continental Cretaceous-Tertiary boundary clays from the Western Interior of the USA. *Geochim Cosmochim Acta* **56**: 1695-1703.

Schmitz B, Andersson P, Dahl J (1988) Iridium, sulfur isotopes and rare earth elements in the Cretaceous-Tertiary boundary clay at Stevns Klint, Denmark. *Geochim Cosmochim Acta* **52**: 229-236.

Schneider J-L, Le Ruyet A, Chanier F, Buret C, Ferriere J, Proust J-N, Rosseel J-B (2001) Primary or secondary distal volcaniclastic turbidites: How to make the distinction? An example from the Miocene of New Zealand (Mahia Peninsula, North Island). *Sediment Geol* **145**(1-2): 1-22.

Schulte P (1999) Geologisch-sedimentologische Untersuchung des Kreide/Tertiär (K/T)-Übergangs im Gebiet zwischen La Sierrita und El Toro, Nuevo Léon, Mexiko. *Unpublished Master Thesis*, Universität Karlsruhe: 1-134.

Schulte P, Stinnesbeck W, Kontny A, Stüben D, Kramar U, Harting M (2002) Multiple (immiscible) melt phases of mafic composition in Chicxulub impact ejecta from northeastern Mexico: New constraints on target lithologies. *EOS Trans AGU* **83(47)** (Fall Meeting Supplement): #OS22C-0293.

Schulte P, Stinnesbeck W, Stüben D, Kramar U, Berner Z, Keller G, Adatte T (2003) Fe-rich and K-rich mafic spherules from slumped and channelized Chicxulub ejecta deposits at the northern La Sierrita area, NE Mexico. *Int Jour Earth Sci* **92**(1): 114-142.

Schumacher R, Schmincke H-U (1991) Internal structure and occurrence of accretionary lapilli – A case study at Laacher See Volcano. *Bull Volcanol* **53**(8): 612-634.

Schumacher R, Schmincke H-U (1995) Models for the origin of accretionary lapilli. *Bull Volcanol* **56**(8): 626-639.

Schuraytz BC, Sharpton VL, Marín LE (1994) Petrology of impact-melt rocks at the Chicxulub multiring basin, Yucatán, Mexico. *Geology* **22**(10): 868-872.

See TH, Wagstaff J, Yang V, Hörz F, McKay GA (1998) Compositional variation and mixing of impact melts on microscopic scales. *Meteor Planet Sci* **33**(4): 937-948.

See TH, Galindo C, Golden DC, Yang V, Mittlefehldt DW, Hörz FP (1999) Major-element composition of ballistically dispersed melts from Meteor Crater, AZ (abstract). *Lun Planet Sci* **30**: #1633 (CD-ROM).

Senftle FE, Thorpe AN, May L, Barkatt A, Adel Hadadi MA, Marbury GS, Izett GA, Sigurdsson H, Maurrasse FJ (1993) Magnetic properties and Mössbauer analyses of glass from the K-T boundary, Beloc, Haiti (abstract). *Lun Planet Sci* **24**: 1275-1276.

Shanmugam G (1996) High density turbity currents: Are they sandy debris flows? *Jour Sediment Res* **66**(1): 2-10.

Shanmugam G (2002) Ten turbidite myths. *Earth-Sci Rev* **58**(3-4): 311-341.

Shanmugam G, Lehtonen LR, Straume T, Syversten SE, Hodgkinson RJ, Skibeli M (1994) Slump and debris-flow dominated upper slope facies in the Cretaceous of the Norwegian and Northern North Seas (61-67°N): Implications for sand distribution. *Am Ass Petrol Geol Bull* **78**(6): 910-937.

Shata S, Hesse R (1998) A refined XRD method for the determination of chlorite composition and application to the McGerrigle Mountains anchizone in the Quebec Appalachians. *Can Mineralogist* **36**(6): 1525-1546.

Shau YH, Feather ME, Essene EJ, Peacor DR (1991) Genesis and solvus relations of submicroscopically intergrown paragonite and phengite in a blueschist from Northern California. *Contrib Mineral Petrol* **106**(3): 367-378.

Shelley D (1993) Igneous and metamorphic rocks under the microscope. Chapman & Hall, London: 1-445.

Sigurdsson H, Leckie RM, Acton GD (1997) Shipboard Scientific Party: Caribbean volcanism, Cretaceous/Tertiary impact, and ocean climate history: Synthesis of Leg 165. Proceedings of the Ocean Drilling Program. *Initial Reports*: 377-400.

Smit J (1982) Extinction and evolution of planktonic foraminifera after a major impact at the Cretaceous/Tertiary boundary. In: Silver LT, Schultz PH (eds) Geological implications of impacts of large asteroids and comets on the Earth. *Geol Soc Am Spec Pap* **190**: 329-352.

Smit J (1999) The global stratigraphy of the Cretaceous-Tertiary boundary impact ejecta. *Ann Rev Earth Planet Sci* **27**: 75-113.

Smit J, Klaver GT (1981) Sanidine spherules at the Cretaceous/Tertiary boundary indicate a large impact event. *Nature* **292**: 47-49.

Smit J, Kyte FT (1984) Siderophile-rich magnetic spheroids from the Cretaceous-Tertiary boundary in Umbria, Italy. *Nature* **310**: 403-405.

Smit J, Alvarez W, Montanari A, Claeys P, Grajales-Nishimura JM (1996) Coarse-grained, clastic sandstone complex at the K/T boundary around the Gulf of Mexico: Deposition by tsunami waves induced by the Chicxulub impact? In: Ryder G, Fastovsky D, Gartner S (eds) The Cretaceous-Tertiary boundary event and other catastrophes in Earth history. *Geol Soc Am Spec Pap* **307**: 151-182.

Smit J, Alvarez W, Montanari A, Swinburn NHM, Van Kempen TM, Klaver GT, Lustenhouwer WJ (1992a) "Tektites" and microkrystites at the Cretaceous Tertiary boundary: Two strewn fields, one crater? *Lun Planet Sci* **22**: 87-100.

Smit J, Montanari A, Swinburn NHM, Alvarez W, Hildebrand AR, Margolis SV, Claeys P, Lowrie W, Asaro F (1992b) Tektite-bearing, deep-water clastic unit at the Cretaceous-Tertiary boundary in northeastern Mexico. *Geology* **20**(1): 99-103.

Soria AR, Liesa CL, Mata MP, Arz JA, Alegret L, Arenillas I, Meléndez A (2001) Slumping and a sandbar deposit at the Cretaceous-Tertiary boundary in the El Tecolote section (northeastern Mexico): An impact-induced sediment gravity flow. *Geology* **29**(3): 231-234.

Soria AR, Liesa CL, Mata MP, Arz JA, Alegret L, Arenillas I, Meléndez A (2002) Reply: "Slumping and a sandbar deposit at the Cretaceous-Tertiary boundary in the El Tecolote section (northeastern Mexico): An impact-induced sediment gravity flow". *Geology* **30**(4): 383.

Stähle V (1972) Impact glasses from the suevite of the Nördlinger Ries. *Earth Planet Sci Lett* **17**: 275-293.

Steiner MB, Walker JD (1996) Late Silurian plutons in Yucatán. *Jour Geophys Res* **101**(B8): 17727-17735.

Stinnesbeck W, Keller G (1996) K/T boundary coarse-grained siliciclastic deposits in northeastern Mexico and northeastern Brazil: Evidence for mega-tsunami or sea-level changes? In: Ryder G, Fastovsky D, Gartner S (eds) The Cretaceous-Tertiary boundary event and other catastrophes in Earth history. *Geol Soc Am Spec Pap* **307**: 197-209.

Stinnesbeck W, Keller G, Adatte T, López-Oliva J-G, MacLeod N (1996) Cretaceous-Tertiary boundary clastic deposits in NE Mexico: Bolide impact or sea-level lowstand? In: MacLeod N, Keller G (eds) The Cretaceous-Tertiary boundary mass extinction: Biotic and environmental events. Norton Press, New York: 471-517.

Stinnesbeck W, Barbarin JM, Keller G, López-Oliva J-G, Pivnik DA, Lyons JB, Officer CB, Adatte T, Graup G, Rocchia R, Robin E (1993) Deposition of channel deposits near the Cretaceous-Tertiary boundary in northeastern Mexico: Catastrophic or "normal" sedimentary deposits? *Geology* **21**(7): 797-800.

Stinnesbeck W, Schulte P, Lindenmaier F, Adatte T et al. (2001) Late Maastrichtian age of spherule deposits in northeastern Mexico: Implication for Chicxulub scenario. *Can Jour Earth Sci* **38**(2): 229-238.

Stix J (1991) Subaqueous, intermediate to silicic-composition explosive volcanism: A review. *Earth-Sci Rev* **31**(1-2): 21-53.

Stöffler D (1971) Progressive metamorphism and classification of shocked and brecciated crystalline rocks at impact craters. *Jour Geophys Res* **76**(23): 5541-5551.

Stöffler D, Hecht L, Kenkmann T, Schmitt RT, Wittmann A (2003) Properties, classification, and genetic interpretation of the allochthonous impact formations of the ICDP Chicxulub drill core YAX-1 (abstract). *Lun Planet Sci* **34**: #1553 (CD-ROM).

Stow DAV, Mayall M (2000) Deep-water sedimentary systems: New models for the 21st century. *Mar Petrol Geol* **17**(2): 125-135.

Stow DAV, Johansson M (2000) Deep-water massive sands: Nature, origin and hydrocarbon implications. *Mar Petrol Geol* **17**: 145-174.

Stow DAV, Reading HG, Collinson JD (1996) Deep seas. In: Reading HG (ed) Sedimentary environments: Processes, facies and stratigraphy. Blackwell Science, Oxford: 395-454.

Strachan LJ (2002) Slump-initiated and controlled syndepositional sandstone remobilization: An example from the Namurian of County Clare, Ireland. *Sedimentology* **49**(1): 25-41.

Stroncik NA, Schmincke H-U (2002) Palagonite – A review. *Int Jour Earth Sci* **91**(4): 680-697.

Stüben D, Kramar U, Berner Z, Eckhardt J-D, Stinnesbeck W, Keller G, Adatte T, Heide K (2002) Two PGE anomalies above the Cretaceous/Tertiary boundary at Beloc/Haiti: Geochemical context and consequences for the impact scenario. In: Koeberl C, MacLeod KG (eds) Catastrophic events and mass extinctions: Impacts and beyond. *Geol Soc Am Spec Pap* **356**: 163-188.

Sturkell E, Ormö J, Nõlvak J, Wallin Å (2000) Distant ejecta from the Lockne marine-target impact crater, Sweden. *Meteor Planet Sci* **35**(5): 929-936.

Sweet AR, Braman DR, Lerbekmo JF (1999) Sequential palynological changes across the composite Cretaceous-Tertiary (K-T) boundary claystone and contiguous strata, western Canada and Montana, USA. *Can Jour Earth Sci* **36**(5): 743-768.

Tada R, Nakano Y, Iturralde-Vinent MA, Yamamoto S et al. (2002) Complex tsunami waves suggested by the Cretaceous-Tertiary boundary deposit at the Moncada section, western Cuba. In: Koeberl C, MacLeod KG (eds) Catastrophic events and mass extinctions: Impacts and beyond. *Geol Soc Am Spec Pap* **356**: 109-124.

Tada R, Iturralde-Vinent MA, Matsui T, Tajika E et al. (2003) K/T boundary deposits in the paleo-western Caribbean Basin. In: Bartolini C, Buffler RT, Blickwede JF (eds) The Gulf of Mexico and Caribbean region: Hydrocarbon habitats, basin formation and plate tectonics. *Am Ass Petrol Geolog Spec Mem* (in press).

Thorpe AN, Senftle FE, May L, Barkatt A, Adel-Hadadi MA, Marbury GS, Izett GA, Maurrasse FR (1994) Comparison of the magnetic properties and Mössbauer analysis of glass from the Cretaceous-Tertiary boundary, Beloc, Haiti, with tektites. *Jour Geophys Res* **99**(5): 10,881-10,886.

Toon OB, Zahnle K, Morrison D, Turco RP, Covey C (1997) Environmental perturbations caused by the impacts of asteroids and comets. *Rev Geophys* **35**(1): 41-78.

Treiman AH (1989) Carbonatite magma: Properties and processes. In: Bell K (ed) Carbonatites: Genesis and evolution. Unwin Hyman, London, UK: 89-104.

Tsikalas F, Gudlaugsson ST, Faleide JI (1998) Collapse, infilling, and postimpact deformation at the Mjolnir impact structure, Barents Sea. *Geol Soc Am Bull* **110**(5): 537-552.

Tucker ME, Wright VP (1992) Carbonate sedimentology. Blackwell Science, Oxford: 1-482.

Utzmann A, Hansteen TH, Schmincke H-U (2002) Trace element mobility during sub-seafloor alteration of basaltic glass from Ocean Drilling Program site 953 (off Gran Canaria). *Int Jour Earth Sci* **91**(4): 661-679.

Vajda V, Raine JI, Hollis CJ (2001) Indication of global deforestation at the Cretaceous-Tertiary boundary by New Zealand fern spike. *Science* **294**: 1700-1702.

Varenkamp JC, Thomas E (1982) Chalcophile elements in Cretaceous-Tertiary boundary sediments: Terrestrial or extraterrestrial? In: Silver LT, Schultz PH (eds) Geological implications of impacts of large asteroids and comets on the Earth. *Geol Soc Am Spec Pap* **190**: 461-467.

Verma HC, Upadhyay C, Tripathi A, Tripathi RP, Bhandari N (2002) Thermal decomposition pattern and particle size estimation of iron minerals associated with the Cretaceous-Tertiary boundary at Gubbio. *Meteor Planet Sci* **37**(7): 901-909.

Ward WC, Keller G, Stinnesbeck W, Adatte T (1995) Yucatán subsurface stratigraphy: Implications and constraints for the Chicxulub impact. *Geology* **23**(10): 873-876.

Warme JE, Morgan M, Kuehner H-C (2002) Impact-generated carbonate accretionary lapilli in the Late Devonian Alamo breccia. In: Koeberl C, MacLeod KG (eds) Catastrophic events and mass extinctions: Impacts and beyond. *Geol Soc Am Spec Pap* **356**: 489-504.

Wdowiak TJ, Armendarez LP, Agresti DG, Wade ML, Wdowiak YS, Claeys P, Izett GA (2001) Presence of an iron-rich nanophase material in the upper layer of the Cretaceous-Tertiary boundary clay. *Meteor Planet Sci* **36**(1): 123-133.

Weidie AE, Murray GE (1967) Geology of Parras Basin and adjacent areas of northeastern Mexico. *Am Ass Petrol Geol Bull* **51**(5): 678-695.

Weidie AE, Wolleben JA, McBride EF (1972) Late Cretaceous depositional systems in Northeastern Mexico. *Gulf Coast Ass Geol Soc Transact* **22**: 323-329.

Werner T, Borradaile GJ (1998) Homogeneous magnetic susceptibilities of tektites: Implications for extreme homogenization of source material. *Phys Earth Planet Inter* **108**(3): 235-243.

Wignall PB (2001) Large igneous provinces and mass extinctions. *Earth-Sci Rev* **53**(1-2): 1-33.

Worm HU, Banerjee SK (1987) Rock magnetic signature of the Cretaceous-Tertiary boundary. *Geophy Res Lett* **14**(11): 1083-1086.

Yancey TE (1996) Stratigraphy and depositional environments of the Cretaceous/Tertiary boundary complex and basal section, Brazos River, Texas. *Gulf Coast Ass Geol Soc Transact* **46**: 433-442.

Yancey TE (2002) Carbonate ejecta spherules in Cretaceous-Tertiary boundary deposits, Brazos River, Texas (abstract). Geol Soc Am, Annual Meeting: #178-12.

3. The Cretaceous-Paleogene transition at Brazos, Texas: Chicxulub ejecta, depositional events, and sea-level changes

3.1 Introduction

Sediments covering the Cretaceous-Paleogene (K-P) transition in sections and cores from the northwestern Gulf of Mexico frequently comprise a complex depositional sequence (Fig. 3.1 and Bohor, 1996; Gartner, 1996; Keller and Stinnesbeck, 1996; Smit et al., 1996). This unique K-P succession shows a characteristic stacking pattern with basal high-energy and ejecta-rich deposits overlain by multiple sets of sandy deposits. However, the exact depositional nature of these K-P sequences in the Gulf of Mexico area and their biostratigraphic age is subject to controversial discussion.

Typical examples for this clastic K-P succession can be found at the outer-shelf Brazos River area in Texas (cf. Rocchia et al., 1996; Yancey, 1996), the inner-shelf sections in south-central Alabama (Moscow Landing, Braggs, Antioch Church, cf. Donovan et al., 1988 and Chapter 4), outer-shelf to upper bathyal sections in central to northeastern Mexico (Chapter 2 and Smit et al., 1996; Stinnesbeck et al., 1996), and the DSDP Leg 77 in the western Gulf of Mexico (Alvarez et al., 1992).

In these sites, the clastic K-P succession disconformably overlies late(st) Maastrichtian shelf sediments and includes: (i) basal, single, or multiple coarse deposits, which contain large amounts of diverse ejecta phases (e.g., spherules, carbonate clasts) presumably derived from the Chicxulub impact on the Yucatán peninsula, southern Mexico. In addition, the basal parts bear large rip-up clast from the underlying formations that indicate high-energy transport. This basal, ejecta-rich deposit may grade upward into, or is followed by, (ii) single or multiple layers of fine, well-sorted sand or sandstone, often rich in foraminiferal shells. These sand layers show an upward-decrease in transport-energy, are bioturbated, especially in their uppermost parts, and, finally, may gradually or abruptly give way to (iii) marls or shales of (reworked?) Maastrichtian or, more commonly, Danian age. Frequently, multiple iridium-anomalies are present, starting in the upper sandy deposits and reaching into the overlying sediments.

One set of authors has correlated these siliciclastic deposits to the latest Maastrichtian sea-level lowstand about 300-200 ka pre-K-P (Keller and Stinnesbeck, 1996; Keller et al., 1997; Stinnesbeck et al., 1996), whereas other authors have interpreted them as tsunami deposits, immediately linked to the Chicxulub impact (Smit et al., 1996; Arz et al., 2001; Soria et al., 2001; Alegret et al., 2002b). Also, they are regarded as turbidites and debris flows, probably
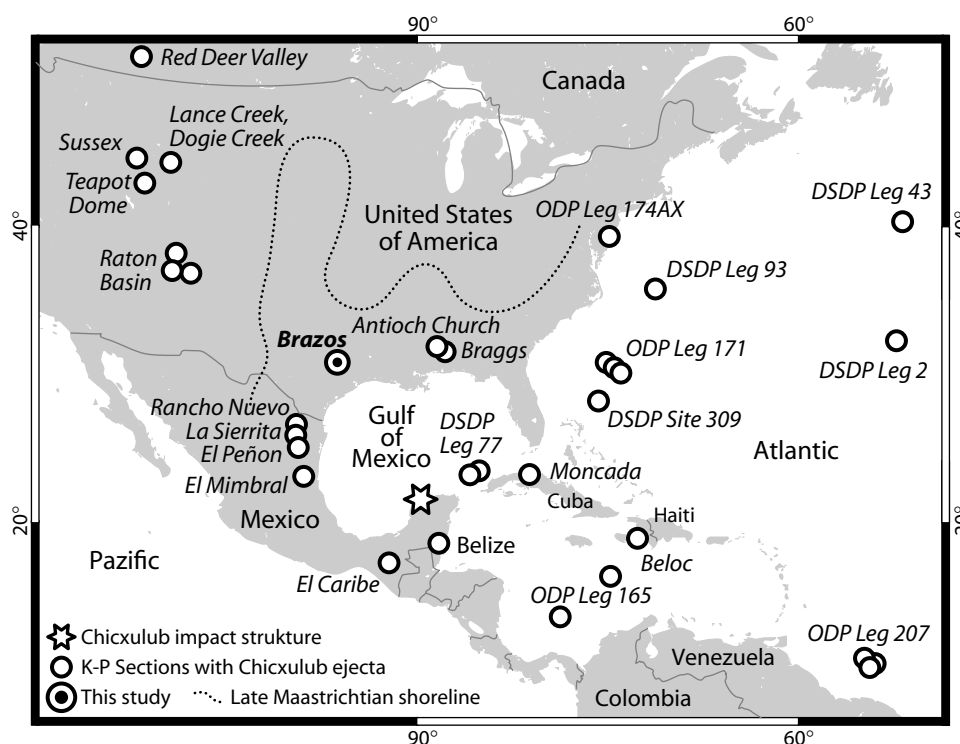
Figure 3.1 Gulf of Mexico with adjacent areas and K-P boundary sections referred to in this study. Position of Latest Cretaceous shoreline and Western Interior Seaway according to Kennedy et al. (1998).
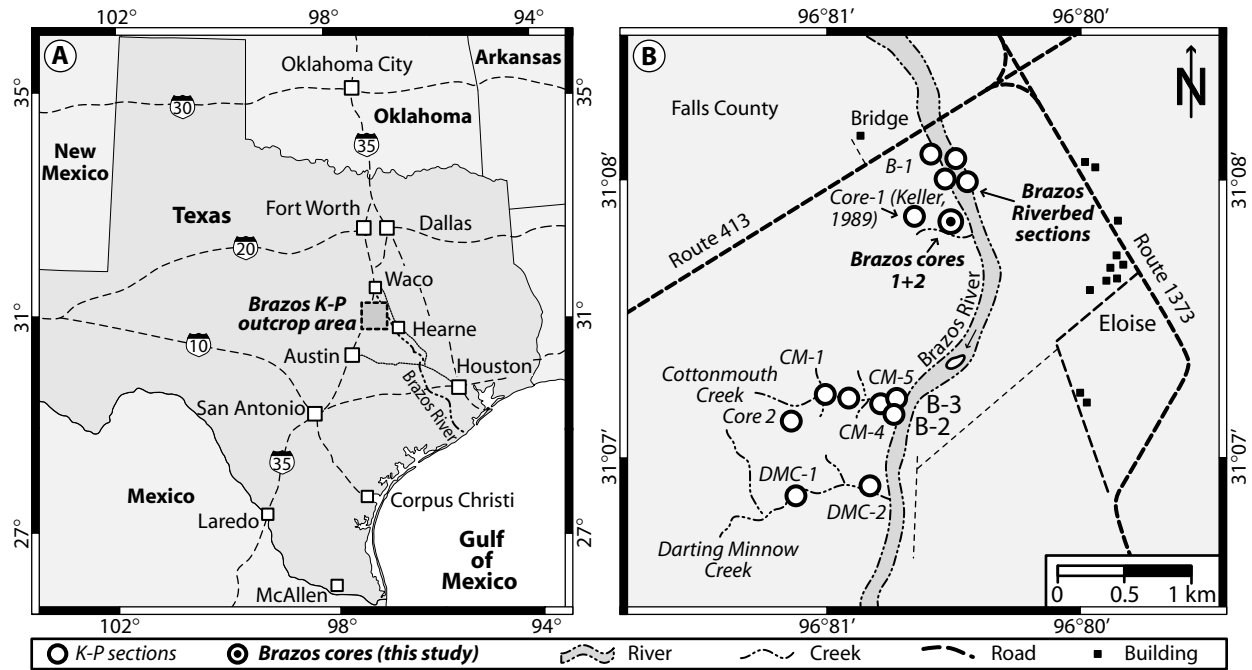
Figure 3.2 (**A**) Map of Texas and (**B**) close-up of the Brazos area with the localities of outcrops and cores.

related to the Chicxulub impact or postimpact processes (e.g., crater collapses or major storm events, cf. Bohor, 1996; Yancey, 1996; 1997). However, considering the extensive geographic distribution of these depositional sequences and their complex stratal architecture, the question arises as if it is possible to give 'one' universally applicable explanation to the driving forces that generated this characteristic depositional sequence in these K-P sections, and if they are related to one or more depositional events. Particularly, in view of their different setting within deep, separate (foreland) basins and shallow shelf environments in distinct tectonic provinces of the Gulf of Mexico (e.g., Sohl et al., 1991; Goldhammer and Johnson, 2001).

Recent studies have stimulated this controversy. For instance, the paleowater depth of K-P sections in northeastern Mexico is now considered between 500-1000 m (Alegret et al., 2001; 2002a; 2002b; Arz et al., 2001), which is difficult to reconcile with a tsunami-wave origin (e.g., Dawson and Shi, 2000). However, deposits triggered by tsunami-related backwash currents may be highly variable and have been observed in bathyal sites of the Mediterranean (so-called "homogenites", e.g., Cita and Aloisi, 2000; Scheffers and Kelletat, 2003). On the other hand, considering a deposition during lowered sea level, sequence stratigraphic studies have shown that clastic deposits in shelfal to slope settings can be generated through the entire 'sea-level cycle' (Burgess and Hovius, 1998; Burgess et al., 2000; Talling,

1998; Plink-Björklund and Steel, 2002). Hence, they are not necessarily restricted to distinct lowlands, though they may be more frequent during times of coastal progradation (e.g., Van Wagoner et al., 1990; Van Wagoner, 1995). However, high-resolution stratigraphic studies have revealed divergent and even contradictory trends in sea-level behavior during the latest Maastrichtian and earliest Danian: Some studies showed a transgressive interval across the K-P boundary in the western Atlantic (e.g., Olsson et al., 2002), others concluded from studies of the K-P transition in the Tethyan realm (e.g., El Kef, Tunisia) that the K-P boundary corresponds to a maximum flooding surface (Adatte et al., 2002a; 2002b; Stüben et al., 2002a), whereas Speijer and van der Zwaan (1996), Tribovillard et al. (2000), Peryt et al. (2002), and Alegret et al. (2003), pointed out that no particular proximal-distal facies trends occurred during this period.

For the Gulf of Mexico, and particularly for the Brazos K-P section, a pronounced sea level lowstand almost coinciding with the first appearance of early Paleocene microfossils was suggested by Keller (1989a; 1989b; 1992), though in later studies, Keller and Stinnesbeck (1996), and Stinnesbeck et al. (1996), concluded that this lowstand occurred during the latest Maastrichtian and suggested that rising sea-levels characterize the K-P boundary. In contrast, Barrera and Keller (1990) concluded that no particular facies change occurred across the K-P boundary, in keeping with the results of Yancey (1996), who

observed no evidence for major sea-level fluctuations for this period, and placed a sequence boundary in the earliest Danian.

The shallow-shelf setting of the well-known Brazos-River K-P sections in central Texas provides an excellent opportunity to reconstruct environmental changes, including sea-level fluctuations during the K-P transition. However, geochemical and mineralogical parameters, and particularly the petrology of Chicxulub ejecta components in the event deposit, have yet rarely been considered, despite providing excellent opportunities to reconstruct environmental changes through time and for correlation with other K-P sections.

In this study, two new cores drilled close to the Brazos River outcrops are investigated. The two cores combined constitute an expanded succession of 15 m of late Maastrichtian and early Danian strata. This multidisciplinary study (i) documents the lithology and stratigraphy of these cores, added by paleoecological aspects, (ii) examines the sedimentological and petrological characteristics to distinguish between sedimentary processes that caused the event deposit and evaluates the origin and characteristics of the Chicxulub ejecta phases, and (iii) analyzes the mineralogical and geochemical composition to evaluate possible or postulated changes in the environmental conditions during the K-P transition with a focus put on sea-level fluctuations.

3.1.1 Previous results from K-P studies at Brazos, Texas

Some 15-20 Cretaceous-Paleogene outcrops and cores from the Brazos riverbed, the adjacent Cottonmouth Creek, and the Darting Minnow Creek are currently documented in the Brazos area (Fig. 3.2). Previous studies have addressed biotic and sedimentological parameters, including biostratigraphy (Jiang and Gartner, 1986; Keller, 1989a, 1989b; Keller et al., 1993; MacLeod and Keller, 1991; Olsson and Liu, 1993), lithostratigraphy and depositional environments (Bourgeois et al., 1988; Smit et al., 1996; Yancey, 1996; Heymann et al., 1998), iridium enrichment (Hansen et al., 1993b; Evans et al., 1995; Rocchia et al., 1996; Heymann et al., 1998), and faunal changes during the K-P transition (Jiang and Gartner, 1986; Hansen et al., 1987; Hansen et al., 1993a; Hansen et al., 1993b; Keller, 1989a, 1989b; Harries, 1999; Kennedy et al., 2001).

The conclusions of these studies may reach from full agreement, up to widely disparate or even contradictory opinions. Among the points that are

agreed to by most studies are the following (see Fig. 3.3 for details): (i) the presence of multiple iridium anomalies starting in the topmost part(s) of the event deposit and extending into the overlying shales, (ii) the absence of a distinct ferruginous and mm-thick boundary clay (with spherules, Ni-rich spinels, etc.) in the Brazos sections, (iii) The presence of a 10-20 cm thick shale interval with uncertain stratigraphic age that overlies the event deposit and underlies sediments of the earliest Paleocene, and (iv) deposition of the event deposit did apparently not result from a single event, but took place during a longer period, though, the amount of time involved in its formation has been debated controversially.

The points upon which no consensus was reached include: (i) the position of the K-P boundary with respect to the event deposit, (ii) the evidence for the presence of impact ejecta in the event deposit, (iii) the mode of origin of the interval above the event deposit, whether long-term or rapid deposition by settling from tempestites, and finally, (iv) the origin of the event deposit itself, whether tsunami- or tempestite-generated or resulting from deposition during a sea-level lowstand.

3.1.2 Locality and geological setting

The Brazos cores were drilled in close proximity at the right side of the Brazos River, about 370 m downstream from the Texas Highway 413 Bridge, which is located near the crossing between Texas Highway 413 and 1773 in south-central Texas (Fig. 3.2). Consequently, the Brazos cores are situated in close proximity to the 'Brazos River sections' that are located in the river floor and banks, about 100 m to the northeast (Hansen et al., 1987; 1993a; 1993b; Yancey, 1996).

The Brazos River Valley is underlain by mildly attenuated continental crust (e.g., Ross and Scotese, 1988), and has been gradually subsiding since the middle of the Mesozoic (see Galloway et al., 1991; Sohl et al., 1991). The region is known for nearly continuous, and predominantly siliciclastic sedimentation during the K-P transition (Davidoff and Yancey, 1993). In addition, the Brazos area is located in the 'entrance' to the Western Interior Seaway, which during most of the Cretaceous connected the Gulf of Mexico with the intra-continental parts of this seaway across large parts of the Dakotas and Nebraska, though significantly reduced through the late Cretaceous (see Fig. 3.1 and Kennedy et al., 1998; Sweet and Braman, 2001).
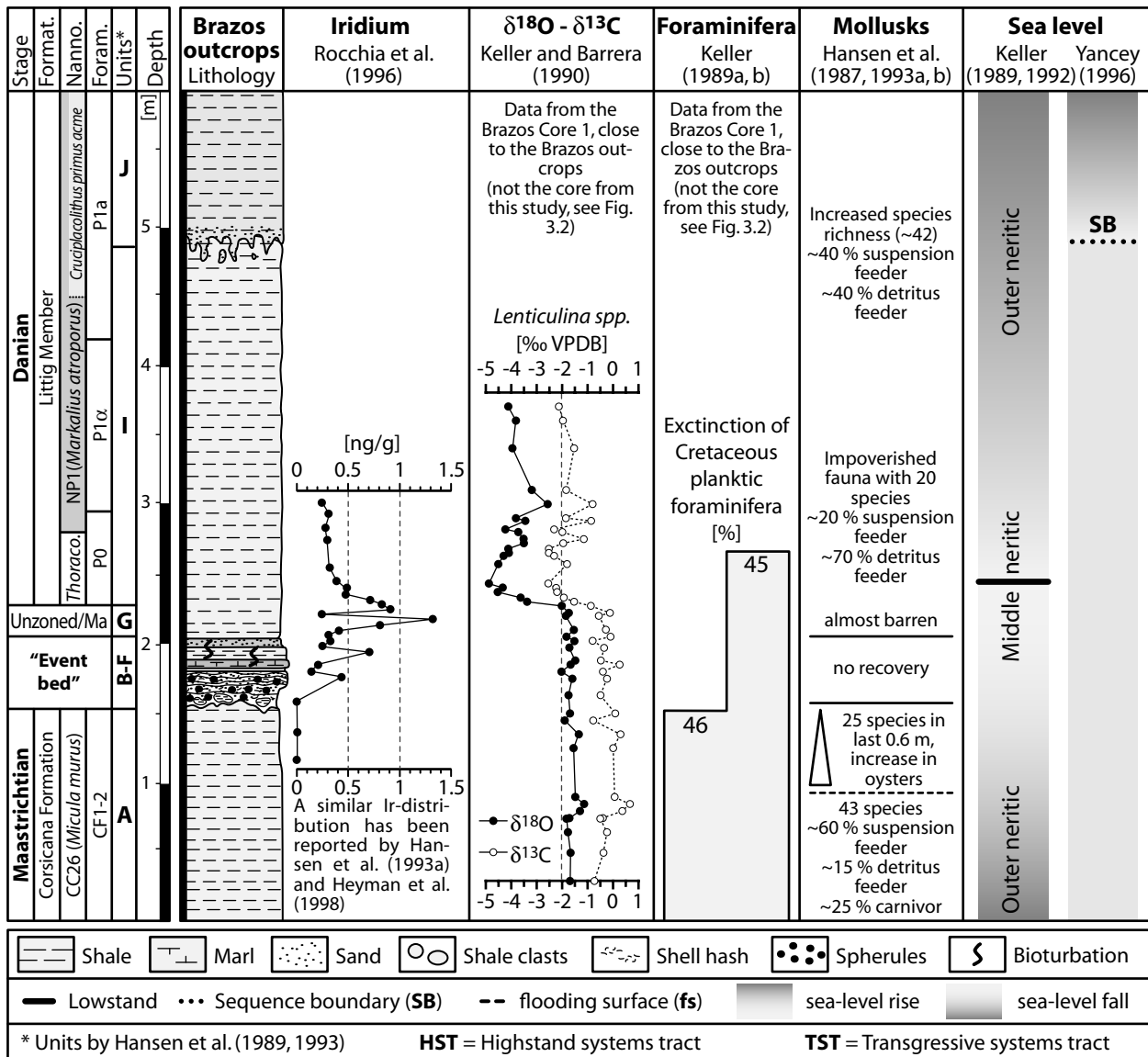
Figure 3.3 Composite stratigraphic section with the summary of previous results: Planktic foraminifera stratigraphy is from a Brazos core by Keller (1989a), calcareous nannofossil zonation is from the Brazos River outcrop from Jiang and Gartner (1986). The iridium-, stable isotope-, molluscan- data, and the sea-level interpretations have been correlated between by the author. Note: (i) the bioturbation of the event bed is only shown in the paper by Hansen et al. (1987). No bioturbation is mentioned in the subsequent papers by this group (Hansen et al., 1993b; 1993a), and in the papers provided by Keller (1989a; 1989b) or Yancey (1996). (ii) An exact correlation of Ir-peaks and δ^{13}C excursions is difficult, since no collection of paired samples exists on which both measurements were made. However, there appears to be a consensus that the lowermost of a series of peak Ir concentration starts already within the top of the 'event deposit, and that the uppermost Ir anomalies are close to the first appearance of earliest Danian planktic foraminifers and calcareous nannofossils (Keller, 1989a; Beeson et al., 1994; Rocchia et al., 1996).

According to Galloway (1989), the provenance of sediments in the Texas area can be assigned to the Great Plain area and the northern part of the Rio Grande rift. The western part of the remnant Ouachita Mountains might also have contributed sediment (e.g., Winker, 1982). Pulses of sediment input to the northwestern margin of the Gulf of Mexico coincided with episodes of distant tectonism in the Rocky Mountains and culmination of the NW-SE Laramide orogeny (Galloway, 1989). Quantities of sediment supply to the Texas portion

of the Gulf coast have generally been higher than the development of accommodation space on the continental shelf, resulting in an outward prograding shelf margin and an overall shallowing trend from the latest Cretaceous to the Late Eocene (Davidoff and Yancey, 1993). Therefore, the end Cretaceous to Paleogene marine sediments at the Brazos river site reflect a general trend of environmental change from mid-outer shelf settings during the latest Cretaceous-early Paleocene (shelf-slope break at approximately 100 km down-dip of the Brazos river outcrops) to

non-marine by the Eocene (basinward migration of the shelf-slope break). These general trend of environmental change at the Brazos area and progradation of the Paleogene shelf margin has been modified substantially by variations in sediment supply and changes in eustatic sea level (cf. Galloway, 1989). However, this progradational facies trend via strong sediment input might have dominated over regional sea-level trends, which suggest a transgressive event during the K-P transition in the Dakotas (Johnson, 2002), in the Carolinas (Hargrove and Engelhardt, 1997), and in Alabama (Chapter 4 and Baum and Vail, 1988; Donovan et al., 1988).

3.2 Analytical techniques

The following analytical techniques were used to characterize the sediments of the K-P transition in the Brazos cores, Texas; for the geochemical and mineralogical analyses, samples were dried, crushed, and finely ground in an agate mill.

Biostratigraphy: Samples were prepared for planktic foraminiferal biostratigraphic analysis by using two size fractions (38-63 μm and >63 μm) after methods given by Pardo et al. (1996), and for qualitative and quantitative benthic foraminiferal analysis after methods given by Speijer et al. (1996). The planktic and benthic foraminifera were analyzed by Robert Speijer, University of Bremen.

For nannofossil biostratigraphy, sample material was ultrasonically cleaned in a weak ammonium solution for 3 minutes. The resulting suspension was allowed to settle for 3 minutes and the water decanted. The deposit was then again brought into suspension and a few drops spread over a graphitic scanning electron microscope (SEM) stub. After drying and coating with gold, the stub was observed in a SEM at 2.5 K magnification. The calcareous nannofossils were analyzed by Hartmut Mai, University of Bremen.

Nonclay and clay mineralogy was analyzed by X-ray diffractometry (XRD) at the Geological Institute of the University of Neuchâtel, Switzerland, with a SCINTAG XRD 2000 diffractometer and Cu-kα-radiation. Diffractograms were evaluated with the MacDIFF software (freeware by R. Petschick, University of Frankfurt, for details see Petschick et al., 1996) and methods outlined in Appendix 3.1. The semiquantitative estimation of the relative abundance of the clay minerals was conducted by using the ratios of the weighted peak areas of smectite (weighting factor '1'), chlorite ('2'), illite ('4'), and

kaolinite ('2') from glycolated specimen. In order to ease comparison with non-weighted datasets, the raw-data, including peak position, height, and area, is given in the Appendix 3.3.

Major elements were determined by wavelength-dispersive X-ray fluorescence spectrometry (WDS) at the Institute for Mineralogy and Geochemistry, University of Karlsruhe, with a SRS 303 AS XRF. For these analyses, fused glass discs were prepared from a mixture of 1 g ignited powder of each sample and 4 g of SPECTROMELT. Major elements were evaluated by a fundamental parameter calibration procedure.

Trace elements (Cr, Ni, Cu, Zn, As, Rb, Sr, Y, Zr, Ba, La, Ce, and Pb) were analyzed from bulk powder samples (5 g) by energy-dispersive X-ray fluorescence spectrometry (EDS) with a SPECTRACE 5000 X-ray analyzer at the Institute for Mineralogy and Geochemistry, University of Karlsruhe. Trace elements were determined using a Compton and intensity matrix correction procedure. Detailed analytical procedures, detection limits, and standards used were compiled by Kramar (1997).

Electron microprobe: Wavelength-dispersive (WDS) and energy-dispersive (EDS) electron microprobe analyses, as well as back-scattered electron (BSE) images were performed with a CAMECA SX50 microprobe on polished, carbon-coated thin sections at the Laboratory for Electron Microscopy, University of Karlsruhe. Detailed sample preparation techniques and analytical methods are summarized in Reed (1996). The SX50 microprobe is equipped with four crystal spectrometers, an EDS system and an electron backscatter detector. Quantitative (WDS) microprobe analyses were carried out using the crystals TAP (Si, Al), PET (Ti, Ca, K, P), RAP (Mg, Na) and LiF (Fe, Mn). All quantitative major element analyses were calibrated with the following standards: Fe: Fe_2O_3; Si: Wollastonite; Mg: MgO; K: Orthoclase; Ca, Al: Anorthite; Ti: $MnTiO_3$; Na: Albite; Ni: NiO. Accelerating voltage was set to 15-20 kV with a primary beam of 15 nA and counting times of 20-40 seconds were used per element. Detection limits are in the range between 0.5 and 1 wt‰. Oxide percentages were calculated using the ZAF correction program and natural silicate and oxide standards.

Figure 3.4A Stratigraphy, lithology, and biostratigraphy of the Brazos core 1, combined with the lithological units shown in Hansen et al. (1993b) and Yancey (1996) and the sequence stratigraphic interpretation (see discussion). Biostratigraphy is provided by Robert Speijer (planktic and benthic foraminifera), Bremen, and Hartmut Mai (calcareous nannoplankton), Bremen. A key to the lithologic symbols is provided in Fig. 3.3.

3.3 Results

3.3.1 Lithology and sedimentology

Detailed descriptions of Brazos K-P outcrops and cores, including the event deposit, have been provided by previous studies and their lithology, has been subdivided into units A through J by Hansen et al. (see Fig. 3.3 and Hansen et al., 1987; 1993a). Almost all of these units are present in the two Brazos cores, hence this subdivision is also applied in this study; additionally, the corresponding description of the lithological units by Yancey (1996, e.g., 'BCB', see below) is given in parenthesis. These studies have revealed a distinct lateral variability in thickness and extent of the individual beds that may be of importance for their sedimentological interpretation (see Yancey, 1996), and are only in part amenable to a corehole analysis.
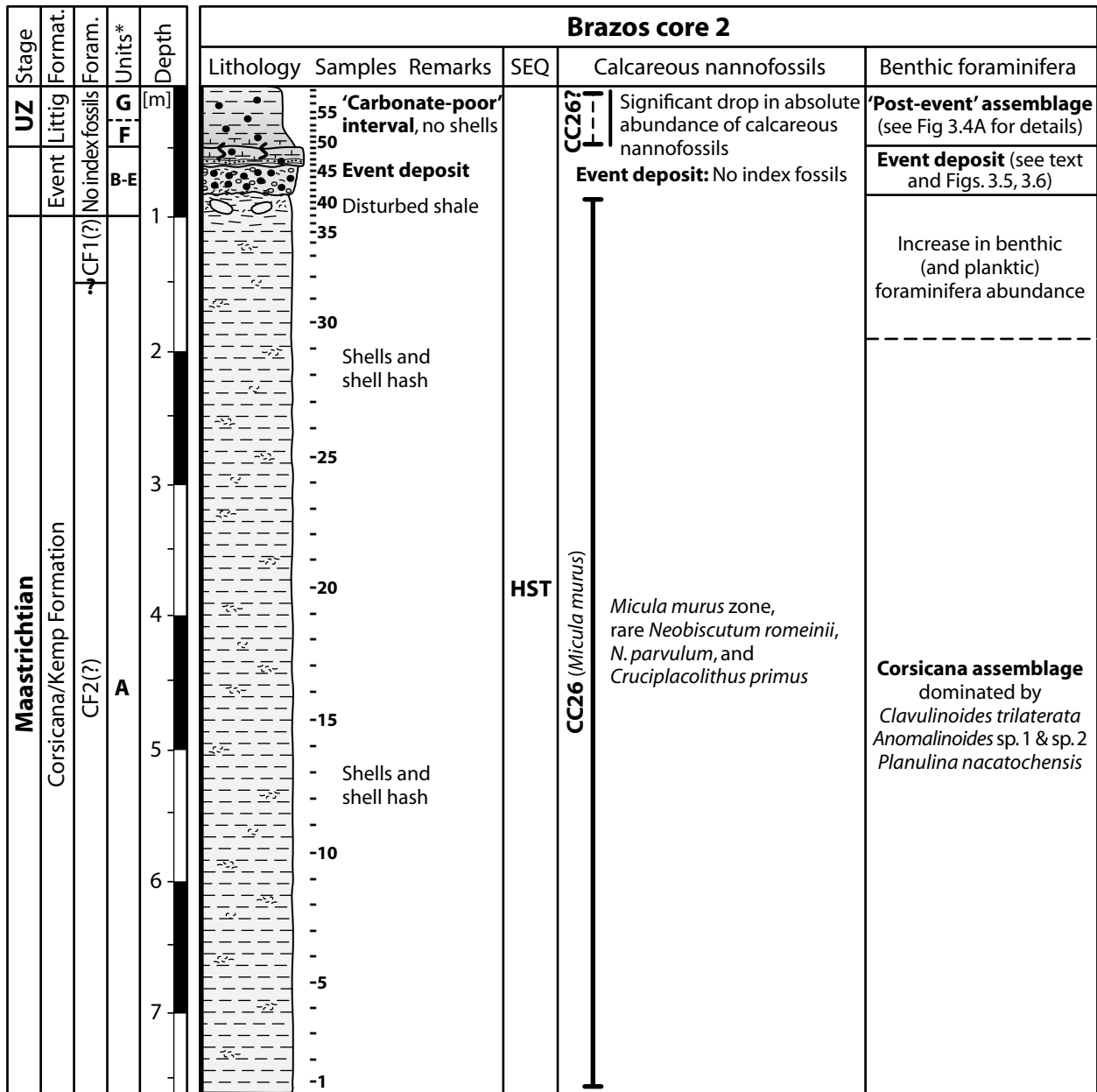
Figure 3.4B Stratigraphy, lithology, and biostratigraphy of the Brazos core 2 in combination with the lithological units shown in Hansen et al. (1993b) and Yancey (1996) and the sequence stratigraphic interpretation (see discussion). Biostratigraphy provided by Robert Speijer (planktic and benthic foraminifera), Bremen, and Hartmut Mai (calcareous nannoplankton), also from Bremen. A key to the lithologic symbols is provided in Fig. 3.3 and a detailed lithology of the event deposit is shown in the Figs. 3.5 and 3.6.

Brazos core 1 comprises 0.5 m of disturbed late Maastrichtian shales, a 10 cm-thick part of the spherule-rich event deposit, a 1.6 m thick (carbonate-poor) shale interval of unclear biostratigraphic age, and a 6-m thick early Danian part. Brazos core 2 includes predominantly late Maastrichtian shales (about 7 m thick) and yields a more expanded record of the event deposit (0.5 m thick), though only a small proportion of the carbonate-poor shales overlying it (0.5 m). Based on the lithology of the event deposit, both cores can be paralleled and, in combination, provide an expanded record of the K-P transition at Brazos. The detailed lithology of both cores is

given in Fig. 3.4; the event deposit is depicted in the Figs. 3.5, and 3.6.

Unit A: The late Maastrichtian Corsicana/Kemp Formation (unit A) comprises the lower 0.5 and 8 m of core 1 and 2, respectively. This formation consists of friable shale, which is slightly laminated and of dark grey-brown color. The Corsicana shales are slightly fossiliferous and include shell hash and small mollusks; evidence for bioturbation is generally rare. In both cores, the uppermost part (20-40 cm) of these shales is devoid of lamination and strongly disturbed.

The spherule-rich event deposit consists of a complex succession of several cm- to 10-cm thick subunits. Brazos core 1 yielded only the upper part(s) of the event deposit including units E and f, which are sharply overlain by the basal shales of the Littig Member (unit G). In contrast, Brazos core 2 contains the entire 'suite' of characteristic subunits, as described by Hansen et al., (1987; 1993b) and Yancey (1996) for other K-P sections from the Brazos area.

Unit B (BCB, basal conglomerate bed) is 10 cm thick and overlies unit A disconformably with a diffuse, transition (see Figs. 3.5, 3.6). It consists of 10 cm thick brown disturbed shales that contain cm-sized shale clasts. It is rich in shell hash and shows no lamination.

Unit C (SCB, spherulitic conglomerate bed) is a 8 cm thick spherule-rich layer, speckled with green, black, red, white, grey mm-sized clasts of various origins. The grain-size of the components in this unit shows a normal grading into a sand-silt-sized upper part.

Unit D (GSB, granular sand bed) consists of 0.5 to 1 cm-thick thin silty-sandy layers that are intercalated in the upper part of unit C and lower part of unit E.

Unit E (HCS, hummocky sandstone unit) is a 10-cm thick package of alternating layers of light grey, silty and calcareous sands. These layers show planar lamination and very low amplitude wavy bedding; in the upper part, more pronounced asymmetric current (climbing) ripples are present. This unit contains some spherules as well as rusty concretions, in addition to several prominent *Ophiomorpha* or *Thalassinoides* burrows that have diameters of 0.5-1 cm, and are infilled with mud.

Unit F (CCH, calcareous clayey bed) is 6-cm thick, massive, and indurated calcareous marl that grades upward into unit G. It shows no bioturbation or lamination; some spherules and rusty concretions as well as pyrite are present.

Unit G is the basal part of the Littig Member of the Kincaid Formation and comprises 1.6 m of sediments overlying the event deposit in core 1 and the uppermost 0.5 m in core 2. It is fissile and laminated, almost unfossiliferous dark brown clayey shale that contains abundant pyrite, rusty concretions, and rare altered spherules and carbonate chips. This shale is generally devoid of fossils and no bioturbation has been observed in this unit.

Unit H is a cm-thick sandy layer that is intermittently present in some Brazos outcrops immediately above the event deposit, though it was not observed in the Brazos cores of this study.

Unit I is the upper part of the Littig Member of the Kincaid Formation, conformably overlies unit G, and has about 6 m in thickness in the Brazos core 1. This unit is carbonate-rich, sandy-silty shale of brown to light grey color with increasing bioturbation, carbonate content, and shells (thin mollusk shells and shell hash) upward. The uppermost meter of this unit is slightly sandier, contains some glauconite, and is bioturbated by cm-thick *Thalassinoides* burrows (MSB or DSB, middle or dirty sandstone bed). In its topmost part, a pyrite- and iron oxide-rich layer is present (RPH, rusty pyrite concretion horizon).

Unit J comprises the topmost part of core 1 and consists of slightly fossiliferous (shell hash, small mollusks, sea urchin spines), shale, which is slight laminated, of brown color, and moderately bioturbated. According to Yancey (1996), unit J may belong to the Pisgah Member of the Kincaid Formation.

3.3.2 Petrography of the K-P event deposit

In order to reveal more details on the petrology and sedimentology of the spherule-rich sandy layer, results from petrographic thin-sections, backscattered electron (BSE) images, and qualitative electron microprobe analysis were incorporated. The complementary results from the quantitative electron microprobe analysis are given in Section 3.3.6.

The spherule-rich basal part of the event deposit shows a chaotic, microbreccia-like texture with high variability in grain-size and rare preferred orientation of grains (Fig. 3.7). The component shapes range from rounded particles to extreme elongated-irregular fragments without any distinct abrasion-textures. No apparent diagenetic overprint (cementation) has been observed and the components are 'loosely' floating in a micritic matrix with abundant pore-space. The grain sizes of the components vary in a broad range from about 0.1 to 2 mm in diameter.

The following components were encountered in the spherule-rich basal part of the K-P event deposit (see Figs. 3.7 and 3.8) and are listed in order of decreasing abundance:

(1) Rounded to elongated (blocky) and schlieren-rich brown to green spherules and irregular to highly flaser-like fragments. Either opaque or green-brown color in plain light, in part with high birefringence under crossed nicols. They have similar shapes and forms to other K-P spherules found in
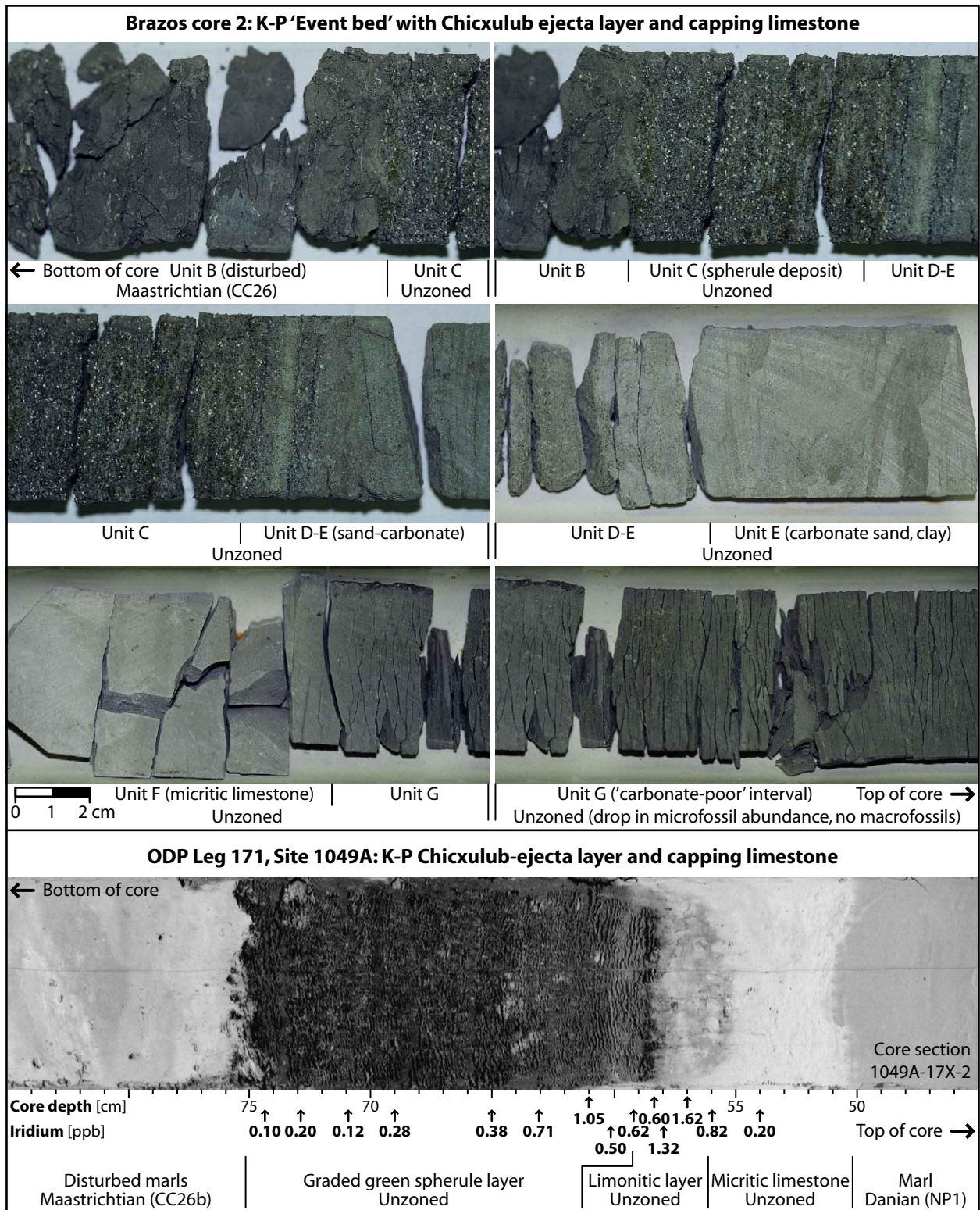
Figure 3.5 Core photos illustrating the lithology and associated units of the event deposit in the Brazos core 2 according to Hansen et al. (1993b). Note distinct overlap of core photos. Below, the spherule-bed at the ODP Leg 1171, Site 1049 is shown for comparison: it reveals a quite similar succession of disturbed Maastrichtian marls, spherule layer, and micritic limestone as in the Brazos core, albeit the ODP core furnishes no sandy intervals as in the Brazos cores. Note that iridium-values at this site are elevated already in the spherule bed, whereas at Brazos, the Ir-enriched zone usually starts at the top of the event deposit within unit E and extends 20-25 cm in the overlying shells (Hansen et al., 1993b; Martínez-Ruiz et al., 2001a,c). Photo from the Ocean Drilling Program (Norris et al., 2001). Biostratigraphy is from Self-Trail (2001).
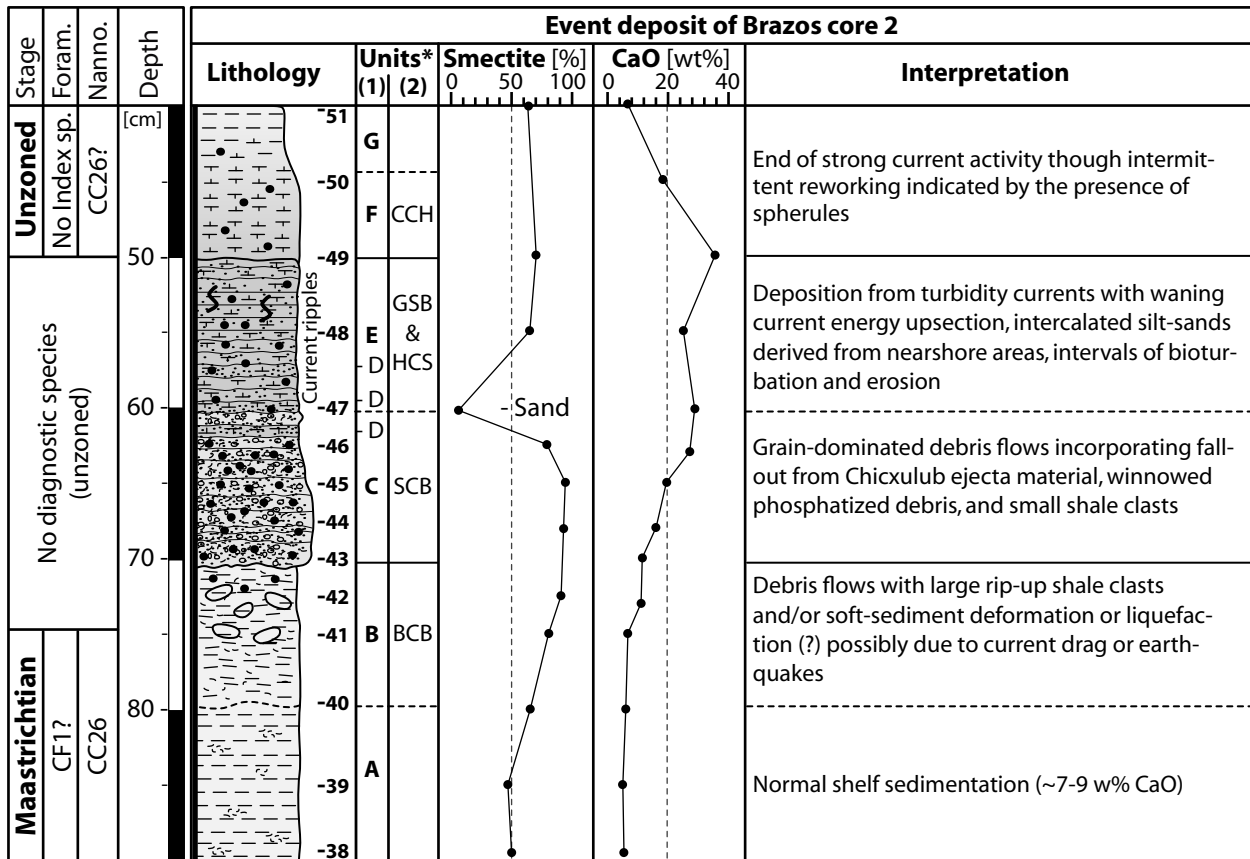
Figure 3.6 Detailed lithology and subdivision of the event deposit and correlation with the units (*) assigned by: (1) Hansen et al. (1993b) and (2) Yancey (1996): BCB, basal conglomerate bed; SCB, spherulitic conglomerate bed; GSB, granular sand bed; HCS, hummocky sandstone unit; CCH, calcareous clayey bed. A legend is provided in Fig. 3.3.

Mexico and Alabama (see Chapter 2 and 4). These particles are frequently fringed by calcite with outward radiating crystals. Some of these spherules are pseudomorphical replacement by numerous tiny pyrite crystals. They show internal structures including vesicles, flow-patterns, and lamellae.

(2) Carbonate fluorapatite (CFA), including rounded to irregular shaped grains, mollusk shell debris, fish teeth, and bone remains.

(3) Tiny mm-sized limestone clasts with 'lapilli-like' accretionary features.

In addition, benthic foraminifera, glauconite, abundant pyrite, iron oxides (hematite, goethite), and rare plant (?) remains have been encountered in the

spherule-rich basal part of the event deposit. In addition, fine sand- to silt-sized quartz grains, and feldspar grains are present in the spherule bed, though they are mostly confined to the distinct thin sand-silt layers of unit D. Among these constituents, pyrite is quite prominent, since it occurs as not only dispersed euhedral crystals dispersed, but also pyrite pseudomorphological replaces spherules and constitutes pyrite framboids of 20-50 μm in diameter.

3.3.3 Biostratigraphy and paleoecology

The biozonation used in this study is based on the schemes provided by Martini (1971) and Perch-Nielsen (1985) for calcareous nannofossils and

Figure 3.7 (page 99) Thin section photos of lithologies from the event deposit in the Brazos cores showing characteristic features of microfacies and components in plane-polarized light. (**A**) and (**B**) Microbreccia-like microfacies of the spherule deposit (unit C) with spherules, opaque phases, limestone clasts, accretionary lapilli, phosphatized particles, and fossil debris (sample BZC2-43). Note near-absence of quartz or feldspar. (**C**) Altered, brown spherules and fragments (unit C, BZC2-43). Spherules are hollow and show thin internal lamellae of Ti-Fe-rich oxide phases. (**D**) Irregular smectitic fragment with opaque inclusions (BZC2-42, unit C). Note schlieren with flow-structures and opaque inclusions. (**E**) Two limestone (?) clasts and one phosphatized particle (unit C, BZC2-43). (**F**) Lithoclast with concentric internal structure interpreted as accretionary lapilli (unit C, BZC2-42). (**G**) Carbonaceous 'sandstone' from unit D-E above the spherule deposit (BZC2-46). Components include smectitic clasts, limestone clasts, opaque phases, phosphatized detritus, and foraminifera, in a micritic matrix. Note rare presence of quartz or feldspar. (**H**) Silty layer incised in the upper fine-grained part of the micritic limestone from unit D-E (BZC1-10). The well-sorted siltstone contains opaque phases, phosphatized detritus, and fossil fragments as accessory components.
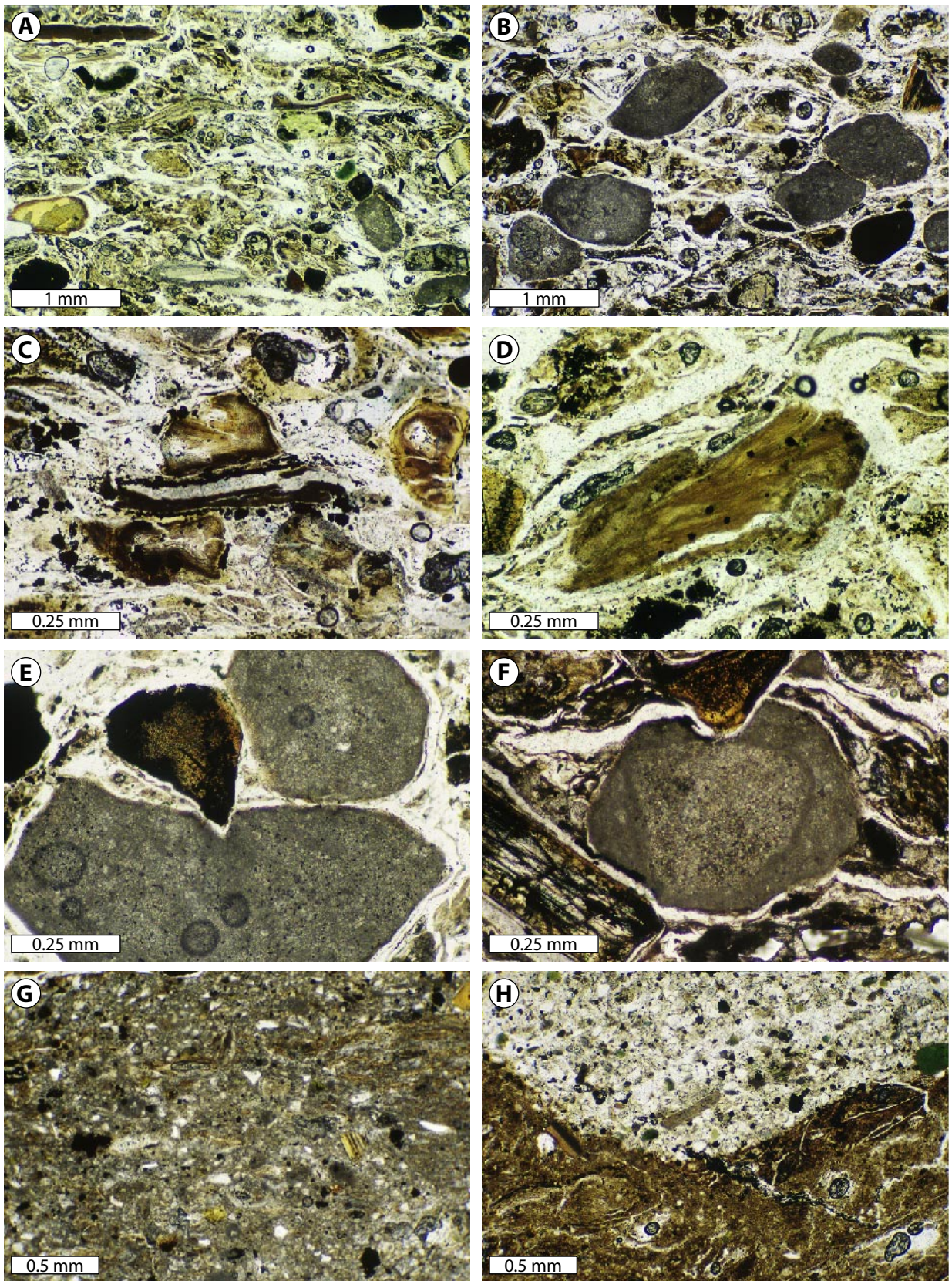
Figure 3.7 (caption on page 98).

Berggren et al. (1995) for planktic foraminifera with added refinements for the late Cretaceous zonation by Pardo et al. (1996). Preservation of coccolithospheres and planktic foraminiferal tests is generally excellent, with only rare glauconite or pyrite infillings in the foraminifera. Therefore, surface textures and morphological features of calcareous nannofossils and planktic, as well as benthic foraminifera are easily identifiable, allowing a high-resolution stratigraphy of the K-P transition and, specifically, for the earliest Danian which is shown in Fig. 3.4. In this figure, benthic foraminifera faunal data were included to constrain potential paleoecological and water-depth changes.

Late Maastrichtian

The interval from the lower part of Brazos core 1 and core 2 up to the event deposit shows a stable, very diverse (~45 species) latest Maastrichtian nannofossil assemblage of the *Micula murus* zone (CC26). This results agrees with previous studies by Jiang and Gartner (1986), who have assigned the interval below the event deposit to the *Micula murus* zone as well, though in their report, this biozone extends to about 18 m (!) below the event deposit. The index fossil for the latest Maastrichtian subzone CC26b, *Micula prinsii* (Self-Trail, 2001), was not detected during this study, though Jiang and Gartner (1986) reported the intermittent and very rare occurrence of *M. prinsii* concomitant to the occurrence of *M. murus* throughout the 18 m below the event deposit. Hence, it is not clear if the upper part of the Biozone CC26 is indeed absent in the Brazos cores.

The finding of single occurrences of Paleogene coccoliths (and foraminifera) below the event deposit in the Brazos outcrops by Montgomery et al. (1992) have not been confirmed by other biostratigraphic studies (e.g., Olsson and Liu, 1993), including ours. However, related to recent observations by Mai et al. (2003) from the Antioch Church core (Alabama), El Kef (Tunisia), and Geulhemmerberg (the Netherlands), tiny specimens of *Neobiscutum romeinii*, *Neobiscutum parvulum,* and *Cruciplacolithus primus* have been observed in the first sample of core 2, about 8 m below the event deposit. These cal-

careous nannofossils have long been used as index fossils for the earliest Paleogene, though recent studies show their consistent presence already in latest Maastrichtian sediments during the uppermost part of the *M. murus* Zone (CC26, Mai et al., 2003). At the Elles K-P section, Tunisia, their first occurrence roughly parallels the first occurrence of *M. prinsii* (Gardin, 2002).

The planktic foraminifera in the basal part of core 2, up to 0.5 m below the event deposit, represent an impoverished Maastrichtian assemblage with low number of species and individuals. This fauna is largely dominated by heterohelicids and guembelitrids with subordinate hedbergellids and globigerinoids, as well as very rare *Globotruncana* and *Rugoglobigerina*. However, no index foraminifera for the late(est) Maastrichtian have been encountered (e.g., *Abathomphalus mayaroensis* or *Plummerita hantkeninoides*). However, the absence of *Gansserina gansseri* in this interval suggests a Biozone CF2 age, since this zone is defined for interval spanning the LAD of *G. gansseri* at the top of the *Pseudoguembelina hariaensis* Zone (CF3), and the FAD of *P. hantkeninoides* or *Plummerita reicheli*, which both mark the latest Maastrichtian Biozone CF1 (Pardo et al., 1996). For the interval spanning the 0.5 m below the event deposit in both cores, the presence of *P. reicheli* may tentatively suggest a Biozone CF1 age (Pardo et al., 1996).

For th planktic foraminifera record, these data is in part consistent with previous results from Keller (1989a; 1989b), including (i) the general absence of *A. mayaroensis*, and (iii) the presence of an impoverished latest Maastrichtian foraminiferal fauna below the event deposit. However, Keller (Fig. 9 in 1989a) reported the sporadic occurrence of *P. reicheli* in an interval extending 24 m below the 'event deposit', even paralleling the occurrence of *G. gansseri* (Biozone CF3 in the scheme of Keller et al., 1995), whereas in the Caravaca section, Spain, *P. reicheli* is observed about 3.5 m below the K-P boundary (Biozone CF1), well above the last occurrence of *G. gansseri* (Pardo et al., 1996). Therefore, the position of the base of CF1 about 0.5 m below the event deposit is regarded as tentative.

Figure 3.8 (page 101) Backscattered electron (BSE) images of components from the spherule-rich deposit at the base of the event deposit in the Brazos cores (unit C). Abbreviations: Smectite, Sm; Pyrite, Py; Calcite, Cz. (**A**) Spherule, which is pseudomorphically replaced by tiny pyrite crystals. (**B**) Framboidal pyrite. (**C**) and (**D**) Flaser-like clayey (smectite) fragments. Note flow-structure and delicate outlines as well as abundance of bright (opaque) phases. (**E**) and (**F**) Details of clayey clasts with internal flow-structures (in E) and Ti-rich lamellae (in F). (**G**) and (**H**) Flaser-like clayey fragments enveloping carbonate fragments and vice versa. Note similarity to textures from spherule deposits in northeastern Mexico (Chapter 2).
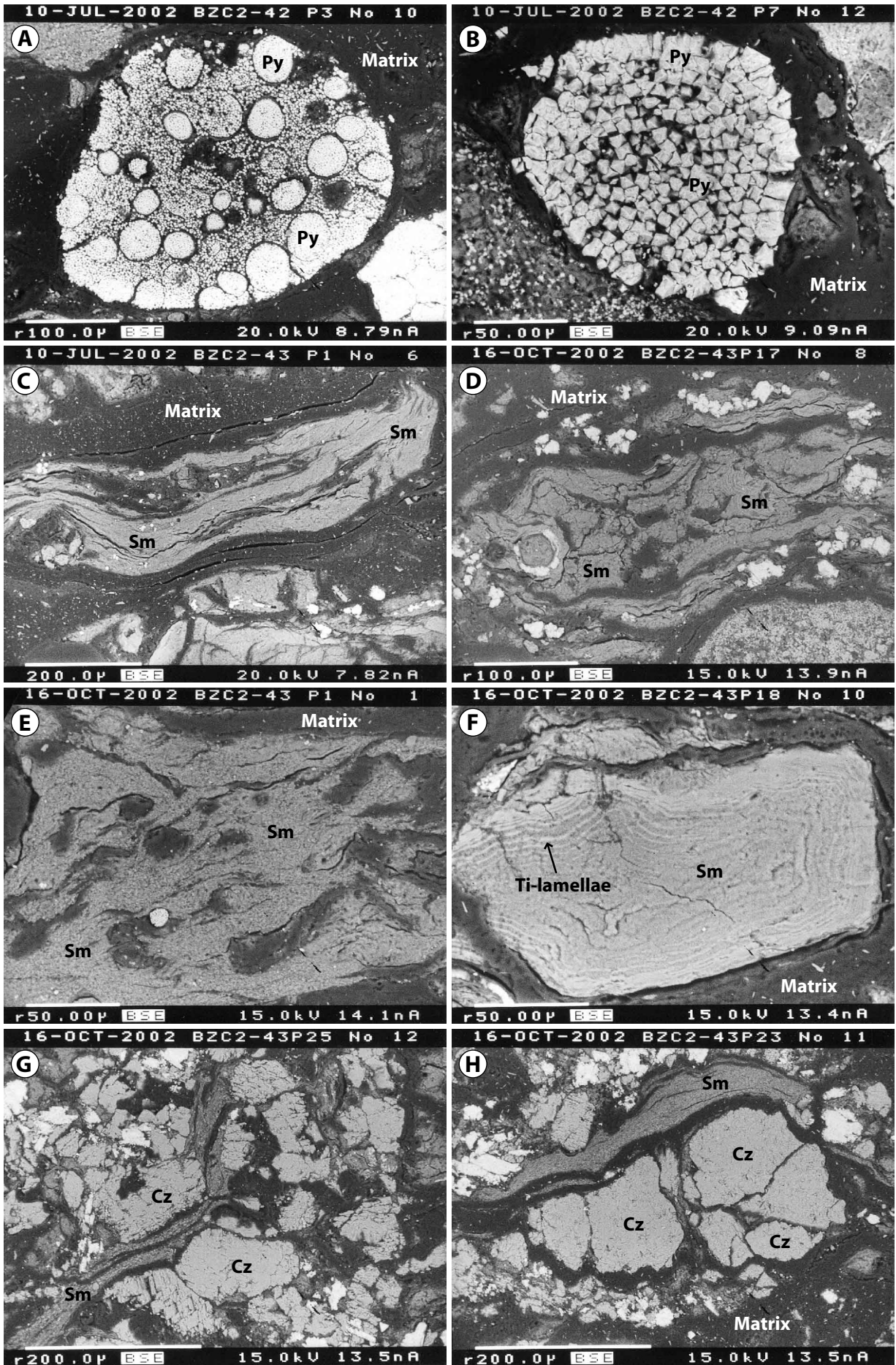
Figure 3.8 (caption on page 100).

The Maastrichtian benthic foraminiferal fauna is very stable up to the event deposit. The fraction >125 *μ*m is dominated by *Clavulinoides trilatera*, *Anomalinoides* sp. 1 and sp. 2 and *Planulina nacatochensis*, together constituting up to 90 % of the benthic assemblage.

K-P event deposit and 'carbonate-poor interval'

In the K-P event deposit (units B-F), an accurate biostratigraphy is difficult to assess since calcareous nannofossils and planktic foraminifera are rare and/or obviously reworked. Therefore, this interval is considered as unzoned.

In the 1.6 m-thick carbonate-poor interval (unit G) immediately above the K-P event deposit, the absolute abundance of calcareous nannofossils species and individuals is drastically reduced, and the nannofossils constitute an impoverished late Cretaceous fauna, though no Paleocene nannoplankton species have been encountered. This result agrees with Jiang and Gartner (1986), though they figured a nannofossil-poor interval overlying the event deposit of about 20-30 cm in thickness and positioned the K-P boundary atop of the nannofossil-poor interval in the Brazos River outcrop. A similar drop in absolute abundance of calcareous nannofossils has been observed in many K-P sections immediately above the iridium-defined K-P boundary (e.g., at El Kef, Tunisia), and often this abundance reduction precedes the first appearance of Paleogene species (see discussions in Gartner, 1996; Pospichal, 1996). Since it is impossible to judge whether the Cretaceous nannofossil species found in the carbonate-poor interval represent an indigenous or reworked fauna (Gartner, 1996), and since the FAD of common earliest Danian nannoplankton marker species (e.g., *Biscutum romeinii*, *B. parvulum*, and *Markalius astroporus*), does not necessarily coincide with the K-P boundary marked by other physical criteria (Gartner, 1996), it is difficult to constrain definitely the age of the carbonate-poor unit G in the Brazos cores by calcareous nannofossils.

Considering planktic foraminifera, the carbonate-poor interval (unit G) is also difficult to assign to a particular biozone because planktic foraminifera are very rare and no index species have been detected (analogous to observations on a nearby core by Keller, 1989a; 1989b; Keller et al., 1993). The remaining foraminifera fauna is, however, well preserved, and this interval furnishes a heterohelicid- and guembelitrid-dominated assemblage. These results are also in line with previous results from Keller (1989a; 1989b), who observed the presence of a strongly impoverished foraminifera fauna (reduction of 30-50 % of species), as well as the absence of *P. reicheli* in the 25 cm thick interval above the event deposit (in her Brazos core 1), though she considered this interval as latest Maastrichtian and hence, placed the K-P boundary atop of this unit.

The benthic foraminifera show a sudden faunal change and a distinct new assemblage ('post-event' fauna) immediately above the event deposit: *Pseudouvigerina* sp. 1 was the first species to appear. It was followed by *Eponides elevatus*, *Cibicides newmanae*, and *Cibicides* sp. 1. Benthic species typical for the Corsicana Formation below the event deposit are becoming increasingly rare throughout this interval (see Fig. 3.4A for details).

Early Danian

The first 'unequivocally' Danian sediments of the Brazos cores have been identified by the first occurrence of the calcareous nannofossil *Biantholithus sparsus* at 1.6 m above the event deposit in core 1. Brazos core 2 yielded no Danian species in the 0.5-m thick interval above the event deposit. The presence of *B. sparsus* in Brazos core 1 suggests a zone NP1 age for the sediments above the carbonate-poor interval. In addition, abundant (reworked?) Cretaceous species, blooms of *Operculodinella operculata* (*Thoracosphaera operculata*, a calcareous dinoflagellate cyst) and *Braarudosphaera bigelowii* are present. These blooms are a characteristic feature of many K-P boundary sections during the Biozone NP1 (Gartner, 1996; Gardin and Monechi, 1998; Gardin, 2002). However, the blooms of *B. bigelowii*, and *N. romeinii* bloom are contemporaneous to Biozone P0 at the Brazos core 1 (see below), and occur generally above P0 during Biozone P1a-P1b in several K-P sections elsewhere (e.g., El Kef and Elles, Tunisia, Gubbio, Italy Caravaca, Spain, Gartner, 1996; Gardin and Monechi, 1998; Gardin, 2002).

In the interval above the *T. operculata* and *B. bigelowii* blooms, acmes of *N. romeinii* followed by *N. parvulum* are concomitant to an upward decreasing number of reworked Cretaceous species. A bloom of *C. primus* follows the acme of *N. parvulum*. The uppermost meter of Brazos core 1 is marked by an acme of *Futyania petalosa* with only a few reworked Cretaceous coccoliths. The index marker of the *Cruciplacolithus tenuis* Zone (NP2) was not observed, though the acme of *F. petalosa* is characteristic for the upper part of Biozone NP1
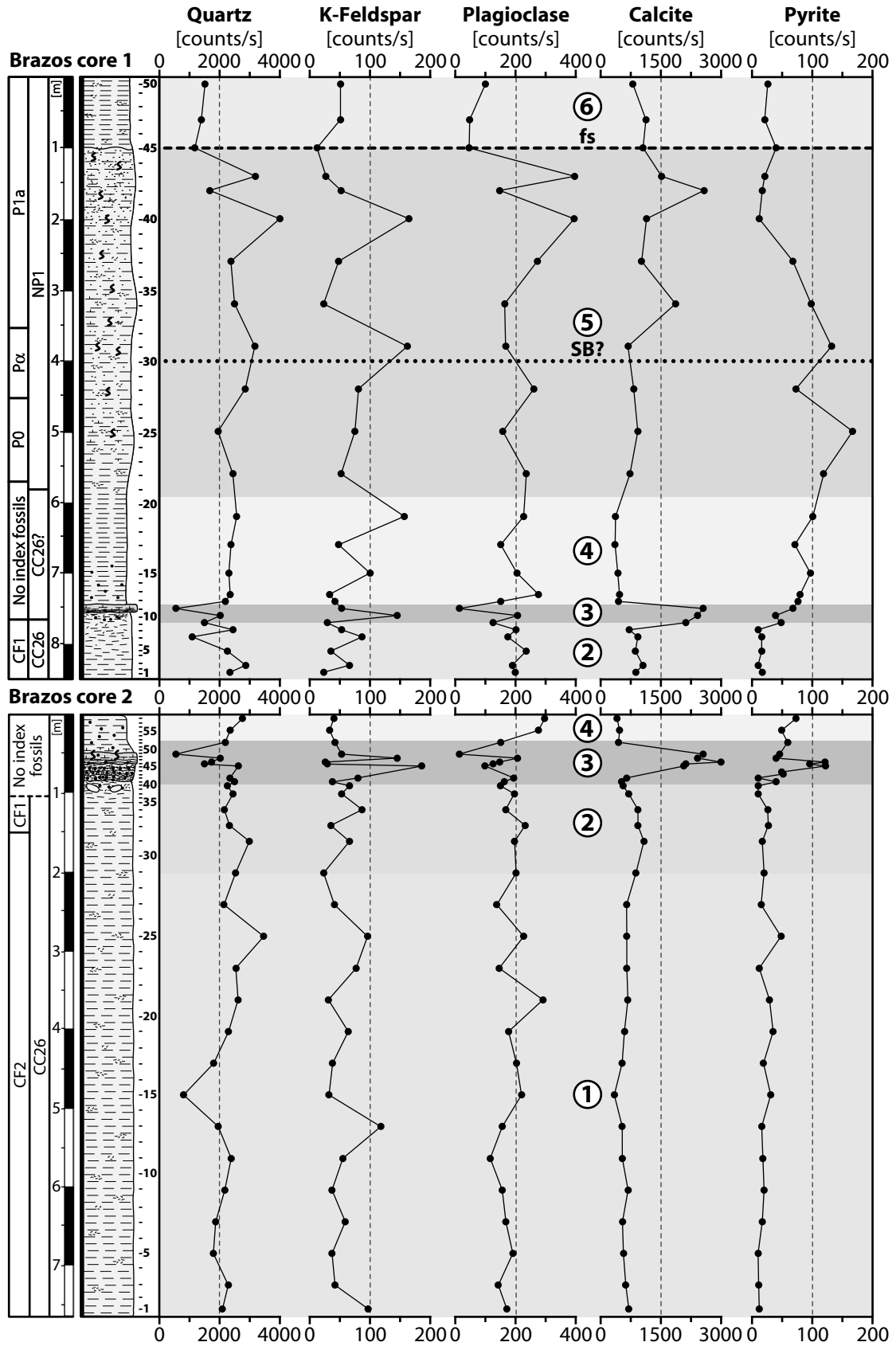
Figure 3.9 Nonclay minerals of the two Brazos cores as determined from bulk rock X-ray diffractometry. The grey shadings correspond to the event deposit and the intervals with prominent changes as discussed in the text. A legend to the lithologic symbols is provided in Fig. 3.3.
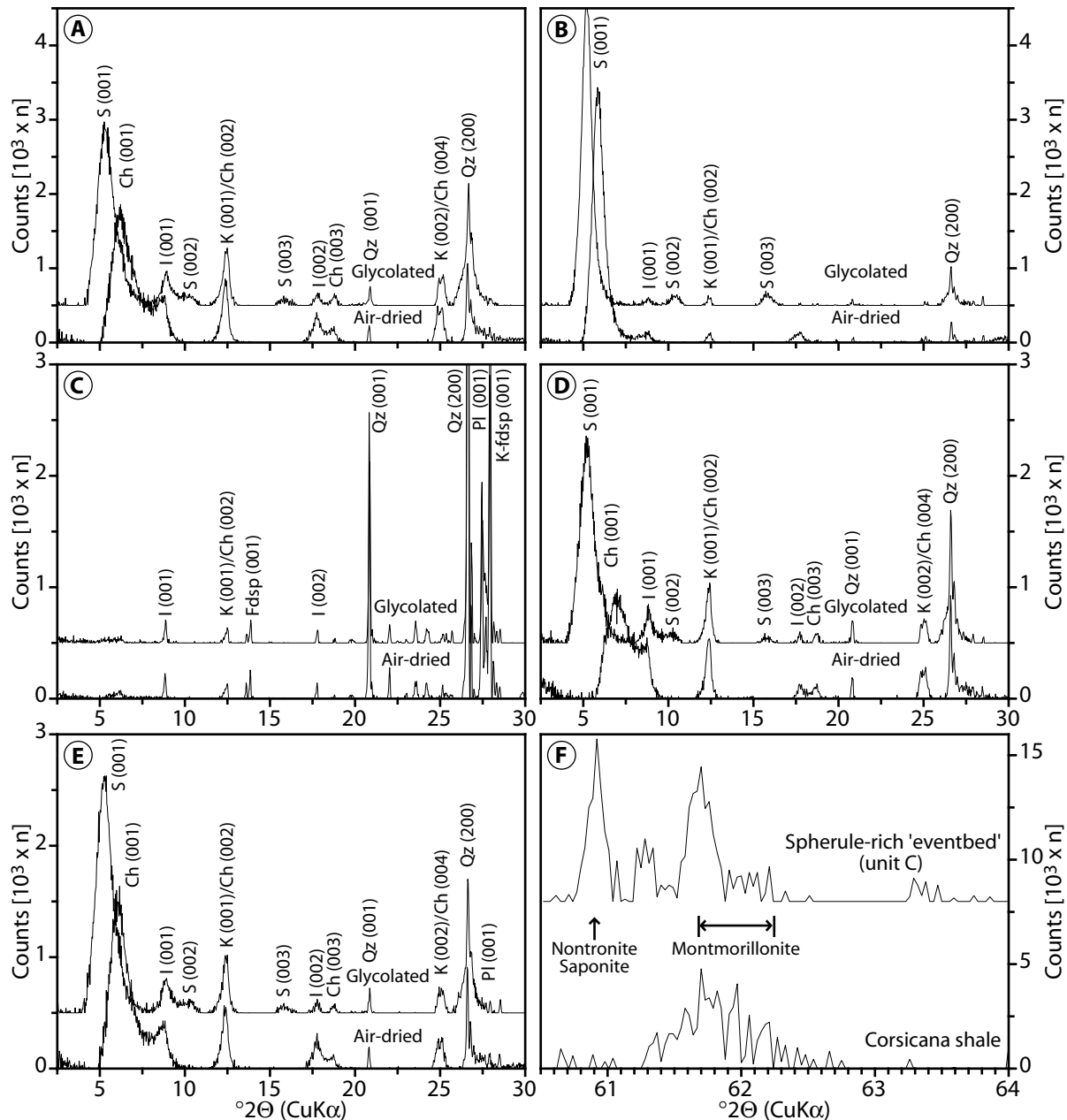
Figure 3.10 Representative X-ray diffraction (XRD) patterns of the <2 μm fraction (air-dried and ethylene glycol-solvated). (**A**) Shale of the Corsicana Formation below the event deposit (sample BZC2-19). (**B**) Spherule-rich event deposit (BZC2-45). (**C**) Sand-silt layer within the event deposit (BZC2-47). (**D**) Shales of the carbonate-poor interval (BZC2-14). (**E**) Early Danian shales (BZC1-22). The diffractogram in (**F**) shows the position of the (060) peaks in the range from 61-64 °2Θ derived from the bulk powder XRD analysis of the montmorrilionite-rich shale of the Corsicana Formation below the event deposit (BZC2-19) compared to the nontronit-/saponite-rich event deposit (BZC2-45).

and the lower part of Biozone NP2. A remarkably similar succession of calcareous nannofossil acme-subzones has been obtained for the Brazos section by Jiang and Gartner (1986), and for the Elles section, Tunisia, by Gardin (2002).

The earliest tiny Paleocene planktonic foraminifera, including *Globoconusa* and *Eoglobigerina* which are indicative of Biozone P0, are present about 1.8 m above the event deposit in core 1. In addition, very rare rugoglobigerinids and heterohelicids occur in this interval. No Danian species has been found

in the interval above the event deposit in core 2. The first occurrence of *Parvularugoglobigerina eugubina* and *Parvularugoglobigerina longiapertura* at 20-40 cm above the base of Biozone P0 marks the beginning of Biozone Pα (Berggren et al., 1995) or P1a (Keller et al., 1995). The planktic foraminifera *Parasubbotina pseudobulloides* was not found and therefore, it was not possible to subdivide biozone P1a into P1a(1) and P1a(2), based on the FAD of this species (Keller et al., 1995). The absence of *P. eugubina* in the topmost 3.6 m of core 1 suggests a
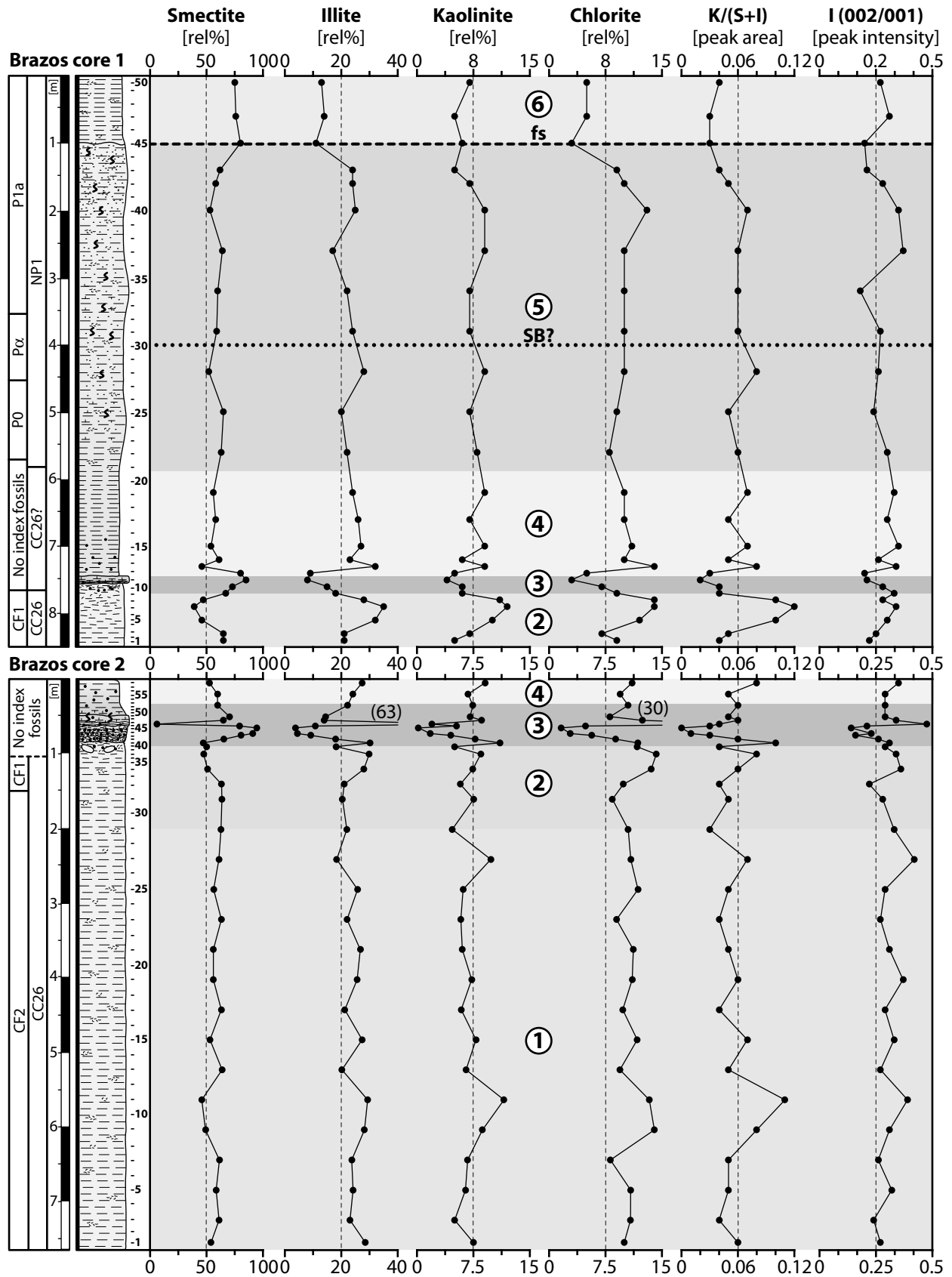
Figure 3.11 Clay mineralogy of the two Brazos cores: semiquantitative determination of clay mineral phases from X-ray diffractometry of the insoluble residue of the <2 μm fraction. Grey shadings correspond to intervals with prominent changes as discussed in the text. Data is given in relative percent of the clay fraction with correction factors (Biscaye, 1965). A key to the lithologic symbols is provided in Fig. 3.3.

Biozone P1a (Berggren et al., 1995), or P1b (Keller et al., 1995) age for this interval. These results are well comparable to the findings of Keller (1989a; 1989b), though her FAD of Paleocene species is about 25 cm above the event deposit in the Brazos core studied by her, which is much lower than the 1.6 m in the Brazos core 1 of this study.

With the appearance of *Alabamina midwayensis* and *Anomalinoides midwayensi*s during biozone Pα-P1a, a typical benthic "Midway-fauna" was established; other common taxa are *Anomalinoides acutus* and *Gyroidina subangulata*. Only a few other species, for instance *Pulsiphonina prima*, *Cibicidoides alleni*, and *Lenticulina rotulata*, are observed in this interval. The base of the Pisgah Member is associated with a minor change in the benthic foraminiferal assemblage: *Hoeglundina eocenica* first appears and few rare species disappear (*Clavulinoides trilatera*, *Pseudouvigerina* sp., and *Cibicides* sp. 1).

In conclusion, these results are consistent with several previous studies, proving the remarkable reproducibility of stratigraphic data in the Brazos area, Texas. The composition of calcareous nannofossil and planktic foraminifera assemblages indicates stable environmental conditions up to the event deposit and a significant drop in species and individual abundance in the interval immediately overlying the event deposit. However, strongly contrasting faunal or evolutionary trends exist beginning with the onset of new Paleocene species during Biozone NP1 and P0-P1a: The Danian planktic foraminifera faunas are characterized by the successive appearance of newly evolved species, whereas the calcareous nannofossil flora is characterized by strong consecutive blooms of various nannofossil species that, for the most part, originated already during the late Maastrichtian.

3.3.4 Mineralogical phases

The nonclay minerals identified in the bulk powder fraction include quartz and calcite, with minor amounts of feldspar (K-feldspar and plagioclase) and pyrite (Fig. 3.9 and raw data in Appendix 3.2), as well as accessory hematite. Plagioclase is dominant over K-feldspar in most samples. In the late Maastrichtian interval below the event deposit, calcite is remarkably constant and shows a slight increase in the uppermost part. The other nonclay phases show only insignificant fluctuations and no apparent long-term trends. The event deposit is characterized by an abrupt increase of calcite (doubling of counts per second) and pyrite, concomitant to a decreased

quartz and plagioclase content. Above the event deposit, in the carbonate-poor interval, abundances of mineral phases step back to 'pre-event values', though calcite shows slightly lower values and pyrite increases significantly. Between the base of the earliest Danian (Biozone NP1 and P0) and the pyritized horizon in the upper part of Brazos core 1, the calcite, quartz, and feldspar content is strongly fluctuating with high peak values, though the pyrite content decreases. In the uppermost meter of Brazos core 1, above the pyritized horizon, the contents of calcite, quartz, and feldspar decrease abruptly.

The clay mineral assemblage of both Brazos cores is characterized by strong predominance of smectite, which comprises generally about 50-75 rel% of the clay fraction (Figs. 3.10, 3.11A, B and raw data in Appendix 3.3). Additional components include illite (~20 rel%) and about equal amounts of chlorite and kaolinite (5-15 rel%, each). Mixed layer clay minerals, for instance illite-smectite, illite-chlorite, and chlorite-smectite, appear throughout both cores in trace amounts (generally below 1-5 rel%), and have therefore not been included in the quantitative analysis. The variations in the relative abundance of clay minerals through time reveal two major results:

First, there are no substantial long-term changes in the clay mineral composition as, from a quantitative and qualitative point of view, the clay mineral association of the shale intervals in both cores is the same for late Maastrichtian and early Danian shales, with only subtle fluctuations. These fluctuations are in a range of ±5-10 rel%, which is well within the error range of the methodology used (Petschick et al., 1996).

Second, significant short-lived changes, however, are associated with the event deposit, which shows a prominent 10-20 rel% smectite detriment in its lower disturbed and reworked part, in addition to a strong increase of smectite in its upper, spherulitic and calcareous part (up to 95 rel%). The contents of the other clay minerals, including chlorite, illite, and kaolinite, are each a mirror image of the smectite curve. The thin silt-sand layers intercalated in the event deposit are almost devoid of smectite and kaolinite.

To constrain possible source regions and transport paths details on the specific mineralogical properties of the predominant clay minerals were incorporated, besides the electron microprobe measurements of individual components (Tables 3.1-3.3). The smectite generally shows medium- to well-defined peaks with a crystallinity index (FWHM, full width at half maximum peak height above background, Kübler,
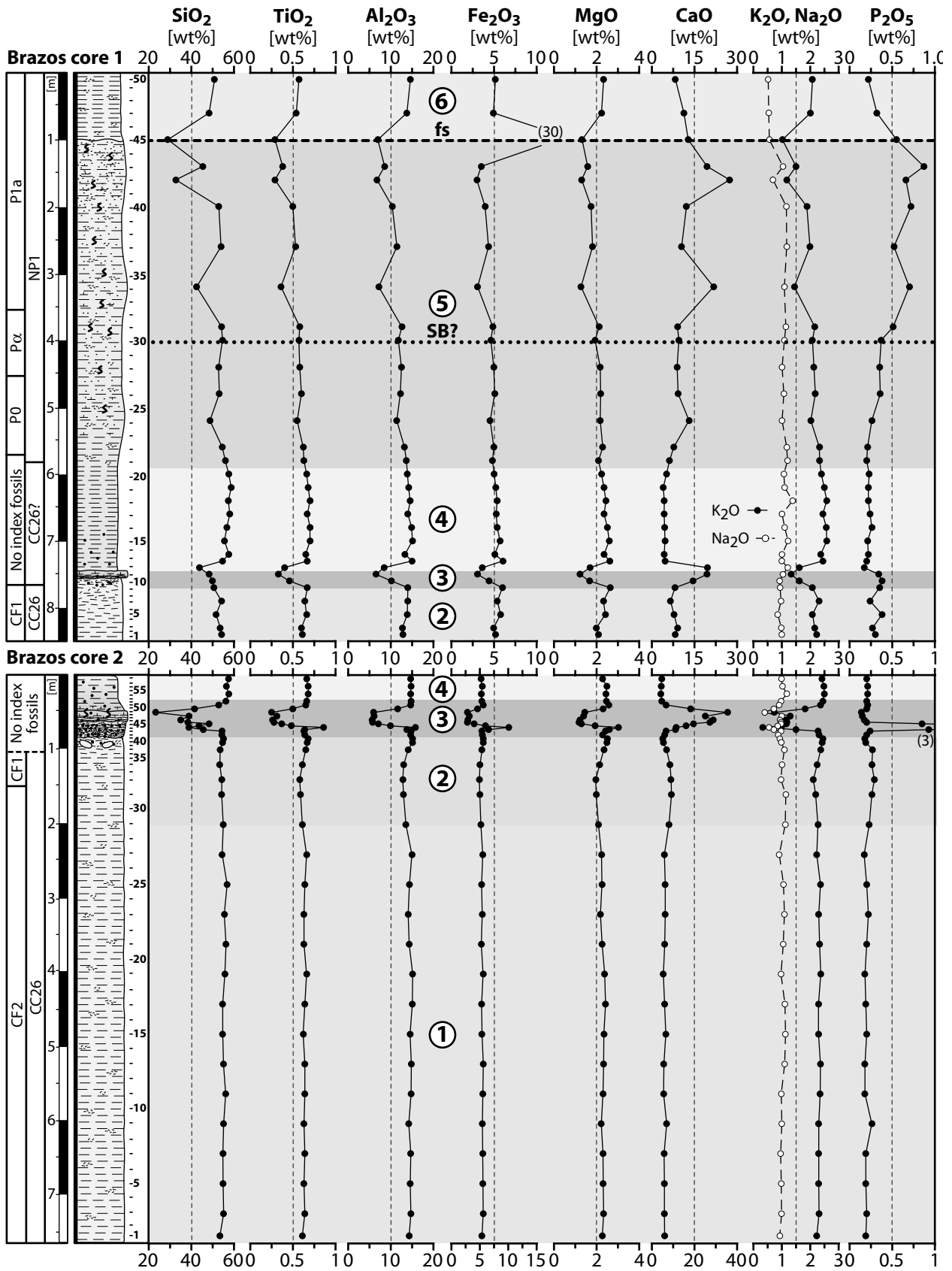
Figure 3.12A Major elements of the two Brazos cores, determined by wavelength-dispersive X-ray fluorescence spectrometry (WDS). The numbers in circles (1 to 6) refer to the lithologically and compositionally distinct intervals outlined in the text. All Fe is given as Fe_2O_3. A key to the lithologic symbols is provided in Fig. 3.3.
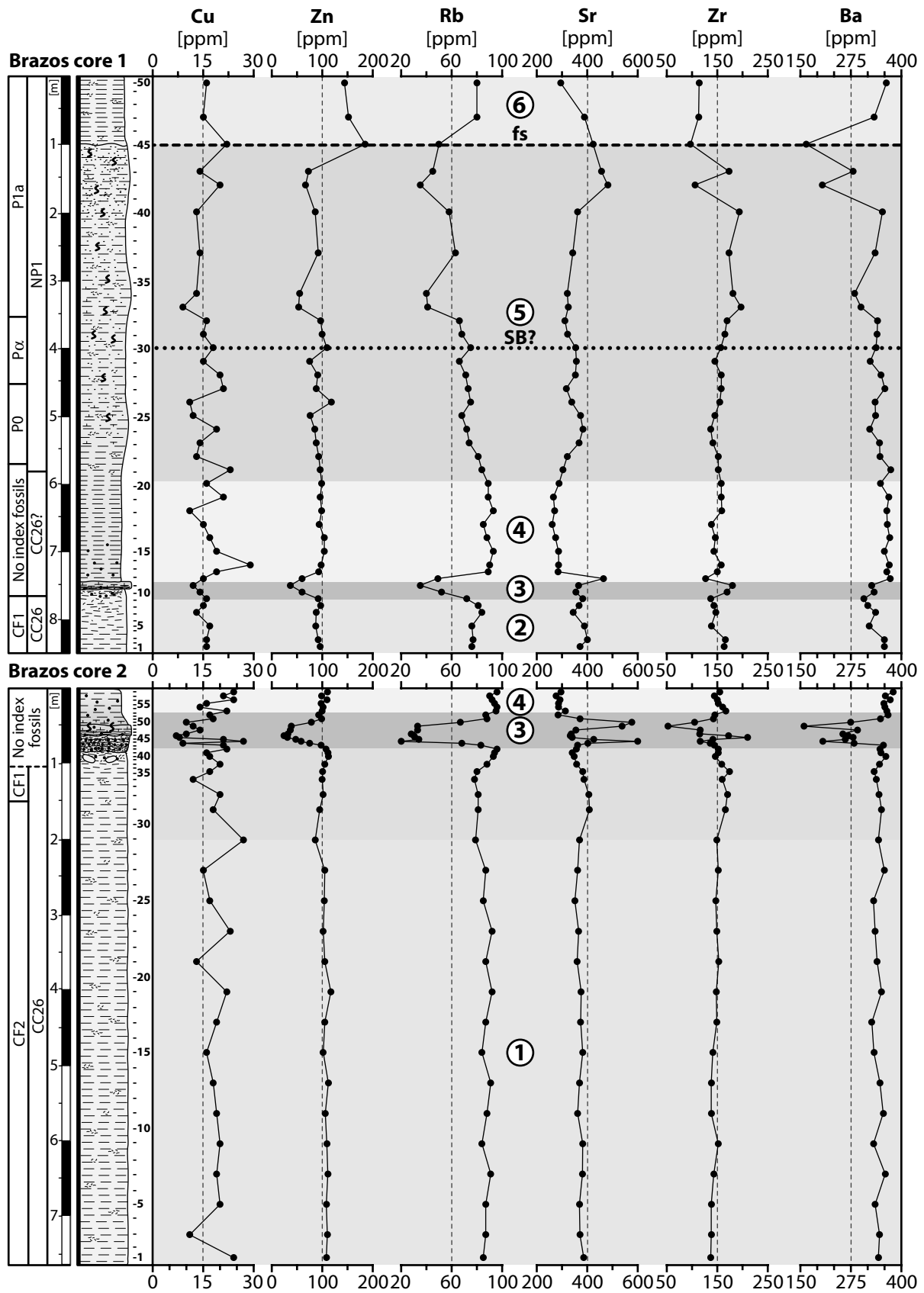
Figure 3.12B Trace elements (Cu, Zn, Rb, Sr, Zr, and Ba) of the two Brazos cores determined by energy-dispersive X-ray fluorescence spectrometry (EDS). The numbers in circles (1 to 6) refer to the lithologically and compositionally distinct intervals outlined in the text. All Fe is given as Fe_2O_3. A key to the lithologic symbols is provided in Fig. 3.3.
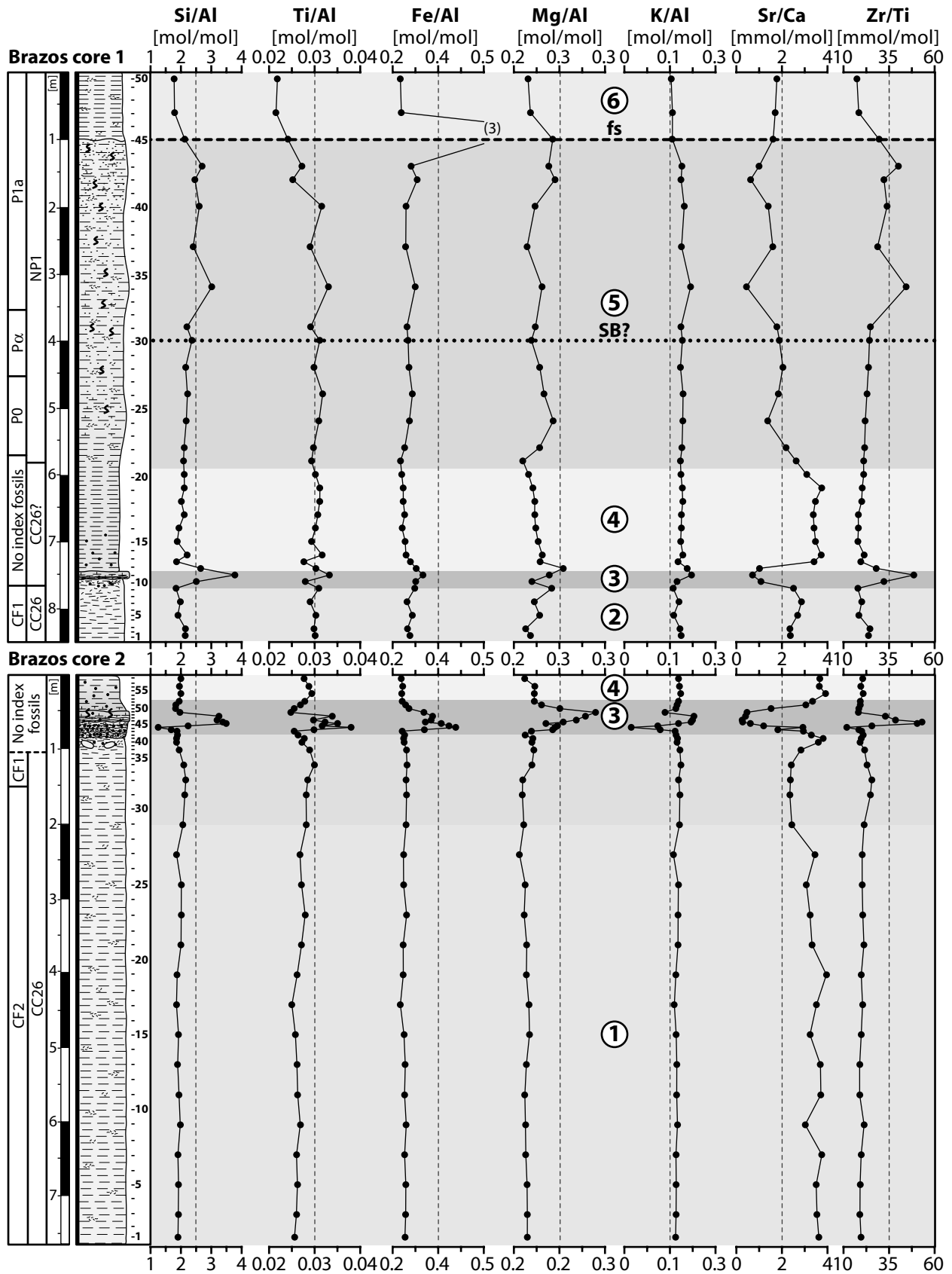
Figure 3.12C Ratios of selected major elements against Al, in addition to the Sr/Ca and Zr/Ti ratio of the two Brazos cores. The numbers in circles (1 to 6) refer to the lithologically and compositionally distinct intervals outlined in the text. All Fe is given as Fe_2O_3. A key to the lithologic symbols is provided in Fig. 3.3.

1987; Moore and Reynolds, 1997) of about 1-1.3 °2Θ, indicating a certain degree of disorder, typical for detrital smectites (see Fig. 3.10). Deviations from these crystallinity values occur in the event deposit, where significant lower crystallinity index values (FWHM ~0.6 to 0.8 °2Θ) imply a higher degree of 'crystallinity' and may suggest that a large part of this smectite formed as an authigenic phase from the alteration of glassy ejecta material, as also revealed by EMP analysis.

Additional constrains on the qualitative classification of the smectites comes from their (060) reflections in bulk rock powder samples (Moore and Reynolds, 1997), as shown in the Fig. 3.10F: The smectite in the shale above and below the event deposit is characterized by (060) peaks in the range between 61.6 to 62.3 °2Θ, indicative of dioctahedral smectites (e.g., montmorillonite). In contrast, samples from the event deposit show prominent peaks at about 60.9 and 61.2 °2Θ, which may indicate the presence of nontronite and/or saponite (Moore and Reynolds, 1997). The 'octahedral character' of the illites was determined by using the illite (002/001) peak intensity ratio. It varies little over the whole in-

terval of both cores (Fig. 3.11), and shows a median value of 0.3 (±0.1). This indicates the dominance of dioctahedral illite over trioctahedral illite since high illite (002/001) ratios (>0.4) correspond to Al-rich ('muscovitic') illites, whereas values <0.15 correspond to 'biotitic' illites (Bengtsson and Stevens, 1998). This result is confirmed by the average c-lattice constant of about 9.95 Å, pointing to a 'muscovitic' character for the illites as well (values <9.98 Å, Petschick et al., 1996).

3.3.5 Major and trace element stratigraphy

The geochemical data from analyses performed on both Brazos cores are presented in Figs. 3.12A-C and in the Appendices 3.4 and 3.5. The Fig. 3.12C also shows whole-rock concentrations of selected major elements normalized to aluminum as an index of the relative abundance of detrital phases in addition to the Sr/Ca and the Zr/Ti ratios. In the shales and mudstones that predominate the lithofacies of the Brazos cores, compositional changes are generally subtle. They are linked to variations in the elements incorporated into biogenic carbonate, including Ca, P, Sr, and Ba (e.g., Tucker and

Table 3.1 Summarized results of the microprobe analyses and calculated mineralogical formulae of spherules and fragments of smectite- and chlorite-like composition from the Brazos core 2 spherule bed. Smectite analyses (P3 to P19) have been normalized to $O_{10}(OH)_2$, whereas chlorite analyses (P9 to P22) have been normalized to $O_{10}(OH)_8$. Abbreviations: Tetra, tetrahedral; Octa, octahedral; Inter, interlayered.

Sample	2-43	2-43	2-42	2-43	2-43	2-43	2-43	2-43	2-42	2-43	2-43	2-43	2-43
#	P3	P2	P9	P4	P30	P28	P16	P35	P5	P19	P9	P8	P22
	wt%	wt%	wt%	wt%	wt%	wt%	wt%	wt%	wt%	wt%	wt%	wt%	wt%
SiO$_2$	59.29	59.46	60.83	59.03	57.58	55.81	55.79	57.53	53.87	33.56	30.69	31.13	30.36
TiO2	0.19	0.19	0.15	0.16	0.37	0.39	1.26	0.99	0.06	0.61	0.31	0.21	2.00
Al$_2$O$_3$	23.31	22.21	24.40	23.87	23.29	23.67	24.15	23.57	22.87	18.22	16.90	17.09	15.94
FeO	0.71	0.70	0.70	0.76	0.70	0.63	0.74	0.70	4.07	18.77	21.19	21.69	21.64
MgO	3.90	4.16	4.03	3.75	3.91	3.67	2.76	3.55	4.56	7.05	8.05	10.51	9.03
CaO	0.03	0.06	0.04	0.04	0.07	0.05	0.07	0.05	0.10	0.13	0.16	0.15	0.27
Na$_2$O	0.08	0.04	0.05	0.01	0.05	0.09	0.08	0.08	0.09	0.09	0.11	0.13	0.09
K$_2$O	1.25	1.15	1.23	1.14	1.12	1.12	1.19	1.17	0.90	0.23	0.28	0.27	0.14
Total	88.80	88.11	91.44	88.82	87.11	85.46	86.11	87.69	86.56	78.80	77.73	81.21	79.54
numbers of cations per half structural unit cell													
Si	3.88	3.93	3.87	3.87	3.85	3.80	3.78	3.82	3.71	3.70	3.52	3.43	3.43
Al(IV)	0.12	0.07	0.13	0.13	0.15	0.20	0.22	0.18	0.29	0.30	0.48	0.57	0.57
∑ (Tetra)	4.00	4.00	4.00	4.00	4.00	4.00	4.00	4.00	4.00	4.00	4.00	4.00	4.00
Al(VI)	1.68	1.66	1.70	1.71	1.68	1.71	1.71	1.67	1.57	2.07	1.81	1.65	1.56
Fe	0.04	0.04	0.04	0.04	0.04	0.04	0.04	0.04	0.23	1.73	2.03	2.00	2.05
Mg	0.38	0.41	0.38	0.37	0.39	0.37	0.28	0.35	0.47	1.16	1.38	1.73	1.52
Ti	0.02	0.02	0.01	0.02	0.04	0.04	0.13	0.10	0.01	0.10	0.05	0.03	0.34
∑ (Octa)	2.12	2.12	2.13	2.13	2.15	2.16	2.16	2.16	2.28	5.07	5.28	5.41	5.46
Ca	0.00	0.00	0.00	0.00	0.00	0.00	0.00	0.00	0.00	0.01	0.01	0.01	0.02
Na	0.01	0.00	0.00	0.00	0.00	0.01	0.01	0.01	0.01	0.01	0.01	0.01	0.01
K	0.09	0.08	0.08	0.08	0.08	0.08	0.09	0.08	0.07	0.03	0.03	0.03	0.02
∑ (Inter)	0.09	0.09	0.09	0.08	0.09	0.09	0.09	0.09	0.08	0.04	0.06	0.05	0.04
Fe/(Fe+Mg)	0.09	0.09	0.09	0.10	0.09	0.09	0.13	0.10	0.33	0.60	0.60	0.54	0.57

Table 3.2 Mineralogical formulas calculated from representative smectite analysis (normalized to $O_{10}(OH)_2$) from the spherule deposits in the Brazos core 2 compared to smectite analysis from K-P boundary spherules and K-P clay layers. Abbreviations: Tetra, tetrahedral; Octa, octahedral; Inter, interlayered. References: (1) Koeberl and Sigurdsson (1992); (2) Bauluz et al. (2000); (3) Martínez-Ruiz et al. (2001c); (4) Klaver et al. (1987); (5) Ortega-Huertas et al. (1998).

Locality	Brazos Texas	Brazos Texas	Beloc Haiti	Beloc Haiti	ODP 1049A W-Atlantic	DSDP 390B W-Atlantic	Stevns Klint Denmark	Agost Spain
Material	Spherule	Spherule	Spherule	Spherule	Spherules	Spherule	K-P Clay	K-P Clay
Reference	This study	This study	(1)	(2)	(3)	(4)	(2)	(5)
			numbers of cations per half structural unit cell					
Si	3.93	3.71	4.00	3.91	3.66	3.74	3.96	3.60
Al(IV)	0.07	0.29	0.00	0.09	0.34	0.26	0.04	0.40
$\sum$ (Tetra)	4.00	4.00	4.00	4.00	4.00	4.00	4.00	4.00
Al(VI)	1.66	1.57	1.17	1.04	1.84	1.26	1.29	1.40
Fe	0.04	0.23	0.37	0.44	0.71	0.63	0.24	0.48
Mg	0.41	0.47	0.68	0.62	0.48	0.27	0.69	0.20
Ti	0.02	0.01	0.06	0.01	0.03	0.05	0.01	0.01
$\sum$ (Octa)	2.12	2.28	2.29	2.11	3.06	2.22	2.23	2.09
Ca	0.00	0.00	0.12	0.36	0.02	0.01	0.15	0.02
Na	0.00	0.01	0.00	0.01	0.01	0.07	0.00	0.01
K	0.08	0.07	0.01	0.13	0.22	0.21	0.00	0.39
$\sum$ (Inter)	0.09	0.08	0.13	0.50	0.25	0.29	0.15	0.42
Fe/(Fe+Mg)	0.09	0.33	0.35	0.42	0.60	0.70	0.26	0.71

Wright, 1992), versus the 'detrital' fraction, including the elements Si, Ti, Al, K, Rb, and Zr, which are predominantly bound to terrigeneous minerals (e.g., Murray and Leinen, 1993). These changes might be ultimately related to variations in productivity, detrital input, relative sea level, and/or the proximity to the shoreline (e.g., Bohacs, 1998; Macquaker et al., 1998; Schutter, 1998; Jarvis et al., 2001). The following trends and abundance patterns have been observed in the Brazos cores and are highlighted in stratigraphic order in Figs. 3.12A-C.

Interval 1: The lower six meters of the Maastrichtian shales in the Brazos core 2 contain, at average, about 55 wt% SiO_2, 14 wt % Al_2O_3, 6 wt % CaO, and 5.4 wt % FeO. In addition, 2.5 wt% of MgO and K_2O, respectively, are present, whereas Na_2O is less than 1 wt%. These amounts of geochemical phases are distinguished from the composition of the "North American shale composite" ("NASC" Gromet et al., 1984), by significantly higher CaO as well as lower SiO_2 and Al_2O_3 values in the Brazos shale. This part of the Brazos core 2 generally furnishes Sr and Ba contents of 300-400 ppm, Zn, Rb, and Zr contents between 80-150 ppm, and low Cu, As, and Pb content (close to the detection limits, ~5-20 ppm). In summary, the element abundances throughout the lower six meters of Brazos core 2 show only insignificant fluctuations and no distinct compositional changes occur, as sustained by constant element/Al, Sr/Ca, and Zr/Ti ratios.

Interval 2: Above the relative uniform basal part of the Brazos core 2, the 1-m thick interval from 1

to 2 m in core depth immediate below the event deposit, shows slightly increasing contents of CaO, Sr, and P_2O_5, as well as reduced Sr/Ca ratios, suggesting either decreasing detritus input or a slight increase in productivity.

Interval 3: The basal breccia-like part of the event deposit shows slightly increasing detrital input (e.g., elevated TiO_2, Al_2O_3, MgO, and Rb contents), increasing Sr/Ca ratios, and decreasing contents of phases bound to carbonates (e.g., CaO, P_2O_5, Sr, and P). Therefore, it is analogous in composition to the shales from the interval (1) outlined above. Above this basal part, and associated with the spherule-rich bed, an amplified carbonate (and partly Sr) content is concomitant to strong depletion of all other elements, suggesting dilution by carbonate input. However, the increasing ratios of Si, Ti, Fe, and Mg against Al suggest a distinct change of the detrital composition. This interval also shows an abrupt lowering of the Sr/Ca ratio and a significant positive anomaly of P_2O_5 as well as lower K_2O in its basal (spherule-rich and microconglomeratic) part. All elements and element ratios decrease gradually to pre-event values in the upper part of the event deposit and in the capping marl layer. Very similar trends, though with lower peak highs, are found in the event deposit of Brazos core 1.

Interval 4: The carbonate-poor, 1.2-m thick shale interval above the event deposit, shows a >50 % drop of the carbonate contents, and a twofold increase of the Sr/Ca ratio, when compared to the late Maastrichtian shales below the event deposit.

Table 3.3 Mineralogical formulas of representative chlorite analysis normalized to $O_{10}(OH)_8$ from the event bed in Brazos core 2 and from spherule deposits in northeastern Mexico (see Table 2.4 for details). Abbreviations: Tetra, tetrahedral; Octa, octahedral; Inter, interlayered.

Locality	Brazos Texas	Brazos Texas	La Sierrita NE Mexico	El Mimbral NE Mexico
Material	Spherule	Spherule	Spherule	Spherule
Reference	This study	This study	Chapter 2	Chapter 2
	numbers of cations per half structural unit cell			
Si	3.43	3.43	3.06	3.40
Al(IV)	0.57	0.57	0.94	0.60
$\sum$ (Tetra)	4.00	4.00	4.00	4.00
Al(VI)	1.65	1.56	1.78	1.51
Fe	2.00	2.05	2.07	1.67
Mg	1.73	1.52	1.65	2.27
Ti	0.03	0.34	0.01	0.00
$\sum$ (Octa)	5.41	5.46	5.51	5.45
Ca	0.01	0.02	0.03	0.06
Na	0.01	0.01	0.01	0.01
K	0.03	0.02	0.04	0.02
$\sum$ (Inter)	0.05	0.04	0.07	0.09
Fe/(Fe+Mg)	0.54	0.57	0.56	0.42

Concomitant to this decrease in carbonate, which is probably related to a decrease in productivity and fossil contents, geochemical phases associated with terrigeneous detritus show slightly higher abundances than in the marls below the event deposit. In the upper part of the carbonate-poor interval, the shales become gradually enriched in carbonate.

Interval 5: Above the first appearance of Paleogene microfossils, and concomitant to the onset of multiple subsequent calcareous nannoplankton blooms during the lower five meters of nannofossil zone NP1, a series of maxima in carbonate content (CaO >20 wt%) and elevated P_2O_5 contents is present suggesting enlarged productivity. In the upper two meters of this interval (1 to 3 m core depth), the element ratio of Si plotted against Al is considerably higher, though other detrital phases (e.g., TiO_2, Rb) are not elevated, pointing to increased input of silica-rich phases (e.g., quartz). Its top is marked by an iron oxide- and pyrite-rich layer (>20 wt% FeO), though no further element anomalies have been observed in this layer.

Interval 6: Overlying the pyrite-rich horizon, in the topmost meter of Brazos core 1 the amount of Al_2O_3, MgO, K_2O, and Rb increases substantially, suggesting an increase in terrigeneous detritus, probably derived from clay minerals or feldspars, since the ratio of Si against Al decreases in this interval. The significant lower Zr/Ti ratios throughout this in-

terval sustain a change in the detritus composition. In addition, the CaO and P_2O_5 content are lower: the detriment of these phases may be linked to the reduced macrofossil-content in this interval.

3.3.6 Electron microprobe analysis

To reveal more details on the sedimentology and petrology of the event deposit, the electron microprobe (EMP) analysis was used combination with backscattered electron (BSE) images. Of particular interest has been the origin of the smectite and carbonate enrichment in the event deposit that has been recognized by the mineral and major element analysis. Some 3-6 points were analyzed on each individual spherule and fragment and in addition, several linescans were accomplished across ejecta particles to assure good average values and a reasonable measure of compositional variability. The stoichiometric conversion of oxide-weight percentage into molar abundance of cations yields reasonable cation sums for both smectites and chlorites, indicating that the mineral analyses are affirmative. The results of the EMP analysis, however, show low oxide totals, typically between 70-90 wt%. This implies copious amounts of low-Z materials, commonly H_2O or CO_2, and hence, the altered spherules are thoroughly hydrated and oxidized. In addition, submicroscopic porosity and irregular surfaces may be substantial, leading also to low oxide totals. Con-

Figure 3.13 (page 113) Two electron microprobe linescans (wavelength-dispersive X-ray fluorescence spectrometry) illustrating the major element phases of components from the spherule deposit (unit C, sample BZC2-43) in the Brazos core 2. All Fe is given as FeO. (**A**) Smectite-chlorite-bearing fragment with TiO_2-rich schlieren, presumably of impact-ejecta origin. (**B**) Carbonate-silicic clast (fish bone?) with carbonate infilled vesicle (?). The origin of these particles in not clear yet (see text for discussion).
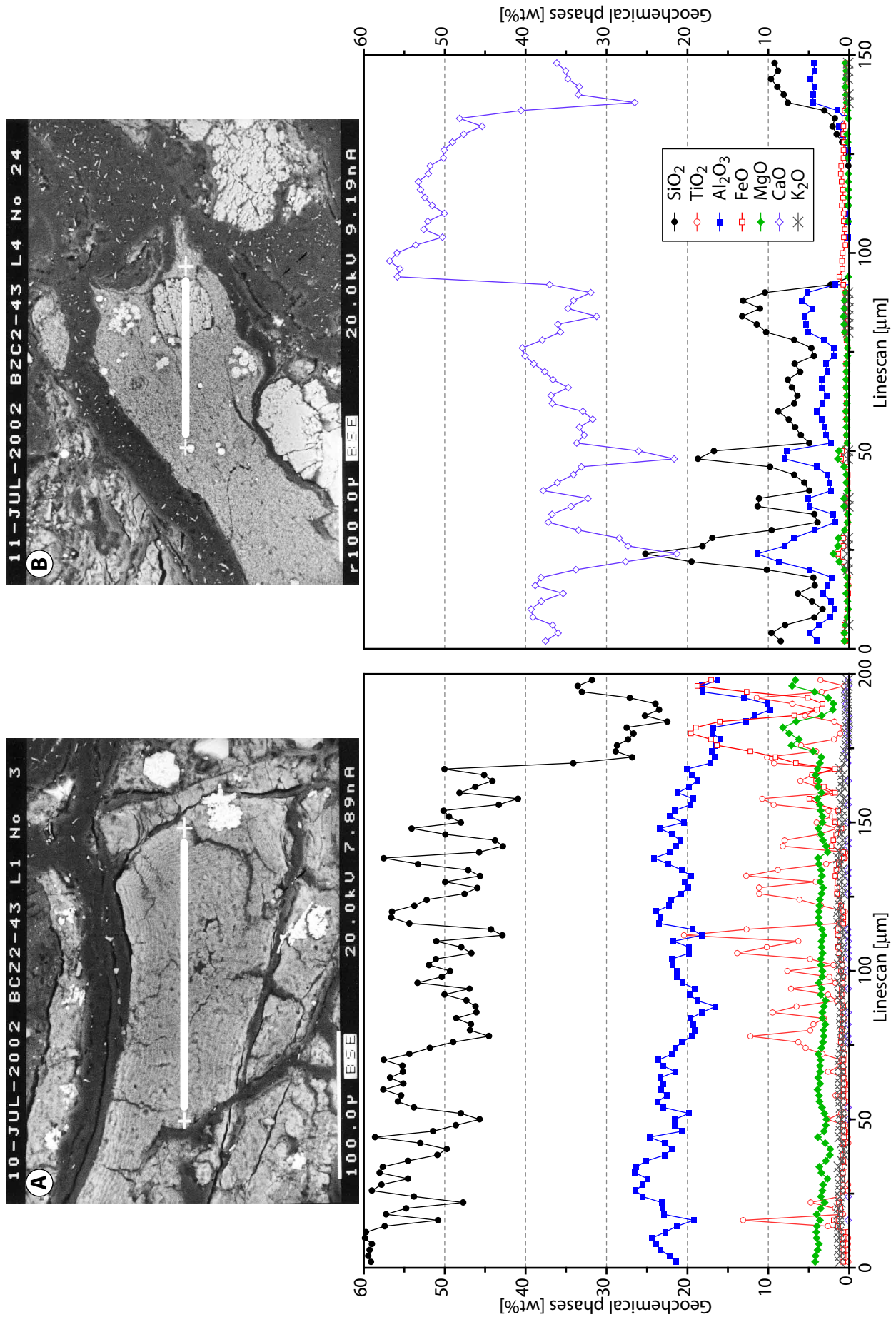
Figure 3.13 (caption on page 112).

sequently, analyses totaling <75 wt% were rejected, and oxide totals are purposefully given in Table 3.1 to illustrate the substantial alteration of these materials. The following geochemically distinct phases were found in the spherule bed of the Brazos core 2 and are shown in Table 3.1 and in Fig. 3.13. A comparison with smectites and chlorites found in spherule beds from other K-P sections is provided in the Tables 3.2 and 3.3.

Smectite spherules: They have high SiO_2 (55-60 wt%), Al_2O_3 (20-25 wt%), MgO (3-5 wt%) and show minor values for K_2O (~1 wt%), FeO (1-2 wt%), whereas Na_2O, TiO_2, CaO, are generally below 0.5 wt%. They contain iron-hydroxides (e.g., hematite crystals), pyrite crystals, and schlieren of TiO_2 (up to 10 wt%) and FeO (up to 7 wt%). In addition, schlieren and inclusions of low SiO_2 (30 wt%), high FeO (20 wt%), and high MgO (10 wt%) are present. Their totals are between 80-90 wt%. According to Newman (1987), these compositions are comparable to Mg-enriched dioctahedral smectite as shown by the characteristic cation sums when normalized to $O_{10}(OH)_2$. The $(Al+Fe)^{VI}/Mg^{VI}$ ratio of 1.7/0.4 substantiates this classification (Grauby et al., 1993). Following the geochemical criteria provided by Güven (1988), these smectites belong to the beidellite-nontronite series. However, sums for the cations occupying the octahedral sites exceed the ideal value of two by 0.1-0.3 and indicate a slight trioctahedral character of the smectite (Newman and Brown, 1987).

Chlorite spherules: They have high amounts of FeO (18-22 wt%) and MgO (7-12 wt%) and considerable lower SiO_2 (30-35 wt%) and Al_2O_3 (15-20 wt%) contents compared to the smectite spherules outlined above. The oxides K_2O, Na_2O, TiO_2, and CaO are generally between 0.5 to 1 wt% and their totals sum up to 75-85 wt%. Normalization to $O_{10}(OH)_8$, showed cation sums indicative for chlorite (Newman and Brown, 1987; Bailey, 1988). Their number of octahedral cations per formula unit is between 5 and 6, with mean values of about 5.4. This composition corresponds to an intermediate composition between di,trioctahedral chlorites (5 cations) and trioctahedral chlorites (5.5-6.1 cations Newman and Brown, 1987). The predominance of Fe in the octahedral layer points to a mineralogical composition that is analogous to chlorites of the chamosite group. However, the high silica content (Si >3-3.4 per formula unit), an Al^{VI} (1.5-2) content much larger than Al^{IV} (0.3-0.6) content, and a total octahedral occupation much lower than 6 cations (5-5.5), suggests that

some corrensite or smectite interlayers are present (Shau et al., 1991).

Glauconite: The glauconite grains from the spherule bed are rich in SiO_2 (~50 wt%) and FeO (~25 wt%), and have about 10 wt% Al_2O_3, as well as a MgO and K_2O contents of about 5 wt%, which is in keeping with published glauconite compositions (e.g., Odin and Fullagar, 1988; Amorosi, 1995). The K_2O content in glaucony defines the maturity of the mineral and serves to estimate the duration of particular diagenetic conditions that allowed authigenetic growth (e.g., Odin and Fullagar, 1988; Amorosi, 1995; 1997): the average K_2O contents of the glauconite at the Brazos event deposit is between 3-6 wt%, suggesting a slightly evolved glauconite maturity and a time for its formation between 10 to 30 ka.

Si- and Ca-rich ribbon-like grains: They consist mainly of SiO_2 (5-25 wt%) and CaO (10-30 wt%), added by minor Al_2O_3 and MgO (<2 wt%), though with low total oxides (generally <60 wt%), implies the presence of considerable amounts of volatile phases, probably due to strong alteration. The origin of these particles is not clear yet, but owed to their shapes and forms, including the faint occurrence of internal filaments, they may be considered as organic remains, though they contain almost no phosphorus.

3.4 Interpretation and discussion

3.4.1 Deposition of the K-P event deposit

The clastic unit consists of a complex stacked sequence including a smectite-rich, coarse-grained basal spherule deposit overlain by a bioturbated coarse carbonate-smectite-rich layer intercalated by thin silt-sand-rich layers, and finally capped by a micritic limestone. Accordingly, it consists of coarser sediments than the overlying and underlying deposits and each unit has anomalous sedimentary features compared to the enclosing lithologies. These characteristics qualify this succession to be considered as an event deposit (e.g., Einsele, 1998). Previous studies have explained this peculiar succession by various depositional processes including the well-known assignation as an impact-generated tsunami deposit by Bourgeois et al. (1988), which was also proposed by subsequent studies (Smit et al., 1996). Further interpretations included deposition by a series of debris flows and tempestites (Yancey, 1996), presumably during the late Maastrichtian sea-level lowstand (Keller, 1989a; 1989b; 1992; Keller

and Stinnesbeck, 1996). In a first step, the sedimentological characteristics of the individual units with respect to the underlying depositional processes will be interpreted (see overview in Figs. 3.4, 3.6). In a second step, the sedimentological data from the Brazos cores against common shelfal depositional mechanisms is discussed.

Unit A: The uniform, laminated shales of the Maastrichtian Corsicana Formation (unit A), with occasional shell (debris) accumulations, are interpreted as 'muds' deposited somewhat between, or slightly below, fair-weather and storm wave base; storm-driven currents probably led to intermittent reworking of shells (Hansen et al., 1987; 1993b; Kerr and Eyles, 1991). However, no distinct sand- or silt-layers have been observed, suggesting that reworking by currents acted on a local scale. The lamination of the shales may record subtle changes in the texture and discharge of suspended sediment or may be a later, diagenetic texture (Schieber, 1998).

The thin interval of 'deformed' shales, which underlie the event deposit in both Brazos cores, and the absence of lamination and bioturbation in this interval, may provide evidence that some kind of (soft-?) sedimentary deformation has occurred (e.g., Collinson, 1994; Maltman, 1994). This disturbance may be associated with or induced by, the strong currents that were active during deposition of the overlying 'conglomeratic' interval because either cyclic strain induced by periodic high currents, and/or current drag may both lead to sediment failure via downslope transport (Decker, 1990; Guiraud and Plaziat, 1993; Alfaro et al., 2002). Alternatively, seismic energy may induce analogous disturbance patterns.

Unit B: The sedimentologic characteristics of the basal unsorted 'conglomeratic' layer (unit B), including chaotic bedding and large grain-size variations, meet the criteria suggested by various authors to be indicative of an origin from a debris flow (e.g., Einsele, 1991; Mulder and Cochonat, 1996; Iverson, 1997; Mulder and Alexander, 2001). A similar conclusion was drawn by Yancey (1996) for the basal part of the event deposit. The size of the shale clasts may be indicative of the current energy that was associated with the debris flow, though this is certainly difficult to judge from a cored section, and for the Brazos cores, their size may be tentatively estimated to be in the range of some cm in diameter. However, Yancey (1996 and written comm. 2003) as well as Hansen et al. (1987; 1993b), have observed large outsized shale clasts (up to 1.2 m diameter) in this unit

that require high current energy to be transported and suggest a local origin from nearby areas on the seafloor (Johansson and Stow, 1995).

Unit C: The slightly laminated and graded coarse spherule-rich unit C lacks bedding and sorting characteristics typical of primary fallout (e.g., Fisher and Schmincke, 1984; Bitschene and Schmincke, 1991), but shows characteristics of deposition from grain-dominated debris flows with decreasing current energy (e.g., Mulder and Cochonat, 1996; Mulder and Alexander, 2001; Iverson, 1997), in line with the interpretation of Yancey (1996) for this interval.

The spherules, accretionary limestone clasts (lapilli), shale clasts, phosphatized particles, and sand-sized carbonaceous material, as well as the thin intercalated layers of micaceous silt-sand grains (unit D), suggest that a mixture of materials from different source areas occurred during sedimentation of this unit:

(1) The ejecta spherules, fragments, and accretionary limestone clasts probably derived via air-water fallout from the Chicxulub impact in southern Mexico (see below) and were subject only to minor local reworking since the highly irregular outlines of ejecta material preclude long-term lateral transport on the sea floor (d'Atri et al., 1999). Specifically, the accretionary spherules are relative fragile clasts and oppose considerable lateral transport on the sea-floor since they are interpreted to have an analogous genetically history to volcanogenic 'lapilli' (Pope et al., 1999; Yancey, 2002), and therefore, probably originated by accretion of dust particles resulting from moisture and electrostatic fields in turbulent ash clouds (Gilbert and Lane, 1994; Schumacher and Schmincke, 1995; Warme et al., 2002).

(2) The intercalated silt-sands probably originated from more proximal coastal areas.

(3) The rounded phosphatized particles, which obviously cause the distinct phosphorus peak (up to 3 wt%) in this unit, may be explained either by winnowing and lateral reworking of the coarse amount of the upper layer of unconsolidated sediments from adjacent areas or by reworking of lag horizons (Schieber, 1998).

Unit D and E: The sedimentological features of the carbonaceous-smectitic, sand-sized, laminated, and rippled unit E with the intercalated coarser sand-silt layers of unit D mark a change of the hydrodynamic conditions, compared to the underlying units. Their characteristics imply deposition from suspension during multiple subsequent steps of waning current

Table 3.4 Defining sedimentological criteria in support of incised valley fill, tsunami, or tempestite deposi-

Incised valley fill or shelf channel/fan deposit
An array of criteria for the recognition and identification of lowstand deposits that are typically confined to 'incised valleys' has been provided by Dalrymple et al. (1994) and Van Wagoner (1988; 1990) with further refinements added by Zaitlin et al. (1994) and Catuneanu (2002):
(i) 'Incised valleys' are elongate erosional features that are larger than a single channel (regional extent) and erosion has been caused by river action during a relative sea-level fall.
(ii) The base of the incised valley represents a sequence boundary that may be mantled by a pebbly lag and/or characterized by burrows. Therefore, the incised valley fill ('ivf') belongs to the lowstand systems tract.
(iii) The basal deposits generally shows an abrupt seaward shift of facies relative to those beneath the erosion surface, leading to a juxtaposition of more proximal and more distal sedimentary facies. They constitute the upper part of an upward-coarsening profile in a marine succession and include the coarsest sediment fraction of shelf sections.
(iv) The depositional valley fill ('ivf') may begin to accumulate near the end of the lowstand, but typically contains sediments deposited during the succeeding transgression with fluviatile or estuarine facies overlain by marine sands and shales in outer shelf areas.

Offshore tsunami sequence
Tsunami waves cause highly localized patterns of sedimentation and erosion in dependence of coastal/shelf morphology and resulting from strongly varying current velocities and directions (Cita et al., 1996; Einsele, 1998; Waythomas and Neal, 1998; Dawson and Shi, 2000; Goff et al., 2001; Carey et al., 2001):
(i) Strongest evidence for tsunami deposition comes from unusual coastal and onshore sand layers that occur several hundred meters land inward.
(ii) Strong erosion and sediment re-deposition on the shelf associated with erosional surfaces, bimodal current directions and multiple stacked sets of contrasting local-distal material in a sedimentary sequence may be caused by episodes of landward inundation of individual tsunami waves alternating with periods where strong backwash currents occur, even without direct tsunami wave interference with the sea floor. However, strong erosion during backwash may erase such evidence.
(iii) 'Boulder deposits' in shallow to intermediate shelf areas are frequently associated with tsunami waves and found embedded within sheets of tsunami-deposited sand.
(iv) Strong backwash currents may transport huge amounts of sediments far offshore, resulting either in 'homogenites' or in turbidite-like deposits in basinal setting (Cita et al., 1996; Cita and Aloisi, 2000).

Offshore tempestite sequence
A typical 'idealized' offshore tempestite succession has been compiled from Aigner (1985), Einsele (1991), Johnson (1996), and Myrow (1996) and comprises the following significant steps. Note, however, that each step, and preferential phase (iii) and (iv), may show large variability in sedimentary characteristics and may be subject to varying degrees of bioturbation.
(i) A basal erosion surface cut by combined oscillatory and unidirectional flow, possibly with gutter casts, sole marks, and intraclasts of pebbles, shells or mudstone may indicate storm erosion.
(ii) A hummocky cross-bedded and graded interval, possibly combined with parallel horizontal laminated layers, indicates the deposition during oscillatory currents and the main storm phase.
(iii) Wave ripples indicate waning storm energy and a return to lower flow regime with oscillatory to unidirectional currents.
(iv) Post-storm/fair-weather mud deposition ('mud blanket') that reflects either the final suspension fallout of storm-derived material or the return to normal background sedimentation.

energy as also indicated by hummocky ripples in the basal part (upper flow regime) and climbing ripples in the upper part (lower flow regime, e.g., Einsele, 1991; Shanmugam, 1997; Shiki et al., 2000). The smectite- and carbonate-rich composition of unit E and the intercalated quartz-mica-dominated sand-silt layers suggest that intermittent influx from nearshore areas alternated with influx from relatively fine-grained ejecta material (compared to the basal spherule bed) via air-water settling or reworking from adjacent areas. The burrows in this unit are confined to the topmost part of the sequence and, as indicated by the mud infill, apparently originated from a (probably eroded) horizon of different sediment composition. This characteristic may suggest an erosional surface atop of unit E, since the overlying carbonate-rich unit F is of a distinctly different, light-grey color.

The fine-grained micritic limestone (unit F) atop of this sequence grades into the overlying shales of unit G, and marks the end of strong current activity. The origin of unit F with gradually decreasing carbonate contents upsection is not clear since it could represent either fine-grained carbonaceous ejecta material from local reworking, though no particular smectite enrichment was encountered in this layer. Alternatively, this limestone is made of inorganically precipitated micrite, since it contains only few microfossils and no evidence for particular nannofossil blooms.

In summary, it appears as if a complex sedimentary sequence is preserved in the event deposit (units B-E, Figs. 3.5, 3.6) with ordered successive stages of (i) strong currents associated with debris flows and probably sediment disturbance (unit B), (ii) deposition of locally reworked coarse ejecta that

originally derived via air-water fallout to the sea-floor (unit C), followed by (iii) intermittent periods of sand-silt deposition (unit D), and finally, deposition of finer-grained ejecta material (unit E). This series of sedimentary events is analogous to other K-P sections in the Brazos area, though a distinct variability in thickness and extension of individual units exists (see Fig. 7 in Yancey, 1996). The 'ordered' succession of coarse ejecta particles overlain by finer-grained (sand-silt sized) ejecta suggests an upward decrease in the depositional energy. However, this distinct sequence with intermittent drastic changes in the provenance of the sediments makes it very unlikely that the event deposit was deposited via a single instantaneous event. The comparison with previously envisaged depositional mechanisms, specifically with sedimentary characteristics of incised valley ('lowstand') deposits, tsunamites, and tempestites, which are summarized in Table 3.4, reveals the following conclusions:

Sea-level lowstand deposits: The complex stacking pattern of the event deposit in the Brazos core 2 and the ordered succession of specific depositional mechanisms in this cm-thick layered 'coarse ejecta – (terrigeneous detritus) – finer-grained ejecta' sequence, as well as the absence of bioturbation in the units B-D, is difficult to explain simply by an abrupt facies change from proximal to distal settings. In addition, there is no further evidence for abrupt changes in the proximal-distal setting of the Brazos area from the mineralogical and geochemical data for the interval immediately above and below the event deposit (see last part of discussion). The stable late Maastrichtian benthic foraminifera assemblage also provides no evidence for gradual shallowing during deposition of the Corsicana Formation below the event deposit. This does not rule out, however, that relative sea level may have fluctuated since it cannot be excluded that a lowering of sea level occurred during the time represented by a possible hiatus at the base of the event deposit, though the duration of this hiatus is not resolvable via the biostratigraphic data (see below).

Tsunamites and tempestites: The high variability of tsunami (or tsunami-related) and of storm-generated event deposits makes it difficult to point out characteristics for either depositional mechanism. Particularly, since the stacked pattern in the upper part of the event deposit (Yancey, 1996 observed up to 5 graded sand-silt layers) suggests that a series of depositional events, hence, a series of tempestites or tsunamis (?) would be needed, which makes it quite

difficult to constrain the basic sedimentary controls. Moreover, the effects of a series of tsunamis or storms in the particular regional setting in the Western Interior Seaway, are currently not known, and probably difficult to estimate (e.g., Scheffers and Kelletat, 2003), though it is likely that the 'buffering' effects of such an extended water mass may have modulated substantially the behavior of tsunami- and tempestite-generated currents.

The debris-flow and turbidite characteristics of the event deposit in the Brazos cores, with intercalated distinct thin sand layers and hummocky stratification in the upper part (see also Yancey, 1996), may suggest strong currents with possible intermittent changes in the provenance area of the sediment, and upward decreasing current energy, which both are typical features for tsunami deposits in shelf settings, as outlined in Table 3.4. However, similar features are also associated with tempestite deposition and, according to Yancey (1996), the well sorting of the sand-silt layers in the Brazos outcrops suggests long duration of uniform high-energy levels; such conditions are difficult to bring into accord with deposition from tsunami waves. Consequently, the variability of tsunami and tempestite deposits, both sharing many common characteristics, does not allow for a clear distinction between the underlying processes, particularly from a cored section.

Therefore, the preferred explanation of the event deposit (unit C to E) is that it was deposited by debris flows of coarse ejecta spherules (unit C), followed by turbidite deposition from fine-grained and suspended ejecta material (unit E). Deposition of these units was punctuated by brief intervals of change in the provenance area associated with deposition of sand-silt-sized terrigeneous detritus (unit D).

3.4.2 Impact origin of the K-P event deposit

Spherules and fragmentary clasts, as well as the accretionary limestone particles, are the most prominent components of the event deposit. The vesiculated spherules and fragmentary clasts are generally altered to clay minerals (smectite and chlorite) and contain Ti-rich schlieren, while some individuals are pseudomorphically replaced by pyrite. In contrast, the lapilli-like grains are composed of microspar calcite and show weak concentric accretionary banding. However, the morphological characteristics of these ejecta spherules and fragments are similar to particles found in Chicxulub ejecta deposits in sections and cores of the Gulf of Mexico and adjacent areas (e.g., Alvarez et al., 1992; Smit et

al., 1996; Stüben et al., 2002b). In addition, similar accretionary clasts have been described by Yancey (2002) from the Brazos outcrop, as well as from several spherule deposits in the Caribbean (Pope et al., 1999; Salge et al., 2000), and in northeastern Mexico (Chapter 2). By analogy, these similarities imply an impact origin for the spherules and fragments, as well as for the lapilli in the event deposit of the Brazos cores. A comprehensive in-depth outline of the origination process of these ejecta particles is provided in Schulte et al. (2003) and in Chapter 2 of this thesis and will not be repeated here. Hence, the most prominent features of these components will be discussed, as well as analogies and differences to ejecta particles from K-P sections on a regional to global scale.

Alteration of Chicxulub ejecta

A distinct diagenetic overprint is indicated by the complete alteration of the ejecta material to clay minerals, as outlined above. However, the complex petrological and mineralogical composition of the event deposit, combined with preservation of many petrological details, suggests that diagenetic effects were relatively minor and did not obliterate primary compositionally trends. This interpretation is inline with the very moderate (<50 m!) burial-depth of the sediments at Brazos, which is far beyond the depth (>2 km) that is commonly required for intensive clay mineral transformation (e.g., from smectite to illite-smectite and to illite, Hower et al., 1976). The extensive pyrite formation in the spherule bed of Brazos core 2 appears to be restricted to the basal part of the event deposit (unit C). No particular evidence for severe anoxic conditions in the interval above and below the event deposit has been found as suggested by low abundances of high redox-sensitive trace elements (Cu, As, Ni, Mo) and benthic foraminifera assemblages (Tyson and Pearson, 1991; Calvert and Pedersen, 1993; Nijenhuis et al., 1999), albeit pyrite concentrations are slightly elevated throughout the event deposit and in unit G (Fig. 3.9).

The pyrite formation in the basal event deposit may be interpreted to be the product of sulfate-reducing bacteria during *in-situ*, transient bacteria blooms subsequent to deposition (Wilson and Roberts, 1999; Grimes et al., 2002). In addition, secondary pyrite nucleation and growth in the sediment, well below the water-sediment interface, may have also resulted in euhedral pyrite grains and pyrite framboids (Morse and Wang, 1997; Wilkin and Barnes, 1997). Heymann et al. (1998) obtained similar results and

detected even native sulfur (S^0) in considerable amounts in the Brazos spherule beds.

In the Brazos core 2, pyrite crystals frequently constitute framboidal agglomerates (50-100 μm in size) and apparently replaced some of the ejecta particles or covered their surfaces and internal vesicles. These infilled and overgrown framboids may have formed in the sediments because of surface nucleation and continued pyrite growth on spherules (e.g., Wilkin and Barnes, 1997). Remarkably, the replacement and overgrowth appears to be highly selective, and some, mostly vesicular spherules, have been affected, whereas other spherules have been preserved without substitution or pyrite overgrowth. This suggests that isolated chemical microenvironments developed in this part of the event deposit and in individual ejecta particles, reflecting local changes in the pH and Eh conditions in response to availability of ferrous species, sulfide species, and suitable electron acceptors (e.g., Wilkin and Barnes, 1997; Grimes et al., 2002). In addition, it is conceivable that this selective pseudomorphosis reflects an initially different spherule composition, with an original composition that was more amenable to substitution by pyrite (Lev et al., 1998; Li et al., 1998; Grimes et al., 2002). Therefore, it is probably that pseudomorphologically replaced spherules originally had a more iron-rich composition, which released iron during diagenesis (Li et al., 1998) and allowed for pseudomorphical substitution, whereas the originally more Si-rich glassy spherules altered to smectite. Such iron-rich spherules are a prominent component of the Chicxulub ejecta deposits in northeastern Mexico (Chapter 2 and Schulte et al., 2003).

For the Gulf of Mexico area, strong pyritization of spherule deposits is not a common phenomenon, though single pyrite crystals are often observed in spherule deposits from northeastern Mexico or Beloc, Haiti (Schulte et al., 2003). Similarly, spherule deposits in the Western Atlantic show only minor pyritization (Klaver et al., 1987; Martínez-Ruiz et al., 2001b). However, for the spherule-rich basal melt-ejecta layer of the K-P boundary clay couplet in the Western Interior, pyritization, and enhanced sulfur contents has been observed in several sections (e.g., Dogie Creek, Brownie Butte, Gardner and Gilmour, 2002; Maruoka et al., 2002). These authors suggested that the high input of sulfate may have been caused by the sulfate-rich melt ejecta and/or acid rain induced by the Chicxulub impact (see also Retallack, 1996; Griscom et al., 2003; Maruoka and Koeberl, 2003).

Table 3.5 Compilation of clay mineral associations from spherule deposits and basal boundary clays in K-P boundary sections (modified from Ortega-Huertas et al., 2002). Abbreviations: *Layer-type:* SP-EL, spherule-rich ejecta layer; LCL, laminated clay layer ("fireball layer"); LCL-MSP, laminated clay layer with microspherules; BCL, boundary clay layer (above LCL). *Clay mineralogy:* S, smectite; S*, Mg-rich smectite; I, illite; I-S, illite-smectite mixed layer; Ch, chlorite; K, kaolinite; **Boldface**, dominant component.

Location	Layer-type	Clay mineralogy	References
Gulf of Mexico			
El Caribe, Guatemala	EL-SP	**S***, K	Fourcade et al. (1997), Debrabant et al (1999)
Albion Quarry, Belize	EL-SP	**S***	Pope et al. (1999)
NE Mexico	EL-SP	**Ch**, Ch-S, I, I-S, S	Schulte et al. 2003; Chapter 2
Brazos, Texas	EL-SP	**S***, Ch, I	This study
Caribbean Sea			
Beloc, Haiti	EL-SP	**S***	Izett (1991), Kring and Boynton (1991), Koeberl and Sigurdsson (1992), Stüben et al. (2002a)
ODP Leg 165 Sites 999, 1001	EL-SP	**S** (?)	Sigurdsson et al. (1997)
North America (Western Interior)			
Madrid, Starkville, Sugarite, Raton	EL-SP LCL	**K** **S**	Pollastro and Pillmore (1987), Izett (1990), Pollastro and Bohor (1993), Evans et al. (1994a)
Frenchman River	LCL	**S**, K	Lerbekmo et al. (1987)
Atlantic Ocean			
DSDP Leg 93 Site 603B	EL-SP	**S***	Klaver et al. (1987)
ODP Leg 174AX Bass River Site	EL-SP	**S** (?)	Olsson et al. (1997)
ODP Leg 171B Sites 1049-1053	EL-SP	**S***	Martínez-Ruiz et al. (2001c)
DSDP Leg 74 Sites 525-529	BCL	**S**, I, Ch, I-S, K	Robert and Chamley (1990)
DSDP Leg 73 Site 524	BCL	**S**, I, K	Hsü et al. (1982)
Tethyan realm			
Agost, Caravaca; Spain	LCL-MSP BCL	**S*** **S**, K, I	Evans et al. (1994a), Ortega-Huertas et al. (1995; 1998), Kaiho et al. (1999)
El Kef; Tunisia	LCL-MSP BCL	**S**, K, I, Ch **S**, K, I	Ortega-Huertas et al. (1998)
Elles II; Tunisia	LCL BCL	**S***, K, I, Ch **K**, S, Ch, I	Adatte et al. (2002b), Stüben et al. (2002b)
Gubbio; Italy	LCL-MSP BCL	**I**, K, I-S **K**, S, Ch, I, I-S	Rampino and Reynolds (1983), Robert et al. (1990), Montanari (1991)
Petriccio; Italy	LCL-MSP BCL	**S**, I, K **I**, S, K	Montanari (1991), Evans et al. (1994a), Ortega-Huertas et al. (1998)
Koshak; Kazakhstan	BCL	**I**, S, K, Ch	Pardo et al. (1999)
Bjala; Bulgaria	BCL	**S**, K, I, Ch	Adatte et al. (2002a), Preisinger et al. (2002)
Basque-Cantabrian Basin; Spain	LCL BCL	**I**, I-S, K, Ch **I**, Ch, I, I-S, K, Ch	Ortega-Huertas et al. (1995, 1998)
Stevns Klint; Denmark	LCL-MSP BCL	**S*** **S***, I-S, I	Kastner (1984), Elliott (1989), Elliott (1993), Evans et al. (1994a), Bauluz et al. (2000)
Pacific Ocean			
ODP Leg 113 Sites 689-690	BCL	**S**, I, Ch, I-S, K	Robert and Chamley (1990)
Woodside Creek; New Zealand	BCL-MSP	**S**	Evans et al. (1994a)

Reducing conditions in the basal K-P boundary (fallout) clay layer accompanied by pyrite replacement of iron-rich spherules and enhanced sulfate and organic contents has been observed in several K-P sections in the Pacific and the Tethyan realm (Montanari, 1991; Martínez-Ruiz et al., 1992; 1999; Kyte et al., 1996; Tribovillard et al., 2000; Preisinger et al., 2002; Shimoyama and Yabuta, 2002). However, evidence for reducing conditions in these K-P sections is generally restricted to the very base of the boundary clay and has been explained by mass mortality and subsequent accumulation of organic material at the K-P boundary (e.g., Shimoyama and Yabuta, 2002) since there exists no evidence for widespread

anoxia following this boundary during the earliest Danian (see also Tribovillard et al., 2000).

Mineralogical composition of Chicxulub ejecta

Electron microprobe analysis revealed that most spherules and fragments are made of smectite with a distinct Mg-rich composition; in addition, some spherules have a chlorite-like mineralogy (Table 3.1). This composition suggests that the exclusive smectitic composition of this layer (>95 rel% smectite from bulk rock analysis of the <2 μm fraction) may be the result of an authigenic replacement of former glassy spherules and fragments. Mg-rich smectite is a common alteration product of formerly glassy Chicxulub ejecta spherules from K-P sections in the southern Gulf of Mexico, the Caribbean and the Western Atlantic (cf. Table 3.5 and Ortega-Huertas et al., 1998; 2002). The smectite compositions from the Brazos spherules are well within the range given for these ejecta spherules (see comparison in Table 3.2 and Klaver et al., 1987; Bohor and Glass, 1995; Debrabant et al., 1999; Martínez-Ruiz et al., 2001b; 2002; Stüben et al., 2002b). According to these studies, smectite spherules often contain glassy cores that by their geochemical composition point to a progenitor phase of andesitic composition, inline with the composition of the melt fragments in the suevite of the Chicxulub impact structure (see Table 2.4 and Schuraytz et al., 1994; Kettrup et al., 2000; 2003). Consequently, these data suggest that the spherules at Brazos derived via authigenesis from a similar parental phase of probably andesitic composition.

Regional-global correlation of Chicxulub ejecta

A distinct smectite enrichment has also been reported from a number of K-P sections in the eastern Atlantic, the Pacific, and the Tethyan realm to be associated with the basal (mm-thick) ejecta-fallout K-P clay layer and the alteration of microspherules, as summarized in the Tables 2.1 and 3.5 (with references, e.g., Ortega-Huertas et al., 2002). Since local sediment influx (e.g., volcaniclastics) may have overprinted the original signal, and since individual sections may have undergone different diagenetic processes due to local settings (e.g., burial depth, type of enclosing sediments), the significance of the increased quantities of smectite observed at the K-P boundary must be evaluated carefully for each section (see Ortega-Huertas et al., 1995; 1998; Kaiho et al., 1999). Several observations, however, have established a link between the smectite-enrichment and the alteration of microspherules and impact

glass: for instance, in the spherule deposits at Beloc, Haiti, and in the K-P boundary clay at Stevens Klint, Denmark (e.g., Bauluz et al., 2000; Stüben et al., 2002b). Glassy and smectite ejecta particles in both sections show a very similar mineralogy and geochemistry including typically andesitic glass compositions and Ca-Mg-rich smectite compositions (see Table 3.2 and Ortega-Huertas et al., 2002).

Spherules of chlorite mineralogy have rarely been observed from K-P spherule deposits in the Gulf of Mexico and adjacent areas, though in the spherule deposits of northeastern Mexico, they constitute the bulk of the ejecta particles (see Chapter 2 and Schulte et al. 2003). The tabulated mineral compositions of typical chlorite from the Brazos core 2 and from northeastern Mexico in Table 3.3 show that the mineralogical composition of the Fe-Mg-rich di,trioctahedral, and trioctahedral chlorite ejecta particles are within the same range for both locations. For the ejecta from northeastern Mexico, a mafic precursor phase was suggested by previous studies (see Chapter 2 and Schulte et al. 2003), implying that a mafic progenitor may also account for the chlorite spherules in the Brazos area. Consequently, and in concert with the presence of Mg-rich smectite spherules as outlined above, the Brazos area in Texas might have received ejecta material from compositionally different (felsic vs. mafic) areas in the subsurface of Chicxulub impact structure at the Yucatán peninsula. Considering the regional setting of the Brazos area in Texas, between the ejecta strewnfield in northeastern Mexico (mostly mafic precursor phases) and the Western Atlantic (mostly intermediate-felsic precursor phases of andesitic composition), some mixing of different ejecta phases is likely to occur, albeit the bulk altered ejecta phase at Brazos is smectite, probably derived from a precursor of andesitic composition. The distinct compositional range of the ejecta phases might reflect the petrological variability of the basement in the subsurface of the Chicxulub impact structure, as outlined by several previous studies (Kettrup et al., 2000; Kettrup and Deutsch, 2003), and specifically for the northwestern sector of the Chicxulub structure (see Chapter 2).

Geochemical composition of the 'K-P event deposit'

The detrital material in the units C, D, and E of the event deposit is distinct from the enclosing shales by significantly higher ratios of Si, Ti, Fe, Mg, and K against Al, sustaining the presence of a considerable

amount of compositionally diverse and altered impact ejecta of smectite- and chlorite-like mineralogy, as outlined above. The high amounts of carbonate in the units C and E, compared to the enclosing shales, may therefore derive via carbonaceous ejecta-fallout (e.g., limestone clasts, accretionary lapilli, carbonaceous dust, see Chapter 2), whereas the elevated phosphate contents in basal layer of unit C may be explained by the presence of phosphatized particles (e.g., fossil shells) from the sea floor. In addition, the Sr/Ca ratios show a pronounced minimum in the units C, D, and E of the event deposit. This trend may be either related to the detrital input of carbonate with a lower Sr content, or by the recrystallization that generally depletes the Sr concentration in carbonates since Sr^{2+} is preferentially removed from calcite into pore waters (Oberhänsli et al., 1998). A comparison with Sr/Ca trends in other parts of the Brazos cores supports the later explanation, as higher carbonate content is always related to lower Sr/Ca ratios and vice versa.

3.4.3 Evaluation of unconformities

The spherule-rich event deposit in the Brazos cores rests unconformable on late Maastrichtian shales. However, from the cored sections and from the poorly constrained biozonation of the late Maastrichtian interval below the event deposit (i.e., the difficulties in differentiating Biozone CF1-CF2), it is difficult to establish if any erosion of Maastrichtian shales is associated with the sedimentary disturbances in the interval below the event deposit. Nevertheless, for the Brazos area, outcrop studies have revealed that the relief induced by the erosion may reach up to no more than 0.2 to 0.4 m (Hansen et al., 1987; 1993b; Yancey, 1996). This would indicate maximum erosion of late Maastrichtian shales in the range of 40 to 80 ka based on a sedimentation rate of about 0.4-0.5 cm/ka given by Hansen et al. (1993b).

Additional unconformities are present in the upper part of the event deposit, where the mud-infilled burrows in unit D may indicate successive periods of sedimentation and erosion atop of this unit, since these burrows did apparently not originate from the non-bioturbated shales of the overlying carbonate-poor interval. However, again, it is not possible to resolve the duration of this hiatus. A third unconformity may be present at the base of the Pisgah Member and expressed by a pyritized layer, though from biostratigraphic data of planktic and benthic foraminifera (no abrupt faunal changes) and from the 'ordered' pattern of successive calcareous nanno-

plankton blooms it is not clear if this unconformity is associated with a hiatus.

3.4.4 Placement of the K-P boundary

The base of the boundary clay at El Kef, Tunisia, has been defined to mark the position of the global stratotype section and point (GSSP) for the Cretaceous-Paleogene boundary (Cowie et al., 1989). Additional defining criteria were added by subsequent studies and included the presence of peak iridium and siderophile-element concentrations, Ni-rich spinels, goethite and smectite microspherules, as well as the mass extinction of Cretaceous calcareous nannofossils and (tropical) foraminifera immediate below, and the appearance of Paleocene species in the centimeters above this clay layer (see summary in Keller et al., 1995; Remane et al., 1999). In addition, the K-P boundary is marked by a sudden drop of the carbonate content and of the $\delta^{13}C$ isotope ratio, reflecting a sudden drop in carbonate productivity (e.g., Lindinger, 1988).

The petrological, mineralogical, and geochemical analysis of both Brazos cores revealed no evidence for the presence of a distinct mm-thick "boundary clay" with anomalous element-concentrations and a sharp drop in carbonate content, hence, it is difficult to appoint a precise position of the K-P boundary in the Brazos cores. The difficulty in placing the K-P boundary in the Brazos area is underlined by the results of previous studies revealing on the one hand that multiple iridium anomalies exist, beginning in the upper part of the event deposit and extending about 15-25 cm into the overlying shales (Fig. 3.3 and Hansen et al., 1993b; Rocchia et al., 1996; Heymann et al., 1998). On the other hand, these studies showed that the mass extinction of Cretaceous planktic foraminifera is not coincident with the first appearance of Paleogene forms, as observed at El Kef, Tunisia (Keller et al., 1995), but precedes (46 % extinction at base event deposit) and follows (45 % extinction at 25 cm above) the first appearance of Paleogene forms (Fig. 3.3 and Keller, 1989a). Therefore, these previous results are incompatible with an unambiguous definition of the K-P boundary by the criteria outlined above and the simultaneous mass extinction of most Cretaceous forms and first appearance of Paleogene species at one distinct mm-thick layer. Considering the data from the two Brazos cores, three possibilities for placing the K-P boundary are conceivable:

(1) At the first appearance of Paleocene microfossils, about 1.6-1.8 m above the top of the event deposit

as suggested by a number of studies (e.g., Jiang and Gartner, 1986; Keller, 1989a; Keller and Stinnesbeck, 1996; Beeson et al., 1994). These previous investigations showed, the first onset of Paleocene taxa is commonly at about 17-25 cm above the top of the event deposit and almost coincident with the uppermost major iridium spike and the onset of the δ^{13}C shift (see also Hansen et al., 1987; 1993a; 1993b; Rocchia et al., 1996; Heymann et al., 1998). However, in the Brazos core 1 of this study, the interval between the event deposit and the first Paleocene microfossils is much more expanded (about 1.6 m).

(2) At the base of the smectite-rich event deposit concomitant to the first occurrence of Chicxulub ejecta-spherules. This possibility gains support from the morphologically and mineralogical similarity of the spherules at Brazos to Chicxulub ejecta spherules found at, or close to, the K-P boundary in sections from the Gulf of Mexico and adjacent areas (e.g., western Atlantic see Fig. 3.5), though the stratigraphic placement of these spherule deposits is not clear for all localities and spherule deposits occur in different stratigraphic horizons during Biozone CF1 to P1a (e.g., Keller et al., 2001): based on one spherule-bearing section in northeastern Mexico (see Chapter 2 for details), a group of authors suggest that the Chicxulub impact occurred 270 ka before the K-P boundary (as defined by the first occurrence of Paleocene microfossils Stinnesbeck et al., 2001; Keller et al., 2002). Nevertheless, the Brazos spherules bear a morphological similarity to spherules found in the K-P boundary clay at sections in the Western Interior (see Bohor et al., 1987; Bohor and Glass, 1995; Izett, 1990 and Chapter 2) and a mineralogical similarity to microspherules from the basal K-P boundary clay in the western Tethys (see Table 3.3 and Bauluz et al., 2000; Ortega-Huertas et al., 2002). Specifically the iridium-enriched K-P boundary clay in North America, which also contains Ni-rich spinels and abundant shocked mineral fragments, has been linked to the Chicxulub impact by the grain-size distribution pattern of shocked minerals, that show an increase in grain-size towards the Caribbean area (e.g., Izett, 1990; Kring, 1995; Croskell et al., 2002; Kring and Durda, 2002). In addition, U-Pb dating of single shocked zircons from the K-P boundary clay in the Western Interior and from the Haitian spherule deposits at Beloc, as well as from the suevite from the Chicxulub impact structure, revealed similar source ages, suggesting that these zircons

derived from a common basement with an age of about 418±6 Ma and 540±10 Ma (e.g., Krogh et al., 1993a; 1993b; Kamo and Krogh, 1995).

(3) Atop of the event deposit, below the carbonate-poor interval. This option gains support from a drastic drop of the macro-, micro-, and nannofossil abundance concomitant to a reduction in the carbonate contents (from about 8 to 4 wt%), as well as from the benthic faunal turnover during this interval. A drop in carbonate contents due to a strong productivity reduction and a sudden drop of the nannofossil abundance are a characteristic feature of many K-P boundary sections for the earliest Danian (Biozone NP1 and P0, P1a Henriksson, 1996; Gartner, 1996; Speijer and Van der Zwaan, 1996; Gardin and Monechi, 1998; Gardin, 2002; Håkansson and Thomsen, 1999; Culver, 2003). No benthic faunal turnover or major drops in the diversity of calcareous nannoplankton have been observed by these authors for the latest Maastrichtian, preceding the K-P boundary (see discussion in Culver, 2003). The placement of the K-P boundary atop of the event deposit is roughly coincident with the first major iridium spike observed by previous studies (see Fig. 3.3 and Hansen et al., 1987; 1993b; Evans et al., 1995; Rocchia et al., 1996; Heymann et al., 1998). However, in the Brazos cores, a carbonate- and nannofossil-impoverished interval occurs well below (1.6 m) the first appearance of Paleocene microfossils within laminated shales with reworked ejecta-debris.

In summary, it appears that the application of the K-P boundary criteria revealed from the GSSP stratotype in Tunisia is difficult for the K-P transition recorded in the Brazos cores since no particular "K-P boundary clay" with the concurrent presence of several characteristic features of the K-P boundary elsewhere (as outlined above) has been found. In addition, the variable occurrence of traditionally used boundary markers over a distinct sedimentary interval (about 1.6 m), as revealed by this study or previous work gives no support for the unequivocal placement of the K-P boundary in the Brazos cores at 'one' distinct mm-thick horizon because several alternative 'positions' are available, each supported by some valid arguments. Nevertheless, a position of the K-P boundary at the base of the spherule-rich event deposit is in line with several K-P sections in the Atlantic, the Pacific, the Western Interior, and the Tethyan realm, which all show a smectite spherule-rich bed at the immediate K-P boundary, and in which the K-P boundary clay layer has been linked

to the Chicxulub impact event by several mineralogical and geochemical criteria. This position is also in keeping with the onset of the iridium anomaly within the event deposit at the Brazos River K-P localities, as reported by previous studies.

3.4.5 Inferences from clay mineral facies – Paleoclimate

The relatively invariable smectite-dominated clay mineralogy of the shales in the Brazos cores may suggest influx from soils that developed during chemical weathering in warm climates with wet and dry seasons (Chamley, 1989; 1997). On the other hand, smectite may be derived from the alteration of volcanic rocks or via diagenesis. However, considering an origin from volcanic sources, the continuous high abundance of smectite throughout the cores would require a permanent high volcanism in this area for which there is no evidence in this passive continental margin setting. In addition, the sediments in the Texas coastal plain did not suffer deep burial diagenesis. The absence of significant diagenetic overprint other than a transformation of impact glass into smectite and chlorite is documented by the constant, but variable presence of smectite, the near-absence of mixed-layers (e.g., illite-smectite), and the co-existence of smectite with kaolinite and chlorite. Moreover, the smectite in the shales of the Brazos cores is not well crystallized, probably Al-rich (beidelite), and supports a pedogenic, hence inherited origin.

Warm and humid to semiarid climate conditions were reported from paleosol studies from western Texas by Lehman (1990), as well as from Atlantic (Martínez-Ruiz et al., 2001a), and Tethyan (Chamley, 1997) domains throughout the K-P transition. These conditions favored the development of thick continental soils that led to the abundance of (Al-rich) smectites. In addition, smectites may have formed in poorly drained coastal areas resulting from tectonic stability, low continental relief, and warm climate conditions. According to the data reported here, these conditions may have prevailed during the latest Maastrichtian into the early Danian. Therefore, the dominance of smectite indicates a relatively constant, warm, and hydrolyzing climate during these times. The subordinate, albeit consistent amounts of illite, kaolinite, and chlorites imply additional, simultaneous influx from more mature (kaolinite) types of soils and from less evolved (illite, chlorite) types of soils. Consequently, the diverse clay mineral assemblage in the Brazos cores suggests a com-

plex hinterland, probably with variable topography (climates), and/or different lithologies.

3.4.6 Long-term facies trends – Sequence stratigraphic setting

Long-term fluctuations in either mineralogical or geochemical composition appear to be relatively subtle in the Maastrichtian to Danian shales bracketing the event deposit in the Brazos cores. Compositional changes are not as obvious as, for instance, in the shallower settings at central Alabama (see Chapter 4). This is particularly evident for the Corsicana shale (unit A) of the Brazos core 2 below the event deposit, where besides negligible fluctuations in the mineral content and element abundances, no significant long-term compositional, and hence facies trends have been observed, as also supported by a stable microfossil fauna throughout this Corsicana shales. However, minor compositional changes of the Corsicana shales are confined to the 1.5 m immediate below the event deposit, where an elevated carbonate content (from ~6 to 9 wt%) coincides with an increase in the abundance of planktic foraminifera and a related increase of the ratio of planktic to benthic foraminifera, tentatively suggesting a slight increase in productivity.

From the Brazos outcrop sections, it is known that this interval is also associated with an increase in epifaunal suspension feeding bivalves (e.g., oysters), as well as with a drop in the molluscan diversity (see Fig. 3.3 and Hansen et al., 1993b). Its (paleoecological) significance is yet unclear, and a relationship to regional climate changes or even the latest Maastrichtian warming event may exist, though a link is difficult to constrain with the present biostratigraphic resolution. Notably, a similar, though more pronounced increase of the carbonate content, coupled with elevated amounts of planktic foraminifera, is also found in the meters before the basal sandy beds of the Clayton Formation in the Antioch Church core, Alabama (see Chapter 4).

In contrast to the Corsicana shales below the event deposit, the shales of the Brazos core 1 and their mineralogical and geochemical composition during the interval governed by the Littig Member (units G, I), and the Pisgah Member (unit J), show distinct facies trends:

'Carbonate-poor interval' of the Littig Member (unit G): The composition of the laminated, carbonate-poor shales (unit G) indicates a significant change in the sedimentary conditions, when compared to the Corsicana shale interval below the

event deposit. The lowered carbonate content may be explained by a decrease of the biogenic carbonate productivity commonly observed at the K-P boundary (Keller and Lindinger, 1989; Zachos et al., 1989; D'Hondt et al., 1998; Stüben et al., 2002a), since this layer is essentially devoid of macrofossil remains and significantly impoverished in micro- and nanno-fossils. The absence of bioturbation may additionally suggest adverse (dysoxic?) sedimentary conditions (Brett and Allison, 1998), though the mineralogy and chemostratigraphy of this interval provides no particular indices for anoxic conditions as outlined above. Also, elevated terrigenous sediment input and enhanced reworking may have had a similar dilution effect of the carbonate fraction, since the sporadic occurrence of altered spherules, as well as carbonate rock chips throughout this interval, indicates intermittent periods of reworking and redeposition. Significant carbonate dissolution in the carbonate-poor interval appears to be less likely since the (rare) planktic and benthic foraminifera show an excellent preservation.

In terms of possible sea-level changes, Keller (1992) and Beeson et al. (1994) suggested a major sea level lowering (from outer to middle neritic settings), followed by transgression during the interval immediate above the event deposit (unit G). From the data presented in this study, it is difficult to obtain distinct trends: on the one hand, decreased carbonate content may suggest increased terrigenous input and, hence, lowered sea-level or a more proximal setting of the shoreline. On the other hand, these trends may be related to local productivity fluctuations, and consequently may have little expressivity regarding sea-level changes. In addition, the amounts of quartz and feldspar are not elevated throughout unit G, compared to the Corsicana shales below the event deposit, as also reflected by the absence of meaningful trends in the element/aluminum ratios (Fig. 3.12C) that could indicate changes in the composition of the terrigeneous detritus, and hence corroborate proximal-distal trends (e.g., Jarvis et al., 2001).

In conclusion, the mineralogical and geochemical data reveal no positive evidence for distinct facies changes throughout this interval in the Brazos cores. This interpretation is consistent with Jiang and Gartner (1986), Bourgeois et al. (1988), Hansen et al. (1987; 1993a), and Yancey (1996) who all concluded that the bracketing of the event deposit by relatively uniform shales suggest that no significant drop in sea level occurred. Based on element ratios,

a similar conclusion was reached by Tribovillard et al. (2000) for the Tunisian K-P sections.

Littig Member (unit I): Unit I starts with the almost simultaneous occurrence of Paleocene microfossils and distinct nannofossil blooms (Fig. 3.4), as well as with the gradual return of many invertebrates, mainly mollusks (see also Fig. 3.3 and Hansen et al., 1987; 1993b). The carbonate content reaches amounts of the Corsicana Formation immediate upon entry of the Paleogene fauna and rises throughout the Biozone P0, Pα, and P1a, with peak values of 30 wt%. This rapidly increase of the carbonate contents is in contrast to observations from other K-P boundary locations from the Tethyan realm, including El Kef, Tunisia, where the calcite content usually remains low from Biozone P0 through at least the lower part of Biozone P1b (Keller and Lindinger, 1989; Zachos et al., 1989; D'Hondt et al., 1998; Stüben et al., 2002a).

Nevertheless, in sections from the Atlantic and the western Tethys, including Caravaca, Spain, the return to pre-K-P carbonate contents is more rapid and occurs immediate within Biozone P0 or at the base of Biozone P1α (see Fig. 3.5 and Martínez-Ruiz et al., 2001c). The increase of coarser sand-silty detritus throughout this interval, as reflected in the slightly rising quartz and feldspar contents (Fig. 3.9), and by slightly elevated Si, Ti, Fe, and Mg versus Al ratios (Fig. 3.12C), suggest increased proximity to the shoreline (Schutter, 1998). Therefore, a sequence boundary may be placed in the basal part of this unit, though an exact position is difficult to determine, since lithologic changes are gradual.

A position of the sequence boundary between sample 28 and 30 is tentatively suggested, since quartz content and Si/Al ratios are rapidly rising immediate above this interval, which is interpreted as lowstand systems tract (see definitions in the Glossary of Chapter 4Van Wagoner et al., 1990). This interpretation is inline with the positioning of the sequence boundary in the Brazos outcrops by Yancey (1996) within the *P. eugubina* Zone Pα (equivalent to P1a of Keller, 1989), though within the Brazos core 1, no pronounced disconformity exists during this interval. Accordingly, the lowermost 2 m of the Littig Member may be assigned as late, regressive, highstand systems tract (e.g., Van Wagoner et al., 1990).

A closer distance to the shoreline may result from lowered relative sea level, which is in keeping with the increase in benthic macrofauna (mainly shell hash) observed throughout this interval, as reflected

also in the increased phosphorus contents (see also Hansen et al., 1993b). The interval enclosing the proposed sequence boundary (±0.5 m) is also associated with a marked change in the benthic foraminifera fauna (Midway assemblage, see Fig. 3.4A), that may also indicate a changing paleoenvironment, though further detailed studies of this faunal assemblage are required to evaluate possible water depth changes. The sand and glauconite contents (and mica, see Fig. 3.11) increases markedly in the uppermost strongly bioturbated meter of unit I, and quartz reaches peak values (Fig. 3.9), implying a condensed interval (Schutter, 1998).

Pisgah Member (unit J): A pyritized layer overlay by the dark, fissile shales of the Pisgah Member marks the top of the Littig Member. In marked contrast to the underlying unit I, the shales of the Pisgah Member show rare bioturbation. These shales show also a drastic change in their mineralogical and geochemical composition, with decreasing quartz and feldspar contents, increasing smectite, as well as lower Si, Ti, and Mg rations versus Al. In addition, the Zr/Ti ratios have distinctly lower values.

In combination, these geochemical and mineralogical changes suggest a sudden increase in the distance to the shoreline, and hence may imply rising sea level (Van Wagoner et al., 1990; Schutter, 1998), an interpretation which is in line with the elevated smectite contents that are often associated with marine flooding periods (Chamley, 1997; Adatte et al., 2002a). Therefore, the base of the Pisgah Member is interpreted as a flooding surface, overlain by a transgressive systems tract (Van Wagoner et al., 1990; Schutter, 1998). This position is in keeping with the position of the rusty pyrite concretion horizon (RPH) in the Brazos outcrop area by Yancey (1996), who placed this interval also within Biozone P1a (equivalent to P1b of Keller, 1989). However, sections from Alabama, including the Antioch Church core (Chapter 4), reveal no evidence for a pronounced lowstand during Biozone NP1, though several parasequences, each associated with a distinct flooding surface, are present. However, the position of a pronounced (maximum) flooding surface in the upper part of Biozone NP1 is also observed in the Antioch Church core (Chapter 4) and central Alabama (Baum and Vail, 1988; Donovan et al., 1988).

3.5 Conclusions

On the basis of the multidisciplinary evaluation of the K-P transition in the drillcores from Brazos, Texas, conclusions concerning the following issues are presented:

The K-P 'event' deposit and Chicxulub ejecta

(1) The complex, 20 cm-thick graded sedimentary sequence ('K-P event deposit') in the Brazos core 2 is explained by ejecta deposition from debris flows and subsequent turbidite currents, with sudden intermittent provenance changes as indicated by thin intercalated pure quartzose sand-silt layers. This depositional sequence is probably resulting from successive storm or tsunami events. The top of this sequence is bioturbated and overlain by micritic limestone grading into laminated dark shales, suggesting deposition over a longer period.

(2) The basal part of the K-P event deposit contains vesiculated irregular clayey round to more irregular spherules, which are interpreted to derive from a rock melt generated by an impact event. These igneous components are linked by morphological and mineralogical criteria to ejecta deposits from the Chicxulub impact, which in turn are observed at the K-P transition in sections from other areas of the Gulf of Mexico, the Pacific, Northern America (Western Interior), and the western Atlantic.

(3) The ejecta particles are altered to clay minerals and characterized by a distinct compositional variability, including particles of smectite and chlorite composition, even composite particles have been found that show a layered succession of a smectite and chlorite phase. However, smectite spherules are the main altered ejecta phase and their authigenesis presumably led to the high amount of smectite in the basal units of the event deposit (>95 rel%). These smectites are well crystallized, Mg-rich, and compositionally belong to the beidellite-nontronite series. The chlorites in the spherules are Fe-Mg-rich and have a chamosite-like composition, albeit with smectite interlayers.

(4) Tiny accretionary carbonate clasts are ubiquitously present in the basal part of the event deposit, which are interpreted to represent 'lapilli-like' ejecta derived from the accretion of fine carbonaceous dust.

Regional-global correlation of Chicxulub ejecta

(1) The wide compositional range of the altered ejecta spherules is interpreted as an inherited feature and suggests a range of different precursor glass phases of presumably mafic to intermediate character. This compositional spectrum is in keeping with the placement of the Brazos area between northeastern Mexico, which received mainly mafic ejecta phases (altered to chlorite), and between the western Atlantic, which received primary ejecta that derived from rocks of intermediate composition (altered to Ca-Mg-rich smectite). Mg-rich smectite derived from the alteration of microspherules is commonly observed in the basal K-P boundary clay layer in the Tethyan realm as well as in proximal Chicxulub ejecta deposits (Ortega-Huertas et al., 2002).

Sequence stratigraphic setting

(1) No evidence for major proximal-distal facies trends are observed from the lithological, geochemical and mineralogical composition of the uniform and laminated pre- and post-'event deposit' shales.

(2) During the early Danian Biozone P0, multiple criteria (e.g., increased sand content) suggest regressive sea-level behavior and a sequence boundary is tentatively placed within Biozone Pα (P1a of Keller, 1989). The subsequent lowstand systems tract is terminated at a pyritized horizon ("flooding surface") and overlain by the geochemically and mineralogically distinct transgressive systems tract.

(3) The relatively constant clay mineral composition suggests that no major change occurred in the climate conditions at Brazos during the immediate K-P transition. The high smectite contents (>60 rel%) flanked by minor illite, chlorite, and kaolinite points to warm, humid climates with pronounced seasonality, albeit the high diversity of this clay assemblage points to a complex hinterland with different tectonic or morphological compartments.

Position of the K-P boundary

(1) The K-P event deposit is separated from the first occurrence of Paleocene microfossils by an interval of laminated shales (1.6 m) that show a reduced carbonate content, an impoverished planktonic foraminifera and nannofossil fauna, as well as almost no evidence for macrofauna remains, compared to the shales below the event deposit. No evidence for

enhanced dys- or anoxic conditions has been found for this interval by trace-element data. A similar interval is commonly present in the Brazos area, though with about 15 to 25 cm thickness, hence, the origin of this interval and possible reworking processes has to be evaluated within the local context of the Brazos outcrop area.

(2) The absence of a characteristic K-P boundary clay, as revealed by the biostratigraphic, geochemical, and mineralogical data, allows no unequivocal placement for the K-P boundary. Therefore, either the K-P boundary may be placed at the base of the event deposit, concomitant to the first appearance of ejecta spherules in the event deposit, or at the first appearance of Paleocene microfossils, which is about 1.6 m above the event deposit. However, the regional-global correlation of the smectite-rich Chicxulub ejecta in the Brazos cores with the K-P boundary clay elsewhere (e.g., Atlantic, Pacific, Western Interior, Tethys) may argue for a position of the K-P boundary at the base of the spherule-rich event deposit.

(3) During Biozone P0 carbonate values reach and even exceed the carbonate contents of late Maastrichtian shales. This contrasts to other K-P boundary sections, for instance in the Tethyan realm, where the carbonate contents, and hence the productivity usually remains low up to Biozone P1b, though K-P sections in the Atlantic and the Pacific usually show no lowered carbonate contents during these biozones.

K-P faunal turnover

(1) The benthic foraminifera show a stable fauna up to the K-P event deposit, a sudden faunal change in the interval above the event deposit, and a gradual change to a 'Midway' fauna close to the tentatively placed sequence boundary within Biozone Pα (P1a of Keller, 1989).

(2) Calcareous nannofossils show a rich fauna in the latest Maastrichtian shales below the K-P event deposit, an impoverished fauna in the 'carbonate-poor' interval above the event deposit, and an ordered succession of characteristic nannofossil blooms upon entry of the first Paleocene forms. A similar sharp drop in diversity and abundance was observed for the planktic foraminifera in the sediments immediately overlying the event bed, though this faunal group shows no particular blooms of individual species but the successive appearance of newly evolved species during the early Danian.

3.6 References

Adatte T, Keller G, Stinnesbeck W (2002a) Late Cretaceous to early Paleocene climate and sea-level fluctuations: The Tunisian record. *Palaeogeogr Palaeoclimatol Palaeoecol* **178**(3-4): 165-196.

Adatte T, Keller G, Burns S, Stoykova KH, Ivanov MI, Vangelov D, Kramar U, Stüben D (2002b) Paleoenvironment across the Cretaceous-Tertiary transition in eastern Bulgaria. In: Koeberl C, MacLeod KG (eds) Catastrophic events and mass extinctions: Impacts and beyond. *Geol Soc Am Spec Pap* **356**: 231-252.

Aigner T (1985) Storm depositional systems. *Lecture notes in Earth systems* **3**. Springer, Heidelberg: 1-174.

Alegret L, Molina E, Thomas E (2001) Benthic foraminifera at the Cretaceous-Tertiary boundary around the Gulf of Mexico. *Geology* **29**(10): 891-894.

Alegret L, Molina E, Thomas E (2003) Benthic foraminiferal turnover across the Cretaceous/Paleogene boundary at Agost (southeastern Spain): Paleoenvironmental inferences. *Mar Micropaleontol* **48**(3-4): 251-279.

Alegret L, Arenillas I, Arz JA, Molina E (2002a) Environmental changes triggered by the K/T impact event at Coxquihui (Mexico) based on foraminifera. *Neues Jahrb Geol Paläontol Mh* **5**: 295-309.

Alegret L, Arenillas I, Arz JA, Liesa C, Mélendez A, Molina E, Soria AR, Thomas E (2002b) The Cretaceous/Tertiary boundary: Sedimentology and micropaleontology at the El Mulato section, NE Mexico. *Terra Nova* **14**(5): 330-336.

Alfaro P, Delgado J, Estévez A, Molina JM, Moretti M, Soria JM (2002) Liquefaction and fluidization structures in Messinian storm deposits (Bajo Segura Basin, Betic Cordillera, southern Spain). *Int Jour Earth Sci* **91**(3): 505-513.

Alvarez W, Smit J, Lowrie W, Asaro F, Margolis SV, Claeys P, Kastner M, Hildebrand AR (1992) Proximal impact deposits at the Cretaceous-Tertiary boundary in the Gulf of Mexico: A restudy of DSDP Leg 77, Sites 536 and 540. *Geology* **20**(8): 697-700.

Amorosi A (1995) Glaucony and sequence stratigraphy: A conceptual framework of distribution in siliciclastic sequences. *Jour Sediment Res* **B65**(4): 419-425.

Amorosi A (1997) Detecting compositional, spatial, and temporal attributes of glaucony: A tool for provenance research. *Sediment Geol* **109**(1-2): 135-153.

Arz JA, Arenillas I, Soria AR, Alegret L, Grajales-Nishimura JM, Liesa CL, Melendez A, Molina E, Rosales MC (2001) Micropaleontology and sedimentology across the Cretaceous/Tertiary boundary at La Ceiba (Mexico): Impact-generated sediment gravity flows. *Jour South Am Earth Sci* **14**(5): 505-519.

Bailey SW (1988) Chlorites: Structures and crystal chemistry. In: Bailey SW (ed) Hydrous phyllosilicates (exclusive of micas). *Reviews in Mineralogy* **19**. Mineralogical Society of America: 347-403.

Barrera E, Keller G (1990) Stable isotopes evidence for gradual environmental changes and species survivorship across the Cretaceous/Tertiary boundary. *Paleoceanography* **5**(6): 867-890.

Bauluz B, Peacor DR, Elliott WC (2000) Coexisting altered glass and Fe/Ni oxides at the Cretaceous/Tertiary boundary, Stevns Klint (Denmark): Direct evidence of meteorite impact. *Earth Planet Sci Lett* **182**: 127-136.

Baum GR, Vail PR (1988) Sequence stratigraphic concepts applied to Paleogene outcrops, Gulf and Atlantic basins. In: Wilgus CK, Hastings BS, Kendall CG et al. (eds) Sea-level changes: An integrated approach. *Soc Econ Paleont Miner Spec Pub* **42**: 309-327.

Beeson D, Gartner S, Keller G, MacLeod N, Medus J, Rocchia R, Robin E (1994) The KT boundary along the Brazos River, Falls County, Texas: Multidisciplinary stratigraphy and depositional environment. New developments regarding the KT event and other catastrophes in Earth history. *LPI Contribution* **825**. Lunar and Planetary Institute, Houston, Texas: 9-10.

Bengtsson H, Stevens RL (1998) Source and grain-size influences upon the clay mineral distribution in the Skagerrak and northern Kattegat. *Clay Miner* **33**(1): 3-13.

Berggren WA, Kent DV, Swisher CC, Aubry M-P (1995) A revised Cenozoic geochronology and chronostratigraphy. In: Berggren WA, Kent DV, Aubry M-P et al. (eds) Geochronology, time scales, and global stratigraphic correlation. *Soc Econ Paleont Miner Spec Pub* **54**: 129-212.

Biscaye PE (1964) Distinction between kaolinite and chlorite in recent sediments by X-ray diffraction. *Am Mineral* **49**(9-10): 1281-1289.

Biscaye PE (1965) Mineralogy and sedimentation of recent deep-sea clay in the Atlantic Ocean and adjacent seas and oceans. *Geol Soc Am Bull* **76**(7): 803-832.

Bitschene PR, Schmincke H-U (1991) Fallout tephra layers: Composition and significance. In: Heling D, Rothe P, Förstner U et al. (eds) Sediments and environmental geochemistry. Springer, Heidelberg: 48-82.

Bohacs KM (1998) Contrasting expressions of depositional sequences in mudrocks from marine to non marine environments. In: Schieber J, Zimmerle W, Sethi PS (eds) Shales and mudstones: I, Basin studies, sedimentology, and paleontology. Schweizerbart, Stuttgart: 33-78.

Bohor BF (1996) A sediment gravity flow hypothesis for siliciclastic units at the K/T boundary, northeastern Mexico. In: Ryder G, Fastovsky D, Gartner S (eds) The Cretaceous-Tertiary boundary event and other catastrophes in Earth history. *Geol Soc Am Spec Pap* **307**: 183-195.

Bohor BF, Glass BP (1995) Origin and diagenesis of K/T impact spherules – From Haiti to Wyoming and beyond. *Meteoritics* **30**: 182-198.

Bohor BF, Triplehorn DM, Nichols DJ, Millard HTJ (1987) Dinosaurs, spherules, and the "magic" layer: A new K-T boundary clay site in Wyoming. *Geology* **15**(10): 896-899.

Bourgeois J, Hansen TA, Wiberg P, Kauffman EG (1988) A tsunami deposit at the Cretaceous-Tertiary boundary in Texas. *Science* **141**: 567-570.

Brett CE, Allison PA (1998) Paleontological approaches to the environmental interpretation of marine mudrocks. In: Schieber J, Zimmerle W, Sethi PS (eds) Shales and mudstones: I, Basin studies, sedimentology, and paleontology. Schweizerbart, Stuttgart: 301-349.

Burgess PM, Hovius N (1998) Rates of delta progradation during highstands: Consequences for timing of deposition in deep-marine systems. *Jour Geol Soc Lond* **155**(2): 217-222.

Burgess PM, Flint S, Johnson S (2000) Sequence stratigraphic interpretation of turbiditic strata: An example from Jurassic strata of the Neuquen Basin, Argentina. *Geol Soc Am Bull* **112**(11): 1650-1666.

Calvert SE, Pedersen TF (1993) Geochemistry of recent oxic and anoxic marine sediments: Implications for the geological record. *Mar Geol* **113**(1-2): 67-88.

Carey SN, Morelli D, Sigurdsson H, Bronto S (2001) Tsunami deposits from major explosive eruptions: An example from the 1883 eruption of Krakatau. *Geology* **29**(4): 347-350.

Catuneanu O (2002) Sequence stratigraphy of clastic systems: Concepts, merits, and pitfalls. *Jour South Afr Earth Sci* **35**(1): 1-43.

Chamley H (1989) Clay sedimentology. Springer, Heidelberg: 1-623.

Chamley H (1997) Clay mineral sedimentation in the ocean. In: Paquet H, Clauer N (eds) Soils and sediments. Springer, Heidelberg: 269-302.

Cita MB, Aloisi G (2000) Deep-sea tsunami deposits triggered by the explosion of Santorini (3500 y BP), eastern Mediterranean. *Sediment Geol* **135**: 181-203.

Cita MB, Camerlenghi A, Rimoldi B (1996) Deep-sea tsunami deposits in the eastern Mediterranean: New evidence and depositional models. *Sediment Geol* **104**(1-4): 155-173.

Collinson JD (1994) Sedimentary deformation structures. In: Maltman AJ (ed) The geological deformation of sediments. Chapman & Hall, London: 95-125.

Cowie JW, Zieger W, Remane J (1989) Stratigraphic Commission accelerates progress, 1984-1989. *Episodes* **12**(2): 79-83.

Croskell MS, Warner M, Morgan J (2002) Annealing of shocked quartz during atmospheric re-entry. *Geophy Res Lett* **29**(20): 1-4.

Culver SJ (2003) Benthic foraminifera across the Cretaceous-Tertiary (K-T) boundary: A review. *Mar Micropaleontol* **47**(3-4): 177-226.

d'Atri A, Dela Pierre F, Lanza R, Ruffini R (1999) Distinguishing primary and resedimented vitric volcaniclastic layers in the Burdigalian carbonate shelf deposits in Monferrato (NW Italy). *Sediment Geol* **129**(1-2): 143-163.

D'Hondt S, Donaghay P, Luttenberg D, Lindinger M (1998) Organic carbon fluxes and ecological recovery from the Cretaceous-Tertiary mass extinction. *Science* **282**: 276-278.

Dalrymple RW, Boyd R, Zaitlin BA (1994) History of research, valley types and internal organization of incised-valley systems: Introduction to the volume. In: Dalrymple RW, Boyd R, Zaitlin BA (eds) Incised-valley systems: Origin and sedimentary sequences. *Soc Econ Paleont Miner Spec Pub* **51**: 3-10.

Davidoff AJ, Yancey TE (1993) Eustatic cyclicity in the Paleocene and Eocene: Data from the Brazos River valley, Texas. *Tectonophysics* **222**(3-4): 371-395.

Dawson AG, Shi S (2000) Tsunami deposits. *Pure App Geophys* **157**(6-8): 875-897.

Debrabant P, Fourcade E, Chamley H, Rocchia R, Robin E, Bellier J-P, Gardin S, Thiébault F (1999) Les argiles de la transition Crétacé-Tertiaire au Guatemala, témoins d'un impact d'asteroide. *Bull Soc Géol Fr* **170**(5): 643-660.

Decker PL (1990) Style and mechanics of liquefaction-related deformation; lower Absaroka Volcanic Supergroup (Eocene), Wyoming. *Geol Soc Am Spec Pap* **240**: 71.

Donovan AD, Baum GR, Blechschmidt GL, Loutit TS, Pflum CE, Vail PR (1988) Sequence stratigraphic setting of the Cretaceous-Tertiary boundary in central Alabama. In: Wilgus CK, Hastings BS, Kendall CG et al. (eds) Sea-level changes: An integrated approach. *Soc Econ Paleont Miner Spec Pub* **42**: 299-307.

Einsele G (1991) Submarine mass flow deposits and turbidites. In: Einsele G, Ricken W, Seilacher A (eds) Cycles and events in stratigraphy. Springer, Heidelberg: 313-339.

Einsele G (1998) Event stratigraphy: Recognition and interpretation of sedimentary event horizons. In: Doyle P, Bennet M (eds) Unlocking the stratigraphical record: Advances in modern stratigraphy. John Wiley & Sons, New York: 145-194.

Einsele G, Seilacher A (1991) Distribution of tempestites and turbidites. In: Einsele G, Ricken W, Seilacher A (eds) Cycles and events in stratigraphy. Springer, Heidelberg: 377-382.

Elliott WC (1993) Origin of the Mg-smectite at the Cretaceous/Tertiary (K/T) boundary at Stevns Klint, Denmark. *Clays Clay Miner* **41**(4): 442-452.

Elliott WC, Aronson JL, Millard HTJ, Gierlowski-Kordesch E (1989) The origin of the clay minerals at the Cretaceous/Tertiary boundary in Denmark. *Geol Soc Am Bull* **101**(5): 702-710.

Evans NJ, Ahrens TJ, Gregoire DC (1995) Fractionation of ruthenium from iridium at the Cretaceous-Tertiary boundary. *Earth Planet Sci Lett* **134**(1-2): 141-153.

Evans NJ, Gregoire DC, Goodfellow WD, Miles N, Veizer J (1994) The Cretaceous-Tertiary fireball layer, ejecta layer and coal seam: Platinum-group element content and mineralogy of size fractions. *Meteoritics* **29**(2): 223-235.

Fisher RV, Schmincke H-U (1984) Pyroclastic rocks. Springer, Heidelberg: 1-472.

Fourcade E, Alonzo M, Barrillas M, Bellier JP et al. (1997) La limite Crétacé/Tertiaire dans le Sud-Ouest du Petén (Guatemala). *CRAS II* **325**(1): 57-64.

Galloway WE (1989) Genetic stratigraphic sequences in basin analysis II: Application to Northwest Gulf of Mexico Cenozoic basin. *Am Ass Petrol Geol Bull* **73**(2): 143-154.

Galloway WE, Bebout DG, Fisher WL, Dunlap JB, Cabrera-Castro R, Lugo-Rivera JE, Scott TM (1991) Cenozoic. In: Salvador A (ed) The Gulf of Mexico Basin. *The geology of North America* **J**. Geological Society of America, Boulder, Colorado: 245-324.

Gardin S (2002) Late Maastrichtian to early Danian calcareous nannofossils at Elles (Northwest Tunisia): A tale of one million years across the K/T boundary. *Palaeogeogr Palaeoclimatol Palaeoecol* **178**(3-4): 211-231.

Gardin S, Monechi S (1998) Paleoecological change in middle to low latitude calcareous nannoplankton at the Cretaceous/Tertiary boundary. *Bull Soc Géol Fr* **169**(5): 709-723.

Gardner AF, Gilmour I (2002) Organic geochemical investigation of terrestrial Cretaceous-Tertiary boundary successions from Brownie Butte, Montana, and the Raton Basin, New Mexico. In: Koeberl C, MacLeod KG (eds) Catastrophic events and mass extinctions: Impacts and beyond. *Geol Soc Am Spec Pap* **356**: 351-362.

Gartner S (1996) Calcareous nannofossils at the Cretaceous-Tertiary boundary. In: MacLeod N, Keller G (eds) Cretaceous-Tertiary boundary mass extinction: Biotic and environmental changes. Norton Press, New York: 27-48.

Gilbert JS, Lane SJ (1994) The origin of accretionary lapilli. *Bull Volcanol* **56**(5): 398-411.

Goff J, Chagué-Goff C, Nichol S (2001) Palaeotsunami deposits: A New Zealand perspective. *Sediment Geol* **143**(1-2): 1-6.

Goldhammer RK, Johnson CA (2001) Middle Jurassic - Upper Cretaceous paleogeographic evolution and sequence-stratigraphic framework of the northwestern Gulf of Mexico rim. In: Bartolini C, Buffler RT, Cantú-Chapa A (eds) The western Gulf of Mexico basin: Tectonics, sedimentary basins and petroleum systems. *Am Ass Petrol Geolog Spec Mem* **75**: 45-82.

Grauby O, Petit S, Decarreau A, Baronnet A (1993) The beidellite-saponite series: An experimental approach. *Europ Jour Mineral* **5**(4): 623-635.

Grimes ST, Davies KL, Butler IB, Brock F, Edwards D, Rickard D, Briggs DEG, Parkes RJ (2002) Fossil plants from the Eocene London Clay: The use of pyrite textures to determine the mechanism of pyritization. *Jour Geol Soc Lond* **159**(5): 493-501.

Griscom Dl, Beltrán-López V, Pope KO, Ocampo AC (2003) New geochemical insights from electron-spin-resonance studies of Mn^{2+} and SO_3^- in calcites: Quantitative analyses of Chicxulub crater ejecta from Belize and southern Mexico with comparison to limestones from distal Cretaceous-Tertiary boundary sites. In: Koeberl C, Martínez-Ruiz F (eds) Impact markers in the stratigraphic record. *Impact studies.* Springer, Heidelberg: 229-270.

Gromet LP, Dymek RF, Haskin LA, Korotev RL (1984) The "North American shale composite": Its compilation, major and trace element characteristics. *Geochim Cosmochim Acta* **48**(11): 2469-2482.

Guiraud M, Plaziat J-C (1993) Seismites in the fluviatile Bima sandstones: Identification of paleoseisms and discussion of their magnitudes in a Cretaceous synsedimentary strike-slip basin (Upper Benue, Nigeria). *Tectonophysics* **225**: 493-522.

Güven N (1988) Smectites. In: Bailey SW (ed) Hydrous phyllosilicates (exclusive of micas). *Reviews in Mineralogy* **19**. Mineralogical Society of America: 347-403.

Håkansson E, Thomsen E (1999) Benthic extinction and recovery patterns at the K/T boundary in shallow water carbonates, Denmark. *Palaeogeogr Palaeoclimatol Palaeoecol* **154**(1-2): 67-85.

Hansen TA, Farrell BR, Upshaw III B (1993a) The first 2 million years after the Cretaceous-Tertiary boundary in east Texas: Rate and paleoecology of the molluscan recovery. *Paleobiology* **19**(2): 251-265.

Hansen TA, Upshaw III B, Kauffman EG, Gose W (1993b) Patterns of molluscan extinction and recovery across the Cretaceous-Tertiary boundary in east Texas: Report on new outcrops. *Cretaceous Res* **14**(6): 685-706.

Hansen TA, Farrand RB, Montgomery HA, Billman HG, Blechschmidt GL (1987) Sedimentology and extinction patterns across the Cretaceous-Tertiary boundary interval in east Texas. *Cretaceous Res* **8**(3): 229-252.

Hargrove DC, Engelhardt DW (1997) Palynology of the Maastrichtian/Danian boundary at Savannah River Site, South Carolina. *Sediment Geol* **108**(1-4): 121-140.

Harries PJ (1999) Repopulations from Cretaceous mass extinctions: Environmental and/or evolutionary controls? In: Barrera E, Johnson CC (eds) Evolution of the Cretaceous ocean-climate system. *Geol Soc Am Spec Pap* **332**: 345-364.

Henriksson AS (1996) Calcareous nannoplankton productivity and succession across the Cretaceous-Tertiary boundary in the Pacific (DSDP Site 465) and Atlantic (DSDP Site 527) oceans. *Cretaceous Res* **17**(4): 451-477.

Heymann D, Yancey TE, Wolbach WS, Thiemens MH, Johnson EA, Roach D, Moecker S (1998) Geochemical markers of the Cretaceous-Tertiary boundary event at Brazos River, Texas, USA. *Geochim Cosmochim Acta* **62**(1): 173-181.

Hower JC, Eslinger E, Hower ME, Perry EA (1976) Mechanism of burial metamorphism of argillaceous sediment: 1. Mineralogical and chemical evidence. *Geol Soc Am Bull* **87**(5): 725-737.

Hsü KJ, McKenzie JA, He QX (1982) Terminal Cretaceous environmental and evolutionary changes. In: Silver LT, Schultz PH (eds) Geological implications of impacts of large asteroids and comets on the Earth. *Geol Soc Am Spec Pap* **190**: 317-328.

Iverson RH (1997) The physics of debris flows. *Rev Geophys* **35**(3): 245-296.

Izett GA (1990) The Cretaceous/Tertiary boundary interval, Ration basin, Colorado and New Mexico, and its content of shock-metamorphosed minerals: Evidence relevant to the K/T boundary impact-extinction event. *Geol Soc Am Spec Pap* **249**: 1-100.

Izett GA (1991) Tektites in Cretaceous-Tertiary boundary rocks on Haiti and their bearing on the Alvarez impact extinction hypothesis. *Jour Geophys Res* **96**(E4): 20879-20905.

Jarvis I, Murphy AM, Gale AS (2001) Geochemistry of pelagic and hemipelagic carbonates: Criteria for identifying systems tracts and sea-level change. *Jour Geol Soc Lond* **158**(4): 685-696.

Jiang MJ, Gartner S (1986) Calcareous nannofossil succession across the Cretaceous/Tertiary boundary in east-central Texas. *Micropaleontology* **32**(3): 232-255.

Johansson M, Stow DAV (1995) A classification scheme for shale clasts in deep water sandstones. In: Hartley AJ, Prosser DJ (eds) Characterization of deep marine clastic systems. *Geol Soc Lond Spec Pub* **94**: 221-241.

Johnson HD, Baldwin CT (1996) Shallow clastic seas. In: Reading HG (ed) Sedimentary environments: Processes, facies and stratigraphy: 232-280.

Johnson KR (2002) Megaflora of the Hell Creek and lower Fort Union Formations in the western Dakotas: Vegetational response to climate change, the Cretaceous-Tertiary boundary event, and rapid marine transgression. In: Hartman JH, Johnson KR, Nichols DJ (eds) The Hell Creek Formation and the Cretaceous-Tertiary boundary in the northern Great Plains – An integrated continental record of the end of the Cretaceous. *Geol Soc Am Spec Pap* **361**: 329-392.

Kaiho K, Kajiwara Y, Tazaki K, Ueshima M, Takeda N, Kawahata H, Arinobu T, Ishiwatari R, Hirai A, Lamolda MA (1999) Oceanic primary productivity and dissolved oxygen levels at the Cretaceous-Tertiary boundary: Their decrease, subsequent warming, and recovery. *Paleoceanography* **14**(4): 511-524.

Kamo SL, Krogh TE (1995) Chicxulub Crater source for shocked zircon crystals from the Cretaceous-Tertiary boundary layer, Saskatchewan: Evidence from new U-Pb data. *Geology* **23**(3): 281-284.

Kastner M, Asaro F, Michel HV, Alvarez W, Alvarez LW (1984) The precursor of the Cretaceous-Tertiary boundary clays at Stevns Klint, Denmark, and DSDP hole 465A. *Science* **226**: 137-143.

Keller G (1989a) Extended Cretaceous/Tertiary boundary extinctions and delayed population change in planktic foraminifera from Brazos River, Texas. *Paleoceanography* **4**(3): 287-332.

Keller G (1989b) Extended period of extinctions across the Cretaceous/Tertiary boundary in planktonic foraminifera of continental-shelf sections: Implications for impact and volcanism theories. *Geol Soc Am Bull* **101**(11): 1408-1419.

Keller G (1992) Paleoecologic response of Tethyan benthic foraminifera to the Cretaceous-Tertiary boundary transition. In: Takayanagi Y, Saito T (eds) Studies in benthic foraminifera. Tokai University Press, Tokio: 77-91.

Keller G, Lindinger M (1989) Stable isotopes, TOC, and $CaCO_3$ record across the Cretaceous/Tertiary Boundary at El Kef, Tunisia. *Palaeogeogr Palaeoclimatol Palaeoecol* **73**(3-4): 243-265.

Keller G, Stinnesbeck W (1996) Sea-level changes, clastic deposits, and megatsunamis across the Cretaceous-Tertiary boundary. In: MacLeod N, Keller G (eds) Cretaceous-Tertiary boundary mass extinction: Biotic and environmental changes. Norton Press, New York: 415-450.

Keller G, Li L, MacLeod N (1995) The Cretaceous/Tertiary boundary stratotype section at El Kef, Tunisia: How catastrophic was the mass extinction? *Palaeogeogr Palaeoclimatol Palaeoecol* **119**(3-4): 221-254.

Keller G, Barrera E, Schmitz B, Mattson E (1993) Gradual mass extinction, species survivorship, and long-term environmental changes across the Cretaceous-Tertiary boundary in high latitudes. *Geol Soc Am Bull* **105**(8): 979-997.

Keller G, López-Oliva J-G, Stinnesbeck W, Adatte T (1997) Age, stratigraphy and deposition of near-K/T siliciclastic deposits in Mexico: Relation to bolide impact? *Geol Soc Am Bull* **109**(6): 410-428.

Keller G, Adatte T, Stinnesbeck W, Stüben D, Berner Z (2001) Age, chemo- and biostratigraphy of Haiti spherule-rich deposits: A multievent K-T scenario. *Can Jour Earth Sci* **38**(2): 197-227.

Keller G, Adatte T, Stinnesbeck W, Affolter M, Schilli L, López-Oliva J-G (2002) Multiple spherule layers in the late Maastrichtian of northeastern Mexico. In: Koeberl C, MacLeod KG (eds) Catastrophic events and mass extinctions: Impacts and beyond. *Geol Soc Am Spec Pap* **356**: 145-162.

Kennedy WJ, Gale AS, Hansen TA (2001) The last Maastrichtian ammonites from the Brazos River sections in Falls County, Texas. *Cretaceous Res* **22**(2): 163-171.

Kennedy WJ, Landman WJ, Christensen CWA, Hancock JM (1998) Marine connections in North America during the late Maastrichtian: Paleogeographic significance of *Jeletzkytes nebrascensis* Zone cephalopod fauna from the Elk Butte Member of the Pierre Shale, SE Dakota and NE Nebraska. *Cretaceous Res* **19**(6): 745-775.

Kerr M, Eyles N (1991) Storm-deposited sandstones (tempestites) and related ichnofossils of the Late Ordovician Georgian Bay Formation, southern Ontario, Canada. *Can Jour Earth Sci* **28**(2): 266-282.

Kettrup B, Deutsch A (2003) Geochemical variability of the Yucatán basement: Constraints from crystalline clasts in Chicxulub impactites. *Meteor Planet Sci*: (in press).

Kettrup B, Deutsch A, Ostermann M, Agrinier P (2000) Chicxulub impactites: Geochemical clues to the precursor rocks. *Meteor Planet Sci* **35**(6): 1229-1238.

Klaver GT, Van Kempen TMG, Bianchi FR (1987) Green spherules as indicators of the Cretaceous/Tertiary boundary in Deep Sea Drilling Project Hole 603B. Deep Sea Drilling Project. *Initial Reports* **93**: 1039-1047.

Koeberl C, Sigurdsson H (1992) Geochemistry of impact glasses from the K/T boundary in Haiti: Relation to smectites and a new type of glass. *Geochim Cosmochim Acta* **56**: 2113-2129.

Kramar U (1997) Advances in energy-dispersive X-ray fluorescence. *Jour Geochem Exploit* **58**: 73-80.

Kring DA (1995) The dimensions of the Chicxulub impact crater and impact melt sheet. *Jour Geophys Res* **100**(E8): 16,979-16,986.

Kring DA, Boynton WV (1991) Altered spherules of impact melt and associated relic glass from the K/T boundary sediments in Haiti. *Geochim Cosmochim Acta* **55**(6): 1737-1742.

Kring DA, Durda DD (2002) Trajectories and distribution of material ejected from the Chicxulub impact crater: Implications for postimpact wildfires. *Jour Geophys Res* **107**(E8): 1-22.

Krogh TE, Kamo SL, Bohor BF (1993a) Fingerprinting the K/T impact site and determining the time of impact by U-Pb dating of single shocked zircons from distal ejecta. *Earth Planet Sci Lett* **119**(3): 425-429.

Krogh TE, Kamo SL, Sharpton VL, Marin LE, Hildebrand AR (1993b) U-Pb ages of single shocked zircons linking distal K/T ejecta to the Chicxulub crater. *Nature* **366**: 731-734.

Kübler B (1983) Dosage quantitatif des minéraux majeurs des roches sédimentaires par diffraction X. *Cahiers de l'Institute Géologique de Neuchâtel, Suisse* **Série AX, 1.1 & 1.2**

Kübler B (1987) Cristallinité de l'illite, méthodes normalisées de préparations, méthodes normalisées de mesures. **Série ADX**. Cahiers de l'Institute Géologique de Neuchâtel, Suisse: 1-13.

Kyte FT, Bostwick JA, Zhou L (1996) The Cretaceous-Tertiary boundary on the Pacific plate: Composition and distribution of impact debris. In: Ryder G, Fastovsky D, Gartner S (eds) The Cretaceous-Tertiary boundary event and other catastrophes in Earth history. *Geol Soc Am Spec Pap* **307**: 389-401.

Lehmann TM (1990) Paleosols and the Cretaceous/Tertiary transition in the Big Bend region of Texas. *Geology* **18**(4): 362-364.

Lerbekmo JF, Sweet AR, Louis RMS (1987) The relationship between the iridium anomaly and the palnyological floral events at three Cretaceous-Tertiary boundary localities in western Canada. *Geol Soc Am Bull* **99**(9): 325-330.

Lev SM, McLennan SM, Meyers WJ, Hanson GN (1998) A petrographic approach for evaluating trace-element mobility in a black shale. *Jour Sediment Res* **68**(5): 970-980.

Li G, Peacor DR, Essene EJ (1998) The formation of sulfides during alteration of biotite to chlorite-corrensite. *Clays Clay Miner* **46**(6): 649-657.

Lindinger M (1988) The Cretaceous/Tertiary boundaries of El Kef and Caravaca: Sedimentological, geochemical, and clay mineralogical aspects. *PhD Thesis*, ETH Zürich: 1-253.

MacLeod N, Keller G (1991) How complete are Cretaceous/Tertiary boundary sections? A chronostratigraphic estimate based on graphic correlation. *Geol Soc Am Bull* **103**(11): 1439-1457.

Macquaker JHS, Gawthorpe RL, Taylor KG, Oates MJ (1998) Heterogeneity, stacking patterns and sequence stratigraphic interpretation in distal mudstone successions: Examples from the Kimmeridge Clay Formation, UK. In: Schieber J, Zimmerle W, Sethi PS (eds) Shales and mudstones: I, Basin studies, sedimentology, and paleontology. Schweizerbart, Stuttgart: 163-186.

Mai H, Speijer RP, Schulte P (2003) Calcareous index nannofossils (coccoliths) of the earliest Paleocene originated in the late Maastrichtian. *Micropaleontology* **49**(2): 189-195.

Maltman AJ (1994) Deformation structures preserved in rocks. In: Maltman AJ (ed) The geological deformation of sediments. Chapman & Hall, London: 261-303.

Martínez-Ruiz F, Ortega-Huertas M, Palomo-Delgado I (1999) Positive Eu anomaly development during diagenesis of the K/T boundary ejecta layer in the Agost section (SE Spain): Implications for trace-element remobilization. *Terra Nova* **11**(6): 290-296.

Martínez-Ruiz F, Ortega-Huertas M, Palomo-Delgado I (2001a) Climate, tectonics and meteoritic impact expressed by clay mineral sedimentation across the Cretaceous-Tertiary boundary at Blake Nose, Northwestern Atlantic. *Clay Miner* **36**(1): 49-60.

Martínez-Ruiz F, Ortega-Huertas M, Palomo-Delgado I, Barbieri M (1992) The geochemistry and mineralogy of the Cretaceous-Tertiary boundary at Agost (southeast Spain). *Chem Geol* **95**: 265-281.

Martínez-Ruiz F, Ortega-Huertas M, Palomo-Delgado I, Smit J (2001b) K-T boundary spherules from Blake Nose (ODP Leg 171B) as a record of the Chicxulub ejecta deposits. In: Kroon D, Norris RD, Klaus A (eds) Western North Atlantic Paleogene and Cretaceous paleoceanography. *Geol Soc Lond Spec Pub* **183**: 149-161.

Martínez-Ruiz F, Ortega-Huertas M, Palomo-Delgado I, Smit J (2002) Cretaceous-Tertiary boundary at Blake Nose (Ocean drilling Program Leg 171B): A record of the Chicxulub impact ejecta. In: Koeberl C, MacLeod KG (eds) Catastrophic events and mass extinctions: Impacts and beyond. *Geol Soc Am Spec Pap* **356**: 189-200.

Martínez-Ruiz F, Ortega-Huertas M, Kroon D, Smit J, Palomo-Delgado I, Rocchia R (2001c) Geochemistry of the Cretaceous-Tertiary boundary at Blake Nose (ODP Leg 171B). In: Kroon D, Norris RD, Klaus A (eds) Western North Atlantic Paleogene and Cretaceous paleoceanography. *Geol Soc Lond Spec Pub* **183**: 131-148.

Martini E (1971) Standard Tertiary and Quarternary calcareous nannoplankton zonation. In: Farinacci A (ed) Second International Planktonic Conference Proceedings. Technoscienza, Rome: 739-785.

Maruoka T, Koeberl C (2003) Acid-neutralizing scenario after the Cretaceous-Tertiary impact event. *Geology* **31**(6): 489–492.

Maruoka T, Koeberl C, Newton J, Gilmour I, Bohor BR (2002) Sulfur isotopic compositions across terrestrial Cretaceous-Tertiary boundary successions. In: Koeberl C, Ma-

cLeod KG (eds) Catastrophic events and mass extinctions: Impacts and beyond. *Geol Soc Am Spec Pap* **356**: 337-344.

Montanari A (1991) Authigenesis of impact spheroids in the K/T boundary clay from Italy: New constraints for high-resolution stratigraphy of terminal Cretaceous events. *Jour Sediment Petrol* **61**(3): 315-339.

Montgomery HA, Pessagno E, Soegaard K, Smith C, Muñoz I, Pessagno J (1992) Misconceptions concerning the Cretaceous/Tertiary boundary at the Brazos River, Falls County, Texas. *Earth Planet Sci Lett* **109**(3-4): 593-600.

Moore DM, Reynolds RC (1997) X-ray diffraction and the identification and analysis of clay minerals. Oxford University Press, Oxford: 1-378.

Morse JW, Wang Q (1997) Pyrite formation under conditions approximating those in anoxic sediments: II, Influence of precursor iron minerals and organic matter. *Mar Chem* **57**(3-4): 187-193.

Mulder T, Cochonat P (1996) Classification of offshore mass movements. *Jour Sediment Res* **66**(1): 43-57.

Mulder T, Alexander J (2001) The physical character of subaqueous sedimentary density flows and their deposits. *Sedimentology* **48**(2): 269-299.

Murray RW, Leinen M (1993) Chemical transport to the seafloor of the equatorial Pacific Ocean across a latitudinal transect at 135°W: Tracking sedimentary major, trace and rare earth element fluxes at the Equator and the Intertropical Convergence Zone. *Geochim Cosmochim Acta* **57**(21): 4141-4163.

Myrow PM, Southard JB (1996) Tempestite deposition. *Jour Sediment Res* **66**(5): 861-866.

Newman ACD, Brown G (1987) The chemical constitution of clays. In: Newman ACD (ed) Chemistry of clays and cay minerals. *Mineralogical Society Monograph* **6**. Longman Scientific, London: 1-128.

Nijenhuis IA, Bosch HJ, Sinninghe Damsté JS, Brumsack HJ, de Lange GJ (1999) Organic matter and trace element rich sapropels and black shales: A geochemical comparison. *Earth Planet Sci Lett* **169**(3-4): 277-290.

Norris RD, Kroon D, Klaus A (2001) Cretaceous-Paleogene climatic evolution of the western North Atlantic: Results from ODP Leg 171B, Blake Nose. Proceedings of the Ocean Drilling Program. *Scientific Results* **171B**: 1-10.

Oberhänsli H, Keller G, Adatte T, Pardo A (1998) Diagenetically and environmentally controlled changes across the K/T transition at Koshak, Mangyshlak (Kazakstan). *Bull Soc Géol Fr* **169**(4): 493-501.

Odin GS, Fullagar PD (1988) The geologic significance of the glaucony facies. In: Odin GS (ed) Green marine clays. *Developments in sedimentology* **45**. Elsevier, Amsterdam: 295-332.

Olsson RK, Liu G (1993) Controversies on the placement of the Cretaceous-Paleogene boundary and the K/T mass extinction of planktonic foraminifera. *Palaios* **8**: 127-139.

Olsson RK, Miller KG, Browning JV, Habib D, Sugarmann PJ (1997) Ejecta layer at the Cretaceous-Tertiary boundary, Bass River, New Jersey (Ocean Drilling Program Leg 174AX). *Geology* **25**(8): 759-762.

Olsson RK, Miller KG, Browning JV, Wright JD, Cramer BS (2002) Sequence stratigraphy and sea-level changes across the Cretaceous-Tertiary boundary on the New Jersey passive margin. In: Koeberl C, MacLeod KG (eds) Catastrophic events and mass extinctions: Impacts and beyond. *Geol Soc Am Spec Pap* **356**: 97-108.

Ortega-Huertas M, Martínez-Ruiz F, Palomo-Delgado I, Chamley H (1995) Comparative mineralogical and geochemical clay sedimentation in the Betic Cordilleras and Basque-Cantabrian Basin areas at the Cretaceous-Tertiary boundary. *Sediment Geol* **94**(3-4): 209-227.

Ortega-Huertas M, Palomo-Delgado I, Martínez-Ruiz F, Gonzalez I (1998) Geological factors controlling clay mineral patterns across the Cretaceous-Tertiary boundary in Mediterranean and Atlantic sections. *Clay Miner* **33**(3): 483-500.

Ortega-Huertas M, Martínez-Ruiz F, Palomo-Delgado I, Chamley H (2002) Review of the mineralogy of the Cretaceous-Tertiary boundary clay: Evidence supporting a major extraterrestrial catastrophic event. *Clay Miner* **37**(3): 395-411.

Pardo A, Ortiz N, Keller G (1996) Latest Maastrichtian and Cretaceous-Tertiary foraminiferal turnover and environmental changes at Agost, Spain. In: MacLeod N, Keller G (eds) Cretaceous-Tertiary boundary mass extinction: Biotic and environmental changes. Norton Press, New York: 139-171.

Pardo A, Adatte T, Keller G, Oberhänsli H (1999) Palaeoenvironmental changes across the Cretaceous-Tertiary boundary at Koshak, Kazakhstan, based on planktic foraminifera and clay mineralogy. *Palaeogeogr Palaeoclimatol Palaeoecol* **154**(3-4): 247-273.

Perch-Nielsen K (1985) Mesozoic calcareous nannofossils. In: Saunders JB, Bolli HM, Perch-Nielsen K (eds) Plankton stratigraphy. Cambridge University Press, Cambridge: 329-426.

Peryt D, Alegret L, Molina E (2002) The Cretaceous/Paleogene (K/P) boundary at Ain Settara, Tunisia: Restructuring of benthic foraminiferal assemblages. *Terra Nova* **14**(2): 101-107.

Petschick R, Kuhn G, Gingele F (1996) Clay mineral distribution in surface sediments of the South Atlantic: Sources, transport, and relation to oceanography. *Mar Geol* **130**(3): 203-229.

Plink-Björklund P, Steel R (2002) Sea-level fall below the shelf edge, without basin-floor fans. *Geology* **30**(2): 115-118.

Pollastro RM, Pillmore CL (1987) Mineralogy and petrology of the Cretaceous-Tertiary boundary clay bed and adjacent clay-rich rocks, Raton Basin, New Mexico and Colorado. *Jour Sediment Petrol* **57**(3): 456-466.

Pollastro RM, Bohor BF (1993) Origin and clay-mineral genesis of the Cretaceous/Tertiary boundary unit, Western Interior of North America. *Clays Clay Miner* **41**(1): 7-25.

Pope KO, Ocampo AC, Fischer AG, Alvarez W, Fouke BW, Webster CL, Vega FJ, Smit J, Fritsche AE, Claeys P (1999) Chicxulub impact ejecta from Albion Island, Belize. *Earth Planet Sci Lett* **170**(4): 351-364.

Pospichal JJ (1996) Calcareous nannoplankton mass extinction at the Cretaceous/Tertiary boundary: An update. In: Ryder G, Fastovsky D, Gartner S (eds) The Cretaceous-Tertiary boundary event and other catastrophes in Earth history. *Geol Soc Am Spec Pap* **307**: 335-360.

Preisinger A, Aslanian S, Brandstätter F, Grass F, Stradner H, Summesberger H (2002) Cretaceous-Tertiary profile, rhythmic deposition, and geomagnetic polarity reversals of marine sediments near Bjala, Bulgaria. In: Koeberl C, MacLeod KG (eds) Catastrophic events and mass extinctions: Impacts and beyond. *Geol Soc Am Spec Pap* **356**: 213-230.

Rampino MR, Reynolds RC (1983) Clay mineralogy of the Cretaceous-Tertiary boundary clay. *Science* **219**: 495-498.

Reed SJB (1996) Electron microprobe analysis and scanning electron microscopy in geology. Cambridge University Press, Cambridge: 1-199.

Remane J, Keller G, Hardenbol J, Ben Haj Ali M (1999) Report on the international workshop on Cretaceous-Paleogene transitions. *Episodes* **22**(1): 47–48.

Retallack GJ (1996) Acid trauma at the Cretaceous-Tertiary boundary in eastern Montana. *GSA Today* **6**(5): 1-7.

Reynolds RC (1989) Principles and techniques of quantitative analysis of clay minerals by X-ray powder diffraction. In: Pevear DR, Mumpton FA (eds) Quantitative mineral analysis of clays. *CMS Workshop Lectures* **1**. Clay Minerals Society, Boulder, Colorado: 4-36.

Robert C, Chamley H (1990) Palaeoenvironmental significance of clay mineral associations at the Cretaceous-Tertiary passage. *Palaeogeogr Palaeoclimatol Palaeoecol* **79**: 205-219.

Rocchia R, Robin E, Froget L, Gayraud J (1996) Stratigraphic distribution of extraterrestrial markers at the Cretaceous-Tertiary boundary in the Gulf of Mexico area: Implications for the temporal complexity of the event. In: Ryder G, Fastovsky D, Gartner S (eds) The Cretaceous-Tertiary boundary event and other catastrophes in Earth history. *Geol Soc Am Spec Pap* **307**: 279-286.

Ross MI, Scotese CR (1988) A hierarchical tectonic model of the Gulf of Mexico and the Caribbean region. *Tectonophysics* **155**: 139-168.

Salge T, Tagle R, Claeys P (2000) Accretionary lapilli from the K-T boundary site of Guayal, Mexico: Preliminary insights of expansion plume formation (abstract). Meteoritical Society, 63th Annual Meeting: #5124 (CD-ROM).

Scheffers A, Kelletat D (2003) Sedimentologic and geomorphologic tsunami imprints worldwide – A review. *Earth-Sci Rev*: (in press).

Schieber J (1998) Sedimentary features indicating erosion, condensation, and hiatuses in the Chattanooga Shale of central Tennessee: Relevance for sedimentary and stratigraphic evolution. In: Schieber J, Zimmerle W, Sethi PS (eds) Shales and mudstones: I, Basin studies, sedimentology, and paleontology. Schweizerbart, Stuttgart: 187-215.

Schulte P, Stinnesbeck W, Stüben D, Kramar U, Berner Z, Keller G, Adatte T (2003) Fe-rich and K-rich mafic spherules from slumped and channelized Chicxulub ejecta deposits at the northern La Sierrita area, NE Mexico. *Int Jour Earth Sci* **92**(1): 114-142.

Schumacher R, Schmincke H-U (1995) Models for the origin of accretionary lapilli. *Bull Volcanol* **56**(8): 626-639.

Schuraytz BC, Sharpton VL, Marín LE (1994) Petrology of impact-melt rocks at the Chicxulub multiring basin, Yucatán, Mexico. *Geology* **22**(10): 868-872.

Schutter SR (1998) Characteristics of shale deposition in relation to stratigraphic sequence systems tracts. In: Schieber J, Zimmerle W, Sethi PS (eds) Shales and mudstones: I, Basin studies, sedimentology, and paleontology. Schweizerbart, Stuttgart: 79-108.

Self-Trail JM (2001) Biostratigraphic subdivision and correlation of upper Maastrichtian sediments from the Atlantic Coastal Plain and Blake Nose, western Atlantic. In: Kroon D, Norris RD, Klaus A (eds) Western North Atlantic Paleogene and Cretaceous paleoceanography. *Geol Soc Lond Spec Pub* **183**: 93-110.

Shanmugam G (1997) The Bouma sequence and the turbidite mind set. *Earth-Sci Rev* **42**(4): 201-229.

Shau YH, Feather ME, Essene EJ, Peacor DR (1991) Genesis and solvus relations of submicroscopically intergrown paragonite and phengite in a blueschist from Northern California. *Contrib Mineral Petrol* **106**(3): 367-378.

Shiki T, Kumon F, Inouchi Y, Kontani Y, Sakamoto T, Tateishi M, Matsubara H, Fukuyama K (2000) Sedimentary features of the seismo-turbidites, Lake Biwa, Japan. *Sediment Geol* **135**: 37-50.

Shimoyama A, Yabuta H (2002) Mono- and bicyclic alkanes and diamondoid hydrocarbons in the Cretaceous /Tertiary boundary sediments at Kawaruppu, Hokkaido, Japan. *Geochemical Journal* **36**(2): 173-189.

Sigurdsson H, Leckie RM, Acton GD (1997) Shipboard Scientific Party: Caribbean volcanism, Cretaceous/Tertiary impact, and ocean climate history: Synthesis of Leg 165. Proceedings of the Ocean Drilling Program. *Initial Reports*: 377-400.

Smit J, Alvarez W, Montanari A, Claeys P, Grajales-Nishimura JM (1996) Coarse-grained, clastic sandstone complex at the K/T boundary around the Gulf of Mexico: Deposition by tsunami waves induced by the Chicxulub impact? In: Ryder G, Fastovsky D, Gartner S (eds) The Cretaceous-Tertiary boundary event and other catastrophes in Earth history. *Geol Soc Am Spec Pap* **307**: 151-182.

Sohl NF, Martínez ER, Salmerón-Ureña P, Soto-Jaramillo F (1991) Upper Cretaceous. In: Salvador A (ed) The Gulf of Mexico Basin. *The geology of North America* **J**. Geological Society of America, Boulder, Colorado: 205-244.

Soria AR, Liesa CL, Mata MP, Arz JA, Alegret L, Arenillas I, Meléndez A (2001) Slumping and a sandbar deposit at the Cretaceous-Tertiary boundary in the El Tecolote section (northeastern Mexico): An impact-induced sediment gravity flow. *Geology* **29**(3): 231-234.

Speijer RP, Van der Zwaan GJ (1996) Extinction and survivorship of southern Tethyan benthic foraminifera across the Cretaceous/Paleogene boundary. In: Hart MB (ed) Biotic recovery from mass extinction events. *Geol Soc Lond Spec Pub* **102**: 343-371.

Speijer RP, Van der Zwaan GJ, Schmitz B (1996) The impact of Paleocene/Eocene boundary events on middle neritic benthic foraminiferal assemblages from Egypt. *Mar Micropaleontol* **28**(1-2): 99-132.

Stinnesbeck W, Keller G, Adatte T, López-Oliva J-G, MacLeod N (1996) Cretaceous-Tertiary boundary clastic deposits in NE Mexico: Bolide impact or sea-level lowstand? In: MacLeod N, Keller G (eds) The Cretaceous-Tertiary boundary mass extinction: Biotic and environmental events. Norton Press, New York: 471-517.

Stinnesbeck W, Schulte P, Lindenmaier F, Adatte T et al. (2001) Late Maastrichtian age of spherule deposits in northeastern Mexico: Implication for Chicxulub scenario. *Can Jour Earth Sci* **38**(2): 229-238.

Stüben D, Kramar U, Berner Z, Stinnesbeck W, Keller G, Adatte T (2002a) Trace elements, stable isotopes, and clay mineralogy of the Elles II K/T boundary section in Tunisia: Indications for sea level fluctuations and primary productivity. *Palaeogeogr Palaeoclimatol Palaeoecol* **178**(3-4): 321-345.

Stüben D, Kramar U, Berner Z, Eckhardt J-D, Stinnesbeck W, Keller G, Adatte T, Heide K (2002b) Two PGE anomalies above the Cretaceous/Tertiary boundary at Beloc/Haiti: Geochemical context and consequences for the impact scenario. In: Koeberl C, MacLeod KG (eds) Catastrophic events and mass extinctions: Impacts and beyond. *Geol Soc Am Spec Pap* **356**: 163-188.

Sweet AR, Braman DR (2001) Cretaceous-Tertiary palynofloral perturbations and extinctions within the Aquilapollenites Phytogeographic Province. *Can Jour Earth Sci* **38**(2): 249-269.

Talling PJ (1998) How and where do incised valleys form if sea level remains above the shelf edge? *Geology* **26**(1): 87-90.

Tribovillard N, Dupuis C, Robin E (2000) Sedimentological and diagenetical conditions of the impact level of the Cretaceous/Tertiary boundary in Tunisia: No anoxia required. *Bull Soc Géol Fr* **171**(6): 629-636.

Tucker ME, Wright VP (1992) Carbonate sedimentology. Blackwell Science, Oxford: 1-482.

Tyson RV, Pearson TH (1991) Modern and ancient continental shelf anoxia: An overview. In: Tyson RV, Pearson TH (eds) Modern and Ancient Continental Shelf Anoxia. *Geol Soc Lond Spec Pub* **58**: 1-24.

Van Wagoner JC (1995) Overview of sequence stratigraphy of foreland basin deposits: Terminology, summary of papers, and glossary of sequence stratigraphy. In: Van Wagoner JC, Bertram GT (eds) Sequence stratigraphy of foreland basin deposits: Outcrop and subsurface examples from the Cretaceous of North America. *Am Ass Petrol Geol Mem* **64**: 9-21.

Van Wagoner JC, Mitchum RM, Campion KM, Rahmanian VD (1990) Siliciclastic sequence stratigraphy in well logs, cores, and outcrops: Concepts for high-resolution correlation of time and facies. *Methods in Exploration* **7**. Am Ass Petrol Geol, Tulsa, Oklahoma: 1-53.

Van Wagoner JC, Posamentier HW, Mitchum RM, Vail PR, Sarg JF, Loutit TS, Hardenbol J (1988) An overview of the fundamentals of sequence stratigraphy and key definitions. In: Wilgus CK, Hastings BS, Kendall CG et al. (eds) Sea-level changes: An integrated approach. *Soc Econ Paleont Miner Spec Pub* **42**: 39-45.

Warme JE, Morgan M, Kuehner H-C (2002) Impact-generated carbonate accretionary lapilli in the Late Devonian Alamo breccia. In: Koeberl C, MacLeod KG (eds) Catastrophic events and mass extinctions: Impacts and beyond. *Geol Soc Am Spec Pap* **356**: 489-504.

Waythomas CF, Neal CA (1998) Tsunami generation by pyroclastic flow during the 3500-year BP caldera-forming eruption of Aniakchak Volcano, Alaska. *Bull Volcanol* **60**(1): 110-124.

Wilkin RT, Barnes HL (1997) Pyrite formation in an anoxic estuarine basin. *Am Jour Sci* **297**(6): 620-650.

Wilson GS, Roberts AP (1999) Diagenesis of magnetic mineral assemblages in multiply redeposited siliciclastic marine sediments, Wanganui Basin, New Zealand. In: Tarling DH, Turner P (eds) Palaeomagnetism and diagenesis in sediments. *Geol Soc Lond Spec Pub* **151**: 95-108.

Winker CD (1982) Cenozoic shelf margins, northwestern Gulf of Mexico. *Gulf Coast Ass Geol Soc Transact* **32**: 427-448.

Yancey TE (1996) Stratigraphy and depositional environments of the Cretaceous/Tertiary boundary complex and basal section, Brazos River, Texas. *Gulf Coast Ass Geol Soc Transact* **46**: 433-442.

Yancey TE (1997) Tsunamites and bolide impact: Cretaceous-Tertiary boundary deposits, northern shelf of the Gulf of Mexico. Annual Meeting. *Abstracts with Programs* **29**. Geol Soc Am: 142.

Yancey TE (2002) Carbonate ejecta spherules in Cretaceous-Tertiary boundary deposits, Brazos River, Texas (abstract). Geol Soc Am, Annual Meeting: #178-12.

Zachos JC, Arthur MA, Dean WE (1989) Geochemical and paleoenvironmental variations across the Cretaceous/Tertiary boundary at Braggs, Alabama. *Palaeogeogr Palaeoclimatol Palaeoecol* **69**: 245-266.

Zaitlin BA, Dalrymple RW, Boyd R (1994) The stratigraphic organization of incised-valley systems associated with relative sea-level change. In: Dalrymple RW, Boyd R, Zaitlin BA (eds) Incised-valley systems: Origin and sedimentary sequences. *Soc Econ Paleont Miner Spec Pub* **51**: 45-60.

4. Sequence stratigraphy of the Cretaceous to Paleogene transition in Central Alabama: A multidisciplinary evaluation

4.1 Introduction

The Mesozoic to Paleogene sedimentary succession of the Alabama Gulf of Mexico coastal plain comprises a unique geological archive that comprehensively documents the depositional history of a slowly subsiding, passive continental margin. Therefore, and owing to their good preservation, shallow burial depth, and easy accessibility, the sediments of the Alabama coastal plain have been among the 'birthplaces' of the basic concepts of sequence stratigraphy by the Exxon research group and several examples from the Alabama shelf were included in the seminal publications on sequence stratigraphy (e.g., Vail and Mitchum, 1977; Vail et al., 1977; Baum and Vail, 1988; Donovan et al., 1988; Jervey, 1988).

The concept of sequence stratigraphy subdivides sequences into genetically related sedimentary units (systems tracts), including the lowstand, transgressive, and highstand systems tracts, that are interpreted as the sedimentary response to various phases of the sea-level behavior. Hence, the sequence stratigraphic model is a valuable tool for the interpretation of stratigraphic architecture. In addition, related studies showed that unconformity-bound packages of sedimentary strata occur on continental margins worldwide (e.g., Vail et al., 1977; Vail et al., 1991; Haq et al., 1987, 1988; Sarg, 1988; Van Wagoner et al., 1988; Van Wagoner, 1995); it was asserted also

that global sea level, or eustasy, was the dominating factor on the formation of such sequences. Consequently, a global sea-level curve was compiled by Haq et al. (1987; 1988) and many sedimentary successions have been correlated with this 'Haq-curve' (e.g., de Graciansky et al., 1998).

Sections in Alabama have also been incorporated in the eustatic 'Haq-curve' to refine the sea-level history, for instance of the late Maastrichtian and the early Danian (e.g., Baum and Vail, 1988; Donovan et al., 1988). However, forthcoming studies from other areas of the Gulf of Mexico and elsewhere have suggested that the generation of sequences may also be controlled independent of sea level by tectonic processes causing subsidence as well as uplift and erosion (Galloway, 1989a, 1989b; Galloway et al., 2000; Aubry, 1991; Christie-Blick, 1991; Miall, 1997; Dewey and Pitman, 1998; Erikson and Pindell, 1998). In addition, the considerable levels of stratigraphic uncertainty immanent in this sea-level curve, as well as internal inconsistencies, were recognized by Miall (1991; 1992; 1997), Hallam (1992), and Prothero (2001). On the other hand, sequences from the Oligocene along the Western Atlantic shelf correlated well with the Haq et al. record, although they show significantly lower amplitudes, than the values proposed by Haq et al. (Pekar and Miller, 1996; Miller et al., 1997; 1998).
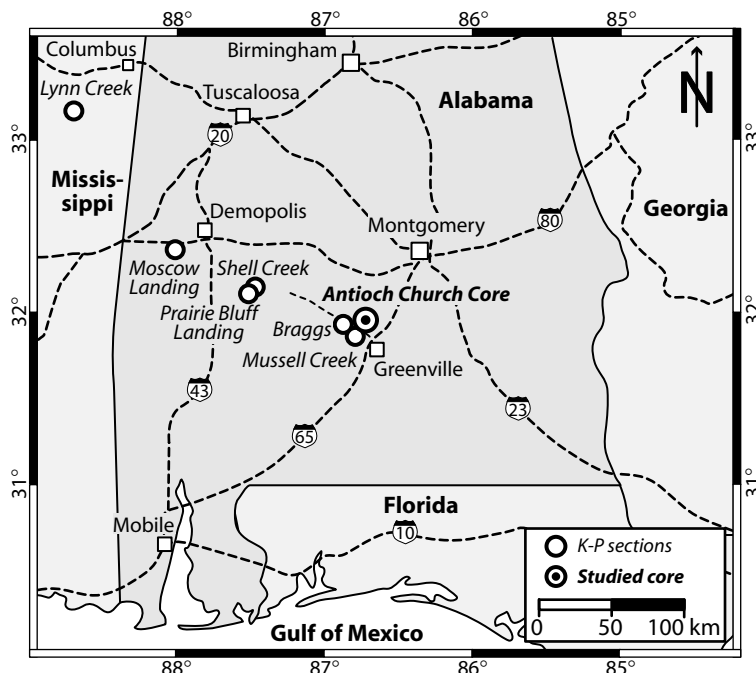
Figure 4.1 Alabama with the location of the Antioch Church core and other K-P sections referred to in this study.

For the late Cretaceous to Danian interval, such inconsistent data becomes evident when comparing various versions of the 'Haq-curve' against sea-level data and sequence stratigraphic analysis from recent papers, particularly for the immediate K-P transition (see Table 4.1 and Keller and Stinnesbeck, 1996; Speijer and Van der Zwaan, 1996; Erikson and Pindell, 1998; Hardenbol and Robaszynski, 1998; Neal and Hardenbol, 1998; Hallam and Wignall, 1999; Miller et al., 2003). However, many of these studies on the Cretaceous-Paleogene transition have aimed at relative sea level ("water depth") at a specific location, rather than conducting a sequence stratigraphic analysis with evaluation of eustatic sea-level behavior through time.

A second prominent aspect of the geology of the Alabama Gulf coast plain has been the K-P boundary, which has been of paramount interest ever since the discovery of a major faunal turnover that characterizes this era boundary in many places worldwide (see Sharpton and Ward, 1990; Ryder et al., 1996; MacLeod et al., 1997; Kiessling and Claeys, 2001). According to Hallam (1999) and Olsson et al. (2002), extensive sea-level changes are often invoked to be among the primary causes for mass extinctions, establishing a direct link between the extinctions at the K-P boundary and the need for detailed sequence stratigraphic studies across the K-P boundary. Particularly, timing, pace, and magnitude of sea-level changes could give information on adverse or stimulating environmental stress during the K-P transition, but must be compared with the characteristics of sea-level fluctuations during other time slices. Therefore, a sequence stratigraphic framework is needed to base any constrains on the environmental impact of sea-level changes on solid ground.

Notably, sea-level fluctuation are certainly not in itself responsible for extinctions events, but extinctions may be related to their negative effects on marine fauna and flora, including the spreading of anoxic bottom waters across the shelf during transgression and habitat loss during regression (e.g., Hallam and Wignall, 1999). Otherwise, the species richness-curve of marine strata would mirror the eustatic curves that have been established for the Cenozoic and Mesozoic, which is obviously not the case (see also sea-level biased biodiversity, Smith et al., 2001).

Additional interest in the K-P boundary deposits of Alabama was attracted by the paper from Alvarez et al. (1980), which proposed a large impact as a major cause of these mass-extinctions. The sedimentary record from Alabama was of primary interest to study the relationships of this impact to the pattern of faunal change, particularly, since it is one of a few globally known shallow to neritic settings that provides an expanded record of the K-P transition (Jones et al., 1987; Zachos et al., 1989; Habib et al., 1992; 1996; Olsson and Liu, 1993; Moshkovitz and Habib, 1993). Consequently, and even before the 180 km in-diameter Chicxulub impact structure on the Yucatán peninsula in southern Mexico has been detected actually around 1990 (e.g., Hildebrand et al., 1991), some authors have re-interpreted siliciclastic K-P deposits along the Gulf of Mexico margin, which were formerly considered as 'incised valley fill' deposits, as impact-generated tsunami/turbidite deposits (e.g., Hansen et al., 1987; Bourgeois et al., 1988; Maurrasse and Sen, 1991; Bohor, 1996; Olsson et al., 1996; Smit et al., 1996). However, this view is not universally accepted and the differentiation of clastic deposition during sea-level lowstand from deposition by tsunamis is still controversially discussed, specifically for the Alabama K-P sections (e.g., Olsson and Liu, 1993; Olsson et al., 1996; Savrda, 1993; Habib et al., 1996; Smit et al., 1996).

The sedimentary succession provided by the Antioch Church core that was drilled close to the famous K-P boundary locations in Braggs and Mussel Creek in central Alabama is an ideal study object: it allows not only to investigate the depositional nature of the K-P transition and to test critically the inferred sea-level variations in magnitude and relative timing, but also, its expanded record encompassing about 4 Ma from the late Maastrichtian calcareous nannoplankton Biozone CC25 to the late Danian Biozone NP4, allows to include the long-term climate record obtained from mineralogical and isotope proxies.

In this study, the results of a multidisciplinary investigation of the Antioch Church core are reported that (i) documents the lithology, microfacies, and biostratigraphy of the core and examine its sedimentological and petrological characteristics in order to establish a sequence stratigraphic framework, (ii) investigates the mineralogical and geochemical record in terms of provenance and variations related to climate, supply, productivity, and/or sea-level changes, and finally, (iii) distinguishes between the sedimentary processes that originated the 'event bed' at the K-P boundary and examine possible links to either the Chicxulub impact, or sea-level fluctuations, or both.

Table 4.1 Compilation of qualitative trends in water depth and sea-level behavior (systems tracts) during the latest Maastrichtian, across the K-P boundary, and during the early Danian.

Location	Late Maastrichtian	Across K-P boundary	Early Danian	References
Gulf of Mexico				
Brazos; Texas	shallowing from outer to middle neritic	shallowing (lowstand)	deepening from middle to outer neritic	Keller (1992)
Brazos; Texas	highstand	highstand-regressive	regressive-transgressive	See Chapter 3
Braggs; Alabama	highstand	lowstand	transgressive	Baum and Vail (1988); Donovan et al. (1988); Mancini and Tew (1993)
Millers Ferry; Alabama	highstand	lowstand	transgressive	Olsson and Liu (1993); Olsson et al. (1996)
NE Mexico	shallowing (200-100 ka pre-K-P)	deepening	no data	Keller et al. (1996)
Western Interior				
Montana, Dakota, Carolina	constant	transgressive	no data	Hargrove et al. (1997); Johnson (2002)
NW Atlantic				
Bass River, New Jersey shelf	highstand (~80 m)	late highstand (~60 m)	lowstand (~60 m)	Sugarman et al. (1995); Olsson et al. (2002)
Tethyan realm				
Stevns Klint; Denmark	shallowing (300 ka pre-K-P)	shallowing	deepening	Schmitz et al. (1992); Surlyk (1997)
Basque Basin; Spain	lowstand fan	lowstand	lowstand	Pujalte et al. (1995)
Agost; Spain	lowstand (400-300 ka pre-K-P)	deepening	deepening, two minor lowstands (P0, P1a)	Pardo et al. (1996)
Agost; Spain	deepening 200 ka pre-K-P	constant	constant	Alegret et al. (2003)
Caravaca; Spain	shallowing from upper bathyal to outer neritic	lowstand	deepening from outer neritic to upper bathyal	Keller (1992)
Negev-Sinai; Israel	upper bathyal to outer neritic depth	shallowing to outer neritic	deepening from outer neritic to upper bathyal	Keller (1992)
El Kef; Tunisia	shallowing from upper bathyal to outer neritic	lowstand	deepening to outer neritic	Keller (1992)
El Kef; Tunisia	shallowing 5-10 ka pre-K-P and shallowing 300 ka pre-K-P	K-P = 'maximum flooding surface'	shallowing - deepening	Li et al. (2000); Adatte et al. (2002a)
El Kef; Tunisia	constant	possible slight shallowing	constant	Speijer and van der Zwaan (1996)
Seldja; Tunisia	shallowing	deepening	shallowing	Keller et al. (1998)
Elles; Tunisia	shallowing at 300-400 ka and 50 ka pre-K-P	K-P = 'maximum flooding surface'	deepening, two minor lowstands (P0, P1a)	Adatte et al. (2002a)
Koshak; Kazakhstan	constant	deepening	shallowing 250 ka post K-P	Pardo et al. (1999)
Bjala; Bulgaria	shallowing	K-P = 'maximum flooding surface'	shallowing -deepening	Adatte et al. (2002b)

4.1.1 Sequence stratigraphy – Definition of key terminology

The purpose of using sequence stratigraphy in this study is to delineate genetically related stratal packages that can be subsequently related to causal events, for instance movement of the shoreline relative to the depositional setting. In addition, it should ease correlation with the extensive literature on Cretaceous-Paleogene depositional systems in Alabama and elsewhere (e.g., Baum and Vail, 1988; Donovan et al., 1988; Davidoff and Yancey, 1993; Miller et al., 1998; Olsson et al., 2002; Soegaard et al., 2002). The

fact, however, that several different sequence stratigraphic models are currently in use, as well as the complex and still non-standardized jargon of this subject, makes it necessary to define the key terms used in this study as shown in the Glossary of this chapter (see also Catuneanu, 2002). In this study, the terminology provided by Posamentier et al. (1988) and Van Wagoner (1995) is employed, because these sequence stratigraphic models were introduced for similar settings on a passive margin. However, it is emphasized that the use of the terms 'lowstand' or 'highstand' systems tract characterizes distinct intervals of relative sea-level behavior through time, but they are not mentioned to indicate 'low' or 'high' (eustatic) sea level, since within a given systems tract relative sea level may vary considerably, not necessarily related to eustatic changes.

Initially, sequence stratigraphic surfaces have been identified by the interpretation of seismic lines aided by calibrations to various physical corehole logs. Thus, a lot of information could be used to infer the regional setting and the spatial 3D geometry of the sediment packages that is important to delineate the history of subsidence and coastal on- or offlap of strata. For a single outcrop or core section, as used in this study, the situation is more complicated since the 'field' or 'core' identification of sequence boundaries and within-trend surfaces has been problematic; they are not simple observations but instead are interpretations of strata. Several of the criteria used are ambiguous with respect to a clear sequence stratigraphic interpretation (e.g., a glauconite-rich layer may be a transgressive surface, a condensed section, or a lag deposit), and, individually, these criteria may not be diagnostic. However, in absence of sustaining seismic data, the pinpointing criteria for the lithological identification of sequence stratigraphic surfaces in shelf sections has been included and summarized in the Glossary.

4.1.2 Locality and geological setting

The Antioch Church Core was cored about 140 m west of Alabama Route 263 and 5 km west of Greenville in Lowndes County, Alabama (Fig. 4.1). The core site is located in a downdip setting about 7.4 km southeast and 3.6 km south of the well known Braggs and Mussel Creek K-P localities, respectively, and was drilled in front of the abandoned building of the Baptist "Antioch Church."

The late Cretaceous to early Paleocene strata of southern and central Alabama constitute a seaward-dipping wedge of sedimentary rocks that reflects the infilling of a slowly, but differentially subsiding depositional basin on the passive southern margin of the North American continent (e.g., Sohl et al., 1991; Mancini and Tew, 1993). Lateral lithofacies changes from west to east indicate that depositional conditions in southwest Alabama during this period were associated with deltaic and marginal marine sediment accumulation, whereas sedimentation in southeast and south-central Alabama was controlled by the presence of a persistent Paleocene carbonate platform that formed over Paleozoic basement rocks and was little affected by salt tectonics. During the early Paleocene, a delta developed in Mississippi and in western Alabama, resulting in increased siliciclastic sedimentation in the western Alabama area (Mancini and Tew, 1993).

For the interval from the latest Maastrichtian to the late Danian, which is 'recorded' in the sediments of the Antioch Church core, Baum and Vail (1988), Mancini and Tew (1993), and Mancini et al. (1996), delineated a distinct succession of three to four unconformities that divide the lower and upper part of the Midway Group into distinct depositional sequences. These unconformity-bound sedimentary sequences are now exposed along the SSE-NWW-trending outcrop belt of Cretaceous and Paleocene units in the Gulf of Mexico coastal plain of Alabama, though local derivations exist in thickness and extent of individual units (see Mancini and Tew, 1993 for details on regional paleogeographic aspects). These depositional sequences are outlined in the following and exemplarily depicted in Fig. 4.3 based on the lithological units of the Antioch Church core; this figure also includes the numerical ages of the unconformities.

Sequence 1: The late Maastrichtian UZGC-5.0 (Upper Zuni A, Gulf Coast) cycle is composed of the Prairie Bluff Formation and represents late highstand or regressive deposits.

Sequence 2: The early Danian TAGC-1.1 (Tejas A, Gulf Coast) cycle, which comprises the basal Clayton Sandstone and limestone as well as the Pine Barren Member of the Clayton Formation: The lower boundary of this sequence in the Gulf Coast Plain area is a type-1 unconformity, with the basal Clayton Sands considered as incised valley fill deposits that developed when sea-level fell below the shelf break. The overlying glaucony-rich Clayton marls or limestones are regarded as transgressive deposits. Their upper termination is marked by a prominent glauconitic 'maximum flooding surface' that separates the retrograding strata below from the

prograding highstand marls and shales of the Pine Barren Member above.

Sequence 3: The early Danian TAGC-1.2 cycle, which includes the 'Turritella Rock', the McBryde Limestone Member of the Clayton Formation, and the basal part of the Porters Creek Formation. In south-central Alabama, the lower boundary of this type-2 sequence is marked by the prominent 'Turritella Rock', which are interpreted as shelf-margin deposits.

Sequence 4: The middle Danian TAGC-1.3 cycle that comprises the upper part (Matthews Landing Marl) of the Porters Creek Formation. In south-central Alabama, however, this formation is only represented by its highstand deposits.

Sequence 5: The late Danian TAGC-1.4 cycle, which is made of the Porters Creek sandstone and basal Oak Hill Member of the Naheola Formation. These sediments are interpreted as shelf-margin and transgressive deposits, respectively.

4.2 Analytical techniques

The following analytical techniques were used to characterize the sediments of the K-P transition in the Antioch Church core, Alabama; for the geochemical and mineralogical analyses, samples were dried, crushed, and finely ground in an agate mill.

Biostratigraphy: For nannofossil biostratigraphy, sample material was ultrasonically cleaned in a weak ammonium solution for 3 minutes. The resulting suspension was allowed to settle for 3 minutes and the water decanted. The deposit was then again brought into suspension and a few drops spread over a graphitic scanning electron microscope (SEM) stub. After drying and coating with gold, the stub was observed in a SEM at 2.5 K magnification. The calcareous nannofossils were analyzed by Hartmut Mai, University of Bremen.

Nonclay and clay mineralogy was analyzed by X-ray diffractometry (XRD) at the Geological Institute of the University of Neuchâtel, Switzerland, with a SCINTAG XRD 2000 diffractometer and Cu-kα-radiation. Diffractograms were evaluated with the MacDIFF software (freeware by R. Petschick, University of Frankfurt, for details see Petschick et al., 1996) and methods outlined in the Appendix 3.1. The semiquantitative estimation of the relative abundance of the clay minerals was conducted by using the ratios of the weighted peak areas of smectite (weighting factor '1'), chlorite ('2'), illite ('4'), and kaolinite ('2') from glycolated specimen. In order to ease comparison with non-weighted datasets, the raw-data, including peak position, height, and area, is given in the Appendix 4.1.

Major elements were determined by wavelength-dispersive X-ray fluorescence spectrometry (WDS) at the Institute for Mineralogy and Geochemistry, University of Karlsruhe, with a SRS 303 AS XRF. For these analyses, fused glass discs were prepared from a mixture of 1 g ignited powder of each sample and 4 g of SPECTROMELT. Major elements were evaluated by a fundamental parameter calibration procedure.

Trace elements (Cr, Ni, Cu, Zn, As, Rb, Sr, Y, Zr, Ba, La, Ce, and Pb) were analyzed from bulk powder samples (5 g) by energy-dispersive X-ray fluorescence spectrometry (EDS) with a SPECTRACE 5000 X-ray analyzer at the Institute for Mineralogy and Geochemistry, University of Karlsruhe. Trace elements were determined using a Compton and intensity matrix correction procedure. Detailed analytical procedures, detection limits, and standards used were compiled by Kramar (1997).

Isotopic ratios of C and O in bulk rock sediment (fine fraction <38 μm) were determined using a fully automated preparation system (MULTIPREP) connected on-line to an Optima isotope ratio mass spectrometer (MICROMASS Limited, UK). The preparation line is based on the standard method by measuring the isotope ratios in CO_2 released by reaction with 100 % phosphoric acid. The samples are dissolved in individual vials, eliminating the risk of cross-contamination from one sample to the next. Certified and calibrated CO_2 gas from a pressure bottle was used as reference gas. Instrumental precision was better than 0.008 for $\delta^{13}C$ and <0.015 for $\delta^{18}O$; accuracy was tested in each analytical batch by running the carbonate standard NBS19. All carbon and oxygen isotope data are reported as δ values relative to the Vienna Pedee belemnite (VPDB) standard.

Rock Eval analysis was performed with a ROCK EVAL 6 pyrolizer at the Geological Institute of Houston, Texas, and at the University of Neuchâtel, Switzerland, following the analytical methods of Langford and Blanc-Valleron (1990). This technique allows for the determination of the total organic carbon (TOC) content. The obtained values were compared with a standard reference sample. Analytical precision for a standard is 0.003 % and reproducibility is 0.02 % for the insoluble residue.
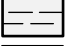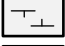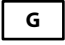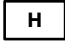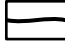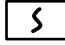
Lithology

Shale		Marl		Sandstone		Limestone		Shells	
Spherules	**G** Glauconite		**H** Hardground		Pyritized layer		Bioturbation		

Systems tracts

LST = Lowstand systems tract   **SMST** = Shelf margin systems tract   **TST** = Transgressive systems tract
HST = Highstand systems tract   **ivf** = Incised valley fill

Sequence stratigraphic surfaces

Sequence boundary: **SB 1** = Sequence boundary type 1 and **SB 2** = Sequence boundary type 2

Flooding ('transgressive') surface (**fs**)   **mfs** = Maximum flooding surface   **cs** = Condensed section

Figure 4.2 Legend to the lithologic columns of the Antioch Church core depicted in this study.

4.3 Results

4.3.1 Lithology and sedimentology

The Antioch Church corehole penetrated 83.7 m of Cretaceous and Cenozoic sediments (Fig. 4.3) and shows of a typical, mixed siliciclastic-carbonate succession. The Cretaceous section is assigned to the late Maastrichtian Prairie Bluff Formation of the lower part of the Midway Group. The Cenozoic section is assigned to the basal Paleocene Clayton Formation, the early Paleocene Porters Creek Formation, and the middle Paleocene Naheola Formation, that all belong to the upper part of the Midway Group. A comprehensive description of lithological, sedimentological, and petrographical characteristics of the Antioch Church core is outlined below; the lithological column, including the gamma-ray log is given in Fig. 4.3. Core depths are given beginning with zero from the top downwards. The Antioch Church core contains a K-P boundary section that is very similar to that at the nearby Braggs outcrop (e.g., Donovan et al., 1988), but provides an expanded succession of the 'incised valley-fill' or 'event bed' at, or close to, the K-P boundary. The detailed lithology of the immediate K-P boundary interval is provided in Fig. 4.4.

Prairie Bluff Formation

The Prairie Bluff Formation in the lowermost part of the Antioch Church core (85.3-80 m) consists of silty-sandy micaceous marls with high micrite

content (50-70 %). Silt-sand grains are subangular quartz, rare feldspar (mostly microcline, rare albite), and shell debris; micas are biotite and muscovite. Grain-sizes of the coarse fraction do not exceed fine sand size. In addition, rounded phosphate and glauconite grains are present, though generally below 5 %. The marl is burrowed and the diffusive, burrow-mottled background fabrics are overprinted by discrete traces including *Planolites*, *Thalassinoides*, and *Chondrites*. Fossils include mollusks and mollusk fragments, for instance, nuculanids (e.g., *Nuculana corbicula*) and oysters. Gastropod shells, including *Acmaea* and the high-spired *Haustator bilira*, as well as scaphopods (e.g., *Dentalium*), fish vertebrae, ostracods, and benthic foraminifera are also present.

In the interval from 80 to 67 m, the Prairie Bluff Formation furnishes dark grey to brown, siltier and sandier parts (up to sandstone layers) interlayered with marl. Towards the top of this interval, marls are increasingly siltier, and contain less carbonate (micrite only 20-25 %), whereas maximum grain-sizes are higher (up to coarse sand), though the petrographic composition of the sand-silt sized grains remains the same. The quantity and kind of glauconite, phosphate, and bioturbation, as well as the fossil content are similar to the interval below.

The topmost 2.45 meters of the Prairie Bluff Formation (67-64.55 m) are in marked contrast with the underlying part as they consist of grey fossiliferous silty-sandy micaceous marls, though these

Figure 4.3 (page 141) Lithology and biostratigraphy of the Antioch Church Core including the sequence stratigraphic interpretation of the units according to previous studies (Baum and Vail, 1988; Donovan et al., 1988; Mancini and Tew, 1993), and the assigned estimations of absolute ages for the individual units and stratigraphic surfaces by calibration of the biostratigraphic data to the geomagnetic time scale by Berggren et al. (1995). In addition, the downhole gamma-ray log along with the interpretation of sequence stratigraphic surfaces according to criteria by Hesselbo (1996) and Catuneanu (2002) is shown. Note that each sequence boundary (and probably also flooding surface) may correspond to a distinct erosional surface, and hence may comprise a hiatus of unknown duration. An explanation to the lithologic symbols is provided in Fig. 4.2 and the detailed lithology of the immediate K-P transition is given in Fig. 4.5.
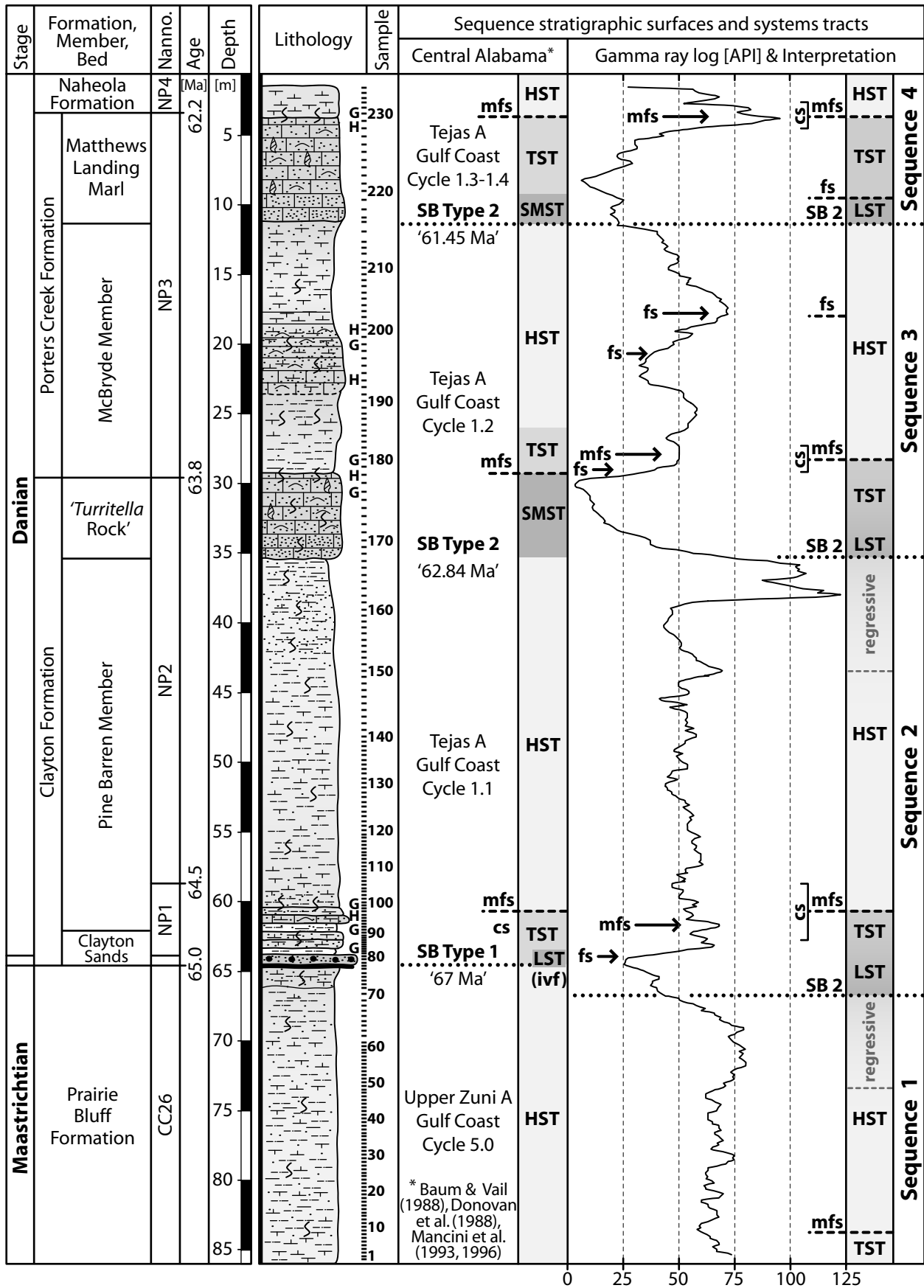
Figure 4.3 (caption on page 140).

1: Prairie Bluff marly shales	3: Pyritized base of Clayton Sands	5: Clayton sandy marls	7: Pine Barren marls
2: Prairie Bluff sandy marls	4: Basal Clayton Sands with spherules	6: Pine Barren marl-limestones	8: Pine Barren shale

K-T 1 and K-T 2 denotes the two possible positions of the K-T boundary (see text for details)
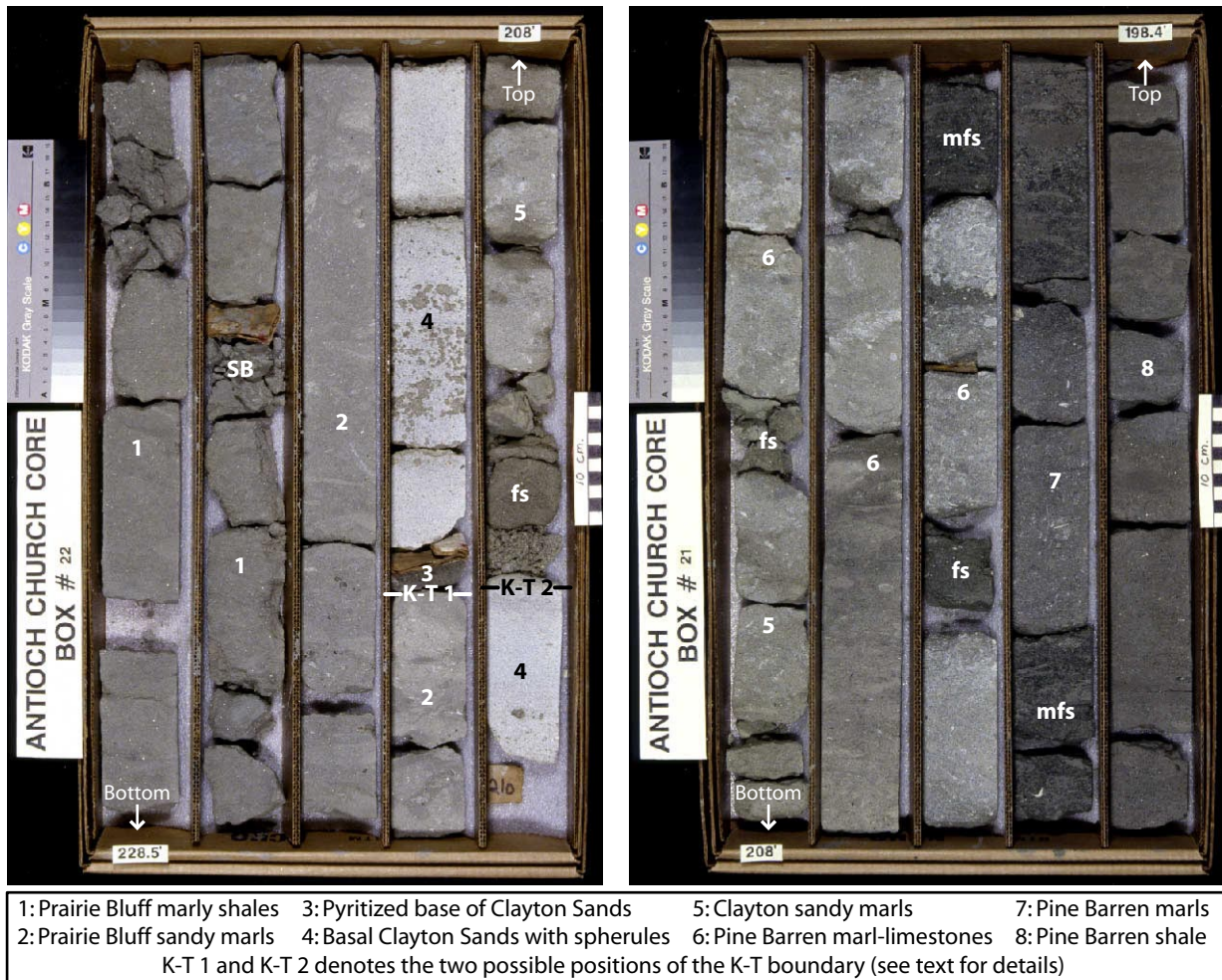
Figure 4.4 Core photos of the K-P transition in the Antioch Church Core (box 22 and box 21) illustrating relevant sedimentary depositional units and sequence stratigraphic surfaces.

marls show a considerable increase in the amount of micrite (50-70 %); the topmost 0.5 m become light-grey, more indurated, and sandier. The marls contain medium to very coarse sand in the topmost layer, immediately below the 'event bed'. Silt and sand grains are made of subangular quartz, rare feldspar (microcline), and shell debris; micas consist of biotite and muscovite flakes. In this interval, the amount of rounded phosphate and glauconite increases significantly up to 10 %. Characteristic fossils include mollusks (with similar faunal elements as mentioned above and as shell fragments), shark teeth, benthic foraminifera, ostracods, echinoderm spines, and bryozoan fragments. The kind and quantity of bioturbation is similar to the intervals below.

Basal Clayton Sands of the Clayton Formation

The marls and shales of the Prairie Bluff Formation are disconformably overlain by the basal Clayton Sands of the Clayton Formation. The lowermost 5 cm of the basal Clayton Sands (at about 64.5 m) are coarse quartz-rich black sandstone with an en-

tirely pyritized matrix (Fig. 4.6A). This pyritized sand layer is almost devoid of carbonate (<2 wt%; Fig. 4.10A) and contains in an entirely pyritized matrix (30-40 %), very coarse angular quartz grains (>50 %), and large grains of feldspar (~5 %), including microcline, orthoclase with tourmaline inclusions, and myrmekite (quartz-feldspar intergrowths that are commonly found in plutonic rocks, e.g., Garcia et al., 1996). In addition, large mica-flakes (~2-4 %: biotite, muscovite), illmenite crystals, spherules (see below), and glauconite grains, as well as rare glauconized and pyritized benthic foraminifera (<2 %) are present.

Above the pyritized sandstone, the interval from 64.5 to 63.8 m furnishes calcitic-cemented, coarse-grained white sandstone. Sedimentary structures observed in the basal Clayton Sands include normal grading with very coarse sand at the base to mean sand-sized grains at the top. The topmost part also shows faint lamination. Bioturbation was not observed throughout this interval. The middle part of this sand bed shows high porosity. The petrographic

Stratigra.	Lithology	Calcareous nannofossils	Sequence stratigraphy and lithologic units

Stratigraphy column (left): Danian; UZ; Maastrichtian. Depth scale [m]: 59, 60, 61, 62, 63, 64, 65, 66, 67, 68.

Lithology depth scale: 110, 105, 100, 95, 90, 85, 80, 77, 75, 70. Markers: H (~95), G-G-G (~95), G (~92), G (~82).

Calcareous nannofossils zones: NP2, NP1, CC26

- FAD *Cruciplacolithos tenuis*
- *Futuyania petalosa* acme
- *Cruciplacolithus primus* acme
- *Neobiscutum parvulum* acme
- *Neobiscutum romeinii* acme
- FAD *Markalius inversus*
- Almost barren (unzoned)
- LAD of *Micula* spp.
- *Micula murus* zone, with rare *Nephrolithus frequens* and *Lithraphridites quadratus*, as well as rare *Neobiscutum romeinii*, *Neobiscutum parvulum*, and *Cruciplacolithus primus*

Sequence stratigraphy and lithologic units:

HST
- **61.5-58 m:** alternating grey calcareous-micaceous silty shales, fossiliferous, phosphatic/glauconitic
- **61.5 m:** green-grey micaceous fossiliferous glauconitic/phosphatic sandstone, bioturbated, FAD *Venericardia* in sample AC97
- **62-61.5 m:** light grey sandy micaceous fossiliferous glauconitic-phosphatic marl, bioturbated, with indurated base

mfs
fs
- **62 m:** 5 cm green glauconitic-phosphatic shale
- **64.25-62.1 m:** green-grey micaceous fossiliferous glauconitic-phosphatic marl, bioturbated

fs
- **64.2 m:** 5 cm green clayey silt, slight glauconitic-phosphatic

fs
LST/TST
- **65.5-64.2 m:** white-grey, normal graded, calcareous, coarse sandstone, indurated, rare fossils, no bioturbation, slight lamination in upper part, rare glauconite-phosphate, rare spherules and calcitic globules. At the base, 3 cm pyrite-rich red coarse sandstone, indurated, no fossils

SB 2
- **66-65.5 m:** grey calcareous silty marl, sandy, glauconitic, fossiliferous, bioturbated

HST
- **69-66 m:** grey silty shale, micaceous, bioturbated

Figure 4.5 Detailed lithology of the immediate K-P transition in the Antioch Church core including the basal Clayton Sands ('event bed'), the detailed nannofossil biostratigraphy, and the lithological description. Abbreviations: UZ, unzoned, LAD, last occurrence data, FAD, first occurrence date. For a legend to the lithologic symbols see Fig. 4.2.

composition of the basal Clayton Sandstone reveals about 50 % quartz, 3-6 % feldspar, 1-3 % muscovite, 35-45 % spar cement, 2-3 % glauconite, and <1 % phosphate grains (Fig. 4.6B-D). Occasionally, plant fragments (charcoal, leaf tissue) are present. The quartz is angular and commonly displays undulatory extinction, subgrains, and edges that look 'embayed' rather than shard-like (Fig. 4.6B). Feldspar compositions range from microcline to albite. These characteristics suggest an igneous source for the minerals, as well as a short transport. Accessory detrital minerals include myrmekite, epidote, and possibly some relict pyroxene, also supporting an igneous and/or metamorphic protolith for the 'sandy' component of this interval.

In the basal Clayton Sands, bioclastic detritus is almost absent; rarely, mollusk fragments, and tiny pyritized planktic foraminifera are present. Occasionally, irregular to rounded marl intraclasts are present; some include tiny planktic foraminifera. A prominent, though rare component of the basal Clayton Sands are 'spherules' that are either mm sized, vesicular brown-green globules (or droplets), or shard-like fragments (Fig. 4.6C, D). Some spher-

ules and fragments are composed entirely of calcite with a thin opaque coating and remains of bubbly inclusions lined by opaque minerals. Another salient constituent of the Clayton Sands are carbonate clasts (up to 2 mm in size) with irregular outlines (Fig. 4.6C). Some of these carbonates show circular opaque inclusions, suggesting a genetic link to the spherules and fragments.

Spherules and carbonate clasts are morphologically similar (size, shape, internal textures etc.) to Chicxulub ejecta spherules found in the basal Clayton Sands of further K-P outcrops in Alabama (e.g., Moscow Landing, Pitakpaivan et al., 1994; Smit et al., 1996), in Texas (Chapter 3 and Smit et al., 1996), and in northeastern Mexico (Chapter 2 and Smit et al., 1996; Schulte et al., 2002; 2003), as well as in the K-P boundary clay of the Western Interior (e.g., in Wyoming, see Bohor et al., 1987; Bohor and Glass, 1995; Izett, 1990 and Chapter 2). By analogy, an origin by the Chicxulub impact on the Yucatán peninsula (southern Mexico) is inferred for the spherules found in the basal Clayton Sands of the Antioch Church core.

Lower Pine Barren Member of the Clayton Formation

The basal Clayton Sands are disconformably overlain by a 10-cm thick, friable, reddish, and fine-grained silty and clayey layer (63.8-63.9 m) that marks the transition to the Lower Pine Barren Member of the Clayton Formation in the Antioch Church core. Overlying the friable shale layer, a green-grey, micaceous, friable, silty-sandy marl is present in the interval from 63.9 to 62.12 m. This marl is rich in phosphate, and glauconite (up to 10 and 15 %) (Fig. 4.6E). It is slightly fossiliferous, including mollusk shell debris (mostly *Ostrea* fragments) and benthic foraminifera, and is thoroughly bioturbated by *Thalassinoides* and *Chondrites*. The top of this marl is indurated, indicating the incipient formation of a hardground.

In the interval from 62.12 to 58 m, the lower Pine Barren Member changes its lithological character from a basal, two cm-thick, friable, reddish and very fine-grained silty and sandy layer with abundant glauconite (up to 40 %), to a 0.5 m thick unit of more indurated and almost pure glauconite sands (>70 % glauconite!), with abundant micrite (20-30 %), and only rare ('sand-sized') quartz grains (Fig. 4.6F-H). This prominent 'glauconite sand' becomes gradually more siltier and more micaceous in the succeeding interval, and finally obtains a marly character due to an increased micrite content in the uppermost two meters (60-58 m). The glauconite replaces pellets, foraminifera, bookmark mica, and bryozoans, or consists of rounded grains without an internal structure (Fig. 4.6G). The bright green and rare pale-brown colors and the rareness of cracks ("critter manure") suggest a juvenile, less evolved state of the glauconite (e.g., Odin and Fullagar, 1988; Amorosi, 1995).

The glauconite-rich interval furnishes bivalves, including *Venericardia* (FAD at 61.3 m), and *Chlamys*, in addition to mollusk shell debris and benthic as well as planktic foraminifera; it is strongly bio-turbated by *Thalassinoides* and *Chondrites*. Within the topmost part, constituents are increasingly cemented by palisade cement and the degree of bioturbation is significantly reduced (Fig. 4.6H). From 57.75 up to 41.4 m, the Pine Barren Member consists of alternating light grey, micaceous, slight sandy marl-siltstones with rare fossils (benthic and planktic foraminifera) and fine sand. The illite content is highly variable (5-40 %) in this interval. Glauconite and phosphate are less abundant, and generally below 5 %. From 41.4 to 35.3 m, the marls of the Pine Barren Member become increasingly sandier and finally siltier. In turn, the amount of bioclastic debris diminishes to almost zero in the topmost part of the Pine Barren Member, which consists of a dark grey, friable, micaceous, and sandy siltstone.

Upper Pine Barren Member of the Clayton Formation ('*Turritella* Rock')

Well-indurated, white-yellow, quartzose sandstones and sandy limestones that range from 35.3 to 29.3 m in core depth disconformably overlie the dark shales of the Pine Barren Member. Due to the abundant presence of the gastropod genus *Turritella*, particularly, *T. mortoni*, this sandstone-limestone bed is commonly referred to as '*Turritella* Rock'. The basal two meters of this limestone bed are essentially bioturbated quartzose sandstone with micritic matrix (Fig. 4.7A). Quartz grains are the predominant component (about 40-50 %) of this sandstone, and show a wide range in grain size between 0.1 to 1 mm, though silt-sized quartz is rare. Most quartz grains have ragged and embayed outlines. Feldspar and illite as well as pyritized or glauconized grains are very rare (less than 10 %). This sandstone yields few fossil remains: mainly benthic foraminifera (mainly rotaliidae and miliolidae), shell fragments (mollusk's, turritellids), echinoderm spines, and very rare dasycladaceans were observed. Frequently, bioclasts show borings and many shells have been dissolved, leaving only residual steinkerns. This sand-

Figure 4.6 (page 145) Thin section microphotographs illustrating compositional and textural characteristics from the Cretaceous-Paleogene transition and the early Danian in the Antioch Church core. All microphotographs in plane-polarized light. (**A**) Pyritized lowermost 5 cm of the basal Clayton Sands. (**B**) Basal Clayton Sands with a large feldspar fragment. (**C**) Spherules and carbonate globules in the basal Clayton Sands. (**D**) Details of a ejecta spherule with globular inclusions. Note strong similarities in size, morphology, and internal features to spherules from various outcrops in northeastern Mexico and Brazos (Texas). (**E**) Sandy limestone above basal Clayton Sands with glauconite and foraminifera, as well as shell and bryozoan fragments. (**F**) Maximum flooding surface with abundant glauconite. Most glauconite is probably derived from fecal pellets. Note bright green color of glauconite, which is indicative of a nascent evolutionary state, involving a short time of formation (<50 ka Amorosi, 1995). (**G**) Detail of a more mature glauconized (mica?) grain from just below the maximum flooding surface with 'concertina-like' structure and incipient iron-oxide formation on internal cracks. Note tiny glauconite-infilled planktic foraminifera in the upper left. (**H**) Glauconite grains with bladed marine cements from the upper condensed section overlying the maximum flooding surface.
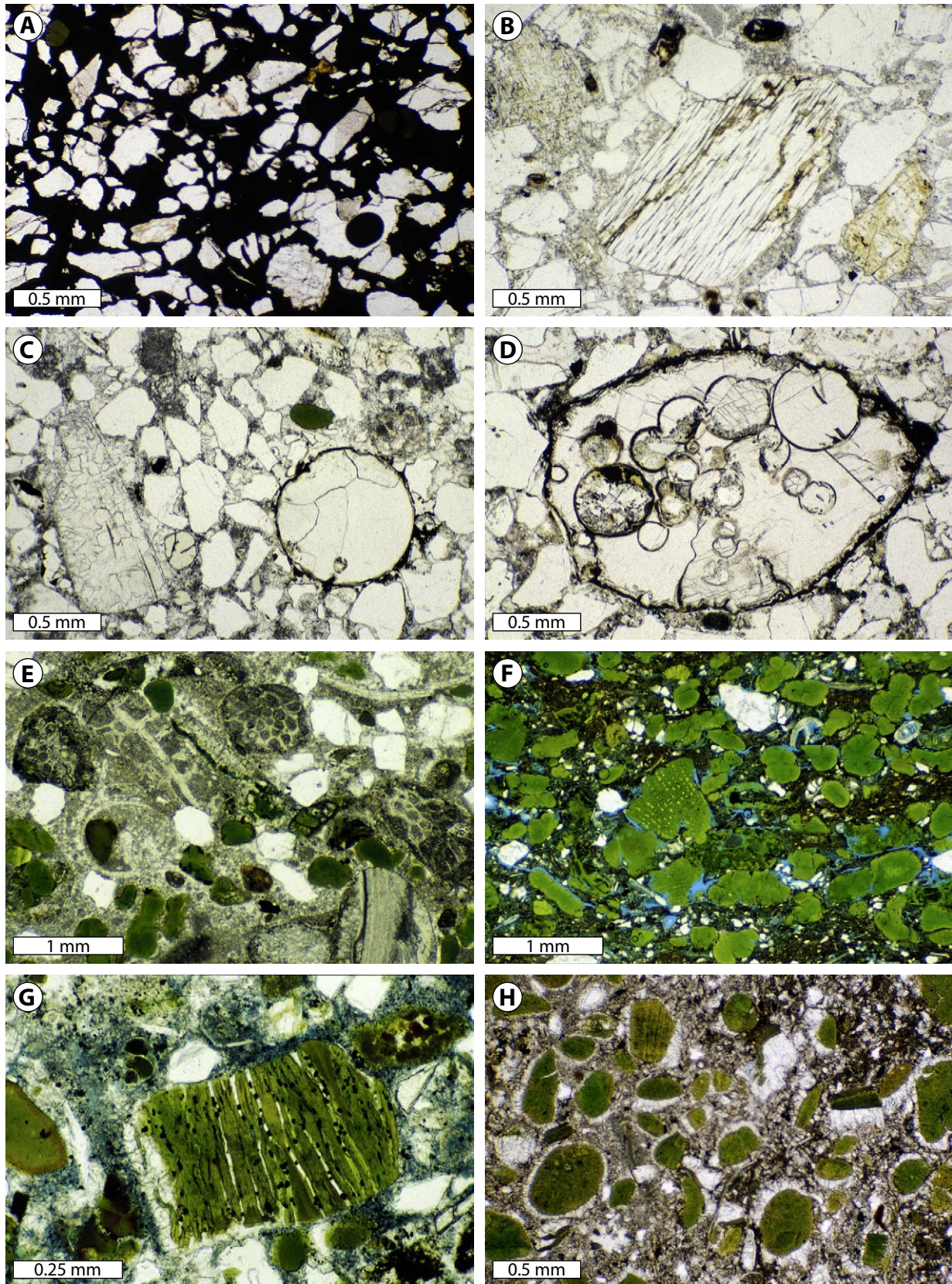
Figure 4.6 (caption on page 144).

stone is characterized by high porosity (10-20 %) and minor fringing cement in cavities.

In the uppermost 4 meters of the 'Turritella Rock', there is an abrupt increase in fossil content, concomitant to a decrease in quartz content, compared to interval below. Therefore, this part of the 'Turritella Rock' is a sandy limestone ("bioclastic packstone"). The faunal assemblage is largely dominated by cm-sized molds of *Turritella* shells or unidentified shell fragments (Fig. 4.7B-H). Additional fossils in this limestone include bivalve fragments (e.g., *Venericardia*, oysters), abundant benthic (mainly rotaliidae and miliolidae) and (very rare) planktic foraminifera, bryozoan fragments, echinoderm spines, sponge spicules, and ostracods. Compared to the lower part of the 'Turritella Rock', the grain size of the fossil debris and shells is strongly increased (up to cm-sized pieces). Other important changes in this upper fossiliferous interval are related to quartz content, which shows a marked decrease upsection reciprocal to an increase of micrite. In addition, pyritized and glauconized particles are prominent constituents of this limestone, as well as large (up to cm-sized) aggregate grains (Fig. 4.7C, D); some ooids have also been observed. Porosity is generally in the range of 20 to 25 %. Notably, iron coatings that are commonly associated with dissolution features line most of the cavities (Fig. 4.7B); spar cement is rarely present in this limestone. Further prominent diagenetic features include 'steinkerns' with internal sediment (micrite, quartz grains) (Fig. 4.7E). Dissolution may have selectively affected certain bioclasts (e.g., predominantly aragonitic turritellids), but may have also been pervasive, and formed caverns of various sizes.

In the 'Turritella Rock', two kinds of micritic cement have been observed: microcrystalline cement (neomorphism), probably related to precipitation from meteoric waters, and dark grey fine micrite. The topmost 20 cm of the 'Turritella Rock' are extremely indurated, slightly enriched in glauconite and phosphate (~10 %, respectively), and bioturbated, indicating a pervasive hardground formation.

In addition, meniscus-shaped and dripstone cement were observed, which both reflect the distribution of water in the vadose zone (Fig. 4.7E, F) (Longman, 1980; Tucker and Wright, 1992). In concert with the presence of *Microcodium* (a calcified fungus), rhizoliths, and iron-rich crusts (Fig. 4.7G, H), this particular cement suggest that emersion of the 'Turritella Rock' above sea level and incipient soil formation took place (Alonso Zarza et al., 1999; Immenhauser et al., 1999; Yilmaz and Altiner, 1999).

Porters Creek Formation

The marly siltstones and marls of the lower Porters Creek Formation (McBryde Member), that cover the interval from 29.3 to 24.4 m in core depth, disconformably overlay the 'Turritella Rock'. Throughout this interval, their character changes from dark grey, fossil-free, shaley siltstone (29.3-28.8 m), to a light grey, slightly shelly marl-rich interval (28.8-27.6 m), back to a dark grey, fossil-free, shaley siltstone (27.6-27.1 m). Finally, these shaley siltstones grades into light grey, calcareous sandy marls that have a mottled texture and are thoroughly bioturbated (27.1-24.2 m). Phosphate and glauconite is very rare in these units and generally below 5 %.

From a core depth of about 24.2 m upward, these strongly bioturbated carbonaceous marls grade into well-indurated sandy and shelly micritic limestones of light-grey and yellow-brown color. Both lithologic units belong to the mid Porters Creek Formation (McBryde Member). These limestones may be classified as bioclastic packstone, though they show significant lower grain size of the detrital and bioclastic components than, for instance the 'Turritella Rock'. They bear many mollusk shells, and shell fragments, specifically of the genus *Ostrea*. Occasionally, shells of the nautiloid *Hercoglossa ulrichi* are present (at 21.9 m). Hence, this limestone bed is called '*Hercoglossa* limestone', whereas gastropods (e.g., turritellids) are rare. Analogous to the 'Turritella Rock'', the topmost part (19-18.5 m) of the McBryde Member is well indurated and burrowed, therefore suggests the presence of a marine hardground, though

Figure 4.7 (page 147) Thin section microphotographs illustrating microfacies characteristics of the 'Turritella Rock' representative for the sandy limestone intervals from the middle to upper Danian units of the Antioch Church core. All microphotographs in plane-polarized light. (**A**) Glauconite-rich sandstone with micrite cement from the basal part of the 'Turritella Rock'. (**B**) Diagenetic textures, including spar/fringed cement and mollusk molds in the upper part of the 'Turritella Rock'. (**C**) and (**D**) upper part of the 'Turritella Rock' with bioclastic debris and 'ghosts' of diagenetically dissolved gastropod shells. (**E**) Fossil 'spirit-level' inside recrystallized gastropod shell. Note accumulation of iron-oxides in the upper part of the shell. (**F**) Dripstone cement below a mollusk shell. (**G**) and (**H**) show steinkerns of gastropod shells with micrite infilling. The upper part of the gastropod is eroded and replaced by a 'foamy' irregular cellular structure interpreted as the fungus *Microcodium*. This structure is commonly an indicator for incipient stages of soil formation, and hence suggests temporarily subaerial exposure of the "*Turritella* Rock."
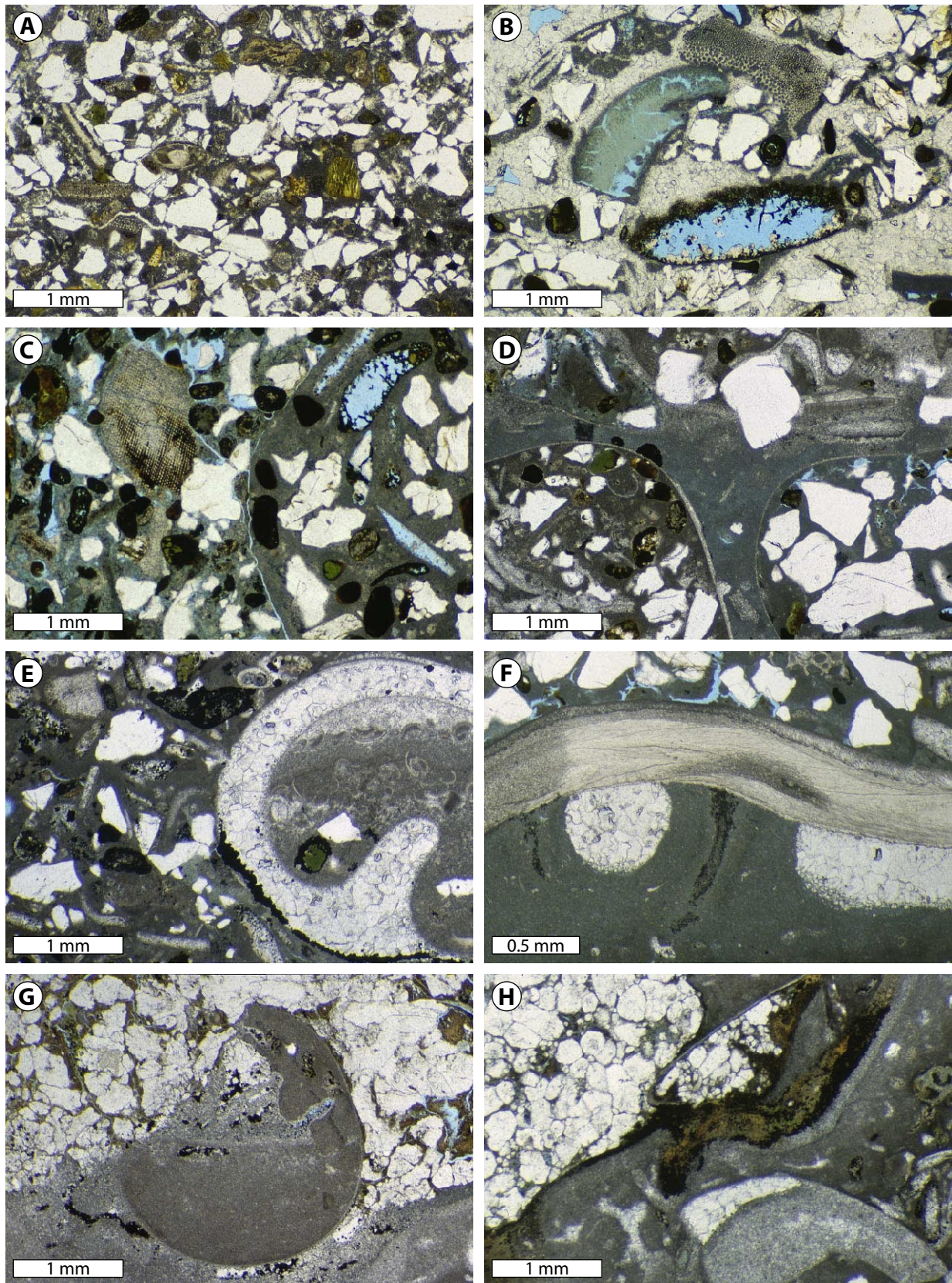
Figure 4.7 (caption on page 146).

no proof for temporary emersion via particular cements or rhizoliths has been found. The quartz and feldspar grains are very coarse in size; there is only rare silt-sized detritus. Phosphate and glauconite is rare in this interval and generally below 5 %. The hardground atop of the 'Hercoglossa limestone' is disconformably overlain by dark grey, fossil-free, friable shaley siltstone, the upper Porters Creek Formation, which grade upward into grey calcareous, slight sandy marls that have a mottled appearance, are bioturbated by *Chondrites* and *Thalassinoides*, and contain only few macrofossil shells or shell debris, but are rich in planktic foraminifera. In the Antioch Church core, the upper Porters Creek Formation covers the interval from 18.6 to 11.5 m.

Matthews Landing Formation

The calcareous marls of the upper Porters Creek Formation grade upward into the indurated sandy limestones of the Matthews Landing Formation, commonly referred to as Matthews Landing Marl Member. These Matthews Landing marls enclose the interval from 11.5 to 4.1 m in core depth and can be divided into two distinct lithologies: A very sandy and shelly coarse-grained, well-indurated basal part (bioclastic packstone; 11.5-10 m) that grades into an upper, fine-grained 'chalky' part with fewer shells and shell debris. This chalky part sporadically bears sandy layers (10-4.1 m). The upper, chalky part of the Matthews Landing marl is again a highly fossiliferous bioclastic packstone, including bivalves (e.g., *Venericardia wilcoxensis*, oysters), gastropods (mainly turritellids), benthic-planktic foraminifera, bryozoan fragments, echinoderm spines, and ostracods. The basal part furnishes many phosphate and glauconite grains (up to 10 %), whereas the upper 'chalky' part is nearly devoid of these authigenic minerals. The uppermost ten centimeters is slightly indurated and burrowed, and enriched in glauconite, suggesting the presence of a marine hardground, but without evidence for emersion above sea level.

Naheola Formation

The topmost 4 meters of the Antioch Church core (4.1-1.8 m) consist of light grey, sandy-silty marls that disconformably overlay the Matthews Landing limestones. This unit belongs to the Oak Hill Member of the late Danian Naheola Formation.

4.3.2 Biostratigraphy

The biostratigraphy of the Antioch Church core is based on the calcareous nannofossil record, which allows a high-resolution correlation within the northern Gulf coast and to K-P boundary sections globally. Calcareous nannofossils reveal an impoverished and poor to modest preserved late Maastrichtian assemblage and more diverse and commonly well-preserved early Danian assemblages, though stratigraphic control in the late Danian part of the core is moderately because of rare presence or absence of index species. For the Maastrichtian, the calcareous nannoplankton zonation used in this study is based on Perch-Nielsen (1985). For the Danian, the zonation provided by Martini (1971) and Berggren et al. (1995) is used. The stratigraphic distribution of calcareous nannofossils is reported in Fig. 4.3; details of the zonation in the K-P transition are depicted in Fig. 4.5. Five calcareous nannofossil zones have been distinguished. These are the *Micula murus* Zone (CC26, late Maastrichtian), the *Markalius inversus* Zone (NP1, earliest Danian), the *Cruciplacolithus tenuis* Zone (NP2, early Danian), the *Chiasmolithus danicus* Zone (NP3, early Danian), and the *Ellipsolithus macellus* Zone (NP4, middle Danian).

Cretaceous

***Micula murus* Zone (CC26):** This biozone is defined from the first occurrence of the nominate species to the first occurrence of *Micula prinsii*. In the Antioch Church core, *M. murus* is rarely, but consistently present throughout the Prairie Bluff Formation, aside from the rare occurrence of *Arkhangelskiella cymbiformis*, *Lithraphidites quadratus*, and *Nephrolithus frequens*, which all are typical for the late Maastrichtian nannofossil assemblage in Alabama (Moshkovitz and Habib, 1993).

No direct evidence has been found in the shales and marls of the Prairie Bluff of the Antioch Church core for the presence of the *Micula prinsii* Subzone (CC26b). Alternatively, the poor to moderate preservation of calcareous nannofossil assemblages in the Prairie Bluff Formation may be responsible for the non-identification of this biozone, since the (very rare) occurrence of this index species, has been reported from several other sections in Alabama, including the nearby Braggs and Mussel Creek sections, where *M. prinsii* occurs in the uppermost 20-40 cm of the Prairie Bluff Formation (e.g., Moshkovitz and Habib, 1993). However, several samples of the Prairie Bluff contain tiny specimens of *Neobiscutum romeinii*, *Neobiscutum parvulum*, and *Cruciplacolithus primus* as far as 12 m below the K-P boundary. These calcareous nannofossils

have long been used as index fossils for the earliest Paleogene, though recent studies reveal their consistent presence already in latest Maastrichtian sediments during the uppermost part of the *M. murus* Zone (Mai et al., 2003). In some localities, their first occurrence roughly parallels the first appearance of *M. prinsii* (CC26b, at Elles, Tunesia, Gardin, 2002). Therefore, it is not certain if the Biozone CC26b is indeed missing at the Antioch Church core, and it is difficult to constrain the extent of the putative hiatus atop of the Prairie Bluff Formation.

Event bed and the K-P boundary

Calcareous nannofossils are rarely present and poorly preserved in the basal Clayton Sands of the Clayton Formation, and no index fossils or characteristic blooms have been observed in this interval (Fig. 4.4). However, Chicxulub impact-spherules (and a smectite-enrichment, see below) are consistently present throughout the 1 m thick Clayton Sands, albeit the pyritized, 5-cm thick basal layer of this clastic deposit reveals none of the particular characteristics of the K-P boundary clay layer observed elsewhere (see Chapter 1), including a distinct siderophile element enrichment (e.g., Ni, Co), a smectite enrichment, and the presence of spherules, shocked quartz, and Ni-spinels (e.g., Pollastro and Bohor, 1993; Bohor and Glass, 1995; Koeberl and Martínez-Ruiz, 2003). The absence of spinels has also been confirmed by a preliminary magnetic susceptibility study (A. Kontny written comm. 2003). Therefore, no direct correlation with the global stratotype section and point (GSSP) at El Kef, Tunisia (Cowie et al., 1989; Remane et al., 1999), in which the K-P boundary is defined at the base of a mm-thick impact-ejecta bearing clay layer that separates Cretaceous and Paleogene strata, is possible. Hence, the K-P boundary may either be placed at the base of the Clayton Sands, coincident with the last occurrence of a Maastrichtian nannofossil fauna. Alternatively, the K-P boundary may be placed at the first appearance of Paleogene taxa, which occurs atop of the Clayton Sands in the Antioch Church core (see below), though other K-P boundary studies in Alabama have shown the presence of earliest Danian microfossils already in these sands (e.g., Olsson and Liu, 1993; Olsson et al., 1996; Mancini and Tew, 1993; Moshkovitz and Habib, 1993). In conclusion, and in absence of iridium-analyses, the basal Claxton sands are considered as an 'unzoned' interval (see Olsson and Liu, 1993).

Paleogene

Markalius inversus **Zone (NP1):** This biozone is defined by the first appearance of Paleogene nannofossils to the first occurrence of *Cruciplacolithus tenuis.* According to the magnetochronological calibration by Berggren et al. (1995), the Biozone NP1 has duration of about 0.5 Ma and spans the interval between 65 and 64.5 Ma, from the middle part of Chron C29R to the middle part of C29N. In this study, the lower boundary of the *M. inversus* Zone is taken at the first appearance of the nominate species. In the Antioch Church core, *M. inversus* has been observed in the samples directly overlying the basal Clayton Sands (at 63.6 m), concomitant to an acme of *N. romeinii* and to the massive disappearance of Maastrichtian nannofossils.

A pronounced *Thoracosphaera* acme at the base of Biozone NP1, which is often observed directly above the K-P boundary clay in many other K-P sections (see overview in Fig. 2 of Gardin, 2002), is not present in the basal Pine Barren Member, suggesting a hiatus and/or erosion atop of the basal Clayton Sands, as also observed by Moshkovitz and Habib (1993) for the Braggs and Mussel Creek sections. Further similarities between these sections and the Antioch Church core are recognized in terms of the FAD of *M. inversus* or other Paleogene nannofossils, which is generally reported at the top, or the topmost 20 cm of the meter-thick Clayton Sands (Moshkovitz and Habib, 1993; Habib et al., 1996; Olsson and Liu, 1993; Olsson et al., 1996). The interval above the basal Clayton Sandstone can be further subdivided by several nannofossil acme zones: From the top of the Clayton Sands up to the interval of maximum starvation at 59.3 m, successive acmes of *N. romeinii*, *N. parvulum*, *C. primus*, and *Futyania petalosa*, have been observed, in addition to the presence of *Prinsius dimorphosus* in the uppermost samples of this interval (see Fig. 4.5 for details). A remarkably analogous succession has been found to occur within Biozone NP1 in several other K-P boundary sections including El Kef, Tunisia, and Brazos, Texas (Gartner and Jiang, 1985; Gartner, 1996; Gardin and Monechi, 1998; Gardin, 2002 and Chapter 3).

Cruciplacolithus tenuis **Zone (NP2):** This interval zone is defined from the first occurrence of *C. tenuis* to the FAD of *Chiasmolithus danicus.* According to the revised Cenozoic geochronology by Berggren et al. (1995), this biozone has duration of about 0.7 Ma and spans the interval between 64.5 and 63.8 Ma from the middle part of C29N to the middle part of C28R. In the Antioch Church core,

the nominate species is present from the surface of maximum starvation at 59.3 m up to the top of the *Turritella* limestone. For the basal limit of the Biozone NP2, this results agree with several previous studies on sections and cores in Alabama by Donovan et al. (1988), Mancini et al. (1989), Mancini and Tew (1993), and Moshkovitz and Habib (1993), who also placed the NP1-NP2 boundary about 5 m above the basal Clayton Sands and slightly (~1 m) above the glauconized interval interpreted as maximum flooding surface.

Chiasmolithus danicus **Zone (NP3):** The base of Biozone NP3 is defined by the first appearance of *C. danicus* and ranges up to the first appearance of *Ellipsolithus macellus.* It spans the interval from 63.8 to 62.2 Ma (middle part of C28R to lower part of C27R) and thus, lasts about 1.6 Ma. In the Antioch Church core, the index species *C. danicus* is difficult to determine unambiguously, and therefore, the first appearance of *Chiasmolithus* sp. in the marls of the McBryde Member, directly overlying the *Turritella* limestone, has been used to tentatively define the base of the Biozone NP3. This stratigraphic assignation agrees well with the results from Mancini et al. (1989), and Mancini and Tew (1993), who placed the NP2-NP3 boundary within or at the top of the '*Turritella* Rock' as well.

Ellipsolithus macellus **Zone (NP4):** The first appearance of *E. macellu*s marks the base of the Biozone NP4, which has duration of 2.5 Ma (62.2 to 59.7 Ma) and covers the lower part of C27R to middle part of C26R. In the Antioch Church core, the index species *E. macellus* is not present, but the occurrence of the species *Ellipsolithus bollii* in the topmost three meters of the core (that corresponds to the Naheola Formation), has been used instead to assign this interval to the Biozone NP4. This result is in rough agreement with Mancini et al. (1989), and Mancini and Tew (1993), who placed the NP3-NP4 boundary at the "middle" part of the Porters Creek Formation.

4.3.3 Gamma-ray log

The standard gamma-ray (GR) curve records the total gamma radiation from all sources (radioactive potassium, thorium, and uranium) within a rock; it is commonly displayed in Gamma-ray American Petroleum Institute ("API") units. Since high potassium, thorium, and uranium generally belongs to the detrital 'fine-fraction' of a sediment, the gamma-ray log proved to be a good indicator of clay content in sedimentary successions (Austin et al., 1998),

though; additionally, potassium may be enriched in authigenic phases (e.g., glauconite) and uranium can also be absorbed by organic matter and phosphate nodules. Correlation with core lithology indicates that, generally, low gamma-ray readings (<30 API) can be interpreted as quartz sands or pure limestones while high gamma-ray values (>80 API) can be related to clay-rich (or organic-rich) shaley lithologies (Hesselbo, 1996; Austin et al., 1998); though these threshold values are not applicable universally, but must be verified with the lithologic description from core cuttings. Sharp GR peaks may be related to glauconite-rich intervals (e.g., condensed sections). These characteristic features make the GR log a valuable tool for the subsurface correlation of well logs and, specifically, in sequence stratigraphic analysis since distinct trends in the gamma-ray logs can be interpreted as facies successions linked to systems tracts and gamma-ray minima or maxima may correspond to particular sequence stratigraphic surfaces (Rider, 1996). However the GR sonde has a vertical resolution between 50-70 cm, leading to 'smoothing' of the GR values, hence, the capabilities of resolving thin interbedded layers of contrasting lithologies is somewhat limited.

The standard gamma-ray log of the Antioch Church core is displayed in Fig. 4.3. It can be subdivided into four intervals ('GR sequences'), each characterized by a stacking pattern of contrasting gamma radiation of variable magnitude: A typical sequence includes first decreasing low GR values through elevated and fluctuating GR readings up to strong increasing GR values. Correlation with the core litholog shows good agreement of low gamma-ray readings with quartz sands or limestones, and high gamma-ray values with shales and glauconite-rich intervals. The boundaries between these intervals do generally correspond to the boundaries between lithologic units, except for the interval preceding the basal Clayton Sands: in this interval, a gradual decrease of the gamma-ray radiation occurs throughout the upper 4 m of the Prairie Bluff Formation, whereas the lithologic change from shale to marl takes not place not until the uppermost two meters. Based on relationships between GR log trends with depth, their association with core lithologies, and the empirical criteria provided by Holmes et al. (1993), Southgate et al. (1993), and Catuneanu (2002), four sequence boundaries and several within-trend surfaces (flooding surfaces) were picked that are marked by arrows in the GR curve (Fig. 4.3). Fig. 4.3 also shows that these results are, mostly,

congruent to the identification of these surfaces based on lithological observations.

4.3.4 Mineralogical phases

The reason for the study of clay mineral assemblages of the Antioch Church core was twofold: on one hand, it is generally assumed that clay mineral assemblages change with increasing distance from the shoreline or delta and therefore may give evidence of relative and eustatic sea level changes (Pearson, 1990; Chamley, 1997; Bengtsson and Stevens, 1998; Schutter, 1998; Srodon, 1999). According to these authors, this behavior partly depends on the different grain-sizes of the clay mineral species ('sorting effect with transportation distance'), as well as on the tendency of distinct clay minerals to agglomerate when entering seawater, leading to faster settling through the water column. Hence, the sequence stratigraphic framework of the Antioch Church core can be tested against compositional changes of the clay mineral assemblage to evaluate proximal-distal facies trends. On the other hand, inherited clay mineral assemblages may record climatic changes in the hinterland and previous studies have suggested and/

or established a link between clay mineral compositions in marine (shelf) sediments adjacent to continental areas with climatic conditions in the terrestrial source areas (Ehrmann et al., 1992; Chamley, 1997; Yuretich et al., 1999; Net et al., 2002). However, this relationship is surely not straightforward since clay mineral assemblages may be altered by a variety of factors that may mask, or even adulterate, potential climatic signals (see critical reviews by Singer, 1984; Thiry, 2000).

Clay minerals identified in the <2 μm fraction of the Antioch Church core and used for semi-quantitative analysis include smectite, chlorite, mica, and kaolinite. Their relative amount varies strongly throughout the core: Smectite and kaolinite are the predominant clay minerals, though kaolinite is virtually absent the upper part of the core. Illites are consistently present throughout the core in minor quantities, whereas the amount of chlorite is confined to a few percent. Mixed-layer clay minerals, including illite-smectite and chlorite-vermiculite, occur only as trace amounts and have therefore not been included in the semiquantitative analysis. In addition, some intervals are characterized by an
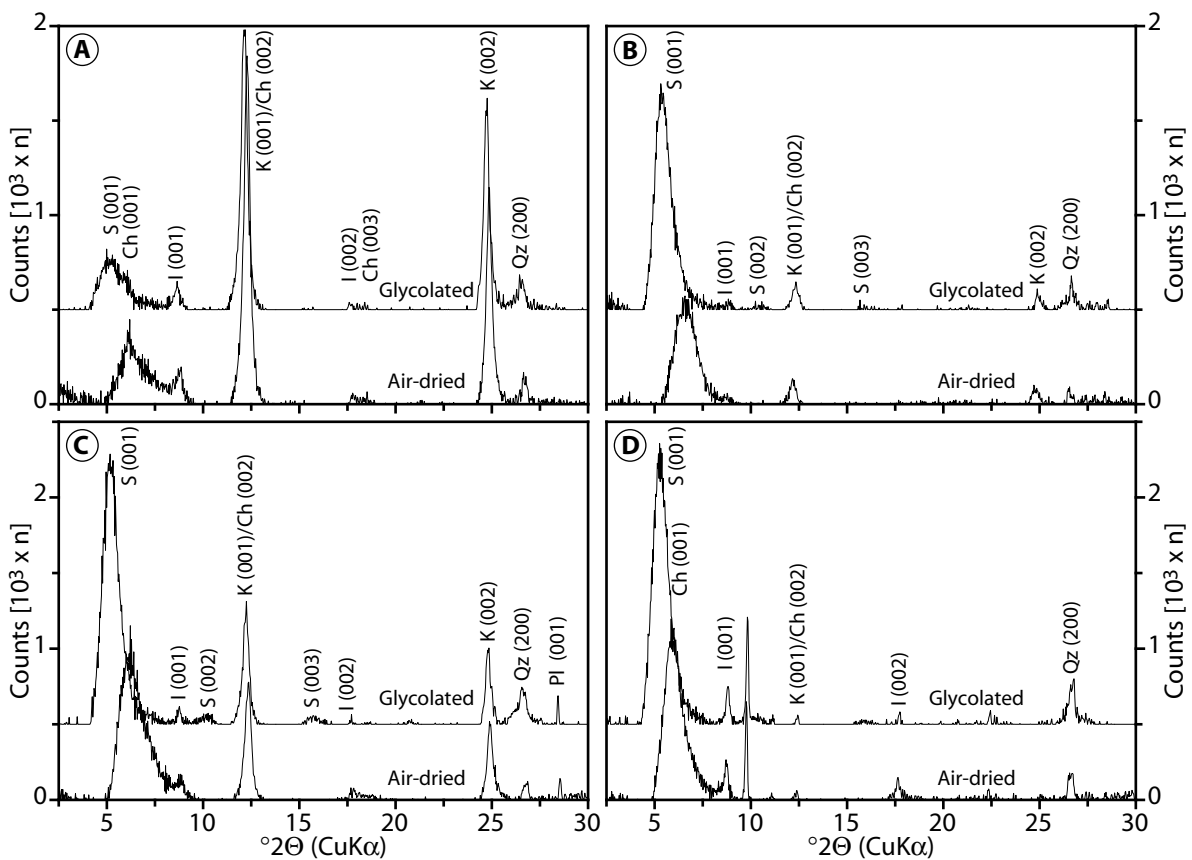
Figure 4.8 Clay mineralogy of the Antioch Church core: Representative X-ray diffraction patterns of the <2 μm fraction (air-dried and ethylene glycol-solvated) showing the three distinct clay mineral assemblages in addition to the smectite-rich basal Clayton Sands (see text for details). (**A**) Prairie Bluff shale (Sample AC82); (**B**) Basal Clayton Sands (AC82); (**C**) Basal Pine Barren Member (AC119); (**D**) McBryde Member (AC194).
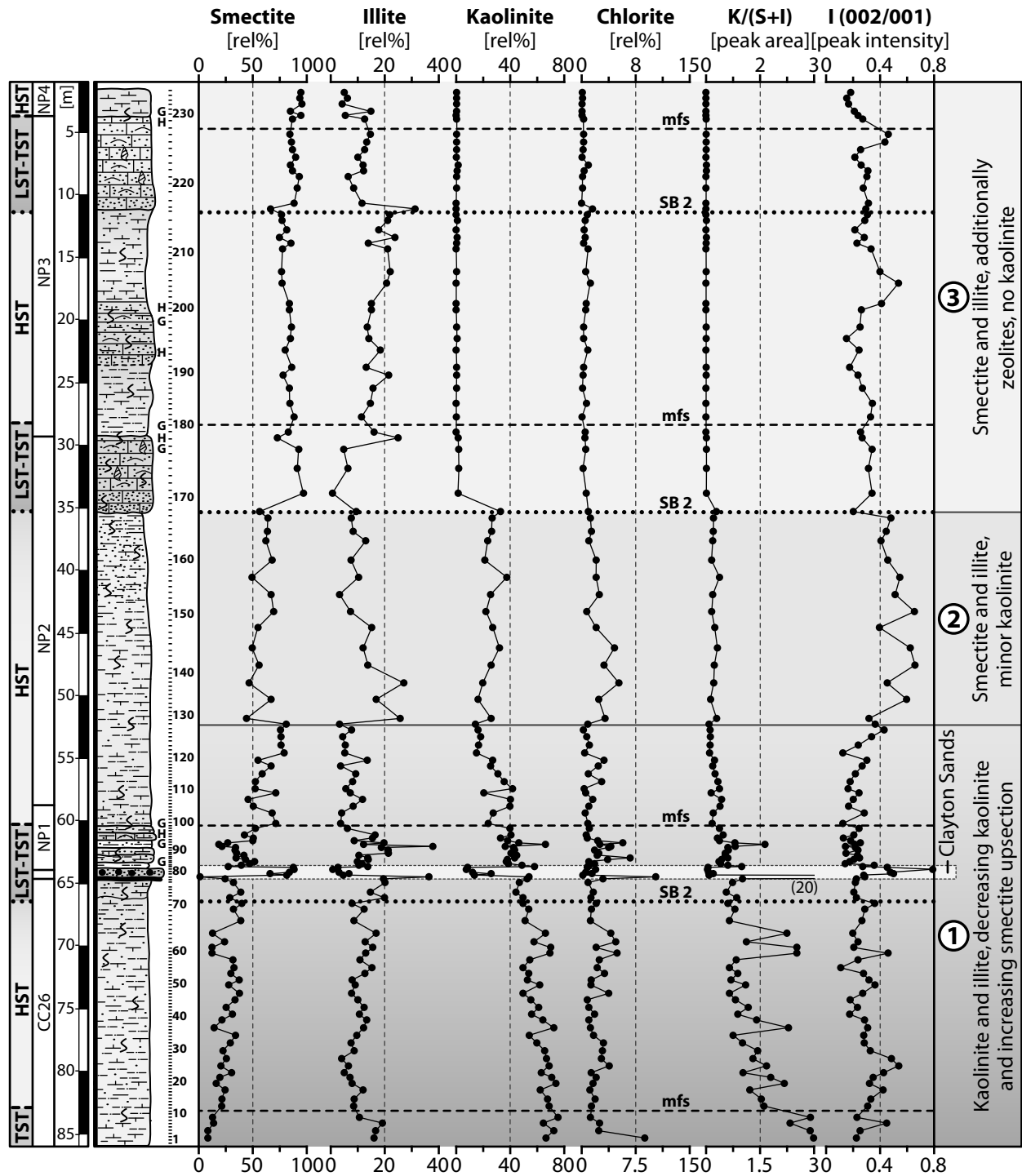
Figure 4.9 Clay mineralogy of the Antioch Church core: Relative abundance of the clay mineral phases determined by X-ray diffractometry of the glycolated <2 μm fraction, including smectite, illite, kaolinite, chlorite, the kaolinite-smectite ratio, and the octahedral character of the illite (002/001 peak intensity ratio). Data is given in relative percent of the clay fraction with correction factors (Biscaye, 1965). Fig. 4.2 includes a key to the lithologic symbols. Nannoplankton zonation and sequence stratigraphic interpretation (see Fig. 4.3) is shown to the left.

abundance of zeolites. Three 'zones' with distinct clay mineralogical assemblages have been identified by the appearance or disappearance of clay mineral phases and are described in stratigraphic order below. The mineralogical characteristics and stratigraphic location of each assemblage are depicted in Fig. 4.9 and representative X-ray diffraction patterns of the <2 μm fraction are illustrated in the Fig. 4.8

(raw data in Appendix 4.1). Additional high-resolution clay-mineral abundances are given for the immediate K-P transition in Fig. 4.11A.

Assemblage 1: A kaolinite + smectite + illite assemblage is present from 85.5 to about 52 m in the Antioch Church core (Fig. 4.9). This assemblage shows a gradual change from a kaolinite-dominated (~70 rel%) clay mineral association with mi-

nor smectite (~15 rel%) in the lowermost part (at ~80 rel%), to a smectite-prevalence (~80 rel%) with only minor amounts of kaolinite (~15 rel%) at about 52 m in core depth (drop in the kaolinite/smectite ratio from 3.5 to 0.1). Several cyclic fluctuations in the range of ±20 rel% are superimposed on this constant shift from a kaolinite to smectite dominated clay mineral composition. Most notably, a distinct peak in kaolinite (from 50 to 75 rel%) occurs during the 71-68 m interval. The illite content shows some fluctuations in the range from 4-20 rel% and averages 10 rel%, whereas chlorite is a minor component and generally below 5 rel%. This interval ranges from the lowermost Maastrichtian up to the lower part of the calcareous nannofossil Zone NP2. This trend is 'interrupted' for the basal Clayton Sands, which show a basal pyritized and jarosite-rich layer and a distinct smectite-enrichment (>80 rel%) with only subordinate amounts of kaolinite (~10 rel%) and illite (~4 rel%; Fig. 4.11A). In the two meters (61-63 m) above the Clayton Sands, a distinct mica-enrichment (25-30 rel%) is present in the condensed section (Fig. 4.11A).

The smectite in this part of the Antioch Church core shows 'full width at half maximum' (FWHM) values in the range of 0.95 to 1.2 °2Θ. In concert with the absence of distinct smectite (002) and (003) reflections in the diffractograms, this indicates at most a moderate crystallization or large crystal sizes of the smectite and suggests a detrital origin. In addition, the poor smectite crystallinity in the basal Clayton Sands gives no evidence for the authigenic neoformation of smectite phase from former glassy phases, contrary to the basal part of the spherule-rich "event bed" at Brazos, Texas (see Chapter 3). The illite (002/001) peak intensity ratio is between 0.2 to 0.4, suggesting an intermediate biotitic to muscovitic octahedral character (Petschick et al., 1996). Higher values (>0.4) of the illite (002/001) intensity ratio are present only in the basal Clayton Sands.

Assemblage 2: A smectite + kaolinite + illite assemblage with prevalence of smectite and kaolinite is present in the Antioch Church core throughout the interval from about 52 m up to the base of the '*Turritella* Rock' at about 28 m (Fig. 4.9). In this interval, smectite averages 58 rel%, kaolinite averages 26 rel%, and illite has mean values of 12 rel%, whereas chlorite is well below 5 rel%. Smectite generally shows well-defined, narrow peaks and the FWHM values increase to average values of 0.8 °2Θ indicating a slightly higher degree of crystallinity or different grain-size compositions as compared to

clay mineral facies of (1). Compared to the lower part of the Antioch Church core, the illite (002/001) peak intensity ratios are considerably higher and show values generally exceeding 0.4, suggesting a muscovite-like 'octahedral character' (Petschick et al., 1996). This result is confirmed by the average c-lattice constant of about 9.9 Å (~8.88 °2Θ) of the illite that indicates a 'muscovitic' character as well (defined by values >9.9 Å, Petschick et al., 1996).

Assemblage 3: A smectite + illite assemblage is present from the base of the '*Turritella* Rock' at 28 m up to the top of the Antioch Church core and furnishes smectite (~85 rel%) largely dominating over illite (~14 rel%), whereas kaolinite and chlorite are virtually absent (<2 rel%; Fig. 4.9). Thereby, the two indurated limestone beds in this interval ('*Turritella* Rock' and Matthews Landing) show slightly higher smectite and lower illite contents. Smectite generally shows well-defined, narrow peaks, and the FWHM values average at 0.7 to 0.8 °2Θ, indicating a slightly higher degree of crystallinity or different smectite grain-size compositions as compared to clay mineral facies of assemblage 1. An additional characteristic component of this interval are zeolites that include clinoptilolite and heulandite, and are constantly present in high quantities from above the '*Turritella* Rock' up to the topmost part of the core (200-800 counts per second, see Appendix 4.1). Except two brief intervals between 16-18 m and 4-6 m, the illite (002/001) peak intensity ratios are between 0.15 and 0.4, pointing to an biotitic to muscovitic octahedral character (Petschick et al., 1996).

4.3.5 Major and trace element stratigraphy

According to studies by Keller et al. (1998), Müller et al. (2001), and Stüben et al (2002), variations of geochemical phases may provide an 'objective tool' at hand to trace even subtle lithofacies changes and, therefore, paleoenvironmental changes within a sedimentary succession. This can be conducted by monitoring elements related to biogenic productivity versus elements typically associated with terrigeneous detritus (e.g., Jeans et al., 1991; Müller et al., 2001; Kastner, 2003). Moreover, geochemical criteria for identifying systems tracts and proximal-distal trends, which ultimately may be related to sea level changes, have been proposed (e.g., Jarvis et al., 2001). These criteria may aid in tackling the sequence stratigraphic framework. In addition, the composition of the detritus-bound geochemical phases may also be used to detect changes in the provenance of the sediments, the hydraulic regime
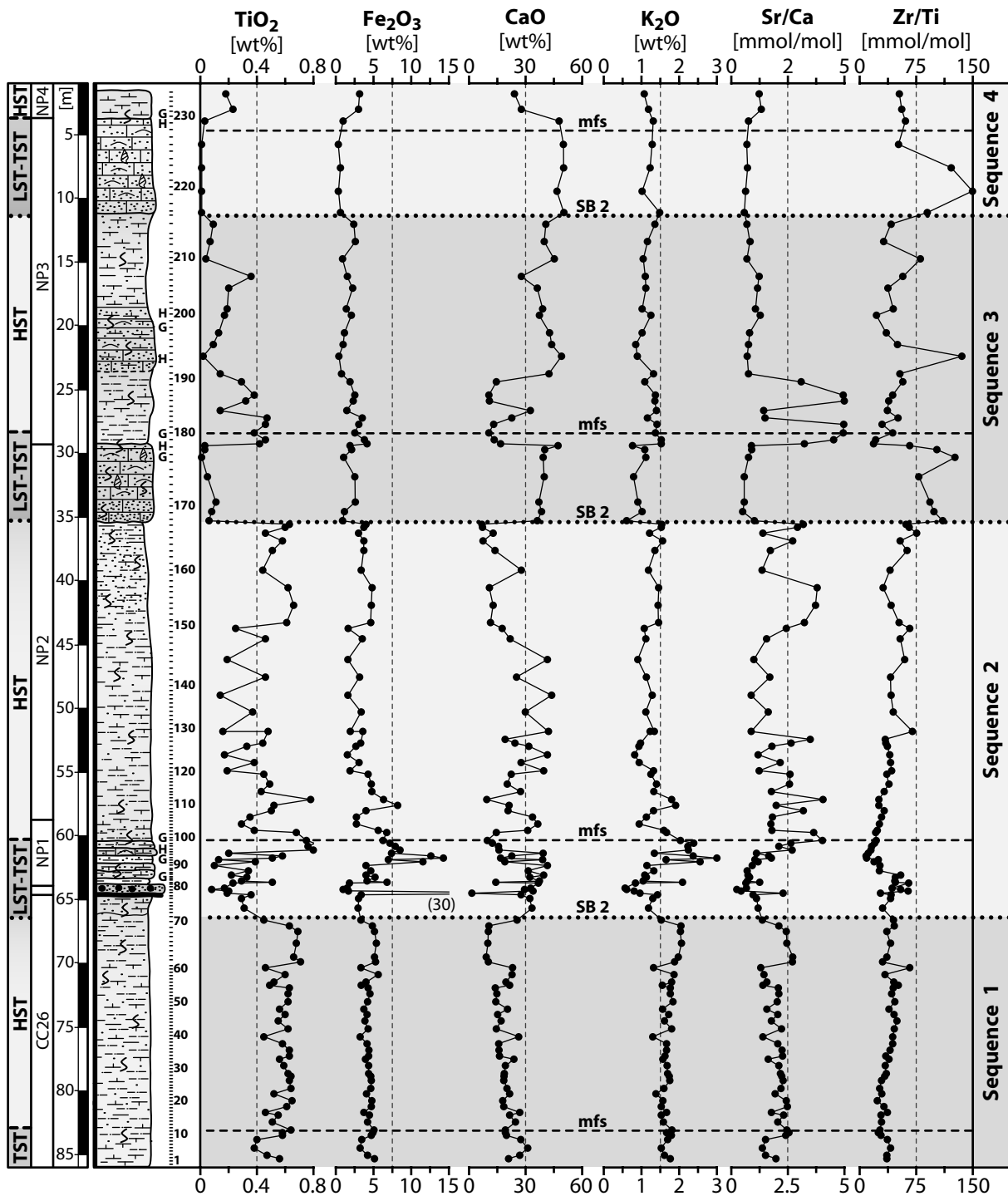
Figure 4.10A Graphical illustration of the results from the energy-dispersive X-ray fluorescence spectrometry (EDS) analysis of the Antioch Church core: Plots of TiO_2, Fe_2O_3, CaO, and K_2O added by the Sr/Ca and Zr/Ti ratios. All Fe is given as Fe_2O_3. Note 'switching' in the element distribution pattern between lithological units and the general subdivision into a lower siliciclastic-dominated part and an upper carbonate-dominated part. A legend is provided in Fig. 4.2. The nannoplankton zonation and sequence stratigraphic interpretation (see Fig. 4.3) is shown in the left columns.

of the source area, and/or the weathering conditions on the adjacent continent (Béllon et al., 1994; Fralick and Kronberg, 1997; Kastner, 2003).

The Si/Al ratio, for instance, is used as an indication of the sand/clay relation (e.g., Thyberg et al., 2000), as Si is mostly found in quartz whereas Al is typically bound to clays, feldspar, and mica. The

Fe content of the sediments can be related to chlorite, pyrite, or siderite as well as iron-rich smectite or mica. The major parts of Ti, K, Rb, and Zr are also bound to the lattices of minerals of terrigeneous origin, including rutile, (K-) feldspar, and zircon (Murray and Leinen, 1993; Young and Nesbitt, 1998). Within this group, Ti and Zr are relatively
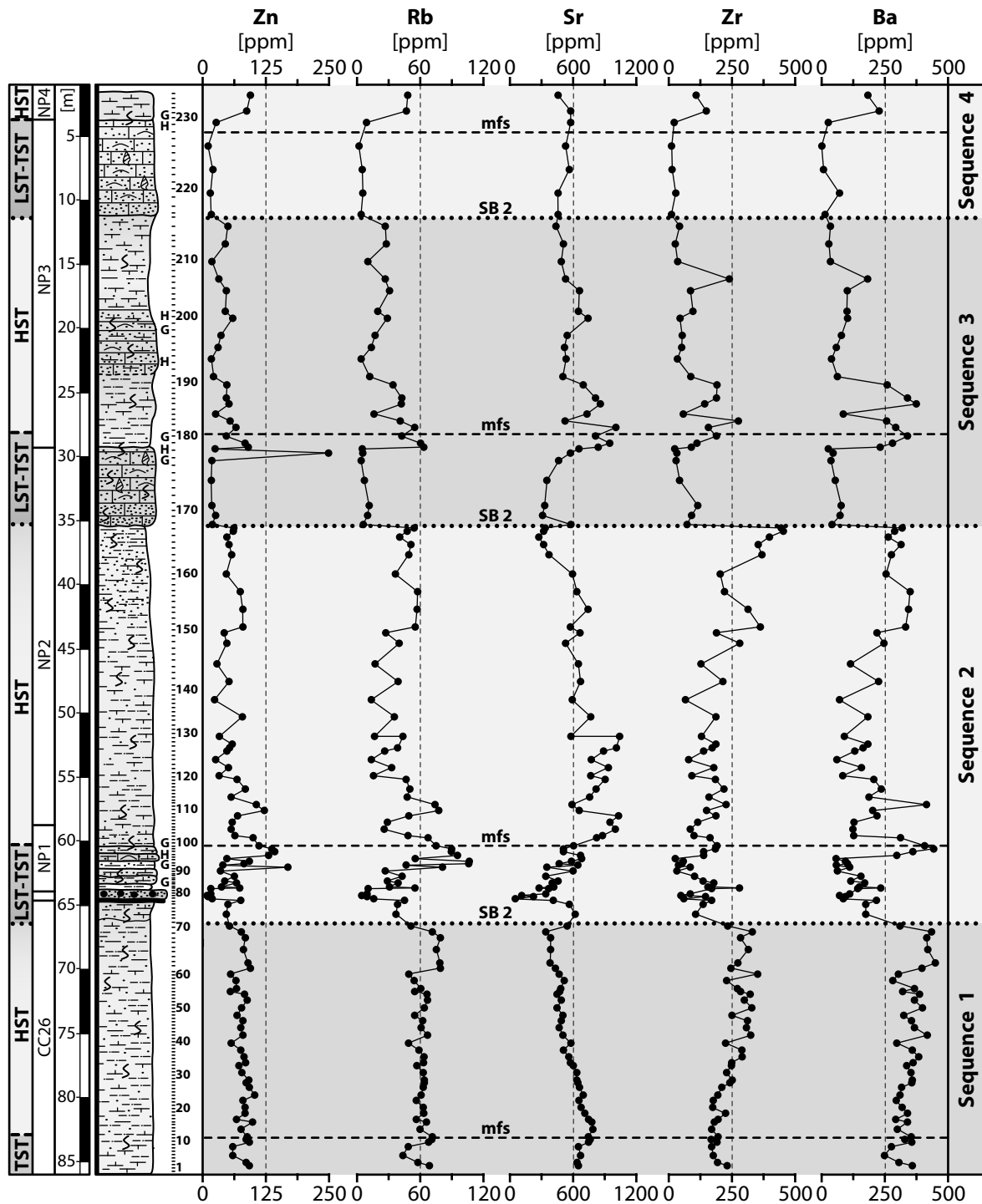
Figure 4.10B Graphical illustration of the results from the energy-dispersive X-ray fluorescence spectrometry (EDS) analysis of the Antioch Church core: Plots of Zn, Rb, Sr, Zr, and Ba. A legend is provided in Fig. 4.2. The nannoplankton zonation and sequence stratigraphic interpretation (see Fig. 4.3) is shown in the left columns.

immobile during weathering (Schroeder et al., 1997; Young and Nesbitt, 1998). The elements Ca, Mg, and Sr, are incorporated into biogenic carbonate (Tucker and Wright, 1992), though Mg and Sr may be bound also to the lattice of mafic terrigeneous minerals or clay minerals. Mn and traces of other metals (e.g., Cu, As) tend to be absorbed on organic matter and to a lesser degree into biogenic carbonate (Jarvis et al., 2001), whereas Ba may either be precipitated as

sulfate from the water column, or is incorporated in clay minerals or feldspar (Schroeder et al., 1997; McManus et al., 1998).

The results from main and trace element analyses by energy-dispersive X-ray fluorescence spectrometry (EDS) of samples from the entire Antioch Church core are shown in Fig. 4.10A, B; the original data is provided in Appendix 4.2. In addition, the Zr/Ti and Sr/Ca ratio is shown in these graphs to
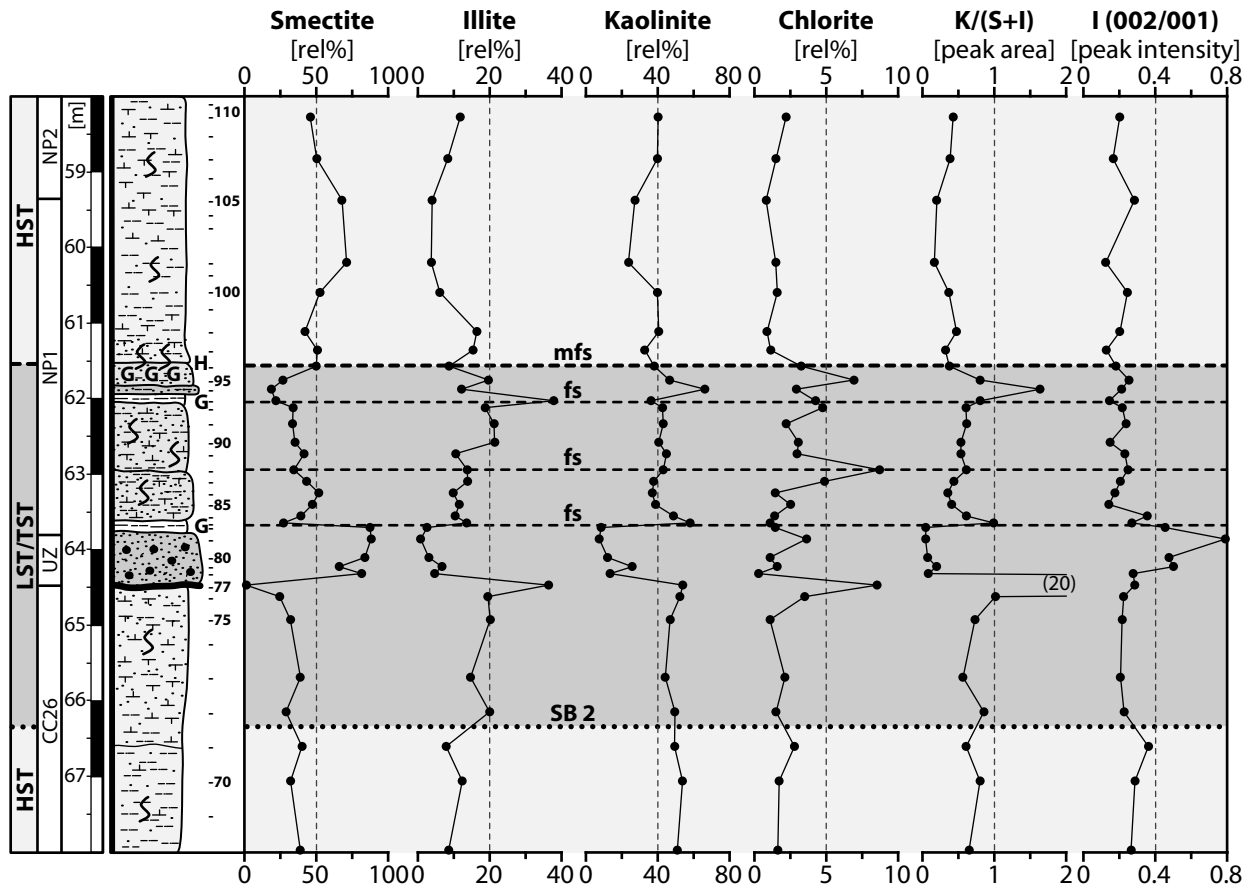
Figure 4.11A Semi-quantitative estimation of the relative distribution of clay mineral phases determined by X-ray diffractometry of the glycolated <2 μm fraction across the immediate K-P transition in the Antioch Church core (from 58-56 m in core depth). Grey shading added in order to ease distinction of lithologic trends. Note distinct smectite and silicate maxima in the basal Clayton Sands and the significant illite enrichment during the condensed section. An explanation to the lithologic symbols is shown in Fig. 4.2 and the nannoplankton zonation and sequence stratigraphic interpretation (Fig. 4.3) is depicted to the left.

depict changes in the terrigeneous and carbonaceous phases, respectively. Several elements (Cu, As, Nb, La, Y), however, showed a close correlation to the Ti contents and have been omitted in the graphs for brevity reasons; yet, their individual amounts are presented in the Appendix 4.2, as well as their correlation coefficient to the Ti contents.

To characterize the immediate K-P transition, additional wavelength-dispersive X-ray fluorescence spectrometry (WDS) analyzes of closely spaced samples from the interval 58 to 68 m across the K-P boundary were conducted and are depicted in Figs 4.11B-C (original values in Appendix 4.3). Selected elements, including Si, Ti, Fe, Mg, and K, have been normalized to aluminum and, together with the Zr/Ti and Sr/Ca ratios, are shown in Fig. 4.11D. The normalization of these elements against Al allows for enhanced monitoring of changes in the detrital composition, since these elements are generally not bound to a carbonate phase.

Element abundances analyzed by EDS for the whole core show two opposing distribution pat-

terns that correspond well to the key 'end Member' lithologies of the Antioch Church core: Silty shale and sandy limestone, with intermediate distribution patterns constituted by marl. The shale intervals are characterized by a low CaO content, generally less than 15 wt%, as well as by peak abundances of almost all other elements and oxides measured (e.g., TiO_2 ~0.5 wt%, Fe_2O_3 ~5 wt%, K_2O ~2 wt%, Rb ~80 ppm, Zr ~300 ppm, Ba ~450 ppm, Sr ~400 ppm). The abundance of elements that are predominantly bound in the lattices of minerals of terrigeneous origin (e.g., Murray and Leinen, 1993), suggest a predominance of clays and other terrigenous detritus in these intervals corresponding to low biogenic productivity or input. The marls and limestones show significant higher values of CaO, which reach 50 wt% (nearly pure calcite) in the limestones, and Sr. Both elements are commonly incorporated into biogenic carbonate, albeit Sr may be also included in feldspars and clays. The concomitant reduction in the quantities of all other elements (except for Sr) that may step back up to the detection limits in
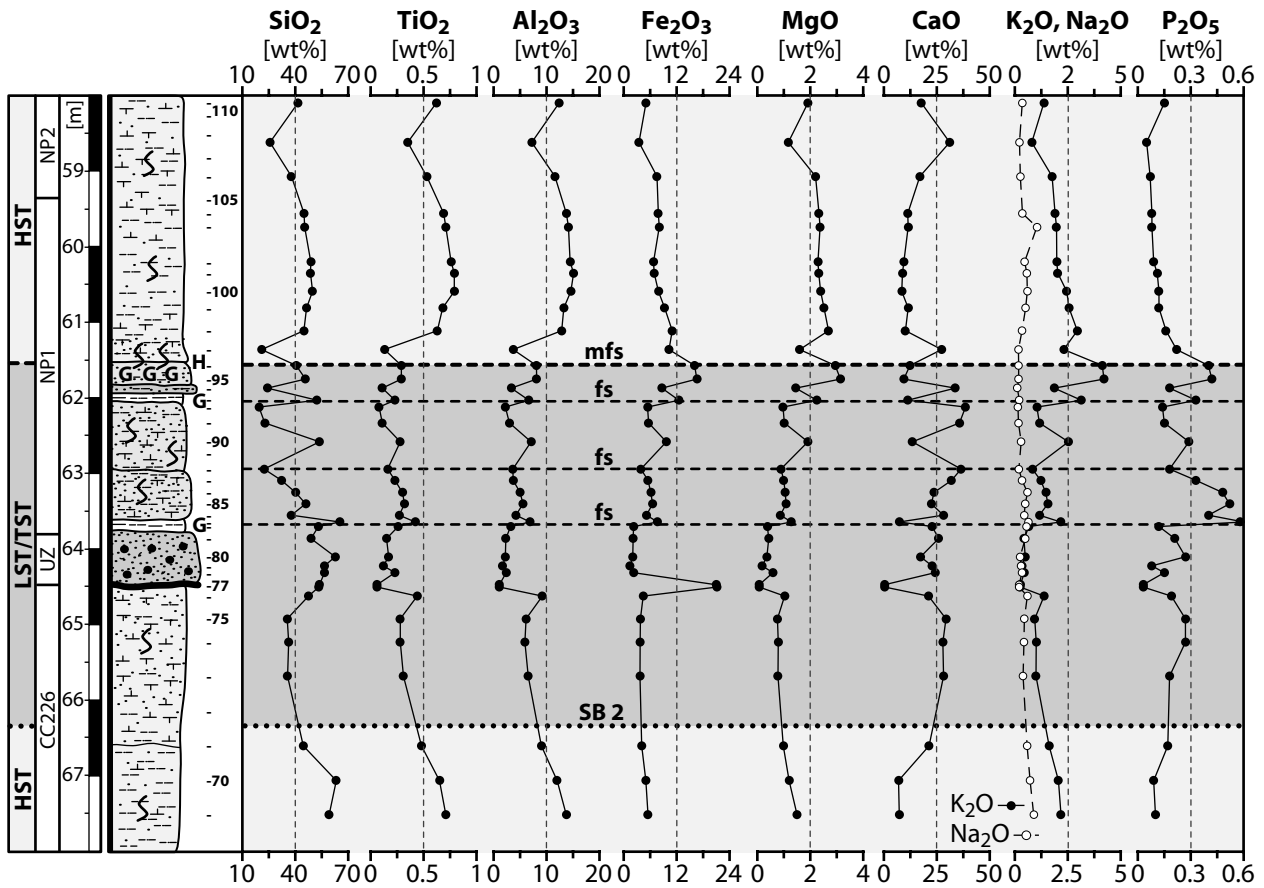
Figure 4.11B Major elements, determined by wavelength-dispersive X-ray fluorescence spectrometry (WDS) across the immediate K-P transition in the Antioch Church core (from 58-56 m in core depth). Grey shading added in order to ease distinction of lithologic trends. An explanation to the lithologic symbols is shown in Fig. 4.2 and the nannoplankton zonation and sequence stratigraphic interpretation (Fig. 4.3) is depicted to the left.

the limestones (e.g., TiO_2, Rb, and Ba), suggests a progressive dilution of the terrigenous fraction by carbonate during intervals of elevated biogenic productivity. These trends are substantiated by high correlation coefficients between the elements (including TiO_2, Fe_2O_3, K, Rb, and Zr) commonly bound to the terrigenous fraction, and CaO (see Table 4.2 and Fig. 4.10). However, Sr shows no significant correlation either with CaO or with TiO_2 (see Table 4.2), and therefore Sr appears to be incorporated in both fractions. The vertical stacking pattern of the shale-marl-limestone successions throughout the Antioch Church core reveals several prominent geochemical trends that are summarized below and shown in Fig. 4.9.

Sequence 1: A steady increase is recognized in the terrigenous fraction during the regressive highstand of the Prairie Bluff Formation (85.5-67 m) with minor superimposed element fluctuations: CaO decreases during this interval from 30 to about 10 wt%, whereas all other element concentrations, except Sr, generally increase.

Sequence 2: In the uppermost, transgressive part of the Prairie Bluff Formation, CaO concentrations abruptly increase up to peak values of 35 wt%, while elements linked with terrigeneous detritus decrease. This trend is punctuated by the cm-thick, pyritized base of the Clayton Sands that has extraordinary high abundances of Fe_2O_3 (>30 wt%), Cu, and As, whereas TiO_2, MnO, Sr, Zr, Zn, and Ba are significant lower than in the enclosing lithologies, and CaO is close to zero (<2 wt%). However, in this pyritized layer, no particular enrichments in Ni or Co (each <50 ppm), have been found in the Antioch Church core that are characteristic for the basal K-P boundary clay elsewhere and interpreted to indicate extraterrestrial-element influx (e.g., Schmitz, 1988, 1992). The overlying basal Clayton Sands are characterized by SiO_2 and CaO contents of ~50 and 25 wt%, respectively, and low amounts of all other major and trace elements, compared to the enclosing shales and limestones. Concomitant to the low amounts of Na_2O and K_2O, indicating scarcity of plagioclase or K-feldspar, these data sustain the initial petrograph-
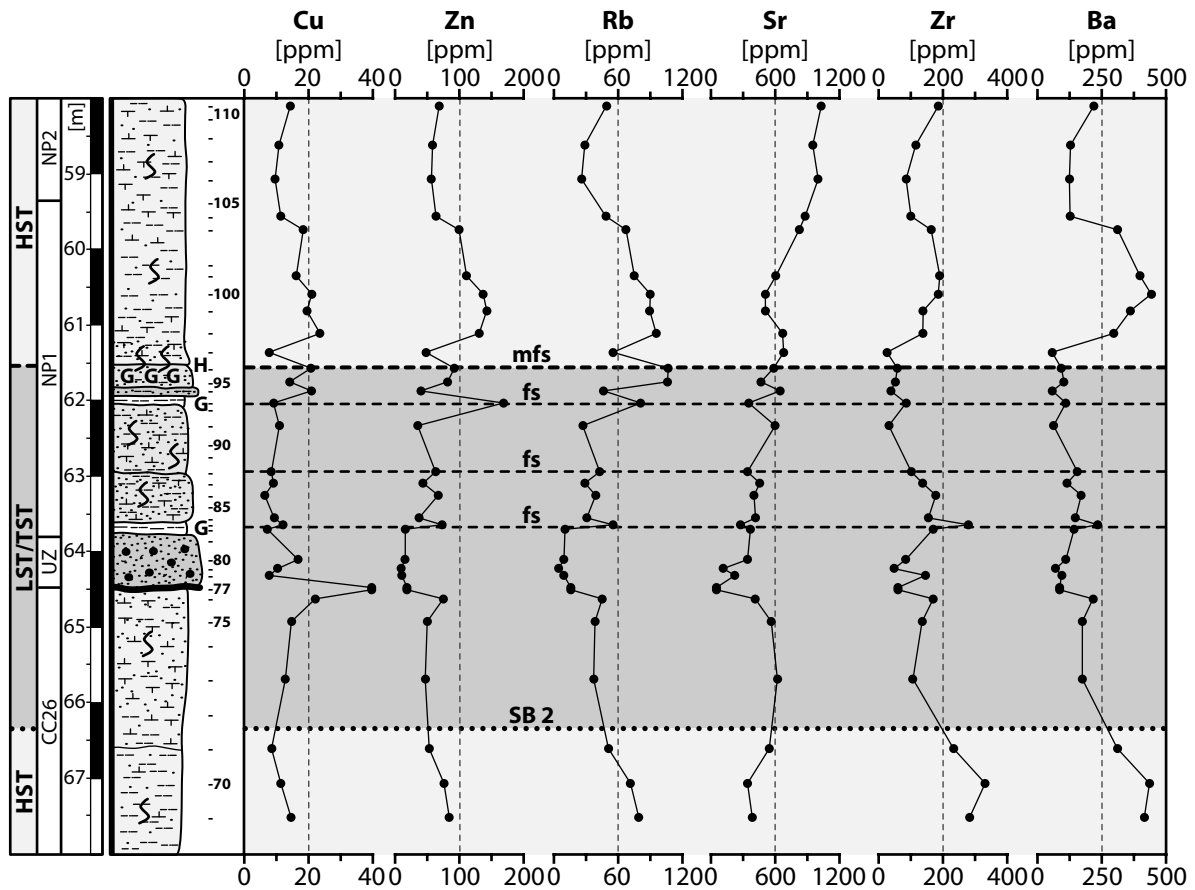
Figure 4.11C Trace elements Cu, Zn, Rb, Sr, Zr, and Ba, determined by energy-dispersive X-ray fluorescence spectrometry (EDS) across the immediate K-P transition in the Antioch Church core (from 58-56 m in core depth). Grey shading added in order to ease distinction of lithologic trends. An explanation to the lithologic symbols is shown in Fig. 4.2 and the nannoplankton zonation and sequence stratigraphic interpretation (Fig. 4.3) is depicted to the left.

ic designation of the basal Clayton Sands as almost 'pure' calcareous and quartzose sand.

In the transgressive interval above the basal Clayton Sands, element abundances switch immediately back to values comparable the latest Maastrichtian Prairie Bluff Formation, though some minor fluctuations occur: most notably phosphorus (~0.6 wt%) peaks and magnesium displays increasing values (from 0.8 to >2 wt%). At about 62 m, the drastic increase in glauconite at the during the condensed section and, particularly, at the maximum flooding surface, is reflected by strong abundance peaks of Fe_2O_3 (up to 15 wt%), K_2O (up to 4.5 wt%), MgO (~3 wt%), P_2O_5 (~0.5 wt%), and Rb (120 ppm), as well as by increased ratios of these elements versus aluminum.

Immediately above the surface of maximum starvation, reduced carbonate values and increased terrigeneous input followed by strong (cyclic?) fluctuations in the carbonate/detritus ratio mark the beginning highstand and parasequences. Notably, the Sr contents and the Sr/Ca ratios show peak values in the interval immediately above the maximum flooding

surface. Significant changes in the abundance of the geochemical phases occur in the uppermost part of the Pine Barren Member, where sediments have low carbonate contents (<10 wt%) and where high values of detrital elements, including TiO_2 (>0.8 wt%) and Zr (~500 ppm), indicate mainly terrigeneous input.

Sequence 3: In contrast to the underlying Pine Barren Member, the '*Turritella* Rock' is almost devoid of elements assigned to terrigeneous-derived minerals (except for quartz, as revealed by the thin-section analysis), and hence, is almost 'pure' quartzose sandstone in the basal 2 m, and sandy limestone in the topmost part. The hardground atop of this limestone package has enhanced Cu, As, and Zn concentrations, possibly indicative of condensed sedimentation, as well as temporary anoxic conditions during the flooding event recognized in the overlaying shales. The overlying highstand deposits reveal increased terrigeneous input and, for instance, Sr values are significantly elevated and reach peak values above 1000 ppm.

Sequence 4: This sequence is characterized by low fluctuations in the element abundances and a
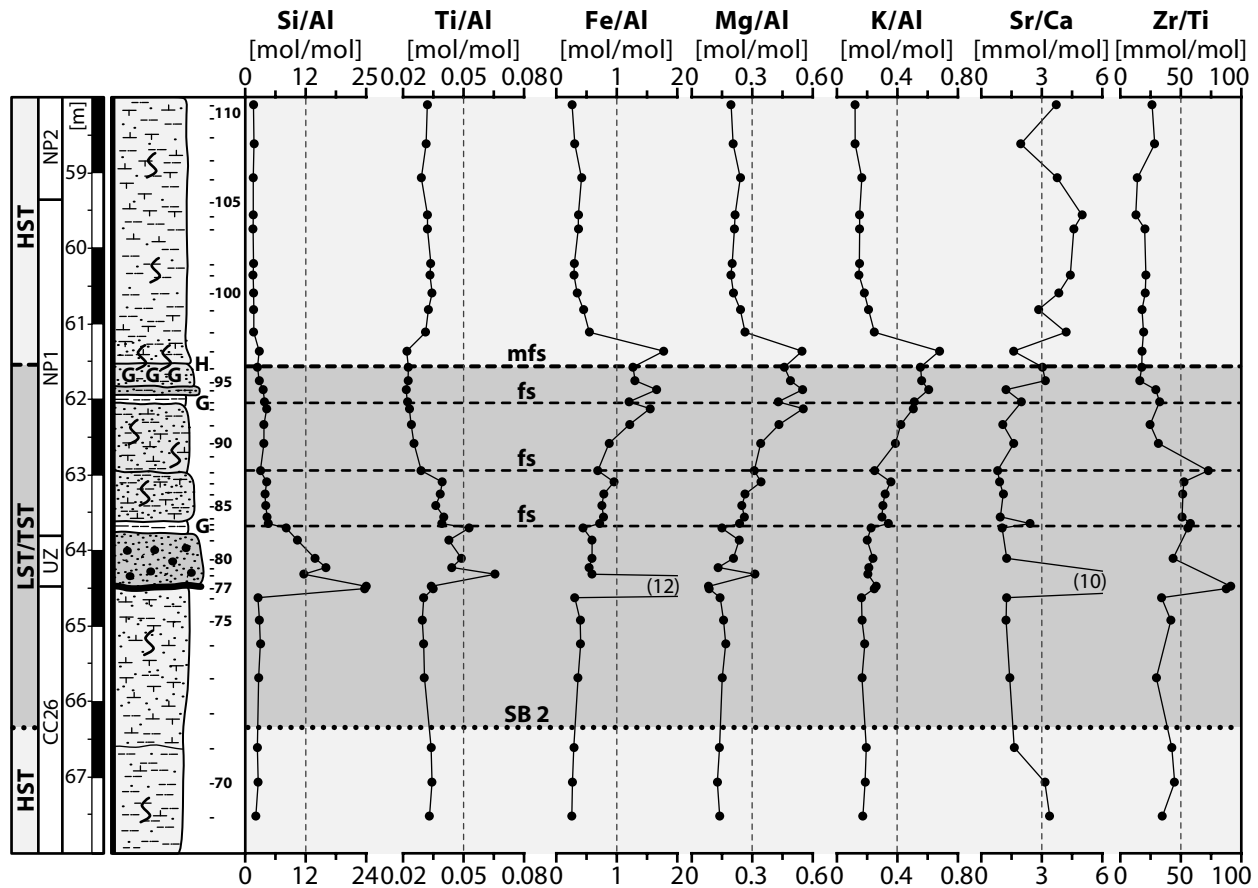
Figure 4.11D Ratios of selected major elements against Al and the Sr/Ca and Zr/Ti ratios across the immediate K-P transition in the Antioch Church core (from 58-56 m in core depth). Grey shading added in order to ease distinction of lithologic trends. An explanation to the lithologic symbols is shown in Fig. 4.2 and the nannoplankton zonation and sequence stratigraphic interpretation (Fig. 4.3) is depicted to the left.

steady high carbonate content; only the marls of the Naheola Formation show a significant increase in elements characteristic of terrigenous detritus.

Factor analysis

The results of the EDS analysis from selected major and trace elements were evaluated by principal factor analysis in order to give a qualitative discrimination between the different lithofacies of the Antioch Church core and to reveal constrains on the nature of the sedimentary source rocks and their variations throughout the time slice studied. Particularly, the transition from the siliciclastic-dominated lower part of the core (from the base up to the top of the Pine Barren Member) towards a carbonate-dominated upper part (incorporating the '*Turritella* Rock', the Porters Creek Formation and the McBryde Member) is of interest, since it is accompanied by a marked change in the clay mineral assemblage. Thus, factors were extracted for the total core (A in Table 4.2), as well as independently for the lower (B), and upper (C) part of the core, to monitor possible changes in the sediment source(s) or in the tectonic regime.

Since the matrix data is not considered to be normally distributed, the parameter-free Spearman rank correlation was used to calculate the principal factors. The pyritized red-layer at the base of the Clayton Sandstone was excluded from the sample set. The resulting factor loadings of selected major and trace elements for these intervals are shown in Table 4.2.

Interval A: Considering the entire Antioch Church core, Factor 1 accounts for 37 % of the relative variance, and generally reflects the opposite trend between the detrital continental input with high positive loadings for elements typically bound in minerals of terrigenous origin (TiO_2, Rb, Y, Zr, Ba), and carbonate-dominated biogenic sedimentation with high negative loadings for the carbonate component (CaO). Sr shows no or very weak loadings, pointing to its association with both, the detrital as well as the carbonate fraction. Factor 2 shows high positive loadings for TiO_2, Fe_2O_3, K_2O, Zn, and Rb, combined with negative loadings for CaO, for the whole core. Therefore, Factor 2 may reflect a possible second detritus source of different compo-

Table 4.2 Varimax rotated factor loadings of the principal component analysis from the Spearman rank correlation matrix with 130 samples and 12 variables of the Antioch Church core. Samples were taken from the energy-dispersive X-ray fluorescence spectrometry (EDS) presented in Appendix 4.2. The following intervals were analyzed: (A) the total bulk samples of the Antioch Church core, (B) the lower part, comprising the interval from 85.5-53.5 m in core depth, and (C) the upper part, comprising the interval from 35.5-1.8 m. *Italics*: factor loadings 0.5-0.6; **boldface**: factor loadings >0.6. The ferruginous layer at the base of the Clayton Sands has been excluded from the analysis.

Elements	(A) Total core			(B) Lower core (85.5-35.5 m)			(C) Upper core (35.5-1.8 m)		
Factor	1	2	3	1	2	3	1	2	3
TiO$_2$	**0.71**	*0.60*	0.31	**0.86**	0.46	0.11	*0.55*	0.39	**0.69**
Fe$_2$O$_3$	0.07	**1.00**	-0.08	*0.51*	-0.19	**0.84**	*0.58*	0.49	0.40
CaO	**-0.74**	*-0.50*	-0.18	**-0.64**	**-0.62**	-0.19	**-0.65**	-0.39	*-0.60*
K$_2$O	0.26	**0.80**	0.11	**0.70**	0.10	*0.56*	-0.16	0.15	**0.73**
Cu	0.24	0.44	0.36	**0.68**	-0.04	0.04	0.47	0.11	0.07
Zn	0.38	**0.76**	0.28	**0.82**	0.06	0.35	0.26	**0.68**	0.46
As	0.19	*0.56*	-0.30	0.05	0.20	**0.68**	**0.88**	0.05	-0.07
Rb	0.46	**0.84**	0.24	**0.86**	0.15	0.46	0.41	*0.58*	**0.66**
Sr	-0.09	0.02	0.38	0.10	-0.35	-0.21	0.21	0.12	**0.82**
Y	**0.76**	0.33	-0.09	0.41	**0.79**	0.14	0.08	**0.88**	0.04
Zr	**0.93**	0.14	-0.12	0.18	**0.95**	-0.06	*0.54*	0.45	0.31
Ba	**0.83**	0.34	0.38	**0.74**	*0.60*	-0.19	*0.55*	0.45	**0.61**
La	**0.81**	0.08	-0.18	0.09	**0.81**	-0.01	0.10	**0.83**	0.26
Ce	**0.88**	0.28	-0.21	0.22	**0.87**	0.12	0.38	**0.79**	0.21
Pb	**0.61**	0.44	0.28	**0.64**	0.37	-0.05	**0.61**	0.22	*0.59*
Expl. variance	5.52	4.59	0.96	4.97	4.27	1.99	3.49	3.94	3.80
Rel. variance	37 %	31 %	6 %	33 %	28 %	13 %	23 %	26 %	25 %

sition and probably more mafic character, compared to the source revealed by Factor 1. Factor 3 accounts for a variance of only 6 % and shows no pronounced factor loadings.

Interval B: In the siliciclastic-dominated lower part of the Antioch Church core, Factor 1 accounts for 33 % of the relative variance and again reflects the reciprocal relationships between terrigeneous (TiO$_2$, K$_2$O, Cu, Zn, Rb, Ba, and Pb) and biogenic sedimentation (CaO). Sr is again associated with both sedimentary fractions. Factor 2 explains 28 % of the variance and has high positive factor loadings for the elements Y, Zr, Ba, La, and Ce, and negative loadings for CaO, hence, the association with a second, more mafic detritus source is not as obvious as outlined for the whole core. Factor 3 accounts for 13 % of the variance) and reveals high positive loadings for Fe$_2$O$_3$, K$_2$O, and As and may be linked with high amounts of mica, particularly glauconite.

Interval C: The carbonate-dominated upper part of the Antioch Church core shows factor loadings, which are markedly different from the two previously explored intervals. For this part, all three factors account for a high degree of variance (23, 25, and 26 %, respectively). In addition, they show moderate positive loadings for elements bound to terrigeneous detritus (TiO$_2$, Fe$_2$O$_3$, Rb, Zr, Ba) and moderate negative factor loadings for CaO. In addi-

tion, Factor 1 has high positive loadings for As and Pb (though these elements are close to the detection limit), whereas Factor 2 reveals high positive loadings for Zn, Y, La, and Ce, and finally, Factor 3 shows high positive loadings for TiO$_2$, K$_2$O, Rb, Sr, Ba, and Pb.

4.3.6 Stable isotopes

Under ideal conditions, the ratio of the stable oxygen and carbon isotopes in 'pristine' marine carbonaceous sediments, revealed either from bulk rock or from fossil shells, may be a sensitive tool to monitor paleoenvironmental changes (e.g., Marshall, 1992; Shackleton et al., 1993; Veizer et al., 1997; Stoll and Schrag, 2000; Stüben et al., 2002). The oxygen isotopic composition of carbonate precipitated in equilibrium with ambient seawater is ultimately related to ocean temperature and global ice volume, whereas the carbon isotopic composition is primarily influenced by biological productivity and the rate of decay of organic matter (e.g., Faure, 1986). During diagenesis, however, primary (biogenic) calcite or aragonite can be dissolved and replaced with secondary calcite of different isotopic composition (Jenkyns et al., 1994; Marshall, 1992; Schrag et al., 1995; Mitchell et al., 1997). Particularly, oxygen isotopic values are prone to postdepositional alteration, which is reflected by lowering of initial oxygen

isotopic values, while carbon isotopic values are less affected by these effects. Indicators of diagenetic change are covariant $\delta^{18}O$ and $\delta^{13}C$ values, as well as covariant $\delta^{18}O$ and CaO values (Marshall, 1992; Mitchell et al., 1997).

For the Antioch Church core, the stable oxygen and carbon isotopic values of the sieved fine fraction ($<36\ \mu m$) display not only large amplitude variations (e.g., $\delta^{18}O$ between -4.5 to -0.5 ‰; $\delta^{13}C$ between -0.5 to $+2$ ‰) and/or significantly scatter throughout the cored interval (see Fig. 4.12, Appendix 4.4),
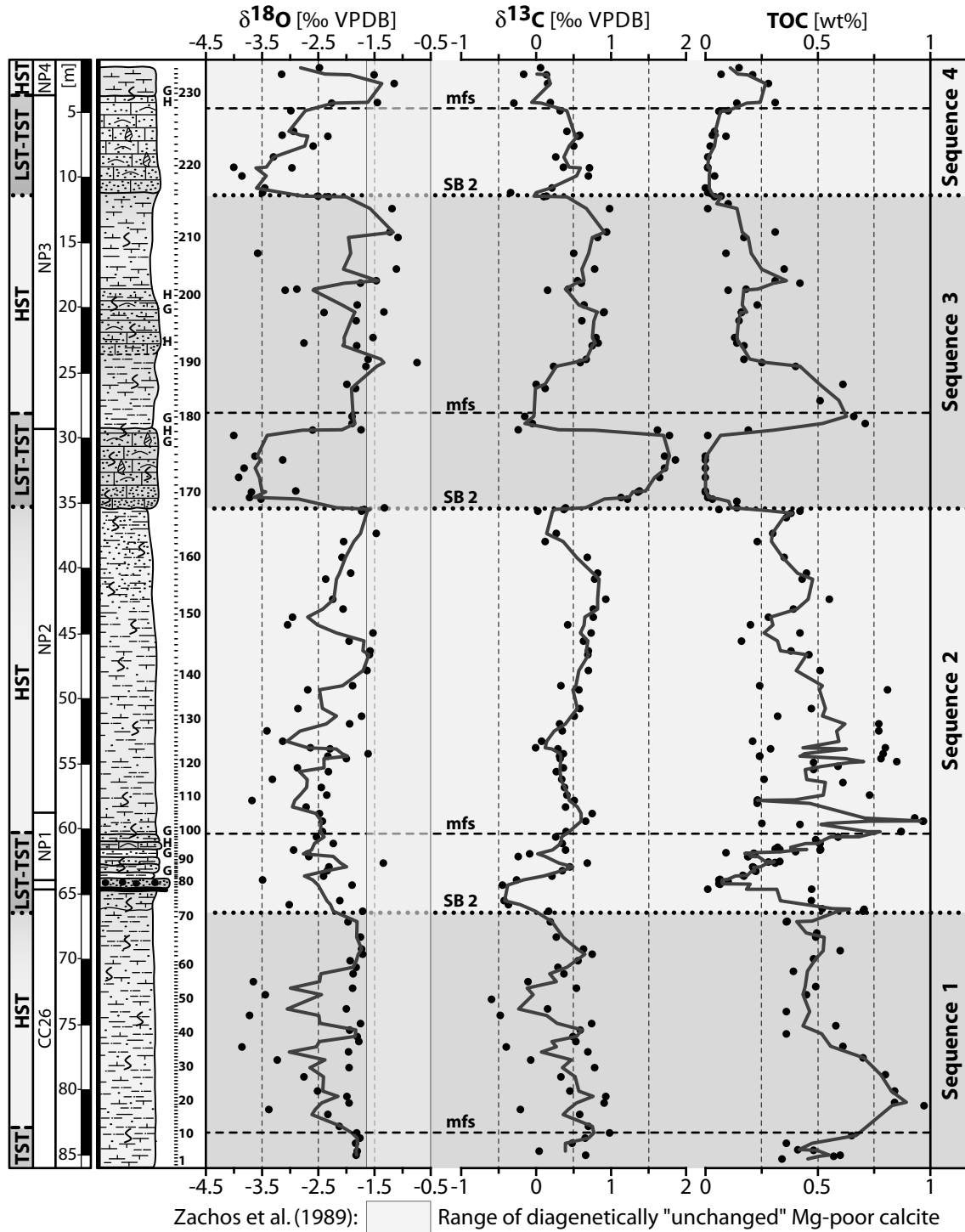
Figure 4.12 Graphical illustration of the results of the stable isotope data ($\delta^{13}C$ and $\delta^{18}O$) of carbonate fine fraction as well as the total organic carbon (TOC) from the Antioch Church core. The black dots show the original data and the grey curves give the three-point average. All δ values are given relative to the VPDB (Vienna Peedee belemnite) standard. The grey shaded area in the $\delta^{18}O$ plot gives the range of 'pristine' low Mg-calcite from mollusk shells revealed by Zachos et al. (1989a), which they considered as unaffected by diagenesis. Fig. 4.2 includes a legend to the lithologic symbols. The nannoplankton zonation and sequence stratigraphic interpretation (Fig. 4.3) is shown to the left.

but also the curve of the $\delta^{18}O$ values closely mirrors the curve of the carbonate content (compare Fig 4.9A and 4.12). Albeit a cross-plot of $\delta^{18}O$ and $\delta^{13}C$ values (not shown) from all samples analyzed shows no correlation (r = 0.02), distinct intervals of the Antioch Church core show a strong correlation between both isotope phases. Particularly, the more indurated and calcareous intervals show significant lighter $\delta^{18}O$ values than the shale intervals. These lighter values may represent variations in the paleoenvironment such as higher water temperature, probably during shallowing, and/or enhanced freshwater influx. Alternatively, these values may be an artifact of diagenesis or reflected a mixed signal of these factors. However, the very low $\delta^{18}O$ values are more likely explained by alteration because of the higher diagenetic potential of the limestones compared to the shales. The latter are less vulnerable to recrystallization because their clay content reduces porosity, whereas the former have been strongly recrystallized (aragonite dissolution), probably enhanced by meteoritic water during emersion above sea level (e.g., the "*Turritella* Rock").

Further support for diagenetic influx derives from comparison with literature data from the nearby Braggs section, for which Zachos et al. (1989) has shown that individual, not recrystallized mollusk shells have generally heavier $\delta^{18}O$ values in the range between –1 and –2 $\delta^{18}O$ (shown in Fig. 4.12). So, the excursions to light $\delta^{18}O$ values may represent diagenetically changed isotope values, since these light values would require rather unrealistic drops in temperature (see Zachos et al., 1989 for details). In summary, these isotope data suggest a strong diagenetic overprint, and consequently, no paleotemperature estimates from the stable oxygen isotope record of the Antioch Church core are given. However, according to Zachos et al. (1989) and Baum et al. (1994), some paleoenvironmental trends may be obtained from the isotope curves:

During the late Maastrichtian Prairie Bluff, curves of $\delta^{18}O$ and $\delta^{13}C$ have congruent trends, though both show large amplitude scattering between values of ±1 ‰: In the lower part of the Prairie Bluff, a gradual shift to lighter ratios occurs from about –2 to –2.8 ‰ $\delta^{18}O$ and +0.6 to –0.1 ‰ $\delta^{13}C$. A strong shift to heavier values of the ^{18}O and ^{13}C ratios (–2 and +0.6 ‰) is present in the upper part of the Prairie Bluff followed by a decrease up to the Clayton Sands, where smallest values for both isotope ratios are reached (–2.5 and +0.2 ‰). However, the strong negative $\delta^{13}C$ shift, commonly associated

with the K-P boundary (e.g., Lindinger, 1988; Kaiho et al., 1999; Stüben et al., 2002), is not recorded in the Antioch Church core; its absence was also demonstrated for the nearby Braggs section by Zachos et al. (1989). This lack is probably the result of a hiatus at the K-P transition, where sediments of the Biozone NP1 rest directly upon the Clayton sands.

Upsection from the basal Clayton Sands, $\delta^{18}O$ show fluctuating, but steadily decreasing values and, just above the maximum flooding surface, values of –2.8 ‰ are reached, whereas $\delta^{13}C$ shifts to heavier values (+0.8 ‰) during this interval. Throughout the Pine Barren Formation up to the base of the '*Turritella* Rock' $\delta^{18}O$ is fluctuating and shifts to heavier values (–1.8 ‰). In contrast, the $\delta^{13}C$ shows only slight variations and decreases just below '*Turritella* Rock' to +0.2 ‰.

The '*Turritella* Rock' is characterized by sharp and strong negative ($\delta^{18}O$) and positive ($\delta^{13}C$) shifts, with minimum and maximum values of –4 ‰ and +1.6 ‰, respectively. Atop of this limestone and at the transition to the shales of the Porters Creek Formation, both stable isotope ratios shift immediately back towards their former values in the upper Pine Barren Formation. This rapid and recursive shift of both isotopes is suggestive of strong diagenetic overprint (dissolution of shells, influx of meteoric waters), though the "warming" indicated by the low $\delta^{18}O$ values, as well as the increased productivity revealed by the high $\delta^{13}C$ ratios, is also in keeping with the strongly lowered sea-level during this interval. Similar trends of the isotope ratios, though with generally lower amplitudes are present in the during the McBryde Member of the Porters Creek Formation and the Matthews Landing marl, suggesting less pronounced changes in the depositional environment.

4.3.7 Total organic carbon

The TOC content reflects the quantity of organic matter and is associated with metabolic processes and the decay of plants and animals (e.g., De Leeuw et al., 1995), albeit organically bound hydrogen, sulphur, and nitrogen can contribute up to 50 % of the total sedimentary organic matter (Tissot and Welte, 1984). In immature samples, 1 wt% TOC usually corresponds to 1.5-2 wt% organic matter. The average organic carbon content of the sediments of the Antioch Church core is generally low and comprises about 0.5 wt% TOC for the siliciclastic-dominated Maastrichtian to middle Danian samples (sequence 1 and 2), whereas during the middle Danian, carbon-

ate-dominated part (sequence 3 and 4), the average is less than 0.1 wt% TOC (except for the highstand periods), hence considered as background noise, and indicating effective shutoff of terrigeneous input (Ricken, 1996). However, in the Antioch Church core, an elevated TOC content typically corresponds to the early highstand systems tract, with peak values at the maximum flooding surface, whereas lowest TOC values are associated with the lowstand systems tract and the late (regressive) highstand systems tract.

4.4 Interpretation and discussion

4.4.1 Sequence stratigraphic setting

In the first section of the discussion, a synoptic evaluation of the well-established sequence stratigraphic framework for central Alabama against the lithological and paleontological results, as well against the geochemical and clay mineralogical record of the Antioch Church core is provided and schematically depicted in Fig. 4.13.

Sequence 1

The first sequence, or to be more accurate, upper part of a sequence, comprises the Prairie Bluff Formation that is inferred to represent a highstand systems tract (Mancini et al., 1996). In the lowermost, more calcareous part of this sequence in the Antioch Church core, a diverse marine fauna, including planktic foraminifera, represent open-marine conditions (Fig. 4.13). According to Mancini et al. (1996 Fig. 10), this part of the Antioch Church core may be correlated to the maximum flooding surface in the Prairie Bluff Formation that is in the upper part of the *A. cymbiformis* Zone (CC25) or the lower part of the *M. murus* Zone (CC26). This maximum flooding surface and overlying highstand depositional systems tract of the Prairie Bluff Formation are recognized throughout central Alabama and eastern Mississippi (Mancini et al., 1996).

Further upsection, the sandy shales and marls of this sequence show a marked increase in the amounts of elements bound to terrigeneous minerals including TiO_2, K_2O, Rb, Zr, and Ba, as well as a decrease in carbonate (Figs. 4.3, 4.10). An increasingly shaley (or condensed) character is also revealed by the fore-stepping gamma log motif in the upper part of this sequence (Fig. 4.3). This increase in siliciclastic detritus upsection is coupled with reduced diversity in marine fossils and almost absence of planktic foraminifera, and culminates about 67-70 m in core depth. The latter interval may be interpreted as a distinct regressive phase, which is marked by very low CaO and Sr values. These strongly lowered Sr-values contrast with enhanced Zr values and may suggest increased winnowing of fine clayey particles and enrichment of residual minerals, probably resulting from enhanced current activity and winnowing during lowered sea level. In summary, these patterns suggest a general shallowing-upward trend during this (regressive) highstand systems tract, linked with a progradational facies development, and more pronounced input of terrigenous detritus.

Sequence 2

The second sequence comprises the uppermost part of the Prairie Bluff Formation, the basal Clayton Formation, and the Pine Barren Member of the Clayton Formation (Fig. 4.3 and Baum and Vail, 1988; Donovan et al., 1988; Mancini et al., 1989; Mancini and Tew, 1993). Its basal surface is about two meters below the basal Clayton Sands within the Prairie Bluff Formation and characterized by a sudden increase in grain-size of terrigeneous detritus and bioclasts, in carbonate content (10 to >30 wt%), and in fossil diversity, including the incursion of planktic foraminifera (Fig. 4.13). This drastic change is reflected also in a pronounced back-stepping gamma log motif (Fig. 4.3). In concert, these criteria suggest a change in the depositional environments to conditions that are more open-marine with reduced terrigeneous input, and therefore indicate the presence of a sequence boundary associated with a transgressive event (merging "SB" and "fs") and probably deepening (Figs. 4.3, 4.10).

This sequence boundary is classified as type-2 sequence boundary sensu Van Wagoner et al. (1988; 1990), since no evidence for subaerial exposure or fluviatile influx was observed. Accordingly, the basal part of this sequence is interpreted as transgressive systems tract. Though from the literature survey, no lithofacies evidence has been presented for a lowstand or transgressive event preceding the deposition of the basal Clayton Sands in Alabama, a similar lithological succession and gamma-ray log has been revealed for the nearby USGS Braggs core #1 (Donovan et al., 1988). Notably, evidence for a possible transgressive event, starting during the upper part of the *M. murus* Zone (CC26), well before the K-P boundary, has also been found at the Brazos cores, Texas (see Chapter 3), as well as in the

Western Atlantic coastal plain (ODP 174AX, Olsson et al., 2002).

This transgressive systems tract is punctuated by the basal Clayton Sands, which have long been considered as bar sands or incised valley fill deposits genetically linked to a sea-level lowstand (e.g., Baum and Vail, 1988; Donovan et al., 1988; Mancini et al., 1989; Mancini and Tew, 1993), alternatively, they have been interpreted as tsunami deposit associated with the Chicxulub impact (e.g., Olsson et al., 1996; Smit et al., 1996). In any case, within a sequence stratigraphic framework, the basal Clayton Sands are placed in a transgressive systems tract. However, the rocks below and above the Clayton Sands include marine fossils, and most importantly, planktic foraminifera and calcareous nannofossils indicative of open-marine conditions (see also Olsson and Liu, 1993). This may constrain the magnitude of facies changes in response to sea-level fluctuations and hence may suggest that sea level did not fall beyond the shelf break, though previous studies have concluded otherwise (e.g., Baum and Vail, 1988; Donovan et al., 1988).

Above the basal Clayton Sands, the lowermost part of the Pine Barren Member reveals a stacked set of thin fine-grained shale intervals (10 wt% CaO) enclosing dm-thick sandy and bioclast-rich marls (30 wt% CaO). In the geochemical record, as well as in the relative abundances of clay minerals, these 'shale-marl couplets' are reflected by rapid fluctuations: a stepped upsection-increase in TiO_2, and particularly in Fe_2O_3, K_2O, Rb, and Sr, associated with a significant increase in mica and TOC, reflects the increasing presence of authigenic mineral phases (e.g., glauconite) and organic matter (Figs. 4.8-11). This increase culminates about four meters above the base of the Clayton Sands, where strata consist of 50-75 % (!) glauconite grains. Above this glauconite layer (marked by a prominent peak in the gamma log), the glauconite content rapidly decreases and sediments become silty-sandy on the detriment of carbonate contents. Therefore, the shale intervals are here interpreted as flooding surfaces, each interval associated with a sudden decrease of detritus input in the overlying marls (Van Wagoner et al., 1988; 1990). These shale-marl couplets may be considered as parasequences that record slight variations in sediment input, distal-proximal setting, and/or relative sea level.

In summary, these lithofacies, mineralogical, and geochemical pattern mark a condensed interval bracketing a maximum flooding surface, which separates the transgressive systems tract below from the prograding highstand systems tract above and includes several parasequences (Fig. 4.13). An analogous pattern and about similar position of the maximum flooding surface during the upper part of the *M. inversus* Zone (NP1) has been observed in sections throughout Alabama (Baum and Vail, 1988; Donovan et al., 1988; Loutit et al., 1988; Van Wagoner et al., 1988; 1990).

The progradational highstand systems tract of sequence 2 is marked by enhanced siliciclastic input, starting immediately above the maximum flooding surface. Throughout the lower parts of the highstand, thin shale-marl-limestone couplets that are reflected by low-amplitude cycles in the gamma-ray log, suggest slight variations in detritus input versus carbonate productivity and may be interpreted as parasequences (Figs. 4.3, 4.11). Remarkably, the lower part of the highstand shows two distinct 'stacked' patterns of increasing Sr values (from 600 to 1200 ppm), which distinguishes this interval from the shales and marls of the upper part of the highstand systems tract that show significant lower Sr contents (about 300 ppm). An analogous arrangement of Sr abundance was found in the highstand systems tract of sequence 1.

In the upper part of the highstand systems tract, distinct trends include a reduction in carbonate content and progressively increasing terrigenous input. Specifically, the silty shale in the uppermost ten meters of the Pine Barren Member reveals a pronounced increase (almost doubling) in the amounts of elements typically bound in detrital minerals (TiO_2, Fe_2O_3, K_2O, Rb, and Ba; Fig. 4.10). The sharp decrease of the Sr contents in the uppermost meter, which correlates well with peak Zr values, and a prominent backstepping gamma log motif (>120 API), as well as with almost zero CaO content, marks a minimum in productivity and/or a maximum in detritus input (Figs. 4.3, 4.10). The distinct pattern of Sr and Zr abundances is related to low may suggest increased winnowing of fine clayey particles and enrichment of residual minerals, probably because of enhanced current activity during lowering of relative sea level. A significantly reduced productivity is also shown by the very low $\delta^{13}C$ values during this interval. Consequently, the uppermost shaley part of the Pine Barren Member of the Clayton Formation is interpreted as regressive highstand systems tract associated with a rapid seaward progradation of facies belts and suppression of biogenic carbonate formation (Van Wagoner et

al., 1988; 1990). A similar conclusion was drawn by Mancini et al. (1989), and Mancini and Tew (1993).

In conclusion, the sequence 2 includes a rapid transgressive event with low sedimentation rates during the K-P transition. The transgressive part is about 8 m thick and corresponds to Biozone NP1 with about 0.5 Ma in duration. In contrast, the subsequent highstand systems tract, which corresponds to Biozone NP2, is about 25 m thick and has a duration of 0.5-0.6 Ma, suggesting an almost threefold

increase of sedimentation rates, related to the progradational development of strata.

Sequence 3

The deposition of the 'Turritella Rock' records a pronounced change in the depositional mode, hydrodynamic regime, and mineralogical composition of the sediment. The basal part of the 'Turritella Rock' is dominated by poorly sorted quartz sand and fossil debris in a micritic matrix, whereas fine-
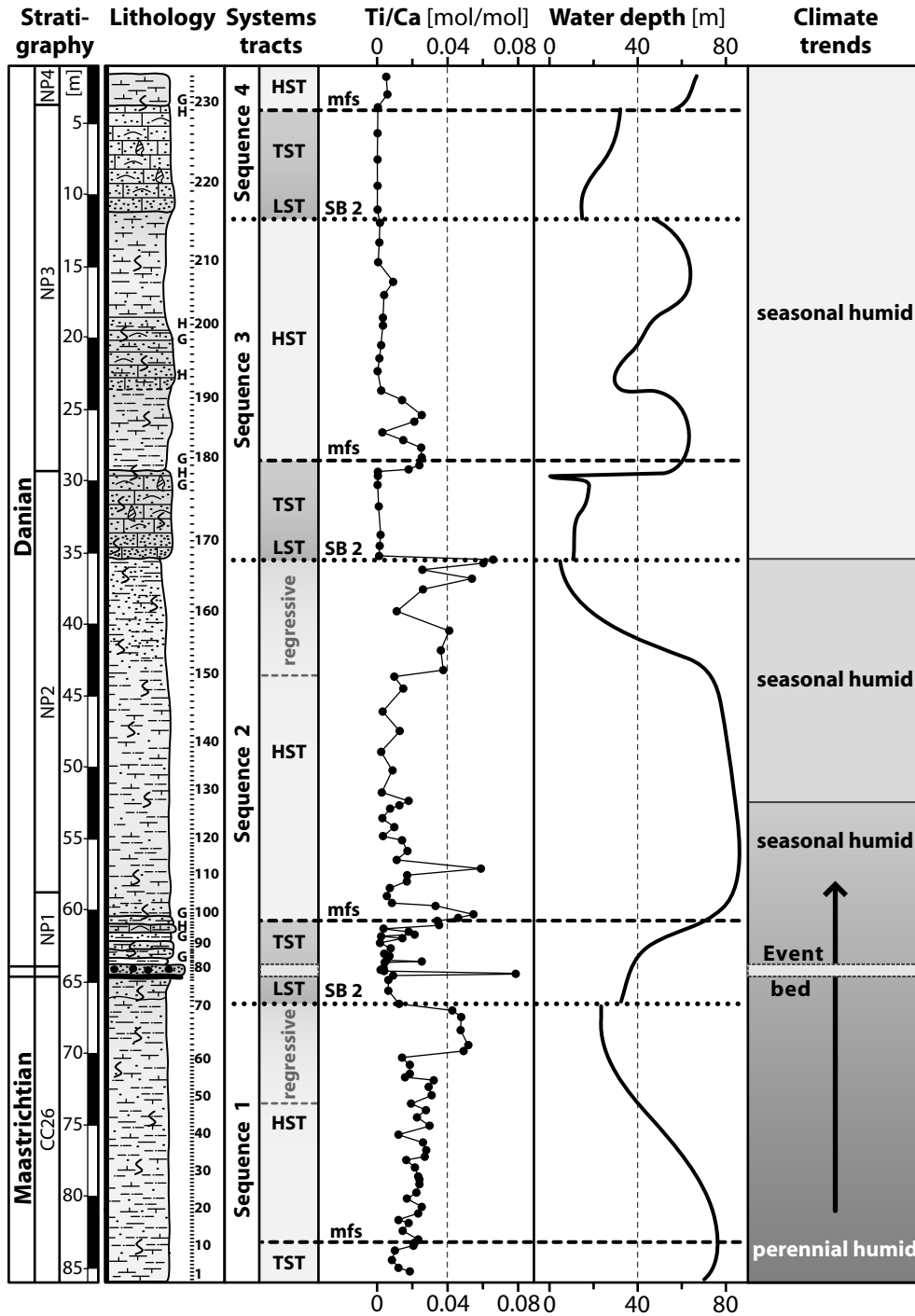
Figure 4.13 Summary diagram with facies trends, the derived sequence stratigraphic interpretation and sea-level history as well as paleoclimate trends from the clay mineralogical composition. A legend to the lithologic symbols is shown in Fig. 4.2. The nannoplankton zonation outlined in Fig. 4.3 is depicted to the left.

grained (clayey) terrigeneous detritus is considerably diminished as shown by very low abundances of Fe_2O_3, K_2O, and Rb, suggesting that the detritic component is made almost entirely of quartz. Therefore, an elevated energy regime is inferred during deposition the '*Turritella* Rock', compared to the underlying shales, which took place in conjunction with the abrupt shutoff of fine-grained terrigeneous detritus. In addition, the strong opposite shifts of the $\delta^{13}C$ and $\delta^{18}O$ values associated with the '*Turritella* Rock', as well as similar, though smaller shifts in the limestone intervals above, suggest strong warming (light $\delta^{18}O$ values), and the presence of surface waters with heavy $\delta^{13}C$ values (Kroopnick, 1980). This shallowing was probably associated with temporary emergence and influx of surface waters in the vadose zone, as also indicated by the petrologic studies (Fig. 4.7).

In summary, these observations provide good arguments to consider the base of the '*Turritella* Rock' as a type-2 sequence boundary, which is overlain by a lowstand and transgressive systems tract. An analogous conclusion was drawn by Mancini et al. (1989), and Mancini and Tew (1993), though the '*Turritella* Rock' was termed 'shelf margin systems tract' by these authors. The vertical sedimentary succession within this sand-limestone package also corroborates a 'transgressive' sea-level behavior, mainly owed to the upward increase in micrite and glauconite concurrent to a significant decrease in the quartz content (Fig. 4.7). Beginning with the onset of the '*Turritella* Rock' the sediment is entirely dominated by smectite and mica, whereas kaolinite is almost absent, which is in marked contrast to the more diverse clay mineral association immediately below. The dominance of fine-grained smectite and illite over coarser kaolinite suggests trapping of coarser detritus (kaolinite) in nearshore areas. Conditions of low detrital input may have also favored the *in-situ* growth of lathed smectite particles, as for instance observed in chalky marine sediments from France (Deconinck and Chamley, 1995). Alternatively, a marked change in the sediment input (provenance) took place, as outlined in the section on paleoclimate trends.

The limestones of the '*Turritella* Rock' are overlain by a shale interval that, on a first glance, corresponds in composition and abundance of petrological and geochemical phases to the shales immediately below these limestones (Figs. 4.9, 4.10). A closer look, however, shows small, but significant differences: The elevated Sr as well as markedly

reduced Zr concentrations suggest variations in the provenance of these shales, though elevated Sr may also be linked the slight productivity increase, since it is associated with both, the carbonate fraction and the detrital fraction of elements, as revealed by the factor analysis. A similar pattern of element abundances has been observed for the beginning of the highstand of sequence 2. Hence, such trace element patterns may be a characteristic feature that allows distinguishing the early highstand (high Sr >800 ppm, 'normal' Zr <200 ppm) from the late, regressive, highstand (low Sr <400 ppm, high Zr >300 ppm). In addition, the $\delta^{13}C$ and $\delta^{18}O$ shifts suddenly back to 'pre-*Turritella* Rock' values.

Baum and Vail (1988) have linked the more negative values of the carbon isotopes ratio above hardgrounds associated with condensed sections to the upward movement of the oxygen minimum during maximum rates of sea-level change. Therefore, an oxygen minimum zone may have encroached upon the outer shelf. An immediate switchback from heavy to light $\delta^{13}C$ values has been observed above the surface of maximum starvation for several limestone-shale sequences from Paleogene outcrops in the Alabama Gulf coast plain (Baum and Vail, 1988). Therefore, and in combination with the fore-stepping pattern of the gamma log response and maximum TOC values, this shale interval marks a condensed section bracketing a maximum flooding surface and hence the beginning of the highstand systems tract (Fig. 4.3, 4.12). This carbonate-rich interval is recognized throughout eastern and western Alabama (Mancini and Tew, 1993). It may demonstrate the initial establishment of a carbonate-dominated system overlying a siliciclastic-dominated system.

The marly limestones and marls of the McBryde Member show a similar succession of lithofacies when compared to the '*Turritella* Rock', suggesting a related pattern of basal sequence boundary, subsequent lowstand or transgressive systems tract, followed by a highstand systems tract (Figs. 4.3, 4.12). In this sequence, however, the lithofacies development, as well as the lower amplitudes of the gamma log readings, suggest that environmental changes are not as pronounced as in the sequence 3 below: The lowered fossil content, as compared to the '*Turritella* Rock', as well as the significantly smaller grain-size of the components, and increased amounts of silicic and clayey detritus in the upper part of the marly limestone interval, suggest less pronounced proximal-distal trends, and probably more open-marine conditions with lower energy of the hydraulic re-

gime, hence this 'sequence' is considered as a para-sequence.

Open-marine conditions are also indicated by the presence of nautiloids (*H. ulrichi*), and abundant planktic foraminifera in the marl intervals. Remarkably, the abundance of glaucony and other iron-rich minerals are significantly reduced, as well as the porosity. A flooding surface is recorded by a prominent peak in the gamma log atop of the limestone interval, as well as a peak in the TOC values, and occurred in conjunction with elevated planktic foraminiferal abundances.

Sequence 4

This sequence includes the Matthews Landing marls and the Naheola Formation. Again, the lithofacies succession of this sequence shows a pattern that is comparable to sequence 3 and 4, suggesting a recurring series of basal sequence boundary and subsequent transgressive systems tract followed by a highstand systems tract (Figs. 4.3, 4.12). However, some differences to the underlying sequences may be noted: Glauconite and pyrite are very rare in the limestones, and the porosity is significantly reduced (<5 %), suggesting conditions that are more open-marine during deposition of this limestone-marl sequence.

4.4.2 Sequence stacking patterns and magnitude of facies change

The maximum environmental shift during deposition of a sedimentary sequence, as identified from component lithofacies, defines the magnitude of the sedimentary sequence ("maximum shift of facies", see Yang and Kominz, 2002). This magnitude is an indicator of the maximum shoreline movement relative to a site and can be used to characterize a sequence to aid in its correlation, as well as to constrain the magnitude of related sea-level changes. In the Antioch Church core, the lithofacies switch between two 'end-member lithologies', namely, bioclastic, sandy limestone, and clayey shale (Fig. 4.3).

During the transgressive interval, progradational parasequences, composed of bioclastic packstone (e.g., '*Turritella* Rock') accumulated in middle to outer shelf settings, contemporaneously to the trapping of terrigeneous clastics in coastal facies of the inner shelf. The reduced input or even shutoff of terrigeneous detritus promoted carbonate production in the middle to outer shelf settings, which probably took place in isolated platforms mounts or bar-like mounds or shoals (see Fig. 12 in Yang and Kominz, 2002 for a well-illustrated example). These back-stepping, transgressive carbonate accumulations were eventually drowned and buried by shales of the condensed section when increased water depth hindered (macrofossil) carbonate productivity.

During the highstand systems tract, carbonate production dominated on the middle to outer shelf but was diluted by influx of terrigeneous detritus (clay and silt) and resulted in the accumulation of silty and marly carbonates. In the late regressive highstand, increased terrigeneous supply subdued largely carbonate productivity. Consequently, this pattern may be indicative of 'reciprocal' sedimentation, reflecting a marked 'partitioning' in the dominant sediment type and deposition style with respect to relative sea-level behavior (Southgate et al., 1993; Wright and Burchette, 1996). Studies of such mixed systems suggest that carbonate sedimentation prevails during relative sea-level rises and highstands, while siliciclastic sedimentation dominates during lowstands when carbonate production is largely shut down, an observation that is in keeping with the observations from the Antioch Church core.

Considering the magnitude of changes in the depositional environment of the Antioch Church core, lithofacies changes are mostly associated with shifts from inner-middle shelf to outer shelf settings (Fig. 4.13). The presence of vadose marine cements (and probably fungi associated with incipient soil formation) atop of the '*Turritella* Rock' (Fig. 4.7), suggests a brief interval of significant shoaling with temporary emersion. However, this evidence is restricted to this particular sequence in the Antioch Church core, and has not been observed in the sequences below and above (Fig. 4.13). In addition, there is no indication for estuarine or fluvially induced deposits in the Antioch Church core. The sandstone intervals (e.g., the basal Clayton Sands) generally contain marine fossils, as well as glaucony. Therefore, these sands are referred to as marine sands without associated evidence for subaerial shelf exposure (e.g., microkarstification), or estuarine-fluvial settings (e.g., rhythmic tidal bundles). On the other hand, evidence for water depth exceeding those typical of outer shelf deposits or even off-shelf deposits has not been found (Baum and Vail, 1988), and according to Mancini et al. (1989), and Mancini and Tew (1993), such deposits are not represented in the late Cretaceous to early Paleogene strata of central Alabama.

In conclusion, these observations suggest that changes of the depositional environment operated

for the most part within marine settings and, there, within a small lateral range. In absence of data from paleo-water depth proxies (e.g., benthic foraminifera), it is difficult to constrain absolute changes in water depth. Estimates may be derived, however, from the lithofacies in the Antioch Church core as schematically depicted in Fig. 4.13: in the sandy bioclastic limestones, fossils appear to be reworked from nearshore settings (e.g., algae) and the large grain size of the constituents suggests a high-energy environment, probably within storm wave base or within wave base (i.e., <25 m, Tucker and Wright, 1992). A position within storm wave base is particularly inferred for the 'Turritella Rock'. In contrast, condensed shale intervals with abundant planktic foraminifera and low energy regime, may have been deposited well beyond storm wave base, probably in a water depth about 60-80 m as inferred from studies at the nearby Braggs outcrop (Baum and Vail, 1988; Donovan et al., 1988; Olsson et al., 1996). For the silty shale intervals in the upper highstand systems tract, immediate below the sequence boundary, it is difficult to assign a distinct water depth range, though the poor macrofaunas and the sparse occurrence of planktic foraminifera may tentatively suggest a shallow water depth, in-between 20 to 40 m, which is in the range given by Olsson et al. (1996) for the upper part of the Prairie Bluff Formation at Millers Ferry. Therefore, changes in sea level appear to be in the range between 20 to 40 m for the lower, siliciclastic-dominated part of the Antioch Church core, whereas the upper, carbonate-dominated part 'suffered' from slightly higher magnitudes of sea-level changes, in the range between 40 to 60 m.

4.4.3 Regional and global correlation of sequences

Preconditions for the correlation of sequence boundaries and the succession of systems tracts between coeval marine sections are: (i) a precise identification of the corresponding sequence stratigraphic surfaces and (ii) a tight chronostratigraphic framework. Both criteria are, however, difficult to establish for most parts of the sedimentary record of the Antioch Church core because of:

(1) The different behavior of the sedimentary system in response to changes in proximity of the shoreline, detrital input, and/or paleobathymetry: In the siliciclastic-dominated basal part, the sedimentary system acts in a more 'robust' way, with a range of intermediate lithologies (e.g., marls), whereas the carbonate-dominated system shows, almost, a bimodal distribution of lithofacies. This has also been interpreted as 'reciprocal' sedimentary pattern as outlined above and documents the more rapid 'give-up' of these facies (Southgate et al., 1993; Strasser et al., 1999).

(2) According to examples from mixed carbonate-siliciclastic systems (e.g., Flood and Orme, 1988; Strasser et al., 1999; Sanders and Höfling, 2000; Yang and Kominz, 2002), carbonate-rich facies tend to occur in a diverse patch-like distributed pattern on the shelf ("compartmentalization"), with intermittent areas of mainly siliciclastic sedimentation. Hence, a vertical succession must be established within a regional framework to distinguish changes produced by local facies shifts from regional sea-level trends.

(3) The poor biostratigraphic control, particularly for the Maastrichtian and middle-late Danian part (exacerbated by the shallow water setting), makes it difficult to assign a biostratigraphic age to the enclosed sequence stratigraphic surfaces. Sequence stratigraphic surfaces occur either during nannofossil zones and/or coincide with first/last occurrences of zonal marker fossils. In addition, these sequence stratigraphic surfaces are often associated with an unconformity at which most likely a hiatus of unknown extension exists (even subaerial exposure). This problem was recognized by Baum and Vail (1988) and they concluded that a sequence boundary must not be dated at their upper shelf extension (i.e., the setting of the Antioch Church core), but rather in deeper marine settings at their 'correlative conformity', to obtain reliable age estimates.

(4) Flooding and maximum flooding 'surfaces' are difficult to tie to 'discrete' lithologic surfaces, but instead enclose a distinct (condensed) sedimentary interval, usually 10 to 40 cm in thickness. The same applies to the regressive intervals in the Antioch Church core, during which relative sea level was possibly lowest and terrigeneous input at maximum – these intervals have usually gradual transitions to the underlying deposits of the highstand – complicating the assignation of a point in time referred to as "lowstand".

This excursion highlights the problems in dating sequence stratigraphic surfaces in the shallow shelf setting of the Antioch Church core and consequently, it is difficult to assign particular biozone 'ages' to these surfaces. Despite these limitations, the succession of systems tracts, and hence sea-level behavior across distinct time lines may be compared with

trends in other sections enclosing the late Maastrichtian to late Danian period. Particularly, since the availability of many high-resolution lithostratigraphic studies with a detailed (bio-) stratigraphy, in combination with paleo proxies constraining water-depth (e.g., benthic foraminifera), makes the K-P transition an attractive subject to address sea-level fluctuations (see Table 4.1):

Prominent sequence stratigraphic studies include the Haq et al. (1987; 1988) cycle chart, which incorporates the detailed studies of Donovan et al. (1988) and Baum and Vail (Baum and Vail, 1988) for the late Maastrichtian to upper Danian interval in Alabama. This cycle chart was 'updated, refined and extended' by the comprehensive de Graciansky et al. (1998) study on European basins. In addition, Erikson and Pindell (1998) provided a detailed sequence stratigraphic study on from South America. In addition, several comprehensive studies also addressed and evaluated sea-level changes throughout the late Maastrichtian to Danian period, as summarized in Table 4.1, though only a few of these studies provided a sequence stratigraphic framework and/or evaluation of (local) paleo-water depth changes against (global) eustatic changes. Hence, one must bear in mind that the apparent lowering of 'relative' (local) sea level during a progradation may operate during 'constant' eustatic sea level (e.g., Miall and Miall, 2001).

Late Maastrichtian Biozone CC26: For the upper part of the late Maastrichtian Biozone CC26, the sequence chart provided by Haq et al. (1987; 1988), reveals one major lowstand at 66.3 Ma (Ma4) and another less pronounced lowstand at 65.4 Ma (Ma5) followed by a transgressive interval during the K-P transition. In the eustatic curve provided by Donovan et al. (1988), however, this succession of sequences was 'switched', giving a minor lowstand at 66.3 Ma (Ma4) and major lowstand at 65.4 Ma (Ma5). However, these results oppose the sequence chart compiled by Hardenbol and Robaszynski (1998), which includes one sequence boundary (Ma5, in the lower third of Biozone CC26) at 66.5 Ma, about 1.5 Ma before the K-P boundary. A sequence stratigraphy study from the Venezuela shelf, conducted by Erikson and Pindell (1998) has also shown only 'one' sequence boundary to occur in the middle Maastrichtian, about 2-3 Ma pre-K-P. Additional constrains were made by Keller and Stinnesbeck (1996): They suggested a major se-level lowstand some 100-200 ka pre K-P, associated with deposition of siliciclastic units in the Gulf of Mexico. However,

recent papers by these authors have readjusted their former interpretations and distinct sandstone units that have been interpreted as lowstand deposits in their earlier papers are now considered as significant younger (50 ka pre-K-P, see Stinnesbeck et al., 2001), though the data from other Tethyan sections that also show this sea-level lowstand have not changed (Pardo et al., 1996; Alegret et al., 2003).

The late Maastrichtian strata of the Antioch Church core reveal a distinct lowering of water depth during progradational highstand conditions associated with increased siliciclastic input. It is, however, not possible to give a reasonable 'timing' for this lowering of relative sea level, other than that it occurred somewhere during the upper part of Biozone CC26, because of the gradual development of these shallow depositional conditions across several meters in the Antioch Church core and in absence of the uppermost Maastrichtian Biozone CC26b. Therefore, this lowstand may have occurred during the interval from 500 to 300 ka preceding the K-P boundary.

K-P transition and early Danian: For the K-P transition and the early Danian, the Haq et al. (1987; 1988) sea-level chart shows a transgressive interval across the K-P boundary, in keeping with Keller and Stinnesbeck (1996), who implied a transgression across the K-P boundary, and further minor lowstands at 50 ka as well as 250 ka post-K-P, well within Biozone NP1. Studies by Erikson and Pindell (1998) in northern South America pointed to a minor lowstand extending across the K-P boundary, followed by gradually rising sea level in the early Danian, analogous to Hardenbol and Robaszynski (1998), who suggested a sea-level lowstand at the K-P boundary followed by two minor sequences in the early Danian, with sequence boundaries dated at 64.6 Ma (Da1; middle part of NP1), 64 Ma (Da2, middle part of NP2) (Neal and Hardenbol, 1998). The sediments of the Antioch Church core show strong evidence for a lowstand and/or transgressive trend across the K-P boundary, which culminated during the earliest Danian up to about 0.5 Ma post K-P (maximum flooding surface atop of Biozone NP1), and was followed by a highstand systems tract during Biozone NP2.

Middle to upper Danian: The sequence stratigraphy middle to upper Danian was compiled by Neal and Hardenbol (1998) and contained a sequence boundary at 63 Ma (Da3; middle part of NP3), and a sequence boundary in the upper Danian at 61.5 Ma (Da4; middle part of NP4). In contrast, the Haq et al. (1987; 1988) curve contains only one major low-

stand at 63 Ma, which corresponds approximately to the Da3 sequence boundary. In contrast, the middle and upper Danian strata in the Antioch Church core show several sea-level fluctuations (two sequence boundaries during this period, with more pronounced changes in the water depth than recorded in the early Danian sediments. However, a switch of the depositional system (from siliciclastic to carbonate dominated), and the different behavior of the sedimentary system in response to water depth or proximity changes make an evaluation difficult.

As a bottom line, it appears that the derivation of an affirmative 'global' curve is currently in 'flux' and, with the many closely spaced trends derived from the literature data for this period (Table 4.1), it would be possible to make a correlation of the sequence boundaries and sea-level trends derived from the Antioch Church core (and even for Alabama, see Mancini and Tew, 1993), with some of those proposed in these studies. Consequently, mo constrains for global correlation are inferred from the data obtained during this study.

4.4.4 Depositional nature of the K-P event bed

The basal Clayton Sands consists of a one-meter thick, moderately to poorly sorted, faintly normal graded sandstone body with a pyritized base that overlies the sandy marls of the uppermost Prairie Bluff Formation. Its upper part shows slight lamination, and bioturbation is not present. Therefore, this sandstone is interpreted to reflect rapid deposition under high-energy traction transport as debris flow with waning-flow conditions preserved at the laminated top (e.g., Mulder and Alexander, 2001). The absence of burrowing may be a sign of rapid deposition, as further shown by the poorly sorted nature, the rip-up clasts, and absence of erosionally amalgamated subunits. Successive events may have removed any burrowed zone at the top of this bed, but likelier, the whole bed may have been deposited in a very short time. These characteristics qualify this sandstone to be considered an 'event bed' (e.g., Einsele, 1998).

The pyrite-rich and ferruginous basal layer of the Clayton Sands is, with exception of the pyritized matrix, compositionally related to the carbonaceous sands above, but is totally devoid of carbonate or fossil tests. In addition, bulk rock X-ray diffractometry showed the additional presence of goethite and jarosite. Jarosite is a potassium-iron-sulfate that forms by oxidization of pyrite, which produces sulfuric acid that attacks illite and K-feldspar, and liber-

ates potassium (Moore and Reynolds, 1997). Jarosite is a weathering product of organic-rich black shales and mudstones. Therefore, the presence of these minerals may indicate increased organic matter associated with deposition of the sandstone and/or a subsequent period of anoxic conditions that both promoted the formation of pyrite. Suboxic or anoxic conditions may also be suggested by elevated Cu (40 ppm), As (300 ppm), and Pb (35 ppm) concentrations, compared to the enclosing lithologies (e.g., Leventhal, 1998; Nijenhuis et al., 1999). Remarkably, jarosite and goethite are a common component of the marine and terrestrial K-P boundary clay layer (e.g., Evans et al., 1994; Martínez-Ruiz et al., 1999; Tribovillard et al., 2000; Wdowiak et al., 2001). However, no increased amount of trace elements (e.g., Ni, Cr, Co) that may be linked to extraterrestrial influx was found (cf. iridium analysis of Donovan et al. 1988).

The Clayton Sandstone above this pyritized sand layer is nearly 'pure' quartzose and carbonaceous sand with a sparitic matrix and contains ejecta spherules, glauconite, and rare (tiny) planktic foraminifera, though fossil debris is rare. In addition, this unit is impoverished in fine-grained (clayey) siliciclastic detritus, as also revealed from geochemical analysis. This composition suggests derivation from shore-nearshore, shallow-water areas with concomitant admixture of ejecta-fallout material. During high-energy transport, winnowing may have been intense and led to the comprehensive removal of fine-grained detritus. Events capable of generating such deposits are usually storms or tsunamis, which may create intense offshore-directed backflows through buildup of water masses along the coast (Myrow and Southard, 1996; Einsele, 1998; Dawson and Shi, 2000). These strong backflow currents may transport large quantities of sand towards outer shelf areas.

The 'triggering' cause(s) of these events is, however, difficult to constrain from the limited data of a cored section. The presence of rare ejecta particles may suggest that deposition occurred subsequently to fallout deposition of ejecta material from the Chicxulub impact at the Yucatán peninsula in southern Mexico. In this context, and by analogy to other K-P boundary sections (Table 3.1), a smectite-enrichment has been observed, for instance for the Brazos K-P section (Chapter 3), as well as at several K-P boundary sections associated with ejecta fallout and spherules or microspherules (Tables 2.1, 3.5 and Smit, 1999; Bauluz et al., 2000; Ortega-Huertas et al., 2002; Koeberl and Martínez-Ruiz, 2003). For

the basal Clayton Sands, however, smectite authigenesis from a glassy progenitor is difficult to conclude from the mineralogical data and not supported by the sporadic occurrence of spherules. In addition, sandstone intervals within the Antioch Church core are often enriched in smectite compared to the enclosing lithologies (Fig. 4.9).

In summary, an origin by a brief depositional event is concluded for the basal Clayton Sands in the Antioch Church core, instead of aggradation during long periods. This interpretation is in line with observations from other K-P sections in the Gulf Coast plain of Alabama where the basal Clayton Sandstones have been considered as 'event deposits' associated with elevated current energies and deposition of chaotic boulder (>1 m in diameter!) beds (e.g., at Moscow Landing Habib et al., 1996; Olsson and Liu, 1993; Olsson et al., 1996; Smit et al., 1996). However, the proposed 'event character' of these sandstones does not concur with the sea-level lowstand or early transgressive phase during its deposition, which, to the contrary, may have even promoted generation of event beds during storms or tsunamis. The observations by Savrda (1993) in support of long-term deposition of the Clayton Sands in the Mussel Creek K-P section may be explained by the different nature of these sands in the Mussel Creek outcrop, compared to the Antioch Church core. Thin section analysis, as well as data from Savrda (1993), shows that these sandstones are highly micaceous, strongly bioturbated (about similar to Fig. 4.6E), and contain no ejecta material (e.g., spherules). Therefore, they may rather correspond to the bioturbated sandy limestones of the Clayton or Pine Barren Formation, which overly the Clayton Sands in the Antioch Church core.

The comparison to the Mussel Creek K-P section may also shed light on the problems for constraining the depositional nature of the K-P sections in Alabama: namely, that they show different lithological characteristics and even different depositional ages in different outcrops (see overview in Mancini et al., 1989; Mancini and Tew, 1993). Consequently, a 'unique' or 'single-event' origin for the K-P boundary deposits in Alabama appears to be not justified by the sedimentological data and a multitude of causes may be responsible for their origin (storms, tsunamis, sea-level fluctuations).

4.4.5 Inferences from clay mineral facies – Paleoclimate

The diversity of clay mineral assemblages identified in the sediments of the Antioch Church core may reflect either a detrital or a diagenetic origin. For that reason, evaluation of these clay mineral assemblages with respect to paleoenvironmental signals first requires investigation and assessment of diagenetic features. Particularly, because the clay facies of the Antioch Church core show a significant decrease of smectite with increased core depth (Fig. 4.9), an observation that may indicate enhanced diagenetic overprint with increased burial depth (Hower et al., 1976).

However, the sediments of the Antioch Church core did not suffer deep burial (at maximum several hundred meters) and there is no concomitant increase in illite-smectite, illite, and chlorite that each would indicate smectite transformation to chlorite and illite during burial diagenesis (Hower et al., 1976; Chamley, 1989). Moreover, a low burial diagenetic overprint throughout the Antioch Church core is documented by the co-existence of smectite with high kaolinite content. Since most of these clay minerals, including kaolinite, illite, and chlorite are not very sensitive to slight or moderate depths of burial (Chamley, 1989), and since clay minerals in the Alabama Gulf coast region were apparently not affected by volcano-hydrothermal activity, the clay mineral facies of the Antioch Church core are mainly considered to be detrital in origin, though minor smectite authigenesis may have occurred in sandy intervals (Fig. 4.9). The clay mineral assemblage therefore reflects processes taking place in their source area or processes associated with their transport path (Kübler, 1997).

Kaolinite

Kaolinite, and increasingly smectite upsection, dominates the late Maastrichtian to early Danian clay mineral assemblage of the Antioch Church core. At the base of the 'Turritella Rock', however, kaolinite disappears suddenly. Kaolinite formation requires intensive chemical weathering in soils of humid low-latitude regions, involving warm to tropical temperatures and high rates of water percolation through feldspar and other minerals in source rocks with high Si-Al content (Weaver, 1989; Chamley, 1989; 1997; Robert and Chamley, 1990). The percolation rate may be either resulting from a high gradient in the source area or high precipitation and under intensive, tropical weathering condition, kaolinite may form rapidly (within years). The sudden disappearance of kaolinite from values between 20 % to almost zero at the base of the 'Turritella Rock' may be related to changes in the current sys-

tem, switching of delta lobes or provenance, instead of climate changes in the hinterland. Alternatively, these changes may be related to a progressive landward shift of the shoreline and subsequent longer transportation paths, which both allowed preferred settling of the 'coarser' clay mineral fraction, i.e., kaolinite ahead of the 'finer' clay particles (smectite and mica). According to Chamley (1989), the augmentation of smectite abundance over kaolinite is frequently associated with offshore settings and transgressive periods.

Smectite

The origin of smectites is more controversial, and three main origins in marine deposits may be considered (i) submarine alteration of volcanic material, (ii) early diagenetic authigenesis, and (iii) reworking of exposed soils and sediments (Chamley, 1989; 1997; Deconinck and Chamley, 1995). Considering an origin from volcanic sources, the continuous high abundance of smectite throughout the core, (almost) independent from sequence stratigraphic setting or lithologic changes, would require a permanent high volcanism in this area for which there is no evidence in this passive continental margin setting. This argument is inline with the absence of any volcanic remains in the sediments of the Antioch Church core. Even the presence of zeolites is not exclusively associated with volcanic rocks (Deconinck and Chamley, 1995), but suggests some diagenesis through water-rock interaction in the uppermost part of the Antioch Church core. Therefore, at the present state, there is no convincing argument linking the smectite to volcanic activity. The very low detrital input in the limestone intervals (e.g., *Turritella* Rock'), may have favored the authigenetic formation of smectite particles, as for instance observed for pelagic basins (e.g., Deconinck and Chamley, 1995). However, high sedimentation rates and high water energy throughout these intervals provides counter arguments against a primary authigenic origin, and rather suggests that the smectites are inherited phases, though some augmentation of the smectite content owed to diagenetic effects cannot be excluded (e.g., Vanderaveroet and Deconinck, 1997). Smectite forms during chemical weathering in soils of warm climates, but it mainly develops in climates that have wet and dry seasons and that have less water percolation than needed for kaolinite formation (Chamley, 1989; 1997).

Mica

Micas usually derive by mainly physical weathering and erosion of a micaceous parent rock and are contributed as a less-altered detrital mineral from the existing bedrock or soils (Chamley, 1989; 1997). The high illite content throughout the Antioch Church core, which is elevated at condensed sections and maximum flooding surfaces, suggest relative proximity to the parent rocks, as also revealed by the non-rounded nature of the quartz detritus. However, some illite may be linked to authigenic processes (glauconitization) during times of reduced sedimentation, possibly associated with alternating oxic-anoxic conditions in the sediment (e.g., Amorosi, 1995; Vanderaveroet and Deconinck, 1997).

In conclusion, the clay mineral data show a change from kaolinite-dominated clay mineral assemblage to smectite-dominated facies (Fig. 4.13). This change started in the late Maastrichtian and gradually developed up to the middle Danian. The gradual nature of this change, almost independent of lithology and position in the sequence stratigraphic framework, suggests an inherited signal without larger influx of proximity to the shoreline. Therefore, this succession may be interpreted as a change from almost tropical climates with high year-round precipitation and percolation to subtropical to semiarid climates with lower precipitation, usually seasonal, and lower water percolation (Gibson et al., 2000). Following Gibson et al. (2000), such a climate change may also be associated with a general temperature decrease. However, the lack of detailed clay mineral as well as stable isotope studies from the Alabama Gulf coast province for this period prevents from evaluation of these climatic trends within a regional context. Such an evaluation and comparison could give evidence whether a shift in regional climates happened, or if these changes were associated with local changes in the depositional system.

Regional-global correlation

Reconstructions from paleomagnetic information places this region about 30° northern latitude (Hay et al., 1999) and therefore in middle subtropical climate belts during late Cretaceous times. Further constrains on the paleoclimate in the region of the Gulf of Mexico during the uppermost Cretaceous to early Paleocene comes from outcrops in the Difunta Group, northeastern Mexico. For this area, McBride (1974) has found evidence for sub-humid

Glossary: Definitions of sequence stratigraphic terms primarily used for siliciclastic depositional systems and criteria for their identification (Loutit et al., 1988; Van Wagoner et al., 1988; 1990; Erikson and Pindell, 1998; Miller et al., 1998; Catuneanu, 2002). Note that in carbonate-dominated depositional systems, the situation is complicated since the water depth of a given site may have little bearing on its proximity to the shoreline (e.g., Southgate et al., 1993).

Sequence stratigraphy and system tracts

The study of rock relationships within a time-stratigraphic framework of repetitive genetically linked strata bounded by surfaces of erosion or nondeposition, or their correlative conformity. A sequence is defined as a relative conformable succession of genetically linked strata bounded by unconformities or their correlative conformities. Systems tracts are a linkage of contemporaneous depositional systems, forming the subdivision of a sequence.

Relative sea level

Sea level defined qualitatively as with respect to the crust or some datum within the sedimentary succession, and inferred on this basis to control the space available for sediment to accumulate (accommodation). As such, this term accounts for the effects of eustasy, subsidence, and sediment supply.

Transgression/Regression

Landward/seaward/ movement of the shoreline, because of variations in sediment supply, sea level, and/or subsidence. Therefore, transgression and regression may be caused by processes other than sea-level changes.

Lowstand systems tract (LST)

It is bounded below by a sequence boundary and above by a transgressive surface. The lowstand unit has an assemblage of seaward building sediments. In shallow ramp settings, it is characterized by regression of the shoreline and by a forestepping (migrating basinward) to aggradational arrangement of sedimentary units. It forms during the early stage of base level rise when the rate of rise is outpaced by the sedimentation rate. This systems tract commonly includes the coarsest fraction of marine sections. It may be interpreted as representing deposition during a relatively lowstand of sea level, but this systems tract can be identified independent of any assumptions or inferences about sea level.

Transgressive systems tract (TST)

It is bounded below by a transgressive surface and above by a condensed interval (maximum flooding surface). The transgressive unit is characterized by transgression of the shoreline and by a backstepping (migrating landward) arrangement of sedimentary units. It may be interpreted as representing deposition during a relatively rapid sea-level rise, but the stratigraphic element can be identified independent of any assumptions or inferences about sea level.

Highstand or regressive systems tract (HST, RST)

It is bounded below by a condensed interval, and above by a sequence boundary. The highstand unit is characterized by progradation of the shoreline and by an aggradational to forestepping arrangement of sedimentary units. It may be interpreted as representing deposition during a relatively high stand of sea level, but this systems tract can be identified independent of any assumptions or inferences about sea level.

Condensed section

A thin marine stratigraphic interval characterized by very slow depositional rates, and typically associated with relatively deep-water sedimentation. Sediment starvation may be associated with a time of maximum flooding in nearshore areas. Specific attributes include: concentrations of pelagic organisms, burrowing, carbonate hardgrounds, and glauconite/phosphate.

Type 1 sequence boundary (subaerial unconformity)

Lithological discontinuity that is used as sequence boundary. It is a surface of erosion or nondeposition created during base level fall by subaerial processes such as fluvial incision, sediment bypass, or pedogenesis. It may be identified by: (i) a sharp increase in grain size (generally associated with incised valley deposition), (ii) a sharp increase of the inferred energy regime across the surface, (iii) an inferred basinward shift of facies, (iv) evidence of a progression or pattern within successive beds, (v) evidence of subaerial exposure, e.g., soil/root horizons, karst features, and (vi) lag deposits resting on the sequence boundary. Note that in shelf settings beyond the reach of subaerial unconformities, the primary indicator of a sequence boundary may be the basinward shift of facies and the increase in grain size.

Type 2 sequence boundary

Lithological discontinuity that is used as sequence boundary. It is a surface of erosion or nondeposition created during base level fall though in contrast to the type 1 sequence boundary, there is no evidence of fluvial incision, i.e., sea level did not fall below the shelf break. It may be identified by similar criteria as mentioned above, though without evidence of subaerial exposure. Note the difficulties in distinguishing type 1 and type 2 sequence boundaries in settings beyond the reach of subaerial unconformities.

Maximum flooding surface (mfs)

Lithological conformable discontinuity that is used as system tract boundary. It marks the end of shoreline transition; hence, this surface separates retrograding strata below from prograding strata above. It is generally associated with the condensed interval due to sediment starvation. This surface is placed at the top of a fining-upward (transgressive) succession and is characterized by burrows, marine cementation, and abundance of glaucony or phosphate in the strata enclosing the mfs, associated with a rich planktic and benthic fauna. It is marked by 'hot' intervals in the gamma-ray log.

Transgressive surface

Lithological discontinuities within systems tracts. This surfaces separates younger from older strata across which there is evidence of an abrupt increase in water depth. Criteria include (i) decrease/increase in grain size, (ii) increase in planktic organisms, and (iii) marked by a hardground.

to semi-arid climates with seasonal wet and dry periods (from the presence of palm leaves, caliche-like soils, iron-oxide rich red beds). These observations are agreeing with data from Lehmann (1989; 1990) for southern Texas who suggested that the climate in this region may have fluctuated between regimes of humid and semiarid character. Both studies are in keeping with the climate range shown by the clay mineral data of the Antioch Church core, though they provided no temporal framework to assess the regional climate variations over time.

Viewed in a global context, comparable clay mineral studies were conducted by Bolle and Adatte (2001) and Adatte et al. (2002a) on several sections in the southern to boreal Tethys. These clay mineral studies focused on the climate evolution during the late Cretaceous-early Paleocene and revealed a relatively uniform climate in the Tethyan with the dominance of warm, perennially wet conditions, which led to the formation of thick kaolinitic soils. However, distinct trends in the Tunisian sections across the K-P boundary included an increase for kaolinite throughout this interval, probably related to increased humidity (Adatte et al., 2002a). This trend was followed by a series of alternating warm humid and seasonal temperate climate during the early Danian. This culminating period of maximum humidity during the immediate K-P transition is not observed for the clay mineral assemblage of the Antioch Church core, which instead revealed a pronounced trend towards drier, more seasonal climates. A similar strong climate trend towards drier condition was, however, observed from the late Paleocene (>Biozone NP6) in the Tethyan realm, and climates became progressively more arid as documented by an increase in smectite and decrease in kaolinite (see Bolle and Adatte, 2001 with references).

4.5 Conclusions

Considering the results of this multidisciplinary investigation of the Antioch Church core, central Alabama, the following conclusions can be drawn on the nature of the Maastrichtian to Danian transition:

Sequence stratigraphic setting

(1) In the sediments of the Antioch Church core, a trend is recognized from a siliciclastic-dominated depositional system in the late Maastrichtian-early Danian, to a carbonate-dominated depositional system during the middle Danian. This change may be related to the establishment of a stable carbonate

platform on the Alabama shelf during the early Paleocene, as shown by Mancini et al. (1993).

(2) Four depositional sequences, or parts of sequences, were distinguished in the mixed carbonate and siliciclastic sediments of the Antioch Church core for the late Maastrichtian to middle Danian period. In this mixed depositional system on the Alabama shelf, siliciclastic sedimentation dominated during the late (regressive) highstand and subsequent lowstand systems tract, when carbonate production was largely shut down, and carbonate sedimentation prevailed during the transgressive and the early highstand systems tract, when terrigeneous detritus was mostly trapped in nearshore areas. This vertical stacking pattern is known as "reciprocal sedimentation" (Southgate et al., 1993).

(3) The vertical succession of component lithofacies suggests that the 'magnitude' of relative sea-level changes was largest during the middle Danian sequences (temporal emergence), whereas magnitudes are less pronounced during the late Maastrichtian-early Danian and the upper Danian sequences.

(4) The changes in terrigeneous input and energy-level during a sequence are reflected by characteristic changes in the major and trace element composition, as well as in the TOC content of the sediments. Along with the gamma-ray log response, these changes allow for a detailed internal subdivision of the depositional sequence. Particularly, it was found that shales of the late (regressive) highstand and shales of the condensed section bracketing the maximum flooding surface are distinguished by a negative correlated pattern of characteristic Sr and Zr abundances.

(5) The lithofacies, paleoecology of fossils, and characteristic abundance pattern of geochemical phases during each systems tract, suggest that these sequences formed during variations in relative water depth, and hence, are not the (exclusive) product of variations in terrigeneous supply.

Clay minerals and paleoclimate

(1) Clay minerals of the Antioch Church core comprise mainly varying proportions of smectite, kaolinite, and illite. Three distinct clay mineral facies were distinguished: (i) a kaolinite-dominated facies with a general upward increase in the relative abundance of smectite concomitant to a relative decrease in kaolinite, (ii) a kaolinite-smectite-rich facies, and (iii) a smectite-illite-dominated facies. The latter facies was established at the transition to

a carbonate-dominated sedimentary system (top of Biozone NP3).

(2) The general trends in clay mineral abundances are not exclusively related to lithological changes, though minor compositional changes occur (i) at lithologic transitions (e.g., sand-rich strata show elevated smectite contents) and (ii) coincident to sequence stratigraphic surfaces. Hence, the compositional variations in the clay mineral assemblages likely resulted mainly from paleoclimate variations in the source area, and to a minor degree from the position relative to the coastline. This climate change may have included a change from humid conditions with year-round precipitation to semi-arid climates with pronounced seasonality.

K-P event bed

(1) At, or close to the K-P boundary, a siliciclastic 'event bed' (basal Clayton Sands) is intercalated within a transgressive systems tract and contains rare ejecta-particles (spherules) that are morphologically similar to ejecta from the Chicxulub impact found in K-P sections from the Gulf of Mexico area, the Western Atlantic, the Pacific, and the K-P boundary clay in Northern America (Western Interior).

(2) The depositional nature of the 'K-P event bed' and its precise age is difficult to constrain from the Antioch Church core, and tsunami- or storm-triggered mechanisms are possible. However, these depositional mechanisms operated during lowered sea level within a transgressive systems tract.

4.6 References

Adatte T, Keller G, Stinnesbeck W (2002a) Late Cretaceous to early Paleocene climate and sea-level fluctuations: The Tunisian record. *Palaeogeogr Palaeoclimatol Palaeoecol* **178**(3-4): 165-196.

Adatte T, Keller G, Burns S, Stoykova KH, Ivanov MI, Vangelov D, Kramar U, Stüben D (2002b) Paleoenvironment across the Cretaceous-Tertiary transition in eastern Bulgaria. In: Koeberl C, MacLeod KG (eds) Catastrophic events and mass extinctions: Impacts and beyond. *Geol Soc Am Spec Pap* **356**: 231-252.

Alegret L, Molina E, Thomas E (2003) Benthic foraminiferal turnover across the Cretaceous/Paleogene boundary at Agost (southeastern Spain): Paleoenvironmental inferences. *Mar Micropaleontol* **48**(3-4): 251-279.

Alonso Zarza AM, Sanz ME, Calvo JP, Estevez P (1999) Calcified root cells in Miocene pedogenic carbonates of the Madrid Basin: Evidence for the origin of *Microcodium* b. *Sediment Geol* **116**(1-2): 81-97.

Alvarez LW, Alvarez W, Asaro F, Michel HV (1980) Extraterrestrial cause for the Cretaceous-Tertiary extinction. *Science* **208**: 1095-1108.

Amorosi A (1995) Glaucony and sequence stratigraphy: A conceptual framework of distribution in siliciclastic sequences. *Jour Sediment Res* **B65**(4): 419-425.

Aubry M-P (1991) Sequence stratigraphy: Eustasy or tectonic imprint? *Jour Geophys Res* **96**(4): 6641-6679.

Austin JA, Christie-Blick N, Malone MJ (1998) Initial reports of Leg 174A. Proceedings Ocean Drilling Program. *Initial Reports* **174A**: 1-147.

Bauluz B, Peacor DR, Elliott WC (2000) Coexisting altered glass and Fe/Ni oxides at the Cretaceous/Tertiary boundary, Stevns Klint (Denmark): Direct evidence of meteorite impact. *Earth Planet Sci Lett* **182**: 127-136.

Baum GR, Vail PR (1988) Sequence stratigraphic concepts applied to Paleogene outcrops, Gulf and Atlantic basins. In: Wilgus CK, Hastings BS, Kendall CG et al. (eds) Sea-level changes: An integrated approach. *Soc Econ Paleont Miner Spec Pub* **42**: 309-327.

Baum JS, Baum GR, Thompson PR, Humphrey JD (1994) Stable isotopic evidence for relative and eustatic sea-level changes in Eocene to Oligocene carbonates, Baldwin County, Alabama. *Geol Soc Am Bull* **106**(6): 824-839.

Béllon AS, Mosser C, Roquin C, Pardo ES (1994) Geochemical characterization of sedimentary basins by statistical analysis: The Mio-Pliocene sequences of the Vera Basin, SE Spain. *Chem Geol* **116**(2): 229-243.

Bengtsson H, Stevens RL (1998) Source and grain-size influences upon the clay mineral distribution in the Skagerrak and northern Kattegat. *Clay Miner* **33**(1): 3-13.

Berggren WA, Kent DV, Swisher CC, Aubry M-P (1995) A revised Cenozoic geochronology and chronostratigraphy. In: Berggren WA, Kent DV, Aubry M-P et al. (eds) Geochronology, time scales, and global stratigraphic correlation. *Soc Econ Paleont Miner Spec Pub* **54**: 129-212.

Bohor BF (1996) A sediment gravity flow hypothesis for siliciclastic units at the K/T boundary, northeastern Mexico. In: Ryder G, Fastovsky D, Gartner S (eds) The Cretaceous-Tertiary boundary event and other catastrophes in Earth history. *Geol Soc Am Spec Pap* **307**: 183-195.

Bohor BF, Glass BP (1995) Origin and diagenesis of K/T impact spherules – From Haiti to Wyoming and beyond. *Meteoritics* **30**: 182-198.

Bohor BF, Triplehorn DM, Nichols DJ, Millard HTJ (1987) Dinosaurs, spherules, and the "magic" layer: A new K-T boundary clay site in Wyoming. *Geology* **15**(10): 896-899.

Bolle M-P, Adatte T (2001) Paleocene-early Eocene climatic evolution in the Tethyan realm: Clay mineral evidence. *Clay Miner* **36**: 249-261.

Bourgeois J, Hansen TA, Wiberg P, Kauffman EG (1988) A tsunami deposit at the Cretaceous-Tertiary boundary in Texas. *Science* **141**: 567-570.

Catuneanu O (2002) Sequence stratigraphy of clastic systems: Concepts, merits, and pitfalls. *Jour South Afr Earth Sci* **35**(1): 1-43.

Chamley H (1989) Clay sedimentology. Springer, Heidelberg: 1-623.

Chamley H (1997) Clay mineral sedimentation in the ocean. In: Paquet H, Clauer N (eds) Soils and sediments. Springer, Heidelberg: 269-302.

Christie-Blick N (1991) Onlap, offlap, and the origin of unconformity-bounded depositional sequences. *Mar Geol* **97**(1-2): 35-56.

Cowie JW, Zieger W, Remane J (1989) Stratigraphic Commission accelerates progress, 1984-1989. *Episodes* **12**(2): 79-83.

Davidoff AJ, Yancey TE (1993) Eustatic cyclicity in the Paleocene and Eocene: Data from the Brazos River valley, Texas. *Tectonophysics* **222**(3-4): 371-395.

Dawson AG, Shi S (2000) Tsunami deposits. *Pure App Geophys* **157**(6-8): 875-897.

de Graciansky P-C, Hardenbol J, Jacquin T, Vail PR (1998) Mesozoic and Cenozoic sequence stratigraphy of European basins. *Soc Econ Paleont Miner Spec Pub* **60**: 786.

De Leeuw JW, Frewin NL, Van Bergen PF, Sinninghe Damsté JS, Collinsin ME (1995) Organic carbon as a palaeoenvironmental indicator in the marine realm. In: Bosence DWJ, Allison PA (eds) Marine palaeoenvironmental analysis from fossils. *Geol Soc Lond Spec Pub* **83**: 43-71.

Deconinck JF, Chamley H (1995) Diversity of smectite origins in Late Cretaceous sediments: Example of chalks from northern France. *Clay Miner* **30**(4): 365-379.

Dewey JF, Pitman WC (1998) Sea-level changes: Mechanisms, magnitudes and rates. In: Pindell JL, Drake CL (eds) Paleogeographic evolution and non-glacial eustasy, northern South America. *Soc Econ Paleont Miner Spec Pub* **58**: 1-16.

Donovan AD, Baum GR, Blechschmidt GL, Loutit TS, Pflum CE, Vail PR (1988) Sequence stratigraphic setting of the Cretaceous-Tertiary boundary in central Alabama. In: Wilgus CK, Hastings BS, Kendall CG et al. (eds) Sea-level changes: An integrated approach. *Soc Econ Paleont Miner Spec Pub* **42**: 299-307.

Ehrmann WU, Melles M, Kuhm G, Grobe H (1992) Significance of clay mineral assemblages in the Antarctic Ocean. *Mar Geol* **107**: 149-173.

Einsele G (1998) Event stratigraphy: Recognition and interpretation of sedimentary event horizons. In: Doyle P, Bennet M (eds) Unlocking the stratigraphical record: Advances in modern stratigraphy. John Wiley & Sons, New York: 145-194.

Erikson JP, Pindell JL (1998) Sequence stratigraphy and relative sea-level history of the Cretaceous to Eocene passive margin of northeastern Venezuela and the possible tectonic and eustatic causes of stratigraphic development. In: Pindell JL, Drake CL (eds) Paleogeographic evolution and non-glacial eustasy, northern South America. *Soc Econ Paleont Miner Spec Pub* **58**: 261-281.

Evans NJ, Gregoire DC, Goodfellow WD, Miles N, Veizer J (1994) The Cretaceous-Tertiary fireball layer, ejecta layer and coal seam: Platinum-group element content and mineralogy of size fractions. *Meteoritics* **29**(2): 223-235.

Faure G (1986) Principles of isotope geology. John Wiley & Sons, New York: 1-589.

Flood PG, Orme GR (1988) Mixed siliciclastic/carbonate sediments of the northern Great Barrier Reef Province, Australia. In: Doyle LJ, Roberts HH (eds) Carbonate – clastic transitions. *Developments in sedimentology* **42**. Elsevier, Amsterdam: 175-205.

Fralick PW, Kronberg BI (1997) Geochemical discrimination of clastic sedimentary rock sources. *Sediment Geol* **113**(1-2): 111-124.

Galloway WE (1989a) Genetic stratigraphic sequences in basin analysis I: Architecture and genesis of flooding-surface bounded depositional units. *Am Ass Petrol Geol Bull* **73**(2): 125-142.

Galloway WE (1989b) Genetic stratigraphic sequences in basin analysis II: Application to Northwest Gulf of Mexico Cenozoic basin. *Am Ass Petrol Geol Bull* **73**(2): 143-154.

Galloway WE, Ganey-Curry PE, Li X, Buffler RT (2000) Cenozoic depositional history of the Gulf of Mexico basin. *Am Ass Petrol Geol Bull* **84**(11): 1743-1774.

Garcia D, Pascal ML, Roux J (1996) Hydrothermal replacement of feldspars in igneous enclaves of the Velay granite and the genesis of myrmekites. *Europ Jour Mineral* **8**: 703-717.

Gardin S (2002) Late Maastrichtian to early Danian calcareous nannofossils at Elles (Northwest Tunisia): A tale of one million years across the K/T boundary. *Palaeogeogr Palaeoclimatol Palaeoecol* **178**(3-4): 211-231.

Gardin S, Monechi S (1998) Paleoecological change in middle to low latitude calcareous nannoplankton at the Cretaceous/Tertiary boundary. *Bull Soc Géol Fr* **169**(5): 709-723.

Gartner S (1996) Calcareous nannofossils at the Cretaceous-Tertiary boundary. In: MacLeod N, Keller G (eds) Cretaceous-Tertiary boundary mass extinction: Biotic and environmental changes. Norton Press, New York: 27-48.

Gartner S, Jiang MJ (1985) The Cretaceous/Tertiary boundary in east-central Texas. *Gulf Coast Ass Geol Soc Transact* **35**: 373-380.

Gibson TG, Bybell LM, Mason DB (2000) Stratigraphic and climatic implications of clay mineral changes around the Paleocene/Eocene boundary of the northeastern US margin. *Sediment Geol* **134**: 65-92.

Habib D, Moshkovitz S, Kramer C (1992) Dinoflagellate and calcareous nannofossil response to sea-level change in Cretaceous-Tertiary boundary sections. *Geology* **20**(2): 165-168.

Habib D, Olsson RK, Liu C, Moshkovitz S (1996) High-resolution biostratigraphy of sea-level low, biotic extinction, and chaotic sedimentation at the Cretaceous-Tertiary boundary in Alabama, north of the Chicxulub crater. In: Ryder G, Fastovsky D, Gartner S (eds) The Cretaceous-Tertiary boundary event and other catastrophes in Earth history. *Geol Soc Am Spec Pap* **307**: 243-252.

Hallam A (1992) Phanerozoic sea level changes. Columbia University Press, New York: 1-266.

Hallam A, Wignall PB (1999) Mass extinctions and sea-level changes. *Earth-Sci Rev* **48**(3-4): 217-250.

Hansen TA, Farrand RB, Montgomery HA, Billman HG, Blechschmidt GL (1987) Sedimentology and extinction patterns across the Cretaceous-Tertiary boundary interval in east Texas. *Cretaceous Res* **8**(3): 229-252.

Haq BU, Hardenbol J, Vail PR (1987) Chronology of fluctuating sea levels since the Triassic. *Science* **235**: 1156-1167.

Haq BU, Hardenbol J, Vail PR (1988) Mesozoic and Cenozoic chronostratigraphy and cycles of sea-level change. In: Wilgus CK, Hastings BS, Kendall CG et al. (eds) Sea-level changes: An integrated approach. *Soc Econ Paleont Miner Spec Pub* **42**: 71-108.

Hardenbol J, Robaszynski F (1998) Introduction to the Upper Cretaceous. In: de Graciansky P-C, Hardenbol J, Jacquin T et al. (eds) Mesozoic and cenozoic sequence stratigraphy of European basins. *Soc Econ Paleont Miner Spec Pub* **60**: 329-332.

Hargrove DC, Engelhardt DW (1997) Palynology of the Maastrichtian/Danian boundary at Savannah River Site, South Carolina. *Sediment Geol* **108**(1-4): 121-140.

Hay WW, DeConto RM, Wold CN, Wilson KM, Voigt S, Schulz M, Wold AR, Dullo WC, Ronov AB, Balukhovsky AN, Soeding E (1999) Alternative global Cretaceous paleogeography. In: Barrera E, Johnson CC (eds) Evolution of the Cretaceous ocean-climate system. *Geol Soc Am Spec Pap* **332**: 1-47.

Hesselbo SP (1996) Spectral gamma-ray logs in relation to clay mineralogy and sequence stratigraphy, Cenozoic of the Atlantic margin, offshore New Jersey. Proceedings of the Ocean Drilling Program. *Scientific Results* **150**: 411-422.

Hildebrand AR, Penfield GT, Kring DA, Pilkington M, Camargo AZ, Jacobsen SB, Boynton WV (1991) Chicxulub Crater: A possible Cretaceous/Tertiary boundary impact crater on the Yucatán peninsula, Mexico. *Geology* **19**(9): 867-871.

Holmes AE, Christie-Blick N (1993) Origin of sedimentary cycles in mixed siliciclastic systems: An example from the Canning Basin, Western Australia. In: Loucks RG, Sarg JF (eds) Carbonate sequence stratigraphy: Recent developments and applications. *Am Ass Petrol Geol Mem* **57**: 181-212.

Hower JC, Eslinger E, Hower ME, Perry EA (1976) Mechanism of burial metamorphism of argillaceous sediment: 1. Mineralogical and chemical evidence. *Geol Soc Am Bull* **87**(5): 725-737.

Immenhauser A, Schlager W, Burns SJ, Scott RW, Geel T, Lehmann J, van der Gaast S, Bolder-Schrijver LJA (1999) Late Aptian to late Albian sea-level fluctuations constrained by geochemical and biological evidence (Nahr Umr Formation, Oman). *Jour Sediment Res* **69**(2): 434-446.

Izett GA (1990) The Cretaceous/Tertiary boundary interval, Ration basin, Colorado and New Mexico, and its content of shock-metamorphosed minerals: Evidence relevant to the K/T boundary impact-extinction event. *Geol Soc Am Spec Pap* **249**: 1-100.

Jarvis I, Murphy AM, Gale AS (2001) Geochemistry of pelagic and hemipelagic carbonates: Criteria for identifying systems tracts and sea-level change. *Jour Geol Soc Lond* **158**(4): 685-696.

Jeans CV, Long D, Hall MA, Bland DJ, Cornford C (1991) The geochemistry of the Plenus Marls at Dover, England: Evidence of fluctuating oceanographic conditions and of glacial control during the development of the Cenomanian-Turonian $\delta^{13}C$ anomaly. *Geol Mag* **128**(6): 603-632.

Jenkyns HC, Gale AS, Corfield RM (1994) Carbon- and oxygen-isotope stratigraphy of the English Chalk and Italian Scaglia and its palaeoclimatic significance. *Geol Mag* **131**(1): 1-34.

Jervey MT (1988) Quantitative geological modeling of siliciclastic rock sequences and their seismic expression. In: Wilgus CK, Hastings BS, Kendall CG et al. (eds) Sea-level changes: An integrated approach. *Soc Econ Paleont Miner Spec Pub* **42**: 47-69.

Johnson KR (2002) Megaflora of the Hell Creek and lower Fort Union Formations in the western Dakotas: Vegetational response to climate change, the Cretaceous-Tertiary boundary event, and rapid marine transgression. In: Hartman JH, Johnson KR, Nichols DJ (eds) The Hell Creek Formation and the Cretaceous-Tertiary boundary in the northern Great Plains – An integrated continental record of the end of the Cretaceous. *Geol Soc Am Spec Pap* **361**: 329-392.

Jones DS, Mueller PA, Bryan JR, Dobson JP, Channell JET, Zachos JC, Arthur MA (1987) Biotic, geochemical and paleomagnetic changes across the Cretaceous/Tertiary boundary at Braggs, Alabama. *Geology* **15**(4): 311-315.

Kaiho K, Kajiwara Y, Tazaki K, Ueshima M, Takeda N, Kawahata H, Arinobu T, Ishiwatari R, Hirai A, Lamolda MA (1999) Oceanic primary productivity and dissolved oxygen levels at the Cretaceous-Tertiary boundary: Their decrease, subsequent warming, and recovery. *Paleoceanography* **14**(4): 511-524.

Kastner M (2003) Oceanic minerals: Their origin, nature of their environment, and significance. *Proc Natl Acad Sci* **96**(7): 3380-3387.

Keller G (1992) Paleoecologic response of Tethyan benthic foraminifera to the Cretaceous-Tertiary boundary transition. In: Takayanagi Y, Saito T (eds) Studies in benthic foraminifera. Tokai University Press, Tokio: 77-91.

Keller G, Stinnesbeck W (1996) Sea-level changes, clastic deposits, and megatsunamis across the Cretaceous-Tertiary boundary. In: MacLeod N, Keller G (eds) Cretaceous-Tertiary boundary mass extinction: Biotic and environmental changes. Norton Press, New York: 415-450.

Keller G, Adatte T, Stinnesbeck W, Stüben D, Kramar U, Berner Z, Li L, von Salis Perch-Nielsen K (1998) The Cretaceous-Tertiary transition on the shallow Saharan Platform of southern Tunisia. *Geobios* **30**(7): 951-975.

Kiessling W, Claeys P (2001) A geographic database approach to the KT boundary. In: Buffetaut E, Koeberl C (eds) Geological and biological effects of impact events. *Impact Studies.* Springer, Heidelberg: 83-140.

Koeberl C, Martínez-Ruiz F (2003) The stratigraphic record of impact events – A short overview. In: Koeberl C, Martínez-Ruiz F (eds) Impact markers in the stratigraphic record. *Impact studies.* Springer, Heidelberg: 1-40.

Kramar U (1997) Advances in energy-dispersive X-ray fluorescence. *Jour Geochem Exploit* **58**: 73-80.

Kroopnick P (1980) The distribution of ^{13}C in the Atlantic Ocean. *Earth Planet Sci Lett* **49**: 469-484.

Kübler B (1997) Concomitant alteration of clay minerals and organic matter during burial diagenesis. In: Paquet H, Clauer N (eds) Soils and sediments. Springer, Heidelberg: 327-362.

Langford FF, Blanc-Valleron M-M (1990) Interpreting Rock-Eval pyrolysis data using graphs of pyrolizable hydrocarbons vs. total organic carbon. *Am Ass Petrol Geol Bull* **74**(6): 799-804.

Lehmann TM (1989) Upper Cretaceous (Maastrichtian) Paleosols in Trans-Pecos Texas. *Geol Soc Am Bull* **101**(2): 188-203.

Lehmann TM (1990) Paleosols and the Cretaceous/Tertiary transition in the Big Bend region of Texas. *Geology* **18**(4): 362-364.

Leventhal JS (1998) Metal-rich black shales: Formation, economic geology and environmental considerations. In: Schieber J, Zimmerle W, Sethi PS (eds) Shales and mudstones: II, Petrography, petrophysics, geochemistry, and economic geology. Schweizerbart, Stuttgart: 255-282.

Li L, Keller G, Adatte T, Stinnesbeck W (2000) Late Cretaceous sea level changes in Tunisia: A multi-disciplinary approach. *Jour Geol Soc Lond* **157**: 447-458.

Lindinger M (1988) The Cretaceous/Tertiary boundaries of El Kef and Caravaca: Sedimentological, geochemical, and clay mineralogical aspects. *PhD Thesis*, ETH Zürich: 1-253.

Longman MW (1980) Carbonate diagenetic textures from nearsurface diagenetic environments. *Am Ass Petrol Geol Bull* **64**(4): 461-487.

Loutit TS, Hardenbol J, Vail PR, Baum GR (1988) Condensed sections: The key to age determination and correlation of continental margin sequences. In: Wilgus CK, Hastings BS, Kendall CG et al. (eds) Sea-level changes: An integrated approach. *Soc Econ Paleont Miner Spec Pub* **42**: 183-213.

MacLeod N, Rawson PF, Forey PL, Banner FT et al. (1997) The Cretaceous-Tertiary biotic transition. *Jour Geol Soc Lond* **154**(2): 265-292.

Mai H, Speijer RP, Schulte P (2003) Calcareous index nannofossils (coccoliths) of the earliest Paleocene originated in the late Maastrichtian. *Micropaleontology* **49**(2): 189-195.

Mancini EA, Tew BH (1993) Eustasy versus subsidence: Lower Paleocene depositional sequences from southern Alabama, eastern Gulf Coastal Plain. *Geol Soc Am Bull* **105**(1): 3-17.

Mancini EA, Tew BH, Smith CC (1989) Cretaceous-Tertiary contact, Mississippi and Alabama. *Jour Foraminif Res* **19**(2): 93-104.

Mancini EA, Puckett TM, Tew BH (1996) Integrated biostratigraphic and sequence stratigraphic framework for Upper Cretaceous strata of the eastern Gulf Coastal Plain, USA. *Cretaceous Res* **17**(6): 645-669.

Marshall JD (1992) Climatic and oceanographic isotopic signals from the carbonate rock record and their preservation. *Geol Mag* **129**(2): 143-160.

Martínez-Ruiz F, Ortega-Huertas M, Palomo-Delgado I (1999) Positive Eu anomaly development during diagenesis of the K/T boundary ejecta layer in the Agost section (SE Spain): Implications for trace-element remobilization. *Terra Nova* **11**(6): 290-296.

Martini E (1971) Standard Tertiary and Quaternary calcareous nannoplankton zonation. In: Farinacci A (ed) Second International Planktonic Conference Proceedings. Technoscienza, Rome: 739-785.

Maurrasse FJ, Sen G (1991) Impacts, tsunamis, and the Haitian Cretaceous-Tertiary boundary layer. *Science* **252**: 1690-1693.

McBride EF (1974) Significance of color in red, green, purple, olive, brown and gray beds of Difunta Group, northeastern Mexico. *Jour Sediment Petrol* **44**(3): 760-773.

McManus J, Berelson WM, Klinkhammer GP, Johnson KS et al. (1998) Geochemistry of barium in marine sediments: Implications for its use as a paleoproxy. *Geochim Cosmochim Acta* **62**(21-22): 3453-3473.

Miall AD (1991) Stratigraphic sequences and their chronostratigraphic correlation. *Jour Sediment Petrol* **61**(4): 497-505.

Miall AD (1992) Exxon global chart: An event for every occasion? *Geology* **20**(9): 787-790.

Miall AD (1997) The geology of stratigraphic sequences. Springer, Heidelberg: 1-433.

Miall AD, Miall CE (2001) Sequence stratigraphy as a scientific enterprise: The evolution and persistence of conflicting paradigms. *Earth-Sci Rev* **54**(4): 321-348.

Miller KG, Browning JV, Pekar SF, Sugarman PJ (1997) Cenozoic evolution of the New Jersey coastal plain: Changes in sea level, tectonics, and sediment supply. Proceedings of the Ocean Drilling Program. *Scientific Results* **150X**: 361-373.

Miller KG, Mountain GS, Browning JV, Kominz MA, Sugarman PJ, Christie-Blick N, Katz ME, Wright JD (1998) Cenozoic global sea level, sequences, and the New Jersey transect: Results from coastal plain and continental slope drilling. *Rev Geophys* **36**(4): 569-601.

Miller KG, Wright JD, Sugarman PJ, Browning JV, Kominz MA, Hernández JC, Olsson RK, Feigenson MD, Sickel WV (2003) Late Cretaceous chronology of large, rapid sea-level changes: Glacioeustasy during the greenhouse world. *Geology* **31**(7): 585–588.

Mitchell SF, Ball JD, Crowley SF, Marshall JD, Paul CRC, Veltkamp CJ, Samir AM (1997) Isotope data from Cretaceous chalks and foraminifera: Environmental or diagenetic signals? *Geology* **25**(8): 691-694.

Moore DM, Reynolds RC (1997) X-ray diffraction and the identification and analysis of clay minerals. Oxford University Press, Oxford: 1-378.

Moshkovitz S, Habib D (1993) Calcareous nannofossil and dinoflagellate stratigraphy of the Cretaceous-Tertiary boundary, Alabama and Georgia. *Micropaleontology* **39**(2): 167-191.

Mulder T, Alexander J (2001) The physical character of subaqueous sedimentary density flows and their deposits. *Sedimentology* **48**(2): 269-299.

Müller J, Oberhänsli H, Melles M, Schwab M, Rachold V, Hubberten H-W (2001) Late Pliocene sedimentation in Lake Baikal: Implications for climatic and tectonic change in SE Siberia. *Palaeogeogr Palaeoclimatol Palaeoecol* **174**(4): 305-326.

Murray RW, Leinen M (1993) Chemical transport to the seafloor of the equatorial Pacific Ocean across a latitudinal transect at 135°W: Tracking sedimentary major, trace and rare earth element fluxes at the Equator and the Intertropical Convergence Zone. *Geochim Cosmochim Acta* **57**(21): 4141-4163.

Myrow PM, Southard JB (1996) Tempestite deposition. *Jour Sediment Res* **66**(5): 861-866.

Neal JE, Hardenbol J (1998) Introduction to the Paleogene. In: de Graciansky P-C, Hardenbol J, Jacquin T et al. (eds) Mesozoic and Cenozoic sequence stratigraphy of European basins. *Soc Econ Paleont Miner Spec Pub* **60**: 87-90.

Net IL, Alonso MS, Limarino CO (2002) Source rock and environmental control on clay mineral associations, Lower Section of Paganzo Group (Carboniferous), Northwest Argentina. *Sediment Geol* **152**(1-2): 183-199.

Nijenhuis IA, Bosch HJ, Sinninghe Damsté JS, Brumsack HJ, de Lange GJ (1999) Organic matter and trace element rich sapropels and black shales: A geochemical comparison. *Earth Planet Sci Lett* **169**(3-4): 277-290.

Odin GS, Fullagar PD (1988) The geologic significance of the glaucony facies. In: Odin GS (ed) Green marine clays. *Developments in sedimentology* **45**. Elsevier, Amsterdam: 295-332.

Olsson RK, Liu G (1993) Controversies on the placement of the Cretaceous-Paleogene boundary and the K/T mass extinction of planktonic foraminifera. *Palaios* **8**: 127-139.

Olsson RK, Liu C, van Fossen M (1996) The Cretaceous-Tertiary catastrophic event at Millers Ferry, Alabama. In: Ryder G, Fastovsky D, Gartner S (eds) The Cretaceous-Tertiary boundary event and other catastrophes in Earth history. *Geol Soc Am Spec Pap* **307**: 263-277.

Olsson RK, Miller KG, Browning JV, Wright JD, Cramer BS (2002) Sequence stratigraphy and sea-level changes across the Cretaceous-Tertiary boundary on the New Jersey passive margin. In: Koeberl C, MacLeod KG (eds) Catastrophic events and mass extinctions: Impacts and beyond. *Geol Soc Am Spec Pap* **356**: 97-108.

Ortega-Huertas M, Martínez-Ruiz F, Palomo-Delgado I, Chamley H (2002) Review of the mineralogy of the Cretaceous-Tertiary boundary clay: Evidence supporting a major extraterrestrial catastrophic event. *Clay Miner* **37**(3): 395-411.

Pardo A, Ortiz N, Keller G (1996) Latest Maastrichtian and Cretaceous-Tertiary foraminiferal turnover and environmental changes at Agost, Spain. In: MacLeod N, Keller G (eds) Cretaceous-Tertiary boundary mass extinction: Biotic and environmental changes. Norton Press, New York: 139-171.

Pardo A, Adatte T, Keller G, Oberhänsli H (1999) Palaeoenvironmental changes across the Cretaceous-Tertiary boundary at Koshak, Kazakhstan, based on planktic foraminifera and clay mineralogy. *Palaeogeogr Palaeoclimatol Palaeoecol* **154**(3-4): 247-273.

Pearson MJ (1990) Clay mineral distribution and provenance in Mesozoic and Tertiary mudrocks of the Moray Firth and northern North Sea. *Clay Miner* **25**(4): 519-541.

Pekar S, Miller KG (1996) New Jersey Oligocene "icehouse" sequences (ODP Leg 150X) correlated with global δ^{18}O and Exxon eustatic records. *Geology* **24**(6): 567-570.

Perch-Nielsen K (1985) Mesozoic calcareous nannofossils. In: Saunders JB, Bolli HM, Perch-Nielsen K (eds) Plankton stratigraphy. Cambridge University Press, Cambridge: 329-426.

Petschick R, Kuhn G, Gingele F (1996) Clay mineral distribution in surface sediments of the South Atlantic: Sources, transport, and relation to oceanography. *Mar Geol* **130**(3): 203-229.

Pitakpaivan K, Byerly GR, Hazel JE (1994) Pseudomorphs of impact spherules from a Cretaceous-Tertiary boundary section at Shell Creek, Alabama. *Earth Planet Sci Lett* **124**(1): 49-56.

Pollastro RM, Bohor BF (1993) Origin and clay-mineral genesis of the Cretaceous/Tertiary boundary unit, Western Interior of North America. *Clays Clay Miner* **41**(1): 7-25.

Posamentier HW, Jervey MT, Vail PR (1988) Eustatic controls on clastic deposition I – Conceptual framework. In: Wilgus CK, Hastings BS, Kendall CG et al. (eds) Sea-level changes: An integrated approach. *Soc Econ Paleont Miner Spec Pub* **42**: 109-124.

Prothero DR (2001) Magnetostratigraphic tests of sequence stratigraphic correlations from the Southern California Paleogene. *Jour Sediment Res* **71**(4): 526-536.

Pujalte V, Baceta J-I, Dinarès-Turell J, Orue-etxebarria X, Parés J-M, Payros A (1995) Biostratigraphic and magnetostratigraphic intercalibration of latest Cretaceous and Paleocene depositional sequences from the deep-water Basque Ba-

sin, western Pyrenees, Spain. *Earth Planet Sci Lett* **136**(1-2): 17-30.

Remane J, Keller G, Hardenbol J, Ben Haj Ali M (1999) Report on the international workshop on Cretaceous-Paleogene transitions. *Episodes* **22**(1): 47–48.

Ricken W (1996) Bedding rhythms and cyclic sequences as documented in organic carbon-carbonate patterns, Upper Cretaceous, Western Interior, USA. *Sediment Geol* **102**(1-2): 131-154.

Rider MH (1996) The geological interpretation of well logs. Whittles Publishing, Caithness, Great Britain: 1-361.

Robert C, Chamley H (1990) Palaeoenvironmental significance of clay mineral associations at the Cretaceous-Tertiary passage. *Palaeogeogr Palaeoclimatol Palaeoecol* **79**: 205-219.

Ryder G, Fastovsky D, Gartner S (eds) (1996) The Cretaceous-Tertiary event and other catastrophes in Earth history. *Geol Soc Am Spec Pap* **307**: 1-556.

Sanders D, Höfling R (2000) Carbonate deposition in mixed siliciclastic-carbonate environments on top of an orogenic wedge (Late Cretaceous, Northern Calcareous Alps, Austria). *Sediment Geol* **137**(3-4): 127-146.

Sarg JF (1988) Carbonate sequence stratigraphy. In: Wilgus CK, Hastings BS, Kendall CG et al. (eds) Sea-level changes: An integrated approach. *Soc Econ Paleont Miner Spec Pub* **42**: 155-181.

Savrda CE (1993) Ichnosedimentologic evidence for a non-catastrophic origin of Cretaceous-Tertiary boundary sands in Alabama. *Geology* **21**(12): 1075-1078.

Schmitz B (1988) Origin of microlayering in worldwide distributed Ir-rich marine Cretaceous/Tertiary boundary clays. *Geology* **16**(12): 1068-1072.

Schmitz B (1992) Chalcophile elements and Ir in continental Cretaceous-Tertiary boundary clays from the Western Interior of the USA. *Geochim Cosmochim Acta* **56**: 1695-1703.

Schmitz B, Keller G, Stenvall O (1992) Stable isotope and foraminiferal changes across the Cretaceous/Tertiary boundary at Stevns Klint, Denmark: Arguments for long-term oceanic instability before and after bolide impact. *Palaeogeogr Palaeoclimatol Palaeoecol* **96**: 233-260.

Schrag DP, DePaolo DJ, Richter FM (1995) Reconstructing past sea surface temperatures: Correcting for diagenesis of bulk marine carbonate. *Geochim Cosmochim Acta* **59**(11): 2265-2278.

Schroeder JO, Murray RW, Leinen M, Pflaum RC, Janecek TR (1997) Barium in equatorial Pacific carbonate sediment: Terrigenous, oxide, and biogenic associations. *Paleoceanography* **12**(1): 125-146.

Schulte P, Stinnesbeck W, Kontny A, Stüben D, Kramar U, Harting M (2002) Multiple (immiscible) melt phases of mafic composition in Chicxulub impact ejecta from northeastern Mexico: New constraints on target lithologies. *EOS Trans AGU* **83**(47) (Fall Meeting Supplement): #OS22C-0293.

Schulte P, Stinnesbeck W, Stüben D, Kramar U, Berner Z, Keller G, Adatte T (2003) Fe-rich and K-rich mafic spherules from slumped and channelized Chicxulub ejecta deposits at the northern La Sierrita area, NE Mexico. *Int Jour Earth Sci* **92**(1): 114-142.

Schutter SR (1998) Characteristics of shale deposition in relation to stratigraphic sequence systems tracts. In: Schieber J, Zimmerle W, Sethi PS (eds) Shales and mudstones: I, Basin studies, sedimentology, and paleontology. Schweizerbart, Stuttgart: 79-108.

Shackleton NJ, Hall MA, Pate D, Meynardier L, Valet P (1993) High-resolution stable isotope stratigraphy from bulk sediment. *Paleoceanography* **8**(2): 141-148.

Sharpton VL, Ward PD (eds) (1990) Global catastrophes in Earth history: An interdisciplinary conference on impacts,

volcanism, and mass mortality. *Geol Soc Am Spec Pap* **247**: 1-631.

Singer A (1984) The paleoclimatic interpretation of clay minerals in sediments – A review. *Earth-Sci Rev* **21**(4): 251-293.

Smit J (1999) The global stratigraphy of the Cretaceous-Tertiary boundary impact ejecta. *Ann Rev Earth Planet Sci* **27**: 75-113.

Smit J, Alvarez W, Montanari A, Claeys P, Grajales-Nishimura JM (1996) Coarse-grained, clastic sandstone complex at the K/T boundary around the Gulf of Mexico: Deposition by tsunami waves induced by the Chicxulub impact? In: Ryder G, Fastovsky D, Gartner S (eds) The Cretaceous-Tertiary boundary event and other catastrophes in Earth history. *Geol Soc Am Spec Pap* **307**: 151-182.

Smith AB, Gale AS, Monks NEA (2001) Sea-level change and rock-record bias in the Cretaceous: A problem for extinction and biodiversity studies. *Paleobiology* **27**(2): 241-253.

Soegaard K, Ye H, Halik N, Daniels A, Arney J, Garrick S (2002) Stratigraphic evolution of latest Cretaceous to early Tertiary Difunta foreland basin in northeast Mexico: Influence of salt withdrawal on tectonically-induced subsidence from the Sierra Madre Oriental. In: Bartolini C, Buffler R, Blickwede J (eds) The Gulf of Mexico and Caribbean region: Hydrocarbon habitats, basin formation and plate tectonics. *Am Ass Petrol Geolog Spec Mem* (in press).

Sohl NF, Martínez ER, Salmerón-Ureña P, Soto-Jaramillo F (1991) Upper Cretaceous. In: Salvador A (ed) The Gulf of Mexico Basin. *The geology of North America* **J**. Geological Society of America, Boulder, Colorado: 205-244.

Southgate PN, Kennard JM, Jackson MJ, O'Brian PE, Sexton MJ (1993) Reciprocal lowstand clastic and highstand carbonate sedimentation, subsurface Devonian Reef complex, Canning Basin, Western Australia. In: Loucks RG, Sarg JF (eds) Carbonate sequence stratigraphy: Recent developments and applications. *Am Ass Petrol Geol Mem* **57**: 157-179.

Speijer RP, Van der Zwaan GJ (1996) Extinction and survivorship of southern Tethyan benthic foraminifera across the Cretaceous/Paleogene boundary. In: Hart MB (ed) Biotic recovery from mass extinction events. *Geol Soc Lond Spec Pub* **102**: 343-371.

Srodon J (1999) Use of clay minerals in reconstructing geological processes: Recent advances and some perspectives. *Clay Miner* **34**(1): 27-37.

Stinnesbeck W, Schulte P, Lindenmaier F, Adatte T et al. (2001) Late Maastrichtian age of spherule deposits in northeastern Mexico: Implication for Chicxulub scenario. *Can Jour Earth Sci* **38**(2): 229-238.

Stoll HM, Schrag DP (2000) High-resolution stable isotope records from the Upper Cretaceous rocks of Italy and Spain: Glacial episodes in a greenhouse planet? *Geol Soc Am Bull* **112**(2): 308-319.

Strasser A, Pittet B, Hillgaertner H, Pasquer J-B (1999) Depositional sequences in shallow carbonate-dominated sedimentary systems: Concepts for a high resolution analysis. *Sediment Geol* **128**(2): 201-221.

Stüben D, Kramar U, Berner Z, Stinnesbeck W, Keller G, Adatte T (2002) Trace elements, stable isotopes, and clay mineralogy of the Elles II K/T boundary section in Tunisia: Indications for sea level fluctuations and primary productivity. *Palaeogeogr Palaeoclimatol Palaeoecol* **178**(3-4): 321-345.

Sugarman PJ, Miller KG, Bukry D, Feigenson MD (1995) Uppermost Campanian-Maestrichtian strontium isotopic, biostratigraphic, and sequence stratigraphic framework of the New Jersey coastal plain. *Geol Soc Am Bull* **107**(1): 19-37.

Surlyk F (1997) A cool-water carbonate ramp with bryozoan mounds: Late Cretaceous-Danian of the Danish Basin. In: James NP, Clarke JAD (eds) Cool-water carbonates. *Soc Econ Paleont Miner Spec Pub* **56**: 293-307.

Thiry M (2000) Palaeoclimate interpretation of clay minerals in marine deposits: An outlook from the continental origin. *Earth-Sci Rev* **49**(1): 201-221.

Thyberg BI, Jordt H, Bjørlykke K, Faleide JI (2000) Relationships between sequence stratigraphy, mineralogy and geochemistry in Cenozoic sediments of the northern North Sea. In: Nøttvedt A (ed) Dynamics of the Norwegian margin. *Geol Soc Lond Spec Pub* **167**: 245-272.

Tissot BP, Welte DH (1984) Petroleum formation and occurrence. Springer, Heidelberg: 1-699.

Tribovillard N, Dupuis C, Robin E (2000) Sedimentological and diagenetical conditions of the impact level of the Cretaceous/Tertiary boundary in Tunisia: No anoxia required. *Bull Soc Géol Fr* **171**(6): 629-636.

Tucker ME, Wright VP (1992) Carbonate sedimentology. Blackwell Science, Oxford: 1-482.

Vail PR, Mitchum RMJ (1977) Seismic stratigraphy and global changes of sea level: Part 1, Overview. In: Payton CE (ed) Seismic stratigraphy – Applications to hydrocarbon explorations. *Am Ass Petrol Geol Mem* **26**: 51-52.

Vail PR, Mitchum RMJ, Thompson SL (1977) Seismic stratigraphy and global changes of sea level: Part 3, Relative changes of sea level from coastal onlap. In: Payton CE (ed) Seismic stratigraphy – Applications to hydrocarbon explorations. *Am Ass Petrol Geol Mem* **26**: 63-81.

Vail PR, Audemard F, Bowman SA, Eisner PN, Perez CG (1991) The stratigraphic signatures of tectonics, eustasy and sedimentology – An overview. In: Einsele G, Ricken W, Seilacher A (eds) Cycles and events in stratigraphy. Springer, Heidelberg: 617-659.

Van Wagoner JC (1995) Overview of sequence stratigraphy of foreland basin deposits: Terminology, summary of papers, and glossary of sequence stratigraphy. In: Van Wagoner JC, Bertram GT (eds) Sequence stratigraphy of foreland basin deposits: Outcrop and subsurface examples from the Cretaceous of North America. *Am Ass Petrol Geol Mem* **64**: 9-21.

Van Wagoner JC, Mitchum RM, Campion KM, Rahmanian VD (1990) Siliciclastic sequence stratigraphy in well logs, cores, and outcrops: Concepts for high-resolution correlation of time and facies. *Methods in Exploration* **7**. Am Ass Petrol Geol, Tulsa, Oklahoma: 1-53.

Van Wagoner JC, Posamentier HW, Mitchum RM, Vail PR, Sarg JF, Loutit TS, Hardenbol J (1988) An overview of the fundamentals of sequence stratigraphy and key definitions. In: Wilgus CK, Hastings BS, Kendall CG et al. (eds) Sealevel changes: An integrated approach. *Soc Econ Paleont Miner Spec Pub* **42**: 39-45.

Vanderaveroet P, Deconinck JF (1997) Clay mineralogy of Cenozoic sediments of the Atlantic City borehole, New Jersey. Proceedings of the Ocean Drilling Program. *Scientific Results* **150X**: 49-57.

Veizer J, Bruckschen P, Pawellek F, Diener A, Podlaha OG, Carden GAD, Jasper T, Korte C, Strauss H, Azmy K, Ala D (1997) Oxygen isotope evolution of Phanerozoic seawater. *Palaeogeogr Palaeoclimatol Palaeoecol* **132**(1-4): 159-172.

Wdowiak TJ, Armendarez LP, Agresti DG, Wade ML, Wdowiak YS, Claeys P, Izett GA (2001) Presence of an iron-rich nanophase material in the upper layer of the Cretaceous-Tertiary boundary clay. *Meteor Planet Sci* **36**(1): 123-133.

Weaver CE (1989) Clays, muds and shales. *Developments in sedimentology* **44**. Elsevier, Amsterdam: 1-819.

Wright VP, Burchette TP (1996) Shallow-water carbonate environments. In: Reading HG (ed) Sedimentary environments: Processes, facies and stratigraphy. Blackwell Science, Oxford: 325-394.

Yang W, Kominz MA (2002) Characteristics, stratigraphic architecture, and time framework of multi-order mixed siliciclastic and carbonate depositional sequences, outcropping Cisco Group (Late Pennsylvanian and Early Permian), Eastern Shelf, north-central Texas, USA. *Sediment Geol* **154**(1-2): 53-87.

Yilmaz IO, Altiner D (1999) Use of sedimentary structures in the recognition of sequence boundaries in Upper Jurassic-Upper Cretaceous peritidal carbonates of the western Taurides, Turkey. *Int Geol Rev* **43**(8): 736-753.

Young GM, Nesbitt HW (1998) Processes controlling the distribution of Ti and Al in weathering profiles, siliciclastic sediments and sedimentary rocks. *Jour Sediment Res* **68**(3): 448-455.

Yuretich R, Melles M, Sarata B, Grobe H (1999) Clay minerals in the sediments of the Lake Baikal: A useful climate proxy. *Jour Sediment Res* **69**(3): 588-596.

Zachos JC, Arthur MA, Dean WE (1989) Geochemical and paleoenvironmental variations across the Cretaceous/Tertiary boundary at Braggs, Alabama. *Palaeogeogr Palaeoclimatol Palaeoecol* **69**: 245-266.

5. Synthesis: The Cretaceous-Paleogene transition and Chicxulub ejecta in the northwestern Gulf of Mexico

The multidisciplinary investigation of the K-P transition in the northwestern Gulf of Mexico area provided the following results.

5.1 Chicxulub ejecta: Composition and regional-global correlation

The spherules found in K-P drillcores and outcrop sections from the northwestern Gulf of Mexico area correspond morphologically to glass-smectite spherules found in the K-P transition of the Gulf of Mexico, Northern America (Western Interior), the western Atlantic, and the eastern Pacific (see papers in Sharpton and Ward, 1990; Ryder et al., 1996; Koeberl and MacLeod, 2002; Koeberl and Martínez-Ruiz, 2003). The particular morphological features (smooth and globular outlines) and internal textures (vesicles, mamillary structures, schlieren) of these spherules, as well as other petrological, mineralogical and geochemical characteristics (as outlined below) indicate that they have been generated by the Chicxulub impact event on the Yucatán peninsula in southern Mexico. This impact event formed a circular multiring structure of about 180 km in diameter (e.g., Morgan et al., 1997). The target at the impact site consisted of shallow water and up to 3 km thick Cretaceous carbonate platform sediments, resting on continental crust composed of different crystalline rocks (granites, gneisses, schists, amphibolites, e.g., Sharpton et al., 1996; Kettrup and Deutsch, 2003).

The mineralogical and geochemical composition of the ejecta spherules found in the western Gulf of Mexico area reflects the specific lithologic succession at the Chicxulub impact site, albeit this study revealed distinct localized compositional trends for the ejecta from northeastern Mexico, Texas, and Alabama. Considering the 'small' area governed by this study, and the generally assumed 'homogenization' of ejecta material during impact events, these compositional trends for the silicic ejecta phases are surprising. Specifically it was found that:

(1) a predominance of Si-Al-K-rich glass spherules exists in the southernmost El Mimbral outcrop in Mexico, pointing to precursor rocks of intermediate mafic-felsic character. In addition, Fe-Mg-rich chlorite spherules suggest mafic precursor lithologies. This locality bears also evidence for liquid immiscibility between the compositionally distinct melt phases ('tektite in tektite' texture) as well as

between silicic phases and carbonate. The presence of μm-sized metallic and sulfidic Ni-Co-(Ir-?) rich inclusions suggest a possible contamination by meteoritic material.

(2) in the northern outcrops at El Peñon and La Sierrita, Mexico, the Chicxulub ejecta is dominated by Fe-Mg-rich chlorite spherules, though with low amounts of the Si-Al-K-rich glass phase found at El Mimbral. Immiscibility features of the diverse melt phases and Ni-Co-rich inclusions are also present in these locations.

(3) at Brazos, Texas, ejecta-spherules are mainly composed of Mg-rich smectite, though (rare) chlorite spherules are also present. The particular smectite composition is similar to smectite spherules found at the K-P boundary in the Petén basin, Guatemala (Debrabant et al., 1999), in Beloc, Haiti (Koeberl and Sigurdsson, 1992), and at the Blake Nose Plateau, Western Atlantic (Martínez-Ruiz et al., 2002). For these localities, an andesitic precursor phase was postulated based on the presence of Si-rich glass spherules of andesitic composition.

Besides these silicic and ejecta phases, the main ejecta phase at northeastern Mexico and Texas (by weight-percentage) is carbonate. The high amount of CaO in the spherule deposits in northeastern Mexico (bulk rock analysis: 25-45 wt %) and in Texas (30-40wt %), suggest that this area may have received ejecta mainly from shallow carbonaceous lithologies of the Yucatán peninsula.

Carbonaceous ejecta phases were dispersed as unshocked clasts, as melt, and constitute accretionary lapilli-like clasts. Several petrographic characteristics (presence of carbonate globules and quenched 'feathery calcite') give evidence for ubiquitous carbonate-silicate liquid immiscibility in the ejecta. The microspar in the spherule deposits in northeastern Mexico and their matrix-supported texture suggests that fine-grained, microcrystalline carbonate and spherules were ejected and deposited simultaneously. The origin of this microcrystalline calcite is not clear yet: it may have originated either from dust dispersed by the impact event, or as secondary calcite derived from the recombination of CO_2 and solid oxides (CaO). Though evaporites (anhydrite and gypsum) are assumed to be a major component of the Yucatán carbonate platform, no particular evidence for these lithologies has been

found, but diagenesis and dissolution may have biased the record in the ejecta deposits.

The localized compositional pattern of silicic ejecta phases and the textural evidence for liquid immiscibility suggests that upon dispersion of the ejecta by the impact event, hot and molten ejecta phases were mutually mixed, though no homogenization of the specific ejecta melt phases occurred. Such homogenization is evident, for instance at Beloc Haiti, where the Si-rich glasses of andesitic composition show a continuous mixing line with a CaO-rich endmember (Koeberl and Sigurdsson, 1992; Stüben et al., 2002). Therefore, ejecta at northeastern Mexico presumably derived from less-energetic parts of the ejecta curtain. In addition, the wide composition range of ejecta phases (e.g., SiO_2 24-50 wt%, Al_2O_3 16-32 wt%, FeO 2-35 wt%) points to a complex geology of the target area, including mafic to felsic basement, specifically at the northwestern sector of the Chicxulub impact structure. This result confirms previous studies that also concluded a lithologically complex basement for the subsurface of the Chicxulub impact structure (e.g., Kettrup et al., 2000; Kettrup and Deutsch, 2003).

The specific compositional range of the Chicxulub ejecta phases found in the northwestern Gulf of Mexico, as well as the results of the petrologic and rock magnetic characteristics, suggest that ejecta spherules and fragments have also several compositional aspects in common with ejecta-derived material ('microspherules' and 'microkrystites') found in the basal layer of the K-P boundary clay in the Western Interior (e.g., Dogie Creek, Wyoming), the Atlantic (Zumaya, Spain) and Tethyan realm (e.g., Stevens Klint, Denmark) (Smit et al., 1992; Smit, 1999; Ortega-Huertas et al., 2002; Koeberl and Martínez-Ruiz, 2003). These aspects include the presence of (i) Mg-rich smectite, (ii) potassium-enriched phases, (iii) altered K-feldspar and pyroxene crystallites with fibroradial texture, and (iv) fine-grained iron- and iron-titanium oxides.

5.2 Sedimentology of Chicxulub ejecta deposits

The spherule deposits at northeastern Mexico, Texas, and Alabama are associated with a calcareous and siliciclastic event bed or event deposit that bears evidence for high-energy deposition from debris flows and turbidity currents. The lithology and thickness

of the ejecta deposits reveal discrete patterns outlined in the following.

Geological mapping of four K-P outcrop areas in **northeastern Mexico** revealed the presence of:

(1) lens-like multiple spherule deposits embedded in late Maastrichtian marls, which are folded or disaggregated (breccia-like). They are up to 4 m thick, locally present only in two outcrop areas (Mesa Juan Perez and El Peñon), and show limited lateral continuity of about 0.5-2 m. These deposits consist of mm-cm sized spherical to drop-shaped vesiculated spherules, angular to filamentous ejecta-fragments and abundant carbonate. They are interpreted as primary ejecta fallout deposits that have been affected by subsequent local slumps-slides, liquefaction, and debris flows; welded components suggest an initial ground surge-like ejecta-dispersion mode.

(2) a 10-100 cm thick spherule deposit that is characterized by wide lateral continuity, constitutes the base of a channelized, multiple debris-flow sand-siltstone deposit and is present in all K-P outcrop areas in northeastern Mexico. These spherule deposits at the base of a channelized sandstone sequence are thickest (up to 100 cm) in the southernmost outcrop at El Mimbral, and are thinning to 20-40 cm in the northernmost outcrops at La Sierrita and Rancho Nuevo. They are of similar petrologic composition to the spherule deposits (1), though slightly enriched in terrigeneous detritus, reflecting influx from proximal shelf areas.

Petrological, mineralogical, and geochemical criteria suggest that ejecta components from both types (1 and 2) of spherule deposits are similar and originated from one impact event, namely the Chicxulub impact, with multiple deposits produced by subsequent remolding, reworking, and redeposition. The compositional similarity of these types of spherule deposits and the absence of abrasion-features of the ejecta-components indicates almost contemporaneous formation, with no significant time interval between original deposition and reworking or remolding.

At **Brazos**, **Texas**, a 10 cm thick spherule deposit is present, overlain by another 10 cm-thick layer rich in fine-grained spherule- and carbonate-clasts, and with intercalated cm-thick sand-silt layers. The top of this sequence is bioturbated and overlain by micritic limestone grading into laminated dark shales. This depositional sequence is explained by ejecta deposition from debris flows and subsequent turbidite currents, resulting from successive storm or tsunami

events, with sudden intermittent provenance changes as indicated by the sand-silt layers.

In the **Antioch Church core**, **central Alabama**, only few spherules are present within a sandstone bed, and no distinct spherule layer was observed. For the emplacement of the sandstone bed, a tsunami- or storm-triggered mechanism is possible.

In conclusion, the pattern of decreasing thickness of ejecta deposits with increasing distance from the Chicxulub structure is in keeping with the thickness distribution of spherule deposits in the West Atlantic, although reworking and resedimentation may have influenced the thickness of the ejecta material locally. These spherule-rich deposits have about 10-15 cm thickness at Blake Nose, ODP Site 171, offshore eastern Florida, (Martínez-Ruiz et al., 2002), about 6 cm thickness at the Bass River ODP Site 174AX in New Jersey (Olsson et al., 1997), and about 2-3 cm at the K-P localities in the Western Interior (e.g., in Colorado, Wyoming, Montana, Sweet et al., 1999). Also, there is a distinct trend of decreasing ejecta grain-size with increasing distance from the Chicxulub structure: grain size of the spherules is largest at the El Mimbral locality (mm-cm-sized spherules) and smallest at Texas and Alabama (sub-mm-sized spherules). In comparison, at Blake Nose, spherules are 1-2 mm in size, at Bass River, 0.2-1 mm, and in the Western Interior about 0.5-1 mm (references above).

Although this distinct ejecta distribution pattern suggests a common and single source for the ejecta-spherules in northwestern Gulf of Mexico and the K-P boundary clay by the Chicxulub impact event, the complex lithostratigraphy of the K-P event bed and event deposit implies that the ultimate causes for these event deposits are probably highly variable and acted over a distinct period. Specifically, an origin by 'one' discrete impact-generated tsunami appears to be unlikely in view of the complex sedimentology and internal subdivision of these deposits. Moreover, the stratigraphy of the ejecta deposits in northeastern Mexico and Texas reveals that the timing of spherule deposition relative to the first appearance of Paleocene microfossils subsequent to the K-P boundary is difficult to constrain:

The spherule deposits in **northeastern Mexico** are locally embedded within latest Maastrichtian marls (Stinnesbeck et al., 2001; Keller et al., 2002), though ubiquitous soft-sediment deformation, post-depositional faulting, and reworking of the ejecta beds (Chapter 2 and Soria et al., 2001; 2002; Schulte et al., 2003) obscures the temporal relationships

between these deposits and the first appearance of Paleocene microfossils, which are found atop of the sand-siltstone deposit (e.g., Keller et al., 1997). Particularly, since no mm-thick ferruginous layer with Ni-rich spinels and smectite spherules (and shocked quartz) that defines the K-P boundary in the Global Stratotype Section and Point (GSSP) at El Kef, Tunisia (Cowie et al., 1989), has been observed in the northeastern Mexican sections. Therefore, further refined sedimentological and biostratigraphical data, which also include the complex local tectonic setting of this area, are called for to resolve this question.

The spherule deposit in the **Brazos core** from **Texas** is separated by 1.6 m of laminated shale from the first appearance of Paleocene microfossils. Since this specific interval is distinctly thinner (15-25 cm) at other localities of the Brazos area (see also Keller, 1989; Hansen et al., 1993; Yancey, 1996), its temporal significance and/or the possibility of enhanced reworking has, however, yet to be evaluated. Analogous to the K-P sections in northeastern Mexico (and Alabama), no mm-thick ferruginous layer with Ni-rich spinels and smectite spherules (and shocked quartz) that defines the K-P boundary in the Global Stratotype Section and Point (GSSP) at El Kef, Tunisia, has been observed at Brazos, Texas.

5.3 Facies trends and sequence stratigraphic setting

The following local facies trends and sequence stratigraphic settings across the Maastrichtian to Danian transition were revealed by lithological, geochemical, and mineralogical criteria:

The deep-water (upper bathyal) lithologies in **northeastern Mexico** and the limited range of outcrops in northeastern Mexico that cover the K-P boundary do not allow to provide well-constrained data on facies and sea-level trends. However, for the K-P transition at the La Sierrita area, no prominent change in clay mineral species (or detritus input) was observed for an interval of several hundred ka across the K-P boundary (see also Lindenmaier, 1999), though a hiatus may have affected this section at the immediate K-P boundary. However, a similar 'smooth' K-P transition with little evidence for drastic facies changes in the marls bracketing the siliciclastic deposit was observed at the El Mulato K-P section near El Peñon (preliminary data by the author).

In the two cores from **Brazos**, **Texas**, that include uniform shales deposited in a middle to outer shelf

setting, no evidence for major proximal-distal facies trends have been observed in the late(st) Maastrichtian shales underlying the event bed, as well as for a 1.6 m-thick shaley interval of unknown stratigraphic age, which is sandwiched between this event deposit and the first occurrence of Paleocene microfossils. Nevertheless, an erosional surface at the base of the spherule-rich event deposit, probably associated with a hiatus, prevented from unequivocal evaluation of these trends. During the early Danian Biozone P0, multiple sedimentological criteria (e.g., increased coarse detritus content) suggest a regressive sea level behavior and a sequence boundary is tentatively placed within Biozone Pα (P1a of Keller, 1989). The subsequent lowstand systems tract is terminated at a flooding surface and overlain by the geochemically and mineralogically distinct transgressive systems tract (see also Yancey, 1996).

In the shallow, inner-shelf sediments of the **Antioch Church core**, **central Alabama**, a trend is recognized from a siliciclastic-dominated depositional system in the late Maastrichtian-early Danian, to a carbonate-dominated depositional system during the middle Danian. This change may be related to the establishment of a stable carbonate platform on the Alabama shelf during the early Paleocene, as shown by Mancini et al. (1993). In summary, four depositional sequences, or parts of sequences, were distinguished in the mixed siliciclastic-carbonate sediments for the late Maastrichtian to middle Danian period. In this mixed depositional system on the Alabama shelf, siliciclastic sedimentation dominated during the late (regressive) highstand and subsequent lowstand systems tract, when carbonate production was largely shut down, and carbonate sedimentation prevailed during the transgressive and the early highstand systems tract, when terrigeneous detritus was mostly trapped in nearshore areas. This vertical stacking pattern is known as "reciprocal sedimentation" (Southgate et al., 1993).

As revealed from the component lithofacies, it appears that the 'magnitude' of relative sea-level changes was largest during the middle Danian sequences (temporal emergence), whereas magnitudes are less pronounced during the late Maastrichtian-early Danian and the upper Danian sequences, though erosional surfaces at sequence boundaries, generally associated with a hiatus, prevent from unequivocal evaluation of these trends. A pronounced sea level lowering was recognized for the interval between 500 and 300 ka pre-K-P, and was followed by a phase of transgressive sea-level behavior across

the K-P boundary. A prominent interval with strongly fluctuating sea-level trends follows the K-P boundary and is associated with condensed sedimentation (bracketing a maximum flooding surface) during the upper part of Biozone NP1, possibly 200-400 ka post-K-P.

In summary, no distinct evidence for hostile or even adverse sedimentary conditions (e.g., dys- or anoxic conditions) was found for the interval bracketing the K-P boundary in all three localities investigated for this study.

5.4 Clay minerals and paleoclimate

The clay mineral species found in the marine K-P sections of northeastern Mexico, Texas, and Alabama show a remarkably complex composition. No unique trend for the northwestern Gulf of Mexico region was found that could be linked to increasingly adverse climatic conditions (e.g., cooling) preceding the K-P boundary. Instead, the complex clay mineral assemblages found in the northwestern Gulf of Mexico suggest highly localized influence from topographically, petrologically, and also probably climatically distinct source regions.

The generally illite- and chlorite-dominated clay mineralogy of the deep-water marls found in the Burgos (and Tampico-Misantla) Basin in **northeastern Mexico** indicates a provenance from areas with rocks of mafic character, associated with dominance of physical over chemical weathering (e.g., Chamley, 1989; 1997; Müller et al., 2001). The provenance of these clay mineral species may be found in the approaching Sierra Madre Oriental to the west, with a pronounced phase of uplift during the K-P transition (e.g., Echanove, 1986; Goldhammer and Johnson, 2001).

The clay mineral composition of the shales bracketing the K-P boundary at **Brazos**, **Texas**, was also relatively constant during an interval of about 1 Ma across the K-P boundary, with major fluctuation restricted to the spherule-rich event bed. Therefore, it is suggested that no major change occurred in the paleoceanographic and/or climate conditions at Brazos during this period across the K-P boundary. The high smectite contents (>60 rel%) flanked by minor illite, chlorite, and kaolinite suggest warm, humid climates with pronounced seasonality, albeit the high diversity of this clay assemblage points to a complex hinterland with different tectonic or topographic compartments.

The clay mineral assemblage of the **Antioch Church core** from **central Alabama**, comprises mainly varying proportions of smectite, kaolinite, and illite and three distinct clay mineral facies were distinguished: (i) a kaolinite-dominated facies with a general upward increase in the relative abundance of smectite concomitant to a relative decrease in kaolinite during the late Maastrichtian into the early Danian, (ii) a kaolinite-smectite-rich facies, during the early Danian, and (iii) a smectite-dominated facies during the late Danian. The latter, smectite facies was established at the transition to a carbonate-dominated sedimentary system (top of Biozone NP3). These general trends in clay mineralogy are not related to lithological changes, though minor compositional changes occur at lithologic transitions (e.g., sand-rich strata show elevated smectite contents) and coincident to sequence stratigraphic surfaces. Therefore, the general compositional variations in the clay mineral assemblages likely resulted mainly from paleoclimate variations in the source area, and to a minor degree from the position relative to the coastline. In conclusion, the climate at Alabama may have changed across the K-P boundary from tropical, humid conditions with year-round precipitation to a distinctly drier semiarid climate with pronounced seasonality. However, it may be inferred that this pronounced change took place already during the Maastrichtian, and Alabama received subsequently kaolinite from reworking of thick kaolinitic soils, though the allover climate has already changed to significantly drier conditions.

5.5 References

Chamley H (1989) Clay sedimentology. Springer, Heidelberg: 1-623.

Chamley H (1997) Clay mineral sedimentation in the ocean. In: Paquet H, Clauer N (eds) Soils and sediments. Springer, Heidelberg: 269-302.

Cowie JW, Zieger W, Remane J (1989) Stratigraphic Commission accelerates progress, 1984-1989. *Episodes* **12**(2): 79-83.

Debrabant P, Fourcade E, Chamley H, Rocchia R, Robin E, Bellier J-P, Gardin S, Thiébault F (1999) Les argiles de la transition Crétacé-Tertiaire au Guatemala, témoins d'un impact d'asteroide. *Bull Soc Géol Fr* **170**(5): 643-660.

Echanove OE (1986) Geología petrolera de la Cuenca de Burgos (Parte 1): Considerations geólogico-petroleras. *Asociatión Mexicana de Geólogos Petroleros Bolletin* **38**: 1-39.

Goldhammer RK, Johnson CA (2001) Middle Jurassic - Upper Cretaceous paleogeographic evolution and sequence-stratigraphic framework of the northwestern Gulf of Mexico rim. In: Bartolini C, Buffler RT, Cantú-Chapa A (eds) The western Gulf of Mexico basin: Tectonics, sedimentary basins and petroleum systems. *Am Ass Petrol Geolog Spec Mem* **75**: 45-82.

Hansen TA, Upshaw III B, Kauffman EG, Gose W (1993) Patterns of molluscan extinction and recovery across the Cretaceous-Tertiary boundary in east Texas: Report on new outcrops. *Cretaceous Res* **14**(6): 685-706.

Keller G (1989) Extended period of extinctions across the Cretaceous/Tertiary boundary in planktonic foraminifera of continental-shelf sections: Implications for impact and volcanism theories. *Geol Soc Am Bull* **101**(11): 1408-1419.

Keller G, López-Oliva J-G, Stinnesbeck W, Adatte T (1997) Age, stratigraphy and deposition of near-K/T siliciclastic deposits in Mexico: Relation to bolide impact? *Geol Soc Am Bull* **109**(6): 410-428.

Keller G, Adatte T, Stinnesbeck W, Affolter M, Schilli L, López-Oliva J-G (2002) Multiple spherule layers in the late Maastrichtian of northeastern Mexico. In: Koeberl C, MacLeod KG (eds) Catastrophic events and mass extinctions: Impacts and beyond. *Geol Soc Am Spec Pap* **356**: 145-162.

Kettrup B, Deutsch A (2003) Geochemical variability of the Yucatán basement: Constraints from crystalline clasts in Chicxulub impactites. *Meteor Planet Sci*: (in press).

Kettrup B, Deutsch A, Ostermann M, Agrinier P (2000) Chicxulub impactites: Geochemical clues to the precursor rocks. *Meteor Planet Sci* **35**(6): 1229-1238.

Koeberl C, Sigurdsson H (1992) Geochemistry of impact glasses from the K/T boundary in Haiti: Relation to smectites and a new type of glass. *Geochim Cosmochim Acta* **56**: 2113-2129.

Koeberl C, MacLeod KG (eds) (2002) Catastrophic events and mass extinctions: Impacts and beyond. *Geol Soc Am Spec Pap* **356**: 1-746.

Koeberl C, Martínez-Ruiz FC (eds) (2003) Impact markers in the stratigraphic record. *Impact Studies*. Springer, Heidelberg: 1-347.

Lindenmaier F (1999) Geologie und Geochemie an der Kreide/Tertiär-Grenze im Nordosten von Mexico. *Unpublished Master Thesis*, Universität Karlsruhe: 1-90.

Mancini EA, Tew BH (1993) Eustasy versus subsidence: Lower Paleocene depositional sequences from southern Alabama, eastern Gulf Coastal Plain. *Geol Soc Am Bull* **105**(1): 3-17.

Martínez-Ruiz F, Ortega-Huertas M, Palomo-Delgado I, Smit J (2002) Cretaceous-Tertiary boundary at Blake Nose (Ocean drilling Program Leg 171B): A record of the Chicxulub impact ejecta. In: Koeberl C, MacLeod KG (eds) Catastrophic events and mass extinctions: Impacts and beyond. *Geol Soc Am Spec Pap* **356**: 189-200.

Morgan JV, Warner MR, Brittan J, Buffler RT et al. (1997) Size and morphology of the Chicxulub impact crater. *Nature* **390**: 472-476.

Müller J, Oberhänsli H, Melles M, Schwab M, Rachold V, Hubberten H-W (2001) Late Pliocene sedimentation in Lake Baikal: Implications for climatic and tectonic change in SE Siberia. *Palaeogeogr Palaeoclimatol Palaeoecol* **174**(4): 305-326.

Olsson RK, Miller KG, Browning JV, Habib D, Sugarmann PJ (1997) Ejecta layer at the Cretaceous-Tertiary boundary, Bass River, New Jersey (Ocean Drilling Program Leg 174AX). *Geology* **25**(8): 759-762.

Ortega-Huertas M, Martínez-Ruiz F, Palomo-Delgado I, Chamley H (2002) Review of the mineralogy of the Cretaceous-Tertiary boundary clay: Evidence supporting a major extraterrestrial catastrophic event. *Clay Miner* **37**(3): 395-411.

Ryder G, Fastovsky D, Gartner S (eds) (1996) The Cretaceous-Tertiary event and other catastrophes in Earth history. *Geol Soc Am Spec Pap* **307**: 1-556.

Schulte P, Stinnesbeck W, Stüben D, Kramar U, Berner Z, Keller G, Adatte T (2003) Fe-rich and K-rich mafic spherules from slumped and channelized Chicxulub ejecta deposits

at the northern La Sierrita area, NE Mexico. *Int Jour Earth Sci* **92**(1): 114-142.

Sharpton VL, Marín LE, Carney JL, Lee S, Ryder G, Schuraytz BC, Ikora P, Spudis PD (1996) A model of the Chicxulub impact basin based on evaluation of geophysical data, well-logs, and drill core samples. In: Ryder G, Fastovsky D, Gartner S (eds) The Cretaceous-Tertiary boundary event and other catastrophes in Earth history. *Geol Soc Am Spec Pap* **307**: 55-74.

Sharpton VL, Ward PD (eds) (1990) Global catastrophes in Earth history: An interdisciplinary conference on impacts, volcanism, and mass mortality. *Geol Soc Am Spec Pap* **247**: 1-631.

Smit J (1999) The global stratigraphy of the Cretaceous-Tertiary boundary impact ejecta. *Ann Rev Earth Planet Sci* **27**: 75-113.

Smit J, Alvarez W, Montanari A, Swinburn NHM, Van Kempen TM, Klaver GT, Lustenhouwer WJ (1992) "Tektites" and microkrystites at the Cretaceous Tertiary boundary: Two strewn fields, one crater? *Lun Planet Sci* **22**: 87-100.

Soria AR, Liesa CL, Mata MP, Arz JA, Alegret L, Arenillas I, Meléndez A (2001) Slumping and a sandbar deposit at the Cretaceous-Tertiary boundary in the El Tecolote section (northeastern Mexico): An impact-induced sediment gravity flow. *Geology* **29**(3): 231-234.

Soria AR, Liesa CL, Mata MP, Arz JA, Alegret L, Arenillas I, Meléndez A (2002) Reply: "Slumping and a sandbar deposit at the Cretaceous-Tertiary boundary in the El Tecolote section (northeastern Mexico): An impact-induced sediment gravity flow". *Geology* **30**(4): 383.

Southgate PN, Kennard JM, Jackson MJ, O'Brian PE, Sexton MJ (1993) Reciprocal lowstand clastic and highstand carbonate sedimentation, subsurface Devonian Reef complex, Canning Basin, Western Australia. In: Loucks RG, Sarg JF (eds) Carbonate sequence stratigraphy: Recent developments and applications. *Am Ass Petrol Geol Mem* **57**: 157-179.

Stinnesbeck W, Schulte P, Lindenmaier F, Adatte T et al. (2001) Late Maastrichtian age of spherule deposits in northeastern Mexico: Implication for Chicxulub scenario. *Can Jour Earth Sci* **38**(2): 229-238.

Stüben D, Kramar U, Berner Z, Eckhardt J-D, Stinnesbeck W, Keller G, Adatte T, Heide K (2002) Two PGE anomalies above the Cretaceous/Tertiary boundary at Beloc/Haiti: Geochemical context and consequences for the impact scenario. In: Koeberl C, MacLeod KG (eds) Catastrophic events and mass extinctions: Impacts and beyond. *Geol Soc Am Spec Pap* **356**: 163-188.

Sweet AR, Braman DR, Lerbekmo JF (1999) Sequential palynological changes across the composite Cretaceous-Tertiary (K-T) boundary claystone and contiguous strata, western Canada and Montana, USA. *Can Jour Earth Sci* **36**(5): 743-768.

Yancey TE (1996) Stratigraphy and depositional environments of the Cretaceous/Tertiary boundary complex and basal section, Brazos River, Texas. *Gulf Coast Ass Geol Soc Transact* **46**: 433-442.

Appendix

Appendix 1.1 The grain-size data of shocked quartz found in the K-P boundary clay layer and in spherule deposits at, or close to the K-P boundary. Data for reconstructed distances from Chicxulub impact site are from Croskell et al. (2002) and Kring and Durda (2002). Note that shocked quartz grains are largest in the Gulf of Mexico, the Caribbean, the eastern Pacific, and the northern America area, whereas their grain size is smallest in the Tethyan and western Pacific K-P sections. References are given in Chapter 1.

Location	Distance	Mean size	Max size	References
	km	μm	μm	
Gulf of Mexico				
El Mimbral, Mexico	700 - 800	–	680	Smit et al. (1992, 1996)
DSDP Leg 77 Site 536, 540	200 - 400	210	–	Alvarez et al. (1992)
Moncada; Cuba	400 - 500	240	–	Tada et al. (2002)
Caribbean Sea				
Beloc; Haiti	860 - 910	150	530	Izett (1991); Hildebrand and Stansberg (1992); Kring et al. (1994)
North America				
Berwind Canyon, Clear Creek North, Raton Basin; Colorado; New Mexico	2200 - 2300	160-200	760	Izett (1990); Schmitz (1992)
Brownie Butte; Montana	2980 - 3180	150	500	Bohor and Izett (1986); Izett (1990); Schmitz (1992)
Teapot Dome, Dogie Creek, Sussex;Wyoming	2640 - 2740	140	500-560	Izett (1990); Schmitz (1992)
Morgan Creek, Frenchman River; Saskatchewan	3350 - 3550	220	480-530	Izett (1990); Lerbekmo et al. (1999)
Red Deer Valley; Alberta	3840 - 3940	260	550	Izett (1990)
Atlantic Ocean				
ODP Leg 174AX Bass River Site	2900	–	200-300	Olsson et al. (1997)
DSDP Leg 93 Site 603B	2540 - 2640	–	300	Izett (1990)
Biarritz, Zumaya; Spain	3500 - 4000	–	250	Doehne and Margeolis (1990); Schmitz (1992)
Tethyan realm				
Caravaca; Spain	6800 - 7000	90	190	Izett (1990); Schmitz (1992); Kring (1995); Kring and Durda (2002)
Agost; Spain	6500 - 6700	90	–	Izett (1990)
Stevns Klint, Nye Kløv; Denmark	7500 - 7700	110	150-180	Izett (1990); Bohor and Izett (1986); Schmitz (1992)
Petriccio; Italy	8100 - 8300	120	–	Izett (1990); Montanari (1991)
Gubbio; Italy	8100 - 8300	120	190	Bohor and Izett (1986); Izett (1990); Montanari (1991); Schmitz (1992)
Pontedazzo; Italy	8460 - 8660	-	120	Bohor and Izett (1986); Montanari (1991)
Pacific Ocean				
LL44-GPC3	5800	≤ 50	320	Bostwick (1996)
ODP Site 886	6450	≤ 50	225	Bostwick (1996)
DSDP Leg 62 Site 465	7900	≤ 50	212	Schmitz (1992); Bostwick (1996)
DSDP Leg 86 Site 576	9100	≤ 50	190	Bostwick (1996)
DSDP Leg 86 Site 577	9600	≤ 50	90	Bostwick (1996)
DSDP Leg 91 Site 596	9700	≤ 50	150	Bostwick (1996)
ODP Leg 130 Site 803	11000	≤ 50	125	Bostwick (1996)
Woodside Creek; New Zealand	13900 - 14100	–	110	Izett (1990); Schmitz (1992)

Appendix 2.1 Raw X-ray diffraction data from the glycolated <2 μm fraction of spherule deposits in northeastern Mexico and of Méndez/Velasco marls in the Los dos Plebes K-P section. Abbreviations as follows: S, smectite; Ch, chlorite; I, illite; I-S, illite-smectite; Ch-S, chlorite-smectite mixed layers; Int, peak height (in counts per second). Abbreviations for section names are given in the text.

		S(001)		Ch(oo1)+Ch-S		I-S(001-002)		I(001)+I-S		Ch(002)		Ch(oo3)		Ch(004)	
		°2Θ	Int.	°2Θ	Int.	°2Θ	Int.	°2Θ	Int.	°2Θ	Int.	°2Θ	Int.	°2Θ	Int.
MJP1B-3	MF 1	5.4	10	6.28	394	–	<5	8.67	75	12.51	640	18.79	119	25.18	332
MJP1C-2	MF 1	–	<5	6.21	938	–	<5	8.78	61	12.45	1477	18.78	310	25.12	680
MJP1C-3	MF 1	–	<5	6.21	568	–	<5	8.77	119	12.49	1136	18.74	226	25.13	353
MJP1C-4	MF 1	–	<5	6.15	1523	–	<5	8.86	42	12.4	3921	18.7	1076	25.05	2166
MJP3A-3	MF 1	–	<5	6.2	754	–	<5	8.68	16	12.41	1203	18.66	250	25.12	545
MJP3A-4	MF 1	–	<5	6.19	2002	–	<5	8.69	15	12.39	2133	18.62	626	25.08	1250
MJP3A-5	MF 1	–	<5	6.22	1631	–	<5	8.89	64	12.44	2642	18.71	656	25.12	1378
MJP3A-8	MF 1	–	<5	6.18	2856	–	<5	8.87	109	12.4	4848	18.78	1217	25.13	2672
MJP3A-6	MF 1	–	<5	6.19	1313	–	<5	8.79	79	12.42	2801	18.69	672	25.11	1661
MAS1-2	MF 1	–	<5	6.27	399	–	<5	8.79	13	12.51	1515	18.78	342	25.16	955
MAS2-2	MF 1	–	<5	6.27	255	–	<5	8.63	154	12.47	437	18.75	68	25.18	260
LPD3-14	MF 1	–	<5	6.26	547	–	<5	8.6	115	12.48	1041	18.76	211	25.18	621
MJP1A-15	MF 3	5.37	18	6.19	398	–	<5	9.03	43	12.45	1114	18.74	279	25.14	665
MJP1A-14	MF 3	5.5	12	6.22	384	–	<5	8.68	25	12.45	1011	18.73	235	25.12	577
SRS-1	MF 3	2.21	45	6.23	33	–	<5	8.98	55	12.47	86	15.58	27	25.28	107
SRS-2	MF 3	5.2	13	6.31	451	–	<5	8.76	46	12.5	766	18.71	176	25.24	605
MAS1-14	MF 3	5.42	25	6.37	323	–	<5	8.77	43	12.46	471	18.66	120	25.25	532
LPD2-2	MF 3	5	12	6.25	18	7.43	154	8.64	76	12.37	69	18.52	22	25.2	37
EPO2A-2	Lime	5.8	752	–	<5	–	<5	8.95	30	12	10	–	<5	25.4	21
EPO2D-3	MF 1	5.24	32	6.3	31	–	<5	8.5	78	12.5	13	18.3	31	25.29	64
EPO2E-2	MF 1	5.27	176	6.2	24	7.8	31	8.6	31	12.4	12	18.6	10	25.3	10
EPO2E-8	MF 1	5.3	103	6.3	70	–	<5	8.8	73	12.5	44	18.7	10	25.3	36
EPO2F-3	MF 1	5.29	125	6.1	210	–	<5	9.1	200	12.35	63	18.3	27	25.32	25
EPO2A-3	MF 3	5.28	109	6.24	75	7.7	20	9.21	54	12.33	12	18.19	12	25.3	28
EPO2A-4	MF 3	5.11	110	6.17	336	7.8	106	9.21	141	12.3	58	18.59	12	25.25	44
EPO2A-6	MF 3	5.05	219	5.99	246	7.65	82	9.26	223	12.4	17	18.05	10	25.29	24
EPO2B-3	MF 3	5.5	60	6.3	268	8.33	25	9.4	24	12.49	79	18.59	10	25.41	51
ELM1-3	MF 1	–	<5	6.1	378	6.91	202	9.4	199	12.42	293	18.76	55	25.22	105
ELM2-3	MF 1	–	<5	6.12	155	7.43	85	9.06	50	12.38	176	18.67	49	25.1	93
ELM2-4	MF 1	–	<5	6.11	742	7.31	35	8.78	51	12.36	469	18.69	105	25.06	211
ELM1-5	MF 1	–	<5	6.04	249	6.86	205	9.52	185	12.34	162	18.68	15	25.26	69
ELM2-6	MF 2	–	<5	6.16	260	7.49	202	8.9	55	12.39	171	18.65	44	25.3	142
ELM1-7	MF 3	5.3	138	6.05	615	–	<5	9.08	80	12.32	295	18.62	62	25.17	102
LDP1-22	Marl	–	<5	6.32	758	–	<5	8.8	877	12.62	460	18.92	59	25.32	122
LDP1-21	Marl	–	<5	6.33	401	–	<5	8.78	605	12.56	220	18.82	43	25.27	110
LDP1-20	Marl	–	<5	6.37	286	–	<5	8.78	489	12.54	16	18.78	25	25.29	104
LDP1-19	Marl	–	<5	6.33	79	–	<5	8.87	138	12.56	50	18.78	10	25.3	71
LDP1-18	Marl	–	<5	6.27	186	–	<5	8.79	540	12.51	183	18.75	42	25.24	176
LDP1-17	Marl	–	<5	6.28	248	–	<5	8.85	504	12.53	228	18.81	38	25.29	146
LDP1-16	Marl	–	<5	634	134	–	<5	8.76	460	12.5	124	18.71	24	25.25	144
LDP1-15	Marl	–	<5	6.32	385	–	<5	8.98	360	12.6	296	18.9	30	25.33	123
LDP1-14	Marl	–	<5	6.25	555	–	<5	8.98	403	12.53	567	18.85	124	25.27	256
LDP1-13	Lime	–	<5	6.29	160	–	<5	8.8	228	12.52	136	18.83	13	25.26	80
LDP1-12	Marl	–	<5	6.33	334	–	<5	8.83	352	12.53	271	18.84	46	25.25	111
LDP1-11	Marl	–	<5	6.35	55	7.00	31	8.86	229	12.53	77	18.87	32	25.25	93
LDP1-10	Marl	–	<5	6.31	73	7.00	45	8.86	255	12.53	111	18.8	13	25.28	102
LDP1-9	Marl	–	<5	6.19	125	–	<5	8.88	280	12.5	117	18.84	20	25.29	104
LDP1-8	Marl	–	<5	6.33	182	–	<5	8.85	686	12.52	197	18.78	61	25.28	227
LDP1-7	Marl	–	<5	6.34	70	7.00	48	8.79	275	12.5	87	18.84	16	25.29	106
LDP1-6	Marl	5.16	134	6.32	153	–	<5	8.93	523	12.5	116	18.7	35	25.3	123
LDP1-5	Marl	5.2	301	6.29	586	–	<5	9.03	461	12.63	332	18.85	45	25.86	197
LDP1-4	Marl	–	<5	6.32	139	–	<5	8.88	340	12.53	128	18.76	19	25.33	96
LDP1-3	Marl	5.28	210	6.29	521	–	<5	9.05	305	12.6	241	18.83	18	25.38	97
LDP1-2	Marl	–	<5	6.39	38	–	<5	8.91	150	12.57	40	18.78	10	25.33	62
LDP1-1	Marl	–	<5	6.29	82	–	<5	8.87	256	12.53	96	18.86	14	25.28	88

Appendix 2.2 Analytical results: **(A)** WDS and **(B)** EDS data of major and trace elements from bulk rock samples of spherule deposits in the Rancho Nuevo (RNO), La Sierrita (MJP, LDP, MAS), El Peñon (EPO) and El Mimbral (MIM) area. Results are grouped according to their microfacies-types and localities. Total Fe is reported as Fe_2O_3. LOI is loss of ignition. Abbreviations as follows: MF, microfacies-type of spherule deposit; Det-lim, Detection limit. Abbreviations for section names are given in the text.

(A) WDS	MF	SiO₂	TiO₂	Al₂O₃	Fe₂O₃	MnO	MgO	CaO	Na₂O	K₂O	P₂O₅	LOI	Total
		wt%	wt%	wt%	wt%	wt%	wt%	wt%	wt%	wt%	wt%	wt%	wt%
RNO1-1	MF 3	35.87	0.80	14.07	10.39	0.05	2.43	15.16	0.86	1.98	0.16	18.92	100.70
RNO1-2	MF 3	35.19	0.78	13.84	9.35	0.04	2.17	16.48	0.90	2.07	0.13	19.56	100.51
RNO1-3	MF 3	32.66	0.73	12.78	8.65	0.03	2.00	15.25	0.99	1.92	0.11	25.31	100.45
RNO1-4	MF 3	31.43	0.49	8.23	3.84	0.08	1.02	27.99	1.07	1.71	0.11	24.02	99.97
RNO1-5	MF 3	35.45	0.79	14.33	9.31	0.04	2.19	17.70	0.81	2.04	0.13	19.23	102.02
LDP3-14	MF 1	15.24	0.35	9.03	9.46	0.11	4.17	33.62	0.08	0.61	0.10	27.00	99.77
MAS1-2	MF 1	9.41	0.27	5.95	7.89	0.09	3.74	37.16	0.03	0.11	0.08	34.06	98.79
MAS2-2	MF 1	14.34	0.38	9.08	10.62	0.07	4.51	26.45	0.05	0.38	0.11	31.68	99.67
MJP1B-3	MF 1	16.79	0.55	10.32	12.31	0.09	5.61	27.76	0.06	0.34	0.12	26.35	100.30
MJP1C-2	MF 1	11.54	0.61	10.52	13.50	0.08	5.66	31.89	0.14	0.40	0.11	25.94	100.39
MJP1C-3	MF 1	17.50	0.85	11.36	13.16	0.09	5.72	25.81	0.21	0.76	0.14	24.02	99.61
MJP1C-4	MF 1	3.75	0.18	4.10	6.00	0.18	2.28	45.93	0.09	0.13	0.09	36.64	99.38
MJP3A-4	MF 1	6.92	0.18	6.50	10.00	0.14	2.94	40.02	0.10	0.15	0.08	32.73	99.76
MJP3A-5	MF 1	10.05	0.53	10.92	14.77	0.11	5.03	32.31	0.44	0.44	0.11	27.16	101.87
MJP3A-6	MF 1	8.78	0.21	4.63	6.54	0.14	1.88	42.45	0.35	0.26	0.08	35.37	100.69
MJP3A-8	MF 1	9.89	0.43	8.04	11.94	0.09	3.38	34.69	0.59	0.38	0.10	30.09	99.62
MJP1A-3	MF 2	31.61	0.56	11.33	8.81	0.08	3.26	27.17	0.77	1.70	0.14	16.52	101.96
MJP1A-11	MF 2	43.48	0.51	11.10	5.03	0.05	2.22	17.68	1.45	2.01	0.15	16.68	100.36
MJP1A-16	MF 2	44.48	0.59	12.85	4.94	0.05	2.51	15.35	1.55	2.66	0.15	15.23	100.37
MJP1A-18	MF 2	47.89	0.67	14.90	7.02	0.04	3.29	11.22	1.11	2.67	0.42	12.96	102.20
MJP2B-10	MF 2	34.70	0.47	10.78	5.29	0.08	3.30	23.92	0.82	1.81	0.14	21.79	97.38
MJP2B-12	MF 2	25.23	0.40	7.98	4.47	0.05	2.60	26.56	0.54	1.31	0.10	28.14	103.10
MJP2B-8	MF 2	28.79	0.52	10.80	8.00	0.06	3.95	19.13	0.58	1.31	0.11	27.39	100.64
LDP2-2	MF 3	15.16	0.35	6.55	6.74	0.13	2.08	35.74	0.15	0.41	0.07	32.38	99.76
MAS1-14	MF 3	22.60	0.34	8.50	8.99	0.12	3.63	31.24	0.49	0.37	0.14	27.00	103.42
MJP1A-13	MF 3	41.37	0.85	14.41	12.69	0.03	5.85	10.15	1.37	1.23	0.12	12.62	100.70
MJP1A-14	MF 3	22.30	0.38	7.81	8.18	0.10	2.88	29.61	0.76	0.53	0.11	26.97	99.63
MJP1A-15	MF 3	39.43	0.84	15.66	15.18	0.03	6.87	7.54	1.02	0.89	0.05	11.79	99.30
MJP1A-17	MF 3	40.12	0.94	15.09	11.60	0.03	4.86	10.42	0.76	2.04	0.15	13.15	99.17
MJP2B-23	MF 3	38.52	0.99	14.82	14.48	0.05	4.09	9.82	0.76	0.68	0.15	12.12	96.48
SRS-1	MF 3	16.38	0.33	7.78	7.10	0.11	2.89	31.81	0.19	0.75	0.07	30.00	97.41
SRS-2	MF 3	22.32	0.27	8.20	8.38	0.08	3.47	28.56	0.57	0.39	0.11	26.33	98.68
MJP1A-10	Marl	40.58	0.52	11.10	4.13	0.05	1.94	18.50	1.13	2.25	0.12	19.66	99.97
MJP1A-12	Marl	42.23	0.48	10.50	4.62	0.05	1.98	18.00	1.21	1.96	0.14	17.29	98.46
MJP1B-9	SLL	50.33	0.21	6.32	2.83	0.05	0.94	19.76	2.32	0.37	0.13	18.02	101.29
MJP2B-3	SLL	30.21	0.25	5.57	2.50	0.10	0.72	36.33	1.70	0.77	0.09	22.07	100.30
MJP1B-11	Unit 2	43.67	0.18	5.65	1.55	0.09	0.61	23.16	2.57	0.32	0.09	22.99	100.87
MJP2B-6	Unit 2	37.07	0.17	4.87	1.71	0.09	0.36	25.87	2.65	0.29	0.08	28.18	101.36
EPO2D-3	MF 1	15.58	0.46	9.94	7.36	0.20	2.50	33.83	0.95	1.51	0.11	28.77	101.21
EPO2E-2	MF 1	21.72	0.49	9.40	6.18	0.10	1.95	30.37	0.35	1.87	0.08	27.98	100.50
EPO2E-8	MF 1	16.53	0.38	7.27	5.54	0.15	2.06	35.40	0.10	1.20	0.07	31.62	100.34
EPO2F-3	MF 1	19.50	0.46	8.44	4.58	0.15	1.94	33.15	0.51	1.80	0.07	29.89	100.47
EPO2A-3	MF 3	21.99	0.50	7.77	7.97	0.13	1.77	31.32	0.68	0.89	0.07	27.47	100.56
EPO2A-4	MF 3	17.11	0.34	8.53	9.87	0.13	2.39	32.13	0.41	0.60	0.08	28.29	99.90
EPO2A-6	MF 3	16.95	0.40	7.35	7.65	0.17	1.70	33.10	0.57	0.75	0.07	30.25	98.96
EPO2B-3	MF 3	26.87	0.50	10.11	11.01	0.08	2.58	23.92	1.10	0.82	0.16	23.39	100.55
EPO2A-2	Lime	15.17	0.16	3.43	1.54	0.06	0.48	42.09	0.43	0.55	0.03	36.15	100.10
EPO2A-5	SLL	56.80	0.32	8.07	2.20	0.04	0.62	15.40	3.98	0.51	0.13	13.16	101.24
EPO2A-7	Unit 2	39.58	0.22	5.27	1.58	0.10	0.37	26.44	2.56	0.36	0.10	22.15	98.75
ELM1-3	MF 1	16.74	0.38	7.48	4.14	0.11	2.41	35.66	0.27	1.28	0.10	30.54	99.10
ELM1-5	MF 1	15.84	0.27	5.90	3.73	0.12	1.82	37.67	0.34	1.05	0.07	33.62	100.42
ELM2-3	MF	19.96	0.37	7.84	5.61	0.09	3.17	28.20	0.47	1.25	0.14	33.45	100.53
ELM2-4	MF 1	11.76	0.35	7.43	7.62	0.10	4.07	37.15	0.16	0.60	0.13	30.74	100.12
ELM2-6	MF 2	17.33	0.32	5.88	3.75	0.11	1.63	37.20	0.60	1.03	0.10	32.45	100.42
ELM1-7	MF 3	19.51	0.28	5.95	3.95	0.12	1.98	35.42	1.15	0.86	0.11	31.01	100.34
ELM2-5	SLL	18.89	0.19	6.06	3.44	0.12	1.59	36.46	0.88	1.01	0.06	31.73	100.43
ELM1-8	Unit 2	51.40	0.26	6.54	3.02	0.05	0.89	19.05	2.26	0.60	0.11	16.07	100.25

Appendix 2.2 (B) (caption on page 189).

(B) EDS	MF	Cu	Zn	As	Rb	Sr	Y	Zr	Ba	La	Ce	Pb
		ppm	ppm	ppm	ppm	ppm	ppm	ppm	ppm	ppm	ppm	ppm
Det-lim		5	4	5	10	1	3	5	5	10	10	5
RNO1-1	MF 3	22	84	9	49	260	26	160	215	20	32	26
RNO1-2	MF 3	25	78	10	53	275	28	155	130	25	15	24
RNO1-3	MF 3	26	52	5	54	420	12	110	140	10	23	17
RNO1-4	MF 3	23	72	6	54	380	19	88	7170	<10	26	10
RNO1-5	MF 3	21	76	10	51	270	26	150	130	20	25	21
LDP3-14	MF 1	17	63	<5	13	500	17	63	6030	<10	<10	<5
MAS1-2	MF 1	21	71	<5	<10	580	10	47	160	19	25	<5
MAS2-2	MF 1	16	58	<5	18	470	15	48	2510	<10	<10	<5
MJP1B-3	MF 1	26	58	<5	10	550	10	72	320	10	30	8
MJP1C-2	MF 1	25	68	<5	10	600	12	77	215	12	31	<5
MJP1C-3	MF 1	25	54	<5	26	485	18	110	190	<10	30	<5
MJP1C-4	MF 1	11	24	<5	<10	610	17	34	160	14	24	<5
MJP3A-4	MF 1	14	53	<5	<10	330	14	32	105	<10	29	<5
MJP3A-5	MF 1	23	72	<5	15	350	15	64	140	12	28	<5
MJP3A-6	MF 1	13	47	<5	<10	470	10	29	270	<10	19	<5
MJP3A-8	MF 1	14	64	5	12	410	12	60	605	<10	13	<5
MJP1A-3	MF 2	14	46	<5	28	490	15	56	190	14	28	<5
MJP1A-11	MF 2	22	59	<5	70	490	17	100	180	<10	45	<5
MJP1A-16	MF 2	17	61	5	90	320	19	95	190	20	43	5
MJP1A-18	MF 2	27	82	5	94	300	26	110	215	19	54	<5
MJP2B-10	MF 2	22	83	<5	60	430	16	82	220	18	38	<5
MJP2B-12	MF 2	19	76	<5	61	420	14	78	210	22	23	<5
MJP2B-8	MF 2	21	78	<5	51	390	16	92	370	10	26	<5
LDP2-2	MF 3	22	50	<5	12	430	12	30	1760	14	26	5
MAS1-14	MF 3	17	53	<5	10	410	15	72	400	10	27	<5
MJP1A-13	MF 3	20	63	<5	40	360	15	175	115	12	34	8
MJP1A-14	MF 3	19	76	<5	61	420	14	78	205	22	23	<5
MJP1A-15	MF 3	32	99	6	28	180	10	150	96	11	38	9
MJP1A-17	MF 3	37	110	6	68	320	20	140	180	22	33	5
MJP2B-23	MF 3	31	78	<5	23	230	19	145	660	11	38	6
SRS-1	MF 3	24	81	8	23	620	15	58	4030	<10	<10	<5
SRS-2	MF 3	11	50	<5	10	480	15	71	4560	<10	<10	<5
MJP1A-10	Marl	25	76	<5	83	425	17	95	200	26	55	8
MJP1A-12	Marl	23	56	<5	72	475	18	95	175	21	44	7
MJP1B-9	SLL	12	26	6	11	410	10	80	100	12	19	5
MJP2B-3	SLL	16	39	<5	24	58	13	70	165	<10	24	<5
MJP1B-11	Unit 2	11	23	6	10	405	10	96	90	11	12	<5
MJP2B-6	Unit 2	16	27	7	29	500	11	75	150	10	27	12
EPO2D-3	MF 1	16	40	7	39	600	11	68	2850	<10	<10	<5
EPO2E-2	MF 1	20	40	<5	45	740	14	70	760	13	25	5
EPO2E-8	MF 1	17	42	<5	32	800	21	61	4170	<10	23	<5
EPO2F-3	MF 1	27	33	<5	47	750	15	73	2390	<10	12	<5
EPO2A-3	MF 3	26	64	8	26	570	15	96	330	<10	26	<5
EPO2A-4	MF 3	12	51	6	19	480	14	69	435	14	24	<5
EPO2A-6	MF 3	21	56	8	23	635	15	75	430	10	29	<5
EPO2B-3	MF 3	20	60	<5	21	470	15	96	440	10	23	<5
EPO2A-2	Limes	9	17	<5	14	240	4	27	130	<10	12	<5
EPO2A-5	SLL	17	29	9	14	370	10	130	130	13	34	6
EPO2A-7	Unit 2	8	25	6	10	520	12	105	130	25	33	7
ELM1-3	MF 1	195	51	6	34	410	16	68	72	15	41	5
ELM2-3	MF 1	26	74	<5	36	330	15	71	115	<10	26	<5
ELM2-4	MF 1	17	100	<5	16	350	11	59	60	<10	26	7
ELM1-5	MF 1	15	51	<5	25	400	10	41	52	13	29	<5
ELM2-6	MF 2	27	68	<5	25	445	13	53	73	20	25	6
ELM1-7	MF 3	13	47	6	19	400	12	64	62	<10	16	<5
ELM2-5	SLL	28	50	<5	25	520	9	40	130	25	33	<5
ELM1-8	Unit 2	18	41	175	20	520	8	93	140	17	18	10

Appendix 2.3 Varimax rotated factor loadings of the principal component analysis from the Spearman rank correlation matrix for the geochemical analysis (WDS and EDS) of bulk samples from spherule deposits (data from Appendix 2.2, 70 samples, 16 variables) and Méndez marls (15 samples, 16 variables, data from Lindenmaier, 1999). *Italics*: 0.5-0.6; **boldface** >0.6. LOI, Loss of ignition.

Oxides and elements	Spherule deposits (n = 70)			Méndez marls (n = 15)		
Factor	1	2	3	1	2	3
SiO$_2$	0.41	**0.85**	0.26	-0.03	**0.72**	0.11
TiO$_2$	**0.74**	0.38	0.43	*0.51*	0.34	*0.53*
Al$_2$O$_3$	**0.74**	0.48	0.39	**0.90**	-0.04	-0.30
Fe$_2$O$_3$	**0.86**	-0.32	0.10	**0.77**	-0.09	0.01
MnO	**-0.67**	*-0.53*	-0.14	0.02	**-0.93**	0.15
MgO	**0.85**	-0.18	-0.31	**0.70**	0.27	0.16
CaO	**-0.66**	**-0.64**	-0.28	**-0.78**	-0.48	-0.25
Na$_2$O	0.14	**0.72**	0.23	-0.38	**0.65**	*0.55*
K$_2$O	-0.06	**0.81**	0.42	**0.65**	0.30	0.35
P$_2$O$_5$	0.35	0.44	0.10	-0.16	-0.04	**0.88**
LOI	**-0.66**	**-0.63**	-0.20	*-0.55*	**-0.64**	-0.46
Cu	*0.50*	0.24	0.19	-0.48	-0.06	0.19
Zn	*0.57*	0.21	0.14	-0.25	0.31	0.46
As	-0.01	0.19	**0.78**	*0.60*	-0.22	0.20
Rb	0.01	**0.87**	0.25	**0.80**	0.02	-0.14
Sr	*-0.52*	-0.28	-0.17	**-0.80**	0.43	0.16
Y	0.13	0.33	**0.61**	-0.05	0.07	**0.76**
Zr	**0.64**	0.46	*0.55*	**0.66**	0.00	-0.25
La	0.15	0.44	0.23	-0.02	-0.33	-0.12
Ce	0.44	0.44	-0.21	0.22	0.20	-0.06
Pb	0.30	0.18	**0.72**	-0.01	0.13	-0.12
Explained variance	5.75	5.39	2.94	6.66	3.33	3.07
Relative variance	27 %	26 %	14 %	30 %	15 %	14 %

Appendix 2.4 Sorted factor values for (**A**) factor 1 and (**B**) factor 2 based on the principal component analysis from the Spearman rank correlation matrix for the WDS and EDS analysis of bulk samples from spherule deposits (analytical data in Appendix 2.2). Abbreviations for the section names are given in Chapter 2.

(A)	MF	Factor 1	Factor 2	Factor 3	(B)	MF	Factor 1	Factor 2	Factor 3
MJP1A-15	MF 3	2.69	0.23	-0.45	MJP1A-16	MF 2	-0.39	2.80	-0.78
MJP2B-23	MF 3	2.16	-0.01	0.84	MJP1A-11	MF 2	-0.40	2.14	-0.71
MJP1A-13	MF 3	1.90	0.90	-0.17	MJP1A-17	MF 3	1.43	1.67	0.04
MJP1C-2	MF 1	1.48	-1.77	-0.28	MJP2B-10	MF 2	-0.09	1.53	-0.58
MJP1A-17	MF 3	1.43	1.67	0.04	MJP1A-3	MF 2	-0.12	1.49	-1.46
MJP1C-3	MF 1	1.35	-0.72	-0.18	MJP2B-12	MF 2	-0.40	0.95	-0.50
MJP3A-5	MF 1	1.18	-1.67	-0.37	MJP1A-13	MF 3	1.90	0.90	-0.17
MJP1B-3	MF 1	1.09	-0.55	-1.31	MJP1A-14	MF 3	-0.28	0.87	-0.84
MAS2-2	MF 1	0.61	-0.84	-0.99	RNO1-1	MF 3	0.45	0.79	2.37
RNO-5	MF 3	0.48	0.08	3.32	RNO1-2	MF 3	0.07	0.70	1.20
MJP2B-8	MF 2	0.45	0.63	-0.37	MJP2B-8	MF 2	0.45	0.63	-0.37
RNO1-1	MF 3	0.45	0.79	2.37	RNO1-2	MF 3	0.28	0.54	2.59
RNO1-2	MF 3	0.28	0.54	2.59	EPO2E-2	MF 1	-0.96	0.40	0.65
EPO2B-3	MF 3	0.20	0.03	0.10	ELM2-3	MF 1	-0.49	0.37	-0.54
LDP3-14	MF 1	0.18	-0.99	-0.07	EPO2F-3	MF 1	-1.52	0.32	0.39
MAS1-3	MF 1	0.13	-1.32	-0.64	MJP1A-15	MF 3	2.69	0.23	-0.45
MJP3A-8	MF 1	0.10	-1.31	0.08	RNO1-5	MF 3	0.48	0.08	3.32
RNO1-2	MF 3	0.07	0.70	1.20	MAS1-6	MF 3	-0.01	0.08	-0.82
ELM2-4	MF 1	0.04	-0.69	-0.13	ELM1-5	MF 1	-1.26	0.04	-0.11
MAS1-6	MF 3	-0.01	0.08	-0.82	EPO2B-3	MF 3	0.20	0.03	0.10
MJP2B-10	MF 2	-0.09	1.53	-0.58	ELM2-6	MF 3	-1.06	0.00	-0.38
SRS-2	MF 3	-0.09	-0.21	-0.68	MJP2B-23	MF 3	2.16	-0.01	0.84
MJP1A-3	MF 2	-0.12	1.49	-1.46	EPO2E-8	MF 1	-1.10	-0.11	-0.23
MJP1A-14	MF 3	-0.28	0.87	-0.84	LDP2-3	MF 3	-0.60	-0.18	-1.10
EPO2A-4	MF 3	-0.39	-0.67	0.86	SRS-2	MF 3	-0.09	-0.21	-0.68
MJP1A-16	MF 2	-0.39	2.80	-0.78	EPO2A-3	MF 3	-0.70	-0.22	0.85
MJP1A-11	MF 2	-0.40	2.14	-0.71	ELM1-7	MF 3	-1.10	-0.27	-0.06
MJP2B-12	MF 2	-0.40	0.95	-0.50	EPO2D-3	MF 1	-1.03	-0.49	1.10
ELM2-3	MF 1	-0.49	0.37	-0.54	MJP3A-6	MF 1	-1.18	-0.49	-0.91
SRS-1	MF 3	-0.50	-0.71	0.18	MJP1B-3	MF 1	1.09	-0.55	-1.31
MJP3A-4	MF 1	-0.55	-1.22	-0.35	EPO2A-4	MF 3	-0.39	-0.67	0.86
LDP2-3	MF 3	-0.60	-0.18	-1.10	ELM2-4	MF 1	0.04	-0.69	-0.13
EPO2A-3	MF 3	-0.70	-0.22	0.85	EPO2A-6	MF 3	-0.83	-0.70	0.70
EPO2A-6	MF 3	-0.83	-0.70	0.70	SRS-1	MF 3	-0.50	-0.71	0.18
EPO2E-2	MF 1	-0.96	0.40	0.65	MJP1C-3	MF 1	1.35	-0.72	-0.18
EPO2D-3	MF 1	-1.03	-0.49	1.10	MAS2-2	MF 1	0.61	-0.84	-0.99
ELM2-6	MF 3	-1.06	0.00	-0.38	LDP3-14	MF 1	0.18	-0.99	-0.07
EPO2E-8	MF 1	-1.10	-0.11	-0.23	MJP3A-4	MF 1	-0.55	-1.22	-0.35
ELM1-7	MF 3	-1.10	-0.27	-0.06	MJP3A-8	MF 1	0.10	-1.31	0.08
MJP3A-6	MF 1	-1.18	-0.49	-0.91	MAS1-3	MF 1	0.13	-1.32	-0.64
MJP1C-4	MF 1	-1.21	-1.42	-0.26	MJP1C-4	MF 1	-1.21	-1.42	-0.26
ELM1-5	MF 1	-1.26	0.04	-0.11	MJP3A-5	MF 1	1.18	-1.67	-0.37
EPO2F-3	MF 1	-1.52	0.32	0.39	MJP1C-2	MF 1	1.48	-1.77	-0.28

Appendix 2.5 Summarized electron microprobe analysis from multiple individual points and linescans of single spherules and fragments from La Sierrita, El Peñon, and El Mimbral (average and standard deviation). All data in weight percent; total Fe is given as FeO; SD is standard deviation. Abbreviations for the section names are given in Chapter 2.

Sample	Mineralogy	SiO$_2$	TiO$_2$	Al$_2$O$_3$	FeO	MgO	CaO	Na$_2$O	K$_2$O	Total
	n	wt%	wt%	wt%	wt%	wt%	wt%	wt%	wt%	wt%
MJP1A-15	Chlorite	28.47	0.10	22.47	24.09	10.73	0.61	0.04	0.53	87.10
SD	75	2.55	0.43	1.17	2.12	0.93	0.20	0.03	0.60	2.72
MAS1-14	Chlorite	28.80	0.34	22.29	25.80	9.65	0.79	0.03	0.46	88.17
SD	20	1.65	0.59	0.77	1.18	0.52	0.14	0.01	0.39	1.47
MJP1B-3	Chlorite	27.52	0.18	18.91	30.34	5.40	2.50	0.08	0.47	85.41
SD	76	1.63	0.18	0.82	3.57	0.37	0.25	0.04	0.09	2.46
LDP3-14	K-rich glass	50.23	0.19	29.15	1.88	2.35	0.57	0.10	7.25	91.79
SD	21	1.16	0.13	0.78	0.54	0.29	0.07	0.04	0.21	1.20
SRS-2	K-rich glass	50.12	0.15	29.55	1.49	2.14	0.56	0.10	7.14	91.30
SD	12	0.62	0.10	0.46	0.09	0.07	0.05	0.04	0.19	1.05
MJP1A-14	Chlorite	30.04	0.03	23.04	23.30	10.40	0.64	0.04	0.88	88.42
SD	37	2.32	0.03	1.06	2.14	0.92	0.20	0.02	0.57	1.82
MJP1A-15	Chlorite	28.56	0.08	21.93	27.88	9.49	0.60	0.04	0.45	89.10
SD	22	1.03	0.05	0.71	0.82	0.44	0.09	0.02	0.13	1.29
MJP1A-15	Chlorite	30.84	0.20	21.62	24.97	9.44	0.57	0.03	0.83	88.59
SD	24	1.49	0.18	1.15	2.38	1.01	0.07	0.03	0.52	2.17
MJP1A-15	Carbonate	0.09	0.02	0.03	0.68	0.27	58.38	0.02	0.08	59.79
SD	21	0.11	0.02	0.03	0.12	0.06	1.16	0.02	0.04	1.18
MAS2-2	Carbonate	1.20	0.16	0.71	1.95	0.67	51.74	0.01	0.03	56.50
SD	7	1.92	0.36	0.98	0.96	0.40	4.05	0.02	0.05	1.81
EPO2A-4	Chlorite	30.55	0.02	22.12	24.00	11.13	0.39	0.07	0.24	88.61
SD	56	0.75	0.02	0.48	0.44	0.28	0.08	0.03	0.05	0.97
EPO2E-2	Chlorite	40.62	1.63	22.71	15.33	3.34	1.24	0.09	4.49	89.57
SD	24	4.89	3.05	1.84	4.42	0.71	1.04	0.03	0.76	3.12
EPO2E-2	K-rich glass	52.12	1.96	23.43	3.94	3.99	0.60	0.07	7.65	93.83
SD	24	1.14	1.43	1.53	1.11	0.48	0.38	0.02	0.29	1.22
EPO2F-3	K-rich glass	50.28	0.10	29.76	2.13	2.69	0.87	0.05	6.99	92.89
SD	21	1.55	0.14	1.48	1.54	0.77	0.10	0.02	0.47	1.51
EPO2A-6	K-rich glass	51.06	0.07	27.22	1.60	2.45	0.46	0.07	7.29	90.27
SD	39	0.60	0.02	0.48	0.08	0.08	0.10	0.03	0.16	0.96
EPO2A-4	K-rich glass	46.25	0.38	25.98	10.29	2.60	0.52	0.05	6.52	92.65
SD	10	1.70	0.80	0.63	3.43	0.41	0.12	0.02	0.29	0.61
EPO2A-4	Carbonate	0.78	0.02	0.06	0.65	0.29	55.09	0.02	0.02	56.96
SD	101	2.20	0.09	0.11	0.13	0.08	3.03	0.02	0.04	1.91
EPO2A-4	Carbonate	0.16	0.05	0.03	0.53	0.21	56.86	0.02	0.02	57.89
SD	98	0.31	0.36	0.05	0.14	0.09	1.60	0.02	0.02	1.52
EPO2F-3	Carbonate	0.28	0.02	0.11	0.60	0.35	56.20	0.02	0.04	57.66
SD	32	0.89	0.02	0.37	0.17	0.12	1.89	0.04	0.03	1.89
ELM1-5	Chlorite	33.75	0.11	17.75	19.87	13.85	0.99	0.17	0.46	87.06
SD	75	2.41	0.15	0.98	2.77	1.11	0.21	0.04	0.48	1.45
ELM1-5	Chlorite	30.25	0.04	19.12	23.92	12.24	0.86	0.07	0.39	87.00
SD	23	3.54	0.02	2.48	6.54	0.81	0.34	0.03	0.28	1.87
ELM1-3	Chlorite	36.71	0.39	17.09	16.79	14.88	1.28	0.20	0.48	87.93
SD	22	2.16	0.63	2.05	0.95	1.52	0.41	0.05	0.21	3.98
ELM1-5	Chlorite	40.65	0.26	18.61	15.70	12.65	1.30	0.18	1.32	90.74
SD	32	1.31	0.17	0.66	1.29	0.75	0.18	0.04	0.26	1.97
ELM1-5	Chlorite	39.88	0.20	19.27	16.78	12.81	1.11	0.17	1.30	91.62
SD	35	2.19	0.13	1.20	2.05	1.09	0.19	0.04	0.46	1.79
ELM1-5	Chlorite	26.61	0.03	22.16	25.62	12.14	0.16	0.03	0.06	86.88
SD	37	0.34	0.02	0.30	0.56	0.49	0.12	0.02	0.03	0.70
ELM1-3	Chlorite	34.85	0.12	18.31	16.82	14.49	2.16	0.06	0.47	87.35
SD	26	1.15	0.18	0.93	1.05	1.46	1.28	0.03	0.25	2.25
ELM1-5	K-rich glass	52.64	0.56	26.07	2.52	2.82	0.58	0.06	6.53	91.83
SD	32	1.46	1.98	0.83	0.14	0.15	0.22	0.03	0.18	1.38
ELM1-3	K-rich glass	52.77	0.18	26.49	2.91	2.85	0.32	0.07	6.52	92.14
SD	22	1.10	0.07	0.29	0.15	0.10	0.06	0.02	0.16	1.27
ELM1-5	Carbonate	0.03	0.03	0.02	0.48	0.45	57.46	0.01	0.02	58.54
SD	45	0.08	0.12	0.03	0.10	0.14	0.96	0.02	0.02	0.90
ELM1-4	Carbonate	0.02	0.01	0.01	0.39	0.39	55.84	0.02	0.02	56.73
SD	22	0.02	0.02	0.01	0.19	0.24	1.46	0.01	0.01	1.50

Appendix 3.1 Description of the methods used for qualitative and semiquantitative analysis of nonclay and clay mineralogy by X-ray diffraction.

Sample preparation for bulk-rock analysis
Random powder of the bulk sample is used for characterization of the whole rock mineralogy. Nearly 20 grams of each rock sample was ground with a ''jaw'' crusher to obtain small chips (1–5 mm) of rock. Nearly 5 g were dried at 60° C and then ground again to a homogenous powder with particle sizes, 40 mm. 800 mg of this powder were pressed (20 bars) in a powder holder covered with blotting paper, and then analyzed by XRD.

Sample preparation for clay mineral analysis
Analytical procedure was based on methods developed by Kübler (1987). Ground ships were mixed with de-ionized water (pH 7-8) and agitated. The carbonate fraction was removed with the addition of HCL 10 % (1.25 N) at room temperature for 20 minutes. Ultrasonic disaggregation was done during 3 min intervals. The insoluble residue was washed and centrifuged until a neutral suspension was obtained (pH 7-8). Separation of the <2μm grain-size fraction was obtained by the time-settling method based on Stokes law. The <2μm fraction was then pipetted onto a round glass plate (ø 25 mm) and air-dried at room temperature. XRD analyses from the oriented samples were made from (i) the "air-dried" sample and (ii) after keeping the sample overnight in ethylenglycol solvated conditions (''glycolated sample'').

XRD measurements
All samples were measured with a SCINTAG 2000 goniometer, using CuKα radiation (45 kV, 40 mA) and an automatic sample charger. The XRD measurements were carried out by a step scan with 2 seconds counting time. "Air-dried" samples of the <2μm fraction were measured from 1 to 50 °2Θ, and "glycolated samples" from 1 to 30 °2Θ, whereas bulk rock powder samples were measured from 1 to 65 °2Θ, all measurements were made with a step size of 0.03°.

Analysis of XRD diagrams
The raw (RD) files generated with SCINTAG are transformed in routine by the software (DMS program, v. 2.63) via Kα-stripping, background subtraction, and Fast Fourier noise filter into calculated (NI) diffractograms. Using the graphically oriented computer program 'MacDiff' (Freeware by R. Petschick, Universität Frankfurt), the calculated XRD diagrams were corrected to the d-value of the (002) quartz peak and the basal mineral reflections were analyzed by determining the d-value, intensity, integrated peak area (Σ of counts), and full width at half maximum; peak-asymmetry was allowed. The reflections of the following minerals were considered from the glycolated sample after deconvolution. Note, however, that the term smectite, chlorite, illite, and kaolinite are here used as a general expression for the respective mineral groups.
• **Smectite** (001) at 5.2 °2Θ after graphical removal of the chlorite 6 °2Θ peak from the glycolated sample. A broad peak around 5.2 °2Θ on the glycolated X-ray diffractograms together with a high background in the low-angle shoulder of this peak indicates the presence of interstratifications with illite (I-S).
• **Illite** (001) at 8.83 °2Θ to estimate relative illite content, the c-lattice constant (unit cell dimension), which varies from 'muscovitic' to 'biotitic', and the full width at half maximum (FWHM). The FWHM grade of lattice order and the crystallite size usually referred to as 'crystallinity' is used to determine low temperature metamorphosis of shales or marls, whereas in young sediments, possible source regions, and transport paths can be traced with this method.
• **Illite** (002) at 17.73 °2Θ was determined to approximate the 'octahedral character' by using the (002/001) peak intensity ratio. High (002)/(001) ratios (>0.4) correspond to Al-rich (muscovitic) illites, whereas values <0.15 correspond to biotitic illites (Bengtsson and Stevens, 1998).
• **Chlorite** (002) and **kaolinite** (001)-doublet at 12.4 °2Θ was used to determine their relative content. To resolve the peaks from both minerals, the relative proportion of the respective mineral determined in the deconvoluted doublet at 24.8 and 25.2 °2Θ was applied to the 12.4 °2Θ peak (Biscaye, 1964).
• Interstratified **illite-smectite** (I-S): The appearance of peaks at about >9 °2Θ (I-S 001/002) and <17.73 °2Θ (I-S 002/003) after glycolization indicates the presence of interstratified illite-smectite. The relative proportion of smectite interstratification can be estimated by the use of the Δ °2Θ data (Table 8.3 in Moore and Reynolds, 1997). The presence of a single peak at about 6.5 °2Θ indicates a R1-ordering of the I-S.
• Interstratified **chlorite-smectite** (C-S): In the glycolated sample, a shift of the C002 peak towards lower angles (<12.4 °2Θ) and a shift of the C003 peak towards higher angles (>25.2 °2Θ) indicates the presence of interstratified chlorite-smectite (C-S 002/002 and C-S 004/005). The relative proportion of smectite interstratification can be estimated by the use of the Δ °2Θ data (Table 8.4 in Moore and Reynolds, 1997).
• Interstratified **chlorite-vermiculite** (C-V): The presence of interstratified chlorite-vermiculite is indicated by peaks at 6.5-7.1 °2Θ, 10.8-11.2 °2Θ, and 25.6 °2Θ that do not change upon glycol-solvation. However, these peaks may be similar to illite-vermiculite R1.

Calculation of mineral percentages
The semiquantitative estimation of the relative abundance (rel%) of the clay minerals was conducted by using the ratios of the integrated peak areas of smectite, chlorite, illite, and kaolinite from the glycolated specimen as recommended by Reynolds (1989) and Moore and Reynolds (1997 p. 309). Since the smectite (002) and (003) peaks were either absent or to weak for semiquantitative analysis, the smectite (001) peak was used instead. To account for the use of the low-range smectite (001) peak area for this semiquantitative analysis, which leads to an over-estimation of the smectite content relative to the other clay minerals (Moore and Reynolds, 1997), the weighting correction factors, which were introduced for peak intensity data, by Biscaye (1965) were used (see Petschick et al., 1996 for details of this methodology). The following multiplication factors were used: '1' for smectite, '4' for illite, and '2' for chlorite and kaolinite peak areas. Due to the considerable effects of chemical and structural composition of clay minerals in relation to their spacing characteristics, these weighting factors only provide a first approach to the quantity of a single phase within the clay mineral fraction.

Appendix 3.2 Raw data of the X-ray diffractometry: Nonclay minerals from bulk powder samples.

BZC	Depth	Quartz	K-Felds.	Plagio.	Calcite	Pyrite	BZC	Depth	Quartz	K-Felds.	Plagio.	Calcite	Pyrite
#	m	counts/s	counts/s	counts/s	counts/s	counts/s	#	m	counts/s	counts/s	counts/s	counts/s	counts/s
1-50	10	1515	51	100	803	26	2-49	50	546	53	13	2554	46
1-47	60	1392	51	48	1127	21	2-48	55	2015	145	207	2415	40
1-45	100	1178	12	46	1056	40	2-47	60	1734	26	147	2995	121
1-43	140	3189	27	396	1518	21	2-46	62.5	1502	29	125	2125	96
1-42	160	1673	52	148	2573	17	2-45	65	2621	186	99	2072	122
1-40	200	3995	165	395	1142	12	2-40	80	2347	80	194	644	10
1-37	260	2374	48	272	1021	68	2-39	85	2490	38	162	518	40
1-34	320	2495	23	164	1864	98	2-38	90	2255	66	150	557	10
1-31	380	3168	162	167	680	132	2-37	100	2445	53	196	698	10
1-28	440	2852	81	261	823	73	2-35	120	2154	87	167	930	26
1-25	500	1948	75	158	925	167	2-33	140	2331	35	232	929	27
1-22	560	2438	52	236	730	119	2-31	160	2989	66	197	1077	17
1-19	620	2568	157	227	371	101	2-29	200	2528	23	202	879	20
1-17	660	2378	48	151	360	71	2-27	240	2146	41	138	645	15
1-15	700	2306	100	205	426	97	2-25	280	3466	96	227	651	48
1-12	740	2186	42	151	447	76	2-23	320	2538	77	146	652	12
1-11	750	546	53	13	2554	68	2-21	360	2612	31	291	678	29
1-10	760	2015	145	207	2415	39	2-19	400	2297	64	177	592	35
1-9	770	1502	29	125	2125	48	2-17	440	1807	38	203	535	19
1-8	780	2445	53	201	712	10	2-15	480	805	32	220	340	31
1-7	790	1096	87	174	926	16	2-13	520	1955	118	156	538	16
1-5	810	2255	35	236	863	16	2-11	560	2384	55	116	539	18
1-3	830	2866	66	189	1052	10	2-9	600	2172	37	156	683	20
1-1	840	2348	23	199	875	17	2-7	640	1870	59	168	543	17
2-58	5	2757	40	297	411	73	2-5	680	1791	37	191	567	10
2-55	20	2350	33	276	470	49	2-3	720	2286	42	143	626	11
2-52	35	2186	42	151	447	59	2-1	750	2095	97	171	701	12

Appendix 3.3 Raw X-ray diffraction data from the glycolated <2 μm fraction of the Brazos cores (BZC) 1 and 2. Abbreviations as follows: S, smectite; Ch, chlorite; I, illite; K, kaolinite. "Int." refers to peak height and "Area" refers to the peak area (both in counts per second).

BZC	Depth	S(001)			Ch(001)			I(001)			K(001)/Ch(002)			I(003)		K(002)		Ch(004)	
#	m	°2Θ	Int.	Area	°2Θ	Int.	Area	°2Θ	Int.	Area	°2Θ	Int.	Area	°2Θ	Int.	°2Θ	Int.	°2Θ	Int.
1-50	0	5.27	1513	56534	6.15	203	7226	8.86	176	2464	12.39	258	4385	17.77	47	24.9	93	25.15	62
1-47	60	5.24	1956	71697	6.17	137	4332	8.89	213	3228	12.4	300	5012	17.8	65	24.9	107	25.1	89
1-45	100	5.2	1581	58168	6.17	87	1589	8.87	147	2058	12.39	193	3165	17.77	30	24.9	73	25.15	41
1-43	140	5.3	555	19220	6.13	350	13780	8.85	95	1882	12.43	148	2223	17.78	20	24.95	33	25.15	55
1-42	160	5.3	501	16166	6.1	340	13742	8.87	81	1699	12.44	163	2431	17.76	23	24.94	38	25.16	51
1-40	200	5.29	1430	46839	6.1	666	27873	8.86	249	5615	12.43	527	9480	17.79	88	24.93	169	25.15	222
1-37	260	5.29	1217	39165	6.1	428	17259	8.92	147	2613	12.45	316	5654	17.81	54	24.94	107	25.18	118
1-34	320	5.21	511	16841	6.1	234	9486	8.87	109	1561	12.43	158	2400	17.81	20	24.93	39	25.16	45
1-31	380	5.25	1083	37167	6.05	386	15536	8.87	198	3722	12.42	333	5575	17.79	53	24.93	88	25.17	111
1-28	440	5.3	645	23073	6.2	267	9414	8.93	188	3104	12.47	276	4301	17.82	49	24.95	75	25.16	77
1-25	500	5.26	1233	46670	6.15	181	5497	8.88	205	3618	12.44	327	5512	17.79	49	24.93	92	25.16	109
1-22	560	5.23	1854	64550	6.05	423	16908	8.89	252	5568	12.45	448	8192	17.81	75	24.96	146	25.18	149
1-19	620	5.2	926	36172	6.21	257	8805	8.88	243	3913	12.42	406	6348	17.79	79	24.94	121	25.15	124
1-17	660	5.24	1719	62229	6.19	315	11593	8.91	301	6869	12.49	492	8822	17.8	89	24.95	159	25.17	191
1-15	700	5.22	968	32881	6.1	184	6728	8.84	180	4115	12.43	358	5922	17.79	63	24.91	133	25.13	145
1-14	720	5.23	1573	52281	6.11	309	11975	8.91	230	4858	12.46	437	7234	17.8	60	24.95	119	25.17	164
1-13	730	5.28	1095	36371	6.11	581	23507	8.88	269	6288	12.46	488	8970	17.78	92	24.92	138	25.15	198
1-12	740	5.21	1807	64667	6.19	96	3028	8.89	134	1872	12.43	256	4152	17.8	27	24.9	76	25.13	67
1-11	750	5.28	1179	33595	6.17	268	9959	8.86	66	751	12.39	104	1403	17.77	14	24.9	37	25.17	27
1-10	760	5.26	1597	59104	6.2	271	9020	8.87	179	2946	12.42	319	4989	17.77	50	24.93	92	25.16	102
1-9	770	5.3	1756	64329	6.16	430	16193	8.88	237	4359	12.43	432	7155	17.79	78	24.91	108	25.16	156
1-8	780	5.3	463	16621	6.25	246	9803	8.92	151	2521	12.46	291	4463	17.82	43	24.95	95	25.18	110
1-7	790	5.3	758	24777	6.2	587	22887	8.89	283	5634	12.44	504	8381	17.79	96	24.92	147	25.17	167
1-5	810	5.3	697	28327	6.25	530	26510	8.86	246	4921	12.43	415	6977	17.79	74	24.93	120	25.17	135
1-3	830	5.21	1065	36146	6.16	267	11635	8.89	163	2871	12.44	259	3965	17.71	41	24.93	83	25.18	77
1-1	850	5.22	1644	57127	6.21	292	12431	8.89	218	4742	12.45	376	6085	17.79	47	24.93	95	25.17	131
2-58	5	5.25	1645	62242	6.2	420	15473	8.87	367	8111	12.42	664	11894	17.75	127	24.9	214	25.15	236
2-55	20	5.29	2007	69659	6.2	353	14142	8.91	321	7026	12.45	575	9479	17.79	93	24.94	162	25.2	214
2-52	35	5.24	1041	38670	6.21	219	7211	8.89	192	3604	12.45	355	5801	17.79	55	24.94	107	25.17	135
2-49	50	5.25	1321	45780	6.2	185	7759	8.92	165	2358	12.44	294	4938	17.82	48	24.94	95	25.17	98
2-48	55	5.3	892	30080	6.21	168	7160	8.91	100	1612	12.43	279	4849	17.79	34	24.91	104	25.12	109
2-47	60	5.28	16	391	6.23	25	581	8.85	112	1024	12.46	87	961	17.73	60	24.95	10	25.17	48
2-46	62.5	5.3	784	22971	6.25	146	6002	8.93	68	783	12.45	105	1462	17.84	14	24.95	34	25.17	31
2-45	65	5.23	3973	108526	6.21	59	1758	8.87	69	1095	12.43	85	1040	17.78	10	24.92	5	25.12	21
2-42	72.5	5.2	2805	90470	6.28	24	726	8.84	80	1109	12.41	154	2286	17.7	18	24.89	31	25.11	46
2-41	75	5.27	1380	54955	6.2	154	5669	8.84	105	1571	12.39	211	3451	17.75	17	24.91	45	25.1	60
2-40	80	5.25	1449	50807	6.23	221	9140	8.85	187	3476	12.42	382	6438	17.77	48	24.92	103	25.12	116
2-39	85	5.3	868	29400	6.19	633	28448	8.9	235	4734	12.43	427	7151	17.79	74	24.93	143	25.18	144
2-38	90	5.28	1739	58504	6.22	334	13948	8.93	184	4085	12.51	436	7481	17.82	54	24.98	114	25.18	187
2-37	100	5.24	696	23100	6.25	261	11430	8.85	189	3641	12.42	337	5537	17.76	65	24.89	94	25.14	145
2-35	120	5.25	712	25310	6.24	247	10230	8.9	170	3474	12.41	329	5213	17.81	61	24.92	89	25.15	160
2-33	140	5.26	1491	53286	6.21	382	17974	8.9	231	4425	12.44	384	6574	17.8	51	24.95	88	25.17	133
2-31	160	5.21	1348	47451	6.19	342	15228	8.84	193	3809	12.4	351	5950	17.75	54	24.89	89	25.12	102
2-29	200	5.26	1837	62223	6.19	392	16905	8.88	241	5437	12.46	440	7530	17.79	80	24.92	89	25.17	155
2-27	240	5.24	1352	50507	6.24	311	14680	8.87	210	3810	12.39	474	8564	17.79	88	24.89	193	25.12	181
2-25	280	5.21	1725	65134	6.18	385	17891	8.85	334	7456	12.44	594	10382	17.76	96	24.92	140	25.14	224
2-23	320	5.22	1978	68920	6.19	386	16857	8.87	274	6013	12.49	463	8070	17.77	75	24.91	97	25.16	143
2-21	360	5.22	1990	74178	6.24	430	18785	8.85	349	8843	12.45	649	11398	17.77	107	24.92	157	25.16	261
2-19	400	5.22	2067	76136	6.19	460	21238	8.88	337	8698	12.44	677	12437	17.78	125	24.93	224	25.17	298
2-17	440	5.19	1567	55983	6.18	319	14364	8.87	227	4714	12.44	423	6951	17.77	65	24.91	90	25.16	142
2-15	480	5.23	1307	49885	6.19	472	22828	8.88	322	6437	12.45	564	9195	17.8	106	24.93	138	25.18	196
2-13	520	5.21	1636	54262	6.21	387	17093	8.85	225	4299	12.43	406	6774	17.77	60	24.91	103	25.16	135
2-11	560	5.3	440	19664	6.23	184	6095	8.89	176	3151	12.43	332	5346	17.78	69	24.91	147	25.13	133
2-9	600	5.28	720	26578	6.24	299	12798	8.89	192	3819	12.46	371	6145	17.77	60	24.91	92	25.18	133
2-7	640	5.19	2168	80936	6.17	307	13199	8.86	333	7806	12.43	569	9809	17.79	87	24.9	140	25.19	175
2-5	680	5.23	2274	82141	6.2	505	22235	8.87	369	8479	12.45	696	12129	17.79	117	24.93	189	25.17	277
2-3	720	5.22	1863	62554	6.18	441	19302	8.87	282	5909	12.45	496	8109	17.75	69	24.93	101	25.15	164
2-1	760	5.22	1395	38353	6.26	618	19496	8.87	260	5069	12.43	400	6215	17.77	71	24.92	102	25.16	134

Appendix 3.4 Major element composition of bulk samples from Brazos core (BZC) 1 and 2 as determined by WDS analysis. Total Fe is reported as Fe_2O_3 and LOI is loss of ignition.

Sample	Depth	SiO_2	TiO_2	Al_2O_3	Fe_2O_3	MnO	MgO	CaO	Na_2O	K_2O	P_2O_5	LOI	Total
BZC #	cm	wt%	wt%	wt%	wt%	wt%	wt%	wt%	wt%	wt%	wt%	wt%	wt%
1-50	0	50.89	0.57	14.60	5.16	0.03	2.33	8.29	0.52	2.08	0.22	16.29	100.99
1-47	60	48.33	0.54	13.77	4.93	0.04	2.23	11.28	0.54	2.01	0.32	17.18	101.18
1-45	100	28.99	0.29	6.95	25.48	0.05	1.32	12.80	0.56	1.02	0.55	14.90	92.89
1-43	140	45.32	0.38	8.55	3.49	0.07	1.58	19.43	1.04	1.50	0.87	18.72	100.94
1-42	160	32.70	0.29	6.77	2.98	0.11	1.30	27.37	0.69	1.17	0.66	25.51	99.55
1-40	200	52.90	0.50	10.34	3.95	0.04	1.74	12.18	1.16	1.88	0.72	13.97	99.38
1-37	260	53.91	0.53	11.44	4.35	0.03	1.81	10.47	1.17	1.99	0.52	13.59	99.81
1-34	320	42.48	0.36	7.17	3.08	0.09	1.27	21.71	1.09	1.44	0.70	19.70	99.08
1-31	380	54.20	0.58	12.58	4.86	0.03	2.12	9.01	1.14	2.16	0.51	13.49	100.68
1-30	400	54.58	0.57	11.78	4.63	0.03	1.93	9.50	1.09	2.08	0.37	14.10	100.66
1-28	440	52.77	0.58	12.49	4.96	0.03	2.17	8.88	1.01	2.13	0.35	14.97	100.36
1-26	480	53.13	0.60	12.24	5.08	0.04	2.19	9.25	1.07	2.18	0.36	14.32	100.47
1-24	520	48.71	0.55	11.40	4.55	0.06	2.17	13.08	1.01	2.02	0.26	16.68	100.49
1-22	560	54.52	0.62	13.22	4.97	0.04	2.29	7.69	1.17	2.32	0.21	13.36	100.41
1-21	580	55.92	0.63	13.66	4.83	0.03	2.09	6.22	1.20	2.33	0.20	12.68	99.81
1-20	600	57.52	0.66	13.91	5.01	0.03	2.23	5.14	1.07	2.39	0.23	12.22	100.40
1-19	620	58.74	0.68	14.16	5.21	0.03	2.34	4.02	1.10	2.49	0.22	11.80	100.77
1-18	640	57.36	0.70	14.55	5.36	0.03	2.44	4.37	1.38	2.58	0.22	11.84	100.82
1-17	660	58.02	0.67	14.01	5.26	0.03	2.35	4.31	1.01	2.44	0.24	12.42	100.76
1-16	680	56.63	0.70	14.89	5.38	0.03	2.51	4.49	1.10	2.57	0.26	12.35	100.92
1-15	700	55.54	0.70	15.07	5.70	0.03	2.59	4.60	1.22	2.58	0.21	12.68	100.92
1-14	720	57.64	0.65	13.32	5.08	0.03	2.35	4.34	1.01	2.37	0.22	14.05	101.06
1-13	730	54.58	0.67	14.98	6.06	0.03	2.61	4.65	1.00	2.44	0.20	13.57	100.79
1-12	740	43.73	0.40	8.41	3.65	0.09	1.70	19.50	1.21	1.61	0.17	19.23	99.70
1-11	750	48.22	0.33	6.51	3.06	0.12	1.21	19.34	1.04	1.33	0.34	19.01	100.50
1-10	760	49.95	0.46	10.17	4.39	0.08	1.67	14.47	0.92	1.62	0.38	16.69	100.80
1-09	770	50.49	0.67	14.01	5.98	0.04	2.64	8.14	0.94	2.08	0.35	15.29	100.64
1-07	790	54.12	0.64	13.93	5.39	0.03	2.32	6.57	0.97	2.31	0.24	13.93	100.47
1-05	810	51.59	0.66	13.87	5.77	0.03	2.41	7.79	0.86	2.08	0.38	14.83	100.27
1-03	830	53.60	0.60	12.71	4.95	0.03	1.99	9.00	0.98	2.16	0.27	14.07	100.35
1-01	850	54.17	0.61	12.87	5.18	0.03	2.09	8.28	1.00	2.22	0.30	13.74	100.48
2-58	5	57.46	0.66	14.67	5.23	0.03	2.28	4.55	0.99	2.41	0.20	12.08	100.57
2-56	15	56.53	0.68	14.78	5.40	0.03	2.48	4.51	1.02	2.48	0.21	12.47	100.59
2-54	25	57.47	0.68	14.61	5.27	0.03	2.44	4.15	1.18	2.50	0.21	12.07	100.61
2-52	35	56.21	0.66	14.75	5.35	0.03	2.46	4.74	0.97	2.44	0.20	12.69	100.50
2-51	40	52.80	0.65	14.69	5.59	0.03	2.58	6.68	0.90	2.36	0.21	14.01	100.51
2-50	45	41.51	0.50	11.61	4.62	0.07	2.30	18.23	0.72	1.82	0.20	19.58	101.16
2-49	50	23.22	0.25	6.01	2.85	0.13	1.45	35.55	0.40	0.74	0.14	29.12	99.86
2-48	55	38.78	0.31	6.08	3.16	0.15	1.39	25.07	1.00	1.29	0.15	21.35	98.72
2-47	60	35.01	0.26	5.60	2.86	0.16	1.22	28.81	0.94	1.16	0.17	24.30	100.49
2-46	63	38.28	0.28	5.78	2.79	0.15	1.17	27.16	0.97	1.17	0.20	22.51	100.45
2-45	65	48.36	0.37	7.06	3.98	0.12	1.28	19.49	0.97	1.16	0.85	16.37	100.00
2-44	68	43.53	0.48	9.92	5.99	0.10	1.93	16.04	0.86	1.01	1.59	17.88	99.33
2-43	70	38.83	0.86	15.77	10.07	0.07	3.03	11.47	0.55	0.33	3.23	17.33	101.53
2-42	73	45.50	0.64	13.76	6.55	0.06	2.60	11.08	0.72	1.50	0.93	17.42	100.78
2-41	75	54.34	0.63	14.79	5.36	0.03	2.42	6.72	0.97	2.28	0.24	13.94	101.71
2-40	80	54.29	0.64	14.63	5.47	0.03	2.28	6.02	0.87	2.31	0.20	13.18	99.92
2-39	85	55.14	0.68	15.13	5.60	0.03	2.50	5.05	0.93	2.45	0.18	12.97	100.66
2-38	90	54.69	0.67	15.08	5.61	0.03	2.48	5.42	0.98	2.42	0.19	13.06	100.61
2-37	100	53.52	0.65	14.05	5.39	0.03	2.34	6.88	1.09	2.37	0.27	14.13	100.72
2-35	120	53.35	0.61	13.02	5.04	0.03	2.14	8.53	1.01	2.24	0.26	14.25	100.47
2-33	140	54.29	0.58	12.80	4.90	0.03	1.96	9.03	0.97	2.11	0.29	14.02	101.00
2-31	160	54.23	0.59	12.99	5.00	0.03	1.98	9.21	1.14	2.19	0.26	13.73	101.35
2-29	200	54.96	0.61	13.55	5.18	0.03	2.09	8.04	1.12	2.27	0.23	13.84	101.92
2-27	240	54.48	0.66	14.95	5.51	0.03	2.23	5.88	0.91	2.23	0.17	14.03	101.08
2-25	280	56.78	0.64	14.37	5.31	0.03	2.25	6.28	1.06	2.36	0.20	13.18	102.47
2-23	320	55.44	0.63	14.07	5.42	0.02	2.18	6.28	1.09	2.30	0.22	13.11	100.76
2-21	360	56.29	0.63	14.32	5.26	0.03	2.26	6.03	1.05	2.33	0.20	13.08	101.48
2-19	400	55.71	0.66	15.13	5.57	0.03	2.38	5.40	0.97	2.37	0.18	13.63	102.02
2-17	440	54.71	0.64	15.05	5.31	0.03	2.42	5.96	1.11	2.29	0.19	13.77	101.47
2-15	480	54.72	0.62	14.52	5.39	0.03	2.34	6.55	1.13	2.29	0.20	13.98	101.76
2-13	520	55.07	0.64	14.82	5.61	0.03	2.33	5.64	1.10	2.36	0.18	13.59	101.39
2-11	560	56.10	0.64	14.76	5.53	0.03	2.30	5.51	0.98	2.35	0.18	13.07	101.46
2-09	600	55.15	0.63	14.22	5.45	0.03	2.22	6.95	1.00	2.30	0.26	13.57	101.76
2-07	640	54.78	0.64	14.69	5.51	0.03	2.30	5.73	0.96	2.30	0.19	13.42	100.53
2-05	680	54.89	0.63	14.56	5.55	0.03	2.31	5.89	0.98	2.30	0.19	13.42	100.76
2-03	720	55.16	0.64	14.71	5.59	0.03	2.33	5.88	0.99	2.31	0.20	13.53	101.37
2-01	760	53.38	0.61	14.30	5.38	0.03	2.27	5.99	0.93	2.23	0.19	14.01	99.31

Appendix 3.5 Trace element compositions of bulk samples based on EDS analysis; detection limits according to Kramar (1997). The concentrations of Cr and Ni are generally below the detection limit (50 ppm) and are not listed.

Sample	Depth	Cu	Zn	As	Rb	Sr	Y	Zr	Ba	La	Ce	Pb
BZC #	cm	ppm	ppm	ppm	ppm	ppm	ppm	ppm	ppm	ppm	ppm	ppm
Detect.-limit		5	4	5	10	1	3	5	5	10	10	5
1-50	0	16	144	6	80	295	16	114	363	35	66	11
1-47	60	15	152	5	80	389	19	113	333	25	55	13
1-45	100	22	185	10	50	423	20	97	164	13	51	11
1-43	140	14	73	7	45	456	21	173	280	24	41	<5
1-42	160	20	67	<5	35	481	17	106	204	18	32	8
1-40	200	13	86	10	58	362	21	194	353	31	48	<5
1-37	260	14	92	9	63	343	21	173	335	22	40	8
1-34	320	13	55	8	40	321	14	181	284	11	31	<5
1-33	340	9	53	9	41	325	17	197	300	31	59	<5
1-32	360	16	97	10	66	312	20	169	341	31	54	7
1-31	380	15	100	13	68	322	21	165	340	25	52	<5
1-30	400	18	109	12	75	354	21	157	337	21	66	7
1-29	420	15	75	12	66	357	19	145	323	25	54	<5
1-28	440	20	91	11	71	353	19	158	350	24	50	5
1-27	460	21	88	11	73	317	19	158	359	31	56	6
1-26	480	11	118	12	75	338	22	155	335	41	48	5
1-25	500	12	76	7	68	373	20	145	336	25	53	8
1-24	520	19	85	6	72	383	19	137	322	46	85	9
1-23	540	14	88	9	74	368	19	141	346	27	43	8
1-22	560	13	93	10	81	321	21	152	347	35	60	7
1-21	580	23	96	9	84	304	20	152	374	20	61	11
1-20	600	16	99	9	89	288	21	158	348	24	68	14
1-19	620	21	96	8	89	266	22	158	369	28	69	18
1-18	640	11	99	8	93	271	20	159	364	28	51	12
1-17	660	15	94	11	85	261	21	138	365	27	63	7
1-16	680	17	104	9	88	274	24	146	371	35	58	13
1-15	700	19	104	9	93	286	21	143	358	21	51	14
1-14	720	29	98	11	90	287	20	158	370	30	48	19
1-13	730	19	93	9	89	284	18	150	364	22	43	18
1-12	740	15	60	7	49	464	17	127	372	28	37	6
1-11	750	12	37	7	35	366	18	180	326	28	48	4
1-10	760	14	60	5	52	355	19	169	332	28	51	8
1-09	770	16	92	8	72	382	18	137	307	21	46	7
1-08	780	15	97	10	81	367	19	143	317	35	64	7
1-07	790	13	88	8	84	345	20	147	336	27	47	9
1-05	810	17	87	7	76	388	19	138	320	26	56	11
1-03	830	16	92	8	77	401	20	166	358	32	49	12
1-01	850	16	96	13	76	372	22	164	358	20	54	8
2-58	5	24	110	7	96	296	20	155	380	27	61	14
2-57	10	21	99	6	90	276	20	144	360	27	63	17
2-56	15	24	109	10	92	292	20	150	372	35	82	10
2-55	20	16	98	9	94	287	20	152	357	38	67	13
2-54	25	14	102	9	96	286	22	161	359	30	62	14
2-53	30	22	100	9	95	313	22	167	364	21	52	21
2-52	35	17	93	8	87	285	18	145	367	36	60	10
2-51	40	18	99	10	88	371	20	142	348	21	66	15
2-50	45	10	78	6	67	577	18	105	275	19	58	11
2-49	50	12	39	<5	33	538	14	52	159	22	47	<5
2-48	55	14	37	6	33	355	14	116	291	20	44	8
2-47	60	10	32	7	28	337	15	115	255	33	38	<5
2-46	62.5	7	24	7	30	332	14	172	268	23	57	<5
2-45	65	8	31	7	31	341	25	210	281	40	57	<5
2-44	67.5	21	47	7	34	425	30	141	261	49	74	5
2-43	70	27	58	5	10	615	25	116	206	30	72	2
2-42	72.5	9	75	6	68	402	18	136	283	30	54	11
2-41	75	21	98	6	83	361	18	144	355	47	69	12
2-40	80	22	107	8	96	357	19	152	347	25	60	14
2-39	85	16	111	7	94	341	18	152	350	22	57	14
2-38	90	17	112	7	93	348	18	146	362	36	54	9
2-37	100	20	105	10	88	358	21	159	346	39	68	10
2-36	110	17	101	9	80	382	23	174	333	24	59	9
2-35	120	12	100	9	78	387	20	160	338	30	78	8
2-33	140	20	102	8	81	406	23	170	345	25	57	13
2-31	160	18	95	10	81	409	21	166	351	44	87	8
2-29	200	37	86	9	79	369	18	149	343	35	61	21
2-27	240	15	105	6	87	362	17	152	358	31	55	15
2-25	280	17	104	11	85	351	21	147	331	29	64	5
2-23	320	23	102	7	92	366	20	149	335	27	75	12
2-21	360	13	105	9	87	360	21	153	340	32	66	10
2-19	400	22	117	6	92	376	20	148	351	32	65	16
2-17	440	19	105	6	87	374	21	149	327	38	65	12
2-15	480	16	102	7	84	382	20	141	332	33	76	8
2-13	520	18	112	7	91	369	20	138	347	37	76	10
2-11	560	19	106	10	88	362	19	138	355	30	62	10
2-09	600	20	109	9	84	382	23	152	331	22	63	9
2-07	640	19	111	6	91	381	21	143	360	37	63	12
2-05	680	20	108	9	87	369	20	138	335	37	63	11
2-03	720	11	110	6	87	371	20	138	346	42	70	11
2-01	760	24	108	5	85	386	21	137	343	37	67	12

Appendix 4.1 Raw X-ray diffraction data from the glycolated <2 μm fraction of the Antioch Church core (AC). Abbreviations as follows. S, smectite; Ch, chlorite; I, illite; Zeol, zeolites (heulandite as indicated by the c-lattice constant of 8.95 Å); K, kaolinite. "Int." refers to peak height and "Area" refers to the peak area (both in counts per second).

AC	Depth	S(001)			Ch(002)			I(001)			Zeol		K(001)/Ch(002)			I(002)		K(002)		Ch(003)	
#	m	°2Θ	Int.	Area	°2Θ	Int.	Area	°2Θ	Int.	Area	°2Θ	Int.	°2Θ	Int.	Area	°2Θ	Int.	°2Θ	Int.	°2Θ	Int.
235	1.83	5.21	1733	53112	6.05	114	5107	8.9	55	713	9.89	212	12.49	10	89	17.78	10	–	<5	–	<5
234	2.29	5.24	1801	54286	6.05	116	5908	8.87	72	882	9.92	412	12.49	11	116	17.78	11	–	<5	–	<5
233	2.74	5.29	1704	61488	6.1	115	4714	8.98	60	678	9.94	363	12.55	10	74	17.83	10	–	<5	–	<5
231	3.35	5.3	1869	33446	6.1	180	6825	8.82	115	1459	9.9	259	12.52	10	56	17.8	24	–	<5	–	<5
230	3.66	5.24	949	91216	6.2	171	6013	8.8	115	1296	9.82	468	12.46	10	66	17.72	27	–	<5	25.17	10
229	3.96	5.23	2801	65030	6.2	36	515	8.89	170	2350	9.91	246	12.47	31	320	17.78	46	–	<5	–	<5
227	5.18	5.23	2174	61019	6.1	92	3425	8.83	176	2634	9.88	208	12.46	33	321	17.73	81	–	<5	–	<5
226	5.79	5.23	2128	61019	6.1	181	7240	8.84	186	2360	9.83	206	12.45	33	322	17.73	81	–	<5	–	<5
225	6.40	5.18	2231	68105	6.15	201	6420	8.78	203	2481	9.8	347	12.4	34	315	17.7	52	–	<5	–	<5
224	7.01	5.26	996	38165	6.12	43	1261	8.78	94	1069	9.82	330	12.46	10	48	17.74	20	–	<5	–	<5
223	7.62	5.18	1806	56760	6.1	60	1723	8.82	161	2009	9.83	217	12.3	90	1078	17.73	42	–	<5	–	<5
222	8.08	5.2	2425	72088	6.1	102	3718	8.85	193	2519	–	<5	12.32	48	497	17.74	60	–	<5	––	<5
221	8.53	5.17	3178	96345	6.1	117	2205	8.81	192	1669	–	<5	12.3	36	218	17.72	58	–	<5	–	<5
220	9.45	5.19	3040	111817	6.05	71	2575	8.82	211	2584	–	<5	12.28	21	230	17.73	58	–	<5	–	<5
218	10.67	5.19	2935	85917	6.1	308	12141	8.81	192	2804	–	<5	–	<5	–	17.7	60	24.81	10	25.14	13
217	11.13	5.22	412	21265	6.12	63	1902	8.8	213	2497	9.81	10	12.43	44	365	17.71	63	–	<5	25.18	13
216	11.58	5.23	1686	53398	6.15	199	8357	8.83	255	3808	–	<5	12.45	47	446	17.73	78	–	<5	25.15	13
215	12.04	5.29	1446	51995	6.3	198	7084	8.83	276	3556	–	<5	12.46	64	572	17.73	79	–	<5	–	<5
214	12.80	5.27	1351	46021	6.12	138	5440	8.83	155	2493	9.78	25	12.48	20	180	17.76	33	–	<5	25.22	10
213	13.41	0.32	1160	40195	6.3	154	6111	8.87	222	3208	9.78	12	12.5	45	414	17.73	63	–	<5	–	<5
212	13.87	5.19	2105	67158	6.12	67	2470	8.82	224	2735	9.88	62	12.46	39	352	17.73	51	–	<5	–	<5
211	14.33	5.18	1540	47229	6.1	129	5121	8.78	261	3205	9.79	290	12.41	51	450	17.69	87	–	<5	25.13	23
207	16.15	5.15	725	34019	6.14	45	872	8.84	183	2445	9.86	774	12.48	34	287	17.74	73	24.89	10	25.17	17
205	17.07	5.16	1507	43668	6.1	98	3771	8.77	209	2930	9.8	286	12.41	56	556	17.68	112	–	<5	25.1	12
202	18.68	5.21	3347	106041	6.18	105	3320	8.8	333	4791	9.85	270	12.43	71	725	17.72	137	–	<5	25.19	20
200	19.20	5.23	1142	41009	6.23	154	6186	8.79	153	1837	9.81	308	12.41	24	246	17.61	40	–	<5	25.09	11
198	20.57	5.23	1631	55312	6.13	192	8265	8.8	180	2171	9.82	412	12.42	33	276	17.72	45	–	<5	–	<5
196	21.49	5.25	1326	42785	6.1	152	5315	8.85	158	1789	9.86	362	12.49	32	267	17.76	24	–	<5	–	<5
194	22.40	5.15	1174	36679	6.11	58	2417	8.81	197	2110	9.83	548	12.43	36	333	17.74	48	–	<5	25.16	10
192	23.77	5.2	448	14479	6.1	48	1847	8.8	57	549	9.82	335	12.46	10	73	17.69	10	–	<5	–	<5
190	24.41	5.3	536	22823	6.17	76	2293	8.79	135	1571	9.81	369	12.43	12	94	17.71	32	–	<5	–	<5
188	25.45	5.2	1024	37258	6.15	53	1545	8.83	145	1744	9.81	401	12.5	10	85	17.75	39	–	<5	–	<5
185	26.67	5.17	1912	67753	6.1	66	1922	8.8	257	2950	9.81	215	12.4	46	472	17.71	88	–	<5	25.1	10
182	27.74	5.2	1931	66580	6.1	81	2553	8.79	149	2149	9.85	107	12.43	10	65	17.71	49	–	<5	–	<5
179	28.96	5.2	1703	65050	6.1	122	4218	8.77	247	3152	9.78	172	12.41	37	317	17.68	63	–	<5	25.1	10
177	29.41	5.23	380	16327	6.1	32	813	8.72	142	1400	9.74	74	12.3	26	244	17.64	38	24.78	17	25.07	10
175	30.33	5.17	1296	38501	6.1	106	4034	8.79	44	499	–	<5	12.31	45	586	17.76	15	24.96	11	25.13	10
173	31.85	5.25	510	21317	6.3	31	1006	8.8	32	372	–	<5	12.3	25	272	17.67	10	24.96	14	25.11	10
171	33.83	5.27	2227	69760	–	<5	–	8.97	34	1114	–	<5	12.45	64	919	17.89	22	–	<5	–	<5
169	35.30	5.26	708	28916	6.1	174	5420	8.8	114	1203	–	<5	12.28	560	8745	17.73	23	24.84	302	25.16	12
167	35.81	5.2	2321	84251	6.05	278	12175	8.81	190	2510	–	<5	12.3	1121	18753	17.79	91	24.91	710	25.13	46
165	36.88	5.18	2583	90319	6.13	235	14100	8.78	253	2932	–	<5	12.28	1207	20196	17.73	113	24.93	856	25.1	57
163	37.64	5.25	910	28830	6.25	109	3951	8.91	150	1498	–	<5	12.39	362	5780	17.83	61	24.95	215	25.3	11
160	39.17	5.27	1895	46614	6.16	153	5057	8.9	136	1286	–	<5	12.36	505	8348	17.83	62	24.91	331	25.38	40
157	40.54	5.26	756	19790	6.12	87	2989	8.86	95	1036	–	<5	12.33	464	8096	17.79	52	24.9	427	25.29	25
154	41.91	5.26	4079	118805	6.12	362	14107	8.86	127	1447	–	<5	12.33	1517	26319	17.8	65	24.9	1088	25.12	121
151	43.28	5.24	2441	64977	6.06	262	9407	8.88	185	1717	–	<5	12.36	665	10915	17.81	121	24.91	479	25.17	51
148	44.56	5.33	992	25922	6.17	153	5370	8.92	192	1797	–	<5	12.39	456	7155	17.85	76	24.94	283	25.42	20
145	46.18	5.3	923	26461	6.18	160	5532	8.9	148	1608	–	<5	12.31	617	10351	17.83	92	24.92	509	25.34	64
142	47.55	5.23	952	31607	6.24	181	7450	8.89	176	1950	–	<5	12.36	532	8596	17.81	116	24.92	394	25.28	51
139	48.98	5.21	606	19573	6.2	148	6227	8.91	288	2843	–	<5	12.38	356	5603	17.85	130	24.93	208	25.38	45
136	50.29	5.27	1249	43428	6.14	184	7215	8.86	174	2096	–	<5	12.34	396	6435	17.78	104	24.88	269	25.33	42
133	51.82	5.25	192	11324	6.28	27	412	8.79	110	1640	–	<5	12.25	256	3861	17.76	35	24.75	149	25.26	27
131	52.27	5.28	4551	156524	6.28	57	914	8.86	126	1590	–	<5	12.33	908	15031	17.77	46	24.88	552	25.13	58
129	52.73	5.28	1581	50507	6.11	219	8706	8.88	140	1272	–	<5	12.33	353	5546	17.8	60	24.89	200	25.24	10
127	53.28	5.26	1975	59059	6.13	186	6787	8.84	86	843	–	<5	12.32	475	7515	17.75	29	24.88	306	25.13	19
125	53.95	5.28	1578	49158	6.24	209	7307	8.84	63	870	–	<5	12.33	390	5978	17.79	15	24.87	227	25.15	44
123	54.56	5.21	1755	57337	6.3	277	9388	8.9	80	944	–	<5	12.37	367	5677	17.84	10	24.92	195	25.16	10
121	55.17	5.29	535	18297	6.2	218	9692	8.97	109	1123	–	<5	12.4	346	5318	17.88	33	24.9	169	25.22	17
119	55.60	5.29	1567	50781	6.12	263	10394	8.92	67	704	–	<5	12.38	652	11084	17.86	18	24.95	390	25.21	59
117	56.24	5.25	613	22640	6.3	164	6477	8.9	79	892	–	<5	12.37	386	6224	17.82	17	24.93	204	25.2	12
115	56.85	5.2	436	23081	6.2	130	6075	8.94	79	888	–	<5	12.4	547	8741	17.87	14	24.97	286	25.22	20
113	57.42	5.2	588	25693	6.25	165	6773	8.88	62	692	–	<5	12.34	626	10369	17.86	10	24.92	348	25.29	14
111	57.76	5.19	1386	44949	6.12	150	5656	8.84	111	1138	–	<5	12.31	431	6771	17.73	27	24.88	236	25.27	10
109	58.28	2.28	432	21685	6.2	178	8889	8.87	94	1395	–	<5	12.31	602	10044	17.77	19	24.88	300	25.2	17

Appendix 4.1 (continued from page 199).

AC	Depth	S(001)			Ch(002)			I(001)			Zeol		K(001)/Ch(002)			I(002)		K(002)		Ch(003)	
#	m	°2Θ	Int.	Area	°2Θ	Int.	Area	°2Θ	Int.	Area	°2Θ	Int.	°2Θ	Int.	Area	°2Θ	Int.	°2Θ	Int.	°2Θ	Int.
105	59.38	5.2	2013	66223	6.09	218	8276	8.86	81	970	–	<5	12.33	812	13675	17.81	23	24.91	486	25.17	22
102	60.20	5.16	2109	64188	6.1	153	7146	8.84	80	840	–	<5	12.31	668	11362	17.77	10	24.88	346	25.2	35
100	60.59	5.21	612	19147	6.19	98	3511	8.85	53	558	–	<5	12.32	469	7546	17.78	13	24.89	312	25.18	19
98	61.11	5.22	841	32264	6.16	149	5912	8.86	167	3142	–	<5	12.31	910	15873	17.75	34	24.86	589	25.29	26
97	61.36	5.22	449	15126	6.17	93	3145	8.88	78	1147	–	<5	12.34	307	5072	17.78	10	24.92	175	25.25	12
96	61.57	5.27	871	30479	6.15	136	10024	8.92	99	1322	–	<5	12.39	720	12569	17.88	18	24.9	413	25.23	35
95	61.75	5.3	454	12329	6.11	191	8932	8.85	142	2251	–	<5	12.32	783	12213	17.8	36	24.89	407	25.21	52
94	61.87	5.31	298	10487	6.21	167	5190	8.88	113	1718	–	<5	12.34	1092	19438	17.8	24	24.91	642	25.3	20
93	62.03	5.3	140	5240	6.2	95	2601	8.9	104	2284	–	<5	12.4	303	4898	17.84	15	24.95	185	25.18	18
92	62.12	5.25	181	7688	6.14	83	3027	8.87	83	1063	–	<5	12.34	325	5375	17.81	18	24.9	184	25.16	28
91	62.33	5.2	260	7790	6.19	118	4199	8.93	93	1232	–	<5	12.38	317	5266	17.86	22	24.94	190	25.2	14
90	62.58	5.25	369	12757	6.2	142	5455	8.9	108	1942	–	<5	12.36	463	7929	17.8	16	24.94	260	25.28	15
89	62.73	5.22	782	28117	6.18	108	4002	8.88	134	1773	–	<5	12.32	873	16177	17.78	31	24.92	558	25.29	34
88	62.94	5.27	353	12757	6.15	135	5470	8.88	101	1276	–	<5	12.34	540	9599	17.79	25	24.91	284	25.18	41
87	63.09	5.14	465	16095	6.16	132	4151	8.92	97	1282	–	<5	12.37	451	7906	17.85	20	24.95	246	25.17	22
86	63.25	5.23	502	17356	6.23	31	989	8.84	57	824	–	<5	12.32	321	6448	17.82	10	24.91	166	25.14	10
85	63.40	5.2	546	19312	6.12	83	3280	8.88	85	1176	–	<5	12.33	479	8396	17.83	12	24.92	270	25.13	22
84	63.55	5.3	343	10430	6.23	20	345	8.87	62	689	–	<5	12.33	339	6637	17.76	22	24.93	206	25.2	10
83	63.64	5.3	246	8839	6.11	49	1351	8.82	78	1106	–	<5	12.28	596	9605	17.76	21	24.87	364	25.18	12
82	63.70	5.3	1046	33477	6.22	167	7092	8.94	22	248	–	<5	12.37	111	1891	17.9	10	24.94	63	25.19	16
81	63.86	5.3	269	11191	6.1	15	485	8.89	10	25	–	<5	12.29	44	704	17.82	10	24.92	22	25.24	10
80	64.10	5.32	727	23547	6.12	55	1909	8.89	21	213	–	<5	12.33	115	1851	17.82	10	24.93	72	25.18	10
79	64.22	5.3	225	9977	6.19	33	1044	8.8	20	254	–	<5	12.3	191	2068	17.83	10	24.89	132	25.2	10
78	64.31	5.31	597	24497	6.17	70	2780	8.87	36	347	–	<5	12.32	130	2078	17.79	10	24.91	93	25.21	10
77	64.47	5.3	10	55	6.28	40	703	8.89	35	406	–	<5	12.35	96	1396	17.85	10	24.94	47	25.16	10
76	64.62	5.24	243	8348	6.18	107	4521	8.9	98	1659	–	<5	12.35	524	9508	17.85	22	24.94	314	25.29	19
75	64.92	5.23	437	15249	6.22	123	4701	8.9	158	2401	–	<5	12.35	606	11442	17.84	34	24.94	339	25.29	14
73	65.68	5.21	947	32204	6.1	154	6766	8.89	179	3029	–	<5	12.38	988	19141	17.81	37	24.93	598	25.29	37
72	66.14	5.19	550	21419	6.1	94	3953	8.86	199	3697	–	<5	12.3	971	18931	17.81	45	24.9	575	25.25	24
71	66.60	5.22	1093	38511	6.13	184	7448	8.84	130	1892	–	<5	12.3	1340	25083	17.76	47	24.88	733	25.19	38
70	67.06	5.24	438	17313	6.16	136	4751	8.86	122	1666	–	<5	12.33	845	14970	17.81	35	24.9	471	25.17	21
68	67.97	5.2	694	27063	6.23	94	3465	8.84	117	1491	–	<5	12.31	1026	18272	17.8	31	24.91	607	25.16	16
66	68.98	5.3	176	5912	6.21	205	7301	8.88	106	1976	–	<5	12.35	926	16594	17.83	21	24.91	538	25.2	31
64	69.65	5.3	296	13278	6.19	82	4185	8.86	106	1770	–	<5	12.32	948	17536	17.78	25	24.9	587	25.17	48
62	70.10	5.26	170	7184	6.2	196	10747	8.88	127	2238	–	<5	12.33	1138	20713	17.83	26	24.91	662	25.2	31
60	70.56	5.3	182	7173	6.21	142	7299	8.8	101	1872	–	<5	12.29	1158	21648	17.77	55	24.86	676	25.29	41
58	71.08	5.28	482	21059	6.17	145	4886	8.86	119	1805	–	<5	12.32	1045	19247	17.79	28	24.9	627	25.27	31
56	71.72	5.27	387	15993	6.21	101	3831	8.84	103	1871	–	<5	12.35	712	12925	17.82	11	24.92	394	25.29	20
54	72.18	5.3	383	16652	6.25	115	4053	8.88	130	1782	–	<5	12.34	929	16306	17.83	36	24.91	521	25.25	31
52	72.69	5.22	936	36516	6.18	115	4132	8.86	133	1916	–	<5	12.33	1437	26448	17.8	42	24.92	919	25.3	25
50	73.09	5.18	405	15054	6.1	62	2171	8.8	94	1224	–	<5	12.28	972	17222	17.77	34	24.85	669	25.25	25
48	73.76	5.18	803	31152	6.2	97	3291	8.87	126	1598	–	<5	12.33	1232	22552	17.82	34	24.91	767	25.22	55
46	74.28	5.24	473	19977	6.19	89	3010	8.84	90	1493	–	<5	12.35	927	16778	17.86	16	24.94	513	25.23	10
44	74.89	5.2	353	13814	6.2	100	3072	8.91	125	1676	–	<5	12.37	974	16972	17.85	29	24.95	559	25.23	15
42	75.44	5.14	567	22059	6.15	116	4144	8.85	131	1855	–	<5	12.31	1151	20478	17.79	23	24.88	631	25.15	29
40	75.90	5.2	205	11858	6.17	128	1751	8.8	116	1837	–	<5	12.29	1023	18013	17.76	33	24.83	622	25.22	21
38	76.50	5.22	245	8342	6.13	218	8975	8.81	130	1766	–	<5	12.23	1210	21372	17.76	40	24.84	732	25.2	21
35	77.11	5.3	546	23937	6.15	135	4675	8.89	107	1680	–	<5	12.3	1125	19618	17.77	30	24.88	644	25.24	29
32	77.72	5.25	559	24045	6.16	123	4367	8.86	110	1539	–	<5	12.32	1494	26257	17.77	31	24.89	876	25.2	52
30	78.33	5.25	334	14819	6.18	105	3546	8.83	107	1441	–	<5	12.31	1321	22831	17.77	35	24.88	880	25.22	69
27	78.97	5.2	680	26985	6.1	58	1829	8.81	85	1062	–	<5	12.29	2061	37073	17.73	41	24.86	1659	25.23	78
25	79.55	5.25	553	21626	6.13	185	7472	8.89	110	1727	–	<5	12.34	2129	38922	17.82	59	24.91	1493	25.24	82
23	80.10	5.18	1009	41442	6.17	101	3375	8.84	108	1689	–	<5	12.3	2388	43996	17.8	46	24.87	1654	25.21	50
21	80.47	5.24	597	22846	6.1	223	7733	8.9	140	2095	–	<5	12.35	2360	42656	17.8	49	24.92	1480	25.24	61
19	80.95	5.23	390	15223	6.1	220	8139	8.88	106	1856	–	<5	12.33	1932	35205	17.8	34	24.91	1178	25.19	26
17	81.47	5.21	581	22730	6.12	152	4922	8.88	138	2816	–	<5	12.35	1671	29889	17.84	58	24.92	981	25.29	34
14	82.20	5.25	536	21928	6.1	163	5347	8.89	139	2226	–	<5	12.34	1954	35832	17.81	46	24.93	1219	25.2	36
12	82.75	5.17	606	23806	6.1	140	4780	8.85	143	2367	–	<5	12.32	2105	39429	17.78	44	24.9	1378	25.19	23
8	83.67	5.2	223	8027	6.11	115	4098	8.84	97	1691	–	<5	12.34	1368	24402	17.82	22	24.92	914	25.26	23
6	84.12	5.15	291	11031	6.1	84	3004	8.86	294	3869	–	<5	12.31	1534	27029	17.79	163	24.89	1094	25.26	40
4	84.73	5.13	203	8007	6.16	104	5193	8.74	163	3874	–	<5	12.23	1889	34773	17.73	41	24.81	1124	25.28	37
1	85.31	5.15	196	7945	6.12	120	5725	8.81	170	3696	–	<5	12.28	1886	34675	17.75	38	24.86	1133	25.18	104

Appendix 4.2 Major- and trace-element composition of bulk samples from the Antioch Church core by energy-dispersive X-ray fluorescence spectrometry (EDS). Abbreviations: D-Lim, detection limits (Kramar, 1997); Cor-Ti, correlation factor of elements with the Ti content. All Fe is given as Fe_2O_3.

AC	Depth	TiO_2	Fe_2O_3	MnO	CaO	K_2O	Cu	Zn	As	Rb	Sr	Y	Zr	Ba	La	Ce	Pb
#	m	wt%	wt%	ppm	wt%	wt%	ppm	ppm	ppm	ppm	ppm	ppm	ppm	ppm	ppm	ppm	ppm
D-Lim	–	–	–	–	–	–	5	4	5	10	1	3	5	5	10	10	5
Cor-Ti	–	–	0.64	0.44	-0.88	0.71	0.38	0.62	-0.07	0.89	0.09	0.71	0.75	0.91	0.56	0.73	0.89
235	1.83	0.18	3.15	266	24.13	1.07	14	94	8	48	459	31	108	182	48	78	<5
232	3.05	0.23	2.99	190	27.79	1.18	8	87	5	47	577	32	149	228	39	56	<5
229	3.96	0.03	0.97	204	47.87	1.31	15	27	<5	<10	577	20	21	26	29	52	<5
226	5.79	0.01	0.33	103	50.10	1.28	<5	11	<5	<10	529	8	12	<5	16	20	<5
223	7.62	0.01	0.61	102	50.16	1.23	8	20	<5	<10	563	11	14	8	21	18	<5
220	9.45	0.01	0.36	61	46.56	1.02	<5	15	<5	<10	455	5	28	70	24	24	<5
217	11.13	0.01	0.64	94	50.26	1.48	<5	17	<5	<10	457	4	10	14	21	22	<5
215	12.04	0.09	2.40	50	40.73	1.36	13	50	<5	27	439	11	43	35	22	35	<5
213	13.41	0.07	2.59	50	39.87	1.16	5	45	<5	28	510	8	26	29	22	24	<5
210	14.78	0.04	0.90	38	45.12	1.05	11	19	<5	10	488	7	35	35	<10	<10	<5
207	16.15	0.36	1.51	64	27.74	1.10	13	32	<5	27	528	14	239	182	26	40	5
205	17.07	0.20	2.23	50	36.21	1.12	9	47	5	31	658	12	86	101	28	50	<5
202	18.68	0.19	1.36	57	39.04	1.02	8	45	<5	20	651	10	96	100	25	36	<5
200	19.20	0.17	2.06	50	37.23	1.25	10	59	<5	29	740	8	44	102	19	34	<5
198	20.57	0.13	1.14	48	42.79	1.02	8	36	<5	17	543	8	53	78	31	40	<5
196	21.49	0.09	0.98	41	43.84	0.85	10	30	<5	13	518	7	51	58	17	21	<5
194	22.40	0.02	0.42	53	49.05	0.89	9	17	<5	<10	533	4	34	40	21	24	<5
192	23.77	0.14	0.75	47	42.34	1.32	11	22	<5	12	503	8	87	62	<10	27	<5
190	24.41	0.29	1.88	50	14.50	1.09	11	48	9	34	698	14	192	259	38	64	<5
188	25.45	0.38	2.50	53	10.53	1.37	13	47	8	42	814	12	188	339	39	63	7
187	25.91	0.32	2.31	50	10.75	1.35	25	52	9	42	858	13	142	375	24	44	6
185	26.67	0.14	1.43	121	32.61	1.40	10	25	<5	16	731	7	58	85	13	29	<5
184	27.22	0.47	3.50	221	22.60	1.16	10	54	8	41	525	17	276	256	30	61	8
182	27.74	0.46	3.05	50	12.94	1.41	11	66	7	55	1004	13	157	292	25	47	7
180	28.41	0.38	2.50	50	10.53	1.37	13	47	8	42	814	12	188	339	39	63	7
179	28.96	0.46	3.77	50	13.39	1.52	11	84	13	60	947	11	111	281	29	57	7
178	29.26	0.42	4.14	50	16.61	1.53	18	90	11	63	838	14	89	232	31	37	9
177	29.41	0.03	1.86	157	47.31	0.76	45	25	73	<10	656	5	24	26	14	<10	<5
176	29.72	0.03	2.09	50	40.14	1.09	12	257	184	<10	574	3	31	44	20	28	5
175	30.33	0.01	1.05	50	39.30	1.11	<5	18	6	<10	464	3	29	37	10	10	<5
173	31.85	0.05	2.54	107	39.81	0.79	18	17	17	7	352	5	43	54	<10	29	<5
171	33.83	0.11	2.57	50	37.07	0.91	<5	18	14	11	329	10	115	78	22	54	5
170	34.59	0.08	1.14	50	38.41	1.02	20	25	7	10	308	11	90	74	17	39	<5
169	35.30	0.06	0.91	173	36.29	0.61	19	19	12	<10	578	7	73	40	13	17	<5
168	35.57	0.63	4.01	50	6.77	1.54	15	61	22	54	337	27	445	319	57	102	13
167	35.81	0.60	3.75	159	7.04	1.52	12	60	37	47	321	21	453	289	58	123	10
166	36.27	0.46	3.03	50	12.68	1.21	11	48	13	40	275	20	398	263	46	96	5
165	36.88	0.58	3.72	158	7.53	1.56	11	52	15	51	319	16	353	313	49	89	11
163	37.64	0.51	3.69	156	13.77	1.36	9	58	14	49	371	20	368	277	58	104	8
160	39.17	0.44	3.36	213	27.82	1.18	9	47	15	36	592	16	204	255	30	40	6
157	40.54	0.62	4.81	203	10.72	1.46	14	74	13	57	637	18	220	349	29	65	12
154	41.91	0.66	4.70	198	12.73	1.44	20	79	13	57	740	20	314	343	31	60	11
151	43.28	0.61	4.62	195	11.37	1.45	12	79	9	55	575	23	362	332	44	97	14
150	43.74	0.25	1.64	69	17.60	1.07	9	42	9	27	664	13	188	219	28	60	<5
148	44.56	0.46	3.53	50	21.75	1.12	11	48	9	40	528	18	281	247	29	57	8
145	46.18	0.19	1.60	168	41.56	0.90	13	28	<5	17	650	10	128	114	18	33	<5
142	47.55	0.46	3.14	133	25.12	1.13	12	52	10	39	670	14	215	225	30	53	<5
139	48.98	0.14	1.63	172	43.74	1.28	7	23	<5	13	591	11	66	71	24	29	<5
136	50.29	0.37	3.35	142	29.84	1.11	6	78	6	36	767	19	186	183	38	59	7
133	51.82	0.16	1.92	122	42.05	1.34	<5	33	6	17	578	11	130	89	11	40	<5
130	52.43	0.48	3.60	76	19.12	1.23	13	58	10	44	1043	15	186	183	35	56	8
129	52.73	0.44	3.32	50	24.43	0.98	15	53	10	39	1009	15	172	163	26	57	7
128	52.97	0.33	2.67	113	31.72	0.93	12	48	9	26	890	13	138	131	28	42	<5
126	53.64	0.17	1.56	100	41.51	0.82	10	26	<5	14	772	10	78	59	22	36	<5
124	54.25	0.38	3.08	130	27.60	0.94	10	51	9	33	933	13	178	158	30	51	8
122	54.89	0.19	1.90	81	39.52	1.32	10	32	<5	15	768	11	91	83	25	41	<5
121	55.17	0.45	4.31	91	22.25	1.25	10	68	9	47	903	15	185	207	30	59	9
118	55.93	0.49	4.70	100	20.27	1.40	13	84	12	50	817	15	217	237	30	58	9
116	56.54	0.43	4.75	101	27.31	1.33	9	56	10	48	758	13	159	186	25	58	6

Appendix 4.2 (continued from page 201).

AC	Depth	TiO$_2$	Fe$_2$O$_3$	MnO	CaO	K$_2$O	Cu	Zn	As	Rb	Sr	Y	Zr	Ba	La	Ce	Pb
#	m	wt%	wt%	ppm	wt%	wt%	ppm	ppm	ppm	ppm	ppm	ppm	ppm	ppm	ppm	ppm	ppm
D-Lim	–	–	–	–	–	–	5	4	5	10	1	3	5	5	10	10	5
Cor-Ti	–	–	0.64	0.44	-0.88	0.71	0.38	0.62	-0.07	0.89	0.09	0.71	0.75	0.91	0.56	0.73	0.89
114	57.15	0.78	6.35	268	9.31	1.80	25	106	14	74	591	18	226	415	26	44	15
112	57.61	0.52	8.20	50	21.25	1.90	12	122	10	78	658	13	150	203	16	53	9
110	58.03	0.50	4.02	85	20.71	1.32	14	69	12	49	1030	15	186	219	28	58	9
108	58.52	0.35	2.74	116	33.54	1.13	11	58	6	29	951	10	115	129	22	45	5
106	59.07	0.29	2.74	116	36.57	0.94	10	57	10	26	1001	16	85	124	36	47	<5
104	59.56	0.38	5.63	119	31.21	1.60	11	64	7	48	879	10	101	127	16	28	<5
103	59.74	0.68	6.77	144	14.47	1.67	18	100	10	67	823	13	163	312	26	48	13
101	60.35	0.75	6.25	263	9.64	2.03	16	111	10	75	607	18	190	407	13	71	14
100	60.59	0.81	7.17	305	12.35	2.38	21	137	10	90	507	19	185	442	32	51	<5
99	60.81	0.76	7.90	168	15.60	2.23	19	143	10	89	509	17	139	362	16	77	8
98	61.11	0.80	8.52	181	15.95	2.25	24	131	14	96	668	16	137	297	36	64	<5
97	61.36	0.20	7.37	50	39.29	1.34	8	48	9	55	679	9	26	57	19	42	<5
96	61.57	0.58	12.60	50	22.74	2.37	21	92	22	107	585	16	58	93	22	47	7
95	61.75	0.51	14.27	50	16.77	3.00	14	82	26	106	467	15	52	103	21	49	9
94	61.87	0.13	6.99	50	39.13	1.65	21	40	15	46	644	7	38	58	21	34	6
93	62.03	0.39	11.55	50	19.03	2.55	9	168	29	81	352	13	85	111	13	43	10
91	62.33	0.10	4.02	85	41.63	1.14	11	35	10	27	599	5	32	63	15	27	<5
89	62.73	0.34	4.63	98	31.28	1.33	8	63	12	43	341	12	102	155	21	52	7
87	63.09	0.22	4.02	170	39.50	1.09	9	44	11	29	457	13	137	115	28	58	<5
86	63.25	0.33	5.18	50	32.26	1.13	6	67	16	39	402	20	178	170	35	92	<5
84	63.55	0.29	4.16	176	37.29	1.04	9	37	19	31	416	15	155	148	25	53	<5
83	63.64	0.51	6.79	50	14.21	2.09	12	73	15	55	277	26	279	234	45	108	6
82	63.70	0.23	1.81	191	36.79	0.84	7	16	7	10	368	10	169	143	24	61	<5
80	64.10	0.17	1.50	159	32.66	0.56	17	16	<5	<10	342	8	85	111	18	35	<5
79	64.22	0.08	0.98	146	29.41	0.61	10	9	<5	<10	114	3	48	71	16	25	<5
78	64.31	0.20	1.65	244	33.98	0.81	8	10	<5	<10	224	10	145	94	21	41	9
77	64.50	0.19	30.05	50	1.45	0.96	40	19	300	16	52	3	60	86	<10	26	35
76	64.62	0.36	3.37	215	27.60	1.43	22	75	8	45	413	16	170	216	35	56	12
75	64.92	0.29	3.04	257	32.22	1.30	15	50	6	38	563	12	135	175	20	45	10
73	65.68	0.31	2.96	251	33.34	1.18	13	47	<5	37	620	11	107	174	33	48	8
71	66.60	0.45	3.33	212	25.46	1.53	8	53	7	51	544	19	233	311	28	69	5
70	67.06	0.63	4.85	206	10.41	2.05	11	76	9	72	341	22	331	436	31	75	6
69	67.51	0.69	5.16	219	10.17	2.03	15	84	9	79	386	21	283	415	30	69	11
67	68.43	0.68	5.38	228	10.03	2.06	17	80	8	75	386	20	315	419	39	84	14
65	69.49	0.66	5.10	217	9.01	1.98	18	90	7	79	383	22	273	451	29	75	13
63	69.89	0.71	5.25	223	10.19	1.88	23	95	8	79	430	18	246	396	35	75	13
61	70.35	0.46	3.33	212	23.09	1.32	8	55	5	49	468	25	351	304	43	102	11
59	70.87	0.60	5.60	237	22.79	1.86	12	66	10	54	516	18	229	281	35	68	15
57	71.48	0.52	4.01	255	19.60	1.80	12	67	9	61	482	19	271	368	38	79	7
56	71.72	0.49	3.35	213	21.49	1.55	9	55	6	55	472	18	284	321	33	73	9
55	71.93	0.63	4.28	182	13.79	1.76	13	83	7	67	445	23	322	387	45	88	13
53	72.39	0.62	4.53	192	14.79	1.77	16	88	8	67	487	20	300	366	40	66	10
51	73.00	0.62	4.23	179	14.09	1.83	13	77	8	64	449	24	329	399	52	84	11
49	73.58	0.56	3.72	158	20.50	1.56	10	68	6	55	503	17	250	325	37	83	7
47	74.01	0.60	4.13	175	15.18	1.72	16	79	9	62	486	22	311	355	24	71	10
45	74.52	0.55	3.84	163	16.91	1.61	12	75	7	61	467	20	308	367	42	71	12
43	75.13	0.62	4.26	181	14.50	1.80	13	79	9	67	503	23	324	417	39	95	10
41	75.74	0.45	3.22	204	26.38	1.30	10	57	6	49	578	15	226	298	34	71	9
39	76.29	0.58	4.15	176	15.74	1.66	11	75	9	59	507	20	289	358	47	93	8
36	76.81	0.63	4.39	186	15.96	1.67	18	82	8	64	558	18	290	384	35	86	11
34	77.27	0.63	4.33	183	16.23	1.62	15	85	8	63	575	17	249	362	33	78	13
33	77.51	0.56	3.92	166	23.78	1.57	14	72	6	57	602	17	247	336	35	71	11
31	78.03	0.59	4.35	184	19.37	1.68	11	78	10	63	635	20	228	353	29	70	9
29	78.64	0.62	4.37	92	18.64	1.69	22	91	7	64	636	19	251	358	38	72	11
28	78.85	0.64	4.62	98	18.57	1.74	14	86	10	64	647	18	243	357	44	68	12
26	79.19	0.63	4.71	100	18.52	1.75	18	92	11	63	662	18	209	316	30	64	9
24	79.80	0.64	4.64	98	20.23	1.60	17	103	10	61	694	19	194	310	34	70	14
22	80.22	0.52	4.08	173	21.60	1.39	18	80	10	56	656	18	175	294	35	70	13
20	80.77	0.65	4.75	101	17.83	1.57	18	84	9	63	677	19	174	319	37	76	15
18	81.23	0.61	4.70	199	18.47	1.53	16	83	12	63	713	18	224	340	49	89	11
16	81.69	0.46	3.71	236	26.93	1.66	17	67	6	56	746	17	194	293	18	64	9
15	81.90	0.55	4.46	189	21.53	1.52	16	99	7	66	778	17	179	340	37	74	11
13	82.45	0.51	4.20	178	24.57	1.58	18	76	8	60	789	17	170	300	40	68	11
11	83.06	0.64	5.08	108	19.33	1.81	14	88	10	72	744	15	195	355	41	84	14
10	83.27	0.58	4.90	208	19.19	1.67	16	86	9	71	761	16	167	328	26	70	14
9	83.48	0.58	4.72	200	19.77	1.79	17	92	8	68	745	15	190	356	33	92	12
7	83.82	0.40	3.41	216	27.55	1.69	8	60	6	49	652	14	169	277	30	57	12
5	84.49	0.38	3.24	206	31.00	1.52	13	59	6	44	670	12	176	249	28	67	9
3	85.04	0.47	4.21	178	26.80	1.61	15	86	9	58	637	19	193	305	38	89	10
1	85.31	0.56	5.14	218	21.02	1.77	15	93	9	69	648	19	231	358	32	62	12

Appendix 4.3 Major element contents of bulk samples from the immediate K-P transition in the Antioch Church core as determined by wavelength-dispersive X-ray fluorescence spectrometry (WDS). All Fe is given as Fe_2O_3; LOI is loss of ignition.

AC	Depth	SiO$_2$	TiO$_2$	Al$_2$O$_3$	Fe$_2$O$_3$	MnO	MgO	CaO	Na$_2$O	K$_2$O	P$_2$O$_5$	LOI	Total
#	m	wt%	wt%	wt%	wt%	wt%	wt%	wt%	wt%	wt%	wt%	wt%	wt%
110	57.91	41.47	0.62	12.37	5.05	0.02	1.91	17.74	0.35	1.37	0.15	18.28	99.32
108	58.52	25.65	0.35	7.21	3.46	0.02	1.17	31.09	0.22	0.80	0.05	28.74	98.77
106	59.07	37.83	0.53	11.58	7.55	0.02	2.20	17.01	0.26	1.76	0.07	21.20	100.01
104	59.56	44.97	0.69	13.74	7.85	0.03	2.33	11.28	0.36	1.90	0.08	17.01	100.24
103	59.74	45.31	0.71	14.14	8.06	0.03	2.37	11.48	1.04	1.97	0.08	14.06	99.25
102	60.20	48.79	0.76	14.45	6.76	0.03	2.29	9.44	0.46	1.98	0.09	15.20	100.26
101	60.35	48.62	0.79	15.11	6.91	0.03	2.32	8.79	0.57	2.03	0.11	14.36	99.65
100	60.59	49.79	0.79	14.59	7.87	0.04	2.39	8.45	0.59	2.45	0.12	12.73	99.80
99	60.81	46.38	0.68	13.26	9.29	0.03	2.52	11.48	0.51	2.56	0.12	13.79	100.62
98	61.11	44.88	0.63	12.86	11.00	0.02	2.69	10.19	0.34	2.95	0.16	14.67	100.39
97	61.36	20.89	0.13	3.69	10.27	0.01	1.60	27.30	0.17	2.31	0.22	33.91	100.48
96	61.57	40.49	0.29	8.09	16.07	0.01	2.94	12.34	0.18	4.13	0.40	14.97	99.91
95	61.75	45.80	0.29	8.13	16.58	0.01	3.14	9.42	0.18	4.21	0.42	12.22	100.39
94	61.87	24.18	0.11	3.33	8.66	0.02	1.45	33.69	0.12	1.86	0.18	27.83	101.43
93	62.03	52.35	0.23	6.65	12.50	0.01	2.25	11.28	0.21	3.14	0.33	11.75	100.69
92	62.12	19.41	0.08	2.22	5.40	0.02	0.97	38.57	0.15	1.04	0.14	32.50	100.50
91	62.33	22.70	0.11	2.98	5.65	0.02	1.02	35.72	0.17	1.16	0.15	30.50	100.20
90	62.58	53.73	0.28	7.08	9.67	0.01	1.91	13.49	0.30	2.53	0.29	11.98	101.28
88	62.94	22.32	0.16	3.63	3.90	0.02	0.89	36.46	0.19	0.83	0.18	31.16	99.75
87	63.09	32.19	0.23	3.70	5.52	0.02	1.00	31.96	0.34	1.22	0.33	22.77	99.27
86	63.25	40.19	0.30	5.00	6.14	0.02	1.05	23.68	0.60	1.46	0.48	20.37	99.30
85	63.40	45.87	0.32	5.55	6.55	0.02	1.09	22.44	0.49	1.56	0.52	15.29	99.69
84	63.55	37.75	0.27	4.22	5.16	0.02	0.87	28.10	0.44	1.16	0.40	21.38	99.77
83	63.64	65.10	0.42	6.87	7.68	0.02	1.29	7.34	0.64	2.16	0.60	6.97	99.09
82	63.70	53.09	0.26	3.20	2.24	0.03	0.38	22.83	0.55	0.67	0.12	16.75	100.10
81	63.86	48.92	0.15	2.31	2.14	0.03	0.43	25.85	0.49	0.43	0.21	18.89	99.84
80	64.10	62.61	0.17	2.21	2.05	0.02	0.36	17.34	0.25	0.49	0.27	14.10	99.87
79	64.22	56.57	0.12	1.72	1.46	0.03	0.18	22.70	0.30	0.34	0.08	16.32	99.83
78	64.31	56.56	0.24	2.38	2.21	0.03	0.59	24.18	0.34	0.45	0.15	12.53	99.68
77B	64.47	53.71	0.06	1.09	20.96	0.01	0.07	0.28	0.20	0.26	0.03	21.84	98.51
77A	64.50	53.32	0.06	1.10	21.20	0.01	0.07	0.29	0.20	0.25	0.03	22.01	98.54
76	64.62	47.50	0.44	9.21	4.42	0.04	1.03	21.11	0.59	1.38	0.19	13.86	99.76
75	64.92	35.44	0.28	6.13	3.79	0.03	0.76	29.33	0.45	0.94	0.27	22.29	99.71
74	65.23	36.25	0.28	5.91	3.73	0.04	0.79	27.87	0.43	1.01	0.27	23.70	100.27
73	65.68	35.63	0.31	6.54	3.69	0.03	0.78	28.19	0.39	1.00	0.18	22.90	99.66
71	66.60	44.53	0.48	9.02	4.08	0.04	0.98	21.35	0.58	1.62	0.17	16.89	99.74
70	67.06	63.24	0.65	12.00	5.02	0.03	1.20	6.93	0.72	2.06	0.09	7.62	99.57
69	67.51	59.20	0.71	13.72	5.51	0.03	1.50	7.28	0.89	2.18	0.10	8.93	100.06

Appendix 4.4 Stable isotope data from the fine fraction <36 μm of bulk samples from the Antioch Church core. All δ values are given relative to the VPDB (Vienna Peedee belemnite) standard.

Sample	Depth	δ¹⁸O	δ¹³C	Sample	Depth	δ¹⁸O	δ¹³C	Sample	Depth	δ¹⁸O	δ¹³C
#	(m)	VDPD	VDPD	#	(m)	VDPD	VDPD	#	(m)	VDPD	VDPD
235	1.62	-2.48	0.06	173	31.70	-3.13	1.86	100	60.60	-2.53	0.26
234	2.10	-3.15	-0.17	173	32.31	-3.82	1.71	98	61.10	-2.23	0.35
234	2.16	-1.51	0.14	172	33.04	-3.92	1.65	96	61.60	-2.94	0.39
233	2.83	-1.15	0.15	171	34.08	-2.90	1.38	94	61.90	-2.69	-0.09
229	4.27	-1.45	0.19	171	34.14	-3.69	1.36	92	62.10	-2.67	-0.24
228	4.33	-2.26	-0.30	170	34.56	-3.72	1.13	90	62.60	-1.34	0.68
227	4.91	-2.99	0.32	170	34.69	-3.52	1.22	88	62.90	-2.31	0.45
225	6.49	-2.94	0.41	169	35.36	-1.32	0.39	86	63.20	-2.34	0.35
224	6.80	-3.14	0.58	168	35.48	-1.68	0.37	84	63.60	-2.41	0.21
224	6.86	-2.33	0.56	167	35.60	-1.73	0.02	81	63.90	-3.49	-0.26
223	7.62	-2.59	0.50	164	37.34	-1.47	0.27	78	64.30	-1.90	-0.45
221	8.47	-3.30	0.26	162	37.95	-2.05	0.12	76	65.50	-2.12	-0.43
220	9.24	-4.00	0.36	160	39.17	-2.08	0.68	74	65.80	-3.02	-0.37
220	9.30	-2.97	0.71	158	40.39	-1.92	0.82	72	66.30	-1.71	0.17
219	9.91	-3.86	0.70	156	40.84	-2.37	0.78	70	67.10	-1.97	0.19
218	10.85	-3.45	0.21	153	42.37	-2.24	0.93	68	68.30	-1.75	0.27
217	11.19	-3.49	-0.34	151	43.13	-2.06	0.76	66	69.20	-1.73	0.63
216	11.46	-2.50	0.14	150	43.74	-2.96	0.76	64	69.60	-1.71	0.75
216	11.52	-2.32	0.10	148	44.35	-3.05	0.42	62	70.10	-1.93	0.56
214	12.41	-1.19	0.98	147	44.96	-1.53	0.73	60	70.60	-1.83	0.29
211	14.23	-1.23	0.94	146	45.57	-1.95	0.63	58	71.10	-1.88	0.37
210	14.63	-1.08	0.82	145	46.33	-1.58	0.70	56	71.70	-3.66	-0.11
208	15.85	-3.58	0.50	144	46.63	-1.59	0.69	54	72.20	-1.89	0.54
205	17.07	-1.11	0.78	141	47.85	-1.63	0.70	52	72.70	-3.44	-0.80
204	17.95	-1.47	0.55	139	49.01	-1.89	0.33	48	73.80	-2.00	0.15
203	18.14	-1.75	0.60	138	49.32	-2.69	0.57	46	74.30	-3.72	-0.48
202	18.59	-2.88	0.43	135	50.75	-2.86	0.58	44	74.90	-1.75	0.74
201	18.68	-3.09	0.15	134	51.33	-1.73	0.51	42	75.40	-1.94	0.59
199	19.81	-1.81	0.64	133	51.94	-1.94	0.31	40	75.90	-1.81	0.49
198	20.36	-1.33	0.91	130	52.49	-3.41	0.35	39	76.30	-1.78	0.53
198	20.39	-2.40	0.90	127	53.28	-3.13	0.07	37	76.70	-3.86	-0.40
197	21.03	-1.83	0.61	126	53.77	-2.64	-0.01	35	77.10	-1.96	0.69
194	22.31	-1.53	0.80	125	53.86	-2.29	0.29	32	77.70	-3.23	-0.07
193	22.74	-2.76	0.83	124	54.22	-1.61	0.36	30	78.30	-1.95	0.78
193	22.92	-1.82	0.75	123	54.41	-2.33	-1.00	27	79.00	-2.76	0.33
192	23.96	-1.61	0.67	122	54.60	-2.00	0.32	23	80.10	-2.51	0.45
191	24.23	-0.74	0.59	120	55.30	-2.87	0.36	21	80.50	-1.99	0.93
190	24.51	-1.65	0.23	119	55.60	-2.32	0.27	19	81.00	-1.95	0.91
188	25.88	-1.99	0.00	117	56.20	-3.32	0.34	17	81.50	-3.38	-0.21
186	26.21	-1.84	0.12	115	56.80	-2.45	0.38	15	81.90	-2.33	0.58
180	28.35	-1.90	-0.15	113	57.40	-2.35	0.41	12	82.80	-2.13	0.70
179	28.90	-1.90	-0.05	111	57.80	-3.68	0.51	10	83.30	-1.82	0.98
178	29.38	-1.74	-0.24	109	58.30	-2.72	0.39	8	83.70	-1.76	0.65
177	29.41	-2.60	1.62	107	58.80	-2.48	0.75	6	84.10	-1.84	0.48
176	29.81	-4.00	1.78	105	59.40	-2.43	0.66	4	84.70	-1.81	0.04
174	31.39	-3.63	1.71	102	60.20	-2.43	0.40	1	85.00	-1.83	0.66